

RELEASED FOR PUBLIC AVAILABILITY
MAY 2, 1977

**A METHOD FOR PREDICTING THE STABILITY CHARACTERISTICS
OF AN ELASTIC AIRPLANE**

Volume I—FLEXSTAB Theoretical Description

By A. R. Dusto, G. W. Brune, G. M. Dornfeld, J. E. Mercer,
S. C. Pilet, P. E. Rubbert, R. C. Schwanz,
P. Smutny, E. N. Tinoco, and J. A. Weber

D6-41064-1
October 1974

Distribution of this report is provided in the interest of
information exchange. Responsibility for the contents
resides in the author or organization that prepared it.

Prepared Under Contract No. NAS2-5006 by

Boeing Commercial Airplane Company
Seattle, Washington 98124

and

Boeing Computer Services, Inc.
Seattle, Washington 98124

for

**AMES RESEARCH CENTER
NATIONAL AERONAUTICS AND SPACE ADMINISTRATION**



(NASA-CR-114712) A METHOD FOR PREDICTING
THE STABILITY CHARACTERISTICS OF AN ELASTIC
AIRPLANE. VOLUME 1: FLEXSTAB THEORETICAL
DESCRIPTION (Boeing Commercial Airplane Co.,
Seattle) 653 p HC A99/MF A01
CSCL 010 G3/08
Unclass
25043
A77-23124

CONTENTS

	Page
SUMMARY	1
1.0 INTRODUCTION	1-1
2.0 COORDINATE SYSTEMS AND KINEMATIC DESCRIPTION	2-1
2.1 Introduction	2-1
2.2 Coordinate Systems	2-3
2.2.1 Inertial Axis System	2-3
2.2.2 Body Axis System	2-3
2.2.3 Fluid Axis System	2-3
2.2.4 Reference Axis System	2-6
2.2.5 Stability Axis System	2-6
2.3 Kinematic Description	2-7
2.3.1 Motion Relative to the Inertial Axis System	2-9
2.3.2 Mean Reference Frame	2-9
2.3.2.1 Moving Reference Frame	2-9
2.3.2.2 Moving Axis System as a Mean Reference Frame	2-11
2.3.2.3 Mean Reference Frame Constraint Conditions	2-13
2.3.2.4 Approximate Mean Reference Frame Constraint Conditions	2-15
2.3.2.5 Reference and Perturbation Motions	2-17
2.3.3 Fluid Motions	2-20
2.3.3.1 Surface Boundary Condition	2-20
2.3.3.2 Linearized Surface Boundary Condition	2-24
2.3.3.3 Flow Incidence for a Fixed Surface Geometry in the Fluid Axis System—Case (1)	2-25
2.3.3.4 Flow Incidence Arising From Surface Motion Relative to the Fluid Axis System—Case (2)	2-27
2.3.3.5 Combined Linearized Surface Boundary Condition—Case (3)	2-29
2.3.3.6 Dynamic Pressure and Mach Number Variations	2-30
2.3.4 Wake Motions	2-31
3.0 AERODYNAMICS	3-1
3.1 Introduction	3-1
3.2 Derivation of the Linear Aerodynamic Theory	3-8
3.2.1 Nonlinear Aerodynamic Theory	3-8
3.2.1.1 Flow Equation	3-8
3.2.1.2 Surface Boundary Condition	3-9
3.2.1.3 Wake Boundary Condition	3-9
3.2.1.4 Far-Field Boundary Condition	3-9
3.2.1.5 Pressure Relation	3-9
3.2.1.6 Statement of the Aerodynamic Problem	3-9
3.2.1.7 Aerodynamic Coordinate Systems	3-9
3.2.1.8 Special Notation Related to Spatial Coordinates	3-10

CONTENTS—Continued

	Page
3.2.2 Asymptotic Expansion Method	3-10
3.2.2.1 The Asymptotic Series	3-10
3.2.2.2 Low Frequency Approximation	3-10
3.2.3 Wing-Body Problem	3-11
3.2.4 Analytical Geometry of Wing-Body Problem	3-13
3.2.4.1 Aerodynamic Local Axis Systems	3-13
3.2.4.2 Analytical Geometry of Thin Bodies	3-13
3.2.4.3 Analytical Geometry of Slender Bodies	3-14
3.2.5 Asymptotic Expansion of the Wing-Body Problem	3-16
3.2.5.1 Asymptotic Series	3-17
3.2.5.2 Expansion of the Flow Equation	3-17
3.2.5.3 Expansion of the Thin Body Surface Boundary Condition	3-18
3.2.5.4 Expansion of the Wake Boundary Condition	3-20
3.2.5.5 Expansion of the Slender Body Surface Boundary Condition	3-23
3.2.5.6 Linear First-Order Aerodynamic Theory for the Wing-Body Problem	3-25
3.2.6 Low Frequency Approximation	3-26
3.2.6.1 Simple Harmonic Time Dependence	3-27
3.2.6.2 Asymptotic Series in Frequency	3-27
3.2.6.3 First-Order Approximation to Unsteady Flow	3-28
3.2.6.4 Derivation of the Form of the Solution to the First Order Problems	3-29
3.2.6.5 Solution to the First Order in Frequency Problem	3-36
3.2.6.6 Arbitrary, Slowly Varying, Time Dependence	3-37
3.2.7 Summary of the Linear Wing-Body Problem	3-38
3.2.8 Restrictions on the Validity of the Low Frequency Approximation	3-41
3.3 Formulation as a System of Integral Equations	3-45
3.3.1 General Approach	3-48
3.3.1.1 Formulation as an Integral Equation	3-48
3.3.1.2 Reduction to an Integral on the Mean Surfaces of Thin and Slender Bodies	3-49
3.3.2 Method of Solution for Individual Flow Problems	3-51
3.3.2.1 Isolated Thin Body Thickness Problem	3-52
3.3.2.2 Isolated Thin Body Steady Lifting Problem	3-53
3.3.2.3 Isolated Slender Body Thickness Problem	3-53
3.3.2.4 Isolated Slender Body Steady Lifting Problem	3-54
3.3.2.5 Steady Aerodynamic Induction Problem	3-56
3.3.2.6 Isolated Thin Body Unsteady Lifting Problem	3-57
3.3.2.7 Isolated Slender Body Unsteady Lifting Problem	3-59
3.3.2.8 Unsteady Aerodynamic Induction Problem	3-61
3.3.3 Integral Equations Describing the Aerodynamic Surface Pressure.	3-62

CONTENTS—Continued

	Page
3.4 Numerical Solution	3-67
3.4.1 Paneling Scheme	3-67
3.4.1.1 Local Panel Coordinate Axis Systems	3-69
3.4.1.2 Local Line Segment Coordinate Axis Systems	3-69
3.4.1.3 Panel Geometry	3-70
3.4.1.4 Paneling Arrangement	3-71
3.4.1.5 Image System of Panels and Line Segments	3-72
3.4.1.6 Flow Incidence at Panel Control Points	3-73
3.4.2 Isolated Thin Body Thickness Problem	3-75
3.4.2.1 Isolated Thin Body Thickness Interference Flow Incidence	3-78
3.4.2.2 Isolated Thin Body Thickness Pressure	3-81
3.4.2.3 Isolated Thin Body Thickness Induced Velocity Components	3-82
3.4.3 Isolated Thin Body Steady Lifting Problem	3-90
3.4.3.1 Isolated Thin Body Steady Lifting Interference Flow Incidence	3-94
3.4.3.2 Isolated Thin Body Steady Lifting Pressure	3-96
3.4.3.3 Isolated Thin Body Steady Lift Induced Velocity Components	3-97
3.4.4 Isolated Slender Body Thickness Problem	3-100
3.4.4.1 Isolated Slender Body Thickness Interference Flow Incidence	3-103
3.4.4.2 Isolated Slender Body Thickness Pressure	3-105
3.4.4.3 Isolated Slender Body Thickness Induced Velocity Components	3-107
3.4.5 Isolated Slender Body Steady Lifting Problem	3-110
3.4.5.1 Isolated Slender Body Steady Lift Interference Flow Incidence	3-116
3.4.5.2 Isolated Slender Body Steady Lifting Pressure	3-118
3.4.5.3 Isolated Slender Body Steady Lift Induced Velocity Components	3-120
3.4.6 Steady Aerodynamic Induction Problem	3-129
3.4.6.1 Steady Aerodynamic Induction Potential	3-129
3.4.6.2 Steady Aerodynamic Induction Pressure	3-130
3.4.7 Combined Steady Aerodynamic Problem	3-132
3.4.7.1 Combined Steady Lifting Aerodynamics	3-132
3.4.7.2 Combined Thickness Aerodynamics	3-135
3.4.8 Isolated Thin Body Unsteady Lifting Problem	3-136
3.4.8.1 Isolated Thin Body Unsteady Lifting Interference Flow Incidence	3-138
3.4.8.2 Isolated Thin Body Unsteady Lifting Pressure	3-139
3.4.8.3 Isolated Thin Body Unsteady Lift Induced Velocity Components	3-139

CONTENTS—Continued

	Page
3.4.9 Isolated Slender Body Unsteady Lifting Problem	3-144
3.4.9.1 Isolated Slender Body Unsteady Lifting Interference Flow Incidence	3-145
3.4.9.2 Isolated Slender Body Unsteady Lifting Pressure	3-146
3.4.9.3 Isolated Slender Body Unsteady Lift Induced Velocity Components	3-147
3.4.10 Unsteady Aerodynamic Induction Problem	3-147
3.4.10.1 Unsteady Aerodynamic Induction Potential	3-147
3.4.10.2 Unsteady Aerodynamic Induction Pressure	3-149
3.4.11 Combined Unsteady Aerodynamic Problem	3-150
3.4.12 Leading Edge Thrust Correction	3-153
3.4.12.1 Leading Edge Thrust of a Flat Plate in Subsonic Flow	3-153
3.4.12.2 Surface Correction at the Leading Edge Panel	3-157
3.4.12.3 Leading Edge Correction for Arbitrary Lifting Thin Bodies	3-157
3.4.13 Aerodynamic Effects of Speed Variations	3-160
3.4.14 Empirical Corrections	3-162
3.4.15 Near Field-Far Field Approximation	3-164
3.4.15.1 Aerodynamic Matrices Involved in the Approximation	3-164
3.4.15.2 Near Field Panel Arrangement	3-164
3.4.15.3 Modifications of the Aerodynamic Equations	3-166
3.4.15.4 Application of the Near Field-Far Field Approximation	3-168
3.5 Aerodynamic Force Derivatives	3-168
3.5.1 Aerodynamic Forces	3-168
3.5.1.1 Paneling Scheme Expansion of the Aerodynamic Force and Couple	3-169
3.5.1.2 Aerodynamic Force at a Thin Body Panel	3-171
3.5.1.3 Aerodynamic Force at a Mean Interference Surface Panel of a Slender Body	3-174
3.5.1.4 Aerodynamic Force at a Slender Body Segment	3-176
3.5.1.5 Combined Aerodynamic Panel and Slender Body Segment Forces	3-178
3.5.1.6 Aerodynamic Panel Forces From Leading Edge Correction	3-184
3.5.2 Lifting Pressure Coefficients in Terms of Flow Incidence	3-184
3.5.2.1 Expansion of the Flow Incidence Matrix	3-186
3.5.2.2 Effects of Dynamic Pressure and Mach Number Variations	3-192
3.5.3 Aerodynamic Force Derivative Formulation	3-194
3.5.3.1 Reference State	3-194
3.5.3.2 Perturbation Expansion	3-195
3.5.3.3 Expansion of Leading Edge Correction Terms	3-197
3.5.3.4 Formulation of the Aerodynamic Force Derivatives	3-199

CONTENTS—Continued

	Page
4.0 STRUCTURES	4-1
4.1 Introduction	4-1
4.2 Structural Equations of Motion	4-2
4.2.1 Hamilton's Principle	4-2
4.2.2 Finite Element Method	4-4
4.2.2.1 Finite Element Concepts	4-4
4.2.2.2 Finite Element Approximations and Structural Reference Frame	4-12
4.2.2.3 Hamilton's Principle in Finite Element Form	4-16
4.2.2.4 Derivation of the Equations of Motion	4-18
4.2.2.5 Evaluation of the Lagrange Multipliers	4-20
4.2.3 Equations of Motion for the Steady Reference Flight Condition	4-23
4.2.3.1 Structural Equations in Terms of Flexibility	4-24
4.2.3.2 Inertial Relief	4-25
4.2.4 Equations of Motion for the Unsteady Perturbation Flight Condition	4-26
4.2.4.1 Free Vibration Mode Shapes	4-26
4.2.4.2 Structural Equations of Motion in Terms of Flexibility	4-28
4.2.4.3 Residual Flexibility Formulation	4-28
4.2.5 Simplification Using the Symmetry of an Aircraft	4-32
4.2.6 Deformation of the Aerodynamic Surfaces	4-33
4.2.6.1 Rotational Deformation	4-35
4.2.6.2 Translational Deformation Rate	4-37
4.2.6.3 Surface Deformation at Aerodynamic Control Points	4-37
4.2.7 Forces at the Structural Nodes due to Aerodynamic Surface Pressure	4-39
4.2.8 Propulsion System Forces and Motions	4-45
4.3 Internal Structural Influence Coefficients	4-46
4.3.1 Description of the Elastic Axis and Beam Finite Elements	4-49
4.3.1.1 Thin Body Elastic Axis	4-49
4.3.1.2 Slender Body Elastic Axis	4-52
4.3.1.3 Assembly of Thin and Slender Structural Bodies to Form a Configuration	4-53
4.3.1.4 Elastic Axis Element Stiffnesses	4-54
4.3.1.5 Elastic Axis Element Stiffness Matrices	4-55
4.3.1.6 Composite Stiffness Matrix	4-57
4.3.1.7 Thin Body Finite Element Stiffness Matrices	4-57
4.3.1.8 Thin Body Composite Stiffness Matrix	4-59
4.3.1.9 Slender Body Finite Element Stiffness Matrices	4-63
4.3.1.10 Slender Body Composite Stiffness Matrix	4-65
4.3.1.11 Junction Point Stiffness Matrices	4-66
4.3.1.12 Reference Junction Point for the Structure	4-70

CONTENTS—Continued

	Page
4.3.1.13 Coplanar Thin Body Junction Points	4-71
4.3.1.14 Plane of Structural Symmetry	4-73
4.3.1.15 Special Consideration for Nodes on the Plane of Symmetry	4-73
4.3.2 Reduction of the Composite Stiffness Matrix	4-73
4.3.2.1 Composite Stiffness Matrix Partitions	4-73
4.3.2.2 Structural Node Point Degrees of Freedom	4-75
4.3.3 Displacement Relations for Beam Finite Elements	4-75
4.3.3.1 Constrained Displacement Relations	4-78
4.3.3.2 Example of Combined Constraint Relations	4-81
4.3.3.3 Constrained Displacement Relation for Combined Structure	4-84
4.3.3.4 Independent Elastic Displacement Relations	4-84
4.3.3.5 Thin Structural Bodies—Displacement Relations	4-85
4.3.3.6 Slender Structural Bodies—Displacement Relations	4-87
4.3.4 Deformation of the Aerodynamic Surfaces	4-88
4.3.4.1 Constrained Rotations at Aerodynamic Surfaces	4-88
4.3.4.2 Independent Elastic Rotations at Aerodynamic Surfaces	4-89
4.3.4.3 Evaluation of the Aerodynamic Surface Deformation on Thin Bodies	4-91
4.3.4.4 Evaluation of the Aerodynamic Surface Deformation on Slender Bodies	4-93
4.3.4.5 Elastic Axis Rate of Twist	4-94
4.3.5 Summary of Aerodynamic Surface Deformation Transformations	4-95
4.3.5.1 Subsets of Elastic Axis Nodal Displacement Components	4-95
4.3.5.2 Partitioned Deformation Transformations	4-96
4.3.5.3 Junction Point Partitions	4-97
4.3.5.4 Slender Body Partitions	4-98
4.3.5.5 Thin Body Partitions	4-99
4.3.6 Propulsion System Forces and Motions	4-101
4.3.7 Mass Matrix	4-105
4.3.7.1 Inertially Equivalent Lumped Masses	4-106
4.3.7.2 Lumped Masses on a Thin Body	4-107
4.3.7.3 Nodal Mass Matrix for a Thin Body Node	4-110
4.3.7.4 Lumped Masses on a Slender Body	4-110
4.3.7.5 Nodal Mass Matrix for a Slender Body Node	4-111
4.3.7.6 Nodal Mass Matrices for Junction Point Nodes	4-111
4.3.7.7 Nodal Mass Matrix for a Complete Structure	4-112
4.3.8 Reduction of the Nodal Mass Matrix	4-113
4.3.8.1 Reduction of the Mass Transformation Matrix $[P_m]$	4-113
4.3.8.2 Equilibrium of the Inertial Forces	4-115

CONTENTS—Continued

	Page
4.3.9 Free Vibrations	4-116
4.3.9.1 Reduction to a Standard Eigenvalue Problem	4-117
4.3.9.2 Solution to the Free Vibration Problem	4-118
4.3.9.3 Construction of the Transformation Matrix	4-119
4.3.9.4 Nodal Displacements in Terms of Generalized Coordinates	4-119
4.3.10 Combined Structural Relations	4-121
4.3.10.1 Stiffness Matrices	4-123
4.3.10.2 Flexibility	4-124
4.3.10.3 Residual Flexibility Matrices	4-129
4.4 External Structural Influence Coefficients	4-132
4.4.1 Structural Idealization	4-133
4.4.1.1 Components of Nodal Displacement	4-134
4.4.1.2 Components of Nodal Forces	4-136
4.4.1.3 Symmetric and Antisymmetric Forms	4-137
4.4.1.4 Displacement Relations	4-137
4.4.1.5 Thin Body Displacement Relations	4-137
4.4.1.6 Slender Body Displacement Relations	4-141
4.4.1.7 Aerodynamic Surface Deformation Transformations	4-143
4.4.1.8 Forces at the Structural Nodes Due to Aerodynamic Surface Pressure	4-148
4.4.1.9 Reduction of the Structural Degrees of Freedom	4-150
4.4.1.10 Approximations in the Pressure-Force Transformation Matrix	4-150
4.4.1.11 Slender Body Application	4-150
4.4.1.12 Thin Body Application	4-151
4.4.2 ESIC Coordinate Systems	4-152
4.4.2.1 Arrangement of the ESIC Coordinate Systems	4-154
4.4.2.2 Transformation of Node Point Geometry	4-155
4.4.3 Construction of the Gyroscopic Couple Transformation Matrix	4-155
4.4.4 Matrix Operators Involving Nodal Inertial Forces	
4.4.4.1 Reduction of the Nodal Degrees of Freedom	4-159
4.4.4.2 Approximate Mass Matrix	4-160
4.4.4.3 Computation of the Mean Reference Frame	4-161
4.4.4.4 Computation of the Nodal Inertial Forces	4-161
4.4.4.5 Deletion of Aerodynamic Forces Resulting From Reduced Degrees of Freedom	4-162
4.4.5 Requirements That Supplied Structural Matrices Must Satisfy	4-163
4.4.5.1 Coordinate Systems	4-163
4.4.5.2 Symmetric and Antisymmetric Forms	4-163
4.4.5.3 Admissible Nodal Degrees of Freedom	4-163
4.4.5.4 Flexibility Matrix Requirements	4-163
4.4.5.5 Free Vibration Mode Shapes	4-163
4.4.5.6 Constraining Degrees of Freedom	4-163

CONTENTS—Continued

	Page
4.4.5.7 Nodal Mass Matrix	4-163
4.4.5.8 Rigid Body Mode Shape Matrix	4-163
4.4.5.9 Total Mass-Inertia Matrix	4-164
5.0 STEADY, REFERENCE FLIGHT CONDITION	5-1
5.1 Introduction	5-1
5.2 Equations of Motion for the Steady, Reference Flight Condition	5-2
5.2.1 Specification of the Reference Flight Condition	5-3
5.2.1.1 Coordinated Maneuvers	5-4
5.2.1.2 Quasi-Steady Maneuvers	5-6
5.2.2 Formulation of the Trim Problem	5-7
5.2.2.1 Nonlinear Trim Problems	5-7
5.2.2.2 Nonlinear Aerodynamic Forces	5-8
5.2.2.3 Linear Trim Problem	5-8
5.2.2.4 Linear Aerodynamic Forces	5-10
5.2.2.5 Aerodynamic Derivatives	5-10
5.3 Aerodynamics of the Reference Flight Condition—Aerodynamic Derivatives	5-11
5.3.1 Summary of Linear Aerodynamic and Structural Theories	5-11
5.3.1.1 Linear Structural Equation	5-12
5.3.1.2 Linear Aerodynamic Equations	5-13
5.3.1.3 Combined Aerodynamic and Structural Equations	5-13
5.3.2 Aerodynamic Derivatives for a Flexible Aircraft	5-14
5.3.2.1 Longitudinal Aerodynamic Derivatives for a Flexible Aircraft	5-15
5.3.2.2 Lateral-Directional Aerodynamic Derivatives for a Flexible Aircraft	5-17
5.3.3 Linear Aerodynamic Forces for a Rigid Aircraft	5-18
5.3.3.1 Longitudinal Aerodynamic Derivatives for a Rigid Aircraft	5-18
5.3.3.2 Lateral-Directional Aerodynamic Derivatives for a Rigid Aircraft	5-19
5.3.4 Aeroelastic Increment to the Aerodynamic Derivatives	5-21
5.3.4.1 Expansion of the Aeroelastic Matrix	5-21
5.3.4.2 Expansion of the Longitudinal Aerodynamic Derivatives for a Flexible Aircraft	5-22
5.3.4.3 Expansion of the Lateral-Directional Aerodynamic Derivatives for a Flexible Aircraft	5-24
5.3.5 Nonlinear Aerodynamic Derivatives	5-26
5.3.5.1 Aeroelastic Effects	5-27
5.3.5.2 Nonlinear, Rigid Aircraft Aerodynamic Derivatives	5-27
5.4 Propulsion System Forces	5-34

CONTENTS—Continued

	Page
5.5 Trim Problem Solution	5-41
5.5.1 Methods of Solution	5-41
5.5.2 Linear Trim Problem	5-42
5.5.2.1 Case (1), Specified Flight Path Angle	5-42
5.5.2.2 Case (2), Specified Thrust Amplitude Setting T_1	5-43
5.5.2.3 Longitudinal Motion	5-44
5.5.3 Nonlinear Trim Problem	5-45
5.6 Static Stability Derivatives	5-49
5.6.1 Classification of Static Stability Derivatives	5-49
5.6.1.1 Longitudinal Static Stability Derivatives	5-49
5.6.1.2 Lateral-Directional Static Stability Derivatives	5-49
5.6.2 Nondimensional Form of the Static Stability Derivatives	5-50
5.6.2.1 Nondimensional Longitudinal Static Stability Derivatives	5-50
5.6.2.2 Nondimensional Lateral-Directional Static Stability Derivatives	5-51
5.6.3 Static Perturbation Aerodynamic Forces	5-53
5.6.3.1 Basic Relations Used in the Formulation	5-53
5.6.3.2 Formulation of the Static Perturbation Aerodynamic Forces	5-54
5.6.4 Static Stability Derivative Formulation	5-57
5.6.4.1 Rigid Aircraft Longitudinal Stability Derivatives	5-57
5.6.4.2 Rigid Aircraft Lateral-Directional Static Stability Derivatives	5-60
5.6.4.3 Aeroelastic Increments to the Longitudinal Static Stability Derivatives	5-61
5.6.4.4 Aeroelastic Increments to the Lateral-Directional Static Stability Derivatives	5-63
5.7 Static Stability and Trim Characteristics	5-64
5.7.1 Static Stability Parameters	5-65
5.7.1.1 Stick Speed Stability	5-65
5.7.1.2 Neutral Point	5-66
5.7.1.3 Static Margin	5-67
5.7.1.4 Elevator Angle Per g (Pull-Up)	5-67
5.7.1.5 Elevator Angle Per g (Turn)	5-67
5.7.1.6 Maneuver Point	5-67
5.7.2 Elastic Deformation	5-68
5.7.2.1 Jig Shape Computation	5-68
5.7.2.2 Off-Design Point Flight Condition Shapes	5-69
5.7.3 Static Loads and Pressure Distribution	5-69
5.7.3.1 Static Loads	5-69
5.7.3.2 Reference Flight Condition Aerodynamic Lifting Pressure Distribution	5-71
5.7.3.3 Airloads Due to a Vertical Gust During 1-g Level Flight	5-72

CONTENTS—Continued

	Page
5.8 Implementation of Empirical Aerodynamic Correction Methods	5-73
5.8.1 Correction of the Steady Aerodynamic Influence Coefficients	5-73
5.8.2 Aerodynamic Surface Area Corrections	5-73
5.8.3 Corrections to Flow Incidence and Steady Lifting Pressure	5-75
5.8.3.1 Corrected Reference Flight Condition Aerodynamic Forces	5-75
5.8.3.2 Corrected Longitudinal Aerodynamic Derivatives for a Rigid Aircraft	5-77
5.8.3.3 Corrected Lateral-Directional Aerodynamic Derivatives for a Rigid Aircraft	5-78
5.8.3.4 Corrected Aeroelastic Increments to the Longitudinal Aerodynamic Derivatives	5-79
5.8.3.5 Corrected Aeroelastic Increments to the Lateral-Directional Aerodynamic Derivatives	5-81
5.8.3.6 Corrected Static Perturbation Aerodynamic Force	5-82
5.8.3.7 Corrected Longitudinal Static Stability Derivatives for a Rigid Aircraft	5-84
5.8.3.8 Corrected Lateral-Directional Static Stability Derivatives for a Rigid Aircraft	5-87
5.8.3.9 Corrected Aeroelastic Increments to the Longitudinal Static Stability Derivatives	5-88
5.8.3.10 Corrected Aeroelastic Increments to the Lateral-Directional Static Stability Derivatives	5-90
6.0 UNSTEADY PERTURBATION FLIGHT CONDITION	6-1
6.1 Introduction	6-1
6.2 Unsteady Perturbation Equations of Motion	6-2
6.2.1 Applied Forces	6-3
6.2.1.1 Perturbation Aerodynamic Forces	6-3
6.2.1.2 Perturbation Thrust Forces	6-4
6.2.1.3 Perturbation Gyroscopic Forces	6-5
6.2.1.4 Matrix Formulation of Perturbation Gyroscopic Couples	6-7
6.2.2 Matrix Formulation of the Perturbation Equations of Motion	6-9
6.2.2.1 Nonlinear Rigid Body Perturbation Equations of Motion	6-10
6.2.2.2 Linear Perturbation Rigid Body Equations of Motion	6-11
6.2.2.3 Perturbation Structural Equations of Motion	6-12
6.3 Unsteady Perturbation Aerodynamic Forces	6-12
6.3.1 Basic Aerodynamic and Structural Relations	6-12
6.3.1.1 Basic Structural Relation	6-13
6.3.1.2 Combination of the Aerodynamic and Structural Relations	6-13
6.3.1.3 Approximation to the Leading Edge Correction	6-15

CONTENTS—Continued

	Page
6.3.2 Aerodynamic Force Coefficient Matrices	6-16
6.3.2.1 Longitudinal Motion and Rigid Aircraft	6-18
6.3.2.2 Lateral-Directional Motion	6-20
6.3.2.3 Aeroelastic Increments to the Unsteady Perturbation Aerodynamics	6-23
6.3.2.4 Longitudinal Motion Aeroelastic Increments	6-23
6.3.2.5 Lateral-Directional Motion Aeroelastic Increments	6-25
6.3.3 Combined Aerodynamic Matrices	6-28
6.3.3.1 $[A_1^A]$, Coefficient of $\{V\}_P$	6-28
6.3.3.2 $[A_2^A]$, Coefficient of $\{\dot{V}\}_P$	6-28
6.3.3.3 $[A_3^A]$, Coefficient of $\{u_1\}_P$	6-29
6.3.3.4 $[A_4^A]$, Coefficient of $\{\dot{u}_1\}_P$	6-29
6.3.3.5 $[A_5^A]$, Coefficient of $\{\ddot{u}_1\}_P$	6-30
6.3.3.6 $[a_1]$, Coefficient of $\{V\}_P$	6-31
6.3.3.7 $[a_2]$, Coefficient of $\{\dot{V}\}_P$	6-31
6.3.3.8 $[a_3^A]$, Coefficient of $\{u_1\}_P$	6-32
6.3.3.9 $[a_4^A]$, Coefficient of $\{\dot{u}_1\}_P$	6-32
6.3.3.10 $[a_5^A]$, Coefficient of $\{\ddot{u}_1\}_P$	6-33
6.3.4 Empirically Corrected Aerodynamic Force Coefficient Matrices	6-34
6.3.5 Dynamic Loads and Unsteady Pressure Distribution	6-38
6.3.5.1 Dynamic Structural Loads	6-38
6.3.5.2 Unsteady Pressure Distribution	6-44
6.4 Linear Dynamic Analysis	6-45
6.4.1 Linear Equations of Motion	6-45
6.4.1.1 Coupled Motion and Totally Dependent Structural Behavior	6-47
6.4.1.2 Coupled Motion and Independent Structural Motion	6-48
6.4.1.3 Longitudinal Motion and Totally Dependent Structural Behavior	6-51
6.4.1.4 Lateral-Directional Motion and Totally Dependent Structural Behavior	6-53
6.4.1.5 Longitudinal Motion and Independent Symmetric Structural Motion	6-55
6.4.1.6 Lateral-Directional Motion and Independent Antisymmetric Structural Motion	6-55
6.4.2 Characteristic Equation Rooting	6-56

CONTENTS—Concluded

	Page
6.4.3 Dynamic Stability Characteristics	6-56
6.4.3.1 Times to One-Half and One-Tenth Amplitude	6-57
6.4.3.2 Frequency and Period	6-57
6.4.3.3 Logarithmic Decrement	6-57
6.4.3.4 Undamped Natural Frequency	6-58
6.4.3.5 Damping Ratio	6-58
6.4.3.6 Phase and Amplitude of Modal Coupling	6-58
6.4.4 Dynamic Stability Derivatives	6-59
6.5 Nonlinear Dynamic Analysis	6-64
6.5.1 Nonlinear Equations of Motion	6-64
6.5.2 Nonlinear Aerodynamic Data	6-65
6.5.2.1 Nonlinear Steady Aerodynamic Data	6-67
6.5.2.2 Nonlinear Unsteady Aerodynamic Data	6-68
6.5.2.3 Nonlinear Aerodynamic Data Transformations	6-69
6.5.3 Excitation by Penetration of a Discrete Gust	6-71
6.5.3.1 Coordinate Systems	6-71
6.5.3.2 Aircraft Motion in a Gust Field	6-73
6.5.3.3 Gust Field Velocity Components	6-74
6.5.3.4 Gust Field Flow Incidence	6-76
6.5.3.5 Gust Field Flow Incidence Rate	6-77
6.5.3.6 Gust Incidence Vectors	6-77
6.5.3.7 Sine Wave Gust	6-78
6.5.3.8 One-Minus-Cosine Wave Gust	6-80
6.5.3.9 Modified Square Wave Gust	6-81
6.5.3.10 Gust-Field-Induced Aerodynamic Forces	6-83
GLOSSARY	G-1
APPENDIX A — Symbols	A-1
APPENDIX B — Definition of the Circle-Cross Product Matrix Operator \otimes	B-1
B.1 Introduction	B-1
B.2 Symbols and Definitions	B-1
B.3 Conformability and Operator Definitions	B-3
B.3.1 A Row Operator	B-3
B.3.2 A Column Operator	B-4
B.3.3 An Element Operator	B-5
B.4 Commutative Property of the Operator \otimes	B-6
B.5 Associative Property of the Operator \otimes	B-7
B.6 Distributive Property of the Operator \otimes Over Matrix Addition	B-8
B.7 The Operator \otimes Combined With Standard Matrix Operations	B-10
B.8 Special Considerations of \otimes as it is Used in the FLEXSTAB Program	B-21
B.9 Index to the Uses of the Circle-Cross Product Matrix Operator	
Within the FLEXSTAB Theoretical Development	B-22
B.10 Index to the Explicit Uses of the Circle-Cross Product Matrix Operator	
Within the FLEXSTAB Code	B-22
REFERENCES	R-1

FIGURES

No.		Page
2.2-1	Inertial and Body Axis Systems	2-4
2.2-2	Body, Fluid, and Reference Axis Systems at Time $t = t_0$	2-4
2.2-3	Fluid Axis System as a Portable System	2-5
2.2-4	Body and Stability Axis Systems	2-6
2.3-1	Position and Velocity Relative to Inertial Axis System	2-10
2.3-2	Position and Velocity Relative to a Moving Reference Frame	2-10
2.3-3	Elastic Displacement	2-15
2.3-4	Angle of Flow Incidence	2-23
2.3-5	Mean Wake Surface	2-32
3.1-1	Typical Thin Body-Slender Body Configuration Arrangement	3-1
3.1-2	Thin Body Mean Surface	3-3
3.1-3	Slender Body Mean Centerline	3-3
3.1-4	Mean Interference Surface of a Slender Body	3-4
3.1-5	Typical Aerodynamic Paneling Scheme	3-5
3.2-1	Wing-Body Problem	3-11
3.2-2	Wing-Body Component Arrangement	3-12
3.2-3	Aerodynamic Local Axis System	3-13
3.2-4	Thin Body Section Geometry	3-13
3.2-5	Slender Body Cross-Section Geometry	3-15
3.2-6	Limiting Form of Configuration	3-16
3.2-7	Wake Surface	3-21
3.2-8	Corresponding Points on the Actual and Mean Surfaces of a Slender Body	3-23
3.2-9	Regions of Integration for Subsonic Velocity Potential	3-43
3.2-10	Complex Aerodynamic Load on Circular Wing Oscillating in Pitch About Midchord	3-46
3.2-11	Complex Aerodynamic Load on SST Wing Oscillating in Pitch About Midchord	3-47
3.3-1	Surfaces Surrounding the Flow Field	3-49
3.3-2	Slender Body Cross Section for Classical Slender Body Theory	3-54
3.4-1	Typical Surface Paneling Arrangement	3-68
3.4-2	Typical Centerline Segment Arrangement	3-68
3.4-3	Local Axis System	3-69
3.4-4	Local Centerline Segment Coordinate System	3-70
3.4-5	Typical Mean Surface Panel	3-70
3.4-6	Mean Surface Panel Row	3-71
3.4-7	Slender Body Mean Surface Panels	3-71
3.4-8	Slender Body Mean Surface for a Wing-Body-Tail Combination	3-72
3.4-9	Image System of Panels and Line Segments	3-73
3.4-10	Velocity Components Induced at Panel Control Points	3-75
3.4-11	Mean Surface Panel Area Contained in Mach Fore Cone	3-77
3.4-12	Major Diagonal of a Mean Surface Panel	3-86
3.4-13	Panel With Uniform Vorticity Distribution	3-91
3.4-14	Typical Semi-Infinite Region With Origin at a Panel Corner Point	3-98

FIGURES—Continued

No.		Page
3.4-15	Subsonic Slender Body Thickness Problem Control Point Locations . . .	3-102
3.4-16	Slender Body Isolated Thickness Problem Control Point Locations . . .	3-102
3.4-17	Regions for Evaluating Supersonic Line Sources	3-107
3.4-18	Line Doublet Control Point Locations	3-111
3.4-19	Quadratic Spline Line Doublet Strength Distribution	3-113
3.4-20	Sine Function Variation of C_p on a Slender Body Surface	3-119
3.4-21	Regions of Integration for Vortex Panel in Supersonic Flow	3-143
3.4-22	Lifting Pressure on a Flat Plate	3-154
3.4-23	Approximate Flat Plate Camber	3-155
3.4-24	Drag on Integrated Downwash Vs Camber Analyzed	3-156
3.4-25	Thin Body Leading Edge Panel Geometry	3-159
3.4-26	Example of Near Field—Far Field Approximation	3-165
3.4-27	Near Field Vortex Panel Subdivision	3-165
3.5-1	Slender Body Mean Interference Surface Unit Normal Vector	3-175
3.5-2	Aerodynamic Forces From Interference Pressure on a Slender Body . . .	3-181
3.5-3	Control Surface Hinge Line	3-188
4.2-1	Rigid Body Displacement of the Undeformed Reference Shape of a Structure	4-14
4.2-2	Elastic Axis and Locus of Section Mass Centers of a Typical Horizontal Tail	4-30
4.2-3	Plane of Structural Symmetry	4-32
4.2-4	Elastic Deformation of Aerodynamic Surfaces	4-34
4.2-5	Elastic Deformation of Slender Body Centerline	4-35
4.2-6	Aerodynamic Forces Acting on Aerodynamic Panels and Slender Body Centerline Segments	4-42
4.3-1	Elastic Axes of a Typical Configuration	4-46
4.3-2	Typical Plane Section of a Structural Body	4-47
4.3-3	General Arrangement of Elastic Axis	4-49
4.3-4	Thin Body Elastic Axis Nodes	4-50
4.3-5	Elastic Axis of the N^{th} Thin Body	4-51
4.3-6	Thin Body Elastic Axis at a Junction Point	4-52
4.3-7	Slender Body Elastic Axis Nodes	4-53
4.3-8	Structural Body and Junction Point Designation	4-54
4.3-9	Thin and Slender Structural Body Junction Point Numbering	4-55
4.3-10	Nodal Forces and Displacements at a Node on the N^{th} Thin Body	4-58
4.3-11	Adjoining Finite Elements on the Elastic Axis of a Thin Body	4-60
4.3-12	Thin Body Clamped at its Junction Points	4-62
4.3-13	Nodal Forces and Displacements at Nodes on Slender Bodies	4-63
4.3-14	Slender Body Clamped at its Junction Points	4-66
4.3-15	Junction Point Node Joining Thin Bodies	4-66
4.3-16	Junction Point Joining a Slender Body	4-70
4.3-17	Structural Representation of a Wing Alone	4-71
4.3-18	Coplanar Thin Body Junction Point Connecting Two Thin Structural Bodies Belonging to the Same Thin Aerodynamic Body	4-72

FIGURES—Continued

No.		Page
4.3-19	Thin and Slender Body Beam Finite Elements	4-77
4.3-20	Constrained Displacement of a Thin Body	4-78
4.3-21	Constrained Displacement of a Slender Body	4-79
4.3-22	Example Structural Configuration	4-82
4.3-23	Finite Element of a Thin Structural Body	4-85
4.3-24	Thin Body Finite Element	4-85
4.3-25	Slender Body Beam Finite Element	4-88
4.3-26	Aerodynamic Paneling of a Thin Body	4-91
4.3-27	Beam Section at an Aerodynamic Panel Centroid	4-92
4.3-28	Aerodynamic Segments of a Slender Body	4-93
4.3-29	Typical Engine Installation	4-102
4.3-30	Finite Element Subdivision of the Structural Mass	4-107
4.3-31	Section of a Thin Body Passing Through an Elastic Axis Node	4-108
4.3-32	Lumped Masses on a Thin Body Subdivision	4-109
4.4-1	Deformation of a Configuration	4-135
4.4-2	Typical Thin Body Structure	4-137
4.4-3	Quadrilateral Membrane Finite Element	4-138
4.4-4	Triangular Finite Element	4-138
4.4-5	Typical Slender Body Structure	4-141
4.4-6	Displacement Function for a Slender Body	4-143
4.4-7	Thin Body Having Two Quadrilateral Finite Elements	4-146
4.4-9	Extended Structural Finite Element Boundaries	4-152
4.4-10	ESIC Coordinate Systems	4-154
4.4-11	Engine Structural Support Loads	4-158
5.2-1	Flight Path of an Aircraft	5-4
5.3-1	Stability Axis System of Tabulated Data	5-28
5.3-2	C_L , C_D , and C_m Versus α For Various Longitudinal Control Settings With β , δa , δr Set to Zero	5-30
5.3-3	C_L , C_D , and C_m Versus β For Various Angles of Attack With δe , δa , δr Set to Zero	5-30
5.3-4	C_L , C_D , and C_m Versus δa For Various Angles of Attack With δe , δr , β Set to Zero	5-31
5.3-5	C_L , C_D , and C_m Versus δr For Various Angles of Attack With δe , δa , β Set to Zero	5-31
5.3-6	C_Y , C_ℓ , and C_n Versus β For Various Angles of Attack With δe , δa , δr Set to Zero	5-31
5.3-7	C_Y , C_ℓ , and C_n Versus δa For Various Angles of Attack With δe , δr , β Set to Zero	5-32
5.3-8	C_Y , C_ℓ , and C_n Versus δr For Various Angles of Attack With δe , δa , β Set to Zero	5-32
5.3-9	C_Y , C_ℓ , and C_n Versus β For Various δe With α , δa , δr , δa Set to Zero	5-32
5.4-1	Angular Momentum of Rotating Engines	5-37
5.8-1	Paneling of a Rounded Thin Body Tip	5-74
6.2-1	Propulsion System Rotor	6-6

FIGURES—Concluded

No.		Page
6.5-1	Coordinate System Definition	6-72
6.5-2	Gust Velocity Distribution Relative to Flightpath	6-75
6.5-3	Resolution of Gust on Airplane Surface	6-76
6.5-4	Sine Wave Gust Definition	6-80
6.5-5	One-Minus-Cosine Wave Gust Definition	6-80
6.5-6	Modified Square Wave Gust Definition	6-82

TABLES

No.		Page
2.1-1	Coordinate Axis Systems	2-1
2.2-2	Summary of Fundamental Axis Systems	2-8
3.1-1	Flow Singularity Distributions	3-6
4.3-1	Summary of Structural Node Point Degrees of Freedom	4-76
4.3-2	Massless Independent Degrees of Freedom	4-114
5.6-1	Dimensionalization of Quantities Related to the Stability Derivatives	5-50
6.5-1	Principal Features of the Inertial and Body Axis Systems for Describing a Gust Field	6-71
B.7-1	Case 4: Prematrices and Postmatrices of the Circle-Cross Product Operator .	B-15
B.7-2	Evaluations of an Expression With the Circle-Cross Product and Standard Matrix Operations	B-15
B.7-3	Additional Evaluations of an Expression With the Circle-Cross Product and Standard Matrix Operations	B-20
B.9-1	Uses of Circle-Cross Product in the FLEXSTAB Theoretical Development .	B-22
B.10-1	Uses of Circle-Cross Product in the FLEXSTAB Code	B-23

SUMMARY

A theoretical development of the FLEXSTAB system is presented. The development integrates the theoretical mechanics of a flexible body with a low frequency unsteady aerodynamic theory employing linear influence coefficients based on finite element approximations. The theoretical mechanics resolve the dynamics of flexible aircraft into structural dynamics of free vibration modes superimposed on rigid body dynamics. This resolution is made using a mean reference frame for structural motions and leads to two important features of the FLEXSTAB system: one, a logical merger of quasi-steady and dynamic aeroelasticity through the residual flexibility approximation; and, two, a logical basis for incorporating into the analysis empirical, rigid aircraft aerodynamic data. The aerodynamic theory is applicable to subsonic and supersonic flow and multiple wing-body-tail-nacelle configurations. Aerodynamic influence coefficients are derived using a paneling scheme which lends itself to empirical corrections. Finally, the theoretical aero- and structural dynamics are integrated, conserving energy of the system and thereby yielding equations of motion appropriate to stability evaluation. These equations are expressed for a steady, reference motion to determine trim and static stability. They are also expressed in terms of unsteady perturbations about the reference motion to determine dynamic stability by characteristic roots or by time histories following an initial perturbation or following penetration of a discrete gust flow field.

PRECEDING PAGE BLANK NOT FILMED

PAGE STATUS LOG

<u>Page no.</u>	<u>Most recent date changed</u>	<u>Page no.</u>	<u>Most recent date changed</u>	<u>Page no.</u>	<u>Most recent date changed</u>
xiii	5/1/75				
xiv	5/1/75				
xix	5/1/75				
3-102	5/1/75				
3-199	5/1/75				
5-69	5/1/75				
5-70	5/1/75				
5-70a	5/1/75				
6-38	5/1/75				
6-77	5/1/75				
A-1	5/1/75				
A-26	5/1/75				
B-1	5/1/75				
B-2	5/1/75				
B-3	5/1/75				
B-4	5/1/75				
B-5	5/1/75				
B-6	5/1/75				
B-7	5/1/75				
B-8	5/1/75				
B-9	5/1/75				
B-10	5/1/75				
B-11	5/1/75				
B-12	5/1/75				
B-13	5/1/75				
B-14	5/1/75				
B-15	5/1/75				
B-16	5/1/75				
B-17	5/1/75				
B-18	5/1/75				
B-19	5/1/75				
B-20	5/1/75				
B-21	5/1/75				
B-22	5/1/75				
B-23	5/1/75				
R-2	5/1/75				

~~PRECEDING PAGE BLANK NOT FILMED~~

1.0 INTRODUCTION

Since the early days of aviation, aircraft designers have contended with aeroelastic problems. Combinations of aerodynamic and inertial loads on flexible aircraft structures have caused problems including wing divergence, flutter, and loss of control. Because these aeroelastic problems have caused catastrophic failures, extensive analytical methods have been developed to predict and to prevent their occurrence.

Aeroelasticity also influences stability; however, until recently, the effects were so minor that they could be evaluated satisfactorily by rigid-aircraft stability theory using simple modifications to the stability derivatives. This approach, however, is not valid for the latest, and largest, flexible aircraft designed to operate at high dynamic pressures. The latest transonic and supersonic transports are prime examples. The static stability characteristics of these aircraft are drastically affected by elastic structural deformation. Further, because some of their structural motions have characteristic frequencies nearly as small as those of their rigid body motions, dynamic stability is significantly affected by the dynamics of the structure through unsteady aerodynamic coupling between the rigid body and the structural motions. For these aircraft, a mathematical model based fundamentally on the dynamics of a flexible body is required to predict static and dynamic stability.

The low aspect ratio, thin wing, slender body configurations of large supersonic aircraft pose the most difficult problems. Severe aeroelastic effects on the stability of these aircraft must be evaluated early in the preliminary design period. These aeroelastic effects arise from complex structural deformation shapes in the presence of strong interference flows among the wing, body, nacelles, and tail. Evaluation requires sophisticated structural, aerodynamic, and dynamic analytical methods having a great deal of generality. These analytical methods consist of large digital computer programs with massive data transfer between the programs. The flow time required for the analysis is very large and reduces its effectiveness in the design cycle, if a unified system of analysis is not available. Recognizing these facts, development of the FLEXSTAB Computer Program System was undertaken by The Boeing Company under contract with the NASA-Ames Research Center. The objective was to provide a unified system of computer programs having the required generality.

FLEXSTAB is a system of digital computer programs based on linear theories for evaluating static stability, dynamic stability, trim state, structural loading, and elastic deformation of arbitrary aircraft configurations in subsonic and supersonic flight. The analysis includes structural dynamics in a controls-fixed dynamic analysis of longitudinal and lateral-directional motions. The distinctive features of the FLEXSTAB system are as follows: (1) the system is based on integrated aerodynamic, structural, and dynamic analytical methods valid for virtually every practical aircraft configuration having a plane of symmetry (2) the aerodynamic analysis can readily incorporate empirical and theoretical corrections, and (3) the system includes the low-frequency aerodynamic effects appropriate for evaluating the stability of large aircraft.

The linear aerodynamic analytical method used in the system is essentially that introduced by Woodward (ref. 1-1) for representing supersonic flow about wing-body combinations. However, the method has been extended to include subsonic flow, arbitrary wing-body-nacelle-tail arrangements, and low-frequency unsteady aerodynamics. In addition, the

FLEXSTAB system is formulated to accept aerodynamic data for making corrections to its linear analysis. The data may be in the form of experimental data from wind tunnel force and pressure models, or data from nonlinear analytical methods. The capability for making aerodynamic corrections was deemed essential because nonlinear aerodynamic phenomena nearly always have important effects on the stability of practical aircraft configurations.

The FLEXSTAB system contains a structural finite element method based on beam theory; it will also accept structural properties generated externally by structural programs such as NASTRAN (ref. 1-2). The system has been used in conjunction with the Boeing-SAMECS structural program (ref. 1-3).

The dynamic analysis uses the residual flexibility concept, wherein an arbitrarily selected number of free-vibration structural mode shapes are used as dynamic degrees of freedom and the remaining free-vibration structural mode shapes are treated as quasi-static* degrees of freedom. The latter do not appear explicitly in the dynamic problem, their effect being represented in terms of residual flexibility.

The formulation and programming of the system have been tested by predicting the stability characteristics of typical subsonic and supersonic aircraft. The test aircraft were the Boeing 707-320B, the Boeing B-2707 SST, and the Lockheed YF-12A. Wind-tunnel and flight test data were compared with numerical results to demonstrate the validity of the system. Comparisons were made of the longitudinal and lateral-directional characteristics of the Boeing 707-320B at mid-cruise (Mach number = 0.8), the longitudinal characteristics of the Boeing B-2707 SST at mid-cruise (Mach number = 2.7), and the longitudinal characteristics of the Lockheed YF-12A at Mach numbers = 0.8 and 2.8.

This report, Volume I of four volumes, describes the engineering analysis on which the FLEXSTAB computing program system is based. Volume II is a computer program user's manual. Volume III describes the FLEXSTAB computer program, and Volume IV contains the results computed for the test cases.

It should be noted that the scope of the FLEXSTAB system described in this report is currently being extended. The computer program coding is also being revised. Each version is identified by a decimal number (X.Y), X indicating the technology (or analytical) level, and Y the level of coding pertaining to a given X. The system described in this report is LEVEL 1.02.00.

*A quasi-static degree of freedom is one for which damping and inertial forces are so small as to be negligible.

2.0 COORDINATE SYSTEMS AND KINEMATIC DESCRIPTION

2.1 INTRODUCTION

The objectives of this section are twofold. The first is to introduce the coordinate systems used in the formulation of the FLEXSTAB system. The second is to derive the basic kinematic description used in the FLEXSTAB system analysis.

All coordinate systems used in the formulation are right-handed, rectangular Cartesian and are listed in table 2.1-1. Five of the coordinate systems are termed fundamental axis systems and are completely defined in section 2.2. In addition, local axis systems are introduced in sections 3 and 4 and are used in the aerodynamic and structural derivations contained in those sections.

TABLE 2.1-1.—COORDINATE AXIS SYSTEMS

FUNDAMENTAL AXIS SYSTEMS		
Inertial Axis System— X', Y', Z' —inertial reference frame for structural and rigid body dynamics		
Fluid Axis System— x, y, z —inertial reference frame for aerodynamics		
Body Axis System— X_B, Y_B, Z_B —body-fixed reference frame for rigid body motions		
Reference Axis System— X, Y, Z —body-fixed coordinate system for geometric, structural, and inertial description		
Stability Axis System— X_S, Y_S, Z_S —body-fixed reference frame for stability parameters		
LOCAL AXIS SYSTEMS		
Axis systems	Aerodynamic	Structural
Component Axis Systems	Thin body— X_N, Y_N, Z_N	Thin body— X_N, Y_N, Z_N
	Slender body— X_M, Y_M, Z_M	
Panel or Segment Axis Systems	Thin body panel— $\xi_{Ni}, \eta_{Ni}, \zeta_{Ni}$	Thin body elastic axis segment— x_{Ni}, y_{Ni}, z_{Ni}
	Slender body centerline segment— $\xi_{Mi}, \eta_{Mi}, \zeta_{Mi}$	
	Interference surface panel— $\xi_{Mi}, \eta_{Mi}, \zeta_{Mi}$	

Two of the fundamental axis systems are inertial reference frames. One, termed the Inertial Axis System, is earth fixed and is used as an inertial reference frame for the dynamics of a flexible aircraft. The other, termed the Fluid Axis System, translates with a steady velocity relative to the earth and is the inertial reference frame for aerodynamics. The three remaining fundamental axis systems are mean reference frames; a concept discussed in detail in section 2.3; in general, they are in motion relative to the two inertial reference frames but

are fixed relative to one another. One mean reference frame, termed the Body Axis System, is used as a basis for expanding vector quantities associated with rigid-body motion. The second, termed the Reference Axis System, is used as a coordinate system in the analytic description of geometric, structural, and aerodynamic properties. The third, termed the Stability Axis System, is used as a basis for describing the stability characteristics of an aircraft.

The motions of the three mean reference frames (i.e., the Body, Reference, and Stability Axis Systems) are such that they may be treated as body fixed, even though the aircraft is undergoing elastic deformation, *in which case every material particle of the aircraft is in motion relative to the mean reference frames.* The mean reference frames are given an initial orientation relative to the aircraft when it has a specific deformed shape, e.g., the shape in the design flight condition. Then subsequent motions of the mean reference frames are determined by requiring the kinetic energy of the aircraft motion relative to them to be at a minimum. This requirement yields six conditions determining the translational and rotational velocities of the mean reference frames relative to the Inertial Axis System. If the aircraft is moving as a rigid body then the minimum kinetic energy is zero and the mean reference frames are body fixed. Section 2.3 shows that even when the aircraft is undergoing elastic deformation the mean reference frames have the characteristics of a body-fixed axis system; hence, *the terms "body-fixed axis system" and "mean reference frame" are used interchangeably in the following.*

The introduction of body-fixed axis systems is a necessity for the FLEXSTAB system analysis. Elastic deformation of an aircraft is described in the FLEXSTAB system by equations based on the classical theory of elasticity, reference 2-1. As a result, equations related to the structural properties of an aircraft are derived in terms of a coordinate system relative to which rotations of the structure are very small. Requiring the Reference Axis System to be a mean reference frame satisfies this requirement.

Kinematics based on motions of and motions relative to a mean reference frame are particularly advantageous. Motions of a mean reference frame are governed by equations of motion identical in form to the equations of motion for a rigid aircraft. Consequently, the parameters derived from the equations of motion and used to evaluate stability of a flexible aircraft are identical in physical significance with the parameters used to evaluate stability of a rigid aircraft. Also, because rigid body motions underlie all of the motions involved in the stability analysis, wind tunnel test data acquired from rigid wind tunnel models may be used as direct empirical corrections in the FLEXSTAB system analysis.

The remainder of this section is devoted to deriving kinematic relations associated with the aerodynamics of the FLEXSTAB system. These kinematic relations are derived in section 2.3.3. They relate flow incidence at the surface of an aircraft to its geometric shape, elastic deformation, rigid body motions, and control surface deflections. Section 2.3.3 also contains a derivation of the relations describing variations in the dynamic pressure and Mach number arising from aircraft motions. Finally, relations describing motions of the wake of an aircraft relative to the aircraft are derived in section 2.3.4.

2.2 COORDINATE SYSTEMS

2.2.1 Inertial Axis System

The Inertial Axis System (X' , Y' , Z') is earth fixed and is oriented relative to the earth as shown by figure 2.2-1. The Z' axis is vertical, positive downward. The direction of the X' axis represents an initial heading of the aircraft, and the Y' is oriented to form a right-handed system. The origin of the Inertial Axis System is at some initial location of the aircraft's center of gravity.

2.2.2 Body Axis System

The origin of the Body Axis System (X_B , Y_B , Z_B) is at the aircraft's center of gravity and moves with this center of gravity along the flight path. The X_B, Z_B plane coincides with the undeformed aircraft's plane of symmetry with X_B positive forward and parallel to the undeformed centerline of the fuselage, figure 2.2-1. The orientation of the Body Axis System relative to the Inertial Axis System is described in terms of Euler angles. The notation and arrangement of reference 2-2 are used—the heading angle is denoted as ψ , the pitch attitude as θ , and the angle of bank as ϕ . Ignoring the shift of the origin along the flight path, the Inertial Axis System is related to the Body Axis System by the following transformation:

$$\begin{bmatrix} X' \\ Y' \\ Z' \end{bmatrix} = [T] \begin{bmatrix} X_B \\ Y_B \\ Z_B \end{bmatrix} \quad (2.2-1)$$

where

$[T] =$

$$\begin{bmatrix} \cos\theta\cos\psi & \sin\phi\sin\theta\cos\psi - \cos\phi\sin\psi & \cos\phi\sin\theta\cos\psi + \sin\phi\sin\psi \\ \cos\theta\sin\psi & \sin\phi\sin\theta\sin\psi + \cos\phi\cos\psi & \cos\phi\sin\theta\sin\psi - \sin\phi\cos\psi \\ -\sin\theta & \sin\phi\cos\theta & \cos\phi\cos\theta \end{bmatrix}.$$

2.2.3 Fluid Axis System

The Fluid Axis System (x , y , z) (fig. 2.2-2) is initially aligned with the Body Axis System; however, the origin may be located arbitrarily on the plane of symmetry. The x axis is positive aft; the z axis is positive upward, and the y axis is positive along the right-hand wing. The arrangement is that used in most texts on the subject of aerodynamics, e.g., reference 2-3. The Fluid Axis System moves with a steady velocity, U ($t=t_0$), in the negative x direction and is in motion relative to the Body Axis System. Figure 2.2-2 shows the orientation of the two axis systems at the instant of time under consideration, $t = t_0$. At this instant of time they are related by

$$\begin{aligned} x &= X_{cg} - X_B \\ y &= Y_B \\ z &= Z_{cg} - Z_B \end{aligned} \quad \text{at } t=t_0 \quad (2.2-2)$$

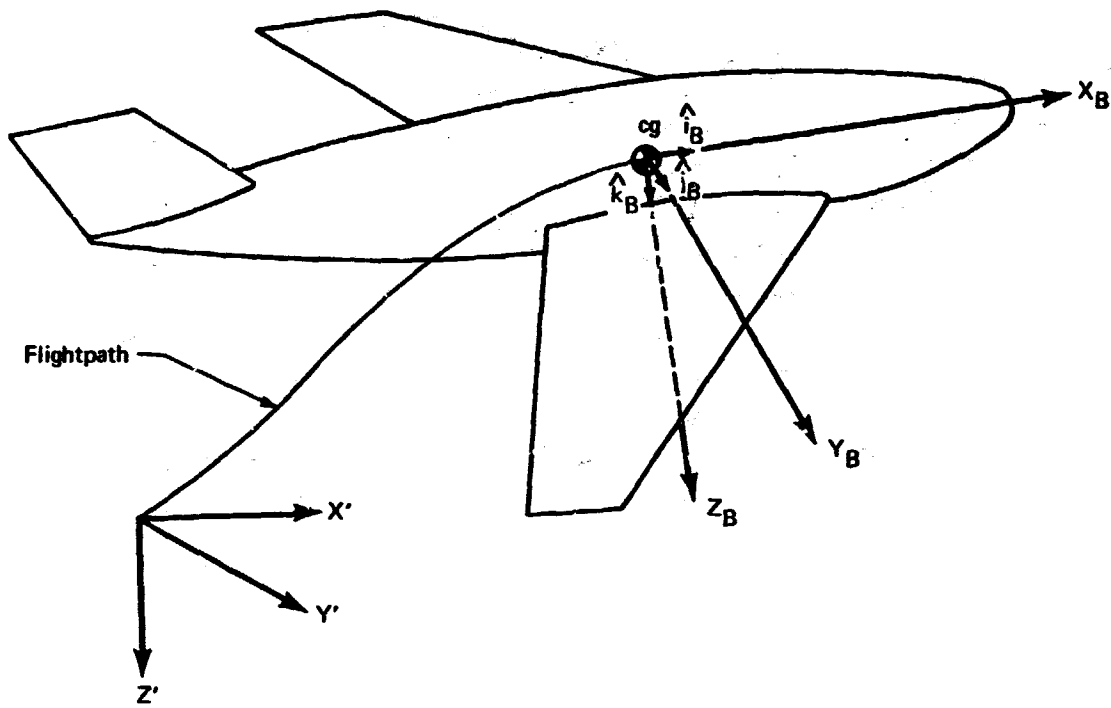


FIGURE 2.2-1.--INERTIAL AND BODY AXIS SYSTEMS

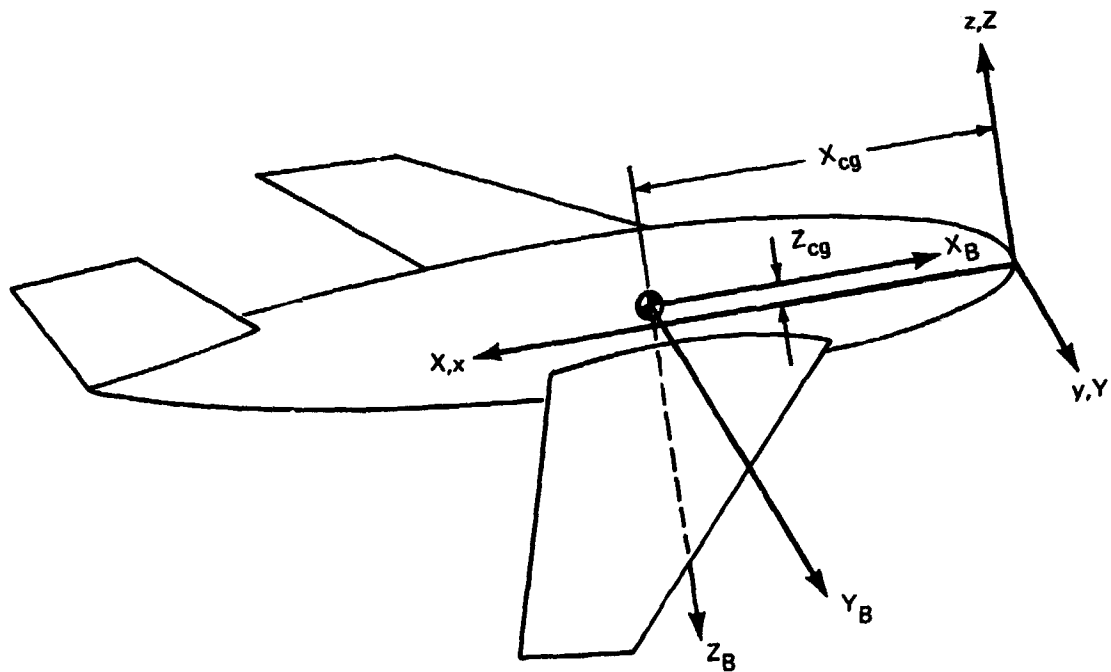


FIGURE 2.2-2.--BODY, FLUID, AND REFERENCE AXIS SYSTEMS AT TIME $t = t_0$

where (X_{cg}, O, Z_{cg}) are the coordinates of the aircraft's center of gravity in the Fluid Axis System.

The Fluid Axis System (fig. 2.2-3) is a portable axis system. The Body Axis System is displaced from the Fluid Axis System as shown by figure 2.2-3 at instants of time following the initial instant of time under consideration. The translational and rotational velocities of the Body Axis System relative to the Inertial Axis System are

$$\vec{V}_C = U\hat{i}_B + V\hat{j}_B + W\hat{k}_B \quad \text{at } t=t_0 \quad (2.2-3)$$

and

$$\vec{\omega} = P\hat{i}_B + Q\hat{j}_B + R\hat{k}_B, \quad \text{respectively;}$$

while the Fluid Axis System is nonrotating and is translating with the steady velocity, $U\hat{i}_B$. Even though nonzero values of V , W , and $\vec{\omega}$ and their time rates of change cause these two axis systems to become separated with time, they are realigned by shifting the Fluid Axis System at any new instant of time under consideration—hence, the term portable axis system.

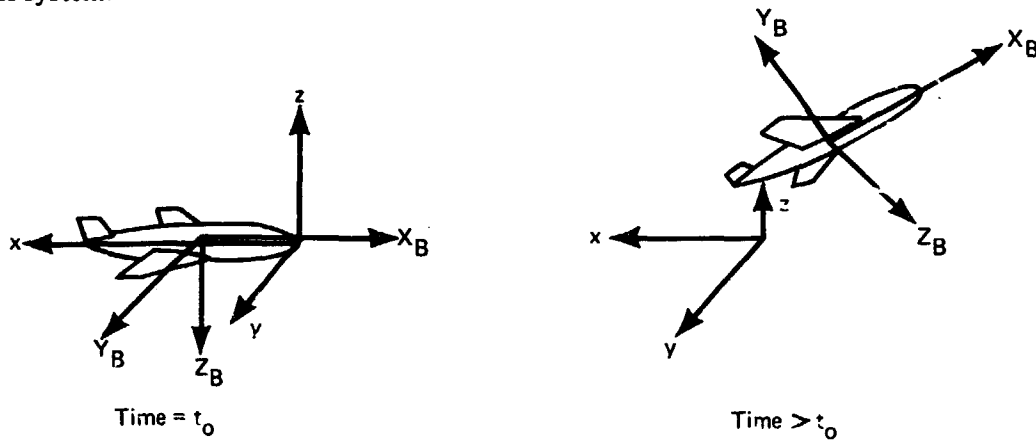


FIGURE 2.2-3.—FLUID AXIS SYSTEM AS A PORTABLE SYSTEM

Since the Fluid Axis System moves relative to the Body Axis System, the velocity of a fluid particle can be described as either velocity \vec{Q} relative to the Fluid Axis System or velocity \vec{V} relative to the Body Axis System. These two velocities are related by the expression

$$\vec{Q} = \vec{V} + \vec{V}_R + \vec{\omega} \times \vec{r} \quad \text{at } t=t_0 \quad (2.2-4)$$

where \vec{r} is the position of the fluid particle relative to the origin of the Body Axis System and

$$\vec{V}_R = V\hat{j}_B + W\hat{k}_B \quad \text{at } t=t_0 \quad (2.2-5)$$

is the velocity of the Body Axis System relative to the Fluid Axis System at time $t = t_0$.

2.2.4 Reference Axis System

The geometry, structural properties, and mass distribution of an aircraft are described in terms of a second body-fixed coordinate system termed the Reference Axis System (X, Y, Z). The Reference Axis System coincides with the Fluid Axis System at the instant of time under consideration ($t = t_0$) and is related to the Body Axis System (X_B, Y_B, Z_B) by a transformation identical with that of equation (2.2-2), viz:

$$\begin{aligned} X &= X_{cg} - X_B \\ Y &= Y_B \\ Z &= Z_{cg} - Z_B \end{aligned} \quad \text{for all } t \quad (2.2-6)$$

The transformation given by equation (2.2-6) holds for all time; thus, the surface of the aircraft may be expressed analytically as

$$G(X, Y, Z, t) = 0 \quad (2.2-7)$$

where the time dependence is only a consequence of elastic deformation and control surface deflections.

2.2.5 Stability Axis System

The Stability Axis System, a third body-fixed axis system, has the origin at an Aerodynamic Moment Reference Point, i.e., the point about which the aerodynamic moments involved in stability derivatives are measured (fig. 2.2-4). The coordinates are denoted as

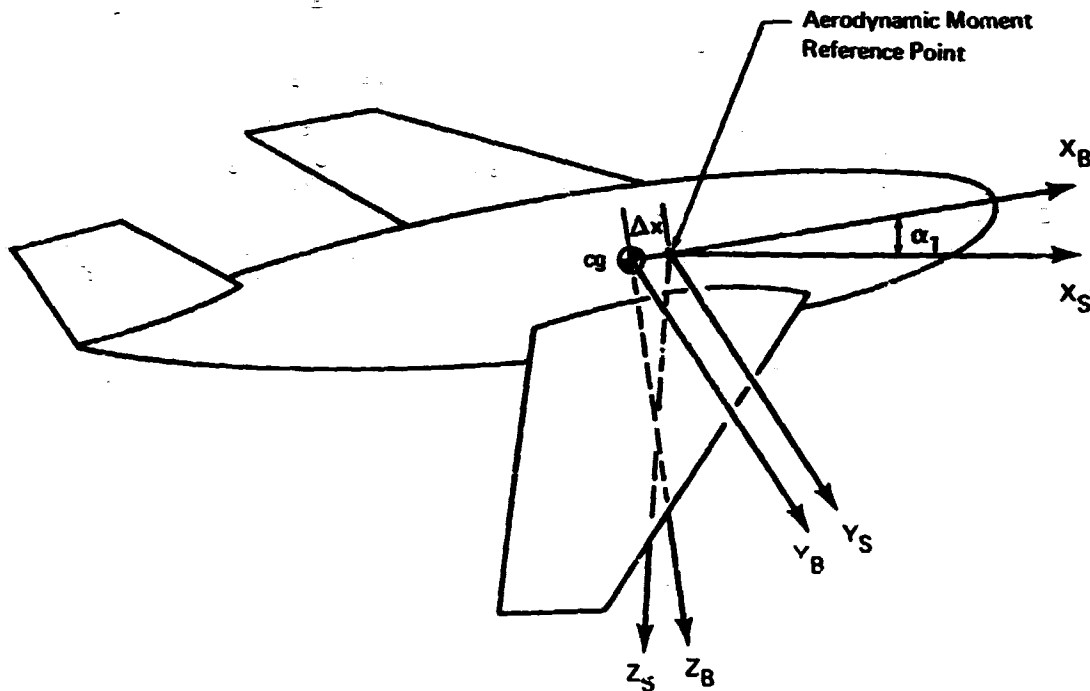


FIGURE 2.2-4.—BODY AND STABILITY AXIS SYSTEMS

X_S, Y_S, Z_S . The X_S axis is positive forward and aligned with the projection of \vec{V}_{C_1} on the aircraft plane of symmetry (see sec. 5). The Y_S axis is positive along the right-hand wing, and Z_S is positive downward. The Stability Axis System is obtained from the Body Axis System by a rotation, α_1 , about the Y_B axis and a translation of the origin, ΔX , from the center of gravity to the Aerodynamic Moment Reference Point, figure 2.2-4. The transformation of coordinates, therefore, is given by

$$\begin{aligned} X_S &= X_B \cos \alpha_1 + Z_B \sin \alpha_1 - \Delta X \cos \alpha_1 \\ Y_S &= Y_B \\ Z_S &= -X_B \sin \alpha_1 + Z_B \cos \alpha_1 + \Delta X \sin \alpha_1 \end{aligned} \quad (2.2-8)$$

The fundamental axis systems and their functions in the FLEXSTAB system analysis are summarized by table 2.2-2.

2.3 KINEMATIC DESCRIPTION

This section contains a development of the kinematics of the FLEXSTAB system describing motions related to the dynamics of a flexible aircraft. The equations governing the dynamics must be expressed in terms of motions relative to an inertial reference frame. The kinematics derived here satisfy this requirement but employ moving axis systems as intermediate frames of reference. Motions relative to inertial reference frames (the Inertial and Fluid Axis Systems) are introduced in sections 2.3.1 and 2.3.3. Moving axis systems (the Body, Reference, and Stability Axis Systems) are introduced in section 2.3.2 where they are given the properties of a mean reference frame—properties which are discussed in detail in section 2.3.2.

In section 2.3.2.1, kinematics are developed for a moving axis system having an unspecified translational and rotational velocity relative to the Inertial Axis System. The velocity of the moving axis system is determined in section 2.3.2.2, by minimizing the kinetic energy of the aircraft apparent to an observer in the moving axis system. The moving axis system is then a mean reference frame. The conditions determining velocity, in section 2.3.2.3, of a moving axis system and making it a mean reference frame are shown to be nonintegrable constraint conditions. These are constraints on the deformation of a flexible aircraft and they are required, in section 4, to develop the dynamic equations from Hamilton's principle. In section 2.3.2.4 an approximation is introduced which makes the constraint conditions integrable. The validity of this approximation is examined in section 2.3.2.5 for two types of motion pertinent to aircraft stability evaluation: (1) steady motion and (2) unsteady perturbation motion about a steady reference motion.

The kinematics of the atmosphere surrounding an aircraft are considered in sections 2.3.3 and 2.3.4. The kinematics of a fluid particle moving along the surface of an elastically deforming aircraft are developed in section 2.3.3. This development leads to the surface boundary condition used in deriving the aerodynamic theory of the FLEXSTAB system in section 3. The surface boundary condition is derived in section 2.3.3.1 and it is linearized for small flow incidence in sections 2.3.3.2 through 2.3.3.5. Section 2.3.3.6 contains a derivation of formulas describing variations in the dynamic pressure and Mach number at the surface of a

TABLE 2.2.2.—SUMMARY OF FUNDAMENTAL AXIS SYSTEMS

Axis system	Description	Transformation
Inertial Axis System— X', Y', Z'	Inertial reference frame, figure 2.2-1	Origin at some initial location of the airplane center of gravity
Body Axis System— X_B, Y_B, Z_B	Body-fixed reference frame for rigid body motion, figure 2.2-1	$\begin{Bmatrix} X_B \\ Y_B \\ Z_B \end{Bmatrix} = \begin{bmatrix} T \end{bmatrix}^{-1} \begin{Bmatrix} X' \\ Y' \\ Z' \end{Bmatrix}$ Equation (2.2-1)
Reference Axis System— X, Y, Z	Body-fixed coordinate system for describing geometric, structural, and inertial properties, figure 2.2-2	$\begin{Bmatrix} X \\ Y \\ Z \end{Bmatrix} = \begin{bmatrix} -1 & 0 & 0 \\ 0 & 1 & 0 \\ 0 & 0 & -1 \end{bmatrix} \begin{Bmatrix} X_B \\ Y_B \\ Z_B \end{Bmatrix} - \begin{Bmatrix} X_{cg} \\ 0 \\ Z_{cg} \end{Bmatrix}$ Equation (2.2-6)
Fluid Axis System— x, y, z	Inertial coordinate system for describing aerodynamic equations, figures 2.2-2 and 2.2-3	$\begin{Bmatrix} x \\ y \\ z \end{Bmatrix} = \begin{bmatrix} -1 & 0 & 0 \\ 0 & 1 & 0 \\ 0 & 0 & -1 \end{bmatrix} \begin{Bmatrix} X_B \\ Y_B \\ Z_B \end{Bmatrix} - \begin{Bmatrix} X_{cg} \\ 0 \\ Z_{cg} \end{Bmatrix}$ Equation (2.2-2)
Stability Axis System— X_s, Y_s, Z_s	Body-fixed reference frame for stability derivatives and other stability parameters, figure 2.2-4	$\begin{Bmatrix} X_s \\ Y_s \\ Z_s \end{Bmatrix} = \begin{bmatrix} \cos \alpha_1 & 0 & \sin \alpha_1 \\ 0 & 1 & 0 \\ -\sin \alpha_1 & 0 & \cos \alpha_1 \end{bmatrix} \begin{Bmatrix} X_B \\ Y_B \\ Z_B \end{Bmatrix} + \Delta X \begin{Bmatrix} -\cos \alpha_1 \\ 0 \\ \sin \alpha_1 \end{Bmatrix}$ Equation 2.2-4

moving aircraft. In section 2.3.4 the kinematics describing motions of an aircraft relative to its wake are developed.

2.3.1 Motion Relative to the Inertial Axis System

In the following an aircraft is considered to be a continuous, flexible body made up of differential mass elements $\rho_A dV$ undergoing motion relative to the Inertial Axis System, figure 2.3-1. The motion is described by a vector field as follows:

$$\begin{aligned} \vec{r}'(\tilde{X}, \tilde{Y}, \tilde{Z}, t) = & X'(\tilde{X}, \tilde{Y}, \tilde{Z}, t) \hat{i}' + Y'(\tilde{X}, \tilde{Y}, \tilde{Z}, t) \hat{j}' \\ & + Z'(\tilde{X}, \tilde{Y}, \tilde{Z}, t) \hat{k}' \end{aligned} \quad (2.3-1)$$

where $\hat{i}', \hat{j}', \hat{k}'$ are the unit base vectors of the Inertial Axis System and the quantities $\tilde{X}', \tilde{Y}', \tilde{Z}'$ are the coordinates of the differential mass element in the Inertial Axis System at a reference instant of time $t = t_0$, i.e., the quantities $\tilde{X}', \tilde{Y}', \tilde{Z}'$ are the Lagrangian coordinates of the differential mass element, pages 29-30 of reference 2-1.

The velocity of the differential mass element is computed from the motion, i.e., equation (2.3-1), as follows:

$$\frac{d\vec{r}'}{dt}(\tilde{X}, \tilde{Y}, \tilde{Z}, t) = \frac{\partial X'}{\partial t} \hat{i}' + \frac{\partial Y'}{\partial t} \hat{j}' + \frac{\partial Z'}{\partial t} \hat{k}' \quad (2.3-2)$$

This expression describes, at time $t \geq t_0$, the velocity (measured relative to the Inertial Axis System) of the differential mass element located at $\tilde{X}', \tilde{Y}', \tilde{Z}'$ at time $t = t_0$. Equation (2.3-2) also defines the operator d/dt as the time rate of change apparent to an observer fixed in the Inertial Axis System.

2.3.2 Mean Reference Frame

In this section the motion relative to the Inertial Axis System, section 2.3.1, is expressed in terms of an intermediate reference frame.

2.3.2.1 Moving reference frame.—Consider a rectangular, Cartesian coordinate system in motion relative to the Inertial Axis System, figure 2.3-2. The origin is at the moving point P_0 and has position $\vec{p}_0'(t)$ relative to the origin of the Inertial Axis System. The position of a differential mass element, equation (2.3-1), is now expressed as

$$\vec{r}' = \vec{p}_0'(t) + \vec{p}(\tilde{\xi}, \tilde{\eta}, \tilde{\zeta}, t) \quad (2.3-3)$$

where $\vec{p}(\tilde{\xi}, \tilde{\eta}, \tilde{\zeta}, t)$ is the position relative to the moving axis system expressed in terms of the Lagrangian coordinates $\tilde{\xi}, \tilde{\eta}, \tilde{\zeta}$, i.e., the coordinates of the mass element in the moving axis system at the reference instant of time $t = t_0$. The relative motion has the following expanded form:

$$\vec{p} = \xi(\tilde{\xi}, \tilde{\eta}, \tilde{\zeta}, t) \hat{i}_p + \eta(\tilde{\xi}, \tilde{\eta}, \tilde{\zeta}, t) \hat{j}_p + \zeta(\tilde{\xi}, \tilde{\eta}, \tilde{\zeta}, t) \hat{k}_p \quad (2.3-4)$$

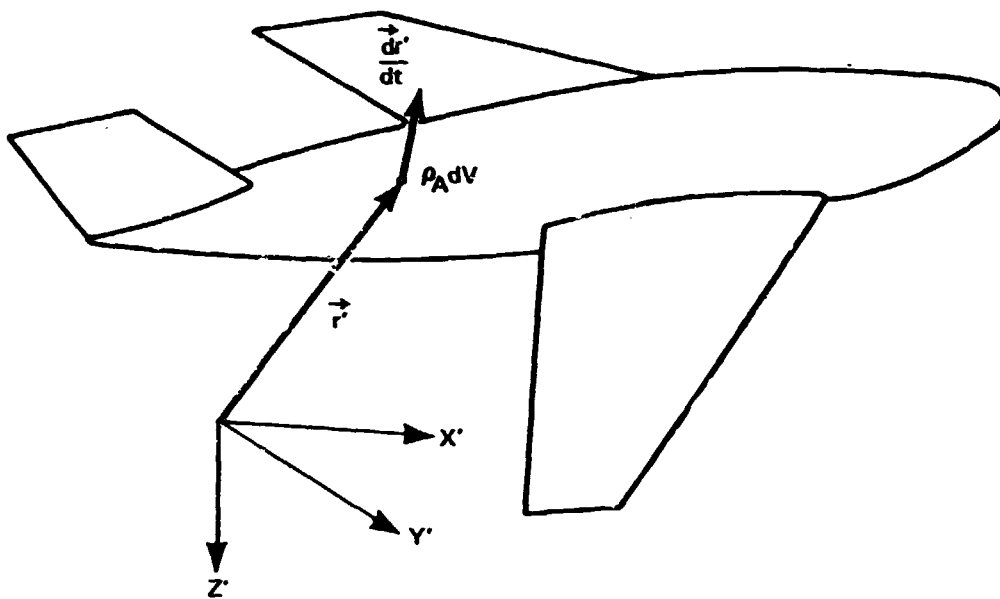


FIGURE 2.3-1.—POSITION AND VELOCITY RELATIVE TO INERTIAL AXIS SYSTEM

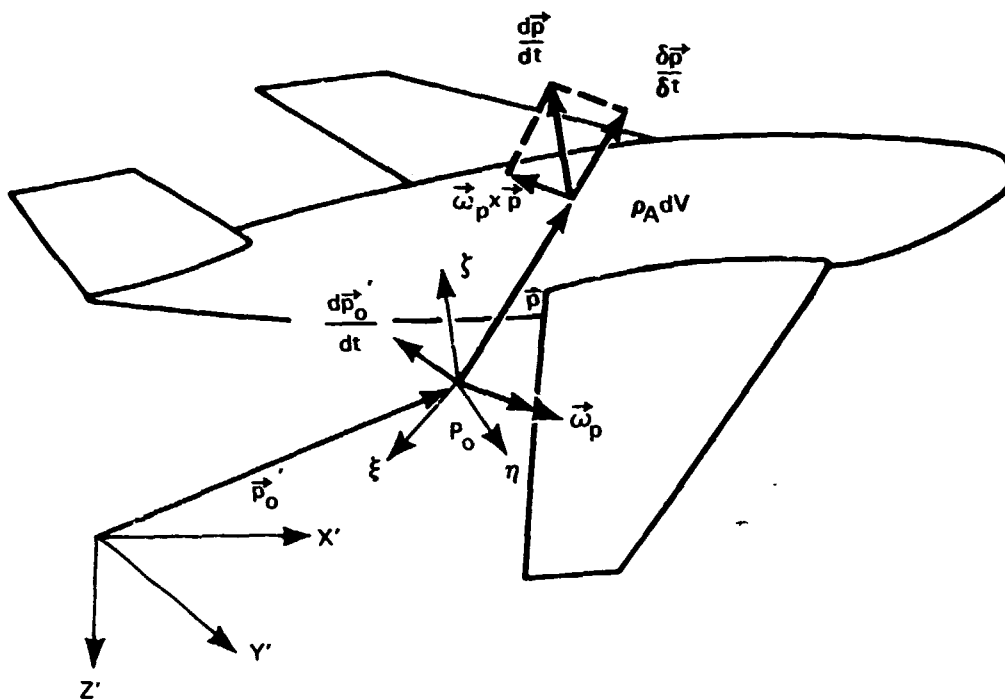


FIGURE 2.3-2.—POSITION AND VELOCITY RELATIVE TO A MOVING REFERENCE FRAME

where $\hat{i}_p, \hat{j}_p, \hat{k}_p$ are the unit base vectors of the moving axis system—time-dependent quantities for an observer in the Inertial Axis System.

The velocity of the mass element relative to the moving axis system is computed from equation (2.3-4) as

$$\frac{\delta \vec{p}}{\delta t} \equiv \frac{\partial \xi}{\partial t} \hat{i}_p + \frac{\partial \eta}{\partial t} \hat{j}_p + \frac{\partial \zeta}{\partial t} \hat{k}_p \quad (2.3-5)$$

This expression describes the velocity (measured relative to the moving axis system) of the mass element located at \vec{p} at time t and located at ξ, η, ζ at time $t = t_0$; equation (2.3-5) also defines the operator $\delta/\delta t$ as the time rate of change apparent to an observer in the moving axis system.

The velocity relative to the Inertial Axis System, equation (2.3-2), may be computed from the motion as given by equation (2.3-3). The result is

$$\frac{d\vec{r}'}{dt} = \frac{d\vec{p}'}{dt_0} + \vec{\omega}_p \times \vec{p} + \frac{\delta \vec{p}}{\delta t} \quad (2.3-6)$$

where

$$\vec{\omega}_p \equiv \omega_\xi \hat{i}_p + \omega_\eta \hat{j}_p + \omega_\zeta \hat{k}_p \quad (2.3-7)$$

is the rotation rate of the moving axis system relative to the Inertial Axis System.

2.3.2.2 Moving axis system as a mean reference frame.—The equations of the preceding section describe motion in terms of an axis system which is translating and rotating with the velocities $d\vec{p}'_0/dt$ and $\vec{\omega}_p$ relative to the Inertial Axis System. In this section six conditions are introduced which determine the components of $d\vec{p}'_0/dt$ and $\vec{\omega}_p$. These conditions make the moving axis system a mean reference frame, references 2-4 and 2-5, and cause the motion of the moving axis system to be such that it is readily identified with a rigid body motion, i.e., the motion appropriate for a body-fixed axis system.

The six conditions are derived from the kinetic energy associated with motion relative to the moving axis system, viz.,

$$K_{rel} \equiv \frac{1}{2} \int_V \frac{\delta \vec{p}}{\delta t} \cdot \frac{\delta \vec{p}}{\delta t} \rho_A dV \quad (2.3-8)$$

and are obtained by minimizing this kinetic energy with respect to the components of $d\vec{p}'_0/dt$ and $\vec{\omega}_p$. The minimizing conditions are represented symbolically by

$$\frac{\partial K_{rel.}}{\partial (d\vec{p}'_0/dt)} = 0 \quad \text{and} \quad \frac{\partial K_{rel.}}{\partial (\vec{\omega}_p)} = 0. \quad (2.3-9)$$

Expanding the relative velocities appearing in the kinetic energy, equation (2.3-8), using equation (2.3-6) leads to

$$K_{rel.} = \frac{1}{2} \int_V \left(\frac{d\vec{r}'}{dt} - \frac{d\vec{p}'_0}{dt} - \vec{\omega}_p \times \vec{p} \right) \cdot \left(\frac{d\vec{r}'}{dt} - \frac{d\vec{p}'_0}{dt} - \vec{\omega}_p \times \vec{p} \right) \rho_A dV.$$

Now, applying the minimizing conditions, equations (2.3-9), to this expression for the kinetic energy yields two vector equations representing six conditions which may be imposed on the six components of $d\vec{p}'_0/dt$ and $\vec{\omega}_p$. These conditions are found to be

$$M \left(\frac{d\vec{r}'_0}{dt} + \vec{\omega}_p \times \vec{R} \right) = \int_V \frac{d\vec{r}'}{dt} \rho_A dV \quad (2.3-10)$$

and

$$M(\vec{R} \times \frac{d\vec{p}'_0}{dt}) + \int_V \vec{p} \times (\vec{\omega}_p \times \vec{p}) \rho_A dV = \int_V \vec{p} \times \frac{d\vec{r}'}{dt} \rho_A dV \quad (2.3-11)$$

where M is the total mass of the aircraft, i.e.,

$$M \equiv \int_V \rho_A dV$$

and \vec{R} is the position of the center of mass relative to the origin of the moving axis system, i.e.,

$$\vec{R} \equiv \frac{1}{M} \int_V \vec{p} \rho_A dV \quad \text{and} \quad \frac{\delta \vec{R}}{\delta t} = 0.$$

The moving axis system is seen to be a mean reference frame if its motion is determined by the following two requirements:

- 1) The momentum of a point mass M at the center of mass moving with the moving axis system is equal to the total linear momentum of the aircraft, i.e.,

$$\int_V \frac{d\vec{r}'}{dt} \rho_A dV.$$

- 2) The angular momentum about the origin of the moving axis system, of the aircraft, as a rigid body, moving with the moving axis system, is equal to the total angular momentum of the aircraft about the origin of the moving axis system, i.e.,

$$\int_V \vec{p} \times \frac{d\vec{r}'}{dt} \rho_A dV.$$

Thus, the moving axis system is a mean reference frame if its coordinates are taken to be Lagrangian coordinates (i.e., fixed to the undeformed aircraft), and if the momentum of the aircraft, as a rigid body, is equated to that of the aircraft as a deforming body.

The physical significance of equations (2.3-10) and (2.3-11) is further borne out when the origin of the moving axis system, now a mean reference frame, is at the center of mass of the aircraft and is taken to be the Body Axis System. When these equations are expanded on the Body Axis System,

$$MV = \hat{j}_B \cdot \int_V \frac{d\vec{r}'}{dt} \rho_A dV, \quad MU = \hat{i}_B \cdot \int_V \frac{d\vec{r}'}{dt} \rho_A dV, \quad (2.3-12)$$

$$MW = \hat{k}_B \cdot \int_V \frac{d\vec{r}'}{dt} \rho_A dV$$

and

$$I_{XX}P - I_{XY}Q - I_{XZ}R = \hat{i}_B \cdot \int_V \vec{r}' \times \frac{d\vec{r}'}{dt} \rho_A dV$$

$$I_{YY}Q - I_{YX}P - I_{YZ}R = \hat{j}_B \cdot \int_V \vec{r}' \times \frac{d\vec{r}'}{dt} \rho_A dV \quad (2.3-13)$$

$$I_{ZZ}R - I_{ZX}P - I_{ZY}Q = \hat{k}_B \cdot \int_V \vec{r}' \times \frac{d\vec{r}'}{dt} \rho_A dV$$

The left-hand members of equations (2.3-12), those following from equation (2.3-10), express the components of momentum of a point mass moving with the velocity of the aircraft center of mass and equate these components to the components of total linear momentum of the aircraft. The left-hand members of equations (2.3-13), those following from equation (2.3-11), express the components of angular momentum of a rigid body rotating about its center of mass. The moments and products of inertia appearing in equations (2.3-13) are computed for the shape of the aircraft at the present instant of time. These quantities are time dependent and have different values at a later instant of time.

If equations (2.3-12) and (2.3-13) are differentiated with respect to time, d/dt , then they can be equated to the components of the applied force resultants at the center of mass, i.e., the total force and couple resultants of the applied forces. The resulting equations can be interpreted as equations of motion governing rigid body degrees of freedom. If, further, as an approximation, the time dependence of the moments and products of inertia are ignored, then these equations reduce to rigid body equations of motion. This approximation is used in the FLEXSTAB system analysis.

2.3.2.3 Mean reference frame constraint conditions.—For the structural theory of section 4, the motion of an aircraft, equation (2.3-1), must be expressed in terms of a displacement field, figure 2.3-3. The displacement field is introduced in terms of the Reference Axis System by expressing the aircraft motion as follows:

$$\vec{r}' = \vec{r}'_O(t) + \vec{r}(\tilde{X}, \tilde{Y}, \tilde{Z}, t) + \vec{d}(\tilde{X}, \tilde{Y}, \tilde{Z}, t) \quad (2.3-14)$$

where \vec{r}' is the position of a differential mass element relative to the Inertial Axis System; $\vec{r}'_O(t)$ is the position of the center of mass relative to the Inertial Axis System:

$$\vec{r}(\tilde{X}, \tilde{Y}, \tilde{Z}, t) \equiv (\tilde{X} - \tilde{X}_{CG})\hat{i} + (\tilde{Y} - \tilde{Y}_{CG})\hat{j} + (\tilde{Z} - \tilde{Z}_{CG})\hat{k} \quad (2.3-15)$$

is the position of the differential mass element relative to the center of mass with the aircraft moving as an undeforming body, $\tilde{X}_{CG}, \tilde{Y}_{CG}, \tilde{Z}_{CG}$ being the Lagrangian coordinates of the center of mass of the undeformed body in the Reference Axis System; and $\vec{d}(\tilde{X}, \tilde{Y}, \tilde{Z}, t)$ is the elastic displacement of the differential mass element from its location in the undeformed shape to its location in the deformed shape.

The components of \vec{r} contain only the Lagrangian coordinates of a differential mass element and the coordinates of the center of mass of the undeformed shape of the aircraft; the components of \vec{r} , therefore, are independent of time for an observer in the Reference Axis System fixed to the undeformed shape. As a result of this, the velocity of a differential mass element is found from equation (2.3-14) as

$$\frac{d\vec{r}'}{dt} = \frac{d\vec{r}'}{dt}_0 + \vec{\omega} \times (\vec{r} + \vec{d}) + \frac{\delta \vec{d}}{\delta t}. \quad (2.3-16)$$

Replacing the velocity vector $\delta \vec{r}' / \delta t$ in the relative kinetic energy expression, equation (2.3-8), by the velocity vector $\delta \vec{d} / \delta t$, the components of $d\vec{r}'_0 / dt$ and $\vec{\omega}$ are chosen to minimize the relative kinetic energy. These operations make the Reference Axis System a mean reference frame and lead to the following conditions on the displacement field:

$$\int_V \frac{\delta \vec{d}}{\delta t} \rho_A dV = \vec{0}$$

and

(2.3-17)

$$\int_V (\vec{r} + \vec{d}) \times \frac{\delta \vec{d}}{\delta t} \rho_A dV = \vec{0}.$$

The conditions on the displacement field given by equations (2.3-17) are used conversely to make the Reference Axis System a mean reference frame. Thus, when the displacement field represents position relative to an undeformed shape fixed with respect to the Reference Axis System, as in equation (2.3-14), and when the displacement field satisfies equations (2.3-17), the Reference Axis System is a mean reference frame. From this point of view (the one adopted in the FLEXSTAB system), equations (2.3-17) can be interpreted as six constraint conditions constraining the motion of the Reference Axis System relative to the moving aircraft. For this reason equations (2.3-17) are called "mean reference frame constraint conditions."

Requiring the Reference Axis System and, therefore, the other body fixed axis systems to be mean reference frames has several interesting consequences. Equations (2.3-17) show that the motion described by the displacement field does not contribute to the total linear and angular momentum as measured by an observer fixed to the Reference Axis System. Also, if the kinetic energy of the aircraft is computed using equation (2.3-16) and if the mean reference frame constraint conditions are applied, the kinetic energy is expressed as a sum: the kinetic energy of a rigid aircraft moving with the Reference Axis System plus the kinetic energy arising from the displacement field, i.e.,

$$K = \frac{1}{2} \frac{d\vec{r}'_0}{dt} \cdot \frac{d\vec{r}'_0}{dt} M + \frac{1}{2} \vec{\omega} \cdot \vec{I} \cdot \vec{\omega} + \frac{1}{2} \int_V \frac{\delta \vec{d}}{\delta t} \cdot \frac{\delta \vec{d}}{\delta t} \rho_A dV$$

where \vec{I} is the inertia tensor and is a function of the displacement field. Also, since there is no kinetic energy due to rigid body motion relative to the Reference Axis System, it follows that, barring the existence of linkages and thermal deformation, motion relative to the Reference Axis System is always accompanied by a change in strain energy; thus, a displacement field satisfying equations (2.3-17) might properly be termed an elastic displacement field. One additional observation is that the total energy of the aircraft apparent to the Reference Axis System (i.e., the sum of the strain energy and the relative kinetic energy) is an absolute minimum. This observation follows from the above and the theorem of minimum strain energy, page 289 of reference 2-1.

The foregoing characteristics of motion relative to a mean reference frame are noteworthy; but the characteristics listed in section 2.1 and demonstrated in section 2.3.2.2 are those of primary importance to the FLEXSTAB system analysis method, viz., the motion of the body fixed axis systems can be identified with that of a rigid body when the motion of the aircraft relative to them satisfies the mean reference frame constraint conditions.

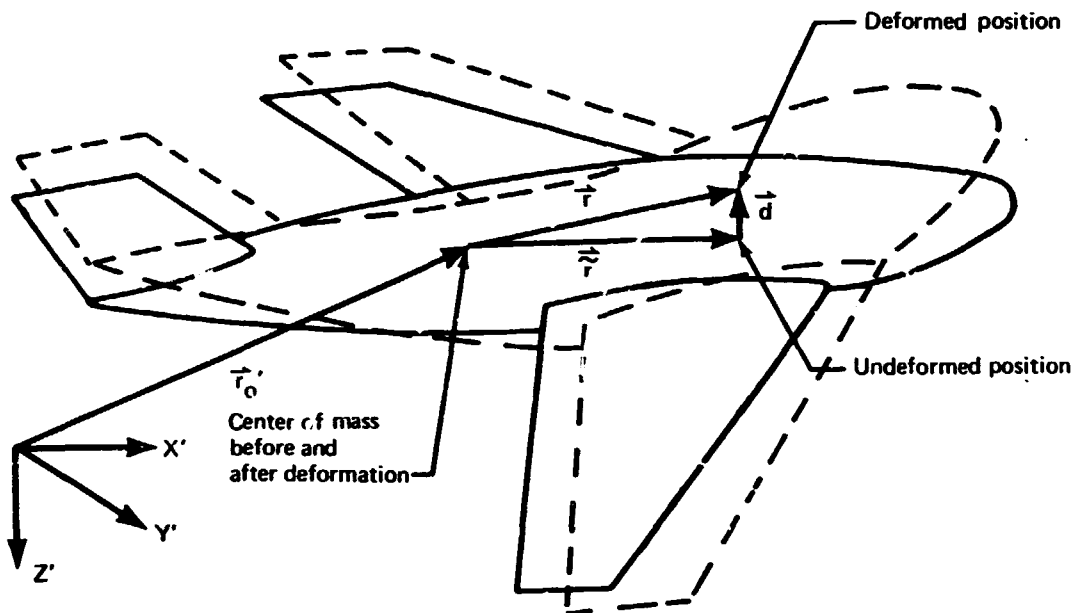


FIGURE 2.3-3.—ELASTIC DISPLACEMENT

2.3.2.4 Approximate mean reference frame constraint conditions.—The FLEXSTAB system is formulated using an approximate form of equation (2.3-17), i.e., the constraint condition which determines the rate of rotation of the mean reference frame. The approximation consists of setting to zero the cross product of the elastic displacement vector with its time rate of change i.e.,

$$\int_V \vec{d} \times \frac{\delta \vec{d}}{\delta t} \rho_A dV = 0$$

This is a valid approximation if the two vectors \vec{d} and $\delta\vec{d}/\delta t$ are nearly parallel; and, for conventional aircraft structural components, this is a valid assumption. Thin lifting surfaces such as wings and tail surfaces are platelike in that the dominant elastic displacement and displacement rate are both normal to a surface and hence parallel. Slender body shapes such as a fuselage are beamlike, with the dominant elastic displacement and displacement rate normal to an elastic axis and in only one direction. Introducing the above approximation into equation (2.3-17), the constraint condition determining the rotation rate of the mean axis system becomes

$$\int_V \vec{r} \times \frac{\delta\vec{d}}{\delta t} \rho_A dV = \vec{0}.$$

The constraint conditions, using the above approximations, are integrable with respect to time and are expressed as follows:

$$\int_V \vec{d} \rho_A dV = \vec{C}_1$$

and

$$\int_V \vec{r} \times \vec{d} \rho_A dV = \vec{C}_2$$

where \vec{C}_1 and \vec{C}_2 are constants of integration. The constants of integration are set to zero and the constraint conditions become (cf., equations 4.73 and 4.74 of reference 2-6)

$$\int_V \vec{d} \rho_A dV = \vec{0}$$

and

$$\int_V \vec{r} \times \vec{d} \rho_A dV = \vec{0}. \quad (2.3-18)$$

The displacement vector contained in equations (2.3-14) is required to satisfy these conditions. Since the elastic displacement field specifies the deformed configuration of the aircraft relative to an undeformed configuration, the six conditions represented by equations (2.3-18) determine a coordinate system in which the coordinates of the undeformed differential mass elements are independent of time, i.e.,

$$\vec{r} = \vec{r}(\tilde{X}, \tilde{Y}, \tilde{Z}).$$

The motions of a flexible aircraft described by equations (2.3-1) and (2.3-14) are related as

$$\vec{r}'(\tilde{X}, \tilde{Y}, \tilde{Z}, t) = \vec{r}'_0(t) + \vec{r}(\tilde{X}, \tilde{Y}, \tilde{Z}) + \vec{d}(\tilde{X}, \tilde{Y}, \tilde{Z}, t) \quad (2.3-19)$$

where $\tilde{X}, \tilde{Y}, \tilde{Z}$ are the Lagrangian coordinates in the Reference Axis System (i.e., the coordinates of the differential mass elements in the reference, undeformed configuration). The constraint conditions, equations (2.3-18), therefore provide the basis for introducing a body-fixed axis system relative to which elastic deformation is measured.

2.3.2.5 Reference and perturbation motions.—In the stability analysis performed by the FLEXSTAB system, the motions described in the preceding are evaluated when an aircraft is in either of two states of motion: (1) a steady reference flight condition and (2) an unsteady perturbation motion about the steady motion of the reference flight condition. In the steady reference flight condition a differential mass element of the aircraft has a velocity relative to the Inertial Axis System which is given by

$$\left(\frac{d\vec{r}'}{dt}\right)_1 = \vec{V}_{C_1} + \vec{\omega}_1 \times \vec{r}_1$$

where $\vec{V}_{C_1} \equiv (d\vec{r}_0'/dt)_1$ and $\vec{\omega}_1$ are the steady translational and rotational velocities of the Body Axis System relative to the Inertial Axis System, equations (2.2-3). In the perturbation motion the perturbation velocity of the differential mass element is given by

$$\left(\frac{d\vec{r}'}{dt}\right)_P = \vec{V}_{CP} + \vec{\omega}_1 \times (\vec{r}_1 + \vec{d}_P) + \vec{\omega}_1 \times \vec{d}_P + \frac{\delta \vec{d}}{\delta t} P.$$

This expression is replaced in the FLEXSTAB system by the following approximation, which neglects the cross product of rotation rate and perturbation displacement:

$$\left(\frac{d\vec{r}'}{dt}\right)_P \approx \vec{V}_{CP} + \vec{\omega}_P \times \vec{r}_1 + \frac{\delta \vec{d}}{\delta t} P. \quad (2.3-20)$$

The consequences of the approximation introduced by equation (2.3-20) are apparent when they are applied to the kinetic energy of an aircraft. The kinetic energy, when the perturbation velocity is given by equation (2.3-20), appears as follows:

$$K = K_1 + K_P \quad (2.3-21)$$

where

$$K_1 \equiv \frac{1}{2} M V_{C_1}^2 + \frac{1}{2} \int_V (\vec{\omega}_1 \times \vec{r}_1) \cdot (\vec{\omega}_1 \times \vec{r}_1) \rho_A dV$$

is the kinetic energy for the steady reference flight condition and

$$\begin{aligned} K_P \equiv & \frac{1}{2} M V_{CP}^2 + M \vec{V}_{CP} \cdot \vec{V}_{C_1} + \frac{1}{2} \int_V [(\vec{\omega}_P + \vec{\omega}_1) \times \vec{r}_1] \cdot (\vec{\omega}_P + \vec{\omega}_1 \times \vec{r}_1) \rho_A dV \\ & + \frac{1}{2} \int_V \frac{\delta \vec{d}}{\delta t} P \cdot \frac{\delta \vec{d}}{\delta t} P \rho_A dV \end{aligned} \quad (2.3-22)$$

is the perturbation kinetic energy. The neglected kinetic energy is given by the following expression:

$$\Delta K_P \equiv \frac{1}{2} \int_V [(\vec{\omega}_1 + \vec{\omega}_P) \times (2\vec{r}_1 + \vec{d}_P) \cdot [(\vec{\omega}_1 + \vec{\omega}_P) \times \vec{d}_P] \rho_A dV. \quad (2.3-23)$$

The approximation, equation (2.3-20), is seen to cause part of the perturbation kinetic energy to be neglected; namely, that which arises from rigid-body rotation in conjunction with a perturbation change in shape.

The kinetic energy which is retained in the formulation is separated into a sum of terms each having a clear physical significance. For the reference flight condition

$$K_1 = K(\vec{V}_{C_1}) + K(\vec{\omega}_1)$$

where

$$K(\vec{V}_{C_1}) \equiv \frac{1}{2} M V_{C_1}^2 \quad (2.3-24)$$

is the reference kinetic energy arising from rigid-body translation and

$$K(\vec{\omega}_1) \equiv \frac{1}{2} \int_V (\vec{\omega}_1 \times \vec{r}_1) \cdot (\vec{\omega}_1 \times \vec{r}_1) \rho_A dV$$

is the reference kinetic energy arising from rigid-body rotation. For the perturbation motion

$$K_P = K(\vec{V}_{C_P}) + K(\vec{\omega}_P) + K(\vec{\dot{d}}_P) \quad (2.3-25)$$

where

$$K(\vec{V}_{C_P}) \equiv \frac{1}{2} M V_{C_P}^2 + M \vec{V}_{C_1} \cdot \vec{V}_{C_P}$$

is the perturbation kinetic energy arising from rigid-body translation,

$$K(\vec{\omega}_P) \equiv \frac{1}{2} \int_V [(\vec{\omega}_P + 2\vec{\omega}_1) \times \vec{r}_1] \cdot (\vec{\omega}_P \times \vec{r}_1) \rho_A dV$$

is the perturbation kinetic energy arising from rigid-body rotation, and

$$K(\vec{\dot{d}}_P) \equiv \frac{1}{2} \int_V \frac{\delta \vec{\dot{d}}_P}{\delta t} \cdot \frac{\delta \vec{\dot{d}}_P}{\delta t} \rho_A dV$$

is the perturbation kinetic energy arising from elastic deformation rate.

The error introduced by the approximation, equation (2.3-20), is related to the perturbation kinetic energy arising from rigid-body rotation. Therefore the validity of the approximation may be evaluated by examining the magnitude of the following ratio:

$$\frac{\Delta K_P}{K(\vec{\omega}_P)} = \frac{\int_V [(\vec{\omega}_1 + \vec{\omega}_P) \times (2\vec{r}_1 + \vec{\dot{d}}_P) \cdot [(\vec{\omega}_1 + \vec{\omega}_P) \times \vec{\dot{d}}_P] \rho_A dV}{\int_V [(\vec{\omega}_P + 2\vec{\omega}_1) \times \vec{r}_1] \cdot (\vec{\omega}_P \times \vec{r}_1) \rho_A dV} \quad (2.3-26)$$

Carrying out the indicated integrations leads to a comparison in terms of physical components. The denominator of equation (2.3-26) becomes

$$K(\vec{\omega}_p) = I_{XX_1}(p^2 + 2pP_1) + I_{YY_1}(q^2 + 2qQ_1) + I_{ZZ_1}(r^2 + 2rR_1) - 2I_{XZ_1}(p + 2P_1)$$

where I_{XX_1} , I_{YY_1} , I_{ZZ_1} , I_{XZ_1} , I_{XY_1} , I_{YZ_1} are the moments and products of inertia in the reference flight condition and p , q , r components of perturbation rotation rate expanded on the Body Axis System, i.e.,

$$\vec{\omega}_p = p\vec{i}_B + q\vec{j}_B + r\vec{k}_B$$

The numerator of equation (2.3-26) becomes

$$\begin{aligned} \Delta K_p = & I_{XX_p}(P_1 + p)^2 + I_{YY_p}(Q_1 + q)^2 + I_{ZZ_p}(R_1 + r)^2 \\ & + 2I_{XZ_p}(P_1 + p)(R_1 + r) + 2I_{XY_p}(P_1 + p)(Q_1 + q) \\ & + 2I_{YZ_p}(Q_1 + q)(R_1 + r) \end{aligned}$$

where I_{XX_p} , I_{YY_p} , I_{ZZ_p} , I_{XZ_p} , I_{XY_p} , I_{YZ_p} are perturbations to the moments and products of inertia arising from perturbation elastic deformation.

The moments of inertia for conventional aircraft configurations (I_{XX_1} , I_{YY_1} , I_{ZZ_1}) in the reference flight condition will be at least an order of magnitude larger than the perturbations I_{XX_p} , I_{YY_p} , I_{ZZ_p} . It follows therefore that the contribution to the error from the terms containing these quantities is negligible if the components of rotation rate in the reference flight condition (P_1 , Q_1 , R_1) have at most the same order of magnitude as their perturbation values, p , q , r . Also, if the elastic deformation in the reference condition is small in comparison to its overall dimensions, all products of inertia contained in the ratio with the exception of I_{XZ_1} are small in comparison to the moments of inertia in the reference flight condition. The products of inertia terms therefore contribute no additional restrictions on the validity of the approximation; and the conditions which must be satisfied for equation (2.3-20) to yield a valid approximation are seen to be as follows:

- 1) $O(P_1) = O(p)$, $O(Q_1) = O(q)$, $O(R_1) = O(r)$
- 2) Perturbation changes to the dimensions must be an order of magnitude less than the dimensions of the aircraft in the reference flight condition.

These conditions are usually satisfied in the case of large aircraft; hence, equation (2.3-20) is taken to be a valid approximation for the FLEXSTAB problem.

The kinematic approximation, equation (2.3-18), and the perturbation expansion about a steady reference flight condition, permit the constraint conditions, equations (2.3-17), to be expressed as follows:

For the reference flight condition,

$$\int_V \vec{d}_1 \rho_A dV = \vec{0}$$

and (2.3-27)

$$\int_V \vec{r} \times \vec{d}_1 \rho_A dV = \vec{0}$$

where $\vec{r} = \vec{r}(\tilde{X}, \tilde{Y}, \tilde{Z})$ describes an undeformed configuration of the aircraft—termed the jig shape—and \vec{d}_1 is the deformation in the reference flight condition; while, for the disturbed flight condition,

$$\int_V \vec{d}_p \rho_A dV = \vec{0}$$

and (2.3-28)

$$\int_V \vec{r}_1 \times \vec{d}_p \rho_A dV = \vec{0}$$

where $\vec{r}_1 = \vec{r}_1(\tilde{X}, \tilde{Y}, \tilde{Z})$ describes the configuration of the aircraft in the reference flight condition.

2.3.3 Fluid Motions

This portion of the kinematic description is aimed at developing formulas describing certain aspects of the fluid motion determined by the geometry of the aircraft and its motion relative to the Fluid Axis System.

2.3.3.1 Surface boundary condition.—The surface of the aircraft having the spatial (i.e., Eulerian) description,

$$G(X, Y, Z, t) = 0, \quad (2.2-7)$$

represents a solid boundary to the fluid; therefore, the velocity of the disturbed fluid must be such that fluid particles do not penetrate the aircraft's surface. This condition represents the surface boundary condition for the fluid flow problem and is expressed analytically for fluid particles located on the surface and having Eulerian coordinates satisfying equation (2.2-7) as follows:

$$\frac{\partial G}{\partial t} + \vec{v} \cdot \vec{\nabla} G = 0 \quad (2.3-29)$$

where \vec{V} is the fluid velocity relative to the Reference Axis System. There is an additional requirement that skin particles at the surface of the aircraft must remain at the surface as it undergoes motion due to elastic deformation or control surface deflection. This surface boundary condition for skin particles whose Eulerian coordinates satisfy equation (2.2-7) is expressed as:

$$\frac{\partial G}{\partial t} + \left(\frac{\delta \vec{d}}{\delta t}\right) \cdot \vec{V}_G = 0 \quad (2.3-30)$$

where $\delta \vec{d}/\delta t$ is the velocity of skin particles relative to the Reference Axis System. Combining equations (2.3-29) and (2.3-30) leads to the following surface boundary condition:

$$\left(\vec{V} - \frac{\delta \vec{d}}{\delta t}\right) \cdot \vec{n} = 0 \quad (2.3-31)$$

where

$$\vec{n} \equiv \vec{\Delta}_G / \sqrt{\vec{\Delta}_G \cdot \vec{\Delta}_G} \quad (2.3-32)$$

is the unit vector normal to the surface.

Recalling the velocity relationship

$$\vec{V} = \vec{Q} - \vec{V}_R - \vec{\omega} \times \vec{r}, \quad \text{at } t=t_0 \quad (2.2-4)$$

the surface boundary condition is expressed as

$$\vec{Q} \cdot \vec{n} = (\vec{V}_R + \vec{\omega} \times \vec{r} + \frac{\delta \vec{d}}{\delta t}) \cdot \vec{n} \quad \text{at } t=t_0 \quad (2.3-33)$$

where \vec{r} is the position vector for a fluid particle on the surface. This form of the boundary condition is appropriate to the stability and control problem because the fluid velocity is related by equation (2.3-33) to the aircraft's velocity, elastic deformation, and control surface deflections. The boundary condition is further developed by letting the fluid velocity \vec{Q} be expressed as a perturbation to a uniform freestream,

$$\vec{Q} = U(\vec{i} + \vec{v}) \quad (2.3-34)$$

where U is the steady translational velocity of the Fluid Axis System relative to the Inertial Axis System. The vector

$$\vec{v} = u\hat{i} + v\hat{j} + w\hat{k} \quad (2.3-35)$$

is the nondimensional perturbation velocity of the fluid expanded on the Reference Axis System. Substituting equations (2.3-34) and (2.3-35) into the surface boundary condition, equation (2.3-33) leads to

$$v_n = -n_x + \frac{1}{U}(\vec{V}_R + \vec{\omega} \times \vec{r} + \frac{\delta \vec{d}}{\delta t}) \cdot \vec{n} \quad (2.3-36)$$

where

$$v_n \equiv \vec{n} \cdot \vec{v} \quad (2.3-37)$$

is the nondimensional component of perturbation velocity normal to the surface.

The velocity vector in the brackets of equation (2.3-36) represents the velocity, relative to the Fluid Axis System, of a point on the deforming surface of the aircraft, i.e.,

$$\vec{V}^S(X, Y, Z, t) \equiv \vec{V}_R(t) + \vec{\omega}(t) \times \vec{r}(X, Y, Z, t) + \frac{\delta \vec{d}}{\delta t}(X, Y, Z, t) \quad (2.3-38)$$

Therefore, equation (2.3-36) may be expressed as

$$v_n = -n_x + \frac{U}{U} \vec{V}^S \cdot \vec{n} \quad (2.3-39)$$

while equation (2.3-33) becomes

$$\vec{Q} \cdot \vec{n} = \vec{V}^S \cdot \vec{n} \quad (2.3-40)$$

These two results, i.e., equations (2.3-39) and (2.3-40), lead to a geometric interpretation of the nondimensional velocity component v_n , relating it to the angle through which the freestream velocity vector $U\hat{i}$ must be perturbed, making the path lines of fluid particles lie along path lines traced by points on the surface. This angle is termed the flow incidence angle.

The flow incidence angle is viewed in figure 2.3-4 for three cases: (1) flow incidence due entirely to geometric slope of the surface, (2) flow incidence due entirely to the velocity of the surface along the surface normal, and (3) a combination of (1) and (2). Taking positive flow incidence to be a positive rotation about the Y-axis, the flow incidence in cases (1) and (2) is as follows:

$$\text{Case (1):} \quad \sin \Psi_1 = -\vec{n} \cdot \vec{v} = n_x \quad (2.3-41)$$

$$\text{Case (2):} \quad \sin \Psi_2 = -\frac{U}{|\vec{Q}_2|} \vec{n} \cdot \vec{v} = -\frac{\vec{V}^S \cdot \vec{n}}{|\vec{Q}_2|}$$

When cases (1) and (2) are combined, i.e., case (3) shown by figure 2.3-4, the flow incidence is given by

$$\begin{aligned} \text{Case (3):} \quad \sin \Psi &= \sin(\Psi_1 + \Psi_2) \\ &= \sin \Psi_1 \cos \Psi_2 + \cos \Psi_1 \sin \Psi_2 \end{aligned} \quad (2.3-42)$$

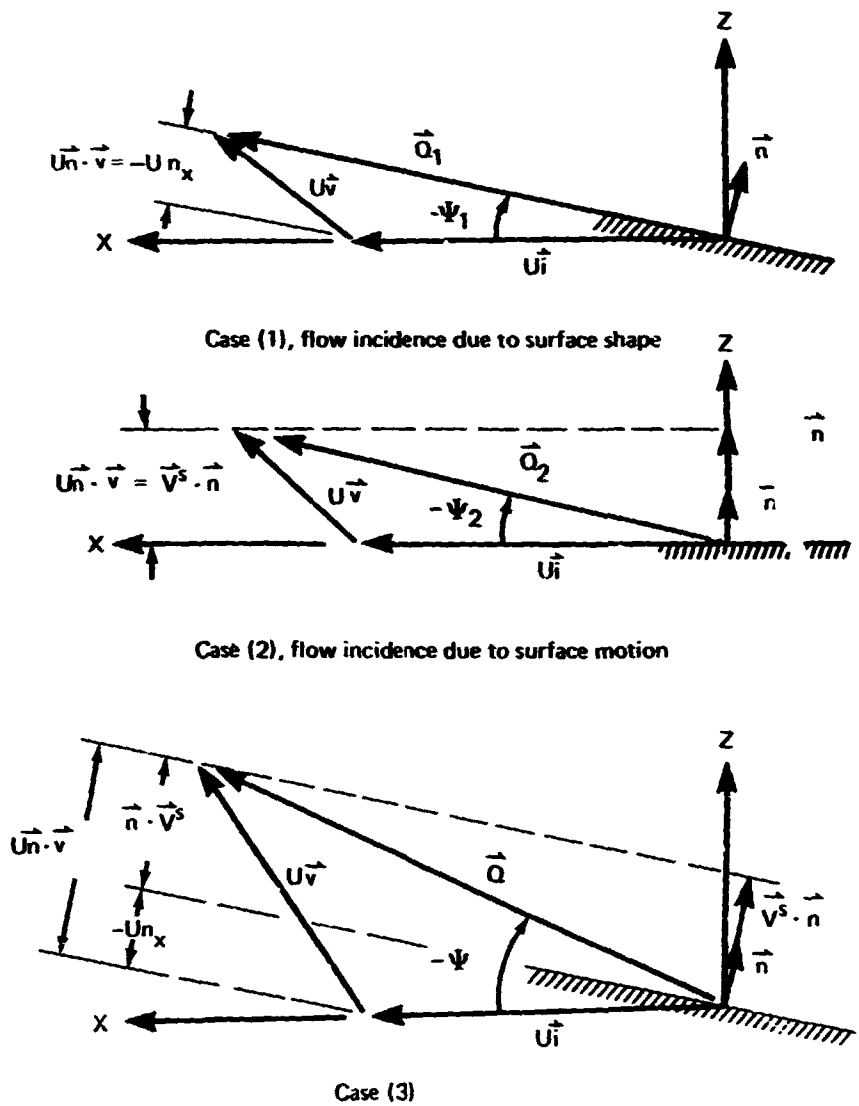


FIGURE 2.3-4.—ANGLE OF FLOW INCIDENCE

where

$$\cos \Psi_1 = \frac{U(1 + u_1)}{|\vec{Q}_1|}$$

and

$$\cos \Psi_2 = \frac{U(1 + u_2)}{|\vec{Q}_2|}$$

2.3.3.2 Linearized surface boundary condition.—The FLEXSTAB system is based on an aerodynamic theory (section 3) which is a linear first-order approximation. This is obtained by assuming

$$|\vec{v}| = O(\epsilon), \quad \epsilon \ll 1 \quad (2.3-43)$$

The theory is applied in the FLEXSTAB system to bodies with nonplanar surfaces which may have any dihedral angle between 0 and 2π radians; thus, the components of the unit normal vector n_Y and n_Z have the following ranges of magnitude:

$$-1 \leq n_Y \leq 1 \quad -1 \leq n_Z \leq 1 \quad (2.3-44)$$

Applying these orders of magnitude to equation (2.3-39), it follows that

$$n_X = O(\epsilon), \quad \frac{V^S}{U} = O(\epsilon), \quad \frac{W^S}{U} = O(\epsilon) \quad (2.3-45)$$

where V^S and W^S are the components of \vec{V}^S expanded on the Reference Axis System.

Expanding the surface boundary condition, equation (2.3-39), leads to

$$v_n = -n_X + \frac{1}{U}(U^S n_X + V^S n_Y + W^S n_Z) \quad (2.3-46)$$

and assuming that

$$\frac{U^S}{U} = O(\epsilon) \quad (2.3-47)$$

(i.e., the X-component of surface velocity arising from the rotation rate and the elastic deformation rate is of order ϵ compared with U) a first-order approximation is obtained by deleting $(U^S/U)n_X = O(\epsilon^2)$,

$$v_n \approx -n_X + \frac{1}{U}(V^S n_Y + W^S n_Z) \quad (2.3-48)$$

Recalling the expressions for flow incidence angle, i.e., equations (2.3-41) and (2.3-42), these expressions are seen to reduce to the following first-order approximations:

$$\begin{aligned}\sin \Psi_1 &\approx \Psi_1 & \sin \Psi_2 &\approx \Psi_2 \\ \cos \Psi_1 &\approx 1 & \cos \Psi_2 &\approx 1\end{aligned}$$

and

$$\Psi \approx \Psi_1 + \Psi_2.$$

From these approximate formulas and equation (2.3-48) the first-order approximation to the flow incidence angle is found to be

$$\Psi = n_X - \frac{1}{U}(V^S n_Y + W^S n_Z). \quad (2.3-49)$$

The process leading to this linear result is considered in detail in the following development. Case (1) and case (2), shown by figure 2.3-4, represent the two mechanisms whereby flow incidence arises at the aircraft surface. In case (1) the flow incidence arises from the geometry of the surface when that geometry in the Fluid Axis System is independent of time. In case (2) the flow incidence arises from motion of the surface relative to the Fluid Axis System. In case (3) the flow incidence arises from a simultaneous occurrence of the two mechanisms of cases (1) and (2). The surface boundary condition, equation (2.3-46), is linearized in the following by first linearizing the two special forms obtained for cases (1) and (2). Once these two special cases are linearized they are combined to obtain the linearized boundary condition for the combined, general case. This approach is used to clarify the development of the linearized boundary condition. Since the results are linear equations, the combined linear boundary conditions are obtained with no loss in generality.

2.3.3.3 Flow incidence for a fixed surface geometry in the Fluid Axis System—

Case (1).—As shown by section 2.3.3.2, the X-component of the unit vector normal to the surface is the quantity which gives rise to flow incidence in case (1). Consider, therefore, the mechanisms which may influence the unit normal vector, viz., the rotation of the surface due to elastic deformation and due to control surface deflection. The unit normal vector is expressed as

$$\begin{aligned}\vec{n} &= \vec{n}^*(\tilde{X}, \tilde{Y}, \tilde{Z}) + \vec{\theta}_E(\tilde{X}, \tilde{Y}, \tilde{Z}, t) \times \vec{n}^*(\tilde{X}, \tilde{Y}, \tilde{Z}) \\ &\quad + \vec{\theta}_C(\tilde{X}, \tilde{Y}, \tilde{Z}, t) \times \vec{n}^*(\tilde{X}, \tilde{Y}, \tilde{Z})\end{aligned} \quad (2.3-50)$$

where

\vec{n}^* is the unit vector normal to the surface before elastic deformation and control surface deflection,

$\vec{\theta}_E \approx 1/2 \vec{\nabla} \times \vec{d}$ is the surface rotation due to elastic deformation, and

$\vec{\theta}_C$ is the surface rotation due to control surface deflection.

The X-component of the unit normal vector is found from equation (2.3-50) to be

$$n_X = \tilde{n}_X + (\theta_{EY} + \delta_{CY})\tilde{n}_Z - (\theta_{EZ} + \delta_{CZ})\tilde{n}_Y \quad (2.3-51)$$

where θ_{EY}, θ_{EZ} are the components of elastic rotation and δ_{CY}, δ_{CZ} are the components of control surface rotation expanded on the Reference Axis System.

An order of magnitude analysis of equation (2.3-51) is made using the assumptions listed by equations (2.3-43) and (2.3-44). Since n_X is of order ϵ and \tilde{n}_Y and \tilde{n}_Z are of order unity, it follows from the independence of $\vec{\theta}_E$ and $\vec{\theta}_C$ that

$$\begin{aligned} \tilde{n}_X &= 0(\epsilon), & \theta_{EY} &= 0(\epsilon), & \theta_{EZ} &= 0(\epsilon), \\ \delta_{CY} &= 0(\epsilon), & \delta_{CZ} &= 0(\epsilon). \end{aligned} \quad (2.3-52)$$

The control surface rotations are expressed in the FLEXSTAB system in terms of three independent control surfaces. Therefore equation (2.3-51) is expressed as

$$n_X = \tilde{n}_X + \theta_{EY}\tilde{n}_Z - \theta_{EZ}\tilde{n}_Y + n_{eX}\delta_e + n_{aX}\delta_a + n_{rX}\delta_r \quad (2.3-53)$$

where n_{eX}, n_{aX}, n_{rX} relate n_X to control surface deflections and the quantities $\delta_e, \delta_a, \delta_r$ are, at most, functions of time and govern the amplitudes of the control surface deflections. The amplitudes of the control surface rotations, δ_{CY} and δ_{CZ} , are, however, restricted to the order of ϵ as in equation (2.3-52).

Combining the first of equations (2.3-41) with equation (2.3-53) and using the first order in ϵ approximation for the sine function, viz.,

$$\sin \psi_1 \approx \psi_1, \quad (2.3-54)$$

the linearized boundary condition in terms of flow incidence arising in case (1) is found as

$$\begin{aligned} \psi_1 &= \tilde{n}_X + \theta_{EY}\tilde{n}_Z - \theta_{EZ}\tilde{n}_Y \\ &+ n_{eX}\delta_e + n_{aX}\delta_a + n_{rX}\delta_r. \end{aligned} \quad (2.3-55)$$

2.3.3.4 Flow incidence arising from surface motion relative to the Fluid Axis System—Case (2).—Consider the expanded form of the surface boundary condition for case (2), viz., the second of equations (2.3-41). Introducing the expanded unit normal vector from equation (2.3-50) leads to

$$\begin{aligned} \Psi_2 = & -\frac{1}{U}\{V^S[\tilde{n}_Y - \theta_{EX}\tilde{n}_Z - \delta_{CX}\tilde{n}_Z + (\theta_{EZ} + \delta_{CZ})\tilde{n}_X] \\ & + W^S[\tilde{n}_Z + \theta_{EX}\tilde{n}_Y + \delta_{CX}\tilde{n}_Y - (\theta_{EY} + \delta_{CY})\tilde{n}_X]\}. \end{aligned} \quad (2.3-56)$$

In the FLEXSTAB system analysis, surface rotations about the X-axis due to elastic deformation and control surface deflections are assumed to have the same order of magnitude as the rotations about the Y- and Z-axes; thus,

$$\begin{aligned} \theta_{EX} &= 0(\epsilon) \\ \text{and} \\ \delta_{CX} &= 0(\epsilon). \end{aligned} \quad (2.3-57)$$

This assumption in conjunction with the assumed ϵ order of magnitude for the following surface velocity component ratios:

$$\frac{V^S}{U} = 0(\epsilon) \quad \text{and} \quad \frac{W^S}{U} = 0(\epsilon)$$

leads to the following first order in ϵ approximation for the flow incidence:

$$\Psi_2 = -\frac{1}{U}(V^S\tilde{n}_Y + W^S\tilde{n}_Z). \quad (2.3-58)$$

This result is related to motions of the aircraft by expanding the velocity components V^S and W^S .

The velocity components V^S and W^S , describing the velocity of the surface relative to the Fluid Axis System, are obtained from equation (2.3-38) as

$$\begin{aligned} \frac{V^S}{U} &= \frac{1}{U}(V - \bar{X}R + \bar{Z}P + \delta d_Y/\delta t) \\ \frac{W^S}{U} &= \frac{1}{U}(-W - \bar{Y}P - \bar{X}Q + \delta d_Z/\delta t) \end{aligned} \quad (2.3-59)$$

The quantities appearing in these expressions are as follows: The coordinates—in the Reference Axis System—of the surface point relative to the center of mass, i.e.,

$$\begin{aligned}
\bar{X} &\equiv X - X_{cg}, \\
\bar{Y} &\equiv Y - Y_{cg}, \\
\text{and } \bar{Z} &\equiv Z - Z_{cg};
\end{aligned}
\tag{2.3-60}$$

the components—expanded on the Reference Axis System—of velocity of the surface point relative to the Reference Axis System, i.e.,

$$\delta d_Y / \delta t \equiv \partial d_Y(\bar{X}, \bar{Y}, \bar{Z}, t) / \partial t$$

and

$$\delta d_Z / \delta t \equiv \partial d_Z(\bar{X}, \bar{Y}, \bar{Z}, t) / \partial t
\tag{2.3-61}$$

and the components of velocity of the Reference Axis System relative to the Fluid Axis System expanded on the Body Axis System, i.e.,

$$V(t), W(t), P(t), Q(t), R(t).
\tag{2.3-62}$$

From an examination of equations (2.3-60), (2.3-61) and (2.3-62) it is apparent that the velocity components, as expressed by equations (2.3-59), are in a form which is a mixture of Eulerian and Lagrangian coordinates. Expressions entirely in terms of Lagrangian coordinates are found by expressing the location of the surface point as

$$\vec{r}(\bar{X}, \bar{Y}, \bar{Z}, t) = \vec{r}(\bar{X}, \bar{Y}, \bar{Z}) + \vec{d}(\bar{X}, \bar{Y}, \bar{Z}, t)$$

so that equations (2.3-59) become

$$\frac{V^S}{U} = \frac{1}{U} [V - (d_X + \bar{X} - X_{cg})R + (d_Z + \bar{Z} - Z_{cg})P + \delta d_Y / \delta t]
\tag{2.3-63}$$

$$\frac{W^S}{U} = \frac{1}{U} [-W - (d_Y + \bar{Y} - Y_{cg})P - (d_X + \bar{X} - X_{cg})Q + \delta d_Z / \delta t].$$

The development to follow is based on the mixed form presented by equation (2.3-59) treating the variables \bar{X} , \bar{Y} , \bar{Z} as Eulerian coordinates while continuing to treat the velocity components $\delta d_Y / \delta t$ and $\delta d_Z / \delta t$ as quantities defined in terms of the Lagrangian coordinates \bar{X} , \bar{Y} , \bar{Z} .

Consider each of the terms contained in the linearized surface boundary condition, equation (2.3-58), letting the elastic displacement field be represented as

$$\vec{d}(\bar{X}, \bar{Y}, \bar{Z}, t) = \vec{\phi}_i(\bar{X}, \bar{Y}, \bar{Z}) u_i(t)
\tag{2.3-64}$$

where $\vec{\phi}_i$ is a mode of structural deformation and u_i is the amplitude of modal deflection. The mode of deformation is chosen such that

$$|\vec{\phi}_i| = O(1)$$

for points X, Y, Z at the aircraft surface. Also, noting that

$$\frac{2\bar{X}}{\bar{c}} = O(1), \quad \frac{2\bar{Y}}{b} = O(1), \quad \frac{2\bar{Z}}{b} = O(1) \quad (2.3-66)$$

where \bar{c} is the reference chord and b is the span of the aircraft it follows from the fact that

$$\psi_2 = O(\epsilon)$$

and from the independence of the velocity components V, W, P, Q, R and \dot{u}_i that

$$\begin{aligned} \hat{P} &\equiv \frac{bP}{2U} = O(\epsilon), \quad \hat{Q} \equiv \frac{\bar{c}Q}{2U} = O(\epsilon), \quad \hat{R} \equiv \frac{bR}{2U} = O(\epsilon), \\ \hat{\dot{u}}_i &\equiv \dot{u}_i / U = O(\epsilon). \end{aligned} \quad (2.3-67)$$

The linearized boundary condition, equation (2.3-58), for case (2), therefore, is expressed as

$$\begin{aligned} \psi_2 = - [& (\beta - \frac{2\bar{X}\hat{R}}{b} + \frac{2\bar{Z}\hat{P}}{b} + \phi_{iY}\hat{\dot{u}}_i) \tilde{n}_Y + \\ & (- \alpha - \frac{2\bar{Y}\hat{P}}{b} - \frac{2\bar{X}\hat{Q}}{\bar{c}} + \phi_{iZ}\hat{\dot{u}}_i) \tilde{n}_Z] \end{aligned} \quad (2.3-68)$$

where $\alpha \equiv W/U$ is the approximate angle of attack, and $\beta \equiv V/U$ is the approximate angle of sideslip.

2.3.3.5 Combined linearized surface boundary condition—Case (3).—The combined linearized surface boundary condition is found by simply adding equations (2.3-55) and (2.3-68) to obtain

$$\begin{aligned} \psi = & \tilde{n}_X + \theta_{EY}\tilde{n}_Z - \theta_{EZ}\tilde{n}_Y + n_{eX}\delta_e + n_{aX}\delta_a + n_{rX}\delta_r - \\ & (\beta - \frac{2\bar{X}\hat{R}}{b} + \frac{2\bar{Z}\hat{P}}{b} + \phi_{iY}\hat{\dot{u}}_i) \tilde{n}_Y \\ & - (- \alpha - \frac{2\bar{Y}\hat{P}}{b} - \frac{2\bar{X}\hat{Q}}{\bar{c}} + \phi_{iZ}\hat{\dot{u}}_i) \tilde{n}_Z. \end{aligned} \quad (2.3-69)$$

Equation (2.3-48) suggests a convenient and compact form for the surface boundary condition to be used in section 3. Each of the quantities, multiplying the small parameters $\alpha, \beta, \hat{P}, \hat{Q}, \hat{R}, \hat{\dot{u}}_i$ in equation (2.3-69), is of order of magnitude unity, and can be incorporated into three terms having the appropriate orders of magnitude by letting

$$\hat{v}\lambda_v(t)\bar{V}(X,Y,Z) \equiv \beta - \frac{2\bar{X}\hat{R}}{b} + \frac{2\bar{Z}\hat{P}}{b} + \phi_{iY}\hat{u}_i \quad (2.3-70)$$

$$\hat{w}\lambda_w(t)\bar{W}(X,Y,Z) \equiv -\alpha - \frac{2\bar{Y}\hat{P}}{b} - \frac{2\bar{X}\hat{Q}}{c} + \phi_{iZ}\hat{u}_i$$

and

$$n_X = \tilde{n}_X + \theta_{EY}n_Z - \theta_{EZ}\tilde{n}_Y + n_{eX}\delta_e + n_{aX}\delta_a + n_{rX}\delta_r \quad (2.3-71)$$

where

$$\hat{v} = 0(\epsilon) \quad \text{and} \quad \hat{w} = 0(\epsilon)$$

while

$$\bar{V}(X,Y,Z) = 0(1), \quad \bar{W}(X,Y,Z) = 0(1).$$

The surface boundary condition is expressed now as the sum of three terms as

$$\psi = n_X - \hat{v}\lambda_v(t)\bar{V}\tilde{n}_Y - \hat{w}\lambda_w(t)\bar{W}\tilde{n}_Z. \quad (2.3-73)$$

This form of the surface boundary condition is used in section 3 to develop the linear aerodynamic theory used in the FLEXSTAB system.

2.3.3.6 Dynamic pressure and Mach number variations.—The aerodynamic analysis of section 3 requires the values of the undisturbed freestream dynamic pressure and Mach number relative to two different reference frames—the Fluid Axis System and the Reference Axis System. The values of the dynamic pressure and Mach number measured in the Fluid Axis System are taken to be reference values and the values apparent to an observer fixed to the Reference Axis System are expressed as variations from these reference values.

The freestream dynamic pressure and Mach number in the Fluid Axis System are given by the definitions

$$\bar{q}_\infty \equiv \frac{1}{2}\rho_\infty \vec{Q} \cdot \vec{Q} \quad \text{and} \quad M_\infty \equiv \frac{|\vec{Q}|}{a_\infty} \quad (2.3-74)$$

while for an observer at the position \vec{r} relative to the aircraft center mass and fixed in the Reference Axis System the freestream dynamic pressure and Mach number are given by the definitions

$$\bar{q} \equiv \frac{1}{2}\rho_\infty \vec{V} \cdot \vec{V} \quad (2.3-75)$$

and

$$M \equiv \frac{|\vec{V}|}{a_\infty}$$

where \vec{Q} and \vec{V} are defined as in section 2.2.3 but evaluated in the undisturbed stream. Introducing the relationship between \vec{Q} and \vec{V} , equation (2.2-4),

$$\bar{q} = \bar{q}_\infty + \frac{1}{2}\rho_\infty \left[2U(\vec{V}_R + \vec{\omega} \times \vec{r}) \cdot \hat{i} + (\vec{V}_R + \vec{\omega} \times \vec{r}) \cdot (\vec{V}_R + \vec{\omega} \times \vec{r}) \right]$$

and

$$M = \frac{1}{a_\infty} \left[U^2 + 2U(\vec{V}_R + \vec{\omega} \times \vec{r}) \cdot \hat{i} + (\vec{V}_R + \vec{\omega} \times \vec{r}) \cdot (\vec{V}_R + \vec{\omega} \times \vec{r}) \right]^{\frac{1}{2}}$$

Assuming the components of \vec{V}_R and $\vec{\omega}$ are small enough that their products may be ignored, first-order expressions for the dynamic pressure and Mach number are found as

$$\bar{q} = \bar{q}_\infty + 2\bar{q}_\infty \frac{1}{U}(Q\bar{Z} + R\bar{Y}) \quad (2.3-76)$$

and

$$M = M_\infty + \frac{M_\infty}{U}(Q\bar{Z} + R\bar{Y}) \quad (2.3-77)$$

where \bar{Y} and \bar{Z} are the coordinates of the point of evaluation relative to the center of mass in the Reference Axis System. The variations in dynamic pressure and Mach number are therefore seen to be

$$\Delta \bar{q} \equiv 2\bar{q}_\infty \frac{1}{U}(Q\bar{Z} + R\bar{Y})$$

and

$$\Delta M \equiv \frac{M_\infty}{U}(Q\bar{Z} + R\bar{Y}).$$

2.3.4 Wake Motions

In addition to the surface boundary condition, the aerodynamic problem involves boundary conditions which must be satisfied on the surface of the aircraft's wake. The kinematic description must therefore contain the location of wake surface. The wake, a surface which emanates from sharp trailing edges of lifting surfaces, may be idealized as a vortex sheet which, by definition, forms a boundary in the flow which fluid particles do not penetrate. The actual wake surface location is therefore not known a priori, because its location depends on the solution to the problem, viz., the motion of the fluid. If it is assumed, however, that the freestream is not disturbed by the presence of the aircraft or the wake itself, the wake location can be described a priori. This fictitious wake surface is termed the Mean Wake Surface, and in formulating the aerodynamic problem the Actual Wake Surface is considered to be deformed about the Mean Wake Surface. The effect of this deformation is negligible for the level of approximation used in the aerodynamic theory. The kinematic description therefore need only locate the Mean Wake Surface.

In section 3 the Mean Wake Surface is taken to be determined from the velocity of the aircraft at the instant of time under consideration. As a result, it is slightly displaced in the X-direction from the surface actually swept out by the path of the trailing edge of a lifting surface, such as a wing, undergoing unsteady motion (fig. 2.3-5). The paths for this and other lifting surfaces are determined by the known history of the aircraft's rigid-body and elastic deformation motions up to the instant of time under consideration, t_0 , when the Fluid and Body Axis Systems are taken to be coincident. For the Mean Wake Surface to be a vortex sheet in the undistributed freestream, it must be displaced from the surface of the trailing edge paths by a distance $\Delta X_0 = (\bar{U} - U) X_0 / U$, where X_0 is the point where the displacement is measured and \bar{U} is the average forward velocity (fig. 2.3-5). At distances X_0 where fluctuations in the wake surface are of significance in the aerodynamic theory, it will be shown that $\Delta X_0 / X_0$ and $\Delta X_0 / \bar{c}$ are small—small enough, in fact, that the effect of the displacement ΔX_0 is shown in the following section to be negligible. The aerodynamic theory presently used in the FLEXSTAB system therefore assumes that the Mean Wake Surface is coincident with the locus of trailing edge positions.

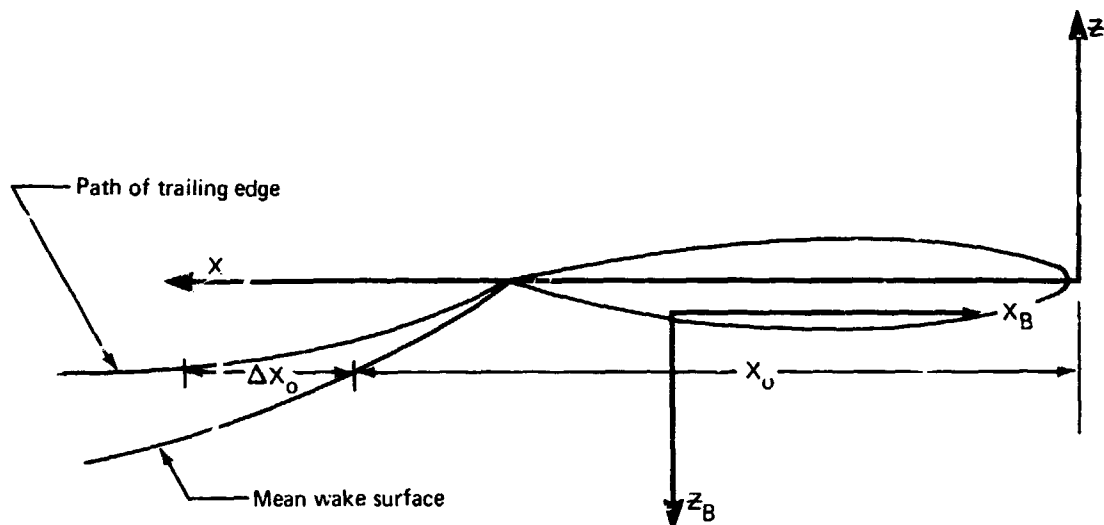


FIGURE 2.3-5.—MEAN WAKE SURFACE

3.0 AERODYNAMICS

3.1 INTRODUCTION

The aerodynamic theory used in formulating the FLEXSTAB system is a linear, first-order, small perturbation approximation to unsteady, inviscid subsonic or supersonic flow. The theory is valid provided the unsteadiness of the flow has reduced frequencies small in comparison to unity—the low frequency approximation of reference 3-1, chapter 4. The theory is applicable to arbitrary aircraft configurations which can be idealized as a collection of components classed either as thin bodies or as slender bodies*, figure 3.1-1.

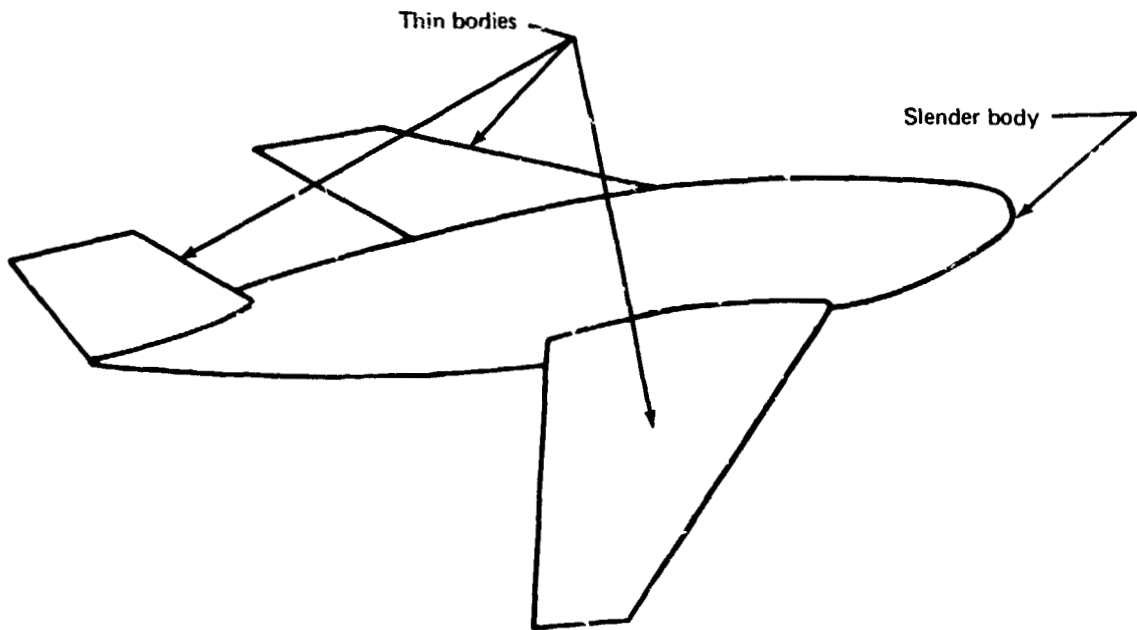


FIGURE 3.1-1.—TYPICAL THIN BODY-SLENDER BODY CONFIGURATION ARRANGEMENT

*Classification of configuration components as thin or slender bodies is based on the relative magnitudes of their thickness and aspect ratios. A thin body is essentially planar having an aspect ratio which is an order of magnitude greater than its thickness ratio. The aspect ratio of a slender body is approximately equal to its thickness ratio, and its actual shape is idealized as an equivalent body of revolution warped by a cambered centerline. Wings, struts, fins, etc., are termed "thin bodies." Fuselages, nacelles, pods, and tip tanks are termed "slender bodies."

The linear aerodynamic theory is derived from the nonlinear theory governing unsteady, continuous, unseparated, inviscid, adiabatic, and irrotational flow as summarized in section 3.2.2. The derivation follows from a sequence of two asymptotic expansions. The nonlinear theory is expanded in section 3.2.5 in terms of small parameters which govern the magnitudes of the disturbances produced in a uniform flow by the presence of the aircraft. In this expansion, the unsteadiness of all time-varying parameters may have reduced frequencies with orders of magnitude equal to unity. A second asymptotic expansion is carried out in section 3.2.6 wherein the small parameters are the reduced frequencies of the time-varying parameters appearing in the first expansion. This expansion leads to the low frequency unsteady aerodynamic theory.

All parameters governing the magnitudes of the flow disturbances are related to quantities contained in the surface boundary condition derived in section 2.3. As shown by equation (2.3-36), the quantities leading to flow disturbances (i.e., flow incidence at the aircraft's surface) arise from two sources - the geometric shape of the aircraft and the motion of the aircraft surface relative to the uniform freestream. Flow incidence due to relative motion of the surface is related to the motion parameters commonly used in stability and control technology, i.e., angle of attack, angle of sideslip, etc.

The geometric shapes of the thin and slender bodies are described analytically in terms of coordinates on "mean" surfaces and lines which are parallel to the freestream. The geometry of a configuration is therefore described entirely in terms of formulas of the following form:

$$\delta_N = \epsilon_N F_N(X, Y, Z)$$

where δ_N is the dimension of the N^{th} body in directions which are transverse to the freestream, $F_N(X, Y, Z)$ is a shape function which has an order of magnitude equal to unity for points (X, Y, Z) on a mean surface or line, and ϵ_N is a small nondimensional parameter. The entire geometric shape collapses to mean surfaces and lines which are aligned with the freestream when all of the parameters ϵ_N are set to zero.

Formulas describing the thickness, camber, and twist of thin lifting surfaces are expressed in terms of coordinates on planar mean surfaces, figure 3.1-2. Ideally, the mean surfaces have generators which lie at the area centroid of each of the airfoil cross sections of thin bodies, figure 3.1-2. The planar mean surfaces cannot be placed at the mathematical mean surface for thin bodies having a smoothly varying dihedral, and thin aerodynamic bodies with varying dihedral are approximated by a sequence of connecting planar mean surfaces.

Slender bodies are described about mean centerlines. The components of a configuration which are designated as slender bodies are idealized as bodies with circular cross sections, the areas of which are equal to the cross-sectional areas of the actual components. The centers of the circular cross sections are located at the area centroids of the actual sections, figure 3.1-3, and the mean centerline parallel to the freestream is at the mean location of the section area centroids. The deviation of the section area centroids from the mean centerline describes the body camber.

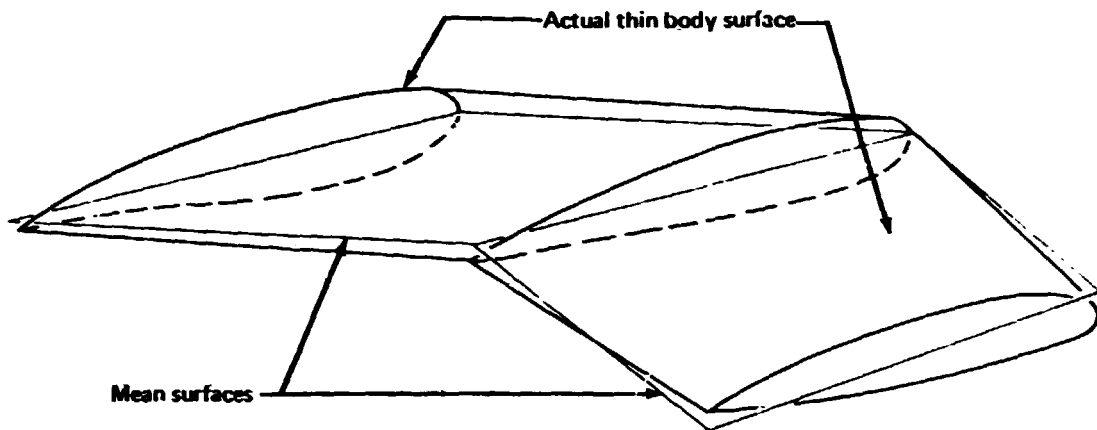


FIGURE 3.1-2.—THIN BODY MEAN SURFACE

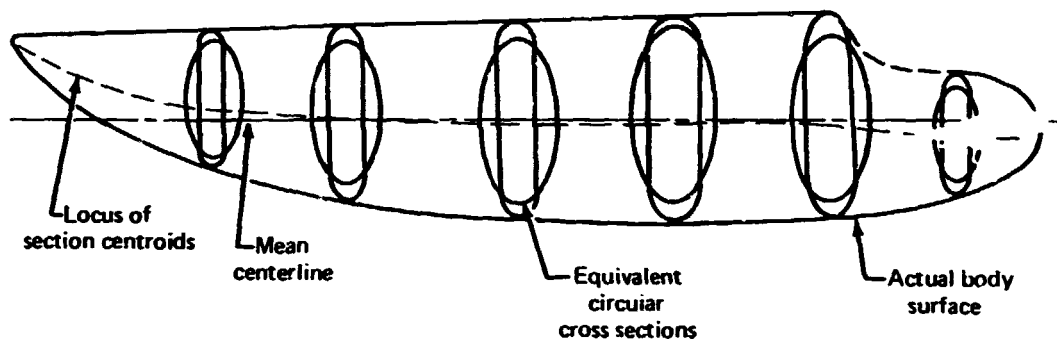


FIGURE 3.1-3.—SLENDER BODY MEAN CENTERLINE

The effects of interference flows between the thin and slender bodies making up a configuration are accounted for on mean interference surfaces. In the case of thin bodies, the mean interference surfaces are identical to the thin body mean surfaces shown by figure 3.1-2. In the case of a slender body, the mean interference surface is a cylindrical surface approximating the actual slender body surface in the region of dominant interference flow, figure 3.1-4.

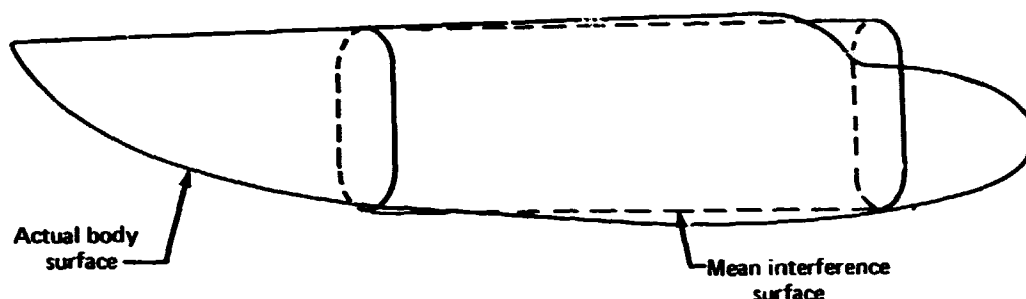


FIGURE 3.1-4.—MEAN INTERFERENCE SURFACE OF A SLENDER BODY

The mathematical problem posed by the linear theory developed in section 3.2 consists of a set of linear boundary value problems, i.e., a set of partial differential equations (viz., the classical small disturbance flow equation) and boundary conditions specified at the mean surfaces and lines. In section 3.3, solutions to the boundary value problems are expressed in terms of integral equations. The flow incidence at the mean surfaces is given by integrals of kernel functions which represent flow singularities (i.e., sources, doublets, and vorticity) distributed on the mean surfaces and mean lines. A solution is constructed by finding the strengths of the flow singularities which produce the flow incidence satisfying the surface boundary conditions. Once this solution is constructed, the aerodynamic surface pressure is computed. This calculation leads to equations relating the surface pressure to the quantities which appear in the surface boundary conditions and which give rise to surface flow incidence, e.g., angle of attack. These final expressions form the basis for computing the stability derivatives required for the FLEXSTAB system analysis.

The FLEXSTAB system determines the strengths of the flow singularity distributions using approximations similar to those of reference 1-1. As shown by figure 3.1-5, the mean surfaces of thin bodies and the mean interference surfaces of slender bodies are subdivided into small quadrilateral panels, while the mean centerlines of slender bodies are subdivided into line segments. Simple distributions of the flow singularities are assumed for the surface panels and centerline segments. The strengths of these simple distributions are governed by unspecified parameters, S_i . The flow singularity, e.g., an element of vorticity (ref. 2-3, eq. 5-34), at the point X_1, Y_1, Z_1 on the panel induces a flow incidence at the point X, Y, Z which can be expressed as follows:

$$\psi^V(X, Y, Z) = -\vec{n} \cdot \vec{\nabla} K^V(X, Y, Z; X_1, Y_1, Z_1) \quad (3.1-1)$$

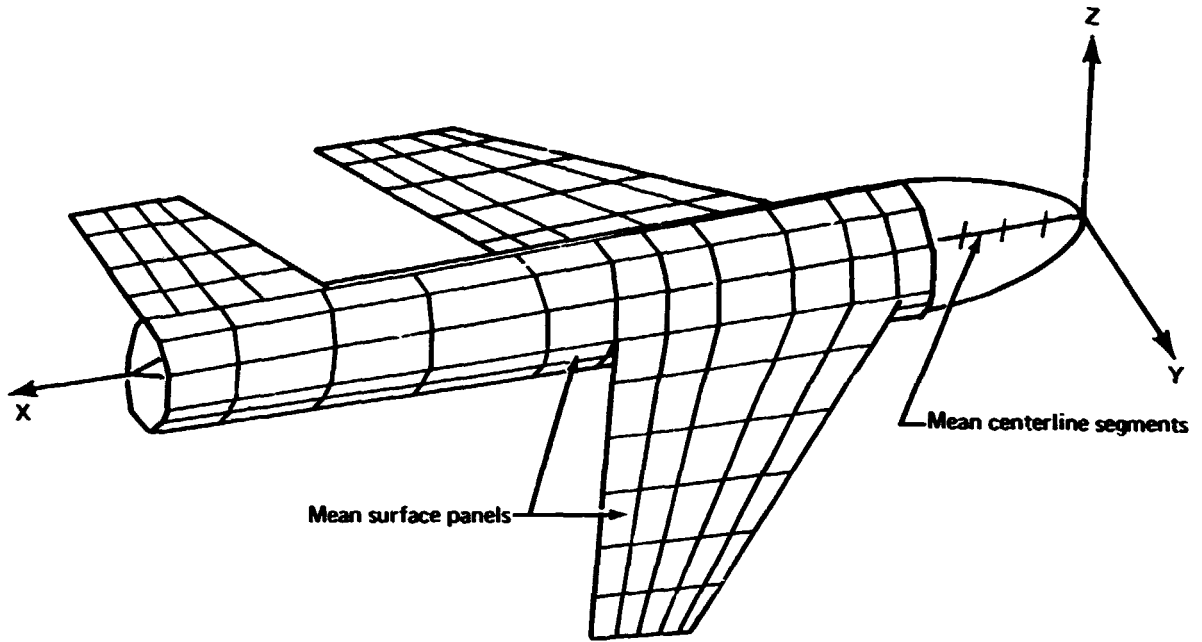


FIGURE 3.1-5.—TYPICAL AERODYNAMIC PANELING SCHEME

Integrating this expression over the i^{th} panel with vorticity distribution strength S_i^V leads to the result

$$\Psi_i^V(X, Y, Z) = a_i^V(X, Y, Z) S_i^V \quad (3.1-2)$$

where

$$a_i^V(X, Y, Z) \equiv - \iint_{S_i} \vec{n} \cdot \vec{\nabla} K^V(X, Y, Z; X_i, Y_i, Z_i) dA$$

and S_i is the surface area of the panel. The aerodynamic influence, a_i^V , at the point X, Y, Z is the flow incidence there due to the vorticity on the i^{th} surface panel.

The flow singularity distributions used in the FLEXSTAB system are summarized in table 3.1-1. Control points, equal in number to the number of unspecified parameters, S_i , are chosen at the surfaces where the boundary conditions are specified. The flow incidence $\Psi_j(X, Y, Z)$ due to each of the panel and line segment flow singularity distributions is evaluated at the control points, thereby generating determinant sets of algebraic equations of the form

$$\Psi_j = \sum_{i=1}^r a_{ji} S_i \quad (3.1-3)$$

TABLE 3.1-1. - FLOW SINGULARITY DISTRIBUTIONS

Region of distribution	Flow singularity	Steady flow X-variations of distribution	
		Subsonic	Supersonic
Thin body mean surfaces	Vorticity	Constant	Constant
	Sources	Linear	Linear
Slender body mean surfaces	Vorticity	Constant	Constant
Slender body centerlines	Doublets	Quadratic	Quadratic
	Sources	Constant	Linear

These equations are expressed in terms of matrices:

$$\{\Psi_j\} = [a_{ji}] \{S_i\} \quad (3.1-4)$$

where $[a_{ji}]$ is an aerodynamic matrix describing the flow incidences induced at control points due to unit strengths of flow singularity distributions.

The aerodynamic matrix is inverted to obtain the following expression:

$$\{S_i\} = [a_{ji}]^{-1} \{\Psi_j\} \quad (3.1-5)$$

where the singularity strengths are now determined from the flow incidence at the control points. Expressions relating the aerodynamic pressure coefficient at the surface to the singularity strengths are derived and appear as matrix equations of the following form:

$$\{C_{P_k}\} = [CPM_{ki}] \{S_i\}. \quad (3.1-6)$$

Combining these expressions with the matrix equations above leads to aerodynamic influence coefficient equations, i.e.,

$$\{C_{P_k}\} = [A_{kj}] \{\Psi_j\} \quad (3.1-7)$$

where the aerodynamic influence coefficient matrix is given by

$$[A_{kj}] = [CPM_{ki}] [a_{ji}]^{-1}. \quad (3.1-8)$$

These expressions represent a solution to the aerodynamic problem solved in the FLEX-STAB system.

The complete method of solution to the aerodynamic problem is derived in section 3.4. The problem is solved in steps following the approach outlined above. Sections 3.4.2 and 3.4.4 contain derivations of the aerodynamic pressures induced by the thickness shapes of slender bodies and thin bodies but with the thickness shapes treated as isolated bodies ignoring the effects of mutual interference. The steady lifting pressure for isolated slender and thin bodies are derived in sections 3.4.3 and 3.4.5, and the solution to the steady aerodynamic induction problem is derived in detail in section 3.4.6. The effects of steady interference from thickness and lift are computed using the solution to the steady aerodynamic induction problem. This computation leads to the solution to the combined steady aerodynamic problem in section 3.4.7, viz., the steady aerodynamic pressures due to thickness and the steady aerodynamic lifting pressures due to camber and steady motions of the aircraft surfaces relative to the freestream.

The method for solving the low frequency unsteady aerodynamic problem is derived in sections 3.4.8 through 3.4.11. The thickness shape of an aircraft is assumed to be steady, and the unsteady aerodynamics are related only to the lifting problem. The combined unsteady aerodynamic problem is treated in section 3.4.11, and the derivation leads to the following expression:

$$\{C_{P_k}\} = [A_{kj}]\{\psi_j\} + [\delta A_{kj}]\{\dot{\psi}_j\} \quad (3.1-9)$$

where the matrix $[\delta A_{kj}]$ is an unsteady aerodynamic influence coefficient matrix relating the time rates of change of flow incidence at control points $\{\dot{\psi}_j\}$ to the aerodynamic pressure coefficients at the vortex panel area centroids. These influence coefficients are independent of frequency (a unique and important characteristic of the low frequency approximation*); they contain the effects of time-varying vorticity in the aircraft's wake and the effects of finite speeds of propagation of flow disturbances—both to a first-order approximation. The frequency dependence appears only because the flow incidence appears as a first-order derivative with respect to time; for harmonic, unsteady motion, the complex pressure is given by

$$\{C_{P_k}^*\} = [A_{kj}^*]\{\psi_j^*\} \quad (3.1-10)$$

where * denotes a complex quantity and

$$[A_{kj}^*] = [A_{kj}] + ik[\delta A_{kj}] \quad (3.1-11)$$

is a complex aerodynamic influence coefficient matrix. This matrix is seen to be a linear function of reduced frequency as a consequence of the harmonic variation of flow incidence.

$$\{\psi_j\} = \{\psi_j^*\} e^{i\omega t}. \quad (3.1-12)$$

The low frequency approximation is valid for arbitrary, slowly varying flow incidence; the complex relations are introduced here only to demonstrate the relationship of the low

*See section 6.1.

frequency unsteady aerodynamic influence coefficients to the complex aerodynamic influence coefficients encountered in solving finite frequency unsteady aerodynamic problems.

Section 3.4.12 derives a leading edge correction which is necessary for the method of solution used in the FLEXSTAB system to yield theoretically correct leading edge suction on thin lifting bodies. Section 3 is completed by sections 3.4.14, 3.4.15, and 3.5 wherein empirical data are introduced and the aerodynamic forces acting on an aircraft are derived from the aerodynamic surface pressure distributions.

3.2 DERIVATION OF THE LINEAR AERODYNAMIC THEORY

3.2.1 Nonlinear Aerodynamic Theory

The complete nonlinear aerodynamic theory consists of a flow equation in terms of an unknown velocity potential, boundary conditions, and a relation governing the pressure coefficient in terms of the unknown velocity potential.

3.2.1.1 Flow equation.—The flow equation is given by equation (1-74) of reference 2-3 as

$$a^2 \nabla^2 \Phi = \frac{\partial}{\partial t} \left[\frac{\partial}{\partial t} (\Phi - \Phi_\infty) + \frac{1}{2} (\vec{\nabla} \Phi)^2 - \frac{1}{2} (\vec{\nabla} \Phi_\infty)^2 \right] + \frac{1}{2} \vec{\nabla} \Phi \cdot \vec{\nabla} (\vec{\nabla} \Phi)^2 - \vec{\nabla} (\Phi - \Phi_\infty) \cdot \frac{\partial}{\partial t} (\vec{\nabla} \Phi_\infty) \quad (3.2-1)$$

where a is the local speed of sound, viz.,

$$a^2 = a_\infty^2 - (\gamma - 1) \left[\frac{\partial}{\partial t} (\Phi - \Phi_\infty) + \frac{1}{2} (\vec{\nabla} \Phi)^2 - \frac{1}{2} (\vec{\nabla} \Phi_\infty)^2 \right], \quad (3.2-2)$$

and Φ is the unsteady velocity potential from which the flow velocity is computed as

$$\vec{Q} = \vec{\nabla} \Phi. \quad (3.2-3)$$

In the analysis to follow the velocity potential Φ is expressed as the sum of a freestream component and a perturbation component. Letting the freestream component be given by

$$\Phi_\infty \equiv Ux, \quad (3.2-4)$$

the perturbed velocity potential is expressed as

$$\Phi = U(x + \phi) \quad (3.2-5)$$

where ϕ is a perturbation velocity potential normalized with respect to the freestream velocity.

3.2.1.2 Surface boundary condition.—The surface boundary condition has previously been developed as equation (2.3-33) and, in terms of the perturbation velocity potential, is expressed as follows:

$$\frac{\partial \phi}{\partial n} = -n_X + \frac{1}{U}(\vec{V}_R + \vec{\omega} \times \vec{r} + \frac{\delta \vec{d}}{\delta t}) \cdot \vec{n} \quad \text{on } G(X, Y, Z, t) = 0. \quad (3.2-6)$$

3.2.1.3 Wake boundary condition.—The wake boundary condition requires that the pressure be continuous across the wake surface, i.e.,

$$[C_p] = 0 \quad \text{on wake surface.} \quad (3.2-7)$$

3.2.1.4 Far-field boundary condition.—The far-field boundary condition requires that perturbations to the freestream propagate outward away from the aircraft surface and that the disturbances either vanish or remain finite at indefinitely large distances from the surface.

3.2.1.5 Pressure relation.—The pressure coefficient,

$$C_p \equiv \frac{p - p_\infty}{q_\infty}, \quad (3.2-8)$$

is given in terms of the velocity potential by equation (1-64) of reference 2-3 as

$$C_p = \frac{2}{\gamma M^2} \left\{ \left[1 - \frac{\gamma-1}{a_\infty^2} \left(\frac{\partial}{\partial t} (\phi - \phi_\infty) + \frac{1}{2} (\vec{V}_\phi)^2 - \frac{1}{2} (\vec{V}_{\phi_\infty})^2 \right) \right]^{\gamma/\gamma-1-1} \right\}. \quad (3.2-9)$$

3.2.1.6 Statement of the aerodynamic problem.—Having the aerodynamic theory expressed as above, the aerodynamic problem may be stated as follows. Given the aerodynamic shape ($G(X, Y, Z, t) = 0$), the surface velocity (U , \vec{V}_R , $\vec{\omega}$ and $\delta \vec{d}/\delta t$), and the wake location contained in the boundary conditions, find the perturbation velocity potential $\phi(X, Y, Z, t)$ satisfying the boundary conditions and the flow equation. The perturbation velocity potential so determined represents a solution to the problem. The aerodynamic surface pressure is computed by substituting the velocity potential into the pressure relation and evaluating the resulting expression at the aerodynamic surface, $G(X, Y, Z, t) = 0$.

3.2.1.7 Aerodynamic coordinate systems.—The aerodynamic theory is developed using only two of the fundamental axis systems defined in section 2.2, viz., the Fluid Axis System and the Reference Axis System, and using local axis systems related to the Reference Axis System by time-independent orthogonal transformations.

3.2.1.8 Special notation related to spatial coordinates. -- The solution to the boundary value problem posed by the aerodynamic theory, i.e., the velocity potential, equation (3.2-5), is derived in the following for the instant of time $t = t_0$. This is the instant of time introduced in section 2.2.2 when the Fluid and Reference Axis Systems are coincident as shown by figure 2.2-2. At this instant of time the spatial coordinates of a point in the Fluid Axis System are identical to the spatial coordinates of the same point in the Reference Axis System. In expressing the velocity potential in the following, the variables x, y, z , therefore, are freely interchanged with the variables X, Y, Z . Also, partial differentiation with respect to the variables x, y, z is freely replaced by partial differentiation with respect to the variables X, Y, Z because time is held fixed in these operations and the equations are entirely in terms of Eulerian, i.e., spatial, coordinates.

To denote spatial variables of integration, several notational devices are used. Spatial variables of integration are sometimes denoted by ξ, η, ζ . At other times a prime in the superscript position or a subscripted one is used to indicate that a spatial variable is a variable of integration. Thus, the notation X', Y', Z' in section 3 denotes Reference Axis System coordinates used as variables of integration. This notation should not be interpreted as indicating coordinates in the Inertial Axis System, which never appears in section 3.

3.2.2 Asymptotic Expansion Method

The linear aerodynamic theory is derived by identifying in the surface boundary condition, equation (3.2-6), small parameters governing the magnitude of the local flow incidence, and by seeking an asymptotic solution to the nonlinear problem valid in the limit as the small parameters approach zero, chapter 3 of reference 2-3. The perturbation velocity potential is expanded in an asymptotic series involving powers of the small parameters. This expansion is substituted into the nonlinear flow equation and boundary conditions of section 3.2.1. Equating terms equal in order of magnitude among the small parameters leads to a sequence of simplified, linear boundary value problems. These problems individually govern the flow associated with each of the small parameters.

3.2.2.1 The asymptotic series. -- The asymptotic series is chosen as

$$\phi = \epsilon_1 \phi_1 + \dots + \epsilon_i \phi_i + \dots + \epsilon_i \epsilon_j \phi_{ij} + \dots, \quad (3.2-10)$$

where ϵ_i denotes any of the small parameters. The first-order potentials are found to be governed by linear partial differential equations of the following form:

$$\beta^2 (\phi_i)_{xx} + (\phi_i)_{yy} + (\phi_i)_{zz} - \frac{2M^2}{U} (\phi_i)_{xt} - \frac{M^2}{U^2} (\phi_i)_{tt} = 0$$

and they are required to satisfy linear boundary conditions imposed at mean locations of the aircraft's surface and its wake.

3.2.2.2 Low frequency approximation. -- A second asymptotic series is chosen assuming that the unsteadiness of the boundary conditions related to the unsteady potentials is slowly varying. The asymptotic expansion is taken to be a complex power series in terms of the frequency of the unsteady surface motion, i.e.,

$$\phi_i e^{i\omega_i t} = [\phi_i^{(0)} + i\bar{\omega}_i \phi_i^{(1)} + \dots] e^{i\omega_i t}$$

where the quantity ω_i is the circular frequency of the i^{th} perturbation potential appearing in the first asymptotic series, equation (3.2-10). The reduced frequency defined in terms of a unit reference length,

$$\bar{\omega}_i \equiv \omega_i / U,$$

is the small parameter in the second asymptotic series, and an asymptotic solution valid in the limit as $\bar{\omega}_i$ approaches zero is sought for the unsteady flow problems. The zeroth and first-order potentials contained in this series are found to be governed by steady flow equations and boundary conditions. The flow equations and wake boundary conditions governing the first-order potentials, however, are found to be inhomogeneous and require the first-order potentials to be related to the surface boundary conditions in a somewhat complicated manner; nevertheless, the first-order potentials are shown to be functions of solutions to steady flow type problems in the general manner shown by section 4.5 of reference 3-1.

3.2.3 Wing-Body Problem

The linear aerodynamic theory used in the FLEXSTAB system is derived from an analysis of a simple configuration consisting of the wing-body combination shown by figure 3.2-1. Although the FLEXSTAB system is applicable to a configuration consisting of an

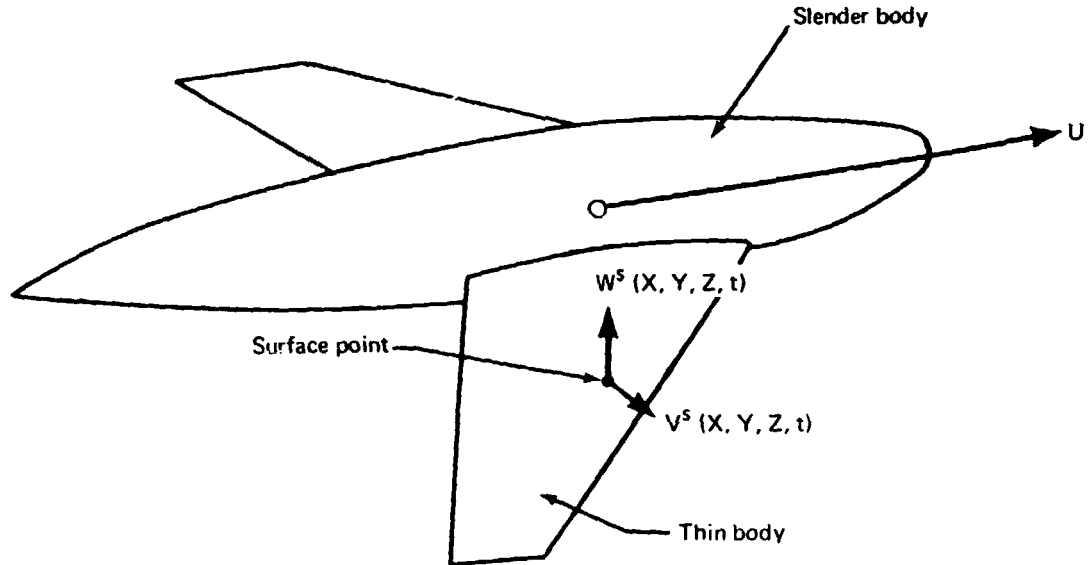


FIGURE 3.2-1.—WING-BODY PROBLEM

arbitrarily arranged assembly of wings, bodies, nacelles, and tails, the aerodynamic theory is readily developed around a simple wing-body combination using the surface boundary condition in the compact form developed in section 2.3.3.3, viz.,

$$\frac{\partial \phi}{\partial n}(X, Y, Z, t) = -n_x(X, Y, Z, t) + \hat{v}\lambda_v(t)\bar{V}(X, Y, Z)n_y + \hat{w}\lambda_w(t)\bar{W}(X, Y, Z)n_z \quad \text{on} \quad G(X, Y, Z, t) = 0. \quad (2.3-73)$$

The aerodynamic problem posed by the wing-body combination with the surface boundary condition given by equation (2.3-73) is referred to hereafter as the Wing-Body Problem.

The geometry of the Wing-Body Problem is described analytically relative to mean locations of the wing and body as shown by figure 3.2-2. The wing, classified as a thin body, is described relative to a planar mean surface, while the body, classified as a slender body, is described relative to a mean centerline and a mean cylindrical surface.

The aerodynamic theory developed around the geometry of the Wing-Body Problem is readily extended by the principle of superposition to the arbitrary configurations dealt with by the FLEXSTAB system. As noted in section 3.2.2, the linear theory is derived by identifying in the surface boundary condition, equation (2.3-73), small parameters governing the magnitude of the local flow incidence at the surface. These parameters are related, in part, to the surface geometry. Again, as noted in the introduction to the aerodynamic theory, section 3.1, the geometry of an arbitrary configuration in the FLEXSTAB system is represented as an assembly of thin and slender bodies, each of which is contained in the Wing-Body Problem. The surface boundary condition of the Wing-Body Problem therefore contains all parameters contained in multiple thin body-slender body

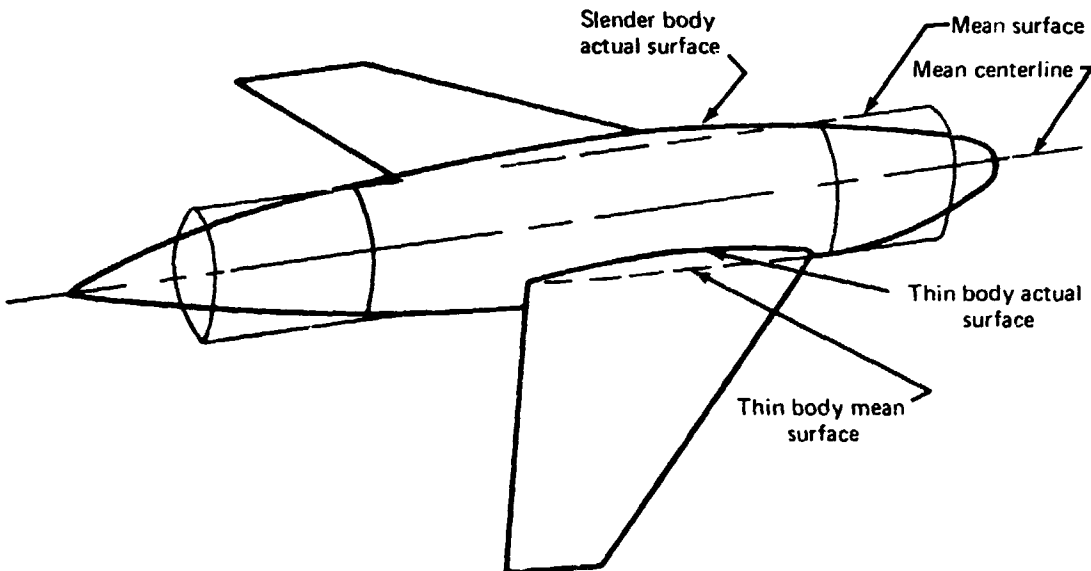


FIGURE 3.2-2.—WING-BODY COMPONENT ARRANGEMENT

configurations. Since the theory being derived is linear, additional potentials $\epsilon_i \phi_i$ associated with additional configuration components may be added to the theory by the principle of superposition. The equations governing the additional potentials will be identical in form to equations contained in the Wing-Body Problem.

3.2.4 Analytical Geometry of Wing-Body Problem

3.2.4.1 Aerodynamic local axis systems.—The geometries of thin and slender bodies are described analytically in terms of local axis systems X_N, Y_N, Z_N —one for each body—with the subscript N indicating that the local axis system is used in the geometric description of the N^{th} body. The origin of the N^{th} local axis system is located by the coordinates $X_N(O), Y_N(O), Z_N(O)$ in the Reference Axis System. The X_N axis is always parallel to the X axis of the Reference Axis System, while the Y_N and Z_N axes are oriented with respect to the Reference Axis System by a positive rotation θ_N about the X_N axis, figure 3.2-3. The transformation from the Reference Axis System to the local axis system of the N^{th} body therefore is given by

$$\begin{aligned} X_N &= X - X_N(O) \\ Y_N &= (Y - Y_N(O)) \cos \theta_N + (Z - Z_N(O)) \sin \theta_N \\ Z_N &= (Y - Y_N(O)) \sin \theta_N + (Z - Z_N(O)) \cos \theta_N. \end{aligned} \quad (3.2-11)$$

3.2.4.2 Analytical geometry of thin bodies.—The geometry of a thin body is described in terms of a local axis system (X_N, Y_N, Z_N) whose $X_N Y_N$ plane coincides with the mean surface of the thin body, figure 3.2-4. The surface of the body is expressed as

$$G(X_N, Y_N, Z_N, t) = Z_N(t) + \tau F(X_N, Y_N) - \theta(t) H(X_N, Y_N) = 0. \quad (3.2-12)$$

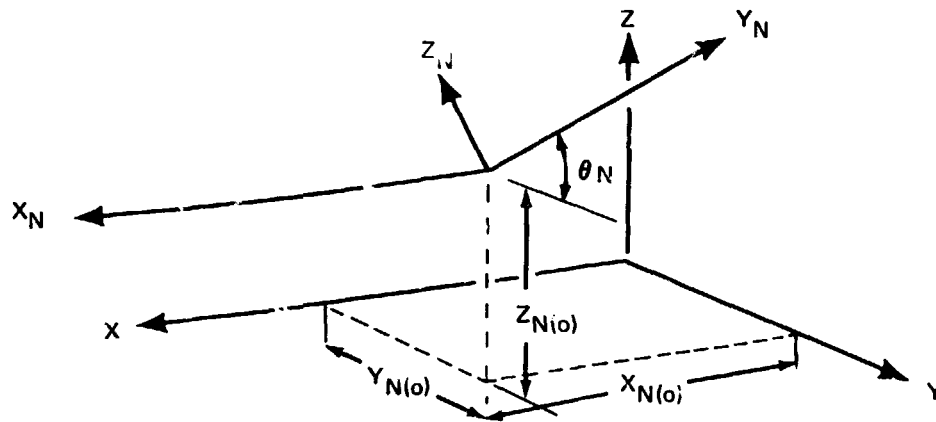


FIGURE 3.2-3.—AERODYNAMIC LOCAL AXIS SYSTEM

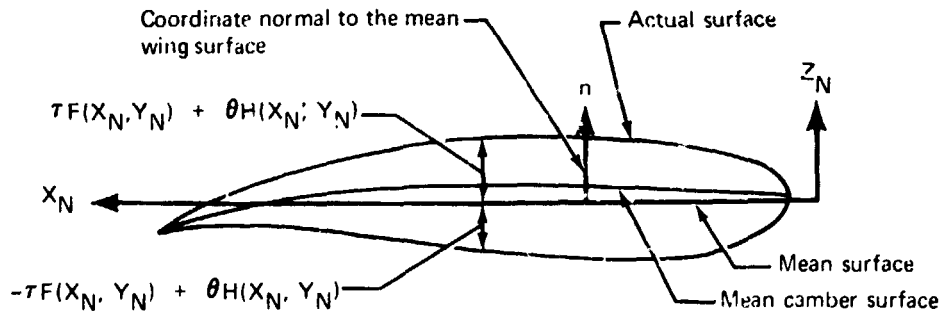


FIGURE 3.2-4.—THIN BODY SECTION GEOMETRY

where $F(X_N, Y_N)$ is an antisymmetric function describing the thickness shape and $H(X_N, Y_N)$ is a symmetric function describing the camber shape including elastic deformation and control surface deflection.

The orders of magnitude assumed for quantities appearing in equation (3.2-12) are as follows:

$$\begin{aligned} F(Y_N, Y_N) &= O(1), \frac{\partial F}{\partial X_N} = O(1), \frac{\partial F}{\partial Y_N} \ll \bar{c} \\ H(X_N, Y_N) &= O(1), \frac{\partial H}{\partial X_N} = O(1), \frac{\partial H}{\partial Y_N} \ll \bar{c} \\ \tau &\ll \bar{c}, \theta \ll \bar{c} \end{aligned} \quad (3.2-13)$$

where \bar{c} is the reference length, e.g., the mean wing chord. The unit vector normal to the surface is found by applying the formula given by equation (2.3-32):

$$\begin{aligned} \vec{n} = & \left\{ -\left[\frac{\partial}{\partial X_N} (\tau F + \theta H) \right] \vec{i} - \left[\frac{\partial}{\partial Y_N} (\tau F + \theta H) \cos \theta_N + \sin \theta_N \right] \vec{j} \right. \\ & \left. - \left[\frac{\partial}{\partial Y_N} (\tau F + \theta H) \sin \theta_N - \cos \theta_N \right] \vec{k} \right\} \quad (3.2-14) \\ & \times \left\{ 1 - \frac{1}{2} \left[\frac{\partial}{\partial X_N} (\tau F + \theta H) \right]^2 - \frac{1}{2} \left[\frac{\partial}{\partial Y_N} (\tau F + \theta H) \right]^2 + \dots \right\} \end{aligned}$$

where the upper (lower) sign implies evaluation at the upper (lower) surface.

3.2.4.3 Analytical geometry of slender bodies.—The geometry of a slender body is described in terms of a local axis system (X_M, Y_M, Z_M) whose X_M axis coincides with the mean centerline of the body, figure 3.2-5. The cross section of the actual body shape is replaced by one which is circular, with the center of the circular section displaced from the mean centerline by the camber shapes:

$$Y_M = b(t)G(X_M)$$

and (3.2-15)

$$Z_M = c(t)I(X_M)$$

where

$$G(X_M) = O(1), I(X_M) = O(1)$$

and (3.2-16)

$$b(t) \ll \bar{c}, c(t) \ll \bar{c}.$$

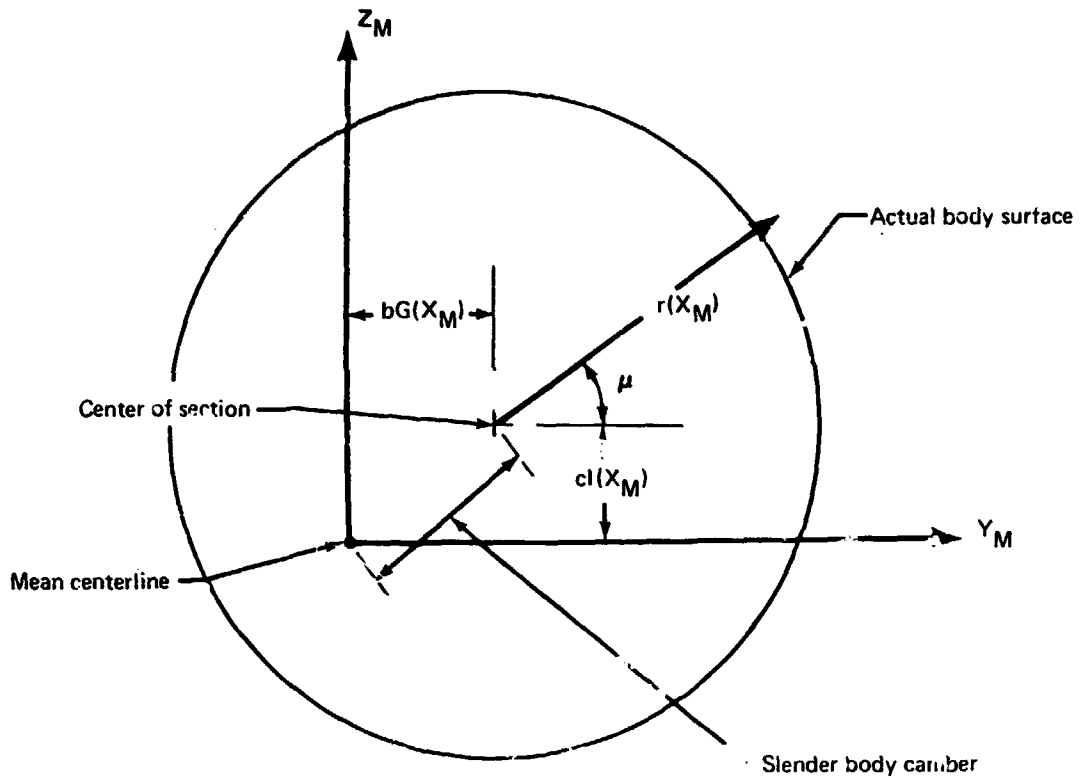


FIGURE 3.2-5.—SLENDER BODY CROSS-SECTION GEOMETRY

For the theoretical development of this section, the slender body is infinitely long with cross section

$$r(X_M) = P + aR(X_M) \quad (3.2-17)$$

where P is a constant,

$$R(X_M) = O(1) \quad (3.2-18)$$

and

$$a \ll \bar{c}.$$

The effects of slender body truncation in the form of a pointed nose and tail are added in a manner similar to that described by reference 1-1, wherein the effects of slender body truncation are patched into the results of the present analysis.

The surface of the slender body is expressed as

$$G(X_M, Y_M, Z_M, t) = -P - aR(X_M) + \left\{ [Y_M - b(t)G(X_M)]^2 + [Z_M - c(t)I(X_M)]^2 \right\}^{\frac{1}{2}} = 0 \quad (3.2-19)$$

and the unit vector normal to the surface is found as

$$\vec{n} = \left\{ -\left[a \frac{dR}{dX_M} + b \frac{\partial G}{\partial X_M} \cos \mu + c \frac{\partial I}{\partial X_M} \sin \mu \right] \vec{i} + \cos \mu \vec{j} + \sin \mu \vec{k} \right\} \quad (3.2-20)$$

$$\times \left\{ 1 - \frac{1}{2} \left[a \frac{dR}{dX_M} + b \frac{\partial G}{\partial X_M} \cos \mu + c \frac{\partial I}{\partial X_M} \sin \mu \right]^2 + \dots \right\}.$$

3.2.5 Asymptotic Expansion of the Wing-Body Problem

When the geometric parameters a , b , c , θ and τ are allowed to vanish, the configuration has the limiting shape shown by figure 3.2-6, i.e., it reduces to mean surfaces which are

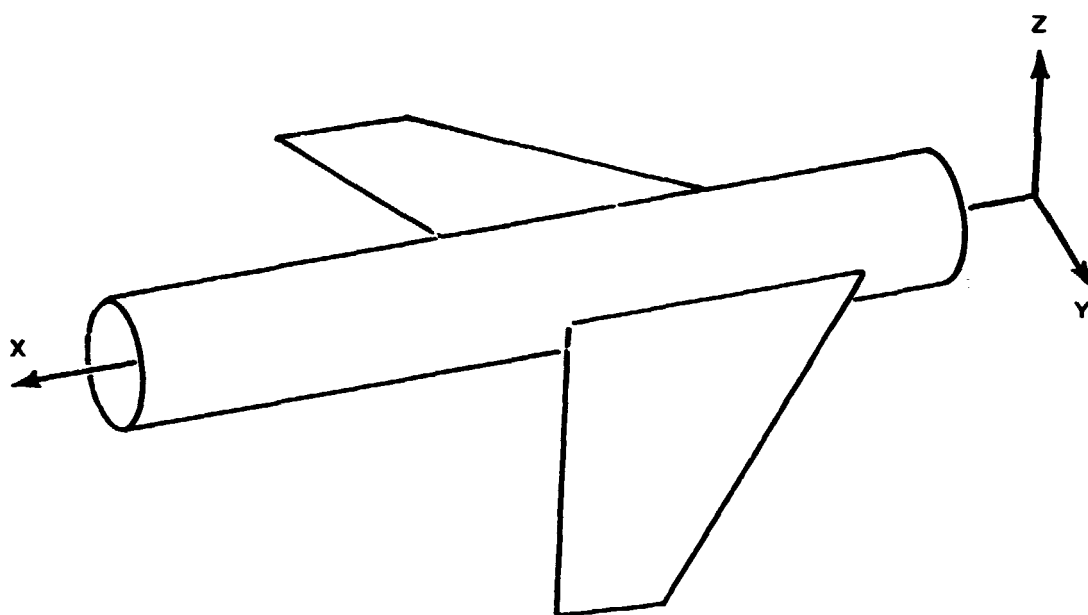


FIGURE 3.2-6—LIMITING FORM OF CONFIGURATION

uncambered and aligned with the X-axis. Letting the time-dependent geometric parameters be expressed as

$$b(t) = \hat{b} \lambda_b(t),$$

$$c(t) = \hat{c} \lambda_c(t),$$

and

$$\theta(t) = \hat{\theta} \lambda_\theta(t). \quad (3.2-21)$$

where $\lambda_b(t)$, $\lambda_c(t)$ and $\lambda_\theta(t)$ and their derivatives have the order of magnitude unity, the parameters which give rise to disturbances to the freestream are as follows:

$$\hat{w}, \hat{v}, \tau, \hat{\theta}, \hat{a}, \hat{c}, \hat{b} \quad (3.2-22)$$

When these parameters are all set to zero, the configuration reduces to the limiting configuration, and flow incidence at the surface vanishes everywhere.

3.2.5.1 Asymptotic series.—The velocity potential, equation (3.2-5), is a parametric function of the perturbation parameters listed by equation (3.2-22), and its asymptotic expansion is chosen to be the following:

$$\phi = U [\hat{w}\phi_1 + \hat{v}\phi_2 + \hat{\tau}\phi_3 + \hat{\theta}\phi_4 + a\phi_5 + b\phi_6 + c\phi_7 + (\text{second and higher order terms})]. \quad (3.2-23)$$

This expression is substituted into the flow equation and the boundary conditions.

3.2.5.2 Expansion of the flow equation.—Substituting the velocity potential given by equation (3.2-23) into the exact flow equation, equations (3.2-1) and (3.2-2), and collecting like-ordered terms in powers of the small parameters, leads to the following:

$$\begin{aligned} & \hat{w} [\beta^2 \phi_{1xx} + \phi_{1yy} + \phi_{1zz} - \frac{2M^2}{U} \phi_{1xt} - \frac{M^2}{U^2} \phi_{1tt}] + \\ & + \hat{v} [\beta^2 \phi_{2xx} + \phi_{2yy} + \phi_{2zz} - \frac{2M^2}{U} \phi_{2xt} - \frac{M^2}{U^2} \phi_{2tt}] + \\ & + \hat{\tau} [\beta^2 \phi_{3xx} + \phi_{3yy} + \phi_{3zz}] + \\ & + \hat{\theta} [\beta^2 \phi_{4xx} + \phi_{4yy} + \phi_{4zz} - \frac{2M^2}{U} \phi_{4xt} - \frac{M^2}{U^2} \phi_{4tt}] + \\ & + a [\beta^2 \phi_{5xx} + \phi_{5yy} + \phi_{5zz}] + \\ & + b [\beta^2 \phi_{6xx} + \phi_{6yy} + \phi_{6zz} - \frac{2M^2}{U} \phi_{6xt} - \frac{M^2}{U^2} \phi_{6tt}] + \\ & + c [\beta^2 \phi_{7xx} + \phi_{7yy} + \phi_{7zz} - \frac{2M^2}{U} \phi_{7xt} - \frac{M^2}{U^2} \phi_{7tt}] + \\ & + (\text{terms of second and higher order}) = 0. \end{aligned} \quad (3.2-24)$$

By definition, the small parameters of the problem are independent of one another (e.g., the magnitude of \hat{w} is not related to the magnitudes of the other parameters). Each of the terms in brackets of equation (3.2-24) therefore must vanish separately. Thus, for the exact nonlinear flow equation (3.2-1) to be satisfied by the velocity potential, equation

(3.2-23), the disturbance potentials ϕ_1 through ϕ_7 must satisfy at least the following linear, partial differential equations:

$$\begin{aligned}
 \hat{w}: \quad & \beta^2 \phi_{1xx} + \phi_{1yy} + \phi_{1zz} - \frac{2M^2}{U} \phi_{1xt} - \frac{M^2}{U^2} \phi_{1tt} = 0 \\
 \hat{v}: \quad & \beta^2 \phi_{2xx} + \phi_{2yy} + \phi_{2zz} - \frac{2M^2}{U} \phi_{2xt} - \frac{M^2}{U^2} \phi_{2tt} = 0 \\
 \tau: \quad & \beta^2 \phi_{3xx} + \phi_{3yy} + \phi_{3zz} = 0 \\
 \hat{\theta}: \quad & \beta^2 \phi_{4xx} + \phi_{4yy} + \phi_{4zz} - \frac{2M^2}{U} \phi_{4xt} - \frac{M^2}{U^2} \phi_{4tt} = 0 \\
 a: \quad & \beta^2 \phi_{5xx} + \phi_{5yy} + \phi_{5zz} = 0 \\
 \hat{b}: \quad & \beta^2 \phi_{6xx} + \phi_{6yy} + \phi_{6zz} - \frac{2M^2}{U} \phi_{6xt} - \frac{M^2}{U^2} \phi_{6tt} = 0 \\
 \hat{c}: \quad & \beta^2 \phi_{7xx} + \phi_{7yy} + \phi_{7zz} - \frac{2M^2}{U} \phi_{7xt} - \frac{M^2}{U^2} \phi_{7tt} = 0
 \end{aligned} \tag{3.2-25}$$

There are, of course, additional partial differential equations contained in the higher ordered terms of equation (3.2-24). These equations are ignored in the present analysis and are, in general, not satisfied by the solution to the aerodynamic problem contained in the FLEXSTAB system; only the first-order flow equations, equations (3.2-25), are considered. The FLEXSTAB system is therefore based on a first-order approximation which is linear as a consequence of the linearity of equations (3.2-25).

3.2.5.3 Expansion of the thin body surface boundary condition.—To express the surface boundary condition in terms of small parameters for the thin body (viz., \hat{w} , \hat{v} , τ , and $\hat{\theta}$) the expanded potential, equation (3.2-23), is substituted into equation (2.3-70) and evaluated at the wing surface. Noting that for spatial differentiation the variables, X, Y, Z and x, y, z , are interchangeable, these operations lead to the following form for the boundary condition:

$$\begin{aligned}
& (-\tau \frac{\partial F}{\partial X_N} \hat{\theta} \lambda_\theta \frac{\partial H}{\partial X_N}) (1 + \hat{w}\phi_{1x} + \hat{v}\phi_{2x} + \tau\phi_{3x} + \hat{\theta}\phi_{4x} + a\phi_{5x} \\
& + \hat{b}\phi_{6x} + \hat{c}\phi_{7x} + \dots) + (\bar{\tau} \sin \theta_N - \tau \frac{\partial F}{\partial Y_N} \cos \theta_N \\
& - \bar{\theta} \tau \frac{\partial H}{\partial Y_N} \cos \theta_N) [-\hat{w}\lambda_v(t) \bar{V} + \hat{w}\phi_{1y} + \hat{v}\phi_{2y} + \tau\phi_{3y} \\
& + \hat{\theta}\phi_{4y} + a\phi_{5y} + \hat{b}\phi_{6y} + \hat{c}\phi_{7y} + \dots] \\
& + (\bar{\tau} \cos \theta_N - \tau \frac{\partial F}{\partial X_N} \sin \theta_N - \bar{\theta} \lambda_\theta \frac{\partial H}{\partial Y_N} \sin \theta_N) \\
& \times [-\hat{w}\lambda_w(t) \bar{W} + \hat{w}\phi_{1z} + \hat{v}\phi_{2z} + \tau\phi_{3z} + \hat{\theta}\phi_{4z} \\
& + a\phi_{5z} + \hat{b}\phi_{6z} + \hat{c}\phi_{7z} + \dots] = 0
\end{aligned} \tag{3.2-26}$$

The values of the potentials at the actual wing surface can be expressed in terms of a Taylor series expansion about the mean wing surface (fig. 3.2-4). Taking a typical expansion, that for ϕ_{1y} , the value of ϕ_{1y} at the actual wing surface is given by

$$\begin{aligned}
\phi_{1y} \Big|_{\text{surface}} = & \phi_{1y}(Z_N = \pm 0) + \left(\frac{\partial \phi_1}{\partial n} \right)_y (Z_N = \pm 0) [\pm \tau F(X_N, Y_N) \\
& + \hat{\theta} \lambda_\theta H(X_N, Y_N)] + (\tau^2, \hat{\theta}^2, \tau \hat{\theta}, \text{ etc.}) \tag{3.2-27}
\end{aligned}$$

where n is a normal coordinate positive upward from the mean wing surface, figure (3.2-4). The plus and minus signs denote upper and lower surface, respectively.

Inserting expansions like that of equation (3.2-27) into equation (3.2-26) and equating orders of magnitudes gives the boundary conditions to be satisfied on the mean surface of the wing. For the various parameters the first-order boundary conditions are as follows:

$$\hat{w}: \quad \frac{\partial \phi_1}{\partial n} = \lambda_w(t) \cos \theta_N \bar{w} \quad (a)$$

$$\hat{v}: \quad \frac{\partial \phi_2}{\partial n} = -\lambda_v(t) \sin \theta_N \bar{v} \quad (b)$$

$$\tau: \quad \frac{\partial \phi_3}{\partial n} = + \frac{\partial F}{\partial X_N} \quad (c)$$

$$\hat{\theta}: \quad \frac{\partial \phi_4}{\partial n} = \lambda_\theta \frac{\partial H}{\partial X_N} \quad (d)$$

(3.2-28)

$$a: \quad \frac{\partial \phi_5}{\partial n} = 0 \quad (e)$$

$$\hat{b}: \quad \frac{\partial \phi_6}{\partial n} = 0 \quad (f)$$

$$\hat{c}: \quad \frac{\partial \phi_7}{\partial n} = 0 \quad (g)$$

where the normal derivative $\partial/\partial n$ is now along the normal to the mean surface:

$$\frac{\partial}{\partial n} = \frac{\partial}{\partial z} \cos \theta_N - \frac{\partial}{\partial y} \sin \theta_N$$

3.2.5.4 Expansion of the wake boundary condition.—The wake boundary condition requires that the pressure coefficient be continuous across the wake surface. Recalling the pressure coefficient, equation (3.2-9), and introducing the expanded potential, it follows that

$$C_P = -2 \left[\frac{\hat{w}}{U} \frac{D\phi_1}{Dt} \bar{w} + \frac{\hat{v}}{U} \frac{D\phi_2}{Dt} \bar{v} + \tau \frac{\partial \phi_3}{\partial x} + \hat{\theta} \frac{D\phi_4}{Dt} + \right. \\ \left. + a \frac{\partial \phi_5}{\partial x} + \hat{b} \frac{D\phi_6}{Dt} + \hat{c} \frac{D\phi_7}{Dt} + \dots \right] \quad (3.2-29)$$

where $D/Dt = \partial/\partial t + U \partial/\partial x$. It remains to evaluate the pressure coefficient on the actual wake surface by expanding the potentials in equation (3.2-29) in terms of a Taylor series expansion about a suitable defining surface whose position is known a priori.

As noted in the discussion on kinematics, the mean wake surface may be located relative to the paths of the trailing edges of lifting surfaces of a configuration. Consider the cylindrical surface which is a downstream continuation of the mean wing surface and which is parallel with the X-axis, figure 3.2-7. This surface is termed the defining surface. The coordinates of points on the mean surface relative to corresponding points on the defining

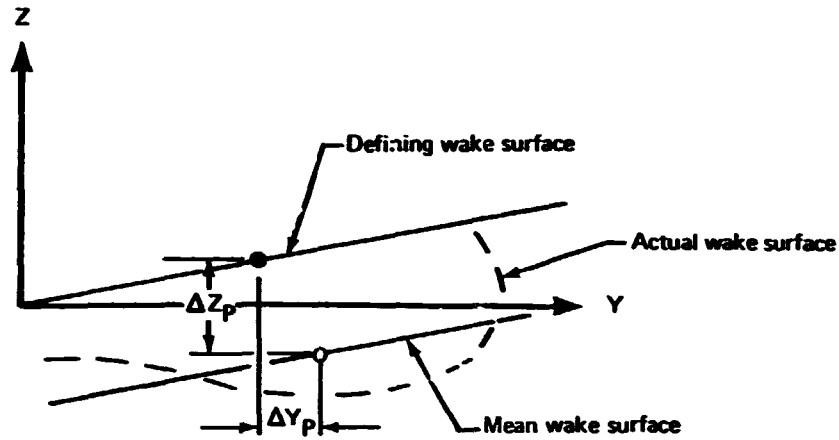


FIGURE 3.2-7.—WAKE SURFACE

surface, ΔX , ΔZ_p , ΔY_p , are found by integrating the unsteady velocities $U\hat{w}\lambda_w(t)$ and $U\hat{v}\lambda_v(t)$ to find the following:

$$\begin{aligned}\Delta Z_p &= - \int_{t-\frac{x}{U}}^t U\hat{w}\lambda_w(\tau) d\tau \\ &= U\hat{w}[-\bar{\lambda}_w(t) + \bar{\lambda}_w(t-x/U)] \\ \Delta Y_p &= - \int_{t-\frac{x}{U}}^t U\hat{v}\lambda_v(\tau) d\tau \\ &= U\hat{v}[-\bar{\lambda}_v(t) + \bar{\lambda}_v(t-x/U)]\end{aligned}\tag{3.2-30}$$

where $\lambda_w(t) = \partial\bar{\lambda}_w/\partial t$ and $\lambda_v(t) = \partial\bar{\lambda}_v/\partial t$. The mean wake surface is displaced in the X-direction as

$$\Delta X = (\bar{U}-U)(t-\frac{x}{U})\tag{3.2-31}$$

where $\bar{U} = U/X \int_{t-U/X}^t U(\tau) d\tau$ is the average forward velocity.

The actual wake surface is deformed about the mean wake surface. The displacement of a point on the actual wake surface from the corresponding point on the mean wake surface is denoted as $\Delta Y, \Delta Z$. The distances ΔY and ΔZ are functions of the small parameters and may be expressed as

$$\begin{aligned}\Delta Y &= \hat{w}\Delta Y_1 + \hat{v}\Delta Y_2 + \tau\Delta Y_3 + \hat{\theta}\Delta Y_4 + a\Delta Y_5 + \hat{b}\Delta Y_6 + \hat{c}\Delta Y_7 + \\ &\quad + (\text{second and higher order terms}) \\ \Delta Z &= \hat{w}\Delta Z_1 + \hat{v}\Delta Z_2 + \tau\Delta Z_3 + \hat{\theta}\Delta Z_4 + a\Delta Z_5 + \hat{c}\Delta Z_6 + \hat{b}\Delta Z_7 + \\ &\quad + (\text{second and higher order terms})\end{aligned}\quad (3.2-32)$$

A second Taylor series expansion in terms of the spatial displacements $\Delta Y, \Delta Z$ is required to express the value of the pressure coefficient on the mean wake surface in terms of its value on the defining wake surface.

Assuming ΔX to be small, the sequence of Taylor series expansions gives rise to second and higher order terms in the expansion of the pressure coefficient. Thus, the pressure coefficient on the defining surface is a first-order approximation to the pressure coefficient at corresponding points of the actual wake surface. Imposing the requirement that the pressure coefficient be continuous across the actual wake surface to all orders of magnitude, i.e., $[[C_p]] = 0$, results in the following boundary conditions to be applied on the defining surface of the wake:

$$\hat{w}: \left[\frac{D\phi_1}{Dt} \right] = 0 \quad (a)$$

$$\hat{v}: \left[\frac{D\phi_2}{Dt} \right] = 0 \quad (b)$$

$$\tau: \left[\frac{\partial \phi_3}{\partial x} \right] = 0 \quad (c)$$

$$\hat{\theta}: \left[\frac{D\phi_4}{Dt} \right] = 0 \quad (d)$$

$$a: \left[\frac{\partial \phi_5}{\partial x} \right] = 0 \quad (e)$$

$$\hat{b}: \left[\frac{D\phi_6}{Dt} \right] = 0 \quad (f)$$

$$\hat{c}: \left[\frac{D\phi_7}{Dt} \right] = 0 \quad (g)$$

(3.2-33)

where $[[\]]$ denotes the discontinuity across the defining surface.

3.2.5.5 Expansion of the slender body surface boundary condition.—Substituting the expression for the unit vector normal to the surface of the slender body, equation (3.2-20), into the surface boundary condition, equation (2.3-70), and evaluating at the surface of the body leads to the following expression:

$$\begin{aligned}
 & -\left(a \frac{dR}{dX_M} + b \lambda \frac{\partial G}{\partial X_M} \cos \mu + \hat{c} \lambda \frac{\partial I}{\partial X_M} \sin \mu\right) (1 + \hat{w} \phi_{1x} + \hat{v} \phi_{2x} + \\
 & + \lambda \phi_{3x} + \hat{\theta} \phi_{4x} + a \phi_{5x} + \hat{b} \phi_{6x} + \hat{c} \phi_{7x} + \dots) + \\
 & + \cos \mu (-\hat{v} \lambda \nabla + \hat{w} \phi_{1y} + \hat{v} \phi_{2y} + \lambda \phi_{3y} + \hat{\theta} \phi_{4y} + \\
 & + a \phi_{5y} + \hat{b} \phi_{6y} + \hat{c} \phi_{7y} + \dots) + \sin \mu (\hat{w} \lambda \nabla \\
 & + \hat{w} \phi_{1z} + \hat{v} \phi_{2z} + \lambda \phi_{3z} + \hat{\theta} \phi_{4z} + a \phi_{5z} + \hat{b} \phi_{6z} \\
 & + \hat{c} \phi_{7z} + \dots) = 0.
 \end{aligned} \tag{3.2-34}$$

The nondimensional perturbation velocity potentials are evaluated at a typical surface point A and this value can be expressed in terms of a Taylor series expansion about the corresponding point A' on the mean surface (fig. 3.2-8).

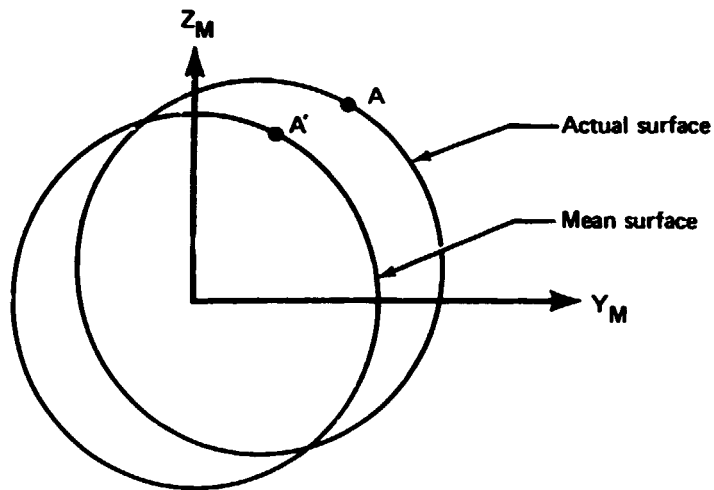


FIGURE 3.2-8.—CORRESPONDING POINTS ON THE ACTUAL AND MEAN SURFACES OF A SLENDER BODY

The nondimensional perturbation velocity potential at point A is therefore given by the expansion about point A' as follows:

$$\begin{aligned}
\phi(A) &= \phi(A') + \frac{\partial \phi(A')}{\partial Y_M} [\hat{b} \lambda_b(t) G(X_M) + a R(X_M) \cos \mu] \\
&\quad + \frac{\partial \phi(A')}{\partial Z_M} [\hat{c} I(X_M) + a R(X_M) \sin \mu] \\
&= \phi(A') + \frac{\partial \phi(A')}{\partial Y_M} \hat{b} \lambda_b(t) G(X_M) + \frac{\partial \phi(A')}{\partial Z_M} \hat{c} \lambda_c(t) I(X_M) \\
&\quad + \frac{\partial \phi(A')}{\partial n} a R(X_M) + \dots
\end{aligned} \tag{3.2-35}$$

Substituting equation (3.2-35) into equation (3.2-34) and equating terms of like order in the small parameters leads to the following system of first-order boundary conditions to be satisfied on the mean surface:

$$\begin{aligned}
\hat{w}: \frac{\partial \phi_1}{\partial n} &= - \lambda_w(t) \bar{W}(X, Y, Z) \sin \mu \\
\hat{v}: \frac{\partial \phi_2}{\partial n} &= - \lambda_v(t) \bar{V}(X, Y, Z) \cos \mu \\
\tau: \frac{\partial \phi_3}{\partial n} &= 0 \\
\hat{\theta}: \frac{\partial \phi_4}{\partial n} &= 0 \\
a: \frac{\partial \phi_5}{\partial n} &= \frac{dR(X_M)}{dX_M} \\
\hat{b}: \frac{\partial \phi_6}{\partial n} &= \lambda_b(t) \frac{G(X_M)}{X_M} \cos \mu \\
\hat{c}: \frac{\partial \phi_7}{\partial n} &= \lambda_c(t) \frac{\partial I(X_M)}{\partial X_M} \sin \mu
\end{aligned} \tag{3.2-36}$$

These are the first-order boundary conditions to be satisfied on the mean surface of the slender body, and n is the outward normal to the mean surface such that the normal derivatives appearing in equation (3.2-36) have the following form:

$$\frac{\partial}{\partial n} \equiv \frac{\partial}{\partial Y_M} \cos \mu + \frac{\partial}{\partial Z_M} \sin \mu \tag{3.2-37}$$

3.2.5.6 Linear First-Order Aerodynamic Theory for the Wing-Body Problem

The first-order aerodynamic theory for the case when the time-varying quantities $\lambda_w(t)$, $\lambda_v(t)$, $\lambda_\theta(t)$, $\lambda_b(t)$, and $\lambda_c(t)$ are of order unity is now completely formulated. The solution is given by the perturbation potential

$$\phi = \hat{w}\phi_1 + \hat{v}\phi_2 + \tau\phi_3 + \hat{\theta}\phi_4 + a\phi_5 + \hat{b}\phi_6 + \hat{c}\phi_7 \quad (3.2-38)$$

and is a first-order approximation to the nonlinear theory stated in section 3.2.1. The velocity potentials ϕ_i ($i = 1, 2, 4, 6, 7$) must satisfy the linear unsteady flow equation

$$\epsilon^2 \phi_{ixx} + \phi_{iyy} + \phi_{izz} - \frac{2M^2}{U} \phi_{ixt} - \frac{M^2}{U^2} \phi_{itt} = 0 \quad (3.2-39)$$

while the velocity potentials ϕ_i ($i = 3, 5$) must satisfy the linear steady flow equation

$$\epsilon^2 \phi_{ixx} + \phi_{iyy} + \phi_{izz} = 0 \quad (3.2-40)$$

Letting S_W and S_B denote, respectively, the mean surfaces of the thin wing and slender body of the Wing-Body Problem and letting the flow incidence from each potential be denoted as

$$\psi_i = -\epsilon_i \frac{\partial \phi_i}{\partial n}, \quad (3.2-41)$$

the surface and wake boundary conditions are summarized as follows:

$$\begin{aligned} \hat{w} : \quad \psi_1 &= -\hat{w}\lambda_w(t) \cos \theta_N \bar{W} && \text{on } S_W \\ &= -\hat{w}\lambda_w(t) \sin \mu \bar{W} && \text{on } S_B \quad (a) \\ \left\{ \frac{D\phi_1}{Dt} \right\} &= 0 && \text{on } W \\ \hat{v} : \quad \psi_2 &= \hat{v}\lambda_v(t) \sin \theta_N \bar{V} && \text{on } S_W \\ &= -\hat{v}\lambda_v(t) \cos \mu \bar{V} && \text{on } S_B \quad (3.2-42) \quad (b) \\ \left\{ \frac{D\phi_2}{Dt} \right\} &= 0 && \text{on } W \\ \tau : \quad \psi_3 &= \tau \frac{\partial F}{\partial X_N} && \text{on } S_W \\ &= 0 && \text{on } S_B \quad (c) \\ \left\{ \phi_3 \right\}_x &= 0 && \text{on } W \\ \hat{\theta} : \quad \psi_4 &= -\hat{\theta}\lambda_\theta(t) \frac{\partial H}{\partial X_N} && \text{on } S_W \\ &= 0 && \text{on } S_B \quad (d) \\ \left\{ \frac{D\phi_4}{Dt} \right\} &= 0 && \text{on } W \end{aligned}$$

$$\begin{aligned} \text{a :} \quad \Psi_5 &= 0 && \text{on } S_W \\ &= -a \frac{dR}{dX_M} && \text{on } S_B \quad (e) \end{aligned}$$

$$[\phi_{5,x}] = 0 \quad \text{on } W$$

$$\begin{aligned} \hat{b} : \quad \Psi_6 &= 0 && \text{on } S_W \\ &= -b\lambda_b(t) \frac{\partial G}{\partial X_M} \cos \mu && \text{on } S_B \quad (f) \end{aligned}$$

$$\left[\frac{D\phi_6}{Dt} \right] = 0 \quad \text{on } W$$

$$\begin{aligned} \hat{c} : \quad \Psi_7 &= 0 && \text{on } S_W \\ &= -\hat{c}\lambda_c(t) \frac{\partial I}{\partial X_M} \sin \mu && \text{on } S_B \quad (g) \end{aligned}$$

$$\left[\frac{D\phi_7}{Dt} \right] = 0 \quad \text{on } W$$

The entire aerodynamic theory for the Wing-Body Problem is expressed in the following compact form:

flow equations,

$$\beta^2 (\phi_i)_{xx} + (\phi_i)_{yy} + (\phi_i)_{zz} - \frac{2M^2}{U} (\phi_i)_{xt} - \frac{M^2}{U^2} (\phi_i)_{tt} = 0;$$

surface boundary conditions,

$$\epsilon_i \frac{\partial \phi_i}{\partial n} = -\Psi_i(X, Y, Z, t) \quad \text{on } S_W + S_B \quad (3.2-43)$$

where $\epsilon_1 = \hat{w}$, $\epsilon_2 = \hat{v}$, $\epsilon_3 = \tau$, $\epsilon_4 = \hat{\theta}$, $\epsilon_5 = a$, $\epsilon_6 = \hat{b}$, $\epsilon_7 = \hat{c}$

and wake boundary conditions,

$$[\phi_{it} + U\phi_{ix}] = 0 \quad \text{on } W$$

where Ψ_i is given by equations (3.2-42) and all derivatives with respect to time vanish for the thickness problems $i=3$ and 5 .

3.2.6 Low Frequency Approximation

The unsteady flow problems posed by equations (3.2-43) are greatly simplified by the low frequency approximation previously referred to in section 3.2.2. Equations (3.2-43) yield a valid approximation when the unsteady flow incidence imposed by the surface boundary conditions has the characteristics

$$\frac{\bar{c}}{U} \frac{\partial}{\partial t} (\psi_i) = 0(1) \quad (3.2-44)$$

and

$$\left(\frac{\bar{c}}{U}\right)^2 \frac{\partial^2}{\partial t^2} (\psi_i) = 0(1)$$

If the unsteadiness is simple harmonic, i.e., if

$$\{\psi_i(X, Y, Z, t) = R\{\psi_i^*(X, Y, Z, \bar{\omega}_i) e^{i\omega_i t}\}, \quad (3.2-45)$$

then equations (3.2-44) imply that the reduced frequency,

$$K_i \equiv \frac{\bar{c}}{U} \omega_i, \quad (3.2-46)$$

may be of order unity. In this section

$$\bar{\omega}_i \equiv \frac{\omega_i}{U} \quad (3.2-47)$$

is taken to be a small parameter, and an asymptotic solution to the unsteady flow problems, equations (3.2-43), valid in the limit as $\bar{\omega}_i$ approaches zero, is sought.

3.2.6.1 Simple harmonic time dependence.—Assuming simple harmonic time dependence as in equation (3.2-45), the unsteady flow problems become as follows:

$$\begin{aligned} \beta^2 \phi_{ixx}^* + \phi_{iyy}^* + \phi_{izz}^* - 2iM^2 \bar{\omega}_i \phi_{ix}^* + M^2 \bar{\omega}_i^2 \phi_i^* &= 0 \\ \frac{\partial \phi_i}{\partial n} &= -\psi_i(X, Y, Z) \quad \text{on } S_W + S_B \\ [i\bar{\omega}_i \phi_i^* + \phi_{ix}^*] &= 0 \quad \text{on } W \end{aligned} \quad (3.2-48)$$

where ϕ_i^* is the complex potential such that

$$\phi_i(X, Y, Z, t) = R\{\phi_i^*(X, Y, Z, \bar{\omega}_i) e^{i\omega_i t}\} \quad (3.2-49)$$

3.2.6.2 Asymptotic series in frequency.—The reduced frequency is identified as a small parameter in the surface boundary condition by noting that the local, complex flow incidence can be expanded in a complex power series as follows:

$$\begin{aligned} \psi_i^* &= \psi_i^{(0)} + i\bar{\omega}_i \psi_i^{(1)} \\ &+ (\text{terms of higher order in } i\bar{\omega}_i) \end{aligned} \quad (3.2-50)$$

Corresponding to this expansion, the asymptotic expansion is chosen as follows:

$$\phi_i^* = \phi_i^{(0)} + i\bar{\omega}_i \phi_i^{(1)} + (\text{terms of higher order in } i\bar{\omega}_i) \quad (3.2-51)$$

Substituting the expansions, equations (3.2-50) and (3.2-51), into the equations governing unsteady flow, i.e., equations (3.2-48), and equating terms of like order in $i\bar{\omega}_i$, leads to the following sequence of simplified flow problems governing the zeroth and first-order potentials:

zeroth order

flow equations,

$$\beta^2 \phi_{ixx}^{(0)} + \phi_{iyy}^{(0)} + \phi_{izz}^{(0)} = 0$$

and boundary conditions,

$$\frac{\partial \phi_i^{(0)}}{\partial n_i} = -\psi_i^{(0)} \quad \text{on } S_W + S_B$$

$$[\phi_{ix}^{(0)}] = 0 \quad \text{on } W$$

(3.2-52)

first order

flow equations,

$$\beta^2 \phi_{ixx}^{(1)} + \phi_{iyy}^{(1)} + \phi_{izz}^{(1)} = 2M^2 \phi_{ix}^{(0)}$$

and boundary conditions,

$$\frac{\partial \phi_i^{(1)}}{\partial n_i} = -\psi_i^{(1)} \quad \text{on } S_W + S_B$$

$$[\phi_{ix}^{(1)}] = -[\phi_i^{(0)}] \quad \text{on } W$$

(3.2-53)

3.2.6.3 First-order approximation to unsteady flow.—The first-order approximation to unsteady flow is obtained by truncating the asymptotic series as follows:

$$\phi_i^* \approx \phi_i^{(0)} + i\bar{\omega}_i \phi_i^{(1)} \quad (3.2-54)$$

This expression yields a valid approximation when the frequency of the local flow incidence is so small that terms of higher order in $i\bar{\omega}_i$ may be neglected by comparison with the zeroth and first-order terms. A direct evaluation of the required smallness of the reduced frequency for equation (3.2-54) to yield a valid approximation is deferred to section 3.2.8, but some insight into the nature of the approximation is gained from an examination of the first-order problems posed by equations (3.2-53).

An interesting physical interpretation of the first-order problems stems from the wake boundary conditions. The implication of this boundary condition follows by noting that $[\phi_i^{(0)}]$ is independent of the X-coordinate, i.e., the distance downstream, because $[\phi_{ix}^{(0)}] = 0$

on W in the zeroth-order problem. It may also be noted that $\llbracket \phi_i^{(0)} \rrbracket$ on W is equal to the strength of the bound vorticity on the surface producing the vortex wake. (See equation (7-38) of reference 2-3.) Recalling that

$$\phi_i \approx (\phi_i^{(0)} + i\bar{\omega}_i \phi_i^{(1)}) e^{i\omega_i t}$$

it follows that to first order in $i\bar{\omega}_i$

$$\frac{1}{U} \llbracket \frac{\partial \phi_i}{\partial t} \rrbracket = i\bar{\omega}_i \llbracket \phi_i^{(0)} \rrbracket$$

and the terms $\llbracket \phi_i^{(0)} \rrbracket$ appearing in the wake boundary conditions of the first-order problems represent the rate of change of bound vorticity in the zeroth-order problems. From the first-order wake boundary conditions, i.e.,

$$\llbracket \phi_{ix}^{(1)} \rrbracket = -\llbracket \phi_i^{(0)} \rrbracket \quad \text{on } W,$$

it follows that there must be a transverse component of vorticity in the wake whose strength is independent of the X -coordinate and is equal to the time rate of change of bound vorticity. In terms of time history the wake has a "memory" limited to the instantaneous flow incidence and time rate of change of flow incidence on the surface. The wake extends to infinity with a transverse component of vorticity which depends only on the time rate of change of surface flow incidence at the instant of time under consideration; thus, the wake vorticity strength varies linearly in the X -direction.

For flows with a supersonic freestream the effect of the limited memory of the wake is not severe since only a small portion of the wake close to a configuration can influence the flow over the configuration. For subsonic flows, however, the situation is quite different because the entire wake influences the flow about the configuration. The influence of distant portions of the wake is greatest for very large aspect ratios, decreasing with decreasing aspect ratio to the slender body theory limit wherein the wake has no first-order influence. The validity of the asymptotic expansion for low frequency motions must depend in some way on the aspect ratio. The question is considered further in section 3.2.8.

3.2.6.4 Derivation of the form of the solution to the first order problems.—The zeroth and first-order problems posed by equations (3.2-52) and (3.2-53) must be solved sequentially because the first-order equations contain inhomogeneous terms which are functions of the solutions to the zeroth-order problems. The zeroth-order problems are seen to be simply the steady flow problems obtained by assuming the local flow incidence on the surface to be steady with the solution given by $\phi_i^{(0)}$. The homogeneous form of the first-order flow equation is seen to be identical to the steady flow equation. Therefore, on letting integrals of this equation be denoted as ϕ_H , the solutions to the zeroth and first-order problems are denoted as follows:

$$\phi_i^{(0)} = \phi_H(x, y, z; -\psi_i^{(0)}) \quad (3.2-55)$$

and

$$\phi_i^{(1)} = \phi_H(x, y, z; -\psi_i^{(1)}) + \phi_{ip}^{(1)}(\phi_i^{(0)}) \quad (3.2-56)$$

where $\phi_{ip}^{(1)}(\phi_i^{(0)})$ denotes a particular integral which is a function of the solution to the zeroth-order problem.

A particular integral to the inhomogeneous flow equation of the first-order problem is given by equation (4.5.1b) of reference 3-1 as follows:

$$\phi_{ip}^{(1)} = \frac{M^2}{\beta^2} x \phi_H(x, y, z; -\psi_i^{(0)}) \quad (3.2-57)$$

This particular integral, when combined with the homogeneous solution and substituted into the boundary conditions of the first-order problem, leads to

$$\begin{aligned} \frac{\partial \phi_H}{\partial n}(x, y, z; -\psi_i^{(1)}) + \frac{M^2}{\beta^2} x \frac{\partial \phi_H}{\partial n}(x, y, z; -\psi_i^{(0)}) \\ = -\psi_i^{(1)} \quad \text{on } S_W + S_E \end{aligned} \quad (3.2-58)$$

and

$$\begin{aligned} \left[\frac{\partial \phi_H}{\partial x}(x, y, z; -\psi_i^{(1)}) \right] - \left[\phi_H(x, y, z; -\psi_i^{(0)}) \right] \\ + \frac{1}{\beta^2} \left[\phi_H(x, y, z; -\psi_i^{(0)}) \right] + \frac{M^2}{\beta^2} x \left[\frac{\partial \phi_H}{\partial x}(x, y, z; -\psi_i^{(0)}) \right] \\ = - \left[\phi_H(x, y, z; -\psi_i^{(0)}) \right] \quad \text{on } W \end{aligned}$$

In the first of equations (3.2-58), the first term cancels the term on the right, leaving the underlined term. The first term in the second of equation (3.2-58) vanishes because of the assumed form of ϕ_H which was used in the zeroth-order problem. The second term cancels the term on the right-hand side, leaving the underlined terms. Thus, to the particular integral given by equation (3.2-57) must be added additional homogeneous terms which cancel the underlined terms appearing in equations (3.2-58).

The additional homogeneous term which will satisfy the surface boundary conditions is given by reference 3-1 and the first-order solution given by reference 3-1 is as follows:

$$\begin{aligned} \phi_i^{(1)} = \underbrace{\phi_H(x, y, z; -\psi_i^{(1)})}_{\text{first homogeneous term}} + \underbrace{\frac{M^2}{\beta^2} [x \phi_H(x, y, z; -\psi_i^{(0)}) - \phi_H(x, y, z; -x \psi_i^{(0)})]}_{\text{particular integral}} \\ \underbrace{- \phi_H(x, y, z; -x \psi_i^{(0)})}_{\text{second homogeneous term}} \end{aligned} \quad (3.2-59)$$

The first homogeneous term provides the solution satisfying the first-order surface boundary condition. The second cancels the flow incidence induced by the particular integral. Equation (3.2-59) corresponds to the result presented as equation (4.5.1b) of reference 3-1; and, as pointed out in reference 3-1, this is a complete solution in the case of supersonic flow about a wing having no subsonic trailing edges, i.e., when the wake boundary condition is eliminated from the problem. Equation (3.2-59) is not a solution in subsonic flow nor in the general case of supersonic flow because it fails to satisfy the wake boundary conditions of the first order problems.

A complete solution to the first-order problems satisfying both the surface and the wake boundary conditions for arbitrary configuration shapes in subsonic and supersonic flow is derived in the following. This derivation proceeds from a formulation of the unsteady flow problems expressed in terms of the acceleration potential defined as

$$\Omega \equiv \frac{D\phi}{Dt}$$

which, to first order, is given by the linear approximation

$$\Omega = \phi_t + U\phi_x \quad (3.2-60)$$

In terms of the acceleration potential the unsteady flow problems are shown by reference 3-2 to be as follows:

flow equations:

$$\beta^2 \Omega_{ixx} + \Omega_{iyy} + \Omega_{izz} - \frac{2M^2}{U} \Omega_{ixt} - \frac{M^2}{U^2} \Omega_{itt} = 0$$

where

$$\beta^2 = 1 - M^2 \quad (3.2-61)$$

boundary conditions:

$$\Omega_i = \Omega_i(X, Y, Z, t) \quad \text{on } S_W + S_B$$

and

$$[\Omega_i] = 0 \quad \text{on } W$$

where Ω_i is required to satisfy the integral equation

$$\Psi_i(X, Y, Z, t) = -\frac{\partial}{\partial n} \int_{-\infty}^X \Omega_i(\xi, Y, Z, t - \frac{X-\xi}{U}) d\xi \quad (3.2-62)$$

for Ψ_i specified on $S_W + S_B$.

The problem formulation consisting of equations (3.2-60) through (3.2-62) has been introduced to obtain a wake boundary condition which is free of first-order time

derivatives—the source of the inhomogeneous term appearing in the wake boundary condition of equations (3.2-53). The first-order time derivative in the flow equation is eliminated by introducing the following transformation of coordinates:

$$\begin{aligned}x' &= \frac{1}{\beta}x \\t' &= \frac{M}{\beta U}x + \beta t\end{aligned}\quad (3.2-63)$$

$$\Omega'_i(x', y, z, t') = \Omega_i(x, y, z, t)$$

so that equations (3.2-61) become

$$\begin{aligned}\Omega'_{ix'x'} + \Omega'_{iyy} + \Omega'_{izz} - \frac{M^2}{U^2} \Omega'_{it't'} &= 0 \\ \Omega'_i &= \Omega'_i(X', Y, Z, t') \quad \text{on } S'_W + S'_P \\ [\Omega'_i] &= 0 \quad \text{on } W'\end{aligned}\quad (3.2-64)$$

Assuming simple harmonic time dependence, i.e., assuming

$$\Omega_i = \Omega_i^* e^{i\omega_i t}, \quad (3.2-65)$$

and multiplying by $e^{i\bar{\omega}_i x}$ so that $d(e^{i\bar{\omega}_i x} \phi^*) = \frac{\Omega_i^*}{U} e^{i\bar{\omega}_i x} dx$, it follows on integration that

$$\psi_i^* = -\frac{1}{U} e^{-i\bar{\omega}_i x} \frac{\partial}{\partial n} \int_{-\infty}^x \Omega_i^* e^{i\bar{\omega}_i \xi} d\xi. \quad (3.2-66)$$

Under the transformation of coordinates, equation (3.2-63), the potential and complex flow incidence become as follows:

$$\Omega'_i = \bar{\Omega}_i^* e^{i\omega_i t'/\beta}$$

and

$$\psi_i^* = -\frac{\beta}{U} e^{-i\bar{\omega}_i \beta x'} \frac{\partial}{\partial n} \int_0^{\beta x'} \bar{\Omega}_i^* e^{i\bar{\omega}_i \xi'/\beta} d\xi' \quad (3.2-67)$$

where

$$\bar{\Omega}_i^* = \Omega_i^* e^{-i\bar{\omega}_i M^2 x'/\beta} \quad (3.2-68)$$

is a modified potential corresponding to that given by equation (2.7.7) of reference 3-1. In these terms equations (3.2-64) become

$$\begin{aligned}\bar{\Omega}'^*_{ix'x'} + \bar{\Omega}'^*_{iyy} + \bar{\Omega}'^*_{izz} + \frac{\bar{\omega}_i^2 M^2}{\beta^2} \bar{\Omega}'^*_i &= 0 \\ \bar{\Omega}'^*_i &= \bar{\Omega}_i^*(X, Y, Z) \quad \text{on } S_W + S_B \\ [\bar{\Omega}'^*_i] &= 0 \quad \text{on } W\end{aligned}\tag{3.2-69}$$

and on returning to the original coordinates, i.e., by substituting $X' = X/\beta$, the unsteady flow problem becomes as follows:

flow equation,

$$\beta^2 \bar{\Omega}^*_{ixx} + \bar{\Omega}^*_{iyy} + \bar{\Omega}^*_{izz} + \frac{M^2 \bar{\omega}_i^2}{\beta^2} \bar{\Omega}^*_i = 0\tag{3.2-70}$$

boundary conditions,

$$\begin{aligned}\bar{\Omega}^*_i &= \bar{\Omega}_i^*(X, Y, Z) \quad \text{on } S_W + S_B \\ [\bar{\Omega}^*_i] &= 0 \quad \text{on } W\end{aligned}$$

where $\bar{\Omega}_i^*(X, Y, Z)$ is required to satisfy

$$\Psi_i^* = -\frac{1}{U} e^{-i\bar{\omega}_i X} \frac{\partial}{\partial n} \int_{-\infty}^X \bar{\Omega}_i^* e^{i\bar{\omega}_i \xi / \beta^2} d\xi\tag{3.2-71}$$

on $S_W + S_B$.

This unsteady flow problem, equations (3.2-70), is physically identical to that posed by equations (3.2-48) and yields an identical solution in terms of the complex velocity potential given by the following:

$$\phi_i^* = -\frac{1}{U} e^{-i\bar{\omega}_i X} \int_{-\infty}^X \bar{\Omega}_i^* e^{i\bar{\omega}_i \xi} d\xi,\tag{3.2-72}$$

when the integrand of equation (3.2-71) is transformed using equation (3.2-68), i.e.,

$$\begin{aligned}\bar{\Omega}_i^* e^{i\bar{\omega}_i \xi / \beta^2} &= \bar{\Omega}_i^* e^{-i\bar{\omega}_i M^2 \xi / \beta^2} e^{i\bar{\omega}_i \xi / \beta^2} \\ &= \bar{\Omega}_i^* e^{i\bar{\omega}_i \xi}\end{aligned}\tag{3.2-73}$$

Thus, if the complex flow incidence appearing in equation (3.2-71) is identical to that appearing in equations (3.2-48), the two problems yield identical complex velocity potentials.

An asymptotic solution to the unsteady flow problem, equations (3.2-70) and (3.2-71), is assumed as follows when the complex flow incidence is expressed in the asymptotic series shown by equation (3.2-50):

$$\bar{\Omega}_i^* = \bar{\Omega}_i^{(0)} + i\bar{\omega}_i \bar{\Omega}_i^{(1)} + (\text{terms of higher order in } i\bar{\omega}_i) \quad (3.2-74)$$

Substituting equations (3.2-50) and (3.2-74) into equations (3.2-70), and equating terms of like order in $i\bar{\omega}_i$, leads to the following sequence of simplified flow problems:

zeroth order:

flow equations,

$$\beta^2 \bar{\Omega}_{ixx}^{(0)} + \bar{\Omega}_{iyy}^{(0)} + \bar{\Omega}_{izz}^{(0)} = 0$$

and boundary conditions,

(3.2-75)

$$\bar{\Omega}_i^{(0)} = \bar{\Omega}_i^{(0)}(X, Y, Z) \quad \text{on } S_W + S_B$$

$$[\bar{\Omega}_i^{(0)}] = 0 \quad \text{on } W$$

first order:

flow equations,

$$\beta^2 \bar{\Omega}_{ixx}^{(1)} + \bar{\Omega}_{iyy}^{(1)} + \bar{\Omega}_{izz}^{(1)} = 0$$

and boundary conditions,

(3.2-76)

$$\bar{\Omega}_i^{(1)} = \bar{\Omega}_i^{(1)}(X, Y, Z) \quad \text{on } S_W + S_B$$

$$[\bar{\Omega}_i^{(1)}] = 0 \quad \text{on } W$$

Both the zeroth and first-order problems are of the steady flow type and the surface boundary conditions are related to the complex flow incidence by expanding equation (3.2-71), i.e.,

$$(\psi_i^{(0)} + i\bar{\omega}_i \psi_i^{(1)} + \dots) = -\frac{1}{U}(1 - i\bar{\omega}_i X + \dots) \frac{\partial}{\partial n} \int_{-\infty}^X (\bar{\Omega}_i^{(0)} + i\bar{\omega}_i \bar{\Omega}_i^{(1)} + \dots) \left(1 + \frac{i\bar{\omega}_i \xi}{\beta^2} + \dots\right) d\xi \quad (3.2-77)$$

Equating terms of like order in $i\bar{\omega}_i$ yields the following:

$$\begin{aligned} \psi_i^{(0)} &= -\frac{1}{U} \frac{\partial}{\partial n} \int_{-\infty}^X \bar{\Omega}_i^{(0)} d\xi \\ \psi_i^{(1)} &= -\frac{1}{U} \left[\frac{\partial}{\partial n} \int_{-\infty}^X \bar{\Omega}_i^{(1)} d\xi + \frac{\partial}{\partial n} \int_{-\infty}^X \bar{\Omega}_i^{(0)} \frac{\xi}{\beta^2} d\xi - \frac{\partial}{\partial n} \int_{-\infty}^X X \bar{\Omega}_i^{(0)} d\xi \right] \end{aligned} \quad (3.2-78)$$

Recalling equation (3.2-60), the complex velocity and acceleration potentials are related as

$$\bar{\Omega}_i^* = i\omega_i \bar{\phi}_i^* + U \bar{\phi}_{ix}^* \quad (3.2-79)$$

where $\bar{\phi}_i^*$ is the modified complex velocity potential

$$\bar{\phi}_i^* = \bar{\phi}_i^* e^{-i\bar{\omega}_i M^2 X / \beta^2} \quad (3.2-80)$$

Substituting the asymptotic series into equation (3.2-79), and equating terms of like order in $i\bar{\omega}_i$, leads to

$$\begin{aligned} \bar{\Omega}_i^{(0)} &= U \bar{\phi}_{ix}^{(0)} \\ \bar{\Omega}_i^{(1)} &= U (\bar{\phi}_{ix}^{(0)} + \bar{\phi}_{ix}^{(1)}) \end{aligned} \quad (3.2-81)$$

Substituting these results into equations (3.2-78) and carrying out the indicated integrations, leads to the following:

$$\begin{aligned} \psi_i^{(0)} &= -\frac{1}{U} \frac{\partial \bar{\phi}_i^{(0)}}{\partial n} \\ \psi_i^{(1)} &= -\frac{M^2}{\beta^2} X \frac{\partial \bar{\phi}_i^{(0)}}{\partial n} - \frac{\partial \bar{\phi}_i^{(1)}}{\partial n} + \frac{1}{\beta^2} \int_{-\infty}^X \frac{\partial \bar{\phi}_i^{(0)}}{\partial n} d\xi \end{aligned} \quad (3.2-82)$$

Applying the procedures leading from equation (3.2-71) to equation (3.2-82) to the expression for the complex velocity potential, i.e.,

$$\phi_j^*(x, y, z) = \frac{1}{U} e^{-i\bar{\omega}_i x} \int_{-\infty}^x \bar{\Omega}_i e^{i\bar{\omega}_i \xi / \beta^2} d\xi, \quad (3.2-83)$$

leads to

$$\phi_i^{(0)} = \bar{\phi}_i^{(0)} \quad (3.2-84)$$

and

$$\phi_i^{(1)} = \frac{M^2}{\beta^2} x \bar{\phi}_i^{(0)} + \bar{\phi}_i^{(1)} - \frac{1}{\beta^2} \int_{-\infty}^x \bar{\phi}_i^{(0)} d\xi \quad (3.2-85)$$

Equations (3.2-82) through (3.2-85) are now combined to find

$$\psi_i^{(0)} = - \frac{\partial \phi_i^{(0)}}{\partial n} \quad \text{on } S_W + S_B \quad (3.2-86)$$

$$\bar{\psi}_i^{(1)} = - \frac{M^2}{\beta^2} x \bar{\psi}_i^{(0)} + \psi_i^{(1)} + \frac{1}{\beta^2} \int_{-\infty}^x \psi_i^{(0)} d\xi \quad \text{on } S_W + S_B \quad (3.2-87)$$

$$\phi_i^{(1)} = \frac{M^2}{\beta^2} x \phi_i^{(0)} + \bar{\phi}_i^{(1)} - \frac{1}{\beta^2} \int_{-\infty}^x \phi_i^{(0)} d\xi \quad (3.2-88)$$

Equations (3.2-81), (3.2-84), and (3.2-86) show that the zeroth-order problem in terms of the acceleration potential stated by equations (3.2-75) and the first of equations (3.2-78) is identical to the original zeroth-order problem in terms of the velocity potential, equation (3.2-52). Equation (3.2-88) yields the desired solution to the first-order problem given by equation (3.2-53) when $\bar{\phi}_i^{(1)}$ is a solution to the homogeneous form of the flow problem with the surface boundary conditions given by equation (3.2-87).

3.2.6.5 Solution to the first order in frequency problem.—Recalling the symbolic notation introduced by equation (3.2-55), the solution to the first-order problem, equation (3.2-88), is expressed as follows:

$$\phi_i^{(1)} = \frac{M^2}{\beta^2} \underbrace{[x \phi_H(x, y, z; -\psi_i^{(0)})]}_{\text{particular integral}} - \underbrace{\phi_H(x, y, z; -x \psi_i^{(0)})}_{\text{second homogeneous term}} +$$

$$\begin{aligned}
& + \underbrace{\phi_H(x, y, z; -\psi_i^{(1)})}_{\text{first homogeneous term}} \\
& - \frac{1}{\beta^2} \underbrace{\left[\int_{-\infty}^x \phi_H(x, y, z; -\psi_i^{(0)}) d\xi - \phi_H(x, y, z; \int_{-\infty}^x \frac{\partial \phi_i^{(0)}}{\partial n} d\xi) \right]}_{\text{third homogeneous term}}
\end{aligned} \tag{3.2-89}$$

Differentiating with respect to the normal to the mean surfaces and evaluating at the mean surface leads directly to

$$\frac{\partial \phi_i^{(1)}}{\partial n} = -\psi_i^{(1)} \quad \text{on } S_W + S_B$$

Thus, the solution satisfies the surface boundary conditions of the first-order problems posed by equations (3.2-53). The third homogeneous term, which appears in equation (3.2-89) but not in the solution given previously by equation (3.2-59), satisfies the first-order wake boundary condition.

The complete solutions are obtained by combining the zeroth and first-order solutions, viz.,

$$\begin{aligned}
\phi_i^* &= \phi_i^{(0)} + i\bar{\omega}_i \phi_i^{(1)} \\
&= \phi_H(x, y, z; -\psi_i^{(0)}) + i\bar{\omega}_i \left\{ \frac{M^2}{\beta^2} \left[x \phi_H(x, y, z; -\psi_i^{(0)}) \right. \right. \\
&\quad \left. \left. - \phi_H(x, y, z; -x\psi_i^{(0)}) \right] - \frac{1}{\beta^2} \int_{-\infty}^x \phi_H(\xi, y, z; -\psi_i^{(0)}) d\xi \right. \\
&\quad \left. - \phi_H(x, y, z; \int_{-\infty}^x \frac{\partial \phi_i^{(0)}}{\partial n} d\xi) \right\} + \phi_H(x, y, z; -\psi_i^{(1)})
\end{aligned} \tag{3.2-90}$$

3.2.6.6 Arbitrary, slowly varying, time dependence. The simple harmonic motion restriction is removed, page 46 of reference 3-1, by noting that the complex power series expansion of the flow incidence, equation (3.2-50), is equivalent to a Taylor series expansion of the time-dependent flow incidence about the present instant of time. Then to first order in frequency

$$\psi_i = (\psi_i^{(0)} + i\bar{\omega}_i \psi_i^{(1)}) e^{i\omega_i t}$$

and

$$\frac{1}{U} \dot{\Psi}_i = i\bar{\omega}_i \Psi_i^{(0)} e^{i\omega_i t}$$

$$\Psi_i^* = \Psi_i^{(0)} + i\bar{\omega}_i \Psi_i^{(1)}$$

Substituting these approximations into equation (3.2-90) leads to the following form for the solution:

$$\begin{aligned} \phi_i = & \phi_H(x, y, z; -\Psi_i) + \frac{M^2}{\beta^2} [x\phi_H(x, y, z; -\dot{\Psi}_i/U) \\ & - \phi_H(x, y, z; -x\dot{\Psi}_i/U)] - \frac{1}{\beta^2} \left[\int_{-\infty}^x \phi_H(\xi, y, z; -\dot{\Psi}_i/U) d\xi \right. \\ & \left. - \phi_H(x, y, z; \int_{-\infty}^x \frac{\partial \phi_H}{\partial n}(\xi, y, z; -\dot{\Psi}_i/U) d\xi) \right] \end{aligned} \quad (3.2-91)$$

The pressure coefficient C_p induced by the flow incidence is the end result required by the FLEXSTAB system and is found for harmonic motion as

$$C_{pi} = -2\epsilon_i (\phi_{ix}^* + i\bar{\omega}_i \phi_i^*) e^{i\bar{\omega}_i t} \quad (3.2-92)$$

while for arbitrary, slowly varying time dependence

$$C_{pi} = -2\epsilon_i \left(\frac{1}{U} \phi_{it} + \phi_{ix} \right). \quad (3.2-93)$$

3.2.7 Summary of the Linear Wing-Body Problem

The linearized Wing-Body Problem is solved by solving a system of linear boundary value problems all of the same form. In each boundary value problem of the system the unknown is a function,

$$\phi_H = \phi_H(x, y, z; -\Psi_H), \quad (3.2-55)$$

which is required to satisfy the following equations: the linear partial differential equation given by

$$\beta^2 (\phi_H)_{xx} + (\phi_H)_{yy} + (\phi_H)_{zz} = 0; \quad (3.2-94)$$

the following mean surface and wake boundary conditions:

$$\frac{\partial \phi_H}{\partial n} = -\Psi_H \quad \text{on } S_W + S_B,$$

$$[(\phi_H)_x] = 0 \quad \text{on } W; \quad (3.2-95)$$

and the far field boundary condition requiring that ϕ_H vanish or be finite on a surface Σ at a large distance from the aircraft. The system of boundary value problems is generated by changing the value of flow incidence distribution, Ψ_H , specified on the mean surfaces $S_W + S_B$. The change is made by setting Ψ_H equal to each one of the following flow incidence distributions:

$$\Psi_i, \quad \dot{\Psi}_i/U, \quad x\dot{\Psi}_i/U$$

and

$$\int_{-\infty}^x \frac{\partial \phi_H}{\partial n} (\xi, y, z; -\dot{\Psi}_i/U) d\xi$$

wherein

$$\begin{aligned} \Psi_1 &= -\hat{w}\bar{W}(X, Y, Z)\lambda_w(t)\cos\theta_N & \text{on } S_W \\ &= -\hat{w}\bar{W}(X, Y, Z)\lambda_w(t)\sin\mu & \text{on } S_B & (a) \\ \Psi_2 &= \hat{v}\bar{V}(X, Y, Z)\lambda_v(t)\sin\theta_N & \text{on } S_W \\ &= -\hat{v}\bar{V}(X, Y, Z)\lambda_v(t)\cos\mu & \text{on } S_B & (b) \\ \Psi_3 &= \hat{\tau}\tau\frac{\partial F}{\partial X}(X, Y, Z) & \text{on } S_W \\ &= 0 & \text{on } S_B & (c) \\ \Psi_4 &= -\hat{\theta}\lambda_\theta(t)\frac{\partial H}{\partial X_N}(X, Y, Z) & \text{on } S_W \\ &= 0 & \text{on } S_B & (d) \\ \Psi_5 &= 0 & \text{on } S_W \\ &= -a\frac{dR}{dX_M}(X, Y, Z) & \text{on } S_B & (e) \end{aligned} \quad (3.2-42)$$

$$\begin{aligned}
 \Psi_6 &= 0 && \text{on } S_W \\
 &= -\hat{b}\lambda_b(t) \frac{\partial G}{\partial X_M}(X,Y,Z) \cos \mu && \text{on } S_B \quad (f) \\
 \Psi_7 &= 0 && \text{on } S_W \\
 &= -\hat{c}\lambda_c(t) \frac{\partial I}{\partial X_M}(X,Y,Z) \sin \mu && \text{on } S_B \quad (g)
 \end{aligned}$$

Once the solutions to the system of boundary value problems are constructed the solution to the Wing-Body Problem is given by

$$\begin{aligned}
 \phi(x,y,z,t) &= \hat{w}\phi_1 + \hat{v}\phi_2 + \tau\phi_3 \\
 &+ \hat{\theta}\phi_4 + a\phi_5 + \hat{b}\phi_6 + \hat{c}\phi_7
 \end{aligned} \quad (3.2-38)$$

where

$$\begin{aligned}
 \phi_i &= \phi_H(x,y,z; -\dot{\Psi}_i) + \frac{M^2}{\beta^2} [x\phi_H(x,y,z; -\dot{\Psi}_i/U) \\
 &- \phi_H(x,y,z; -x\dot{\Psi}_i/U) - \frac{1}{\beta^2} \left(\int_{-\infty}^x \phi_H(\xi,y,z; -\dot{\Psi}_i/U) d\xi \right. \\
 &\left. - \phi_H(x,y,z; \int_{-\infty}^x \frac{\partial \phi_i}{\partial n}(\xi,y,z; -\dot{\Psi}_i/U) d\xi \right)
 \end{aligned} \quad (3.2-91)$$

for $i = 1, 2, 4, 6, 7$ and

$$\phi_i = \phi_H(x,y,z; -\dot{\Psi}_i)$$

for $i = 3, 5$

Having the solution given by equation (3.2-91), the induced aerodynamic pressure is found by substituting the potentials given by equations (3.2-91) into equation (3.2-93), viz.,

$$C_{Pi} = -2\epsilon_i \left(\frac{1}{U} \phi_{it} + \phi_{ix} \right). \quad (3.2-93)$$

By examining this summary of the linear theory developed around the Wing-Body Problem it is readily seen that the theory may be extended to the aerodynamic problem posed by an arbitrary configuration idealized as an assembly of any number of thin and slender bodies. Additional configuration components merely introduce additional mean surface boundary conditions of the same form as those represented by equations (3.2-42). These additional boundary conditions pose additional boundary value problems which must be solved, and the solutions to these additional boundary value problems are simply added to equation (3.2-38).

3.2.8 Restrictions on the Validity of the Low Frequency Approximation

The low frequency approximation is derived in section 3.2.6 as an asymptotic series, equation (3.2-51), in which the small parameter is the reduced frequency of the unsteady flow based on a characteristic length of unity, equation (3.2-47). For the approximation to be valid, the terms of order higher than the zeroth and first-order terms in the asymptotic series must be negligible. A fundamental restriction on the unsteadiness of the surface flow incidence stems from the expansion of the surface boundary conditions, equation (3.2-50). This expansion is a complex power series, and terms of order $\bar{\omega}_i^2$ and higher are neglected in the low frequency approximation; thus, introducing the reference length c_i used in scaling the small parameters listed by equation (3.2-21), the fundamental restriction is given by

$$k_i (\equiv \bar{\omega}_i c_i) \ll 1. \quad (3.2-96)$$

From the discussion of section 3.2.6.3, however, it is readily apparent that there are additional restrictions on the permissible magnitude of the unsteadiness of the flow imposed by the boundary conditions. The additional restrictions have been only partially derived, and the objective of this section is to present those which have been derived and to describe an approach taken to obtain a complete derivation.

The required smallness of the reduced frequency for validity of the low frequency approximation can be determined only by investigating the effects of the higher order terms neglected in the approximation. As noted in section 3.2.6.3, the validity of the approximation is expected to depend on the aspect ratio of a configuration; but, in addition, references 3-3 and 3-4 show that the validity is limited by Mach number as follows:

$$k \ll \frac{1-M^2}{M} \quad \text{for } M < 1 \quad (3.2-97)$$

and

$$k \ll \frac{M^2-1}{M^2} \quad \text{for } M > 1 \quad (3.2-98)$$

The restrictions on the validity of the low frequency approximation, equations (3.2-97) and (3.2-98), are derived from the well-known solutions for unsteady lift on thin bodies in subsonic and supersonic flow, references 3-3 and 3-4. These solutions are valid for $k = O(1)$.

and are given by the complex amplitude of the velocity potential expressed as an integral over the thin body mean surfaces S_W and appear as follows:

For subsonic flow

$$\begin{aligned} \phi^*(x, y, z; k, M) = & -\frac{1}{4\pi} \int_{-\infty}^x \iint_{S_W} \gamma(X_1, Y_1) \\ & \times \frac{\partial}{\partial Z} \left\{ \frac{1}{R} e^{ik(\frac{M}{\beta^2})[M(\xi - X_1) - R]} \right\} dX_1 dY_1 e^{ik(\xi - X)} d\xi \end{aligned} \quad (3.2-99)$$

For supersonic flow

$$\begin{aligned} \phi^*(x, y, z; k, M) = & -\frac{1}{2\pi} \int_{\beta r}^x \iint_{S_W} \gamma(X_1, Y_1) \\ & \times \frac{\partial}{\partial Z} \left\{ \frac{1}{R} e^{ik(M^2/\beta^2)(\xi - X_1)} \cos(k\frac{M}{\beta^2} R) \right\} dX_1 dY_1 e^{-ik(\xi - X)} d\xi \end{aligned} \quad (3.2-100)$$

where

$$R^2 = [(\xi - X_1)^2 + \beta^2(y - Y_1)^2 + \beta^2(z - Z_1)^2],$$

$$r^2 = \beta^2[(y - Y_1)^2 + z^2],$$

and

$\gamma(X_1, Y_1)$ is the unsteady load amplitude.

The limitations of the low frequency approximation are found from the conditions which must be placed on equations (3.2-99) and (3.2-100) to permit a convergent power series expansion of the terms dependent on k . In the supersonic case, equation (3.2-100), the exponential terms contain the following geometric quantities: $(\xi - X_1)$, $(\xi - X)$, and R . These quantities influence the range of validity of the expansion.

Assuming that the potential is to be evaluated in the neighborhood of the thin body, the quantities $|\xi - X_1|_{\max}$, $|\xi - X|_{\max}$, and R_{\max} are of order unity compared with the dimensions of the wing. The exponentials in the integral for the supersonic case may therefore be expanded in powers of k provided

$$k \ll 1 \quad \text{and} \quad k \ll \left| \frac{\beta^2}{M^2} \right|$$

This establishes the inequality given by equation (3.2-98). For the subsonic case, however, it is not clear whether the exponential terms can be expanded in powers of k . The question arises because of the infinite lower limit of the outer integral, equation (3.2-99).

Following the analysis of reference 3-5, the integral for subsonic flow is separated into two parts as follows:

$$\phi^* = \int_{-\infty}^{x-X_0} H(\xi, y, z; k, M) e^{ik(\xi-x)} d\xi + \int_{x-X_0}^x H(\xi, y, z; k, M) e^{ik(\xi-x)} d\xi \quad (3.2-101)$$

where H represents the surface integral in equation (3.2-99). The intervals of integration are shown by figure 3.2-9. The distance X_0 is chosen such that the first integral, referred to in the following as ϕ_{∞}^* , becomes an integration from $-\infty$ to a point some chord lengths ahead of the thin body surface S_W . The second integral, termed ϕ_W^* , is confined to the region occupied by the thin body surface.

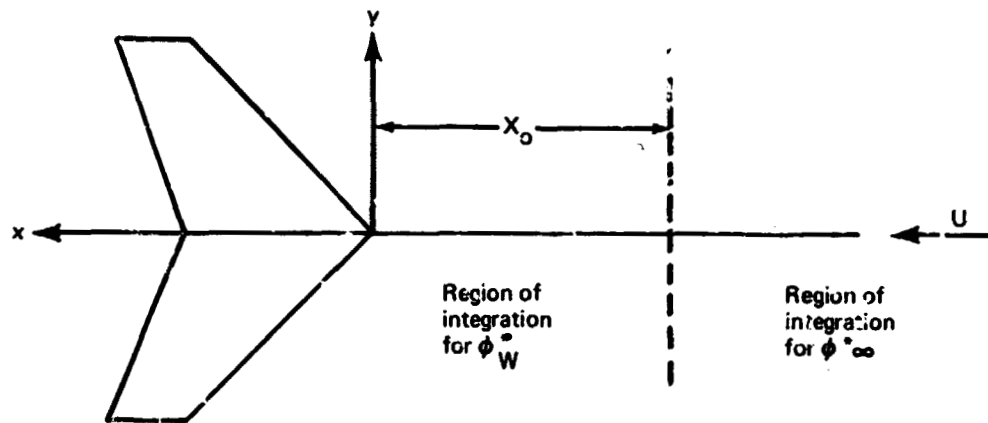


FIGURE 3.2-9.—REGIONS OF INTEGRATION FOR SUBSONIC VELOCITY POTENTIAL

Referring to equation (3.2-99), it is seen that the exponential term in ϕ_W^* may be expanded in powers of k provided

$$k \ll 1 \quad \text{and} \quad k \ll |\beta^2/M_1|$$

This establishes the inequality given by equation (3.2-97).

The contribution to the potential ϕ^* from the far field ahead of the thin body, viz., ϕ_{∞}^* , is approximated by introducing the following assumptions:

$$\beta^2 (y-Y_1)^2 + \beta^2 Z^2 \ll (\xi-X_1)^2$$

and

$$(\xi-X_1)^2 \approx (\xi-X)^2.$$

(3.2-102)

These expressions state analytically the assumption that the potentials are to be evaluated in the region of the thin body and, thus, over a region having dimensions which are small by comparison with X_0 . Performing the differentiation indicated in equation (3.2-99) and introducing the assumptions of equation (3.2-102), the potential ϕ_{∞}^* becomes

$$\begin{aligned} \phi_{\infty}^* &\approx \frac{Z}{4\pi} \iint_{S_W} \gamma(X_1, Y_1) dX_1 dY_1 \\ &\times \int_{-\infty}^{x-X_0} \frac{ikM(x-\xi) + \beta^2}{(x-\xi)^3} e^{-i[k/(1-M)](x-\xi)} d\xi \end{aligned}$$

(3.2-103)

For small reduced frequencies the last integral in equation (3.2-103) becomes

$$\begin{aligned} &\int_{-\infty}^{x-X_0} \frac{ikM(x-\xi) + \beta^2}{(x-\xi)^3} e^{-i[k/(1-M)](x-\xi)} d\xi \\ &= \frac{\beta^2}{2X_0} - i\frac{k}{X_0} + \frac{1}{2}k^2 \ln k + (\text{terms of order } k^2 \text{ and higher}) \end{aligned}$$

(3.2-104)

The relative magnitudes of these terms, however, cannot be established without relating the magnitude of X_0 to the dimensions of the surface S_W .

The magnitude of X_0 is implied by the first of the assumptions listed as equation (3.2-102). Clearly,

$$(\xi-X_1)_{\min} \approx X_0$$

(3.2-105)

Also, since all dimensions are referred to the reference length \bar{c} by having defined $k = \bar{\omega}\bar{c}\beta$, it follows that, when the reference length is taken to be the mean wing chord, a relationship in terms of aspect ratio is found, viz.,

$$\beta^2 (y-Y_1)^2_{\max} \approx \beta^2 (AR)^2.$$

(3.2-106)

Combining equations (3.2-102) with equations (3.2-105) and (3.2-106) leads to the following inequality:

$$\beta AR \ll X_0 \quad (3.2-107)$$

In obtaining the restriction of equation (3.2-97), however, it was assumed that the distance X_0 has the order of magnitude unity. Thus, the expansion of ϕ_{∞}^* given by equation (3.2-104) can only be valid for very small aspect ratios. Assuming $\beta AR \ll 1$, the first real and imaginary terms in the expansion of ϕ_{∞}^* are dominant for $k \ll 1$ and the term $1/2k^2 \ln k$ and all higher order terms in k may be neglected.

The analysis does not provide a reliable estimate of the validity of the first order in frequency approximation for thin bodies having an aspect ratio of order unity or larger. In these cases the expansion of ϕ_{∞}^* shows that the first real term, viz., $\beta^2 2X_0^2$, is of order unity or smaller and, thus, leads to conjecture regarding the admissible magnitude of the term $1/2k^2 \ln k$. The introduction of larger aspect ratios, however, violates the assumptions leading to the inequality expressed by equation (3.2-97), and the magnitude of ϕ_W^* relative to that of ϕ_{∞}^* becomes uncertain as well.

Experience with the method has shown that it gives reliable results for wings of aspect ratio less than 7 in subsonic flow, figures 3.2-10 and 3.2-11. No systematic effort, however, has been carried out to establish the limits of validity for larger aspect ratios. Figure 3.2-10 shows results for a circular wing, $AR = 0.785$, undergoing unsteady pitch oscillations at $M = 0, 0.5$, and 0.9 . The results are in terms of the real and imaginary parts of the lifting pressure. The discontinuous pressure distribution was computed using the low frequency approximation evaluated by the numerical method contained in the FLEXSTAB system, while the continuous distributions were obtained by evaluating equation (3.2-12) using the method of reference 3-6. Figure 3.2-11 shows similar results for the Boeing SST wing planform, $AR = 2.6$ at $M = 0.8$. The comparisons shown by figures 3.2-10 and 3.2-11 indicate that the low frequency approximation is valid for low and moderate aspect ratios. A complete evaluation of the approximation's limitations, however, requires a parametric study involving at least aspect ratio, Mach number, and reduced frequency.

3.3 FORMULATION AS A SYSTEM OF INTEGRAL EQUATIONS

The theoretical development of section 3.2 has led to a system of linear boundary value problems, summarized in section 3.2.7. Solutions to these boundary value problems are numerically evaluated by the FLEXSTAB system. They are constructed in this section in the form of a system of integral equations. The numerical evaluation method—applied to the system of integral equations—is derived in section 3.4.

The solution to the aerodynamic problem is the sum of the velocity potentials $\epsilon_i \phi_i$, equation (3.2-10). Each of these velocity potentials is a linear combination of the functions $\phi_H(x, y, z; -\Psi_H)$, which are solutions to linear boundary value problems, section 3.2.7. The boundary value problems are all of the same form, consisting of the classical steady flow equation and boundary conditions of the type encountered in steady aerodynamic problems.

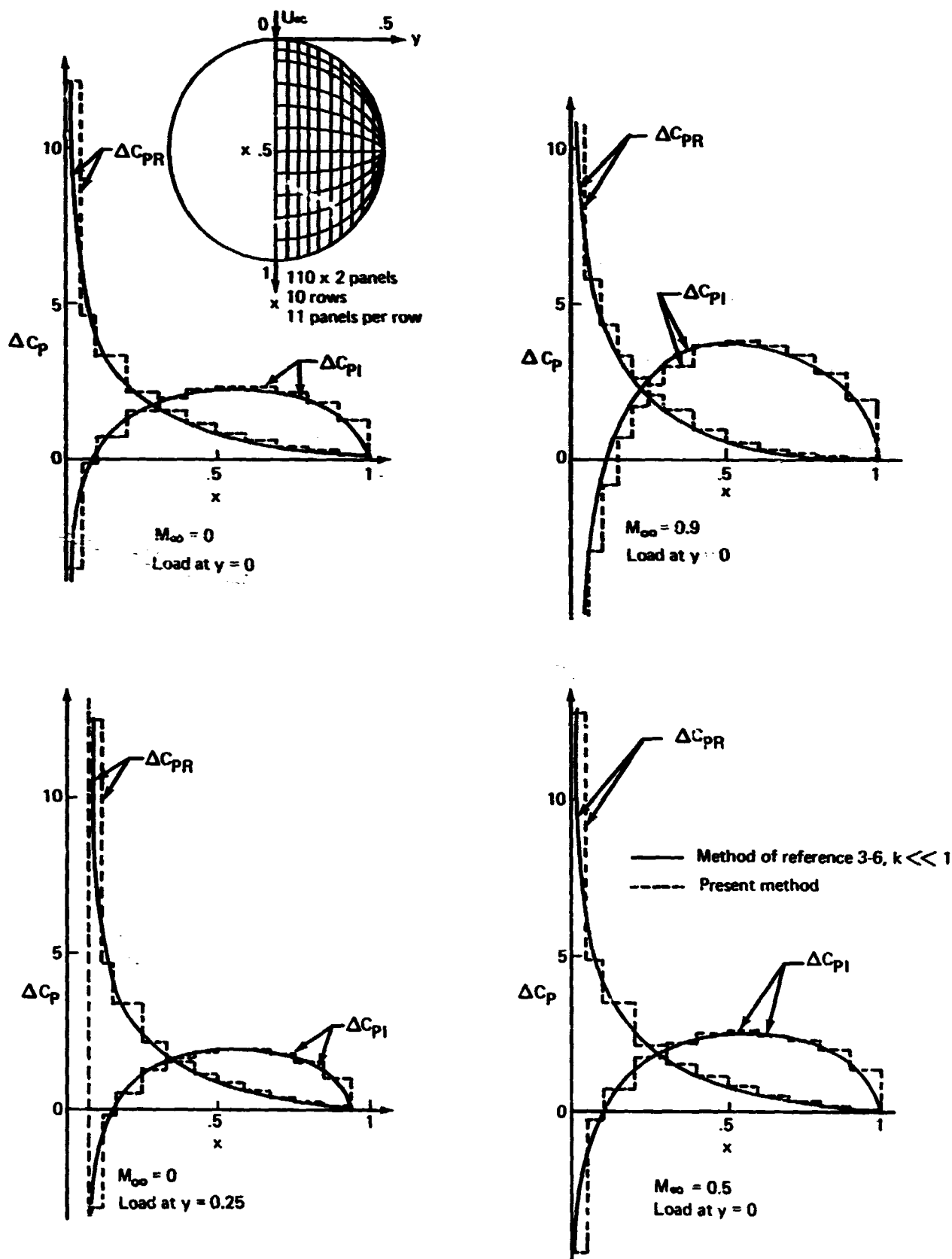


FIGURE 3.2-10.—COMPLEX AERODYNAMIC LOAD ON CIRCULAR WING OSCILLATING IN PITCH ABOUT MIDCHORD

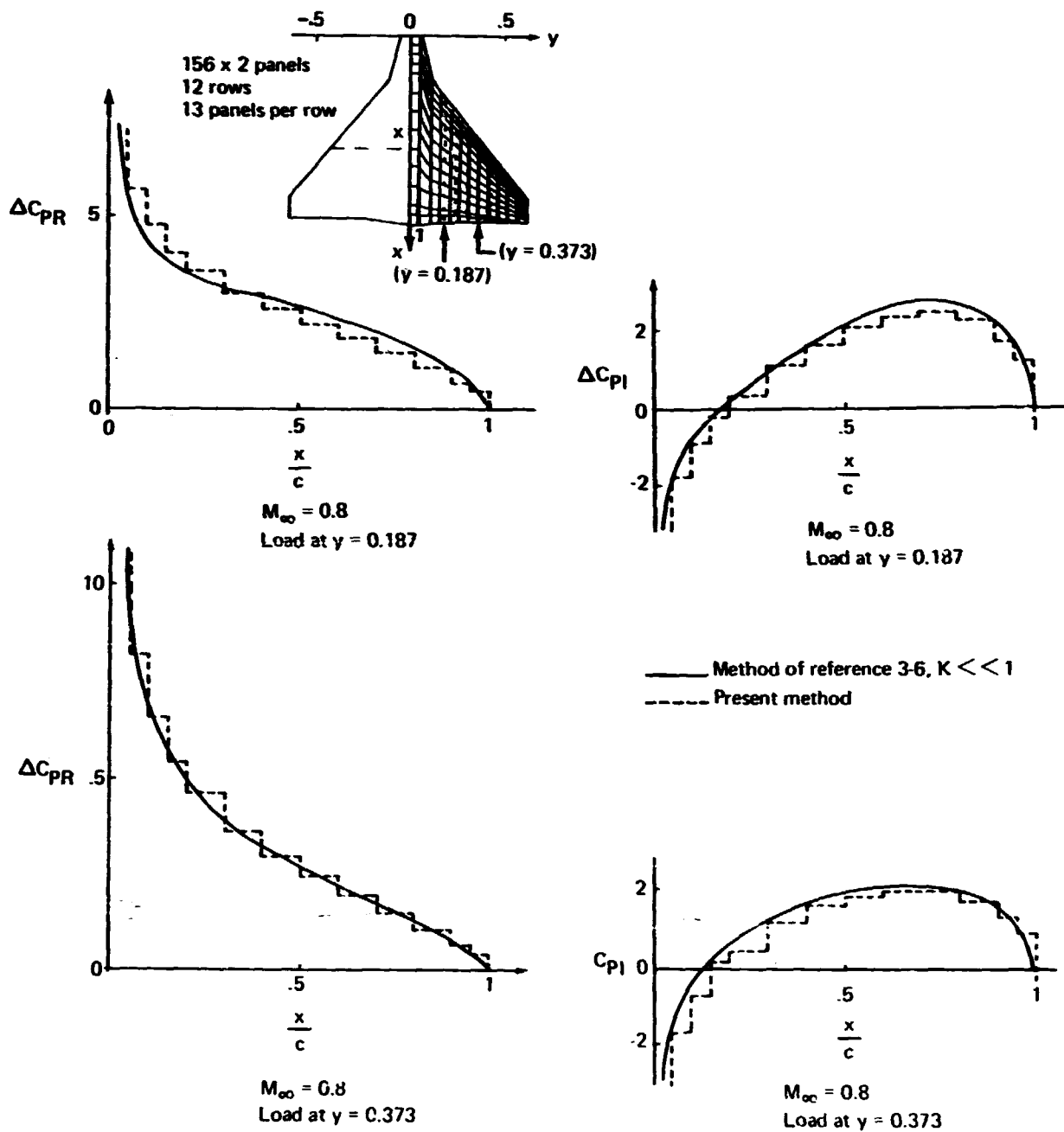


FIGURE 3.2-11.—COMPLEX AERODYNAMIC LOAD ON SST WING OSCILLATING IN PITCH ABOUT MIDCHORD

Following the usual approach, the solutions to these boundary value problems are formulated as integral equations involving integrals of distributions of flow singularities (i.e., sources, doublets, and vorticities) on or interior to the surfaces where the boundary conditions are specified. The aerodynamic problem then becomes one of finding the strengths of the distributions such that the potentials ϕ_H , represented by the integral equations, satisfy the boundary conditions.

Section 3.3.1 describes the general approach taken wherein the integral equations are reduced to integrals on only the mean surfaces of the thin and slender bodies of a configuration. In section 3.3.2, each of the boundary value problems is separated into two parts. One part is a boundary value problem governing the flow about a configuration component isolated in an undisturbed freestream. The second part is a boundary value problem governing the effects of interference. Finally, in section 3.3.3, integral equations governing the aerodynamic surface pressures are derived.

3.3.1 General Approach

3.3.1.1 Formulation as an integral equation.—As shown by reference 2-3 and most theoretical aerodynamics texts, a solution to the homogeneous form of the flow equation, i.e.,

$$\beta^2 (\phi_H)_{xx} + (\phi_H)_{yy} + (\phi_H)_{zz} = 0,$$

in the flow field V enclosed by the surface S can be expressed by the following integral equation:

$$\begin{aligned} \phi_H(x, y, z) = & \iint_S [m(\xi, \eta, \zeta) K^S(x, y, z; \xi, \eta, \zeta) \\ & + \mu(\xi, \eta, \zeta) K^{nD}(x, y, z; \xi, \eta, \zeta)] ds \end{aligned} \quad (3.3-1)$$

where the functions K^S and K^{nD} are, respectively, the expressions for unit sources and doublets located at points ξ, η, ζ on the enclosing surface S' and are given as follows:

Unit source:

$$\begin{aligned} K^S &= -\frac{1}{4\pi} \frac{1}{R} \quad \text{for } M < 1 \\ &= -\frac{1}{2\pi} \frac{1}{R} \quad \text{for } M > 1 \end{aligned} \quad (3.3-2)$$

Unit doublet with axis along the surface normal n :

$$\begin{aligned} K^{nD} &= -\frac{1}{4\pi} \frac{\partial}{\partial n} \left(\frac{1}{R} \right) \quad \text{for } M < 1 \\ &= -\frac{1}{2\pi} \frac{\partial}{\partial n} \left(\frac{1}{R} \right) \quad \text{for } M > 1 \end{aligned} \quad (3.3-3)$$

where

$$R \equiv \sqrt{(x-\xi)^2 + \beta^2[(y-\eta)^2 + (z-\zeta)^2]}$$

The functions $m(\xi, \eta, \zeta)$ and $\mu(\xi, \eta, \zeta)$ specify the strengths of the sources and doublets distributed on S , and a solution to a boundary value problem involving the homogeneous flow equation is constructed by finding the functions m and μ so that ϕ_H satisfies boundary conditions specified everywhere on S .

From section 3.2.7 it is seen that the solution to the Wing-Body Problem, ϕ , given by equation (3.2-91), is the sum of 7 solutions to the homogeneous flow equation. Each of these solutions must satisfy boundary conditions on the mean surfaces of the thin and slender body, $S_W + S_B$, and on the wake surface, W . In addition, the potential ϕ must vanish or remain finite at large distances from the wing-body combination, i.e., on the surface Σ shown by figure 3.3-1. The surface $S_W + S_B + W + \Sigma$, where the boundary conditions are specified, completely encloses the flow field V surrounding the aircraft; hence, each of the boundary value problems which must be solved is of the form which may be solved by solving the integral equation expressed by equation (3.3-1).

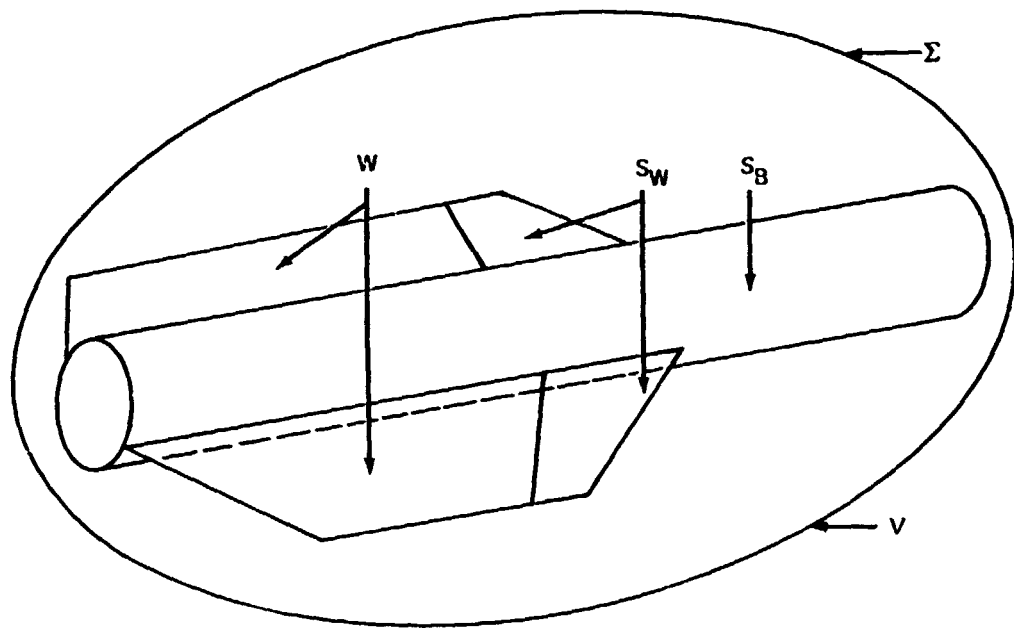


FIGURE 3.3-1.—SURFACES SURROUNDING THE FLOW FIELD

3.3.1.2 Reduction to an integral on the mean surfaces of thin and slender bodies. - There are an indefinite number of different distributions, m and μ , which, when substituted into equation (3.3-1), yield a potential satisfying specific boundary conditions on S . Since the boundary conditions do not determine the distributions uniquely, various arrangements of the distributions may be considered for any one boundary value problem and the analyst is free to

choose an arrangement which appears to offer computational advantages. The arrangement chosen for the FLEXSTAB system is essentially that of reference 1-1 wherein the integral equation, equation (3.3-1), is reduced to an integral on the mean surfaces of thin and slender bodies alone.

The reduction of the integral equation is achieved from a consideration of three characteristics of the boundary conditions and the elementary, singular solutions. First, it is noted that the boundary conditions require that ϕ vanish on the surface Σ in subsonic flow, while in supersonic flow ϕ must vanish on certain portions of Σ and must be determined on the remaining portions of Σ by the distributions on $S_W + S_B + W$. The functions m and μ are therefore set to zero on Σ , leading to

$$\phi_H = \iint_{S_W + S_B + W} (mK^S + \mu K^{nD}) dS$$

Second, sources produce only a symmetric flow disturbance inappropriate to the wake; hence, m is set to zero on W leading to

$$\phi_H = \iint_{S_W + S_B} mK^S dS + \iint_{S_W + S_B + W} \mu K^{nD} dS$$

Third, the integral of the doublets on the wake surface is removed from direct consideration by considering the doublet distribution to be made up of line doublets, i.e., lines of unit doublets lying parallel to the X-axis. These line doublets yield a discontinuity in $\partial\phi/\partial x$ at their ends; and, since the wake boundary condition requires this quantity to be continuous on W , the line doublets are originated on the mean surfaces and extend to infinity in the positive X-direction. As shown by equation (5-35) of reference 2-3, the potential due to these line doublets may be expressed as follows:

$$K^V(x, y, z; \xi, \eta, \zeta) \equiv \int_{\xi}^{\infty} K^{nD}(x, y, z; \xi', \eta, \zeta) d\xi' \quad (3.3-4)$$

where K^V is recognized as the perturbation potential due to an elementary horseshoe vortex of unit strength with bound element located at ξ, η, ζ . Using this result to replace all doublet distributions by distributions of vorticity, the integral equation reduces to

$$\begin{aligned} \phi_H(x, y, z) = & \iint_{S_W + S_B} [m(\xi, \eta, \zeta) K^S(x, y, z; \xi, \eta, \zeta) \\ & + \gamma(\xi, \eta, \zeta) K^V(x, y, z; \xi, \eta, \zeta)] dS \end{aligned} \quad (3.3-5)$$

where $\gamma(\xi, \eta, \zeta)$ is the strength of the vorticity distribution on $S_W + S_B$. Equation (3.3-5) constitutes the desired result—an integral equation in terms of distributions on the surface $S_W + S_B$ alone.

3.3.2 Method of Solution for Individual Flow Problems

Each of the individual flow problems, which are solved in constructing the solution to the aerodynamic problem for a configuration, section 3.2.7, is solved in two steps. Each boundary condition among equations (3.2-97) involving non-zero flow incidence on one of the surfaces S_W or S_B is solved assuming the surface to be isolated from the remainder of the configuration, i.e., ignoring the effects of interference. These isolated thin and slender body solutions yield an interference flow incidence denoted as Ψ_i^{int} at the mean surfaces. This interference flow is suppressed by a vorticity distribution at the mean surfaces determined by the expression

$$\Psi_i^{int} = \iint_{S_W + S_B} \gamma_i^{int} \frac{\partial K^V}{\partial n} dS \quad (3.3-6)$$

Letting the vorticity and source distributions required to satisfy the isolated flow problem be denoted as

$$\gamma_i^{iso} \quad \text{and} \quad m_i^{iso}, \quad (3.3-7)$$

the solution to the problem including the effects of interference is given by

$$\begin{aligned} \phi_H(x, y, z; -\Psi_i) = \iint_{S_W + S_B} [(\gamma_i^{int} + \gamma_i^{iso}) K^V \\ + m_i^{iso} K^S] dS \end{aligned} \quad (3.3-8)$$

The problem given by equation (3.3-6) and solved to determine Ψ_i^{int} is termed the aerodynamic induction problem.

This approach is applied to each of the following problems:

- Isolated thin body thickness (section 3.3.2.1)
- Isolated thin body steady lift (section 3.3.2.2)
- Isolated slender body thickness (section 3.3.2.3)
- Isolated slender body steady lift (section 3.3.2.4)
- Steady aerodynamic induction (section 3.3.2.5)
- Isolated thin body unsteady lift (section 3.3.2.6)
- Isolated slender body unsteady lift (section 3.3.2.7)
- Unsteady aerodynamic induction (section 3.3.2.8)

This development is applicable to arbitrary configurations, not just the Wing-Body Problem. Equations (3.3-6) through (3.3-7) take on the appropriate meaning by letting S_W and S_B represent the total surface area of the mean surfaces of any number of thin and slender bodies, i.e.,

$$S_W = \sum_{I=1}^N S_{WI} \quad (3.3-9)$$

and

$$S_B = \sum_{J=1}^M S_{BJ} \quad (3.3-10)$$

where S_{WI} is the mean surface of the I^{th} thin body and S_{WJ} is the mean surface of the J^{th} slender body.

3.3.2.1 Isolated thin body thickness problem.—The isolated thickness problem for a thin body is discussed in detail in sections 7-2 and 8-2 of reference 2-3. The thickness shape of the i^{th} thin body is given by equation 3.2-12 as follows:

$$Z_I = \tau_I F_I(X_I, Y_I) \quad (3.3-11)$$

in the local axis system of the body. The problem consists of finding the source distribution $m(X_I, Y_I)$ on the mean surface such that the potential

$$\phi_{WI}^S(X_I, Y_I, Z_I) = \iint_{S_{WI}} m(X'_I, Y'_I) K^S(X_I, Y_I, Z_I; X'_I, Y'_I) dX'_I dY'_I \quad (3.3-12)$$

satisfies the boundary condition, equation (3.2-42c),

$$\frac{\partial \phi_{WI}^S}{\partial Z_I} = \pm \tau_I \frac{\partial F_I}{\partial X_I} \quad (3.3-13)$$

on the mean surface of the I^{th} thin body.

As shown by reference 2-3, it follows directly from the properties of the source distribution that the required distribution is

$$m(X_I, Y_I) = \frac{1}{2} \tau_I \frac{\partial F_I}{\partial X_I}(X_I, Y_I). \quad (3.3-14)$$

The solution to the isolated thickness problem for the I^{th} thin body now follows directly as

$$\phi_{WI}^S(X_I, Y_I, Z_I) = \frac{\tau_I}{2} \iint_{S_{WI}} \frac{\partial F_I}{\partial X_I}(X'_I, Y'_I) K^S(X_I, Y_I, Z_I; X'_I, Y'_I) dX'_I dY'_I \quad (3.3-15)$$

3.3.2.2 Isolated thin body steady lifting problem.—In the FLEXSTAB system the steady lifting problem for both subsonic and supersonic flow is solved by finding the appropriate vorticity distribution on the mean surface of the thin body essentially as shown by section 7-3 of reference 2-3, for subsonic flow. The integral equation appears as

$$\phi_{WI}^V(X_I, Y_I, Z_I) = \iint_{S_{WI}} \gamma_O(X'_I, Y'_I) K^V(X_I, Y_I, Z_I; X'_I, Y'_I) dX'_I dY'_I \quad (3.3-16)$$

and the problem consists of finding the vorticity distribution $\gamma(X_I, Y_I)$ such that the potential $\phi_{WI}(X_I, Y_I, Z_I)$ satisfies the thin body surface boundary conditions, equations (3.2-42):

$$\begin{aligned} \frac{\partial \phi_{WI}}{\partial Z_I} &= \hat{W}\lambda_w(t) \cos \theta_I - \hat{V}\lambda_v(t) \sin \theta_I + \theta \lambda_\theta(t) \frac{\partial H}{\partial X_I} \\ &\equiv -\psi_{WI}^V \end{aligned} \quad (3.3-17)$$

on the mean surface S_{WI} for a specified instant of time t , i.e., by solving the integral equation

$$\begin{aligned} \iint_{S_{WI}} \gamma_O(X'_I, Y'_I) \frac{\partial K^V}{\partial Z_I} dX'_I dY'_I &= \hat{W}\bar{W}\lambda_w \cos \theta_I \\ &- \hat{V}\bar{V}\lambda_v \sin \theta_I + \theta \lambda_\theta(t) \frac{\partial H}{\partial X_I} \end{aligned} \quad (3.3-18)$$

for $\gamma_O(X_I, Y_I)$. Substituting the resulting vorticity distribution into equation (3.3-16) yields the desired solution.

3.3.2.3 Isolated slender body thickness problem.—The isolated slender body thickness problem is formulated in the FLEXSTAB system using the boundary conditions of classical slender body theory derived in sections 9.13 and 9.14 of reference 3-7. The slender body thickness boundary condition, given by equation (3.2-42e), is therefore replaced by the following boundary condition:

$$a \frac{\partial \phi_s}{\partial r} = a \frac{dR}{dX_J} (1 + a \frac{\partial \phi_s}{\partial x}) \quad (3.3-19)$$

on the surface S'_{BJ} of an equivalent body of revolution about the mean centerline, figure 3.3-2, where r is the cylindrical coordinate normal to the mean centerline.

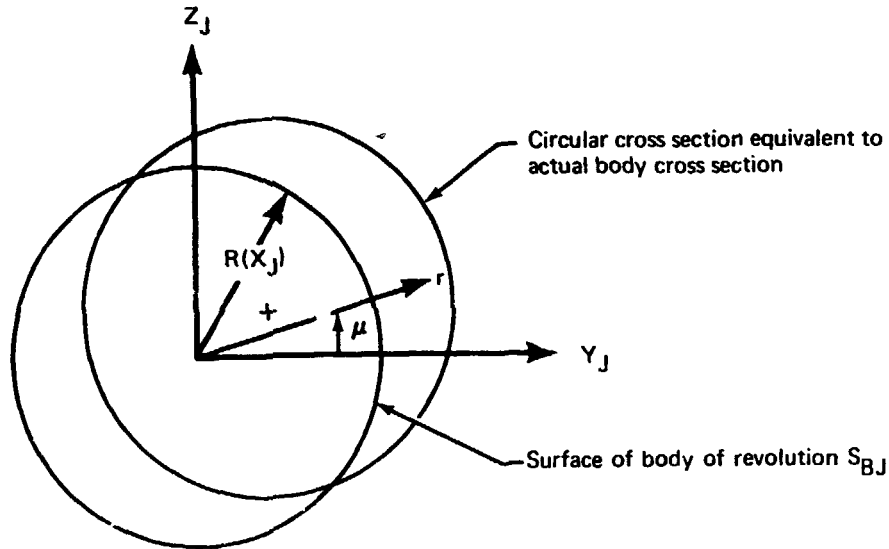


FIGURE 3.3-2.—SLENDER BODY CROSS SECTION
FOR CLASSICAL SLENDER BODY THEORY

The effects of slender body thickness are represented by sources distributed along the mean centerline; thus the perturbation velocity induced by thickness of the J^{th} slender body is given by

$$\phi_{BJ}^S(X_J, Y_J, Z_J) = \int_{L_{BJ}} m(X'_J) K^S(X_J, Y_J, Z_J; X'_J) dX'_J \quad (3.3-20)$$

where L_{BJ} is the length of the slender body centerline. The distribution $m(X'_J)$ is determined by requiring ϕ_{BJ}^S to satisfy equation (3.3-19) on S'_{BJ} , i.e., by solving the integral equation

$$\int_{L_{BJ}} m(X'_J) \left[\frac{\partial K^S}{\partial r} - a \frac{dR}{dX_J} \frac{\partial K^S}{\partial x} \right] dX'_J = a \frac{dR}{dX_J} \quad (3.3-21)$$

for $m(X'_J)$. Substituting the resulting source distribution into equation (3.3-20) yields the desired solution.

3.3.2.4 Isolated slender body steady lifting problem.—As in section 3.3.2.3, the isolated slender body steady lifting problem is formulated using the boundary conditions of classical slender body theory. The boundary conditions given by equations (3.2-42a,b,e,f) are replaced by the following boundary conditions on the surface S_{BJ} shown by figure 3.3-2:

$$\hat{w} \frac{\partial \phi_1}{\partial r} = \hat{w} \lambda_w(t) \sin \mu \quad (a)$$

$$\hat{v} \frac{\partial \phi_2}{\partial r} = \hat{v} \lambda_v(t) \cos \mu \quad (b)$$

$$\hat{b} \frac{\partial \phi_6}{\partial r} = \hat{b} \lambda_b(t) \frac{\partial G_J}{\partial X_J} \cos \mu \quad (c) \quad (3.3-22)$$

$$\hat{c} \frac{\partial \phi_7}{\partial r} = \hat{c} \lambda_c(t) \frac{\partial I_J}{\partial X_J} \sin \mu \quad (d)$$

The solutions to these problems are expressed in terms of doublets distributed along the mean centerline of the body. Using the terminology of section 9.14 of reference 3-7, the problems posed by (a) and (d) represent a cross flow in the Z_J direction, while those posed by (b) and (c) represent a cross flow in the Y_J direction. The Z_J cross-flow problems have the solutions

$$\phi_{BJ}^{ZD}(X_J, Y_J, Z_J) = \int_{L_{BJ}} \mu_0^Z(X_J') K^{ZD}(X_J, Y_J, Z_J; X_J') dX_J' \quad (3.3-23)$$

while the Y_J cross-flow problems have the solutions

$$\phi_{BJ}^{YD}(X_J, Y_J, Z_J) = \int_{L_{BJ}} \mu_0^Y(X_J') K^{YD}(X_J, Y_J, Z_J; X_J') dX_J' \quad (3.3-24)$$

where, in the notation of equation (3.3-3),

$$\begin{aligned} K^{ZD} &\equiv -\frac{1}{4\pi} \frac{\partial}{\partial Z_J} \left(\frac{1}{R} \right) \quad \text{for } M < 1 \\ &\equiv -\frac{1}{2\pi} \frac{\partial}{\partial Z_J} \left(\frac{1}{R} \right) \quad \text{for } M > 1 \end{aligned} \quad (3.3-25)$$

and

$$\begin{aligned} K^{YD} &\equiv -\frac{1}{4\pi} \frac{\partial}{\partial Y_J} \left(\frac{1}{R} \right) \quad \text{for } M < 1 \\ &\equiv -\frac{1}{2\pi} \frac{\partial}{\partial Y_J} \left(\frac{1}{R} \right) \quad \text{for } M > 1 \end{aligned} \quad (3.3-26)$$

The integral equations which must be solved to determine the distributions $\mu_o^Z(X_J)$ and $\mu_o^Y(X_J)$ are as follows:

$$\int_{L_{BJ}} \mu_o^Z \frac{\partial K^{ZD}}{\partial Z_J} dX_J = \hat{w}\lambda_w(t)\bar{W} + \hat{c}\lambda_c(t)\frac{\partial I_J}{\partial X_J} \quad (3.3-27)$$

obtained by evaluating the coordinates μ, r as $\mu = \pi/2$ and $r = Z_J$, figure 3.3-2; and

$$\int_{L_{BJ}} \mu_o^Y \frac{\partial K^{YD}}{\partial Y_J} dX_J = \hat{v}\lambda_v(t)\bar{V} + \hat{b}\lambda_b(t)\frac{\partial G_J}{\partial X_J} \quad (3.3-28)$$

obtained by evaluating the coordinates μ, r as $\mu = 0$, and $r = Y_J$, figure 3.3.2. The isolated slender body steady lifting problem is solved by substituting the resulting doublet distributions into equations (3.3-23) and 3.3-24).

3.3.2.5 Steady aerodynamic induction problem.—Sections 3.3.2.1 through 3.3.2.4 give solutions to the aerodynamic problems posed by configuration components, viz., thin and slender bodies, when they are isolated from one another, ignoring mutual interference between the components. The effects of interference are accounted for in the aerodynamic induction problem, wherein vorticity is distributed on the mean surfaces of all the configuration components to account for the effects of interference. The solution to the problem is therefore given by the following integral equation:

$$\phi_{int}^V(x, y, z) = \iint_{S_W + S_B} \gamma_o^{int}(\xi, \eta, \zeta) K^V(x, y, z; \xi, \eta, \zeta) dS \quad (3.3-29)$$

where ξ, η, ζ is a point on a mean surface, $S_W + S_B$ is the total mean surface, and $\gamma_o(\xi, \eta, \zeta)$ is the vorticity induced by steady aerodynamic interference.

As noted in section 3.3.2, the vorticity appearing in equation (3.2-29) is that required to suppress interference flow induced at the mean surfaces. The interference flow at the mean surfaces is computed as a normal derivative of the potentials representing solutions to the isolated body problems. As an example, consider the solution to the isolated thickness problem for the I^{th} thin body, equation (3.3-15). The interference flow is found by evaluating

$$\psi_{WI}^t(X, Y, Z) = - \frac{\partial \phi_W^S}{\partial n} \quad (3.3-30)$$

at the mean surfaces of all bodies of a configuration except the I^{th} thin body. The resulting flow incidence is set equal in magnitude but opposite in sign to that induced by the vorticity of equation (3.3-29), i.e.,

$$\frac{\partial \phi_{WI}^S}{\partial n}(X, Y, Z) = - \iint_{S_W^+ \cup S_B} \gamma_O^{int}(\xi, \eta, \zeta) \frac{\partial K^V}{\partial n}(X, Y, Z; \xi, \eta, \zeta) dS \quad (3.3-31)$$

This integral equation is solved and the resulting vorticity distribution is substituted into equation (3.3-29). The resulting velocity potential is the solution to the aerodynamic induction problem governing the interference effects from isolated thickness of the l^{th} thin body.

The above operations are carried out for each isolated body problem associated with a configuration. The sum of the potentials for the isolated body problems and their corresponding aerodynamic induction problems constitutes a solution to the steady aerodynamic problem for a complete configuration.

3.3.2.6 Isolated thin body unsteady lifting problem.—The solutions to the unsteady flow problems are all of the form derived in section 3.2.6 and are given by equation (3.2-91), i.e.,

$$\begin{aligned} \epsilon_i \phi_i &= \phi_H(x, y, z; -\dot{\Psi}_i) + \frac{M^2}{\beta^2} [x \phi_H(x, y, z; -\dot{\Psi}_i/U) \\ &- \phi_H(x, y, z; -x \dot{\Psi}_i/U)] - \frac{1}{\beta^2} \left[\int_{-\infty}^x \phi_H(\xi, y, z; -\dot{\Psi}_i/U) d\xi \right. \\ &\quad \left. - \phi_H(x, y, z; \frac{1}{U} \int_{-\infty}^x \frac{\partial \dot{\phi}_H}{\partial z_I} d\xi) \right] \end{aligned} \quad (3.2-91)$$

In the case of the isolated thin body unsteady lifting problem, the first term of equation (3.2-91) represents the solution to the isolated thin body steady lifting problem of section 3.3.2.2, i.e.,

$$\phi_H(x, y, z; -\dot{\Psi}_{WI}^V) = \iint_{S_{WI}} \gamma_O(\hat{X}_I, \hat{Y}_I) K^V(x, y, z; \hat{X}_I, \hat{Y}_I) d\hat{X}_I d\hat{Y}_I \quad (3.3-32)$$

where

$$\dot{\Psi}_{WI}^V \equiv - \frac{\partial \phi_{WI}^V}{\partial z_I} \text{ on } S_{WI}$$

The remainder of the solution to the unsteady problem is represented in terms of three vorticity distributions on the thin body mean surface as follows:

$$\begin{aligned}
& \frac{M^2}{\beta^2} [\kappa \phi_H(x, y, z; -\dot{\Psi}_{WI}^V/U) - \phi_H(x, y, z; -\kappa \dot{\Psi}_{WI}^V/U)] \\
& - \frac{1}{\beta^2} \left[\int_{-\infty}^x H(\xi, y, z; -\dot{\Psi}_{WI}^V/U) - \phi_H(x, y, z; \frac{1}{U} \int_{-\infty}^x \frac{\partial \dot{\phi}_{WI}^V}{\partial Z_I} d\xi) \right] \\
& = \frac{M^2}{\beta^2} \left[\kappa \iint_{S_{WI}} \gamma_1(X_I', Y_I') K^V(x, y, z; X_I', Y_I') dX_I' dY_I' \right. \\
& \quad \left. - \iint_{S_{WI}} \gamma_2(X_I', Y_I') K^V(x, y, z; X_I', Y_I') dX_I' dY_I' \right] \\
& - \frac{1}{\beta^2} \left[\iint_{S_{WI}} \gamma_1(X_I', Y_I') K^V(\xi, y, z; X_I', Y_I') dX_I' dY_I' \right. \\
& \quad \left. - \iint_{S_{WI}} \gamma_3(X_I', Y_I') K^V(x, y, z; X_I', Y_I') dX_I' dY_I' \right]
\end{aligned} \tag{3.3-33}$$

The three vorticity distributions $\gamma_1, \gamma_2, \gamma_3$ are determined by solving the following three integral equations:

$$\begin{aligned}
-\frac{1}{U} \dot{\Psi}_{WI}^V &= \iint_{S_{WI}} \gamma_1 \frac{\partial K^V}{\partial Z_I} dS \\
-\frac{1}{U} \kappa \dot{\Psi}_{WI}^V &= \iint_{S_{WI}} \gamma_2 \frac{\partial K^V}{\partial Z_I} dS \\
\int_{-\infty}^x \iint_{S_{WI}} \gamma_1 \frac{\partial K^V}{\partial Z_I} dS d\xi &= \iint_{S_{WI}} \gamma_3 \frac{\partial K^V}{\partial Z_I} dS
\end{aligned} \tag{3.3-34}$$

The resulting vorticity distributions are then substituted into equation (3.3-33), thereby constructing the unsteady contribution to the isolated thin body lifting problem. The complete solution is obtained by combining equations (3.3-32) and (3.3-33) to obtain

$$\begin{aligned} \phi_{WI}^{UV} = & \iint_{S_{WI}} \gamma_0 K^V dS + \frac{M^2}{\beta^2} [x \iint_{S_{WI}} \gamma_1 K^V dS - \iint_{S_{WI}} \gamma_2 K^V dS] \\ & - \frac{1}{\beta^2} \left[\int_{-\infty}^x \iint_{S_{WI}} \gamma_1 K^V dS - \iint_{S_{WI}} \gamma_3 K^V dS \right] \end{aligned} \quad (3.3-35)$$

This result expresses the potential induced by the isolated thin body subjected to slowly varying flow incidence. Recalling equation (3.3-17), the solution is seen to depend on

$$\psi_{WI}^V = -\hat{w}_w(t) \bar{w} \cos \theta_I + \hat{v}_v(t) \bar{v} \sin \theta_I - \hat{\theta}_\theta(t) \frac{\partial H}{\partial X_I}$$

and

$$\frac{\partial \psi_{WI}^V}{\partial t} = -\hat{w} \frac{\partial \lambda_w(t)}{\partial t} \bar{w} \cos \theta_I + \hat{v} \frac{\partial \lambda_v(t)}{\partial t} \bar{v} \sin \theta_I - \hat{\theta} \frac{\partial \lambda_\theta(t)}{\partial t} \frac{\partial H}{\partial X_I} \quad (3.3-36)$$

3.3.2.7 Isolated slender body unsteady lifting problem.—In the case of the slender body, the general form for solution to the unsteady problems, equation (3.2-92), may be simplified. The solution to the steady component of the flow problem, section 3.3.2.4, induces a continuous velocity potential at the wake surface; hence, the wake boundary condition for the first-order unsteady problem, equation (3.2-53), reduces to

$$[(\phi_{BJ}^D)_x^{(1)}] = 0 \text{ on } W$$

Because of this simplification, the third homogeneous term in the solution to the first-order problem, equation (3.2-89), may be deleted. The form of the solution to the unsteady isolated slender body lifting problem is given by equation (3.2-92) with the final terms in brackets deleted, i.e.,

$$\begin{aligned} \phi_{BJ}^D = & \phi_H(x, y, z; -\psi_{BJ}^D) + \frac{M^2}{\beta^2} [x \phi_H(x, y, z; -\dot{\psi}_{BJ}^D/U) \\ & - \phi_H(x, y, z; -x \dot{\psi}_{BJ}^D/U)] \end{aligned} \quad (3.3-37)$$

where the first term is the steady flow solution of section 3.3.2.4.

The unsteady flow problem is separated into cross-flow problems in the Y_J and Z_J directions as in the case of steady flow, section 3.3.2.4, with the boundary conditions expressed as

$$\begin{aligned}
 \Psi_{BJ}^{YD} &\equiv -\frac{\partial}{\partial r}(\phi_{BJ}^{YD}) = -\hat{v}\lambda_v(t)\bar{V} \cos\mu - \hat{b}\lambda_b(t)\frac{\partial G_J}{\partial X_J} \cos\mu \\
 \dot{\Psi}_{BJ}^{YD} &\equiv -\frac{\partial^2}{\partial t \partial r}(\phi_{BJ}^{YD}) = -\hat{v}\frac{\partial \lambda_v(t)}{\partial t} \bar{V} \cos\mu - \hat{b}\frac{\partial \lambda_b(t)}{\partial t} \frac{\partial G_J}{\partial X_J} \cos\mu \\
 \Psi_{BJ}^{ZD} &\equiv -\frac{\partial}{\partial r}(\phi_{BJ}^{ZD}) = -\hat{w}\lambda_w(t)\bar{W} \sin\mu - \hat{c}\lambda_c(t)\frac{\partial I}{\partial X_J} \sin\mu \\
 \dot{\Psi}_{BJ}^{ZD} &\equiv -\frac{\partial^2}{\partial t \partial r}(\phi_{BJ}^{ZD}) = -\hat{w}\frac{\partial \lambda_w(t)}{\partial t} \bar{W} \sin\mu - \hat{c}\frac{\partial \lambda_c(t)}{\partial t} \frac{\partial I}{\partial X_J} \sin\mu
 \end{aligned} \tag{3.3-38}$$

It is noted that these expressions are evaluated at the surface of the body of revolution shown by figure 3.3-2. The solutions are then given by

$$\begin{aligned}
 \phi_{BJ}^{YD} &= \int_{L_{BJ}} \mu_0^Y(X_J') K^{YD}(X_J, Y_J, Z_J; X_J') dX_J' \\
 &\quad + \frac{M^2}{\beta^2} [X_J \int_{L_{BJ}} \mu_1^Y(X_J') D^{YD}(X_J, Y_J, Z_J; X_J') dX_J' \\
 &\quad - \int_{L_{BJ}} \mu_2^Y(X_J') K^{YD}(X_J, Y_J, Z_J; X_J') dX_J']
 \end{aligned} \tag{3.3-39}$$

where the doublet distributions μ_1^Y and μ_2^Y are required to satisfy the integral equations

$$\begin{aligned}
 \dot{\Psi}_{BJ}^{YD} &= -\int_{L_{BJ}} \mu_1^Y \frac{\partial K^{YD}}{\partial r} dX_J' \\
 X_J \dot{\Psi}_{BJ}^{YD} &= -\int_{L_{BJ}} \mu_2^Y \frac{\partial K^{YD}}{\partial r} dX_J'
 \end{aligned} \tag{3.3-40}$$

and

$$\begin{aligned}
 \phi_{BJ}^{ZD} = & \int_{L_{BJ}} \mu_0^Z(x_J') K^{ZD}(x_J, y_J, z_J; x_J') dx_J' \\
 & + \frac{M^2}{\beta^2} [x_J \int_{L_{BJ}} \mu_1^Z(x_J') K^{ZD}(x_J, y_J, z_J; x_J') dx_J' \\
 & - \int_{L_{BJ}} \mu_2^Z(x_J') K^{ZD}(x_J, y_J, z_J; x_J') dx_J']
 \end{aligned} \quad (3.3-41)$$

and where the doublet distributions μ_1^Z, μ_2^Z are required to satisfy the integral equations

$$\begin{aligned}
 \dot{\Psi}_{BJ}^{ZD} &= - \int_{L_{BJ}} \mu_1^Z \frac{\partial K^{ZD}}{\partial r} dx_J' \\
 x_J \dot{\Psi}_{BJ}^{ZD} &= - \int_{L_{BJ}} \mu_2^Z \frac{\partial K^{ZD}}{\partial r} dx_J'
 \end{aligned} \quad (3.3-42)$$

The solution is constructed by determining the doublet distributions satisfying the integral equations, equations (3.3-40) and (3.3-42), and substituting the results into equations (3.3-39) and (3.3-41).

3.3.2.4 Unsteady aerodynamic induction problem.—The effects of unsteady interference flow are accounted for in the solution to the unsteady aerodynamic induction problem. As in the case of steady interference, section 3.3.2.5, the solution is expressed in terms of vorticity distributed on the mean surfaces of all components of a configuration. The form of the solution is given by equation (3.2-92); hence, in terms of vorticity on the mean surfaces, the solution is given by

$$\begin{aligned}
 \phi_{int}^{UV}(x, y, z) = & \iint_{S_W + S_B} \gamma_0^{int}(\xi, \eta, \zeta) K^V(x, y, z; \xi, \eta, \zeta) dS \\
 & + \frac{M^2}{\beta^2} [x \iint_{S_W + S_B} \gamma_1^{int}(\xi, \eta, \zeta) K^V(x, y, z; \xi, \eta, \zeta) dS -
 \end{aligned}$$

$$\begin{aligned}
& - \iint_{S_W + S_B} \gamma_2^{\text{int}}(\xi, \eta, \zeta) K^V(x, y, z; \xi, \eta, \zeta) dS] \\
& + \frac{1}{\beta^2} \left[\int_{-\infty}^x \iint_{S_W + S_B} \gamma_1^{\text{int}}(\xi, \eta, \zeta) K^V(\xi, y, z; \xi, \eta, \zeta) dS d\xi \right. \\
& \left. - \iint_{S_W + S_B} \gamma_3^{\text{int}}(\xi, \eta, \zeta) K^V(x, y, z; \xi, \eta, \zeta) dS \right] \quad (3.3-43)
\end{aligned}$$

where the interference vorticity distributions are required to satisfy the unsteady interference boundary conditions generated from the isolated body solutions of sections 3.3.2.6 and 3.3.2.7. For the example of unsteady cross flow in the Z_j direction, the integral equations are as follows:

$$\begin{aligned}
\frac{1}{U} \frac{\partial^2 \phi_{BJ}^{ZD}}{\partial t \partial n} &= \iint_{S_W + S_B} \gamma_1^{\text{int}} \frac{\partial K^V}{\partial n} dS \\
\frac{X}{U} \frac{\partial^2 \phi_{BJ}^{ZD}}{\partial t \partial n} &= \iint_{S_W + S_B} \gamma_2^{\text{int}} \frac{\partial K^V}{\partial n} dS \quad (3.3-44) \\
\int_{-\infty}^x \iint_{S_W + S_B} \gamma_1^{\text{int}} \frac{\partial K^V}{\partial n} dS &= \iint_{S_W + S_B} \gamma_3^{\text{int}} \frac{\partial K^V}{\partial n} dS
\end{aligned}$$

Integral equations of the type shown by equation (3.3-44) are solved for each of the isolated body unsteady flow problems, and the interference problem for a complete configuration is solved by substituting the combined interference vorticity distribution into equation (3.3-43).

3.3.3 Integral Equations Describing the Aerodynamic Surface Pressure

The first-order approximation to the aerodynamic pressure is given by equation (3.2-29) (or in compact notation, equation (3.2-93)), and is related to the flow incidence prescribed by the boundary conditions by combining equations (3.2-91) and (3.2-93) to find

$$\begin{aligned}
C_p(x, y, z; \Psi, \dot{\Psi}_i/U) = & -2\{\phi_{H_x}(x, y, z; -\Psi_i) \\
& + \frac{M^2}{\beta^2}[\chi\phi_{H_x}(x, y, z; -\dot{\Psi}_i/U) - \phi_{H_x}(x, y, z; -x\dot{\Psi}_i/U)] \\
& + \frac{1}{\beta^2}\phi_{H_x}(x, y, z; \int_{-\infty}^x \frac{\partial \phi_H}{\partial n}(\xi, y, z; -\dot{\Psi}_i/U) d\xi)\}
\end{aligned} \tag{3.3-45}$$

or for the case of steady flow

$$C_p(x, y, z; \Psi_i) = -2\phi_{H_x}(x, y, z; -\Psi_i)$$

When the low frequency approximation is applied to the problem of an isolated slender body in unsteady flow, a case in which there is no wake, the unsteady pressure coefficient is given by

$$\begin{aligned}
C_p(x, y, z; \Psi_i, \dot{\Psi}_i/U) = & -2\{\phi_{H_x}(x, y, z; -\Psi_i) \\
& + \frac{M^2}{\beta^2}[\chi\phi_{H_x}(x, y, z; -\dot{\Psi}_i/U) - \phi_{H_x}(x, y, z; -x\dot{\Psi}_i/U)] \\
& + \frac{1}{\beta^2}\phi_H(x, y, z; -\dot{\Psi}_i/U)\}
\end{aligned} \tag{3.3-46}$$

For the case of an isolated slender body in steady flow, the induced pressure coefficient is given by equation (3.3-45). The aerodynamic surface pressure is found simply by evaluating these equations at the aerodynamic surfaces. Equations (3.3-44), (3.3-45), and (3.3-46) are formed as integral equations representing aerodynamic surface pressure by combining them with the results of section 3.3.2 as follows.

Isolated thin body thickness pressure: Combining equations (3.3-15) and (3.3-45),

$$C_{P_{WI}}^S(X_I, Y_I, Z_I) = -\tau_I \iint_{S_{WI}} \frac{\partial F_I}{\partial X_I} \frac{\partial K_I^S}{\partial X_I} dX_I' dY_I' \tag{3.3-47}$$

where $Z_I = \pm \tau_I F_I(X_I, Y_I)$ is the thickness shape.

Isolated thin body steady lifting pressure: Combining equations (3.3-16 and (3.3-45).

$$C_{P_{WI}}^V(X_I, Y_I, Z_I) = -2 \iint_{S_{WI}} \gamma_o \frac{\partial K^V}{\partial X_I} dX_I' dY_I' \quad (3.3-48)$$

where $\gamma_o(X_I, Y_I)$ is given by equation (3.3-18).

Isolated slender body thickness pressure: Combining equations (3.3-20) and (3.3-45),

$$C_{P_{BJ}}^S(X_J, Y_J, Z_J) = -2 \int_{L_{BJ}} m \frac{\partial K^S}{\partial X_J} dX_J' \quad (3.3-49)$$

where $m(X_J)$ is given by equation (3.3-21).

Isolated slender body steady lifting pressure: Combining equations (3.3-23) and (3.3-45),

$$C_{P_{BJ}}^{ZD} = -2 \int_{L_{BJ}} \mu_o^Z \frac{\partial K^{ZD}}{\partial X_J} dX_J' \quad (3.3-50)$$

where $\mu_o^Z(X_J)$ is given by equation (3.3-27); and combining equations (3.3-24) and (3.3-45),

$$C_{P_{BJ}}^{YD} = -2 \int_{L_{BJ}} \mu_o^Y \frac{\partial K^{YD}}{\partial X_J} dX_J' \quad (3.3-51)$$

where $\mu_o^Y(X_J)$ is given by equation (3.3-28).

Steady interference pressure: Combining equations (3.3-20) and (3.3-45),

$$C_{P_{int}}^V(X, Y, Z) = -2 \iint_{S_W + S_B} \gamma_o^{int} \frac{\partial K^V}{\partial X} dS \quad (3.3-52)$$

where $\gamma_o^{int}(X, Y, Z)$ is obtained by solving the steady aerodynamic induction problems of which equation (3.3-31) is typical.

Isolated thin body unsteady lifting pressure: Substituting into equations (3.3-44), solutions to the homogeneous flow problems are constructed by solving the integral equations posed by equations (3.3-34). These operations lead to

$$\begin{aligned}
 C_{P_{WI}}^{UV}(X_I, Y_I, Z_I) = & -2 \iint_{S_{WI}} \gamma_0 \frac{\partial K_I^V}{\partial X_I} dS \\
 & -2 \frac{M^2}{\beta^2} [X_I \iint_{S_{WI}} \gamma_1 \frac{\partial K_I^V}{\partial X_I} dS - \iint_{S_{WI}} \gamma_2 \frac{\partial K_I^V}{\partial X_I} dS] \\
 & - \frac{2}{\beta^2} \iint_{S_{WI}} \gamma_3 \frac{\partial K_I^V}{\partial X_I} dS
 \end{aligned} \tag{3.3-53}$$

where $\gamma_1(X_I, Y_I)$, $\gamma_2(X_I, Y_I)$, $\gamma_3(X_I, Y_I)$ are the vorticity distributions found by solving equations (3.3-34).

Isolated slender body unsteady lifting pressure: Substituting into equations (3.3-46), the solutions to the homogeneous flow problems are constructed by solving the integral equations posed by equations (3.3-40). These operations lead to

$$\begin{aligned}
 C_{P_{BJ}}^{YD}(X_J, Y_J, Z_J) = & -2 \int_{L_{BJ}} \mu_0^Y \frac{\partial K_J^{YD}}{\partial X_J} dX_J' - \frac{2}{\beta^2} \int_{L_{BJ}} \mu_1^Y K_J^{YD} dX_J' \\
 & -2 \frac{M^2}{\beta^2} [X_J \int_{L_{BJ}} \mu_1^Y \frac{\partial K_J^{YD}}{\partial X_J} dX_J' - \int_{L_{BJ}} \mu_2^Y \frac{\partial K_J^{YD}}{\partial X_J} dX_J']
 \end{aligned} \tag{3.3-54}$$

where $\mu_1^Y(X_J)$ and $\mu_2^Y(X_J)$ are given by equations (3.3-40); while, for the integral equations posed by equations (3.3-42)

$$\begin{aligned}
 C_{P_{BJ}}^{ZD}(X_J, Y_J, Z_J) = & -2 \int_{L_{BJ}} \mu_c^Z \frac{\partial K_J^{ZD}}{\partial X_J} dX_J' - \frac{2}{\beta^2} \int_{L_{BJ}} \mu_1^Z K_J^{ZD} dX_J' \\
 & -2 \frac{M^2}{\beta^2} [X_J \int_{L_{BJ}} \mu_1^Z \frac{\partial K_J^{ZD}}{\partial X_J} dX_J' - \int_{L_{BJ}} \mu_2^Z \frac{\partial K_J^{ZD}}{\partial X_J} dX_J']
 \end{aligned} \tag{3.3-55}$$

where $\mu_1^Z(X_J)$ and $\mu_2^Z(X_J)$ are the doublet distribution strengths found by solving equations (3.3-42).

Unsteady interference pressure: Combining equations (3.3-42) and (3.3-44),

$$C_{P_{int}}^{UV}(X,Y,Z) = -2 \iint_{S_W + S_B} \gamma_0 \frac{\partial K^V}{\partial X} dS - 2 \frac{M^2}{\beta^2} [X \iint_{S_W + S_B} \gamma_1 \frac{\partial K^V}{\partial X} dS - \iint_{S_W + S_B} \gamma_2 \frac{\partial K^V}{\partial X} dS] + \frac{2}{\beta^2} \iint_{S_W + S_B} \gamma_3 \frac{\partial K^V}{\partial X} dS \quad (3.3-56)$$

where $\gamma_1^{int}(X,Y,Z)$, $\gamma_2^{int}(X,Y,Z)$, $\gamma_3^{int}(X,Y,Z)$ are the vorticity strengths found by solving equations (3.3-44).

3.4 NUMERICAL SOLUTION

For practical aircraft configurations, an exact numerical solution to the integral equations derived in section 3.3 is not possible. An approximate solution is obtained in the FLEXSTAB system using a method based on a paneling scheme. The surfaces and lines of integration are subdivided into small regions as shown by figure 3.4-1. These small regions consist of quadrilateral panels on mean surfaces and line segments on mean centerlines. Simple distribution functions having unknown amplitudes are assumed for the flow singularities (i.e., sources, vorticity, and doublets) on the small regions of integration, and the integration is carried out. These operations reduce the integral equations to algebraic equations in terms of the unknown amplitudes, i.e., the strengths of the distributions. The algebraic equations are chosen to be determinant sets for each of the aerodynamic problems in section 3.3, and they are solved directly.

3.4.1 Paneling Scheme

In using the paneling scheme, the mean surfaces of the thin and slender bodies are subdivided into small panel areas, figure 3.4-1. The mean surface of the I^{th} thin body is covered by nI planes, whence

$$S_{WI} = \sum_{i=1}^{nI} S_{WIi} \quad (3.4-1)$$

where S_{WIi} is the surface area of the i^{th} panel. Similarly, the mean surface of the J^{th} slender body is covered by mJ panels,

$$S_{BJ} = \sum_{j=1}^{mJ} S_{BJj} \quad (3.4-2)$$

The centerlines of the slender bodies are also subdivided, figure 3.4-2; and the subdivisions are line segments of length L_{BJk} . The line segments on the J^{th} slender body centerline, whose number is denoted as $1J$, provide a covering of the centerline. Thus,

$$L_{BJ} = \sum_{K=1}^{1J} L_{BJK} \quad (3.4-3)$$

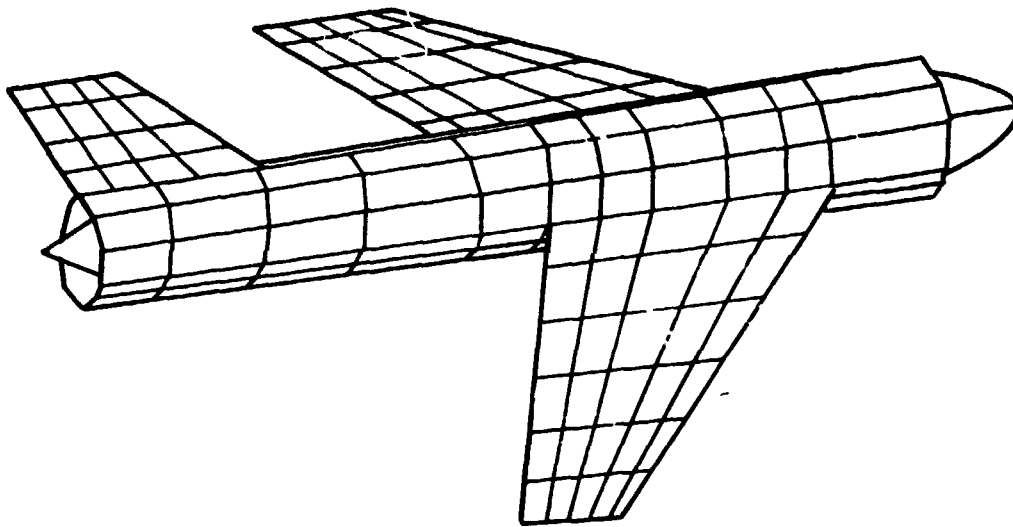


FIGURE 3.4.1— TYPICAL SURFACE PANELING ARRANGEMENT

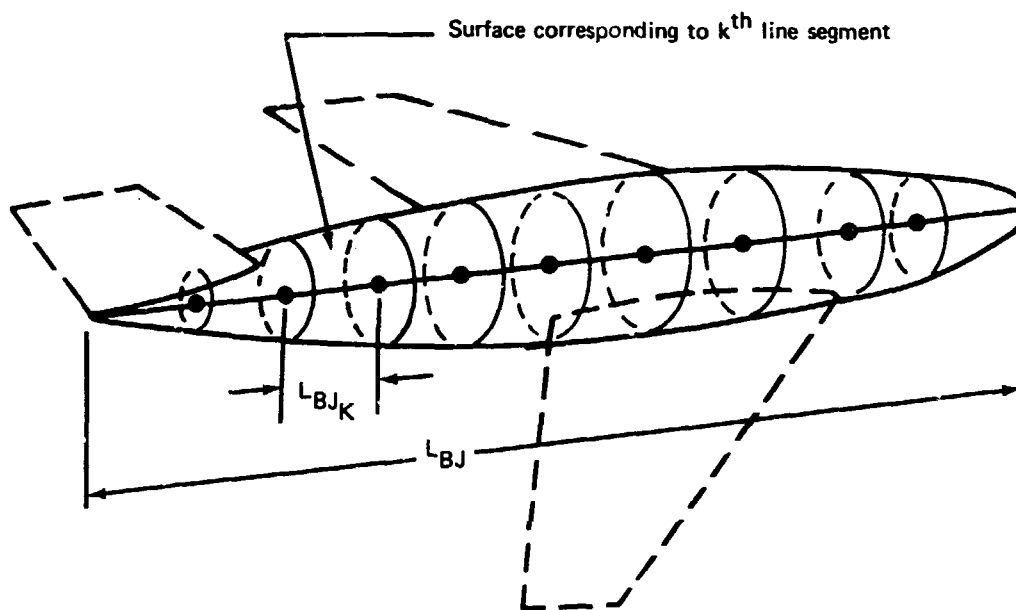


FIGURE 3.4.2.—TYPICAL CENTERLINE SEGMENT ARRANGEMENT

3.4.1.1 Local panel coordinate axis systems.—A local axis system is introduced for each mean surface panel, as shown by figure 3.4-3. For the i^{th} panel on the I^{th} mean surface, the origin of the local coordinate system has the coordinates $X_{Ii}(0)$, $Y_{Ii}(0)$, $Z_{Ii}(0)$ in the Reference Axis System. The surface of the panel is coincident with the ξ_{Ii} - η_{Ii} plane, and θ_{Ii} is the panel dihedral angle. The transformation from the Reference Axis System to the local panel axis system is given by

$$\begin{aligned}\xi_{Ii} &= X - X_{Ii}(0) \\ \eta_{Ii} &= (Y - Y_{Ii}(0))\cos\theta_{Ii} + (Z - Z_{Ii}(0))\sin\theta_{Ii} \\ \zeta_{Ii} &= -(Y - Y_{Ii}(0))\sin\theta_{Ii} + (Z - Z_{Ii}(0))\cos\theta_{Ii}\end{aligned}\quad (3.4-4)$$

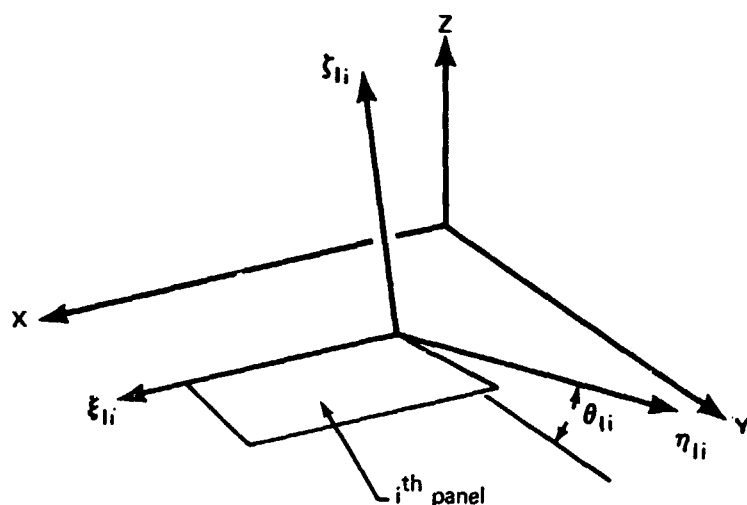


FIGURE 3.4-3.—LOCAL AXIS SYSTEM

3.4.1.2 Local line segment coordinate axis systems.—A local axis system is introduced for each slender body mean centerline segment, figure 3.4-4. For the i^{th} segment of the mean centerline of the J^{th} slender body, the origin of the local axis system has the coordinates $X_{Jj}(0)$, $Y_{Jj}(0)$, $Z_{Jj}(0)$ in the Reference Axis System. The ξ_{Jj} axis is coincident with the mean centerline, and the ξ_{Jj} , η_{Jj} plane may be either parallel with the X, Y plane or the X, Z plane of the Reference Axis System. The transformation from the Reference Axis System to the local line segment axis system is therefore given by

$$\begin{aligned}
\xi_{Jj} &= X - X_{Jj}(0) \\
\eta_{Jj} &= (Y - Y_{Jj}(0))\cos\mu + (Z - Z_{Jj}(0))\sin\mu \\
\zeta_{Jj} &= -(Y - Y_{Jj}(0))\sin\mu + (Z - Z_{Jj}(0))\cos\mu
\end{aligned} \tag{3.4-5}$$

where

$$\mu = 0 \text{ or } \pi/2.$$

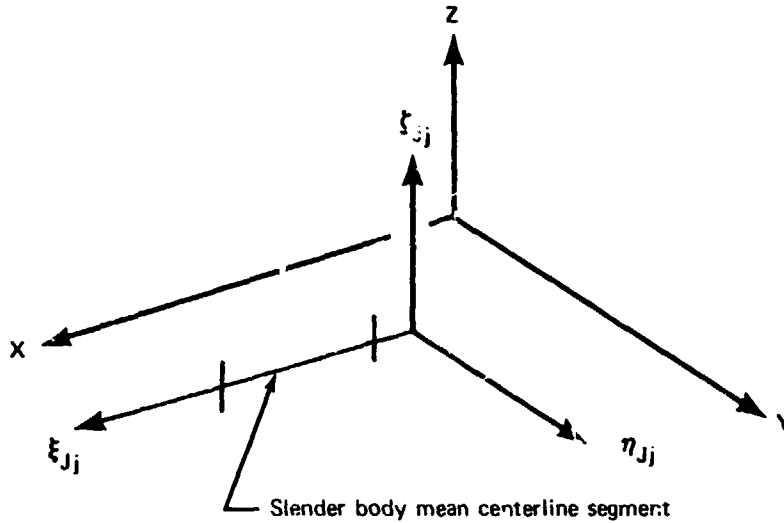


FIGURE 3.4-4.—LOCAL CENTERLINE SEGMENT COORDINATE SYSTEM

3.4.1.3 *Panel geometry.*—A typical mean surface panel is shown by figure 3.4-5. All panels are quadrilaterals with two edges parallel to the X-axis of the Reference Axis System. The panel span is denoted as b_i , and the inboard chord length as c_i . The tangents of the angles of sweep of the leading and trailing edges are denoted as $(d\xi_T/d\eta)_i$ and $(d\xi_L/d\eta)_i$. Finally, a point called a control point is defined for each panel.

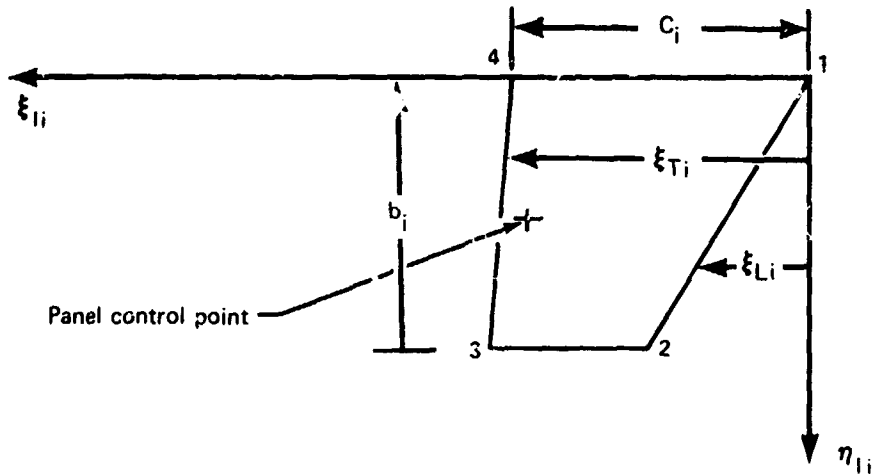


FIGURE 3.4-5.—TYPICAL MEAN SURFACE PANEL

3.4.1.4 Paneling arrangement.—Mean surface panels always occur in rows of constant span as shown by figure 3.4-6. The panel control points to be used later in the development are located along the area centroid line of the panel row, figure 3.4-6. A single control point is located on each panel.

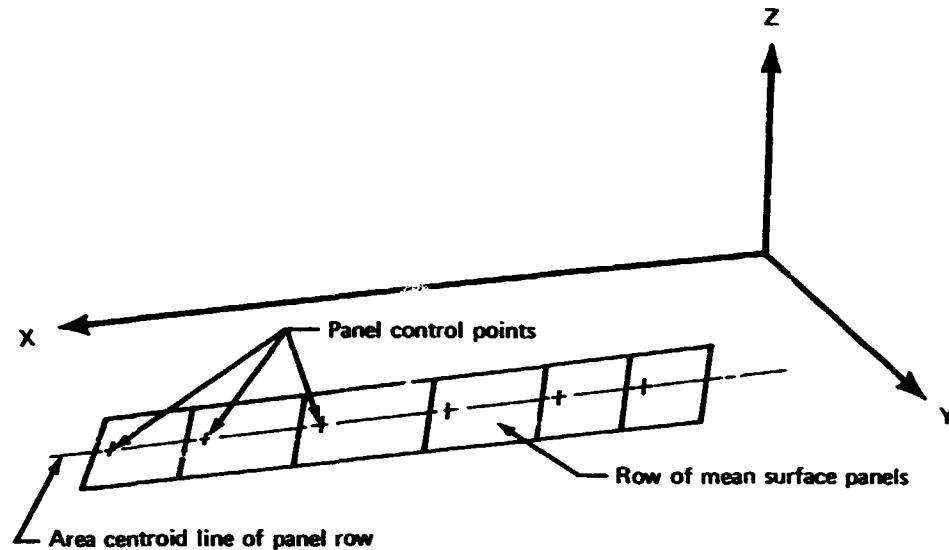


FIGURE 3.4-6.—MEAN SURFACE PANEL ROW

The entire mean surface of every thin and slender body of a configuration is covered by quadrilateral panels as shown by figure 3.4-7, with the panels arranged in streamwise rows parallel to the X-axis. Because the panels are planar surfaces, the mean surfaces of slender bodies must be cylinders with polygonal cross sections, figure 3.4-7.

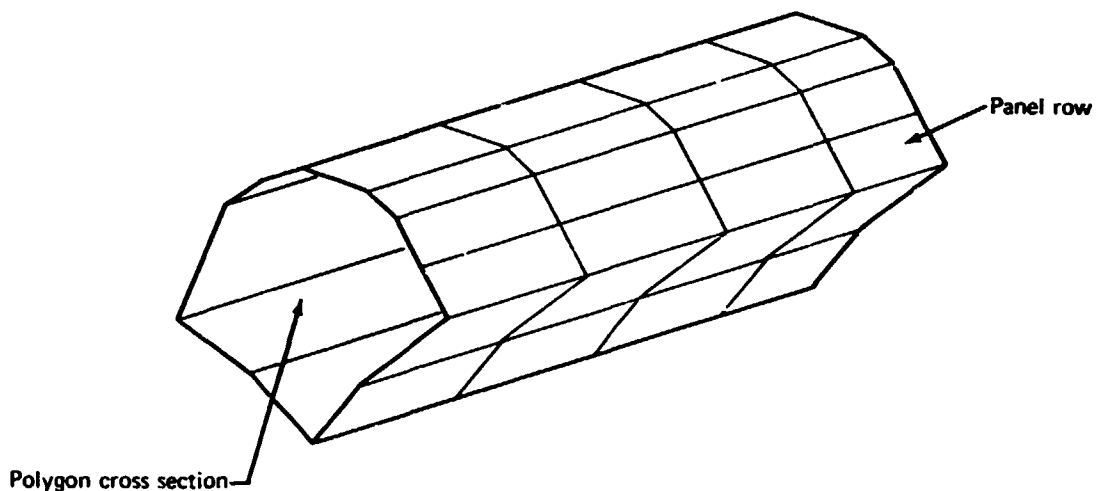
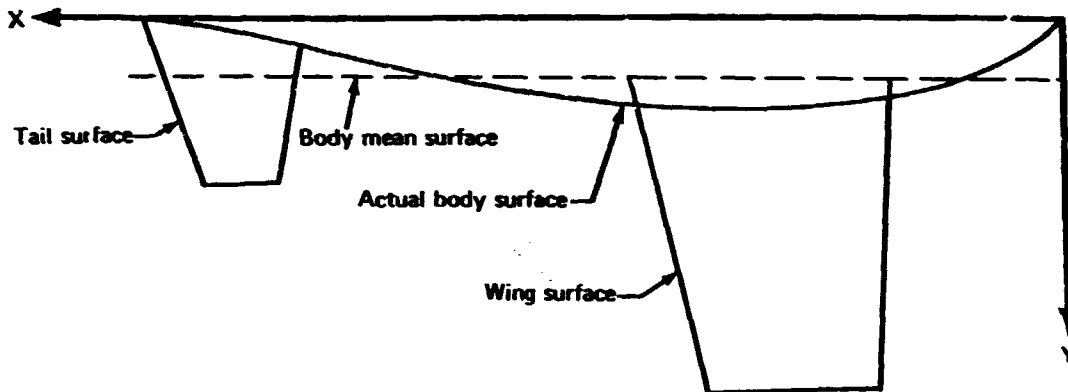


FIGURE 3.4-7.—SLENDER BODY MEAN SURFACE PANELS

The fact that the slender body mean surface must be cylindrical leads to a compromise in representing the mean surface of a wing-body-tail configuration, as shown by figure 3.4-8. Assuming the actual body to be tapered, a portion of the tail surface falls interior to the mean surface of the slender body, while the wing surface must be extended from its actual root location to meet the slender body mean surface.



**FIGURE 3.4-8.—SLENDER BODY MEAN SURFACE
FOR A WING-BODY-TAIL COMBINATION**

3.4.1.5 Image system of panels and line segments.—FLEXSTAB is designed to evaluate aircraft configurations having a plane of geometric, structural, and inertial symmetry. The X,Z plane of the Reference Axis System is the plane of symmetry. As a consequence of the assumed geometric symmetry, the solution to the aerodynamic problem can be expressed in terms of functions either symmetric or antisymmetric in the Y coordinate using the X,Z plane as an image plane.

The geometric symmetry is employed in the paneling scheme. For every mean surface panel or mean centerline segment on the right of the X,Z plane there is a mirror image on the left of the X,Z plane, figure 3.4-9. Only the panels and centerline segments on and to the right of the X,Z plane appear explicitly in the following analysis.

For example, the perturbation velocity potential induced by a flow singularity distributed on the i^{th} panel of the I^{th} thin body is denoted as

$$\phi_{W I i}(X, Y, Z) . \quad (3.4-6)$$

The value of this potential at the control point on the j^{th} panel of the J^{th} slender body mean surface is denoted as

$$\phi_{B J W I j i} \quad (3.4-7)$$

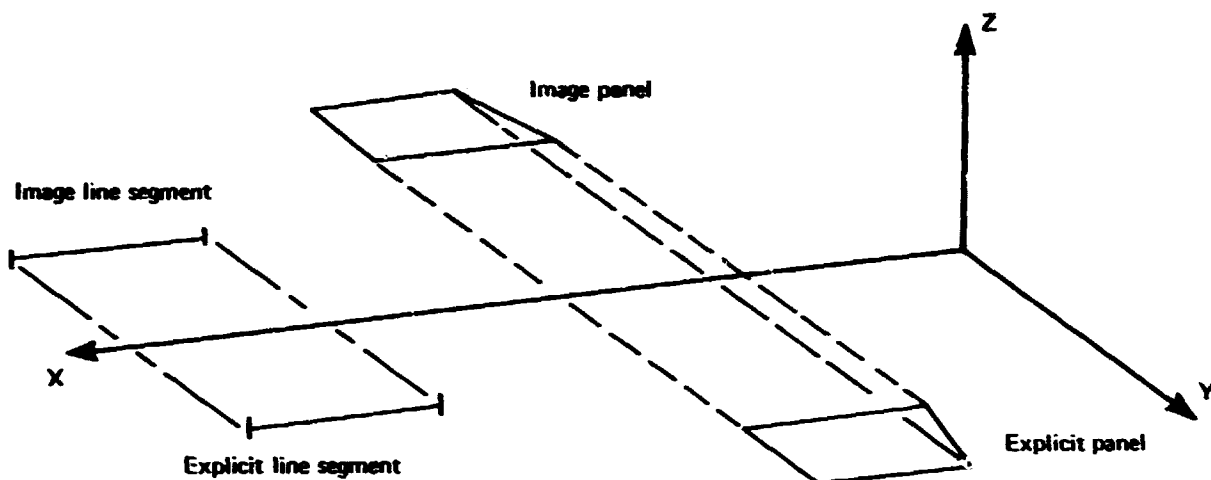


FIGURE 3.4-9.—IMAGE SYSTEM OF PANELS AND LINE SEGMENTS

Letting the coordinates of this control point in the Reference Axis System be denoted as $X(Jj)$, $Y(Jj)$, $Z(Jj)$, the value of the velocity potential at the control point is taken to be

$$\begin{aligned} \phi_{BJWIj} = & \phi_{WII}(X(Jj), Y(Jj), Z(Jj)) \\ & \pm \phi_{WII}(X(Jj), -Y(Jj), Z(Jj)) \end{aligned} \quad (3.4-8)$$

where the second term introduces the contribution to the value of the potential supplied by the image panel, figure 3.4-7. The plus sign for the second term yields a symmetric distribution of the flow singularity, while the minus sign yields an antisymmetric distribution.

All values of velocity potentials and velocity components at control points appearing in the following are obtained using formulations corresponding to the example shown by equation (3.4-8). For brevity of the development, however, all formulas describing these quantities will be expressed for the right side of the aircraft only. When these formulas are evaluated, the reader may infer that they are evaluated in the manner used in equation (3.4-8) whether this is explicitly stated or not.

3.4.1.6 Flow incidence at panel control points.—The first-order boundary conditions of section 3.2 are all in terms of flow incidence evaluated at the mean surfaces. Each of the perturbation potentials must therefore satisfy boundary conditions of the following form at each panel control point:

$$\psi_{BJj} = \frac{\partial \phi}{\partial Y} \sin \theta_{Jj} - \frac{\partial \phi}{\partial Z} \cos \theta_{Jj} \quad (3.4-9)$$

where θ_{Jj} is the dihedral angle, figure 3.4-3, of the j^{th} panel taken for the example to be on the J^{th} slender body.

In the following, the nondimensional velocity components in the Reference Axis System,

$$v = \frac{\partial \phi}{\partial Y} \quad w = \frac{\partial \phi}{\partial Z},$$

are expressed in terms of components expanded on the local axis systems introduced by sections 3.4.1.1 and 3.4.1.2. The latter velocity components are induced by the flow singularities distributed on the mean surface panels and mean centerline segments. If the velocity components are induced by a panel, they are expressed as in the following example:

$$v_{WIi} \equiv \frac{\partial \phi_{WIi}}{\partial \eta_{Ii}} \quad (3.4-10)$$

and

$$w_{WIi} \equiv \frac{\partial \phi_{WIi}}{\partial \zeta_{Ii}}$$

where for the example ϕ_{WIi} is the perturbation velocity potential due to a flow singularity distributed on the i^{th} panel of the I^{th} thin body. If the velocity components are induced by a line segment, for example the k^{th} segment on the centerline of the K^{th} slender body, then they are as follows:

$$v_{r_{BKk}} \equiv \frac{\partial \phi_{BKk}}{\partial r} \quad (3.4-11)$$

and

$$v_{\theta_{BKk}} \equiv \frac{1}{r} \frac{\partial \phi_{BKk}}{\partial \theta}$$

where the coordinates r and θ are those shown by figure 3.4-10.

The velocity components given by equations (3.4-10) and (3.4-11) are transformed to the Reference Axis System and substituted into equation (3.4-9) to obtain the desired flow incidence as follows:

$$\psi_{BJWIji} = v_{BJWIji} \sin(\theta_{Jj} - \theta_{Ii}) - w_{BJWIji} \cos(\theta_{Jj} - \theta_{Ii}) \quad (3.4-12)$$

and

$$\psi_{BJBKjk} = v_{r_{JBKjk}} \sin(\theta_{Jj} - \theta(Jj)) - v_{\theta_{JBKjk}} \cos(\theta_{Jj} - \theta(Jj)) \quad (3.4-13)$$

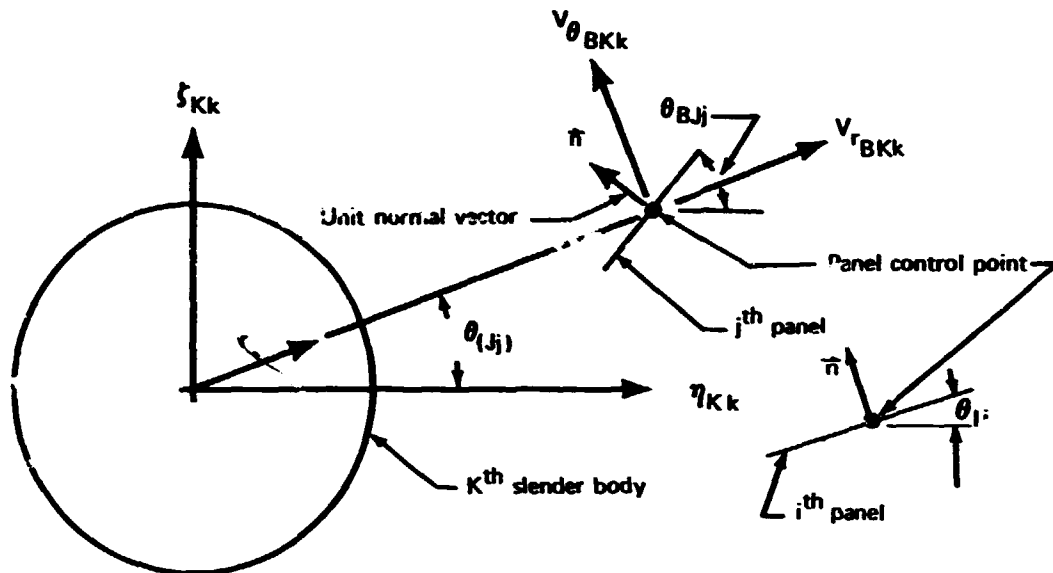


FIGURE 3.4-10.—VELOCITY COMPONENTS INDUCED AT PANEL CONTROL POINTS

3.4.2 Isolated Thin Body Thickness Problem

The solution to the isolated thin body thickness problem is given by section 3.3.2.1 as a source sheet located on the thin body mean surface and as having the following distribution of strength:

$$m(X_I, Y_I) = \frac{1}{2} \tau_I \frac{\partial F_I}{\partial X_I}(X_I, Y_I) \quad (3.4-14)$$

In the FLEXSTAB system the source distribution on each panel, figure 3.4-5, is given by

$$m(\xi_{Ii}, \eta_{Ii}) = S_{WIi}^{CS} + \left\{ \frac{\xi_{Ii} - \left(\frac{d\xi_L}{d\eta} \right)_i \eta_{Ii}}{C_i - \left[\left(\frac{d\xi_L}{d\eta} \right)_i - \left(\frac{d\xi_T}{d\eta} \right)_i \right] \eta_{Ii}} - \frac{1}{2} \right\} S_{WIi}^{LS} \quad (3.4-15)$$

where S_{WIi}^{CS} is the strength of a uniform source distribution and S_{WIi}^{LS} is the strength of a source distribution which varies linearly in ξ_{Ii} .

The strength of the uniform (or constant) part of the source distribution is chosen so that the thin body has the correct thickness at the panel edges along the panel row centroid line, figure 3.4-6. At these points on the i^{th} panel the ordinates of the body thickness shape are denoted as

$Z_I(i) = \tau_I F_I(i)$: ordinate at panel leading edge

$Z_I(i+1) = \tau_I F_I(i+1)$: ordinate at panel trailing edge

Letting \bar{c}_i denote the chord length of the panel along the panel row centroid line, the constant strength part of the source distribution is given by

$$S_{WIi}^{CS} = \frac{1}{2\bar{c}_i} [\tau_I F_I(i+1) - \tau_I F_I(i)] \quad (3.4-16)$$

The thickness shape at an arbitrary point X_I, Y_I on the thin body mean surface is found as

$$\tau_I F_I(X_I, Y_I) = 2 \int_{X_I(L)}^{X_I} m(X'_I, Y_I) dX'_I \quad (3.4-17)$$

where $X_I(L)$ is the coordinate of the leading edge of the thin body at Y_I .

Substituting the source distribution given by equation (3.4-15) into equation (3.4-17) and integrating shows that the thickness shape varies as a quadratic in X_I between the panel edges, but with the thickness at the panel edge solely a consequence of the constant strength part of the source distribution. The quadratic variation is specified by choosing the magnitude of the linearly varying part of the source distribution, viz., S_{WIi}^{LS} . These coefficients are computed by the formula

$$S_{WIi}^{LS} = \left[\frac{S_{WIi+1}^{CS} - S_{WIi-1}^{CS}}{\bar{c}_i + \bar{c}_{i+1/2} + \bar{c}_{i-1/2}} \right] \quad (3.4-18)$$

and lead to an average thickness surface slope on the i^{th} panel equal to the average slope of the thickness shape represented by the constant strength distributions of the panels just forward and aft of the i^{th} panel. The resulting thickness shape consists of a series of quadratics passing through the ordinates of the actual thickness shape at the panel edges.

The solution to the isolated thickness problem is now expressed as follows:

$$\phi_{WI}^S = \sum_{i=1}^{nI} \phi_{WIi}^{CS} S_{WIi}^{CS} + \sum_{i=1}^{nI} \phi_{WIi}^{LS} S_{WIi}^{LS} \quad (3.4-19)$$

where the quantities ϕ_{WIi}^{CS} and ϕ_{WIi}^{LS} are potentials induced by distributions of unit strength. These unit potentials are computed in the local panel axis systems using equation (3.4-4) and, for subsonic and supersonic flow, appear as follows:

Subsonic flow:

$$\begin{aligned}\phi_{WII}^{CS}(\xi_{Ii}, \eta_{Ii}, \zeta_{Ii}) &= \iint_{S_{WII}} K^S(\xi_{Ii}, \eta_{Ii}, \zeta_{Ii}; \xi'_{Ii}, \eta'_{Ii}) d\xi'_{Ii} d\eta'_{Ii} \\ \phi_{WII}^{LS}(\xi_{Ii}, \eta_{Ii}, \zeta_{Ii}) &= \iint_{S_{WII}} g(\xi_{Ii}, \eta_{Ii}) K^S(\xi_{Ii}, \eta_{Ii}, \zeta_{Ii}; \xi'_{Ii}, \eta'_{Ii}) d\xi'_{Ii} d\eta'_{Ii}\end{aligned}\quad (3.4-20)$$

where K^S is given by the first of equations (3.3-2), and from equation (3.3-13),

$$g(\xi_{Ii}, \eta_{Ii}) \equiv \left\{ \frac{\xi_{Ii} - \left(\frac{d\xi_T}{d\eta} \right)_i \eta_{Ii}}{c_i - \left[\left(\frac{d\xi_L}{d\eta} \right)_i - \left(\frac{d\xi_T}{d\eta} \right)_i \right] \eta_{Ii}} - \frac{1}{2} \right\} \quad (3.4-21)$$

Supersonic flow:

$$\begin{aligned}\phi_{WII}^{CS}(\xi_{Ii}, \eta_{Ii}, \zeta_{Ii}) &= \iint_{\Delta S_{WII}} K^S(\xi_{Ii}, \eta_{Ii}, \zeta_{Ii}; \xi'_{Ii}, \eta'_{Ii}) d\xi'_{Ii} d\eta'_{Ii} \\ \phi_{WII}^{LS}(\xi_{Ii}, \eta_{Ii}, \zeta_{Ii}) &= \iint_{\Delta S_{WII}} g(\xi_{Ii}, \eta_{Ii}) K^S(\xi_{Ii}, \eta_{Ii}, \zeta_{Ii}; \xi'_{Ii}, \eta'_{Ii}) d\xi'_{Ii} d\eta'_{Ii}\end{aligned}\quad (3.4-22)$$

where K^S is given by the second of equations (3.3-2) and ΔS_{WII} is that portion of the panel surface area contained in the Mach fore cone extending from the point $P(\xi_{Ii}, \eta_{Ii}, \zeta_{Ii})$, figure 3.4-11.

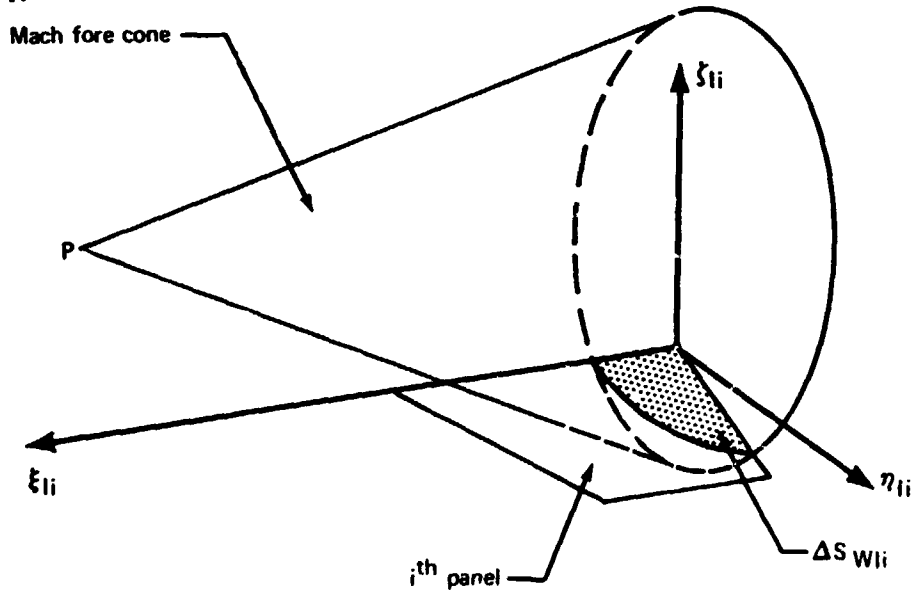


FIGURE 3.4-11.—MEAN SURFACE PANEL AREA CONTAINED IN MACH FORE CONE

3.4.2.1 Isolated thin body thickness interference flow incidence.—The solution to the isolated thin body thickness problem for the I^{th} thin body, equation (3.4-19), may give rise to flow incidence at the mean surfaces of all other thin and slender bodies which are components of the aircraft configuration. This flow incidence is the interference flow incidence described in section 3.3.2, equation (3.3-6), and is computed at all control points of the mean surface panels except those on the I^{th} thin body where it must vanish.

The interference flow incidence is computed by equation (3.4-12). To use this formula, the velocity components shown by equations (3.4-10) must first be computed from the potential describing the solution to the isolated thickness problem, equation (3.4-19). These velocity components are given by

$$v_{WI}^S = \sum_{i=1}^{nI} v_{WII}^{CS} S_{WII}^{CS} + \sum_{i=1}^{nI} v_{WII}^{LS} S_{WII}^{LS} \quad (3.4-23)$$

and

$$w_{WI}^S = \sum_{i=1}^{nI} w_{WII}^{CS} S_{WII}^{CS} + \sum_{i=1}^{nI} w_{WII}^{LS} S_{WII}^{LS}$$

where

$$v_{WII}^{CS} \equiv \frac{\partial \phi_{WII}^{CS}}{\partial \eta_{Ii}}, \quad w_{WII}^{CS} \equiv \frac{\partial \phi_{WII}^{CS}}{\partial \zeta_{Ii}} \quad (3.4-24)$$

$$v_{WII}^{LS} \equiv \frac{\partial \phi_{WII}^{LS}}{\partial \eta_{Ii}}, \quad w_{WII}^{LS} \equiv \frac{\partial \phi_{WII}^{LS}}{\partial \zeta_{Ii}}$$

Evaluating the velocity components at the control points, using the method of section 3.4.1.5, and substituting into equation (3.4-12), leads to the interference flow incidence on the K^{th} thin body mean surface as

$$\psi_{WK}^S = \sum_{i=1}^{nI} a_{WKWIk}^{CS} S_{WII}^{CS} + \sum_{i=1}^{nI} a_{WKWIk}^{LS} S_{WII}^{LS} \quad (3.4-25)$$

and on the J^{th} slender body mean surface as

$$\psi_{BJj}^S = \sum_{i=1}^{nI} a_{BJWIji}^{CS} S_{Wii}^{CS} + \sum_{i=1}^{nI} a_{BJWIji}^{LS} S_{Wii}^{LS} \quad (3.4-26)$$

where, for example, a_{BJWIji}^{CS} is the flow incidence shown by equation (3.4-12) when that equation is evaluated using the potential induced by a uniform source distribution of unit strength on the i^{th} panel of the I^{th} thin body, i.e.,

$$a_{BJWIji}^{CS} \equiv + v_{Wii}^{CS} \sin(\theta_{Jj} - \theta_{Ii}) - w_{Wii}^{CS} \cos(\theta_{Jj} - \theta_{Ii})$$

When evaluated at the control points on all mean surfaces of a configuration and expressed for all thin bodies used in the configuration, equations (3.4-25) and (3.4-26) are expressed in matrix form as follows:

$$\{\psi_{BW}^S\}^{int} = [a_{BW,W}^{CS}] \{S_W^{CS}\} + [a_{BW,W}^{LS}] \{S_W^{LS}\} \quad (3.4-27)$$

where the matrix elements have the following arrangement for a configuration consisting of N thin bodies and M slender bodies:

interference flow incidence matrix,

$$\{\psi_{BW}^S\}^{int} \equiv \begin{bmatrix} \{\psi_{B1}^S\} \\ \vdots \\ \{\psi_{BM}^S\} \\ \hline \{\psi_{W1}^S\} \\ \vdots \\ \{\psi_{WN}^S\} \end{bmatrix} \quad (3.4-28)$$

influence coefficient matrix for uniform source distributions,

$$[a_{BW,W}^{CS}] \equiv \begin{bmatrix} [a_{B1,W1}^{CS}] & \cdots & [a_{B1,WN}^{CS}] \\ \vdots & \ddots & \vdots \\ [a_{BM,W1}^{CS}] & \cdots & [a_{BM,WN}^{CS}] \\ [a_{W1,W1}^{CS}] & \cdots & [a_{W1,WN}^{CS}] \\ \vdots & \ddots & \vdots \\ [a_{WN,W1}^{CS}] & \cdots & [a_{WN,WN}^{CS}] \end{bmatrix}; \quad (3.4-29)$$

source distribution strength matrices,

$$\{S_W^{CS}\} \equiv \begin{bmatrix} \{S_{W1}^{CS}\} \\ \vdots \\ \{S_{WN}^{CS}\} \end{bmatrix} \quad \{S_W^{LS}\} \equiv \begin{bmatrix} \{S_{W1}^{LS}\} \\ \vdots \\ \{S_{WN}^{LS}\} \end{bmatrix} \quad (3.4-30)$$

and influence coefficient matrix for linear source distributions,

$$[a_{BW,W}^{LS}] \equiv \begin{bmatrix} [a_{B1,W1}^{LS}] & \cdots & [a_{B1,WN}^{LS}] \\ \vdots & \ddots & \vdots \\ [a_{BM,W1}^{LS}] & \cdots & [a_{BM,WN}^{LS}] \\ [a_{W1,W1}^{LS}] & \cdots & [a_{W1,WN}^{LS}] \\ \vdots & \ddots & \vdots \\ [a_{WN,W1}^{LS}] & \cdots & [a_{WN,WN}^{LS}] \end{bmatrix} \quad (3.4-31)$$

3.4.2.2 Isolated thin body thickness pressure.—The aerodynamic pressure induced by the isolated thin body thickness problem, a steady flow problem, is computed on the basis of equation (3.3-47). Substituting the solution for the I^{th} thin body, equation (3.4-19), into equation (3.3-47), leads to the pressure distribution

$$C_{P_{WI}}^S = -2 \left[\sum_{i=1}^{nI} u_{WIi}^{CS} S_{WIi}^{CS} + \sum_{i=1}^{nI} u_{WIi}^{LS} S_{WIi}^{LS} \right] \quad (3.4-32)$$

where

$$u_{WIi}^{CS} \equiv \frac{\partial \phi_{WIi}^{CS}}{\partial \xi_{Ii}}, \quad u_{WIi}^{LS} \equiv \frac{\partial \phi_{WIi}^{LS}}{\partial \xi_{Ii}} \quad (3.4-33)$$

This pressure distribution is evaluated at the area centroids of the mean surface panels, and the result for the j^{th} panel centroid is expressed as:

$$C_{P_{WIj}}^S = -2 \left[\sum_{i=1}^{nI} u_{WIji}^{CS} S_{WIi}^{CS} + \sum_{i=1}^{nI} u_{WIji}^{LS} S_{WIi}^{LS} \right] \quad (3.4-34)$$

When expressed for all panel centroids, equation (3.4-34) is expressed in matrix form as

$$\{C_{P_W}^S\}^{iso} = [CPM_{W,W}^{CS}] \{S_W^{CS}\} + [CPM_{W,W}^{LS}] \{S_W^{LS}\} \quad (3.4-35)$$

where $\{S_W^{CS}\}$ and $\{S_W^{LS}\}$ are as defined by equations (3.4-30), while the pressure coefficients at the panel centroids are given by

$$\{C_{P_W}^S\}^{iso} \equiv \begin{bmatrix} \{C_{P_{WI}}^S\}^{iso} \\ \vdots \\ \{C_{P_{WN}}^S\}^{iso} \end{bmatrix} \quad (3.4-36)$$

and the pressure influence coefficient matrices are given by

$$[CPM_{W,W}^{CS}] \equiv \begin{bmatrix} [-2u_{W1,W1}^{CS}] & \cdots & [-2u_{W1,WN}^{CS}] \\ \vdots & \ddots & \vdots \\ [-2u_{WN,W1}^{CS}] & \cdots & [-2u_{WN,WN}^{CS}] \end{bmatrix} \quad (3.4-37)$$

$$[CPM_{W,W}^{LS}] \equiv \begin{bmatrix} [-2u_{W1,W1}^{LS}] & \cdots & [-2u_{W1,WN}^{LS}] \\ \vdots & \ddots & \vdots \\ [-2u_{WN,W1}^{LS}] & \cdots & [-2u_{WN,WN}^{LS}] \end{bmatrix}$$

3.4.2.3 Isolated thin body thickness induced velocity components.—The computations for isolated thin body thickness interference flow incidence and pressure, sections 3.4.2.1 and 3.4.2.2, require the following velocity components:

$$\left. \begin{array}{l} u_{Wli}^{CS} \\ v_{Wli}^{CS} \\ w_{Wli}^{CS} \end{array} \right\} \text{ due to a uniform source distribution on the } i^{\text{th}} \text{ panel}$$

$$\left. \begin{array}{l} u_{Wli}^{LS} \\ v_{Wli}^{LS} \\ w_{Wli}^{LS} \end{array} \right\} \text{ due to a linearly varying source distribution on the } i^{\text{th}} \text{ panel}$$

These components, in terms of the local panel axis system, section 3.4.1.1, are derived in this section.

Again, letting ϕ_{Wli}^{CS} and ϕ_{Wli}^{LS} denote the velocity potential induced by the unit source distributions on the i^{th} panel of the J^{th} thin body, the desired velocity components are found as

$$u_{WII}^{CS} = \frac{\partial}{\partial \xi_{II}} (\phi_{WII}^{CS}) \quad u_{WII}^{LS} = \frac{\partial}{\partial \xi_{II}} (\phi_{WII}^{LS})$$

$$v_{WII}^{CS} = \frac{\partial}{\partial \eta_{II}} (\phi_{WII}^{CS}) \quad v_{WII}^{LS} = \frac{\partial}{\partial \eta_{II}} (\phi_{WII}^{LS})$$

$$w_{WII}^{CS} = \frac{\partial}{\partial \zeta_{II}} (\phi_{WII}^{CS}) \quad w_{WII}^{LS} = \frac{\partial}{\partial \zeta_{II}} (\phi_{WII}^{LS})$$

For supersonic flow the velocity components induced by the source panel distributions are found by the FLEXSTAB system using the formulas given by equations (22) and (27) of Reference 1-1. For subsonic flow the velocity components are developed* as follows:

For the constant strength distribution, the velocity potential induced by the i^{th} panel of the l^{th} thin body is

$$\phi_{WII}^{CS} = -\frac{1}{4\pi} \int_{\eta_1}^{\eta_2} d\eta' \int_{\xi_L}^{\xi_T} \frac{d\xi'}{\sqrt{(\xi - \xi')^2 + \beta^2[(\eta - \eta')^2 + \zeta^2]}} \quad (3.438)$$

where $\xi_L = \xi_1 + \left(\frac{d\xi_L}{d\eta}\right)(\eta' - \eta_1)$ and $\xi_T = \xi_4 + \left(\frac{d\xi_T}{d\eta}\right)(\eta' - \eta_1)$

where the subscripts indicate the coordinates of the panel corner points, figure 3.4-5. The integration with respect to ξ' is carried out to find

$$\phi_{WII}^{CS} = -\frac{1}{4\pi} \int_{\eta_1}^{\eta_2} \ln \frac{L_u + \sqrt{L_u^2 + a^2}}{L_l + \sqrt{L_l^2 + a^2}} d\eta' \quad (3.439)$$

where

$$L_u \equiv \xi - \left[\xi_4 + \left(\frac{d\xi_T}{d\eta}\right)(\eta' - \eta_1) \right]$$

$$L_l \equiv \xi - \left[\xi_1 + \left(\frac{d\xi_L}{d\eta}\right)(\eta' - \eta_1) \right]$$

*To simplify the notation, subscripts are deleted on the symbols denoting the local panel axis system coordinates, (i.e., $\xi_{II}, \eta_{II}, \zeta_{II}$ appear as ξ, η, ζ)

and

$$a^2 \equiv \beta^2 [(\eta - \eta')^2 + \zeta^2]$$

The nondimensional velocity components are computed from this velocity potential as follows:

$$\begin{aligned} u_{WII}^{CS} &= -\frac{1}{4\pi} \int_{\eta_1}^{\eta_2} \left\{ \frac{\sqrt{L_u^2 + a^2} + L_u}{L_u \sqrt{L_u^2 + a^2} + L_u^2 + a^2} \right. \\ &\quad \left. - \frac{\sqrt{L_l^2 + a^2} + L_l}{L_l \sqrt{L_l^2 + a^2} + L_l^2 + a^2} \right\} d\eta' \\ v_{WII}^{CS} &= -\frac{1}{4\pi} \int_{\eta_1}^{\eta_2} \left\{ \frac{\beta^2 (\eta - \eta')}{L_u \sqrt{L_u^2 + a^2} + L_u^2 + a^2} \right. \\ &\quad \left. - \frac{\beta^2 (\eta - \eta')}{L_l \sqrt{L_l^2 + a^2} + L_l^2 + a^2} \right\} d\eta' \\ w_{WII}^{CS} &= -\frac{1}{4\pi} \int_{\eta_1}^{\eta_2} \left\{ \frac{\beta^2 \zeta}{L_u \sqrt{L_u^2 + a^2} + L_u^2 + a^2} \right. \\ &\quad \left. - \frac{\beta^2 \zeta}{L_l \sqrt{L_l^2 + a^2} + L_l^2 + a^2} \right\} d\eta' \end{aligned} \quad (3.440)$$

The integration with respect to η is carried out numerically in the FLEXSTAB system with the singularities in the integrals evaluated using the procedure described in section 5.3 of reference 3-10.

For the linear variation in the source distribution, the velocity potential is given by

$$\phi_{WII}^{LS} = -\frac{1}{4\pi} \int_{\eta_1}^{\eta_2} d\eta' \int_{\xi_L}^{\xi_T} \frac{g'(\xi, \eta') d\xi'}{\sqrt{(\xi - \xi')^2 + \beta^2 [(\eta - \eta')^2 + \zeta^2]}} \quad (3.441)$$

where g' is a linear function of ξ , η and

$$\xi_L = \xi_1 + \left(\frac{d\xi_L}{d\eta}\right)(\eta' - \eta_1) \quad \text{and} \quad \xi_T = \xi_2 + \left(\frac{d\xi_T}{d\eta}\right)(\eta' - \eta_1)$$

Letting $N \equiv -\xi_L - (d\xi_L/d\eta)(\eta - \eta')$ and $D \equiv C - (d\xi_L/d\eta)(\eta - \eta') + (d\xi_T/d\eta)(\eta - \eta')$, the integration with respect to ξ is carried out to find the velocity potential as follows:

$$\begin{aligned} \phi_{WII}^{LS} = & -\frac{1}{4\pi} \int_{\eta_1}^{\eta_2} \left[\frac{N}{D} \ln \left(\frac{\xi - L_u + \sqrt{L_u^2 + a^2}}{\xi - L_1 + \sqrt{L_1^2 + a^2}} \right) \right. \\ & \left. + \frac{1}{D} \left(\sqrt{L_u^2 + a^2} - \sqrt{L_1^2 + a^2} + \xi I(\phi^{CS}) \right) \right] d\eta' \end{aligned} \quad (3.4-42)$$

where $I(\phi^{CS})$ is the integrand of equation (3.4-38). The nondimensional velocity components are found by differentiating ϕ_{WII}^{LS} with respect to ξ, η, ζ to find

$$\begin{aligned} u_{WII}^{LS} = & -\frac{1}{4\pi} \int_{\eta_1}^{\eta_2} \left\{ \frac{N}{D} I(u^{CS}) + \frac{1}{D} \left[-\frac{L_u}{\sqrt{L_u^2 + a^2}} + \frac{L_1}{\sqrt{L_1^2 + a^2}} \right. \right. \\ & \left. \left. + \ln \frac{L_u + \sqrt{L_u^2 + a^2}}{L_1 + \sqrt{L_1^2 + a^2}} + \xi I(u^{CS}) \right] \right\} d\eta' \end{aligned} \quad (3.4-43)$$

$$\begin{aligned} v_{WII}^{LS} = & -\frac{1}{4\pi} \int_{\eta_1}^{\eta_2} \left\{ \frac{N}{D} I(v^{CS}) + \frac{1}{D} \left[-\frac{\beta^2(\eta - \eta')}{\sqrt{L_u^2 + a^2}} + \frac{\beta^2(\eta - \eta')}{\sqrt{L_1^2 + a^2}} \right. \right. \\ & \left. \left. + \xi I(v^{CS}) \right] \right\} d\eta' \end{aligned}$$

$$\begin{aligned} w_{WII}^{LS} = & -\frac{1}{4\pi} \int_{\eta_1}^{\eta_2} \left\{ \frac{N}{D} I(w^{CS}) + \frac{1}{D} \left[-\frac{\beta^2 \zeta}{\sqrt{L_u^2 + a^2}} + \frac{\beta^2 \zeta}{\sqrt{L_1^2 + a^2}} \right. \right. \\ & \left. \left. + \xi I(w^{CS}) \right] \right\} d\eta' \end{aligned}$$

where $I(u^{CS})$, $I(v^{CS})$, $I(w^{CS})$ are the integrands of equations (3.4-40). The integrations indicated in equations (3.4-43) are carried out numerically with the singularities in the integrals evaluated using the procedure of section 5.3 of reference 3-10.

Equations (3.4-40) and (3.4-43) are used to compute the velocity components in the flow field immediately adjacent to the panel containing the source distributions. At larger distances, equations (3.4-40) and (3.4-43) are replaced by approximations which have been shown to yield the numerical accuracy required by the FLEXSTAB system and which require less computational time.

Letting r_0 be the distance from the centroid of the influencing panel to the point where u , v , and w are evaluated, the flow field is separated into near, intermediate and far fields as follows:

$$\begin{aligned} r_0 < 2.45d_0 & : \text{near field} \\ 2.45d_0 < r_0 < 4.0d_0 & : \text{intermediate field} \\ 4.0d_0 < r_0 & : \text{far field} \end{aligned} \quad (3.4-44)$$

where d_0 is the major diagonal of the quadrilateral panel. figure 3.4-12.

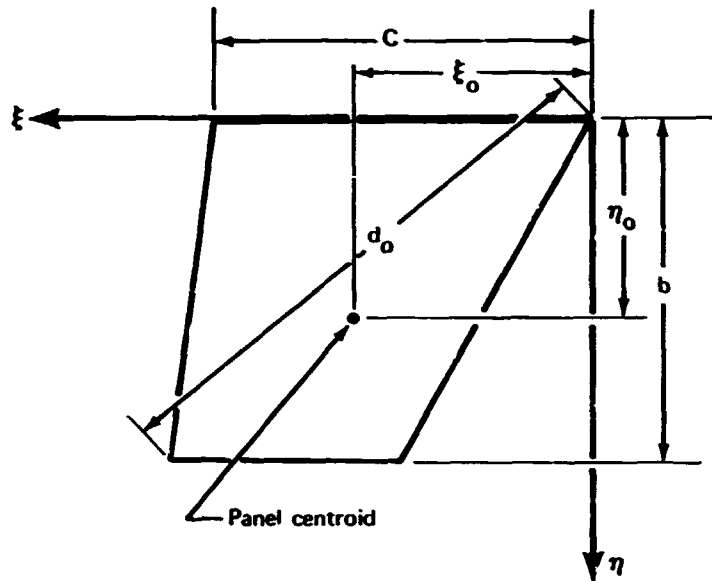


FIGURE 3.4-12.—MAJOR DIAGONAL OF A MEAN SURFACE PANEL

The values of velocity potentials for the two panel source distributions, equations (3.4-38) and (3.4-41), in the intermediate and far fields are expressed in series form. The integrands appearing in equations (3.4-38) and (3.4-41) are expanded in a Taylor series about the area centroid of the panel at ξ_0 , η_0 , figure 3.4-12. Following the expansion, the terms of the series are integrated thereby yielding a series representation for the velocity potentials. For the uniform source panels the series expression is given by

$$\begin{aligned} \phi_{WII}^{CS} = & -\frac{1}{4\pi} \left\{ \frac{1}{R_0} S_{WII} + 3\beta^2 \frac{(\eta - \eta_0)(\xi - \xi_0)}{R_0^5} - I_{\xi_0 \eta_0} \right. \\ & + \beta^2 \left[3 \frac{(\xi - \xi_0)^2}{R_0^5} - \frac{1}{R_0^3} \right] I_{\xi_0 \xi_0} + \frac{\beta^2}{2} \left[\frac{3(\eta - \eta_0)^2}{R_0^5} - \frac{1}{R_0^3} \right] I_{\eta_0 \eta_0} \\ & \left. + (\text{terms of higher order in } \frac{1}{R_0}) \right\} \end{aligned} \quad (3.4-45)$$

where

$$I_{\xi_0 \eta_0} \equiv \iint_{S_{WII}} (\xi - \xi_0)(\eta - \eta_0) d\xi d\eta$$

$$I_{\xi_0 \xi_0} \equiv \iint_{S_{WII}} (\xi - \xi_0)^2 d\xi d\eta$$

$$I_{\eta_0 \eta_0} \equiv \iint_{S_{WII}} (\eta - \eta_0)^2 d\xi d\eta$$

Successive terms in the series are of higher order in terms of the reciprocal of the radial distance

$$R_0 \equiv \sqrt{(\xi - \xi_0)^2 + \beta^2[(\eta - \eta_0)^2 + \zeta^2]};$$

Thus, for points of evaluation ξ, η, ζ for which R_0 is sufficiently large, the higher order terms are negligibly small. For points in the intermediate field the potential is approximated by deleting terms denoted as higher order in equation (3.4-45). For points in the far field only the first term is retained and the potential is approximated as

$$\phi_{WII}^{CS} = -\frac{1}{4\pi} \frac{1}{R_0} S_{WII},$$

i.e., the potential due to a source located at the point ξ_0, η_0 .

The nondimensional velocity components induced by the uniform source distribution on a panel are found by differentiating the potentials, and appear as follows:

For the intermediate field,

$$\begin{aligned} u_{WII}^{CS} = -\frac{1}{4\pi} \left\{ -\frac{\xi - \xi_0}{R_0^3} S_{WII} + \frac{3\beta^2(\eta - \eta_0)}{R_0^5} \left[1 - 5\frac{(\xi - \xi_0)^2}{R_0^2} \right] I_{\xi_0 \eta_0} \right. \\ \left. + \frac{3(\xi - \xi_0)}{2R_0^5} \left[3 - 5\frac{(\xi - \xi_0)^2}{R_0^2} \right] I_{\xi_0 \xi_0} \right. \\ \left. + \frac{3\beta^2}{2R_0^5} (\xi - \xi_0) \left[-\frac{5\beta^2(\eta - \eta_0)}{R_0^2} + 1 \right] I_{\eta_0 \eta_0} \right\} \end{aligned} \quad (3.4-46)$$

$$v_{WII}^{CS} = -\frac{1}{4\pi} \left\{ -\frac{\beta^2(\eta-\eta_0)}{R_0^3} S_{WII} + \frac{3\beta^2(\xi-\xi_0)}{R_0^5} \left[1 - \frac{5\beta^2(\eta-\eta_0)^2}{R_0^2} \right] I_{\xi_0 \xi_0} \right. \\ \left. + \frac{3\beta^2}{2} \frac{(\eta-\eta_c)}{R_0^5} \left[-5 \frac{(\xi-\xi_0)^2}{R_0^2} + 1 \right] I_{\xi_0 \xi_0} \right. \\ \left. + \frac{3\beta^4(\eta-\eta_0)}{2R_0^5} \left[3 - \frac{5\beta^4(\eta-\eta_0)^2}{R_0^2} \right] I_{\eta_c \eta_0} \right\}$$

$$w_{WII}^{CS} = -\frac{1}{4\pi} \left\{ -\frac{\beta^2 \zeta}{R_0^3} S_{WII} - 15\beta^4 \frac{(\xi-\xi_0)(\eta-\eta_c)\zeta}{R_0^7} I_{\xi_0 \eta_0} \right. \\ \left. + \frac{3\beta^2 \zeta}{2R_0^5} \left[1 - 5 \frac{(\xi-\xi_0)^2}{R_0^2} \right] I_{\xi_0 \xi_0} \right. \\ \left. + \frac{3\beta^4 \zeta}{2R_0^5} \left[1 - 5\beta^2(\eta-\eta_0)^2/R_0^2 \right] I_{\eta_0 \eta_c} \right\}$$

For the far field,

$$u_{WII}^{CS} = -\frac{1}{4\pi} \frac{(\xi-\xi_0)}{R_0^3} S_{WII} \quad (3.4-47)$$

$$v_{WII}^{CS} = -\frac{1}{4\pi} \beta^2 \frac{(\eta-\eta_0)}{R_0^3} S_{WII}$$

$$w_{WII}^{CS} = -\frac{1}{4\pi} \beta^2 \frac{\zeta}{R_0^3} S_{WII}$$

A similar development for the linearly varying source strength panels gives the following nondimensional velocity components:

For the intermediate field,

$$\begin{aligned}
 u_{WII}^{LS} = & \frac{1}{4\pi} \frac{\bar{g}}{R_0^3} (\xi - \xi_0) S_{WII} - \frac{1}{4\pi} \left\{ 2 \frac{\bar{g}}{R_0^3} \left[1 - 3 \frac{(\xi - \xi_0)^2}{R_0^2} \right] \right. \\
 & + \frac{3\bar{g}}{2R_0^5} (\xi - \xi_0) \left[3 - 5 \frac{(\xi - \xi_0)^2}{R_0^2} \right] \left. \right\} I_{\xi_0 \xi_0} - \frac{1}{4\pi} \left\{ -\bar{g}_{\xi\eta} \frac{(\xi - \xi_0)}{R_0^3} \right. \\
 & + \bar{g}_{\xi\xi} \frac{\beta^2 (\xi - \xi_0) (\eta - \eta_0)}{R_0^5} + \frac{\bar{g}_\eta}{R_0^3} \left[1 - \frac{3(\xi - \xi_0)^2}{R_0^2} \right] + \frac{3\bar{g}\beta^2}{R_0^5} (\eta - \eta_0) \\
 & \left. \left[1 - 5 \frac{(\xi - \xi_0)^2}{R_0^2} \right] \right\} I_{\xi_0 \eta_0} - \frac{1}{4\pi} \left\{ -\bar{g}_{\eta\eta} \frac{(\eta - \eta_0)}{R_0^3} \right. \\
 & - \frac{2\bar{g}_\eta}{3} \beta^2 \frac{(\xi - \xi_0) (\eta - \eta_0)}{R_0^5} + \frac{3\bar{g}\beta^4}{2} \frac{(\eta - \eta_0)}{R_0^5} \left[3 - 5 \beta^2 \frac{(\eta - \eta_0)^2}{R_0^2} \right] \left. \right\} I_{\eta_0 \eta_0}
 \end{aligned}
 \tag{3.448}$$

$$\begin{aligned}
 v_{WII}^{LS} = & \frac{1}{4\pi} \beta^2 \frac{\bar{g}(\eta - \eta_0)}{R_0^3} S_{WII} - \frac{1}{4\pi} \left\{ -2\bar{g}_\xi \left[\frac{\beta^2}{R_0^3} - \frac{\beta^4 (\eta - \eta_0)^2}{3 R_0^5} \right] \right. \\
 & + \frac{\bar{g}}{2} \left[-\frac{15(\xi - \xi_0)^2 \beta^2 (\eta - \eta_0)}{R_0^7} + 3\beta^2 \frac{(\eta - \eta_0)}{R_0^5} \right] \left. \right\} I_{\xi_0 \xi_0} \\
 & + \left\{ -\bar{g}_{\xi\eta} \beta^2 \frac{(\eta - \eta_0)}{R_0^3} - \bar{g}_\xi \left[\frac{\beta^2}{R_0^3} - \frac{\beta^4 (\eta - \eta_0)^2}{3 R_0^5} \right] + \bar{g}_\eta \left[\frac{\beta^2 (\xi - \xi_0) (\eta - \eta_0)}{3 R_0^5} \right] \right. \\
 & + \bar{g} \left[-\frac{3\beta^2 (\xi - \xi_0)}{R_0^5} - 15\beta^4 \frac{(\eta - \eta_0)^2 (\xi - \xi_0)}{R_0^7} \right] \left. \right\} I_{\xi_0 \eta_0} \\
 & + \left\{ -\bar{g}_{\eta\eta} \frac{\beta^2 (\eta - \eta_0)}{R_0^3} - 2\bar{g}_\eta \left[\frac{\beta^2}{R_0^3} - \frac{\beta^4 (\eta - \eta_0)^2}{3 R_0^5} \right] \right. \\
 & + \frac{\bar{g}}{2} \left[6\beta^4 \frac{(\eta - \eta_0)}{R_0^5} - 15\beta^6 \frac{(\eta - \eta_0)^3}{R_0^7} + \beta^4 \frac{(\eta - \eta_0)}{R_0^5} \right] \left. \right\} I_{\eta_0 \eta_0} \left. \right\}
 \end{aligned}$$

$$\begin{aligned}
w_{WII}^{LS} = & \frac{1}{4\pi} \frac{\beta^2 \bar{g} \zeta}{R_0^3} S_{WII} - \frac{1}{4\pi} \left\{ \frac{\bar{g}}{2} \left[\frac{3\beta^2 \zeta}{R_0^5} - 15\beta^2 \frac{(\xi - \xi_0)^2}{R_0^7} \zeta \right] \right. \\
& + 6\bar{g}_\xi \frac{(\xi - \xi_0)^2 \zeta}{R_0^5} - \bar{g}_{\xi\xi} \frac{\beta^2 \zeta}{R_0^3} \} I_{\xi_0 \xi_0} + \left\{ \frac{3\bar{g}}{2} \left[\frac{\beta^4 \zeta}{R_0^5} \right. \right. \\
& - 5\beta^6 \frac{(\eta - \eta_0)^2 \zeta}{R_0^7} \left. \right] + 3\bar{g}_\eta \frac{(\xi - \xi_0) \beta^2 \zeta}{R_0^5} + 3\bar{g}_\xi \beta^4 \frac{\zeta (\eta - \eta_0)}{R_0^5} \\
& - \bar{g}_{\xi\eta} \frac{\beta^2 \zeta}{R_0^3} \} I_{\xi_0 \eta_0} + \frac{3\bar{g}}{2} \left[\frac{\beta^4 \zeta}{R_0^5} - 5\beta^6 \frac{(\eta - \eta_0)^2}{R_0^7} \zeta \right] \\
& + 6\bar{g}_\eta \beta^4 \frac{\zeta (\eta - \eta_0)}{R_0^5} - \bar{g}_{\eta\eta} \frac{\beta^2 \zeta}{R_0^3} \} I_{\eta_0 \eta_0} \left. \right\}
\end{aligned}$$

For the far field,

$$\begin{aligned}
u_{WII}^{LS} &= - \frac{1}{4\pi} \bar{g} \frac{(\xi - \xi_0)}{R_0^3} S_{WII} \\
v_{WII}^{LS} &= - \frac{1}{4\pi} \bar{g} \beta^2 \frac{(\eta - \eta_0)}{R_0^3} S_{WII} \\
w_{WII}^{LS} &= - \frac{1}{4\pi} \bar{g} \frac{\beta^2 \zeta}{R_0^3} S_{WII}
\end{aligned} \tag{3.449}$$

where \bar{g} , \bar{g}_ξ , \bar{g}_η , $\bar{g}_{\xi\xi}$, $\bar{g}_{\xi\eta}$, and $\bar{g}_{\eta\eta}$ are evaluated at the centroid of the panel, viz., $\xi_{II} = \xi_0$, and $\eta_{II} = \eta_0$.

3.4.3 Isolated Thin Body Steady Lifting Problem

As noted in section 3.3.2.2, the solution to the isolated thin body steady lifting problem is expressed in terms of a vorticity distribution on the mean surface of the thin body as follows:

$$\phi_{WI}^V(X_I, Y_I, Z_I) = \iint_{S_{WI}} \gamma_0(X_I', Y_I') K^V(X_I, Y_I, Z_I; X_I', Y_I') dX_I' dY_I'$$

where the vorticity distribution is required to satisfy the integral equation given by equation (3.3-18). An approximate solution is constructed in the FLEXSTAB system by subdividing the surface of integration into the panels of area S_{WIi} , equation (3.4-1), and by assuming each panel to have a uniform distribution of vorticity and a trailing vortex sheet, figure (3.4-13). The uniform vorticity distribution on the i^{th} panel is expressed as

$$\gamma_o(\xi_{Ii}, \eta_{Ii}) = S_{WIi}^v \text{ for } \xi_{Ii}, \eta_{Ii} \text{ in } S_{WIi} \quad (3.4-50)$$

where S_{WIi}^v is the strength of the uniform distribution. An approximate solution to the problem is then expressed by writing equation (3.3-16) as follows:

$$\phi_{WI}^v(X_I, Y_I, Z_I) = \sum_{i=1}^{n_I} S_{WIi}^v \iint_{S_{WIi}} K^v(X_I, Y_I, Z_I; X_I', Y_I') dX_I' dY_I' \quad (3.4-51)$$

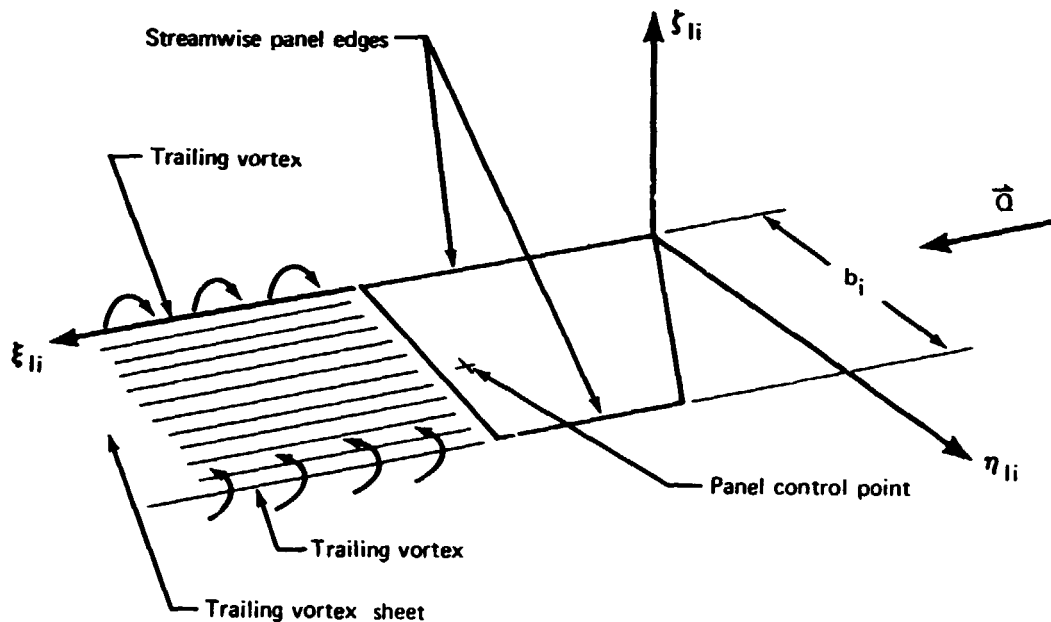


FIGURE 3.4-13.—PANEL WITH UNIFORM VORTICITY DISTRIBUTION

Equation (3.1-18), the integral equation which the velocity potential induced by the vorticity distribution must satisfy, is expressed in terms of the panel vorticity distributions

$$w_{WI}^V = \sum_{i=1}^{nI} a_{WII}^V S_{WII}^V \quad (3.4-52)$$

where w_{WI}^V is given by the boundary condition

$$w_{WI}^V \equiv \hat{w} \bar{w} \lambda_w \cos \theta_I - \hat{v} \bar{v} \lambda_v \sin \theta_I + \hat{\theta} \lambda_\theta \frac{\partial H}{\partial X_I}$$

and

$$-a_{WII}^V(X_I, Y_I, Z_I) \equiv \iint_{S_{WII}} \frac{\partial K^V}{\partial Z_I} dX_I' dY_I'$$

Evaluating the influence functions $a_{WII}^V(X_I, Y_I, Z_I)$ at the control points of the panels on the thin body mean surface leads to

$$w_{WIj}^V = \sum_{i=1}^{nI} a_{WI, WIj}^V S_{WII}^V \quad (3.4-53)$$

where w_{WIj}^V is the nondimensional component of velocity normal to the mean surface at the j th control point. Equation (3.4-53) is expressed in matrix form as follows:

$$\{w_{WI}^V\} = -[a_{WI, WI}^V] \{S_{WII}^V\}, \quad (3.4-54)$$

A second matrix expression is obtained by evaluating the boundary conditions, equation (3.4-52), at the panel centroids. The vortex panel strengths required to satisfy the boundary conditions at the panel centroids are then found as

$$\begin{aligned} \{S_{WI}^V\} = & -[a_{WI, WI}^V]^{-1} \{ \hat{w} \lambda_w \{\bar{w}_{WI}\} \cos \theta_I - \hat{v} \lambda_v \{\bar{v}_{WI}\} \sin \theta_I + \\ & + \hat{\theta} \lambda_\theta \left\{ \frac{\partial H_I}{\partial X_I} \right\} \} \end{aligned} \quad (3.4-55)$$

Finally, the solution to the isolated thin body steady lifting problem is obtained by substituting the values of S_{WII}^V so determined into equation (3.4-51).

Equation (3.4-55) is used as a basis for writing a single matrix equation for an entire aircraft configuration having N thin bodies as follows:

$$\{S_W^v\} = [a_{W,W}^v]^{-1} \{-\hat{w}\lambda_w\{\bar{w}_w\} - \hat{v}\lambda_v\{\bar{v}_w\} + \{\psi_{cw}\}\} \quad (3.4-56)$$

where

$$\{S_W^v\} \equiv \begin{bmatrix} \{S_{W1}^v\} \\ \vdots \\ \{S_{WN}^v\} \end{bmatrix},$$

$$[a_{W,W}^v]^{-1} \equiv \begin{bmatrix} [a_{W1,W1}^v]^{-1} & \text{zeros} & \\ & \cdot & \cdot \\ \text{zeros} & & [a_{WN,WN}^v]^{-1} \end{bmatrix}$$

$$\{\bar{w}_w\} \equiv \begin{bmatrix} \{\bar{w}_{W1}\} \cos\theta_1 \\ \vdots \\ \{\bar{w}_{WN}\} \cos\theta_N \end{bmatrix} \quad \{\bar{v}_w\} \equiv - \begin{bmatrix} \{\bar{v}_{W1}\} \sin\theta_1 \\ \vdots \\ \{\bar{v}_{WN}\} \sin\theta_N \end{bmatrix}$$

$$\{\psi_{cw}\} \equiv -\hat{\theta}\lambda_{\theta} \begin{bmatrix} \frac{\partial H_1}{\partial X} \\ \vdots \\ \frac{\partial H_N}{\partial X} \end{bmatrix}$$

3.4.3.1 Isolated thin body steady lifting interference flow incidence.—As in section 3.4.2.1, the interference flow incidence induced by steady lift on an isolated thin body is computed using the formula given by equation (3.4-12) expressed in terms of velocity components, equation (3.4-10), computed from the solution to the isolated thin body steady lifting problem, equation (3.4-51). These velocity components are given by

$$v_{WI}^v = \sum_{i=1}^{\eta I} v_{WII}^v S_{WII}^v$$

(3.4-57)

and

$$w_{WI}^v = \sum_{i=1}^{\eta I} w_{WII}^v S_{WII}^v$$

where

$$v_{WII}^v \equiv \frac{\partial \phi_{WII}^v}{\partial \eta_{Ii}} \quad \text{and} \quad w_{WII}^v \equiv \frac{\partial \phi_{WII}^v}{\partial \zeta_{Ii}}$$

Evaluating the velocity components at the control points, using the method of section 3.4.1.5, and substituting into equation (3.4-12), leads to the interference flow incidence on the K^{th} thin body mean surface as

$$\psi_{WKk}^S = \sum_{i=1}^{\eta I} a_{WK,WIki}^v S_{WII}^v \quad (3.4-58)$$

and on the J^{th} slender body mean surface as

$$\psi_{BJj}^S = \sum_{i=1}^{\eta I} a_{BJ,WIji}^v S_{WII}^v \quad (3.4-59)$$

where the influence coefficients are given by

$$a_{WK,WIki}^v \equiv v_{WII}^v \sin(\theta_{Kk} - \theta_{Ii}) - w_{WII}^v \cos(\theta_{Kk} - \theta_{Ii}) \quad (3.4-60)$$

and

$$a_{BJ,WIji}^v \equiv v_{WII}^v \sin(\theta_{Jj} - \theta_{Ii}) - w_{WII}^v \cos(\theta_{Jj} - \theta_{Ii}) \quad (3.4-61)$$

When evaluated at the control points on all mean surfaces of a configuration and expressed for the steady lift on N thin bodies of a configuration, equations (3.4-58) and (3.4-59) lead to the following matrix expression:

$$\{\psi_{BW}^v\}^{int} = [a_{BW,W}^v] \{S_W^v\} \quad (3.4-62)$$

where the interference flow incidence matrix is defined as

$$\{\psi_{BW}^v\}^{int} \equiv \begin{bmatrix} \{\psi_{B1}^v\} \\ \vdots \\ \{\psi_{BM}^v\} \\ \hline \{\psi_{W1}^v\} \\ \vdots \\ \{\psi_{WN}^v\} \end{bmatrix} \quad (3.4-63)$$

the aerodynamic influence coefficient matrix is defined as

$$[a_{BW,W}^v] \equiv \begin{bmatrix} [a_{B1,W1}^v] \cdots [a_{B1,WN}^v] \\ \vdots \quad \ddots \quad \vdots \\ [a_{BM,W1}^v] \cdots [a_{BM,WN}^v] \\ \hline [a_{W1,W1}^v] \cdots [a_{W1,WN}^v] \\ \vdots \quad \ddots \quad \vdots \\ [a_{WN,W1}^v] \cdots [a_{WN,WN}^v] \end{bmatrix} \quad (3.4-64)$$

and the vorticity distribution strength matrix is defined as

$$\{S_W^v\} = \begin{bmatrix} \{S_{W1}^v\} \\ \vdots \\ \{S_{WN}^v\} \end{bmatrix}$$

3.4.3.2 Isolated thin body steady lifting pressure.—The aerodynamic pressure induced by the isolated thin body steady lift is given by equation (3.4-48), viz.,

$$C_{P_{WI}}^v(X_I, Y_I, Z_I) = -2 \iint \gamma_0 \frac{\partial K^v}{\partial X_I} dX_I' dY_I'$$

Introducing the approximations leading to the solution to the thin body steady lifting problem given by equation (3.4-51), the induced pressure is found as

$$C_{P_{WI}}^v(X_I, Y_I, Z_I) = -2 \sum_{i=1}^{nI} u_{WII}^v(X_I, Y_I, Z_I) S_{WII}^v \quad (3.4-66)$$

where

$$u_{WII}^v \equiv \iint \frac{\partial K^v}{\partial X_I} dX_I' dY_I' \\ S_{WII}$$

The pressure distribution which gives rise to lift on the thin body is

$$\Delta C_{P_{WI}}^v(X_I, Y_I) \equiv C_{P_{WI}}^v(X_I, Y_I, Z_I = -0) - C_{P_{WI}}^v(X_I, Y_I, Z_I = +0) \quad (3.4-67)$$

where $Z_I = -0$ and $Z_I = +0$ are the coordinates of points on the lower and upper surfaces of the thin body, respectively, figure 3.2-3.

As shown by equation (7-33) of reference 2-3, the lifting pressure distribution on a thin body is directly related to the distribution of vorticity strength as follows:

$$\Delta C_{P_{WI}}^v(X_I, Y_I) = 2\gamma_0(X_I, Y_I) \quad (3.4-68)$$

For the case of uniform vorticity on the panels of a thin body, the lifting pressures on the panels are given by

$$\{C_P^V\}_W = [CPM_{W,W}^V]\{S_W^V\} \quad (3.4-69)$$

where the lifting pressures are defined as

$$\{C_P^V\}_W \equiv \begin{bmatrix} \{C_{P_{W1}}^V\} \\ \vdots \\ \{C_{P_{WN}}^V\} \end{bmatrix} \quad (3.4-70)$$

with

$$\{C_{P_{WI}}^V\} \equiv \begin{bmatrix} \Delta C_{P_{WI1}}^V \\ \vdots \\ \Delta C_{P_{WIn}}^V \end{bmatrix}$$

and $\Delta C_{P_{Wi}}^V$ being the lifting pressure coefficient for the i^{th} panel of the l^{th} thin body—a uniform value of equation (3.4-67) for points on the i^{th} panel. The matrix of pressure influence coefficients $[CPM_{W,W}^V]$ is simply a diagonal matrix with the factor (2) on the diagonal, i.e.,

$$[CPM_{W,W}^V] = +2[I]$$

The matrix of panel vorticity strengths $\{S_W^V\}$ is defined by equation (3.4-65).

3.4.3.3 Isolated thin body steady lift induced velocity components.—In the FLEXSTAB system the nondimensional velocity components appearing in equations (3.4-57) and (3.4-67) are evaluated using equations (26) through (33) of reference 3-8. The expressions for the velocity components are derived in reference 3-8 in terms of integrals over semi-infinite triangular regions having origins at each of the four panel corners, figure 3.4-5. Denoting the value of the potential induced by the vorticity on the k^{th} semi-infinite triangular region as $\phi_{(k)}^V$, the potential induced by a panel of vorticity is obtained by

superimposing the potentials induced by the four semi-infinite triangular regions. The formula representing the potential induced by the i^{th} panel on the l^{th} thin body is as follows:

$$\phi_{Wli}^v = \phi_{Wli(1)}^v - \phi_{Wli(2)}^v + \phi_{Wli(3)}^v - \phi_{Wli(4)}^v$$

where, for example, $\phi_{Wli(2)}^v$ is the potential induced by the semi-infinite triangular region shown by the shaded region in figure 3.4-14.

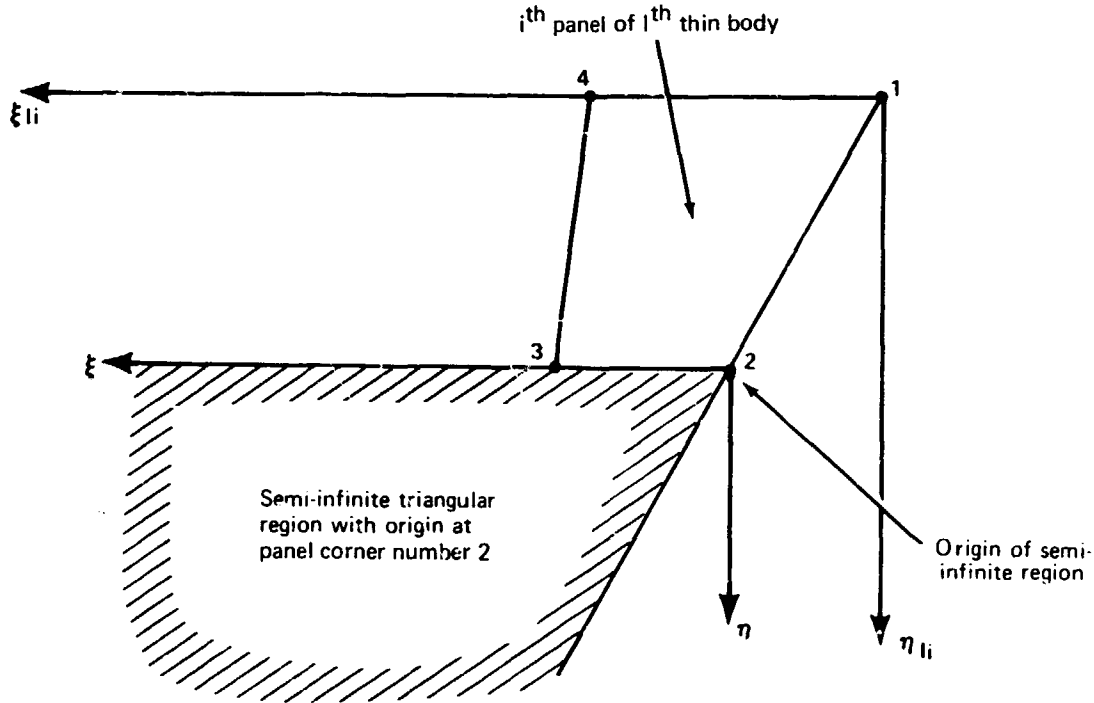


FIGURE 3.4-14.—TYPICAL SEMI-INFINITE REGION WITH ORIGIN AT A PANEL CORNER POINT

The nondimensional velocity components induced by the k^{th} semi-infinite triangular region are given by reference 3-8 for a uniform vorticity strength equal to $(-1/2)$. In the FLEXSTAB system these quantities are computed for a vorticity strength of $(+1)$ and are given by

$$\begin{aligned} u_{Wli(k)}^v &= + \frac{K}{\pi} (F_3 + F_4) \\ v_{Wli(k)}^v &= + \frac{K}{\pi} [L(F_3 + F_4) - \zeta F_6] \\ w_{Wli(k)}^v &= + \frac{K}{\pi} [(L^2 + 1 - M^2)F_2 - L(F_1 - F_5) - \eta F_6] \end{aligned} \quad (3.4-71)$$

where

$$F_1 = \text{R.P.} \left(\log \frac{\xi + d}{|1-M^2| r} \right)$$

$$F_2 = \frac{1}{\sqrt{L^2 + 1 - M^2}} \text{R.P.} \left[\log \sqrt{\frac{\xi' + d'}{|1-M^2| r'}} \right]$$

$$F_3 = \text{R.P.} \left[\tan^{-1} \sqrt{\frac{\xi d}{|1-M^2| r'}} \right]$$

$$F_4 = \tan^{-1}(\eta/\zeta) \text{ for } M < 1$$

$$= 0 \text{ for } M \geq 1$$

$$F_5 = \log \frac{Lr}{r'} \text{ for } M < 1$$

$$= 0 \text{ for } M > 1$$

$$F_6 = \frac{\xi - d}{r^2} \text{ for } M < 1$$

$$= \frac{d}{r^2} \text{ for } M > 1$$

and

$$K = 0.5 \text{ for } M < 1$$

$$K = 1.0 \text{ for } M > 1$$

$$r \equiv \eta^2 + \zeta^2$$

$$d \equiv \xi^2 + (1-M^2)r^2$$

$$\xi' \equiv L\xi + (1-M^2)\eta$$

$$\eta' \equiv \xi - L\eta$$

$$r' \equiv \sqrt{(\xi - L\eta)^2 + (L^2 + 1 - M^2)\zeta^2}$$

$$d' \equiv \sqrt{(\xi')^2 + (1-M^2)(r')^2}$$

$$L \equiv \tan \Lambda$$

while ξ, η, ζ are the coordinates of the point where the velocity components are evaluated relative to the origin of the semi-infinite triangular region.

3.4.4 Isolated Slender Body Thickness Problem

As shown in section 3.3.2.3, the solution to the isolated slender body thickness problem is expressed in terms of a line source distribution on the mean centerline of the slender body, i.e.,

$$\phi_{BJ}^c(X_J, Y_J, Z_J) = \int_{L_{BJ}} m(X_J') K^S(X_J, Y_J, Z_J; X_J') dX_J'$$

where the source distribution is required to satisfy the integral equation given by equation (3.3-21). An approximate solution is constructed in FLEXSTAB by subdividing the line of integration into segments of length L_{BJj} . Equation (3.4-3), assigning source distributions for the segments, and carrying out the indicated integrations. The specific details of these operations differ for subsonic and supersonic flow, and these two cases are treated separately in the following.

Subsonic Case: In subsonic flow a uniform source distribution is assumed for the centerline segments which for the j^{th} segment of the J^{th} slender body mean centerline is expressed as

$$m(\xi_{Jj}) = S_{BJj}^S \quad (3.4-72)$$

where S_{BJj}^S is the strength of the uniform distribution. The approximate solution is obtained by writing equation (3.3-21) as

$$\sum_{j=1}^{NJ} S_{BJj}^S \int_{L_{BJj}} \left[\frac{\partial K^S}{\partial r} - a \frac{dR(X_J)}{dX_J} \frac{\partial K^S}{\partial X_J} \right] d\xi = a \frac{dR(X_J)}{dX_J} \quad (3.4-73)$$

The indicated integrations imply the following velocity components:

$$u_{BJj}^{cs} \equiv \int_{L_{BJj}} \frac{\partial K^S}{\partial X} d\xi$$

and

$$v_{rBJj}^{cs} \equiv \int_{L_{BJj}} \frac{\partial K^S}{\partial r} d\xi \quad (3.4-74)$$

The velocity components are evaluated at control points on the surface of the equivalent slender body of revolution located at the midpoints of the line segments, figure 3.4-15, with the values at the i^{th} control point denoted as

$$v_{r_{BJ,BJij}}^{cs} \quad (3.4-75)$$

Equation (3.4-72) evaluated at the i^{th} control point becomes

$$\sum_{j=1}^{IJ} v_{r_{BJ,BJij}}^{cs} S_{BJj}^{cs} = a \left[1 + \sum_{j=1}^{IJ} u_{BJ,BJij} S_{BJj}^{cs} \right] \frac{dR(Ji)}{dX_J} \quad (3.4-76)$$

where $a(dR/dX_J)(Ji)$ denotes the value of the slender body thickness slope at the i^{th} control point. The required strengths of the source distributions are then expressed in matrix form as

$$\{S_{BJ}^{cs}\} = [BSC_J] \{a(\frac{dR}{dX})_J\} \quad (3.4-77)$$

where

$$[BSC_J] \equiv [v_{r_{BJ,BJij}}^{cs} - a \frac{dR(Ji)}{dX} u_{BJ,BJij}^{cs}]^{-1}$$

and $\{S_{BJ}^{cs}\}$ is the matrix of required source distribution strengths. The solution to the problem is expressed by writing equation (3.2-30) as

$$\phi_{BJ}^S = \sum_{j=1}^{IJ} \phi_{BJj}^{cs} S_{BJj}^{cs} \quad (3.4-78)$$

where

$$\phi_{BJj}^{cs} \equiv \int_{L_{BJj}} K^S d\zeta$$

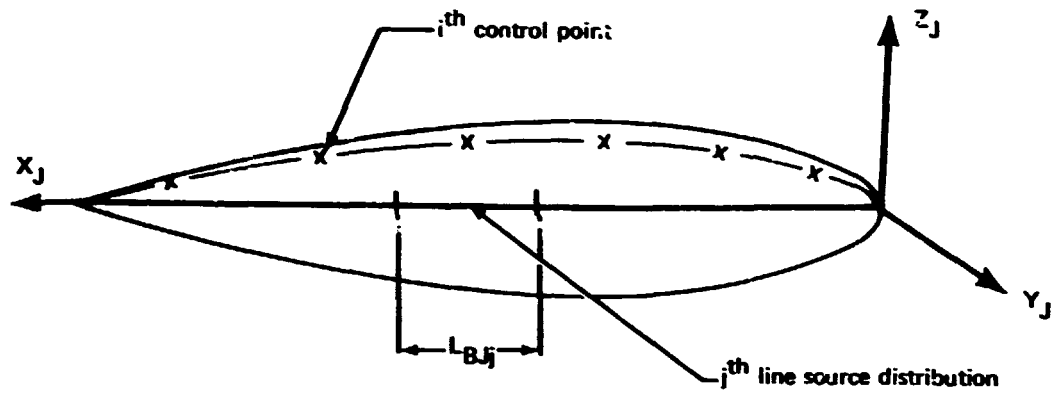


**FIGURE 3.4-15.—SUBSONIC SLENDER BODY THICKNESS
PROBLEM CONTROL POINT LOCATIONS**

Supersonic Case: In supersonic flow the source distributions have a linear dependence on the local centerline segment coordinates ξ_{Jj} shown by figure 3.4-4. The line source for the j^{th} segment of the J^{th} slender body originates at the point $X_{Jj}(0)$. The origin $X_{Jj}(0)$ is determined such that the Mach cone from the origin $X_{Jj}(0)$ passes through the control point for the $(j-1)^{\text{th}}$ slender body segment. Each line source distribution extends to the tail of the slender body at $\xi_{Jj}(T)$. This arrangement is illustrated in figure 3.4-16 and is used for all source distributions except the one which is most forward. This source distribution originates at the slender body nose and varies linearly in strength to the tail. The source distribution on the slender body centerline is therefore the result of superpositioning distributions of the form.

$$\xi_{Jj} S_{BJj}^{LS} \quad \text{for} \quad 0 \leq \xi_{Jj} \leq \xi_{Jj}(T) \quad (3.4-79)$$

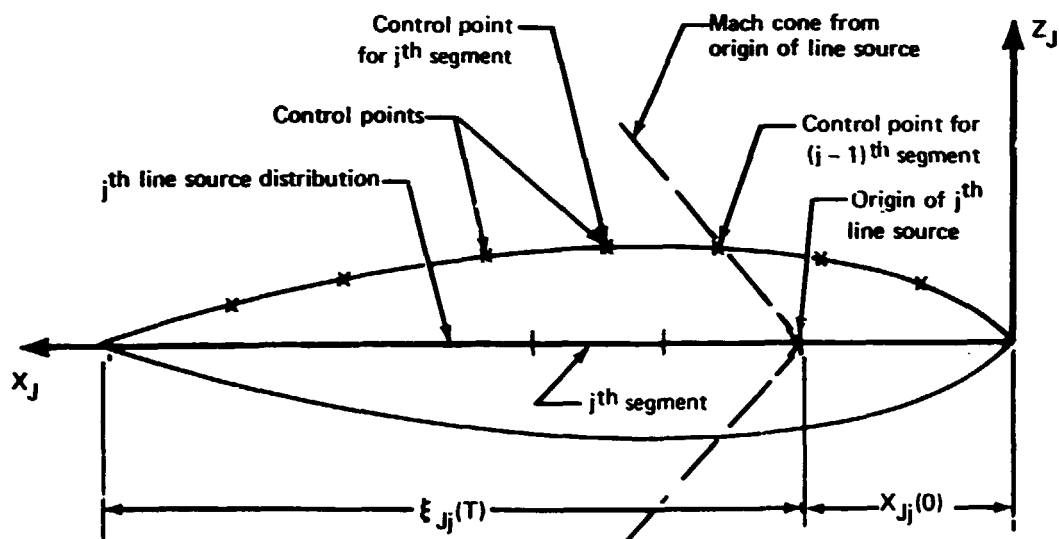


**FIGURE 3.4-16.—SLENDER BODY ISOLATED THICKNESS
PROBLEM CONTROL POINT LOCATIONS**

The velocity components appearing in equation (3.4-74) in the case of supersonic flow are given by

$$u_{BJj}^{LS} \equiv \int_0^{\xi} B_{Jj}^{(T)} \xi \frac{\partial K^S}{\partial X} d\xi \quad (3.4-80)$$

and

$$v_{rBJj}^{LS} \equiv \int_0^{\xi} B_{Jj}^{(T)} \xi \frac{\partial K^S}{\partial r} d\xi$$

The strengths of the source distributions $\{S_{BJ}^{LS}\}$ are obtained from equation (3.4-77), with the matrix $[BSC_j]$ expressed in terms of the velocity components given by equation (3.4-80). Finally, the solution to the problem is expressed by writing equation (3.2-20) as

$$\phi_{BJ}^S = \sum_{j=1}^{1J} \phi_{BJj}^{LS} S_{BJj}^{LS} \quad (3.4-81)$$

where

$$\phi_{BJj}^{LS} \equiv \int_0^{\xi} B_{Jj}^{(T)} K^S d\xi$$

3.4.4.1 Isolated slender body thickness interference flow incidence.—The interference flow incidence induced by thickness of a slender body is computed using equation (3.4-13) expressed in terms of velocity components, equation (3.4-11). These are computed from the solution to the slender body thickness problem given by equation (3.4-78) in subsonic flow and by equation (3.4-81) in supersonic flow. These velocity components are given by

$$v_{rBJ}^S = \sum_{j=1}^{1J} v_{rBJj}^S S_{BJj}^S \quad (3.4-82)$$

and

$$v_{\theta BJ}^S = 0$$

where S_{BJj}^S refers to S_{BJj}^{CS} for subsonic flow and to S_{BJj}^{LS} for supersonic flow, while

$$v_{r_{BJj}}^S \equiv \frac{\partial \phi_{BJj}^S}{\partial r}$$

Evaluating the velocity components at the control points using the method of section 3.4.1.5 and substituting into equation (3.4-13) yields the interference flow on the I^{th} thin body mean surface as

$$\psi_{WII}^S = \sum_{j=1}^{1J} a_{WI, BJij}^S S_{BJj}^S \quad (3.4-84)$$

and on the K^{th} slender body mean surface as

$$\psi_{BKk}^S = \sum_{j=1}^{1J} a_{BK, BJkj}^S S_{BJj}^S \quad (3.4-85)$$

where the influence coefficients are given by

$$a_{WI, BJij}^S \equiv v_{r_{WI, BJij}}^S \sin(\theta_{Ii} - \theta(Jj))$$

and

$$a_{BK, BJkj}^S \equiv v_{r_{BK, BJkj}}^S \sin(\theta_{Kk} - \theta(Jj))$$

When evaluated at the control points on all mean surfaces of a configuration and expressed for the thickness of M slender bodies of a configuration, equations (3.4-84) and (3.4-85) lead to the following matrix expression:

$$\{\psi_{BW}^S\}^{int} = [a_{BW, B}^S] \{S_B^S\} \quad (3.4-87)$$

where the interference flow is described by the matrix

$$\{\psi_{BW}^S\}^{int} \equiv \begin{bmatrix} \{\psi_{B1}^S\} \\ \vdots \\ \{\psi_{BM}^S\} \\ \{\psi_{W1}^S\} \\ \vdots \\ \{\psi_{WN}^S\} \end{bmatrix} \quad (3.4-88)$$

the aerodynamic influence coefficient matrix is defined as

$$[a_{BW,B}^S] \equiv \begin{bmatrix} [a_{B1,B1}^S] \cdots [a_{B1,BM}^S] \\ \vdots \quad \ddots \quad \vdots \\ [a_{BM,B1}^S] \cdots [a_{BM,BM}^S] \\ [a_{W1,B1}^S] \cdots [a_{W1,BM}^S] \\ \vdots \quad \ddots \quad \vdots \\ [a_{WN,B1}^S] \cdots [a_{WN,BM}^S] \end{bmatrix} \quad (3.4-89)$$

and the source distribution strength matrix is defined as

$$\{S_B^S\} \equiv \begin{bmatrix} \{S_{B1}^S\} \\ \vdots \\ \{S_{BM}^S\} \end{bmatrix} \quad (3.4-90)$$

3.4.4.2 Isolated slender body thickness pressure. -The aerodynamic pressure induced by the thickness of an isolated slender body is computed on the basis of equation (3.3-49). Substituting into equation (3.3-49), the solution for the J^{th} slender body, equation (3.4-78) in subsonic flow or equation (3.4-81) in supersonic flow, leads to the pressure distribution

$$C_{p_{BJ}}^S = -2 \sum_{j=1}^{1J} u_{BJj}^S S_{BJj}^S \quad (3.4-91)$$

where the nondimensional velocity component u_{BJj}^S is given by equation (3.4-74) in subsonic flow and by equation (3.4-80) in supersonic flow. This pressure distribution, evaluated on the surface of the slender body, is symmetric about the slender body centerline. The values of the pressure on the slender body surface are computed at points midway between the ends of each centerline segment, figure 3.4-2. For the k^{th} segment the pressures at the points of evaluation are given by

$$C_{P_{BJk}}^S = -2 \sum_{j=1}^{1J} u_{BJ, BJkj}^S S_{BJj}^S \quad (3.4-92)$$

where $u_{BJ, BJkj}^S$ is the X-component of nondimensional velocity at the k^{th} segment due to the source distribution on the j^{th} segment. When expressed for all slender body line segments, equation (3.4-92) is expressed in matrix form as

$$\{C_{P_B}^S\}^{\text{iso}} = [CPM_{B, B}^S] \{S_B^S\} \quad (3.4-93)$$

where $\{S_B^S\}$ is as defined by equation (3.4-90), while the pressure coefficient values at centerline segment midpoints are given by

$$\{C_{P_B}^S\}^{\text{iso}} \equiv \begin{bmatrix} \{C_{P_{B1}}^S\} \\ \vdots \\ \{C_{P_{BM}}^S\} \end{bmatrix} \quad (3.4-94)$$

and the pressure influence coefficients, i.e., the quantities $-2u_{BJ, BJkj}^S$, are expressed in a matrix as

$$[CPM_{B, B}^S] \equiv \begin{bmatrix} [-2u_{B1, B1}^S] \cdots [-2u_{B1, BM}^S] \\ \vdots \quad \ddots \quad \vdots \\ [-2u_{BM, B1}^S] \cdots [-2u_{BM, BM}^S] \end{bmatrix} \quad (3.4-95)$$

3.4.4.3 Isolated slender body thickness induced velocity components.—The computations for isolated slender body thickness interference flow incidence and pressure require the following velocity components:

$$\left. \begin{array}{l} u_{BJj}^{CS} \\ v_{rBJj}^{CS} \end{array} \right\} \text{ due to a uniform distribution of line source in subsonic flow on the } j^{\text{th}} \text{ centerline segment}$$

$$\left. \begin{array}{l} u_{BJj}^{LS} \\ v_{rBJj}^{LS} \end{array} \right\} \text{ due to a linearly varying distribution of line sources in supersonic flow extending aft as shown by figure 3.4-17}$$

Subsonic Case: The velocity potential induced by the line source distributed on the k^{th} segment is given by

$$\phi_{BJk}^{CS} = - \frac{1}{4\pi} \int_0^{L_{BJk}} \frac{d\xi_{JK}}{R} \quad (3.4-96)$$

where

$$R = \sqrt{(\xi_{JK} - \xi_{JK}')^2 + a^2}$$

and

$$a = \beta \sqrt{(\eta_{JK})^2 + (\zeta_{JK})^2}$$

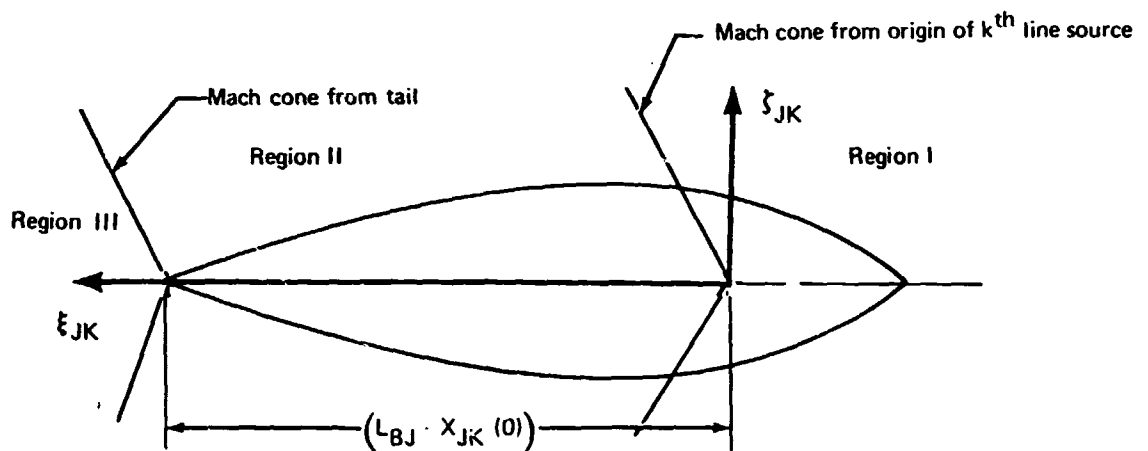


FIGURE 3.4-17.—REGIONS FOR EVALUATING SUPERSONIC LINE SOURCES

Letting

$$\xi_{Jk} - \xi'_{Jk} = a \sinh \sigma \quad (3.4-97)$$

and

$$\xi \equiv \xi_{Jk}, L \equiv L_{BJk}$$

then

$$\phi_{BJk}^{CS} = - \frac{1}{4\pi} \int_{\sinh^{-1}(\frac{\xi}{a})}^{\sinh^{-1}(\frac{\xi-L}{a})} d\sigma \quad (3.4-98)$$

$$= - \frac{1}{4\pi} [\sinh^{-1}(\frac{\xi}{a}) - \sinh^{-1}(\frac{\xi-L}{a})]$$

The components of velocity induced by the line source are found as follows:

$$\begin{aligned} u_{BJk}^{CS} &= \frac{\partial \phi_{BJk}^{CS}}{\partial \xi} = \frac{1}{4\pi} \left[\frac{1}{\sqrt{a^2 + (\xi)^2}} - \frac{1}{\sqrt{a^2 + (\xi-L)^2}} \right] \\ v_{rBJk}^{CS} &= \frac{\partial \phi_{BJk}^{CS}}{\partial r} = \frac{\beta}{4\pi a} \left[\frac{\xi}{\sqrt{a^2 + (\xi)^2}} - \frac{(\xi-L)}{\sqrt{a^2 + (\xi-L)^2}} \right] \\ v_{\theta BJk}^{CS} &= 0 \end{aligned} \quad (3.4-99)$$

Supersonic Case: The velocity potential induced by the k^{th} line source is given by

$$\phi_{BJk}^{LS} = - \frac{1}{2\pi} \int_0^{(\xi-a); (L-X(0))} \frac{\xi' d\xi'}{R} \quad (3.4-100)$$

where

$$R \equiv \sqrt{(\xi - \xi')^2 - a^2}, \quad a \equiv \beta \sqrt{(\eta_{Jr})^2 + (\zeta_{Jk})^2},$$

$$\beta = M^2 - 1, \quad \xi \equiv \xi_{rk}, \quad L \equiv L_{BJ}, \quad X(0) \equiv X_{Jk}^J(0)$$

The first upper limit is applied to region II, figure (3.4-17), and the second to region III. Letting $\xi - a = \cosh \sigma$ as a change of variable, the integration is readily carried out to find the velocity potential for regions II and III of figure 3.4-17 as follows:

For region II

$$\phi_{BJk}^{LS} = \frac{1}{2\pi} \left[\sqrt{(\xi)^2 - a^2} - \xi \cosh^{-1} \left(\frac{\xi}{a} \right) \right] \quad (3.4-101)$$

and for region III

$$\phi_{BJk}^{LS} = \frac{1}{2\pi} \left[\sqrt{(\xi - L + X(0))^2 - a^2} - \xi \cosh^{-1} \left(\frac{\xi - L + X(0)}{a} \right) \right] \quad (3.4-102)$$

The nondimensional velocity components induced by the k^{th} line source in regions II and III are given by the following formulas obtained by differentiating the velocity potential, equations (3.4-101) and (3.4-102).

For region II

$$\begin{aligned} u_{EJk}^{LS} &= - \frac{1}{2\pi} \cosh^{-1} \left(\frac{\xi}{a} \right) \\ v_r^{LS} &= \frac{\beta}{2\pi a} \cdot \sqrt{(\xi)^2 - a^2} \\ v_{\theta}^{LS} &= 0 \end{aligned} \quad (3.4-103)$$

and for region III

$$\begin{aligned}
 u_{BJk}^{LS} &= -\frac{1}{2\pi} \left[\frac{L - X(0)}{\sqrt{(\xi_{Jk} - L_{BJ} + X_{Jk}(0))^2 - a^2}} \right. \\
 &\quad \left. + \cosh^{-1} \left(\frac{\xi - L + X(0)}{a} \right) \right] \\
 v_{rBJk}^{LS} &= \frac{\beta}{2\pi a} \frac{\xi(\xi - L + X(0)) - a^2}{\sqrt{(\xi - L + X(0))^2 - a^2}} \\
 v_{\theta BJk}^{LS} &= 0
 \end{aligned} \tag{3.4-104}$$

3.4.5 Isolated Slender Body Steady Lifting Problem

The isolated slender body steady lifting problem is posed in section 3.3.2.4, where the solution is represented by the potentials induced by two line doublet distributions, viz.,

$$\phi_{BJ}^{ZD}(X_J, Y_J, Z_J) = \int_{L_{BJ}} \mu_0^Z(\xi) K^{ZD}(X_J, Y_J, Z_J; \xi) d\xi$$

and

$$\phi_{BJ}^{YD}(X_J, Y_J, Z_J) = \int_{L_{BJ}} \mu_0^Y(\xi) K^{YD}(X_J, Y_J, Z_J; \xi) d\xi$$

where the line doublet distribution strengths $\mu_0^Z(X_J)$ and $\mu_0^Y(X_J)$ are determined by the integral equations given by equations (3.3-27) and (3.3-28).

An approximate solution is developed in this section following an approach similar to that used in constructing an approximate solution to the isolated slender body thickness problem in section 3.4.4. The slender body mean centerline is subdivided into segments identical to those shown by figures 3.4-15 and 3.4-16. Control points are located relative to the ends of the centerline segments for the cases of subsonic and supersonic flow shown by these figures, but there are two control points for each segment as shown by figure 3.4-18. This arrangement forms two sets of control points—one used to determine the distribution

strength μ_0^Z and the other to determine the distribution strength μ_0^Y —those controlling the Z-doublets are along the meridian line at $\theta = 90^\circ$, while those controlling the Y-doublets are along the meridian line at $\theta = 180^\circ$.

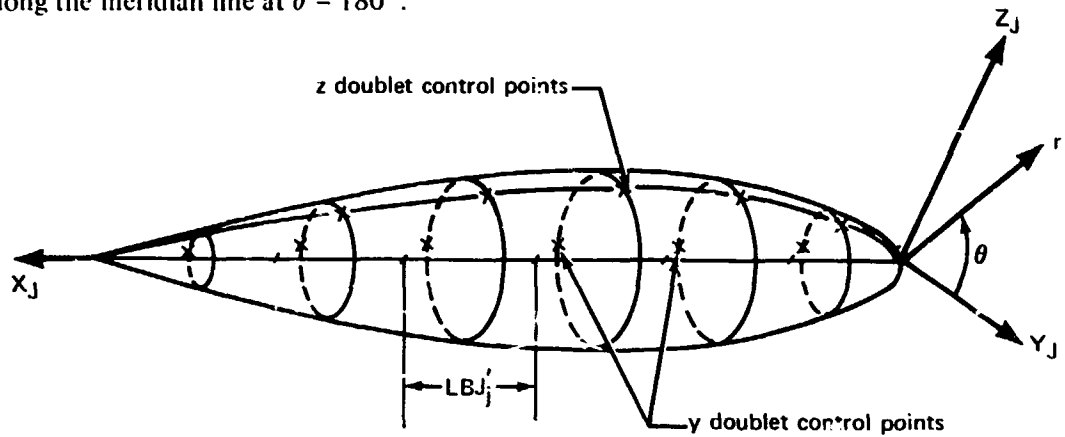


FIGURE 3.4-18.—LINE DOUBLET CONTROL POINT LOCATIONS

The potentials for the unit doublets appearing in equations (3.3-23) and (3.3-24) are found from the potential for a unit source as follows:

$$K^{YD} = -\cos\theta \frac{\partial K^S}{\partial r}$$

and

$$K^{ZD} = \sin\theta \frac{\partial K^S}{\partial r}$$

where θ is the circumferential coordinate shown in figure 3.4-18. To make the following development more compact, these equations are combined into the single expression

$$\kappa \begin{pmatrix} Y \\ Z \end{pmatrix} D = \begin{pmatrix} -\cos\theta \\ \sin\theta \end{pmatrix} \frac{\partial K^S}{\partial r} \quad (3.4-105)$$

where the upper and lower quantities in the brackets are taken to be in correspondence. This notation leads to the integral equations (3.3-23) and 3.3-24) expressed by the single equation

$$\phi_{BJ} \begin{pmatrix} Y \\ Z \end{pmatrix} D = \int_{L_{BJ}} \mu_0 \begin{pmatrix} Y \\ Z \end{pmatrix} \begin{pmatrix} -\cos\theta \\ \sin\theta \end{pmatrix} \frac{\partial K^S}{\partial r} dx_J \quad (3.4-106)$$

The line doublet distribution strengths $\mu_0^{(Y)}(Z)$ are expressed in terms of the mean centerline segments such that

$$\mu_{BJj}^{(Y)}(X_J) S_{BJj}^{(Y)D}$$

represents a distribution associated with the j^{th} segment and $S_{BJj}^{(Y)D}$ is a constant which determines the magnitude of the distribution strength. The functions

$$\mu_{BJj}^{(Y)}(Z)$$

are defined differently for the two cases of subsonic and supersonic flow.

Subsonic Case: In subsonic flow the line doublets are distributed as quadratic splines, figure 3.4-19. Each of the quadratic splines spans three segments of the centerline commencing one segment length forward of the actual nose of the slender body. The distribution associated with the j^{th} segment therefore spans the $(j-1)^{\text{th}}$ segment and the $(j+1)^{\text{th}}$ segment as well, and has the following form:

$$\begin{aligned} \mu_{BJj}^{(Y)} &= h_{Jj-1}(\xi) && \text{for } -L_{BJj} \leq \xi \leq 0 \\ &= h_{Jj-1}(\xi) + h_{Jj}(\xi) && \text{for } 0 \leq \xi \leq L_{BJj} \\ &= h_{Jj-1}(\xi) + h_{Jj}(\xi) + h_{Jj+1}(\xi) && \text{for } L_{BJj} \leq \xi \leq L_{BJj} + L_{BJj+1} \end{aligned} \quad (3.4-107)$$

where

$$\begin{aligned} h_{Jj-1}(\xi) &\equiv (\xi + L_{BJj-1})^2 \\ h_{Jj}(\xi) &\equiv - \frac{(L_{BJj-1} + L_{BJj})(L_{BJj-1} + L_{BJj} + L_{BJj+1})\xi^2}{(L_{BJj})(L_{BJj} + L_{BJj+1})} \\ h_{Jj+1}(\xi) &\equiv \frac{L_{BJj-1}(L_{BJj-1} + L_{BJj} + L_{BJj+1})(\xi - L_{BJj})^2}{(L_{BJj})(L_{BJj+1})} \end{aligned}$$

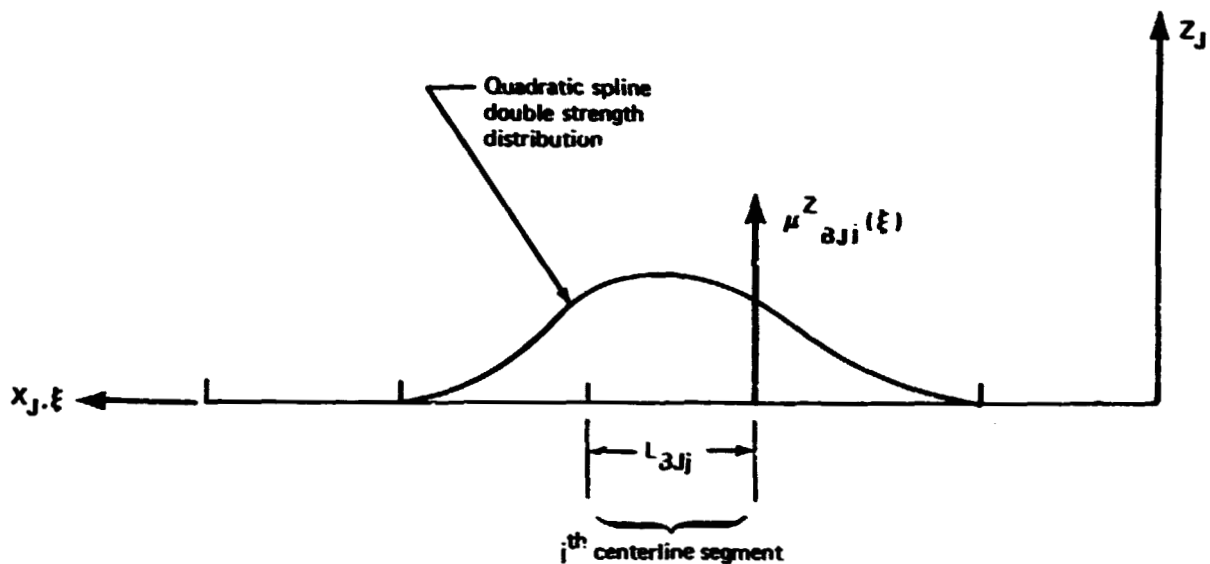


FIGURE 3.4-19.—QUADRATIC SPLINE LINE DOUBLET STRENGTH DISTRIBUTION

Supersonic Case: In supersonic flow a line doublet extends aft from the point of intersection of the body centerline with the Mach fore cone from a control point, figure 3.4-16. The strengths of these line doublets are quadratic in the ξ_{j1} coordinates shown by Figure 3.4-16, and are expressed as

$$\mu_{BJK}^{\left(\frac{Y}{Z}\right)} = (\xi_{JK})^2 S_{BJK}^{\left(\frac{Y}{Z}\right)D} \quad (3.4-108)$$

Each line doublet extends from $\xi_{j1} = 0$ to $\xi_{j1} = \xi_{j1}(T)$, where $\xi_{j1}(T)$ is the coordinate of the body tail shown by figure 3.4-16.

Substituting the distribution strengths, i.e., either equation (3.4-107) or equation (3.4-108), into the expression for the velocity potential, equation (3.4-106), and carrying out the integration over the lengths of the distributions leads to the velocity potential expressed as

$$\phi_{BJ}^{\left(\frac{Y}{Z}\right)D} = \sum_{j=1}^J \phi_{BJj}^{\left(\frac{Y}{Z}\right)D} \quad (3.4-109)$$

The integral equations which must be solved, equations (3.3-27) and (3.3-28), are now expressed as

$$\sum_{j=1}^{1J} w_{BJj}^{ZD} S_{BJj}^{ZD} = -\hat{w}\lambda_w \bar{W} + \hat{c}\lambda_c \frac{\partial I_J}{\partial X_J} \quad (3.4-110)$$

and

$$\sum_{j=1}^{1J} v_{BJj}^{YD} S_{BJj}^{YD} = -\hat{v}\lambda_v \bar{V} + \hat{b}\lambda_b \frac{\partial G_J}{\partial X_J} \quad (3.4-111)$$

where

$$w_{BJj}^{ZD} \equiv \frac{\partial \phi_{BJj}^{ZD}}{\partial r} \quad (3.4-112)$$

and

$$v_{BJj}^{YD} \equiv \frac{\partial \phi_{BJj}^{YD}}{\partial r}$$

Evaluating the velocity components w_{BJj}^{ZD} and v_{BJj}^{YD} at the control points as

$$w_{BjBJij}^{ZD} \quad v_{BjBJij}^{YD} \quad (3.4-113)$$

as well as the functions, \bar{V} , \bar{W} , $\partial I_J / \partial X_J$, and $\partial G_J / \partial X_J$ leads to the following matrix expressions

$$[a_{BJ, BJ}^{ZD}] \{S_{BJ}^{ZD}\} = -\hat{w}\lambda_w \{\bar{W}_{BJ}\} - \hat{c}\lambda_c \left\{ \frac{\partial I_J}{\partial X_J} \right\} \quad (3.4-114)$$

and

$$[a_{BJ, BJ}^{YD}] \{S_{BJ}^{YD}\} = -\hat{v}\lambda_v \{\bar{V}_{BJ}\} - \hat{b}\lambda_b \left\{ \frac{\partial G_J}{\partial X_J} \right\}$$

The matrix expressions given by equations (3.4-114) are solved by inverting the influence coefficient matrices to determine the doublet distribution strengths.

The solutions to equations (3.4-114) are combined into a single matrix equation for an aircraft configuration having M slender bodies. This combined equation is written as follows:

$$\{S_B^D\} = [a_{B,B}^D]^{-1} \left\{ -\hat{w}\lambda_w \{\bar{W}_B\} - \hat{v}\lambda_v \{\bar{V}_B\} + \{\Psi_{cB}\} \right\} \quad (3.4-115)$$

where

$$\{S_B^D\} \equiv \begin{bmatrix} \{S_{B1}^{YD}\} \\ \vdots \\ \{S_{BM}^{YD}\} \\ \{S_{B1}^{ZD}\} \\ \vdots \\ \{S_{BM}^{ZD}\} \end{bmatrix}, \quad (3.4-116)$$

$$[a_{B,B}^D]^{-1} \equiv \begin{bmatrix} [a_{B1,B1}^{YD}]^{-1} & & & & \\ & \ddots & & & \\ & & [a_{BM,BM}^{YD}]^{-1} & & \text{zeros} \\ & & & [a_{B1,B1}^{ZD}]^{-1} & \\ \text{zeros} & & & & \ddots \\ & & & & & [a_{BM,BM}^{ZD}]^{-1} \end{bmatrix} \quad (3.4-117)$$

$$\{\bar{W}_B\} \equiv \begin{bmatrix} 0 \\ \vdots \\ 0 \\ \hline \{\bar{W}_{B1}\} \\ \vdots \\ \{\bar{W}_{BM}\} \end{bmatrix}, \quad \{\bar{V}_B\} \equiv \begin{bmatrix} \{\bar{V}_{B1}\} \\ \vdots \\ \{\bar{V}_{BM}\} \\ \hline 0 \\ \vdots \\ 0 \end{bmatrix}, \quad \{\Psi_{cB}\} \equiv \begin{bmatrix} -\hat{b}\lambda_b \{(\frac{\partial G}{\partial X})_B\} \\ \hline -\hat{c}\lambda_c \{(\frac{\partial I}{\partial X})_B\} \end{bmatrix} \quad (3.4-118)$$

$$\{(\frac{\partial I}{\partial X})_B\} \equiv \begin{bmatrix} 0 \\ \vdots \\ 0 \\ \hline \{\frac{\partial I_1}{\partial X_1}\} \\ \vdots \\ \{\frac{\partial I_M}{\partial X_M}\} \end{bmatrix} \quad \text{and} \quad \{(\frac{\partial G}{\partial X})_B\} \equiv \begin{bmatrix} \{\frac{\partial G_1}{\partial X_1}\} \\ \vdots \\ \{\frac{\partial G_M}{\partial X_M}\} \\ \hline 0 \\ \vdots \\ 0 \end{bmatrix}$$

3.4.5.1 Isolated slender body steady lift interference flow incidence.—The interference flow incidence induced by the steady lift of an isolated slender body is computed using the formula given by equation (3.4-13) with the velocity components, equations (3.4-11), computed from the solution to the isolated slender body steady lifting problem, equation (3.4-109). These velocity components are given by

$$v_{r_{BJ}}^{(Y)} = \sum_{j=1}^J v_{r_{BJj}}^{(Y)} S_{BJj}^{(Y)} \quad (3.4-119)$$

and

$$v_{\theta_{BJ}}^{(Y)} = \sum_{j=1}^J v_{\theta_{BJj}}^{(Y)} S_{BJj}^{(Y)}$$

where the quantities $S_{BJj}^{(Y)}$ are the doublet distribution strengths given by equation (3.4-115) and

$$\begin{aligned} v_{r_{BJj}}^{(Y)} &\equiv \frac{\partial \phi_{BJj}^{(Y)}}{\partial r} \\ v_{\theta_{BJj}}^{(Y)} &\equiv \frac{1}{r} \frac{\partial \phi_{BJj}^{(Y)}}{\partial \theta} \end{aligned} \quad (3.4-120)$$

These velocity components are evaluated at the control points of all mean surface panels of a configuration except for the panels on the interference surface of the J^{th} slender body. This evaluation is carried out using the method of section 3.4.1.5. Substituting the results into equation (3.4-13) yields the interference flow incidence on the I^{th} thin body mean surface as

$$\psi_{WIi}^{(Y)} = \sum_{j=1}^J a_{WI, BJij}^{(Y)} S_{BJj}^{(Y)} \quad (3.4-121)$$

and on the K^{th} slender body mean surface as

$$\begin{aligned} \left(\frac{Y}{Z}\right)_D \Psi_{BKK} &= \sum_{j=1}^{LJ} a_{BK, BJKj} \left(\frac{Y}{Z}\right)_D S_{BJj} \text{ for } K \neq J \\ &= 0 \text{ for } K=J \end{aligned} \quad (3.4-122)$$

where the influence coefficients are given by

$$\begin{aligned} \left(\frac{Y}{Z}\right)_D a_{WI, BJij} &= v_{rWI, BJij} \left(\frac{Y}{Z}\right) \sin (\theta_{Ii} - \theta(Jj)) \\ &\quad - v_{\theta WI, BJij} \left(\frac{Y}{Z}\right)_D \cos (\theta_{Ii} - \theta(Jj)) \end{aligned} \quad (3.4-123)$$

and

$$\begin{aligned} \left(\frac{Y}{Z}\right)_D a_{BK, BJKj} &= v_{rBK, BJKj} \left(\frac{Y}{Z}\right) \sin (\theta_{Kk} - \theta(Jj)) \\ &\quad - v_{\theta BK, BJKj} \left(\frac{Y}{Z}\right)_D \cos (\theta_{Kk} - \theta(Jj)) \end{aligned} \quad (3.4-124)$$

The interference flow given by equations (3.4-121) and (3.4-122) is expressed in matrix form as follows:

$$\{\Psi_{BW}^D\}^{\text{int}} = [a_{BW, B}^D] \{S_B^D\} \quad (3.4-125)$$

where the interference flow is described by the matrix

$$\{\Psi_{BW}^D\}^{\text{int}} \equiv \begin{bmatrix} \{\Psi_{B1}^D\} \\ \vdots \\ \{\Psi_{BM}^D\} \\ \hline \{\Psi_{W1}^D\} \\ \vdots \\ \{\Psi_{WN}^D\} \end{bmatrix} \quad (3.4-126)$$

The influence coefficient matrix is given by

(3.4-127)

$$[a_{BW,B}^D] \equiv \begin{bmatrix} [a_{B1,B1}^{YD}] \cdots \text{zeros} & | & [a_{B1,B1}^{ZD}] \cdots \text{zeros} \\ \vdots & & \vdots \\ \text{zeros} & [a_{BM,BM}^{YD}] & | & \text{zeros} & [a_{BM,BM}^{ZD}] \\ \hline [a_{W1,B1}^{YD}] \cdots [a_{WL,BM}^{YD}] & | & [a_{W1,BM}^{ZD}] \cdots [a_{WL,BM}^{ZD}] \\ \vdots & & \vdots \\ [a_{WN,B1}^{YD}] \cdots [a_{WN,BM}^{YD}] & | & [a_{WN,B1}^{ZD}] \cdots [a_{WN,BM}^{ZD}] \end{bmatrix}$$

and the doublet distribution strengths are given by the matrix

$$\{S_B^D\} \equiv \begin{bmatrix} \{S_{B1}^{YD}\} \\ \vdots \\ \{S_{BM}^{YD}\} \\ \hline \{S_{B1}^{ZD}\} \\ \vdots \\ \{S_{EM}^{ZD}\} \end{bmatrix} \quad (3.4-128)$$

3.4.5.2 Isolated slender body steady lifting pressure.—The aerodynamic pressure induced by steady lift of an isolated slender body is computed on the basis of equations (3.3-50) and (3.3-51). Substituting into equations (3.3-50) and (3.3-51), the solution for the J th slender body, equation (3.4-109), leads to the pressure distributions

$$C_{P_{BJ}}^{ZD} = - 2 \sum_{j=1}^J u_{BJj}^{ZD} S_{BJj}^{ZD} \\ = C_{P_{BJ}}^{ZD}(x) \sin \theta$$

and

$$C_{P_{BJ}}^{YD} = - 2 \sum_{j=1}^J u_{BJj}^{YD} S_{BJj}^{YD} \\ = - C_{P_{BJ}}^{YD}(x) \cos \theta \quad (3.4-129)$$

where the nondimensional velocities u_{BJj}^{ZD} and u_{BJj}^{YD} are as follows:

$$u_{BJj}^{(Y)D} = \frac{\partial \phi_{BJj}^{(Y)D}}{\partial X_j} \quad (3.4-130)$$

The pressure distributions given by equations (3.4.129) vary as sine and cosine functions of the circumferential coordinate θ shown by figure 3.4-20. The pressure is evaluated at the points used as control points in the subsonic form of the problem, figures 3.4-15 and 3.4-18, leading to

$$C_{P_{BJi}}^{ZD} = -2 \sum_{j=1}^{lJ} u_{BJ, BJij}^{ZD} S_{BJj}^{ZD} \quad (3.4-131)$$

and

$$C_{P_{BJi}}^{YD} = -2 \sum_{j=1}^{lJ} u_{BJ, BJij}^{YD} S_{BJj}^{YD} \quad (3.4-132)$$

These results are incorporated into the following matrix equation:

$$\{C_P^D\}_B = [CPM_{B,B}^D] \{S_B^D\} \quad (3.4-133)$$

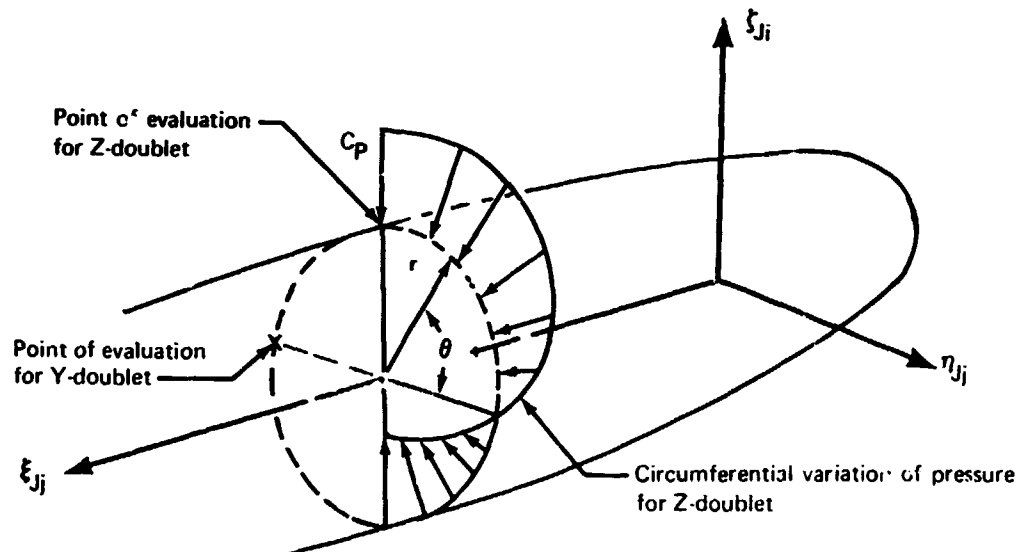


FIGURE 3.4-20.—SINE FUNCTION VARIATION OF C_p ON A SLENDER BODY SURFACE

where $\{S_B^D\}$ is as defined by equation (3.4-128), while the pressure coefficients at the surface points are given by

$$\{C_{P_B}^D\} \equiv \begin{bmatrix} \{C_{P_{B1}}^{YD}\} \\ \vdots \\ \{C_{P_{BM}}^{YD}\} \\ \hline ZD \\ \{C_{P_{B1}}^{ZD}\} \\ \vdots \\ ZD \\ \{C_{P_{BM}}^{ZD}\} \end{bmatrix} \quad (3.4-134)$$

and the pressure influence coefficients are expressed in matrix form as

$$[CPM_{B,B}^D] \equiv \begin{bmatrix} [-2u_{B1,B1}^{YD}] & \text{zeros} & & \\ & \ddots & & \\ \text{zeros} & & [-2u_{BM,BM}^{YD}] & \\ \hline & \text{zeros} & & [-2u_{B1,B1}^{ZD}] & \text{zeros} \\ & & & \ddots & \\ \text{zeros} & & & \text{zeros} & [-2u_{BM,BM}^{ZD}] \end{bmatrix} \quad (3.4-135)$$

3.4.5.3 Isolated slender body steady lift induced velocity components.—The computations for isolated slender body steady lift interference flow and pressure require the following velocity components:

$$\begin{array}{ll} u_{BJj}^{ZD} & u_{BJj}^{YD} \\ v_{rBJj}^{ZD} & v_{rBJj}^{YD} \\ v_{\theta BJj}^{ZD} & v_{\theta BJj}^{YD} \end{array} \quad (3.4-136)$$

As noted in the preceding, these velocity components are computed from the velocity potentials

$$\phi_{BJj}^{YD} \quad \text{and} \quad \phi_{BJj}^{ZD}$$

and these potentials are computed from the potential for a line source as

$$\phi_{BJj}^{YD} = -\cos\theta \frac{\partial \phi^S}{\partial r}{}_{BJj}$$

and

(3.4-137)

$$\phi_{BJj}^{ZD} = \sin\theta \frac{\partial \phi^S}{\partial r}{}_{BJj}$$

The computations differ for subsonic and supersonic flow, as described in the following.

Subsonic Case: In subsonic flow the velocity components are derived from the following potential for a line source of quadratic strength variation distributed on the line $0 \leq \xi \leq L$:

$$\phi_L^S = -\frac{1}{4\pi} \int_0^L \frac{(\xi')^2}{R} d\xi' \quad (3.4-138)$$

where

$$R \equiv \sqrt{(\xi - \xi')^2 + a^2},$$

$$a \equiv \beta r,$$

and

$$r \equiv \sqrt{\eta^2 + \zeta^2}$$

Carrying out the indicated integration leads to

$$\phi_L^S = -\frac{1}{4\pi} \sum_{n=1}^2 (-1)^n \left\{ \frac{4\xi - X_n}{2} d_n - \left(\xi^2 - \frac{a^2}{2} \right) \sinh^{-1} \frac{X_n}{a} \right\}$$

(3.4-139)

where

$$d_1 \equiv X_1^2 + a^2, \quad d_2 \equiv X_2^2 + a^2$$

$$X_1 \equiv \xi, \quad X_2 \equiv \xi - L$$

The differentiation indicated by equations (3.4-137) leads to the potentials for line doublets of quadratic strength variation, on the line $0 \leq \xi \leq L$ as

$$\begin{aligned} \left(\frac{Y}{Z}\right)_D^D \phi_L = \frac{\beta}{4\pi r} \left(\frac{-\cos\theta}{\sin\theta}\right) \sum_{n=1}^2 (-1)^n \left\{ \frac{1}{d_n} [a^2 (2\xi - X_n) \right. \\ \left. + \xi^2 X_n] + a^2 \sinh^{-1} \frac{X_n}{a} \right\} \end{aligned} \quad (3.4-140)$$

Introducing the following definitions for three quadratic distributions:

$$\begin{aligned} \left(\frac{Y}{Z}\right)_D^D \phi_{j-1} \equiv \left(\frac{Y}{Z}\right)_D^D \phi_L \quad \text{for } L = L_{BJj-1} + L_{BJj} + L_{BJj+1} \text{ and} \\ \xi = \xi_{Jj} + L_{BJj-1} \end{aligned}$$

$$\left(\frac{Y}{Z}\right)_D^D \phi_j \equiv \left(\frac{Y}{Z}\right)_D^D \phi_L \quad \text{for } L = L_{BJj} + L_{BJj+1} \text{ and } \xi = \xi_{Jj}$$

$$\left(\frac{Y}{Z}\right)_D^D \phi_{j+1} \equiv \left(\frac{Y}{Z}\right)_D^D \phi_L \quad \text{for } L = L_{BJj+1} \text{ and } \xi = \xi_{Jj} - L_{BJj}$$

the potentials due to a quadratic spline distribution of line doublets about the j^{th} slender body mean centerline segment, figure 3.4-19, are constructed as

$$\left(\frac{Y}{Z}\right)_D^D \phi_{BJj} = \left(\frac{Y}{Z}\right)_D^D \phi_{j-1} + a_j \left(\frac{Y}{Z}\right)_D^D \phi_j + b_j \left(\frac{Y}{Z}\right)_D^D \phi_{j+1} \quad (3.4-141)$$

where the coefficients a_j and b_j are given by the formulas

$$a_j \equiv - \frac{(L_{BJj-1} + L_{BJj})(L_{BJj-1} + L_{BJj} + L_{BJj+1})}{L_{BJj}(L_{BJj} + L_{BJj+1})}$$

and

$$b_J \equiv \frac{L_{BJj-1} (L_{BJj-1} + L_{BJj} + L_{BJj+1})}{L_{BJj} (L_{BJj+1})}$$

The velocity components, equation (3.4-136), for computing the flow incidence and pressure induced by the quadratic spline line doublets are found by differentiating the potential, equation (3.4-141), as follows:

$$\begin{aligned} v_{r_{BJj}}^{(Y)D} &= \frac{\partial}{\partial r} (\phi_{BJj}^{(Y)D}) \\ v_{\theta_{BJj}}^{(Y)D} &= \frac{1}{r} \frac{\partial}{\partial \theta} (\phi_{BJj}^{(Y)D}) \end{aligned} \quad (3.4-142)$$

These operations lead to the desired velocity components given by the following formulas:

$$\begin{aligned} u_L^{(Y)D} &= \frac{1}{4\pi r} \left(\frac{-\cos\theta}{\sin\theta} \right) \sum_{n=1}^2 (-1)^n \left\{ -\frac{X_n}{(d_n)^3} [a^2(2\xi - X_n) + \xi^2 X_n] \right. \\ &\quad \left. + \frac{1}{d_n} [2(a^2 + \xi X_n) + \xi^2] \right\} \\ v_{r_L}^{(Y)D} &= -\frac{1}{r} \phi_L^{(Y)D} + \frac{\beta^2}{4\pi} \left(\frac{-\cos\theta}{\sin\theta} \right) \sum_{n=1}^2 (-1)^n \left\{ -\frac{1}{(d_n)^3} [a^2(2\xi - X_n) \right. \\ &\quad \left. + \xi^2 X_n] + \frac{1}{d_n} (4\xi - 3X_n) + 2\sinh^{-1} \frac{X_n}{a} \right\} \\ v_{\theta_L}^{(Y)D} &= \frac{1}{r} \left(\frac{-\tan\theta}{\cot\theta} \right) \phi_L^{(Y)D} \end{aligned} \quad (3.4-143)$$

where, again,

$$d_1 \equiv X_1^2 + a^2, \quad d_2 \equiv X_2^2 + a^2$$

$$X_1 \equiv \xi, \quad X_2 \equiv \xi - L$$

Evaluating these velocity components at the aerodynamic control points leads to the values of the quantities appearing in the matrices defined by equations (3.4-117), (3.4-127), and (3.4-135).

Supersonic Case: The velocity potentials for the supersonic line doublets are derived, as in the subsonic case, by differentiating the velocity potential for a source having the same strength variation, viz.,

$$\phi_{BJK}^S = - \frac{1}{2\pi} \int_0^{(\xi-a); (L-X(o))} \frac{(\xi')^2 d\xi'}{R} \quad (3.4-144)$$

where

$$R \equiv \sqrt{(\xi_{JK} - \xi_{JK}')^2 - a^2}, \quad a \equiv \beta \sqrt{(\eta_{JK})^2 + (\zeta_{JK})^2},$$

$$\beta \equiv \sqrt{M^2 - 1}$$

$$\xi \equiv \xi_{JK}, \quad L \equiv L_{BJ}, \quad X(o) \equiv X_{JK}(o)$$

and the first upper limit applies to region II, figure 3.4-17, and the second to region III. The indicated integration is more readily carried out by writing the potential as follows:

$$\begin{aligned} \phi_{BJK}^S &= - \frac{1}{2\pi} \int \frac{1}{R} [(\xi' - \xi)^2 + 2(\xi' - \xi)\xi + (\xi)^2] d\xi' \\ &= - \frac{1}{2\pi} [I_2 + 2\xi I_1 + (\xi)^2 I_0] \end{aligned} \quad (3.4-145)$$

where for region II

$$I_0 \equiv \int_0^{\xi-a} \frac{1}{R} d\xi'$$

$$I_1 \equiv \int_0^{\xi-a} \frac{(\xi' - \xi)}{R} d\xi'$$

$$I_2 \equiv \int_0^{\xi-a} \frac{(\xi' - \xi)^2}{R} d\xi'$$

and for region III

$$I_0 \equiv \int_0^{L-X(0)} \frac{1}{R} d\xi'$$

$$I_1 \equiv \int_0^{L-X(0)} \frac{(\xi' - \xi)}{R} d\xi'$$

$$I_2 \equiv \int_0^{L-X(0)} \frac{(\xi' - \xi)^2}{R} d\xi'$$

As in the case of supersonic line sources, a change of variable is introduced as

$$\frac{\xi' - \xi}{a} = \cosh \sigma \quad (3.4-146)$$

The integrations then follow readily to obtain in region II

$$I_0 = \cosh^{-1} \left(\frac{\xi}{a} \right)$$

$$I_1 = - \sqrt{(\xi)^2 - a^2}$$

$$I_2 = \frac{1}{2} [\xi \sqrt{(\xi)^2 - a^2} + a^2 \cosh^{-1} \left(\frac{\xi}{a} \right)]$$

and in region III

$$I_0 = \cosh^{-1} \left(\frac{\xi}{a} \right) - \cosh^{-1} \left(\frac{\xi - L + X(0)}{a} \right)$$

$$I_1 = - \sqrt{(\xi)^2 - a^2} + \sqrt{(\xi - L + X(0))^2 - a^2}$$

$$I_2 = \frac{1}{2} [\xi \sqrt{(\xi)^2 - a^2} + a^2 \cosh^{-1} \left(\frac{\xi}{a} \right) - (\xi - L + X(0)) \sqrt{(\xi - L + X(0))^2 - a^2} - a^2 \cosh^{-1} \left(\frac{\xi - L + X(0)}{a} \right)] \quad (3.4-147)$$

On substituting equations (3.4-146) and (3.4-147) into equation (3.4-145), the supersonic line source potential is found for region II as:

$$\phi_{BJK}^S = -\frac{1}{2\pi} \left\{ \frac{3\xi}{2} d_1 - \sqrt{\left(\xi^2 + \frac{a^2}{2}\right)} \cosh^{-1} \frac{\xi}{a} \right\}$$

and for region III as:

(3.4-148)

$$\phi_{BJK}^S = -\frac{1}{2\pi} \sum_{n=1}^2 (-1)^n \left\{ -\frac{4\xi - X_n}{2} d_n + \left(\xi^2 + \frac{a^2}{2}\right) \cosh^{-1} \frac{X_n}{a} \right\}$$

where

$$d_1 \equiv \sqrt{X_1^2 - a^2}, \quad d_2 \equiv \sqrt{X_2^2 - a^2}$$

$$X_1 \equiv \xi, \quad X_2 \equiv \xi - (L - X(0))$$

The velocity potentials for the line doublets are obtained from the line source potential as

$$\begin{pmatrix} Z \\ Y \end{pmatrix}_D = \begin{pmatrix} -\cos\theta \\ \sin\theta \end{pmatrix} \beta \frac{\partial \phi_{BJK}^S}{\partial a} \quad (3.4-149)$$

Carrying out this operation yields doublet potentials for region II as:

$$\begin{pmatrix} Y \\ Z \end{pmatrix}_D = \frac{\beta}{2\pi} \begin{pmatrix} -\cos\theta \\ \sin\theta \end{pmatrix} \left\{ \frac{\xi}{a} d_1 - a \cosh^{-1} \left(\frac{\xi}{a} \right) \right\} \quad (3.4-150)$$

and for region III as:

$$\begin{aligned} \begin{pmatrix} Y \\ Z \end{pmatrix}_D &= \frac{\beta}{2\pi} \begin{pmatrix} -\cos\theta \\ \sin\theta \end{pmatrix} \sum_{n=1}^2 (-1)^n \left\{ \left[2\xi a - \left(\frac{\xi^2}{a} + a \right) X_n \right] \frac{1}{d_n} \right. \\ &\quad \left. + a \cosh^{-1} \frac{X_n}{a} \right\} \end{aligned} \quad (3.4-151)$$

The required velocity components, equation (3.4-136), are now found by carrying out the following operations on the supersonic doublet potentials, equations (3.4-150) and (3.4-151):

$$\begin{aligned} u_{BJK}^{(Z)D} &= \frac{\partial}{\partial \xi} (\phi_{BJK}^{(Z)}) \\ v_r^{(Z)D} &= \beta \frac{\partial}{\partial a} (\phi_{BJK}^{(Z)}) \\ v_\theta^{(Z)D} &= \frac{1}{r} \frac{\partial}{\partial \theta} (\phi_{BJK}^{(Z)}) \end{aligned} \quad (3.4-152)$$

The velocity components for region I computed from equation (3.4-150) and are found to be

$$\begin{aligned} u_{BJK}^{(Y)D} &= \frac{\beta}{\pi} (-\cos \theta) \frac{d_1}{a} \\ v_r^{(Y)D} &= \frac{\beta^2}{2\pi} (-\cos \theta) \left[-\frac{\xi d_1}{a^2} - \cosh^{-1} \frac{\xi}{a} \right] \\ v_\theta^{(Y)D} &= \frac{1}{r} (-\tan \theta) \phi_{BJK}^{(Y)D} \end{aligned} \quad (3.4-153)$$

For region III the velocity components are found to be given by the following:

(3.4-154)

$$u_{BJK}^{(Y)_D} = \frac{\beta}{2\pi} \begin{pmatrix} -\cos\theta \\ \sin\theta \end{pmatrix} \sum_{n=1}^{\infty} (-1)^n \left\{ \left[2a - \frac{\xi(2X_n + \xi)}{a} \right] \frac{1}{d_n} \right. \\ \left. - \left[2\xi a - \left(\frac{\xi^2}{a} + a \right) X_n \right] \frac{X_n}{(d_n)^3} \right\}$$

$$v_{r_{BJK}}^{(Y)_D} = \frac{\beta^2}{2\pi} \begin{pmatrix} -\cos\theta \\ \sin\theta \end{pmatrix} \sum_{n=1}^{\infty} (-1)^n \left\{ \left[2(\xi - X_n) + \frac{\xi^2 X_n}{a^2} \right] \frac{1}{d_n} \right. \\ \left. + \left[2\xi a^2 - (\xi^2 + a^2) X_n \right] \frac{1}{(d_n)^3} + \cosh^{-1} \frac{X_n}{a} \right\}$$

$$v_{\theta_{BJK}}^{(Y)_D} = \frac{1}{r} \begin{pmatrix} -\tan\theta \\ \cot\theta \end{pmatrix} \phi_{BJK}^{(Y)_D}$$

3.4.6 Steady Aerodynamic Induction Problem

3.4.6.1 Steady aerodynamic induction potential. – As shown by section 3.3.2.5, the solution to the steady aerodynamic induction problem is expressed in terms of vorticity distributed on the mean surfaces of all thin and slender bodies comprising an aircraft configuration, i.e.,

$$\phi^V(x, y, z) = \iiint_{S_W + S_B} \gamma_o^{int}(\xi, \eta, \zeta) K^V(x, y, z; \xi, \eta, \zeta) dS$$

where γ_o^{int} is a solution to the integral equation

$$\psi^{int} = \iiint_{S_W + S_B} \gamma_o^{int} \frac{\partial K^V}{\partial n} dS \quad (3.4-155)$$

wherein ψ^{int} is the interference flow incidence found from the solution to one of the preceding isolated body problems. The solution to the steady aerodynamic induction problem, equation (3.3-29), is expressed in terms of uniform distributions of vorticity on the mean surface panels, equation (3.4-50), as

$$\begin{aligned} \phi^V(x, y, z) = & \sum_{I=1}^N \sum_{i=1}^{nI} \phi_{WII}^V(x, y, z) S_{WII}^V \\ & + \sum_{J=1}^N \sum_{j=1}^{mJ} \phi_{BJj}^V(x, y, z) S_{BJj}^V \end{aligned} \quad (3.4-156)$$

where

$$\phi_{WII}^V(x, y, z) \equiv \iiint_{S_{WII}} K^V(x, y, z; \xi, \eta, \zeta) dS$$

$$\phi_{BJj}^W(x, y, z) \equiv \iiint_{S_{BJj}} K^V(x, y, z; \xi, \eta, \zeta) dS$$

The integral equation which must be solved, equation (3.4-155), is approximated by the following matrix expression similar to equation (3.4-62),

$$\{\psi^{(-)}\}_{BW}^{int} = -[a_{BW, BW}^V] \{S_{BW}^V\}^{int} \quad (3.4-157)$$

where $\{\Psi_{BW}^{(-)}\}^{int}$ is the interference flow incidence at the vortex panels and is given by each of equations (3.4-28), (3.4-63), (3.4-88), and (3.4-126), i.e., the interference flow incidence induced by one of the preceding isolated body problems. The influence coefficient matrix is given by

$$[a_{BW,BW}^V] = \begin{bmatrix} [a_{BW,B}^V] & [a_{BW,W}^V] \end{bmatrix} \quad (3.4-158)$$

where $[a_{BW,W}^V]$ is given by equation (3.4-64) and

$$[a_{BW,B}^V] \equiv \begin{bmatrix} [a_{B1,B1}^V] & \cdots & [a_{B1,BM}^V] \\ \vdots & \ddots & \vdots \\ [a_{BM,B1}^V] & \cdots & [a_{BM,BM}^V] \\ \hline [a_{W1,B1}^V] & \cdots & [a_{W1,BM}^V] \\ \vdots & \ddots & \vdots \\ [a_{WN,B1}^V] & \cdots & [a_{WN,BM}^V] \end{bmatrix} \quad (3.4-159)$$

Finally, the strengths of the vorticity distributions are given by

$$\{s_{BW}^V\} = \begin{bmatrix} \{s_B^V\} \\ \hline \{s_W^V\} \end{bmatrix}, \quad \{s_B^V\} = \begin{bmatrix} \{s_{B1}^V\} \\ \vdots \\ \{s_{BM}^V\} \end{bmatrix}, \quad \{s_W^V\} = \begin{bmatrix} \{s_{W1}^V\} \\ \vdots \\ \{s_{WN}^V\} \end{bmatrix} \quad (3.4-160)$$

The strengths of the vorticity distributions are found by inverting the influence coefficient matrix, i.e.,

$$\{s_{BW}^V\}^{int} = -[a_{BW,BW}^V]^{-1} \{\Psi_{BW}^{(-)}\}^{int} \quad (3.4-161)$$

Substituting the values so obtained into equation (3.4-156) yields the solution to the steady aerodynamic induction problem.

3.4.6.2 Steady aerodynamic induction pressure. -- The aerodynamic pressure induced by the aerodynamic induction problem constitutes the interference pressures induced by the isolated bodies of the preceding sections when they are combined to form a configuration. This pressure is computed by substituting the solution to the problem, equation (3.4-156),

into equation (3.3-52). Carrying out that operation and evaluating the pressure coefficient at the geometric centroid of each mean surface panel leads to the following matrix expression:

$$\{C_{P_{BW}}^V\}^{int} = [CPM_{BW,BW}^V] \{S_{BW}^V\}^{int} \quad (3.4-162)$$

The matrix of pressure coefficients appearing in this expression is given by

$$\{C_{P_{BW}}^V\} = \begin{bmatrix} \{C_{P_B}^V\} \\ \{C_{P_W}^V\} \end{bmatrix}, \quad \{C_{P_B}^V\} = \begin{bmatrix} \{C_{P_{B1}}^V\} \\ \vdots \\ \{C_{P_{BM}}^V\} \end{bmatrix}, \quad \{C_{P_W}^V\} = \begin{bmatrix} \{C_{P_{W1}}^V\} \\ \vdots \\ \{C_{P_{WN}}^V\} \end{bmatrix}$$

where $C_{P_{BJj}}^V \equiv -2u_{BJj}^V$ and $C_{P_{Wli}}^V \equiv -2u_{Wli}^V$.

The pressure influence coefficient matrix is given by

$$[CPM_{BW,BW}^V] \equiv \begin{bmatrix} [CPM_{B,B}^V] & [CPM_{B,W}^V] \\ [CPM_{W,B}^V] & [CPM_{W,W}^V] \end{bmatrix} \quad (3.4-164)$$

where

$$[CPM_{B,B}^V] \equiv [-2u_{BK,BJk}^V]$$

$$[CPM_{B,W}^V] \equiv [-2u_{BJ,WIj}^V]$$

$$[CPM_{W,B}^V] \equiv [-2u_{WI,BJi}^V]$$

$$[CPM_{W,W}^V] \equiv [-2u_{WI,WKik}^V]$$

and the final matrix is identical to the matrix of pressure influence coefficients for the isolated thin body steady lifting problem, equation (3.4-68).

3.4.7 Combined Steady Aerodynamic Problem

The development to this point has produced all of the elements which are used in the FLEXSTAB system to represent steady aerodynamics. In this section these elements are combined to obtain the final matrix expressions used in the FLEXSTAB system to relate aerodynamic surface pressures to the flow incidence described by the surface boundary conditions.

3.4.7.1 Combined steady lifting aerodynamics.—The steady lifting pressure acting on a configuration is the total of the isolated thin and slender body lifting pressures, sections 3.4.2.3 and 3.4.5.2, and the interference pressures. The total steady lifting pressure is expressed as

$$\{C_P\} \equiv \begin{bmatrix} \{C_{PB}^D\} \\ \{C_{PB}^V\} \\ \{C_{PW}^V\} \end{bmatrix} \quad (3.4-165)$$

where $\{C_{PB}^D\}$ is the isolated slender body lifting pressure, equation (3.4-133); $\{C_{PB}^V\}$ is the interference pressure on slender body mean surfaces, equation (3.4-163); and $\{C_{PW}^V\}$ is the combined isolated and interference thin body lifting pressure, equation (3.4-68). The strengths of the flow singularity distribution giving rise to the total pressure are expressed as

$$\{S\} \equiv \begin{bmatrix} \{S_B^D\} \\ \{S_B^V\} \\ \{S_W^V\} \end{bmatrix} \quad (3.4-166)$$

where $\{S_B^D\}$ represents the strengths of the line doublet distributions, equation (3.4-117); $\{S_B^V\}$ the strengths of the vorticity distributions on slender body mean surfaces arising from interference flows, equation (3.4-160); and $\{S_W^V\}$ the sum of the vorticity distribution strength from the isolated thin body lifting problem, equation (3.4-56), and those arising from interference flows, equation (3.4-160). Finally, the lifting pressure is given by

$$\{C_P\} = [CPM]\{S\} \quad (3.4-167)$$

where

$$[CPM] \equiv \begin{bmatrix} [CPM_{B,B}^D] & [0] \\ [CPM_{BW,B}^D] & [CPM_{BW,BW}^V] \end{bmatrix}$$

wherein $[CPM_{BW,BW}^V]$ is defined by equation (3.4-164) while

$$[CPM_{BW,B}^D] \equiv \begin{bmatrix} [CPM_{B,B}^D] \\ [CPM_{W,B}^D] \end{bmatrix}$$

where $[CPM_{W,B}^D] = [0]$ and $[CPM_{B,B}^D] = \begin{bmatrix} [CPM_{BJ,BJ}^D] \end{bmatrix}$

since $[CPM_{BI,BJ}^D] = [0]$ for $I \neq J$, equation (3.4-135)

The relationship between the singularity strengths of equation (3.4-166) and the flow incidence at all control points in the lifting problem is given by

$$\{\Psi'\} = [AIC]\{S\} \quad (3.4-168)$$

where

$$\{\Psi'\} \equiv \begin{bmatrix} \{\Psi_B^D\} \\ \{\Psi_{BW}^V\} \\ \{\Psi_W^V\} \end{bmatrix}$$

and

$$[AIC] \equiv \begin{bmatrix} [a_{B,B}^D] & | & \text{zeros} \\ \hline [a_{BW,B}^D] & | & [a_{BW,BW}^V] \end{bmatrix}$$

The partitions of the matrix $[AIC]$ are given by equation (3.4-117), equation (3.4-127), and the influence coefficients of the aerodynamic induction problem, equation (3.4-159). Equation (3.4-168) represents the basic steady lifting aerodynamic influence coefficient relation of the FLEXSTAB system; however, the term "aerodynamic influence coefficient" is reserved herein for the relationship between lifting pressure and flow incidence.

The aerodynamic influence coefficients are found by combining equations (3.4-167) and (3.4-168) as follows:

$$\{C_p\} = [LSC]\{\Psi'\} \quad (3.4-169)$$

where

$$[LSC] \equiv [CPM][AIC]^{-1} \quad (3.4-170)$$

and

$$[AIC]^{-1} \equiv \begin{bmatrix} [a_{B,B}^D]^{-1} & | & \text{zeros} \\ \hline -[a_{BW,BW}^V]^{-1}[a_{BW,B}^V][a_{B,B}^D]^{-1} & | & [a_{BW,BW}^V]^{-1} \end{bmatrix}$$

The interference flow incidences must vanish at the mean surfaces of slender bodies; thus, the flow incidence matrix $\{\Psi'\}$ is reduced by deleting the elements $\{\Psi_B^V\}$. Also, the columns of the matrix $[LSC]$ multiplying the elements of $\{\Psi_B^V\}$ are deleted from the $[LSC]$ matrix. These operations lead to the combined lifting solution expressed as

$$\{C_p\} = [A]\{\Psi\} \quad (3.4-171)$$

where, from equations (3.4-56) and (3.4-115),

$$\{\Psi\} = -\hat{w}\lambda_w\{\bar{W}\} - \hat{v}\lambda_v\{\bar{V}\} + \{\Psi_c\} \quad (3.4-172)$$

with

$$\{\bar{W}\} \equiv \begin{bmatrix} \{\bar{W}_B\} \\ \{\bar{W}_W\} \end{bmatrix} \quad \{\bar{V}\} \equiv \begin{bmatrix} \{\bar{V}_B\} \\ \{\bar{V}_W\} \end{bmatrix}$$

and

$$\{\Psi_c\} \equiv \begin{bmatrix} \{\Psi_{CB}\} \\ \{\Psi_{CW}\} \end{bmatrix}$$

Equation (3.4-171) yields quantities from which the entire lifting pressure on an aircraft configuration is determined from the steady part of the flow incidence. Following the method of reference (1-1), the thin body partition of equation (3.4-172) is evaluated for flow incidence at panel centroids even though equation (3.4-168) is evaluated for flow incidence at the panel control points. This arrangement has been found empirically to yield a better approximation than when equation (3.4-172) is evaluated at panel control points.

3.4.7.2 Combined thickness aerodynamics.—The pressure induced by thin and slender body thickness is expressed in two parts—the pressure induced on the isolated bodies, sections 3.4.2.2 and 3.4.4.2, and the thickness interference pressure. The isolated thickness pressures are expressed as

$$\{C_P^S\}^{iso} \equiv \begin{bmatrix} \{C_{PB}^S\}^{iso} \\ \{C_{PW}^S\}^{iso} \end{bmatrix} \quad (3.4-173)$$

where $\{C_{PB}^S\}$ is given by equation (3.4-93) and $\{C_{PW}^S\}$ is given by equation (3.4-35). The thickness interference pressure is found by substituting into the aerodynamic induction problem, i.e.,

$$\{C_{PBW}^V\}^{int} = -[CPM_{BW,BW}^V][a_{BW,BW}^V]^{-1}\{\psi_{BW}^S\}^{int}, \quad (3.4-174)$$

the interference flow incidence induced by thin and slender body thickness, equations (3.4-27) and (3.4-87), i.e.,

$$\{\psi_{BW}^S\}^{int} = [TD^S]\{S^S\} \quad (3.4-175)$$

$$[TD^S] \equiv [[a_{BW,B}^S][a_{BW,W}^{CS}][a_{BW,W}^{LS}], \{S^S\} \equiv \begin{bmatrix} \{S_B^S\} \\ \{S_W^{CS}\} \\ \{S_W^{LS}\} \end{bmatrix}$$

3.4.8 Isolated Thin Body Unsteady Lifting Problem

In section 3.3.2.6 the solution to the isolated thin body unsteady lifting problem is expressed in terms of vorticity distributed on the thin body mean surface, equation (3.3-35), and the vorticity distribution is required to satisfy the integral equations given as equation (3.3-34). The vorticity distribution γ_0 is that determined in the steady form of the problem, section 3.4.3; and, like the distribution γ_0 , the distributions γ_1 , γ_2 , and γ_3 which introduce the effects of unsteady flow are assumed to be uniform on each panel, viz.,

$$\left. \begin{aligned} \gamma_1(\xi_{Ii}, \eta_{Ii}) &= S_{WIi}^{V1} \\ \gamma_2(\xi_{Ii}, \eta_{Ii}) &= S_{WIi}^{V2} \\ \gamma_3(\xi_{Ii}, \eta_{Ii}) &= S_{WIi}^{V3} \end{aligned} \right\} \text{ for } \xi_{Ii}, \eta_{Ii} \text{ in } S_{WIi}$$

Having introduced these approximations, the unsteady velocity potential is given by

$$\begin{aligned} \phi_{WI}^{UV}(X_I, Y_I, Z_I) &= \sum_{i=1}^{nI} [\phi_{WIi}^V S_{WIi}^{V1} + \frac{M^2}{\beta^2} (X_I \phi_{WIi}^V S_{WIi}^{V1} \\ &- \phi_{WIi}^V S_{WIi}^{V2}) - \frac{1}{\beta^2} (\int_{-\infty}^{X_I} \phi_{WIi}^V S_{WIi}^{V1} d\xi - \phi_{WIi}^V S_{WIi}^{V3})] \end{aligned} \quad (3.4-176)$$

where

$$\phi_{WIi}^V \equiv \iiint_{S_{WIi}} K^V(X_I, Y_I, Z_I; \xi'_{Ii}, \eta'_{Ii}) d\xi'_{Ii} d\eta'_{Ii}$$

and the integral equation (3.3-34), in terms of the influence functions introduced by equation (3.4-53), become as follows:

$$\begin{aligned} \dot{\psi}_{WI/U} &= \sum_{i=1}^{nI} a_{WIi}^V S_{WIi}^{V1} \\ X_I \dot{\psi}_{WI/U} &= \sum_{i=1}^{nI} a_{WIi}^V S_{WIi}^{V2} \end{aligned} \quad (3.4-177)$$

and

$$\sum_{i=1}^{nI} \left[\int_{-\infty}^{X_I} a_{WIi}^V(\xi, X_I, Y_I) d\xi \right] S_{WIi}^{V1} = \sum_{i=1}^{nI} a_{WIi}^V S_{WIi}^{V3}$$

where $\dot{\Psi}_{WI}^V$ is given by equation (3.3-36).

Equations (3.4-177) are evaluated at the control points of the mean surface panels, and the results are expressed in matrix form as

$$\frac{1}{U} \{\dot{\Psi}_{WI}^V\} = [a_{WI,WI}^V] \{S_{WI}^{V1}\},$$

$$\frac{1}{U} [X_{WI}^V] \{\dot{\Psi}_{WI}^V\} = [a_{WI,WI}^V] \{S_{WI}^{V2}\},$$

and

$$- [f a_{WI,WI}^V] S_{WI}^{V1} = [a_{WI,WI}^V] \{S_{WI}^{V3}\}$$

where the matrix $[X_{WI}^V]$ contains the X_I -coordinates of the panel control points and the matrix $[f a_{WI,WI}^V]$ is formed in the same manner as $[a_{WI,WI}^V]$, but the elements are the result of evaluating

$$- \int_{-\infty}^{X_I} a_{WIi}^V(\xi, Y_I, Z_I) d\xi \quad (3.4-179)$$

at the panel control points. The solution to the problem is constructed by solving equations (3.4-178) for the values of $\{S_{WI}^{V1}\}$, $\{S_{WI}^{V2}\}$, and $\{S_{WI}^{V3}\}$ and substituting the values so determined into equation (3.4-176).

The solutions to equations (3.4-178) are formulated for N thin bodies in a configuration and expressed in a single matrix equation using the notation of equation (3.4-56) as follows:

$$\{S_W^{V1}\} = [a_{W,W}^V]^{-1} \{\dot{\Psi}_W^V\} \frac{1}{U}, \quad (3.4-180)$$

$$\{S_W^{V2}\} = [a_{W,W}^V]^{-1} [X_W^V] \{\dot{\Psi}_W^V\} \frac{1}{U},$$

and

$$\{S_W^{V3}\} = -[a_{W,W}^V]^{-1} [f a_{W,W}^V] [a_{W,W}^V]^{-1} \{\dot{\Psi}_W^V\} \frac{1}{U}$$

where

$$[X_W^V] \equiv \begin{bmatrix} [X_{WI}^V] & \text{zeros} \\ & \ddots \\ \text{zeros} & [X_{WN}^V] \end{bmatrix} \quad (3.4-181)$$

with the panel control point coordinates expressed in the Reference Axis System.

3.4.8.1 Isolated thin body unsteady lifting interference flow incidence.—Each of the vorticity distributions whose strength is determined by equations (3.4-180) induces an interference flow. These interference flows at the panel control points on the mean surfaces of all thin and slender bodies of a configuration are obtained by setting up equations (3.4-180) and (3.4-181) in the form which they have prior to solution. These equations are expressed in terms of the panels on all N thin and M slender bodies of a configuration and appear as follows:

$$\frac{1}{U} \begin{bmatrix} \{\dot{\Psi}_B^V\} \\ \{\dot{\Psi}_W^V\} \end{bmatrix} = \begin{bmatrix} [a_{B,B}^V][a_{B,W}^V] \\ [a_{W,B}^V][a_{W,W}^V] \end{bmatrix} \begin{bmatrix} \{S_B^{V1}\} \\ \{S_W^{V1}\} \end{bmatrix}, \quad (3.4-182)$$

$$\frac{1}{U} \begin{bmatrix} [X_B^V] & [0] \\ [0] & [X_W^V] \end{bmatrix} \begin{bmatrix} \{\dot{\Psi}_B^V\} \\ \{\dot{\Psi}_W^V\} \end{bmatrix} = \begin{bmatrix} [a_{B,B}^V][a_{B,W}^V] \\ [a_{W,B}^V][a_{W,W}^V] \end{bmatrix} \begin{bmatrix} \{S_B^{V2}\} \\ \{S_W^{V2}\} \end{bmatrix},$$

and

$$\begin{bmatrix} [a_{B,B}^V][a_{B,W}^V] \\ [a_{W,B}^V][a_{W,W}^V] \end{bmatrix} \begin{bmatrix} \{S_B^{V1}\} \\ \{S_W^{V1}\} \end{bmatrix} = - \begin{bmatrix} [a_{B,B}^V][a_{B,W}^V] \\ [a_{W,B}^V][a_{W,W}^V] \end{bmatrix} \begin{bmatrix} \{S_B^{V3}\} \\ \{S_W^{V3}\} \end{bmatrix}.$$

The interference flow incidence may now be obtained by determining $\{\dot{\Psi}_B^V\}^{int}$ and the required interference vorticity strengths.

An alternative approach, not used in the steady lifting problem, follows from setting the rates of change of flow incidence at the mean slender body surfaces to zero and solving for the resulting vorticity distribution strengths. This operation yields the strengths required

to represent the isolated thin body lift including interference effects. The operation is deferred, however, to section 3.4.10 where the effects of isolated slender body unsteady lift are also included.

3.4.8.2 Isolated thin body unsteady lifting pressure.—The aerodynamic pressure induced by the isolated thin body unsteady lift is computed on the basis of equation (3.3-53). Substituting the solution for the i^{th} thin body, equation (3.4-176), into equation (3.3-53) leads to the pressure distribution expressed as

$$C_{P_{WI}}^V = -2 \sum_{i=1}^{nI} \{ u_{WIi}^V S_{WIi}^V + \frac{M^2}{\beta^2} [X_I^V u_{WIi}^V S_{WIi}^{V1} - u_{WIi}^V S_{WIi}^{V2}] + \frac{1}{\beta^2} u_{WIi}^V S_{WIi}^{V3} \} \quad (3.4-183)$$

where

$$u_{WIi}^V \equiv \iint_{S_{WIi}} \frac{\partial K^V}{\partial X_I} dX_I' dY_I'$$

Evaluating the lifting pressure distribution, equation (3.4-66), at the surface of the thin body results in the matrix expression

$$\{C_{P_W}^V\} = [CPM_{W,W}^V] \{S_W^V\} + \frac{M^2}{\beta^2} ([X_W^V] [CPM_{W,W}^V] \{S_W^{V1}\} - [CPM_{W,W}^V] \{S_W^{V2}\}) + \frac{1}{\beta^2} [CPM_{W,W}^V] \{S_W^{V3}\} \quad (3.4-184)$$

where the matrices $\{C_{P_W}^V\}$ and $[CPM_{W,W}^V]$ are given by equations (3.4-69) and (3.4-70) and $[X_W^V]$ contains the coordinates of the points where the pressure is evaluated, i.e., the panel geometric centroids.

3.4.8.3 Isolated thin body unsteady lift induced velocity components.—The velocity components induced by the uniform vorticity distribution on a panel are considered in section 3.3.3. It remains, however, to consider the elements of the matrices contained in equations (3.4-182) which are obtained by evaluating equation (3.4-179), i.e.,

$$\int_{-\infty}^{X_J} a_{WII}^v(\xi; Y_J, Z_J) d\xi' = \sin(\theta_J - \theta_I) \int_{-\infty}^{X_J} \iint_{S_{WII}} \frac{\partial K^v}{\partial \eta} d\xi' ds$$

$$- \cos(\theta_J - \theta_I) \int_{-\infty}^{X_J} \iint_{S_{WII}} \frac{\partial K^v}{\partial \zeta} d\xi' ds \quad (3.4-185)$$

where K^v is the potential for an elementary horseshoe vortex (ref. 2-3, equation 5-35) and θ_J is the dihedral angle of the mean surface panel where equation (3.4-185) is evaluated, denoted as θ_{II} in figure 3.4-3.

Expressed in the local panel axis system figure 3.4-5, the potential induced at the point ξ, η, ζ due to an elementary horseshoe vortex with bound element at $\bar{\xi}, \bar{\eta}, \bar{\zeta} = 0$ is for *subsonic flow* (page 87 of reference 2-3):

$$K^v(\xi, \eta, \zeta; \bar{\xi}, \bar{\eta}) \equiv \frac{1}{4\pi} \frac{\zeta}{\sqrt{(\eta - \bar{\eta})^2 + \zeta^2}} \left\{ 1 + \frac{\xi - \bar{\xi}}{\sqrt{(\xi - \bar{\xi})^2 + \beta^2 r^2}} \right\} \quad (3.4-186)$$

and for *supersonic flow* (page 87 of reference 2-3):

$$K^v(\xi, \eta, \zeta; \bar{\xi}, \bar{\eta}) \equiv \frac{1}{2\pi} \frac{\zeta(\xi - \bar{\xi})}{\sqrt{(\eta - \bar{\eta})^2 + \zeta^2}} \left[\frac{1}{\sqrt{(\xi - \bar{\xi})^2 - \beta^2 r^2}} \right] \quad (3.4-187)$$

where

$$r^2 = (\eta - \bar{\eta})^2 + \zeta^2$$

Equation (3.4-185) contains the quantities

$$I_{uWII}^v \equiv \int_{-\infty}^{X_J} \iint_{S_{WII}} \frac{\partial K^v}{\partial \eta} d\xi' ds \quad (3.4-188)$$

and

$$I_{wWII}^v \equiv \int_{-\infty}^{X_J} \iint_{S_{WII}} \frac{\partial K^v}{\partial \zeta} d\xi' ds$$

which are obtained by operating on the potentials given by equations (3.4-186) and (3.4-187). The potentials are first differentiated with respect to η and ξ and then integrated twice with respect to ξ . In subsonic flow, one of these integrations is carried out using the leading and trailing edge coordinates of the panel, figure 3.4-5, as the limits of the integration. In the second integration the limits are $\xi = -\infty$ and the ξ coordinate where the influence of the panel is evaluated. In supersonic flow the first integration is carried out over only that portion of the panel which is contained in the Mach fore cone of the influenced point—the point P shown in figure 3.4-11. The panel is divided into two regions (I and II) as shown by figure 3.4-21 and the limits of integration extend only from the panel leading edge to the line of intersection between the panel and the Mach fore cone in region II.

Subsonic case: In subsonic flow the above operations reduce equations (3.4-188) to the following expressions which are evaluated by numerical integration over the η coordinate:

$$I_{u_{WIi}}^V = \frac{1}{4\pi} \int_0^b \frac{\zeta(\eta-\bar{\eta})}{[(\eta-\bar{\eta})^2 + \zeta^2]^2} \{ (\xi - \xi_T)^2 + (\xi - \xi_T) \sqrt{(\xi - \xi_T)^2 + \beta^2 r^2} \} d\bar{\eta} \quad (3.4-189)$$

$$- \frac{1}{4\pi} \int_0^b \frac{\zeta(\eta-\bar{\eta})}{[(\eta-\bar{\eta})^2 + \zeta^2]^2} \{ (\xi - \xi_L)^2 + (\xi - \xi_L) \sqrt{(\xi - \xi_L)^2 + \beta^2 r^2} \} d\bar{\eta}$$

$$I_{w_{WIi}}^V = \frac{1}{4\pi} \int_0^b \frac{\zeta(\eta-\bar{\eta})}{r^4} \{ (\xi - \xi_T)^2 + (\xi - \xi_T) \sqrt{(\xi - \xi_T)^2 + \beta^2 r^2} \} d\bar{\eta} \quad (3.4-190)$$

$$- \frac{1}{4\pi} \int_0^b \frac{\zeta(\eta-\bar{\eta})}{r^4} \{ (\xi - \xi_L)^2 + (\xi - \xi_L) \sqrt{(\xi - \xi_L)^2 + \beta^2 r^2} \} d\bar{\eta}$$

Supersonic case: In supersonic flow the contributions to the quantities $I_{v_{WIi}}^V$ and $I_{w_{WIi}}^V$ from regions I and II are obtained by numerical integration of the following expressions:

Region I:

$$I_{u_{WIi}}^V = \frac{1}{2\pi} \int_{\eta_1}^{\eta_2} \left\{ \frac{\zeta(\eta-\bar{\eta})(\xi-\xi_T)}{r^4} \sqrt{(\xi-\xi_T)^2 + \beta^2 r^2} \right\} d\bar{\eta} \quad (3.4-191)$$

$$- \frac{1}{2\pi} \int_{\eta_1}^{\eta_2} \left\{ \frac{\zeta(\xi-\xi_L)(\eta-\bar{\eta})}{r^4} \sqrt{(\xi-\xi_L)^2 - \beta^2 r^2} \right\} d\bar{\eta}$$

$$\begin{aligned}
I_{w_{WIi}}^v = & -\frac{1}{2\pi} \int_{\eta_1}^{\eta_2} \left[\frac{(\eta-\bar{\eta})^2 - \zeta^2}{r^4} \right] (\xi - \xi_T) \sqrt{(\xi - \xi_T)^2 - \beta^2 r^2} d\bar{\eta} \\
& - \frac{1}{2\pi} \int_{\eta_1}^{\eta_2} \frac{\beta^2 \zeta^2}{r^4} \frac{(\xi - \xi_T)}{\sqrt{(\xi - \xi_T)^2 - \beta^2 r^2}} d\bar{\eta} \\
& + \frac{1}{2\pi} \int_{\eta_1}^{\eta_2} \frac{\beta^2}{2} \text{Ln} |\xi - \xi_T + \sqrt{(\xi - \xi_T)^2 - \beta^2 r^2}| d\bar{\eta}
\end{aligned}
\tag{3.4-192}$$

$$\begin{aligned}
& + \frac{1}{2\pi} \int_{\eta_1}^{\eta_2} \left[\frac{(\eta-\bar{\eta})^2 - \zeta^2}{r^4} \right] (\xi - \xi_L) \sqrt{(\xi - \xi_L)^2 - \beta^2 r^2} d\bar{\eta} \\
& + \frac{1}{2\pi} \int_{\eta_1}^{\eta_2} \frac{\beta^2 \zeta^2}{r^4} \frac{(\xi - \xi_L)}{\sqrt{(\xi - \xi_L)^2 - \beta^2 r^2}} d\bar{\eta} \\
& - \frac{1}{2\pi} \int_{\eta_1}^{\eta_2} \frac{\beta^2}{2} \text{Ln} |\xi - \xi_L + \sqrt{(\xi - \xi_L)^2 - \beta^2 r^2}| d\bar{\eta}
\end{aligned}$$

Region II:

$$I_{u_{WIi}}^v = \frac{1}{2\pi} \int_{\eta_1}^{\eta_2} \frac{-\zeta(\eta-\bar{\eta})(\xi - \xi_L)}{r^4} \sqrt{(\xi - \xi_L)^2 - \beta^2 r^2} d\bar{\eta}
\tag{3.4-193}$$

$$\begin{aligned}
I_{w_{WIi}}^v = & \frac{1}{2\pi} \int_{\eta_1}^{\eta_2} \frac{[(\eta-\bar{\eta})^2 - \zeta^2]}{2r^4} (\xi - \xi_L) \sqrt{(\xi - \xi_L)^2 - \beta^2 r^2} d\bar{\eta} \\
& + \frac{1}{2\pi} \int_{\eta_1}^{\eta_2} \frac{\beta^2}{2} \{ \text{Ln} |\beta r| - \text{Ln} |\xi - \xi_L + \sqrt{(\xi - \xi_L)^2 - \beta^2 r^2}| \} d\bar{\eta}
\end{aligned}
\tag{3.4-194}$$

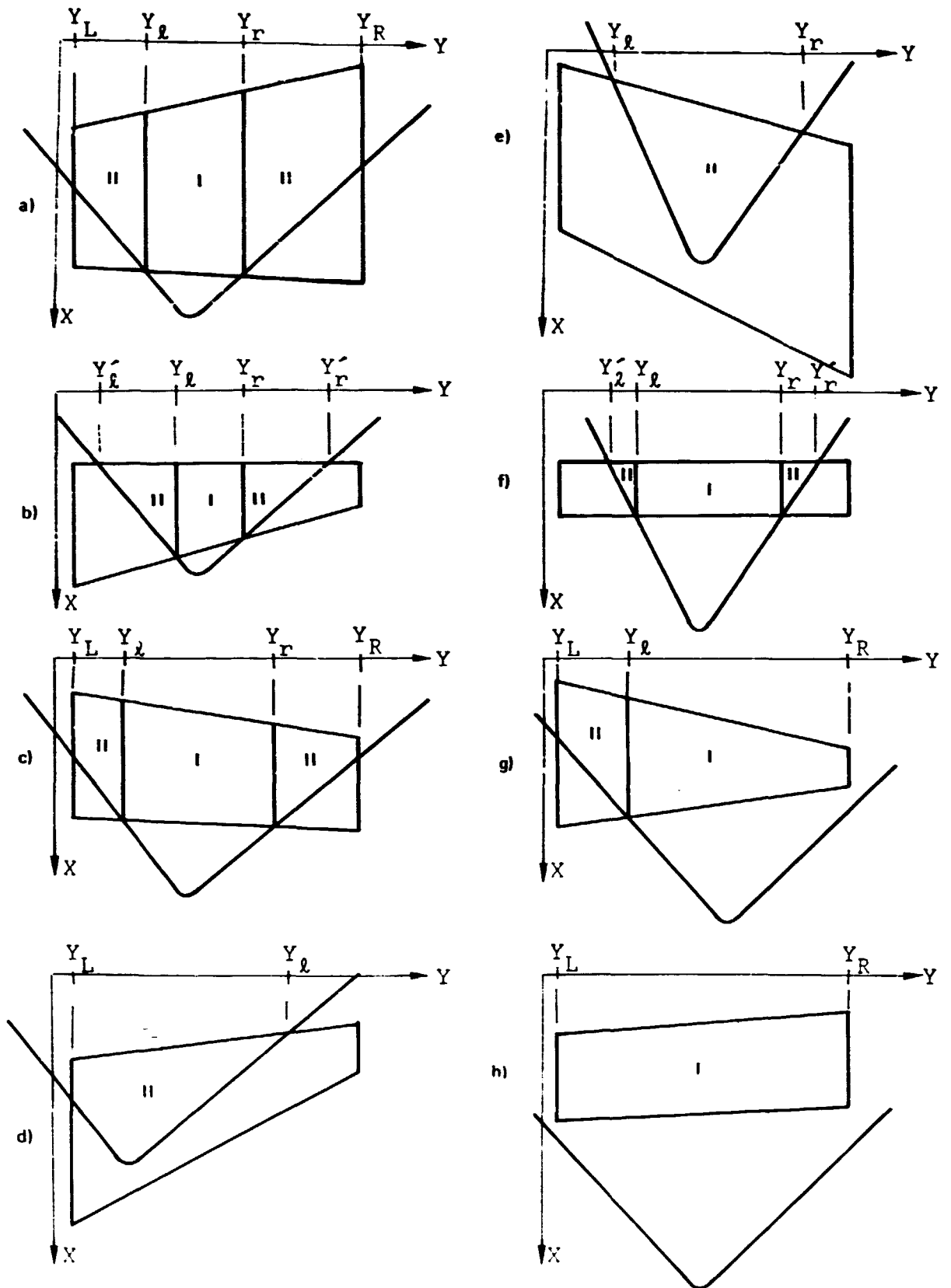


FIGURE 3.4-21.—REGIONS OF INTEGRATION FOR VORTEX PANEL IN SUPERSONIC FLOW

3.4.9 Isolated Slender Body Unsteady Lifting Problem

In section 3.3.2.7 the solution to the isolated slender body unsteady lifting problem is expressed in terms of line doublets distributed on the slender body mean centerline, equations (3.3-39) and (3.3-41), and these line doublet distributions are required to satisfy the integral equations given as equations (3.3-40) and (3.3-42). Letting line doublet distributions have the form introduced in section 3.4.5 for the two cases, subsonic or supersonic flow, the solution to the present problem—equations (3.3-39) and (3.3-41)—is approximated by the following expression:

$$\phi_{BJ}^{YD} = \sum_{j=1}^N \{ \phi_{BJj}^{YD} S_{BJj}^{YD} + \frac{M^2}{\beta^2} [X_j \phi_{BJj}^{YD1} S_{BJj}^{YD1} - \phi_{BJj}^{YD2} S_{BJj}^{YD2}] \} \quad (3.4-195)$$

$$\phi_{BJ}^{ZD} = \sum_{j=1}^N \{ \phi_{BJj}^{ZD} S_{BJj}^{ZD} + \frac{M^2}{\beta^2} [X_j \phi_{BJj}^{ZD1} S_{BJj}^{ZD1} - \phi_{BJj}^{ZD2} S_{BJj}^{ZD2}] \}$$

where ϕ_{BJj}^{YD} and ϕ_{BJj}^{ZD} are as defined in section 3.4.5.

The integral equations, equations (3.3-40) and (3.3-42), which must be solved to determine the doublet distribution strengths, are expressed in terms of the influence coefficients given by equation (3.4-113) and appear as follows:

$$\begin{aligned} \frac{1}{U} \{ \dot{\psi}_{BJ}^{YD} \} &= [a_{BJ,BJ}^{YD}] \{ S_{BJ}^{YD1} \} \\ \frac{1}{U} [X_{BJ}^D] \{ \dot{\psi}_{BJ}^{YD} \} &= [a_{BJ,BJ}^{YD}] \{ S_{BJ}^{YD2} \} \\ \frac{1}{U} \{ \dot{\psi}_{BJ}^{ZD} \} &= [a_{BJ,BJ}^{ZD}] \{ S_{BJ}^{ZD1} \} \\ \frac{1}{U} [X_{BJ}^D] \{ \dot{\psi}_{BJ}^{ZD} \} &= [a_{BJ,BJ}^{ZD}] \{ S_{BJ}^{ZD2} \} \end{aligned} \quad (3.4-196)$$

where the matrix $[X_{BJ}^D]$ contains the X_j coordinates of the line doublet control points. The solution to the problem is constructed by solving equations (3.4-196) for the values of S_{BJj}^{YD1} , S_{BJj}^{YD2} , S_{BJj}^{ZD1} , and S_{BJj}^{ZD2} and substituting the values so obtained into equations (3.4-195).

Equations (3.4-196) are expressed for M slender bodies of a configuration using the matrices introduced by equation (3.4-117). The result is as follows:

$$\frac{1}{U} \{\dot{\Psi}_B^{D1}\} = [a_{B,B}^D] \{S_B^{D1}\}$$

and

(3.4-197)

$$\frac{1}{U} [X_B^D] \{\dot{\Psi}_B^{D2}\} = [a_{B,B}^D] \{S_B^{D2}\}$$

where

$$[X_B^D] = \begin{bmatrix} [X_{B1}^D] & \text{zeros} \\ & \ddots \\ \text{zeros} & [X_{BM}^D] \end{bmatrix} \quad (3.4-198)$$

and the diagonal elements are the line doublet control point coordinates expressed in the Reference Axis System.

3.4.9.1 Isolated slender body unsteady lifting interference flow incidence.—Each of the line doublet distributions whose strength is determined by solving equations (3.4-197) induces interference flow incidence at the mean surfaces of the thin and slender bodies of a configuration. The interference flow incidence is evaluated at the control points of the mean surface panels. The result is expressed in terms of the influence coefficient matrix given by equation (3.4-127) as follows:

$$\frac{1}{U} \{\Psi_{BW}^{D1}\}^{int} = [a_{BW,B}^D] \{S_B^{D1}\}$$

(3.4-199)

and

$$\frac{1}{U} [X^V] \{\Psi_{BW}^{D2}\}^{int} = [a_{BW,B}^D] \{S_B^{D2}\}$$

where

$$[X^V] \equiv \begin{bmatrix} [X_B^V] & [0] \\ [0] & [X_W^V] \end{bmatrix} \quad (3.4-200)$$

and the diagonal elements of this matrix are the coordinates of the mean surface panel control points expressed in the Reference Axis System.

3.4.9.2 Isolated slender body unsteady lifting pressure. – The aerodynamic pressure induced by the isolated slender body unsteady lift is computed on the basis of equations (3.3-54) and (3.3-55). Substituting the solution for the J^{th} slender body, equations (3.4-195), into these equations leads to the pressure distribution expressed as follows:

$$C_{PBj}^{YD} = -2 \sum_{j=1}^{J} \left\{ u_{BJj}^{YD} S_{BJj}^{YD} + \frac{M^2}{\beta^2} [X_J u_{BJj}^{YD} S_{BJj}^{YD1} - u_{BJj}^{YD} S_{BJj}^{YD2}] + \frac{1}{\beta^2} \phi_{BJj}^{YD} S_{BJj}^{YD1} \right\} \quad (3.4-201)$$

$$C_{PBj}^{ZD} = -2 \sum_{j=1}^{J} \left\{ u_{BJj}^{ZD} S_{BJj}^{ZD} + \frac{M^2}{\beta^2} [X_J u_{BJj}^{ZD} S_{BJj}^{ZD1} - u_{BJj}^{ZD} S_{BJj}^{ZD2}] + \frac{1}{\beta^2} \phi_{BJj}^{ZD} S_{BJj}^{ZD1} \right\}$$

where u_{BJj}^{YD} and u_{BJj}^{ZD} are given by equations (3.4-130) and (3.4-131) while ϕ_{BJj}^{YD} and ϕ_{BJj}^{ZD} are given by equations (3.4-115) and (3.4-116) in subsonic flow and equivalent expressions in supersonic flow, see section 3.4.5.

The unsteady pressure induced by the line doublets is evaluated at points on the slender body surface exactly as in section 3.4.5.2 for the case of steady flow. The unsteady pressure induced at these points is expressed in terms of the matrices of section 3.4.5.2 as

$$\{C_{PB}^D\} = [CPM_{B,B}^D] \{S_B^D\} + \frac{M^2}{\beta^2} [X_B^D] [CPM_{B,B}^D] - \frac{2}{M^2} [\phi_{B,B}^D] \{S_B^{D1}\} - \frac{1}{\beta^2} [CPM_{B,B}^D] \{S_B^{D2}\} \quad (3.4-202)$$

where

$$[\phi_{B,B}^D] \equiv \begin{bmatrix} [\phi_{B1,B1}^{YD}] & & & & \\ & \ddots & & & \\ & & [\phi_{BM,BM}^{YD}] & & \text{zeros} \\ & & & [\phi_{B1,B1}^{ZD}] & \\ \text{zeros} & & & & \ddots \\ & & & & & [\phi_{BM,BM}^{ZD}] \end{bmatrix}$$

and the matrices on the diagonal, i.e.,

$$[\phi_{BJ,BJ}^{YD}] \equiv [\phi_{BJ,BJij}^{YD}]$$

and

(3.4-203)

$$[\phi_{BJ,BJ}^{ZD}] \equiv [\phi_{BJ,BJij}^{ZD}],$$

contain the surface point values of the potentials given by equations (3.4-115) and (3.4-116) or their equivalents in supersonic flow. The matrix $[X_B^D]$ contains the X coordinates of the points where the pressure is evaluated in the Reference Axis System.

3.4.9.3 Isolated slender body unsteady lift induced velocity components.—No additional velocity components beyond those used in constructing the solution to the steady flow problem, section 3.4.5, are required in this section; however, the values of the potentials induced by the line doublets are needed to compute the isolated slender body unsteady lifting pressures, section 3.4.9.2. As in the case of steady flow, section 3.4.5, the line doublets are distributed differently for subsonic and supersonic flow.

Subsonic case: In subsonic flow the potential due to one component of the quadratic splines, figure 3.4-19, is given by equation (3.4-140) and the potential for a spline found by superposition in the manner of equations (3.4-141), i.e.,

$$\phi_{BJk}^{(Z)D}(\xi_{Jk}) = \phi_{BJk-1}^{(Z)D}(\xi_{Jk} + L_{BJk-1})$$

(3.4-204)

$$+ a_k \phi_{BJk}^{(Z)D}(\xi_{Jk}) + b_k \phi_{BJk+1}^{(Z)D}(\xi_{Jk} - L_{BJk})$$

Supersonic case: In supersonic flow the potential induced by the k^{th} line doublet is given by equation (3.4-15) in region II, figure 3.4-17, and by equation (3.4-151) in region III.

3.4.10 Unsteady Aerodynamic Induction Problem

3.4.10.1 Unsteady Aerodynamic Induction Potential. As shown by section 3.3.2.8, the solution to the unsteady aerodynamic induction problem is expressed in terms of vorticity distributed on the mean surfaces of all thin and slender bodies comprising an aircraft configuration, i.e.,

$$\begin{aligned} \phi_{int}^{UV} = & \iint_{S_W+S_B} \gamma_0^{int} K^v ds + \frac{M^2}{\beta^2} \left[x \iint_{S_W+S_B} \gamma_1^{int} K^v ds \right. \\ & - \iint_{S_W+S_B} \gamma_2^{int} K^v ds \left. - \frac{1}{\beta^2} \left[\int_{-\infty}^x \iint_{S_W+S_B} \gamma_1^{int} K^v ds d\xi \right. \right. \\ & \left. \left. - \iint_{S_W+S_B} \gamma_3^{int} K^v ds \right] \right] \end{aligned}$$

where the interference vorticity distributions are required to satisfy the integral equations given by equations (3.3-44). The vorticity distributions on each mean surface panel are assumed to be uniform as in the case of the unsteady thin body lifting problem in section 3.4.8; the solution to the problem, equation (3.3-43), is expressed as

$$\begin{aligned} \phi_{int}^{UV}(x,y,z,) = & \sum_{I=1}^N \sum_{i=1}^{nI} \{ \phi_{WII}^v S_{WII}^v + \frac{M^2}{\beta^2} (x \phi_{WII}^v S_{WII}^{v1} \\ & - \phi_{WII}^v S_{WII}^{v2}) - \frac{1}{\beta^2} \left(\int_{-\infty}^x \phi_{WII}^v S_{WII}^{v1} - \phi_{WII}^v S_{WII}^v \right) \} \\ & + \sum_{J=1}^M \sum_{j=1}^{mJ} \{ \phi_{BJj}^v S_{BJj}^v + \frac{M^2}{\beta^2} (x \phi_{BJj}^v S_{BJj}^{v1} \\ & - \phi_{BJj}^v S_{BJj}^{v2}) - \frac{1}{\beta^2} \left(\int_{-\infty}^x \phi_{BJj}^v S_{BJj}^{v1} - \phi_{BJj}^v S_{BJj}^{v3} \right) \} \end{aligned} \quad (3.4-205)$$

The integral equations which must be solved, equations (3.3-34), are expressed in terms of the influence coefficients appearing in sections 3.4.6 and 3.4.8 as follows:

$$\begin{aligned} \{ \dot{\psi}_{BW}^v \} &= [a_{BW,BW}^v] \{ S_{BW}^{v1} \}^{int} \\ \frac{1}{U} [X_{BW}^v] \{ \dot{\psi}_{BW}^v \} &= [a_{BW,BW}^v] \{ S_{BW}^{v3} \}^{int} \\ [a_{BW,BW}^v] \{ S_{BW}^{v1} \} &= - [a_{BW,BW}^v] \{ S_{BW}^{v3} \}^{int} \end{aligned} \quad (3.4-206)$$

where $[a_{WB, WB}^V]$ contains elements obtained by evaluating the expressions

$$\int_{-\infty}^{X_I} a_{WIi}^V(\xi, Y_I, Z_I) d\xi$$

and

$$\int_{-\infty}^{X_J} a_{BJj}^V(\xi, Y_J, Z_J) d\xi$$

at the mean surface control points.

The strengths of the vorticity distributions are found as follows:

$$\{S_{BW}^{v1}\}^{int} = [a_{BW, BW}^V]^{-1} \{\Psi_{BW}^V\} \frac{1}{U} \quad (3.4-207)$$

$$\{S_{BW}^{v2}\}^{int} = [a_{BW, BW}^V]^{-1} [X_{BW}^V] \{\Psi_{BW}^V\} \frac{1}{U}$$

$$\{S_{BW}^{v3}\} = -[a_{BW, BW}^V]^{-1} \left[\int a_{BW, BW}^V [a_{BW, BW}^V]^{-1} \{\Psi_{BW}^V\} \frac{1}{U} \right]$$

Finally, the solution to the unsteady aerodynamic induction problem is obtained by substituting the values of S_{WIi}^{V1} , S_{BJj}^{V1} , S_{WIi}^{V2} , S_{BJj}^{V2} , S_{WIi}^{V3} and S_{BJj}^{V3} so determined into equation (3.4-205).

3.4.10.2 Unsteady aerodynamic induction pressure.—The aerodynamic pressure induced by the unsteady aerodynamic induction problem constitutes the interference pressure induced by the unsteady isolated problems of sections 3.4.8 and 3.4.9. This pressure is computed by substituting the solution to the problem, equation (3.4-205), into equation (3.4-44). Carrying out that operation and evaluating the pressure at the geometric centroids of each mean surface panel leads to the following matrix expression

$$\begin{aligned} \{C_P^{UV}\}^{int} = & [CPM_{BW, BW}^V] \{S_{BW}^V\} + \frac{M^2}{\beta^2} [X_{BW}^V] [CPM_{BW, BW}^V] \{S_{PW}^{v1}\} \\ & - [CPM_{BW, BW}^V] \{S_{BW}^{v2}\} + \frac{1}{\beta^2} [CPM_{BW, BW}^V] \{S_{BW}^{v3}\} \end{aligned} \quad (3.4-208)$$

where the matrices $\{C_P^{UV}\}^{int}$ and $[CPM_{WB, WB}^V]$ are formulated as shown by equations (3.4-163) and (3.4-164) and the matrix $[X_{WB}^V]$ contains on its diagonal the coordinates of the panel area centroids expressed in the Reference Axis System.

3.4.11 Combined Unsteady Aerodynamic Problem

The preceding development provides all elements used in FLEXSTAB to represent unsteady aerodynamics. In this section these elements are combined to obtain the final matrix expressions used in FLEXSTAB to relate aerodynamic surface pressures to the unsteady flow incidence described by the surface boundary conditions.

The unsteady pressure acting on a configuration is the total of the isolated thin and slender body lifting pressures, sections 3.4.8.2 and 3.4.9.2, and the interference pressures. The combined pressure distribution is expressed in terms of equations (3.4-165), (3.4-166), (3.4-167), (3.4-184), (3.4-202), and (3.4-208) and appears as follows:

$$\begin{aligned} \{C_P\} = & [CPM]\{S\} + \frac{M^2}{\beta^2} \left(([DX][CPM] - \frac{2}{M^2}[\phi^D])\{S^1\} \right. \\ & \left. - [CPM]\{S^2\} \right) + \frac{1}{\beta^2}[CPM]\{S^3\} \end{aligned} \quad (3.4-209)$$

where

$$[DX] \equiv \left[\begin{array}{c|c} [X_B^D] & [0] \\ \hline [0] & [X_{BW}^V] \end{array} \right] \quad (3.4-210)$$

the coordinates of the points where the pressure is evaluated, and

$$[\phi^D] \equiv \left[\begin{array}{c|c} [\phi_{B,B}^D] & [0] \\ \hline [0] & [0] \end{array} \right] \quad (3.4-211)$$

The flow singularity strengths appearing in equation (3.4-209) are given by equation (3.4-168) and the following expressions

$$\{S^1\} = [AIC]^{-1} \{\psi'\}_{\frac{1}{U}}, \quad (3.4-212)$$

$$\{S^2\} = [AIC]^{-1} [DX] \{\psi'\}_{\frac{1}{U}}, \quad (3.4-213)$$

and

$$\{S^3\} = -[AIC]^{-1} \left[\int a \right] [AIC]^{-1} \{\dot{\Psi}'\} \frac{1}{U} \quad (3.4-214)$$

where $[a]$ is given by equation (3.4-169),

$$[a] \equiv \begin{bmatrix} [0] & | & [0] & | & [0] \\ \hline [0] & | & [a_{B,B}^v] & | & [a_{B,W}^v] \\ \hline [0] & | & [a_{W,B}^v] & | & [a_{W,W}^v] \end{bmatrix} \quad (3.4-215)$$

Combining equations (3.4-209) through (3.4-215) leads to the solution to the combined unsteady aerodynamic lifting problem as follows:

$$\{C_p\} = [LSC]\{\Psi'\} + [\delta LSC]\{\dot{\Psi}'\} \frac{1}{U} \quad (3.4-216)$$

where

$$[\delta LSC] \equiv \frac{M^2}{\beta^2} \left[([DX][CPM] - \frac{2}{M^2}[\phi^D])[AIC]^{-1} - [CPM][AIC]^{-1}[DX] \right] - \frac{1}{\beta^2} [CPM][AIC]^{-1} \left[\int a \right] [AIC]^{-1} \quad (3.4-217)$$

Deleting the elements $\{\dot{\Psi}_B^V\}$ from $\{\dot{\Psi}'\}$ and deleting the corresponding columns from the $[\delta LSC]$ matrix leads to

$$\begin{aligned} \{C_p\} = [A]\{-\dot{\omega}\lambda_w\{\bar{W}\} - \dot{\phi}\lambda_v\{\bar{V}\} + \{\Psi_C\}\} \\ + [\delta A]\{-\dot{\omega}\lambda_w\{\bar{W}\} - \dot{\phi}\lambda_v\{\bar{V}\}\} \frac{1}{U} \end{aligned} \quad (3.4-218)$$

where $[\delta A]$ is the reduced form of $[\delta LSC]$, i.e., the columns of $[\delta LSC]$ multiplying $\{\Psi_B^V\}$ are deleted. This reduction corresponds to the reduction of $[LSC]$ to the steady aerodynamic influence coefficients $[A]$ of equation (3.4-171). Also, the flow incidence as well as its rate of change follows from equation (3.4-172).

Equation (3.4-217) yields quantities from which the entire unsteady lifting pressure on an aircraft configuration is determined from the unsteady flow incidence imposed by the boundary conditions.

The pitching wings, figures 3.2-10 and 3.2-11, used in section 3.2.8 to demonstrate the accuracy of the low-frequency approximation, are used here to illustrate the application of equation (3.4-217). The geometries of the pitching wings are described in the form

$$G(X, Y, Z) = 0$$

and, expressed in the Fluid Axis System, appears as

$$f(x, z, t) = z - (.5 - x)e^{i\omega t} = 0$$

The flow incidence at the wing surface is found as

$$\psi = \frac{1}{U} \frac{\partial f}{\partial t} + \frac{\partial f}{\partial x}$$

or

$$\psi = [1 - i(.5 - x)\frac{\omega}{U}]e^{i\omega t}$$

and the rate of change of flow incidence, to first order in ω/U , is found to be

$$\frac{1}{U} \dot{\psi} = i\frac{\omega}{U} e^{i\omega t}$$

Substituting the matrix equivalents of these equations into equation (3.4-217), a matrix of complex pressure coefficients is found as

$$\{C_p^*\} = [A][\{1\} - i(.5\{1\} - \{x\})\frac{\omega}{U}] + i\frac{\omega}{U}[\delta A]\{1\}$$

Separating into real and imaginary parts,

$$\text{Re}\{C_p^*\} = [A]\{1\},$$

i.e., the lifting pressure coefficients for the wing having plunging velocity, $w = -U$ (chord lengths/second), and

$$\text{Im}\{C_p^*\} = -[A](.5\{1\} - \{x\})\frac{\omega}{U} + [\delta A]\{1\}\frac{\omega}{U}$$

The first term of the imaginary part contains the lifting pressure coefficients for the wing having a steady pitch rate $Q = U$ (radians per second), and the second term contains the lifting pressure coefficients for the wing having a plunging acceleration $\dot{w} = -U^2$ (chord lengths/(second)²).

3.4.12 Leading Edge Thrust Correction

The FLEXSTAB system contains a correction to the drag force induced on lifting thin bodies. This is a leading edge thrust correction analogous to those usually encountered in the theory of thin lifting surfaces, e.g., reference 3-9, pages 147-148 and 218-223. The correction accounts for the fact that the linear aerodynamic theory of section 3 is not valid in regions where the flow changes rapidly in the x-direction as near wing leading edges. The correction used in FLEXSTAB is demonstrated in the following for the case of an infinite aspect ratio flap plate at angle of attack in a subsonic flow. The correction is then developed for the case of arbitrary thin lifting surfaces.

3.4.12.1 Leading edge thrust of a flat plate in subsonic flow.—The leading edge thrust correction contained in FLEXSTAB is illustrated by considering the pressure distribution induced by subsonic flow over an infinite aspect ratio flat plate at angle of attack to a subsonic flow. The leading edge thrust correction usually encountered in the theory of thin lifting surfaces, references 2-3 and 3-9, is described and then the leading edge thrust correction used in FLEXSTAB is described showing the contrast with thin lifting surface theory.

Figure 3.4-22 shows the lifting pressure distribution induced by the vorticity distribution producing a flow satisfying the boundary conditions of the flat plate, case 1. This vorticity distribution is given by the formula

$$\gamma = \frac{2\alpha}{\sqrt{1-M^2}} \sqrt{\frac{1-x}{x}} \quad (3.4-219)$$

and is seen to become infinite in the region of the leading edge, i.e., as x tends to zero. The lifting pressure is given by

$$\begin{aligned} \Delta C_P &\equiv C_{P_l} - C_{P_u} \\ &= \frac{4\alpha}{\sqrt{1-M^2}} \sqrt{\frac{1-x}{x}} \end{aligned} \quad (3.4-220)$$

Integrating this pressure distribution over the surface yields the following section lift and drag coefficients:

$$C_l = \frac{2\pi\alpha}{\sqrt{1-M^2}} \quad C_d = \frac{2\pi\alpha^2}{\sqrt{1-M^2}}$$

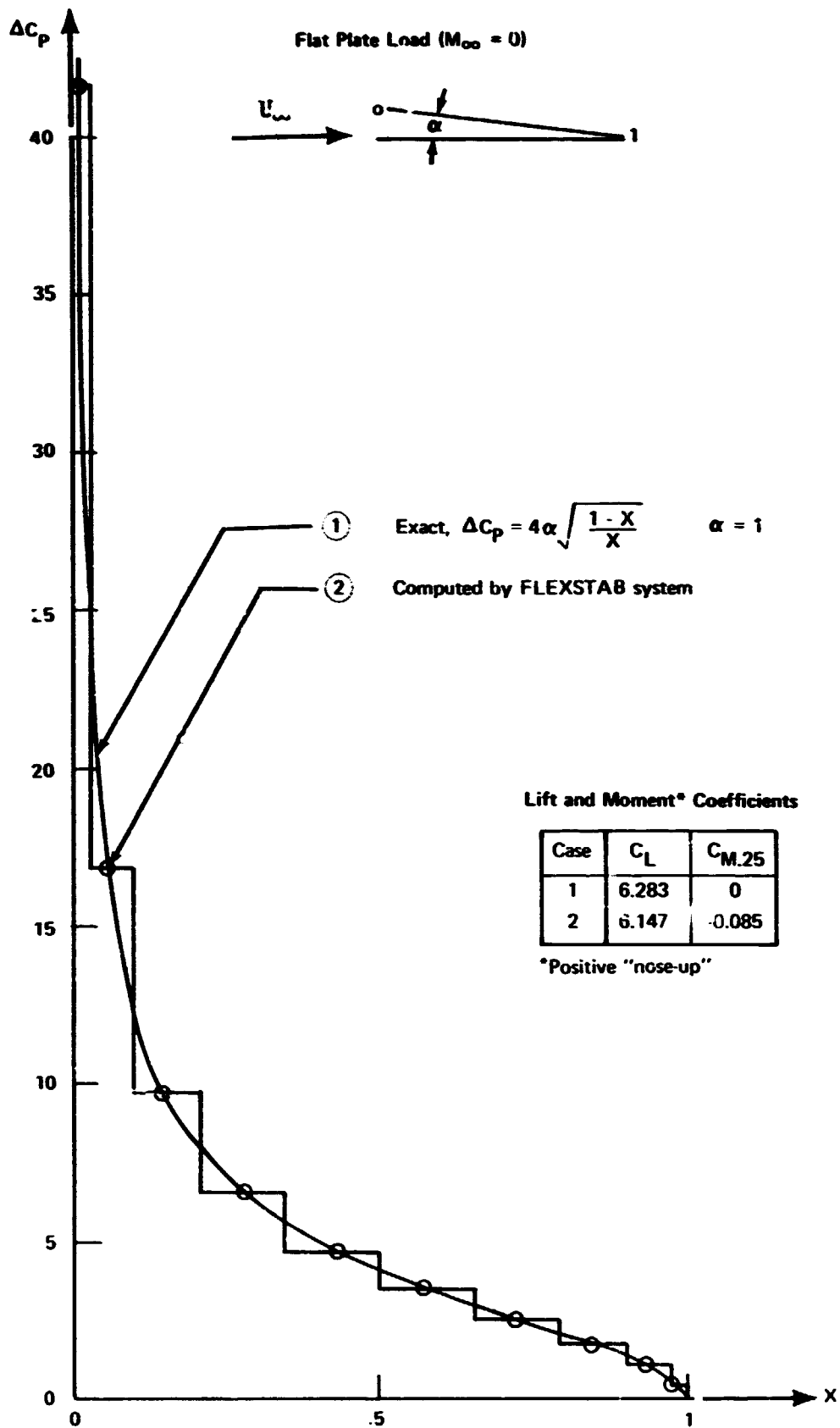


FIGURE 3.4-22.—LIFTING PRESSURE ON A FLAT PLATE

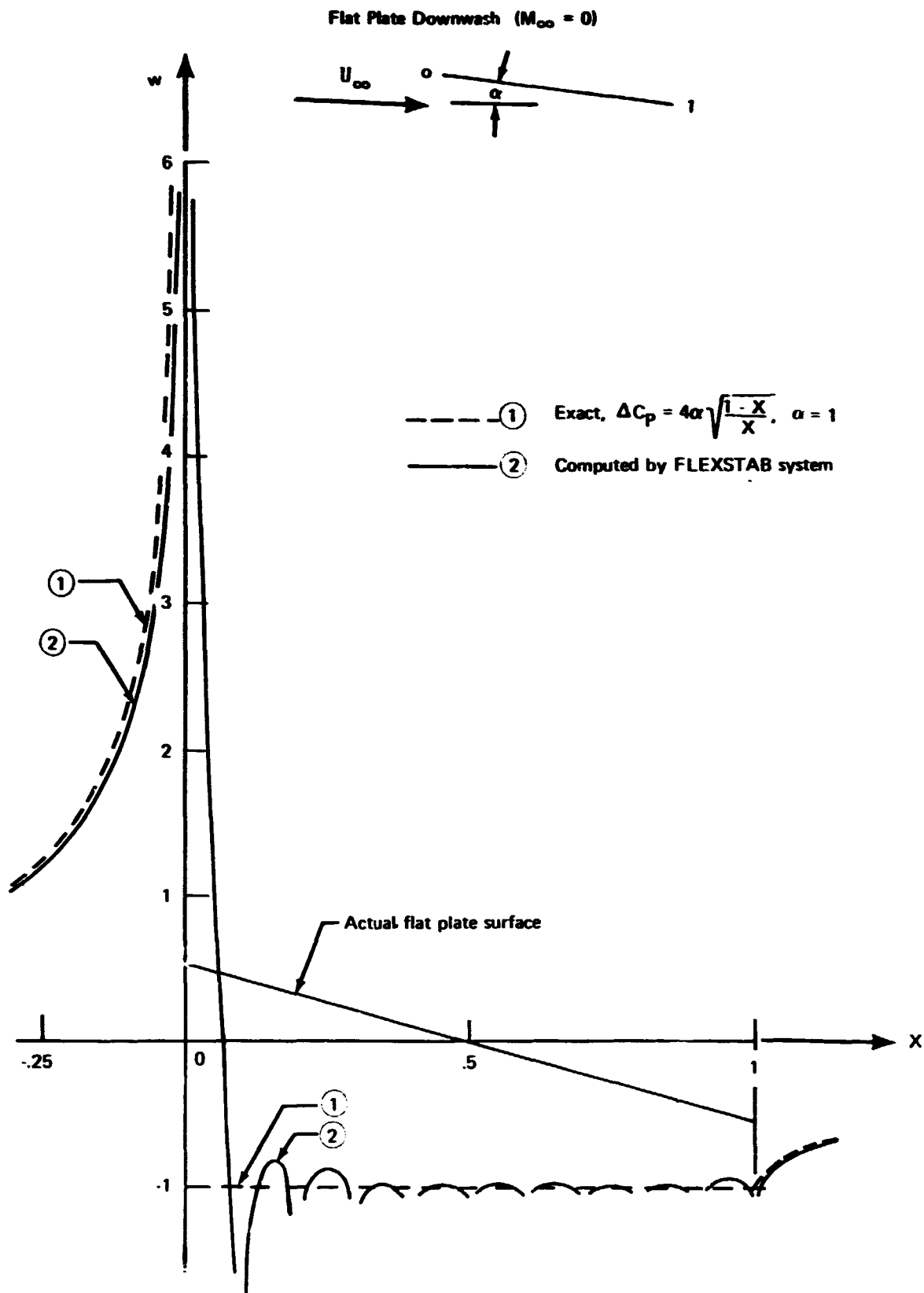
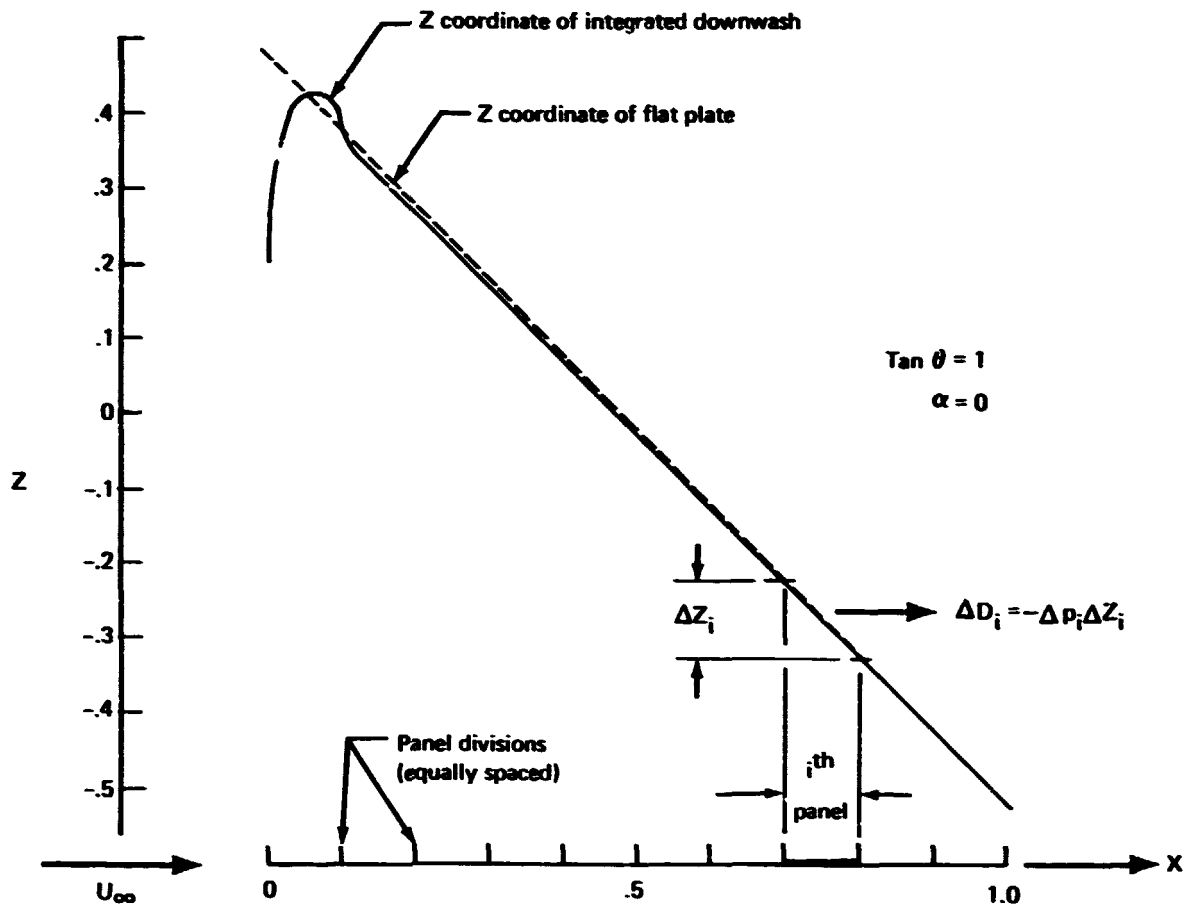


FIGURE 3.4-23.—APPROXIMATE FLAT PLATE CAMBER



Values for $1/2 \rho U_\infty^2 = 1$, $X_{TE} - X_{LE} = 1$

Panel no. i	FLEXSTAB load Δp_i	For flat plate		For integrated downwash	
		Camber increase ΔZ_i	Drag on segment $\Delta D_i = -\Delta p_i \Delta Z_i$	Camber increase ΔZ_i	Drag on segment $\Delta D_i = -\Delta p_i \Delta Z_i$
1	22.378	.1	2.2378	.1780	-3.9845
2	9.8097	.1	.9810	.1130	1.1089
3	7.1907	.1	.7199	.0967	.6961
4	5.6305	.1	.5630	.0977	.5501
5	4.5558	.1	.4556	.0981	.4469
6	3.7255	.1	.3725	.0984	.3665
7	3.0280	.1	.3028	.0985	.2983
8	2.3975	.1	.2398	.0985	.2363
9	1.7785	.1	.1778	.0984	.1750
10	1.0874	.1	.1087	.0979	.1065

Totals, $\Sigma \Delta D_i = 6.1590$

$\Sigma \Delta D_i = 0.0000$

$\Sigma \Delta D_i = \text{FLEXSTAB value of drag} = -0.0633$
(sum of boxed values)
FLEXSTAB

FIGURE 3.4-24.—DRAG ON INTEGRATED DOWNWASH VS CAMBER ANALYZED

The non-zero section drag coefficient is not consistent with inviscid flow theory and arises because the linear theory fails in the region of the leading edge where perturbations to the flow velocity are not small. Following the method of reference 3-9 (pages 147-148 and 218-223), a leading edge correction is computed which just balances the drag, viz.,

$$C_d = - \frac{2\pi\alpha^2}{\sqrt{1-M^2}}$$

This correction is computed by a limiting process involving the infinite pressure at the leading edge.

In the FLEXSTAB system the lifting pressure given by equation (3.4-220) is approximated by the step function shown as case 2 in figure 3.4-22. The lifting pressure is finite at the leading edge so that the limiting process alluded to above yields a leading edge thrust of zero. The leading edge thrust correction in the FLEXSTAB system is a geometric shape correction. The downwashes induced at the flat plate by the two vorticity distributions, i.e., cases 1 and 2, are shown by figure 3.4-23. The downwash computed by FLEXSTAB satisfies the boundary conditions at only a finite number of points; hence, the FLEXSTAB solution yields a surface which approximates the boundary condition surface—the flat plate in this case. If the lifting pressure shown by case 2 of figure 3.4-22 is applied to the surface obtained by integrating the downwash with respect to x , the FLEXSTAB solution will yield lift and drag forces consistent with the boundary condition surface approximation. In this computation, the section drag for the infinite aspect ratio flat plate is found to be zero. The surface found by integrating the downwash, however, as noted, is not that of the flat plate, and the FLEXSTAB leading edge thrust correction is a correction from the surface appearing in the boundary condition (here, the flat plate) to the surface obtained by integrating the downwash.

3.4.12.2 Surface correction at the leading edge panel.—If the downwash from the FLEXSTAB approximate solution for the flat plate is integrated, figure 3.4-24, the surface generated closely approximates the flat plate except at the leading edge panel. If the drag is computed assuming the pressure to act on the flat plate, the value of section drag obtained is $C_d = 6.1950$ —nearly the value 2π obtained from equation (3.4-220). If the pressure is assumed to act on the integrated downwash surface, the section drag value computed is $C_d = 0$. Correcting the leading edge panel shape leads to an approximation yielding $C_d = -0.0633$. This approximation is accepted for the FLEXSTAB system, and the lifting pressure is assumed to act on the boundary condition surface in all areas except at the leading edge panel where it is assumed to act on the surface obtained by integrating the downwash.

3.4.12.3 Leading edge correction for arbitrary lifting thin bodies. The correction procedure described above is valid not only for infinite aspect ratio surfaces but also for the thin bodies used in FLEXSTAB to represent an aircraft configuration. The lifting pressure at

the leading edge panels is assumed to act at the surface generated by integrating the flow incidence: at the remainder of the thin body the lifting pressure is assumed at the actual mean camber surface of the thin body.

The incidence generated by the flow singularities of the aerodynamic representation contains incidence arising from motion of the Body Axis System relative to the Fluid Axis System, section 2.2.3; this incidence, describing a change in direction of the apparent freestream, is not included in the surface shape generation.

The force in the x-direction of the Reference Axis System at the i^{th} leading edge panel of the i^{th} thin body, figure 3.4-25, is found as

$$D_{WII}^V = -\bar{q} \Delta C_{P_{WII}}^V \int_{X_{LWII}}^{X_{TWII}} (w_{WII}^V - \Delta w_{WII}^V) d\xi b_{WII} \quad (3.4-221)$$

where

- b_{WII} is the panel span
- X_{LWII}, X_{TWII} are the coordinates of the panel leading and trailing edges along the panel row centroid, figure 3.4-6
- w_{WII}^V is the component of perturbation velocity along the (normal) coordinate, figure 3.4-3
- Δw_{WII}^V is the normal component of perturbation velocity due to motion of the Body Axis System relative to the Fluid Axis System.

Carrying out the integration results in

$$D_{WII}^V = \bar{q} \Delta C_{P_{WII}}^V [I_{w_{WII}}^V - \Delta I_{w_{WII}}^V C_{WII}] b_{WII}$$

where

$$I_{w_{WII}}^V = -\sum_{j=1}^n \int_{X_{LWII}}^{X_{TWII}} a_{WIIj}^V(\xi, Y_{TII}, Z_{TII}) d\xi S_{WII}^V$$

and the chord of the panel is given by

$$C_{WII} = X_{TWII} - X_{LWII}$$

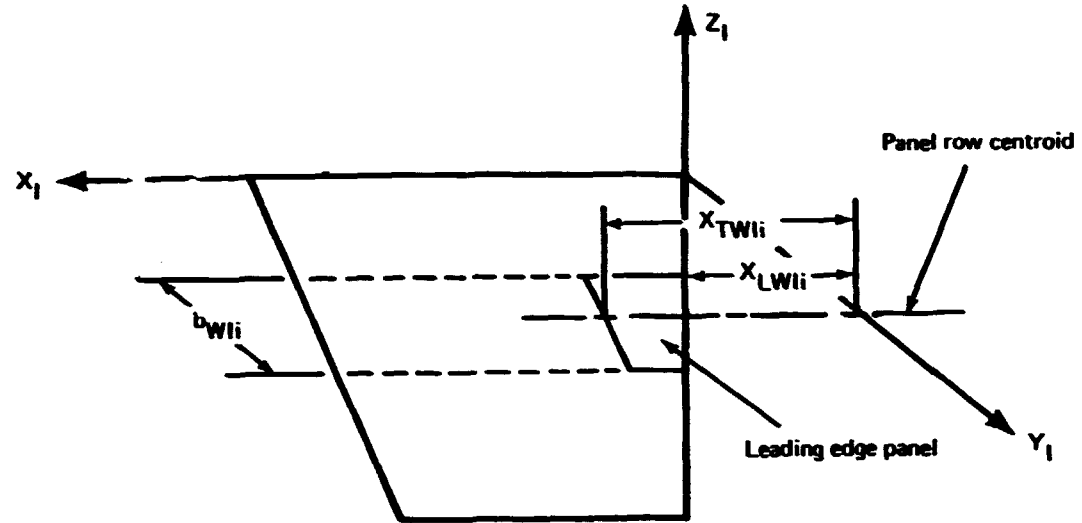


FIGURE 3.4-25.—THIN BODY LEADING EDGE PANEL GEOMETRY

A matrix of integrated flow incidences is formed as

$$\{w_{IW}^V\} = [IDM]\{S_W^V\} \quad (3.4-222)$$

where

$$[IDM] \equiv [- \int_{C_{WIi}} a_{WIj}^V(\xi, Y_{Ii}, Z_{Ii}) d\xi]$$

where $\{S_W^V\}$ represents the vortex panel singularity strengths at thin bodies. This matrix is combined with partitions of zeros to conform with the solution to the combined steady lifting problem, section 3.4.7, equation (3.4-168). This operation leads to the expression

$$\{w_I\} = [ISC_\psi]\{\psi'\}$$

or

$$\{w_I\} = [ISC_\theta]\{\psi\} \quad (3.4-223)$$

where

$$[ISC_\psi] \equiv \begin{bmatrix} [0] & [0] \\ [0] & [IDM] \end{bmatrix} [AIC]^{-1}$$

The matrix $[ISC_\psi]$ is reduced to the matrix $[ISC_\theta]$ eliminating the columns multiplying $\{\psi_B^V\}$ contained in $\{\psi'\}$ but not in $\{\psi\}$, c.f. equation (3.4-218). Using this result, the leading edge panel force per unit panel span is found as follows

$$\{D\} \equiv \bar{q}(\{w_I\} \otimes \{C_p\} + \{\Delta w_I\} \otimes \{C_p\}) \quad (3.4-224)$$

where \otimes denotes element-by-element multiplication between column matrices and $\{\Delta w_I\}$ is the incidence due to relative motion between the Body and Fluid Axis Systems at each leading edge panel multiplied by the panel chord. The matrix $\{\Delta w_I^V\}$ is described in detail in section 3.5. Equation (3.4-224) forms the basis for the leading edge correction.

3.4.13 Aerodynamic Effects of Speed Variations

As shown in section 2.3.3.4, an aircraft is subjected to a variation in Mach number at its surface when it undergoes a change in forward speed or undergoes a pitch or yaw rate,

$$\Delta M(\bar{Y}, \bar{Z}) = \frac{M}{U} [\Delta U + (Q\bar{Z} + R\bar{Y})] \quad (2.3-74)$$

where \bar{Y}, \bar{Z} are the coordinates of a surface point relative to the aircraft center of mass. This variation in local Mach number produces a variation in aerodynamic surface pressure. The entire variation given by equation (2.3-74) is imposed on the isolated body thickness pressures, equation (3.4-173), and leads to the following variation in that pressure distribution:

$$\Delta \{C_P^S\}^{iso} = \left\{ \frac{\partial C_P^S}{\partial M} \right\}^{iso} \left[[I] \Delta U + \{\bar{Z}\} Q + \{\bar{Y}\} R \right] \frac{M_1}{U_1} \quad (3.4-225)$$

where ΔU is the change in forward speed and $\{\bar{Z}\}$ and $\{\bar{Y}\}$ are column matrices of thin body panel centroid coordinates and slender body segment centroid coordinates—body measured relative to the center of mass in the Reference Axis System. The partial derivative of the pressure coefficients is computed by finite difference as

$$\left\{ \frac{\partial C_P^S}{\partial M} \right\}^{iso} \equiv \frac{1}{\Delta M} \left[\{C_P^S\}_{M+\Delta M}^{iso} - \{C_P^S\}_M^{iso} \right]$$

following the approach of sections 3.4.3 and 3.4.4 evaluating all Mach number dependent quantities using the incremental Mach number $M + \Delta M$, i.e.,

$$\begin{aligned} \{C_P^S\}_{M+\Delta M}^W &= [CPM_{W,W}^{CS}]_{M+\Delta M} \{S_W^{CS}\}_{M+\Delta M} \\ &+ [CPM_{W,W}^{LS}]_{M+\Delta M} \{S_W^{LS}\}_{M+\Delta M} \end{aligned} \quad (3.4-226)$$

$$\{C_P^S\}_{M+\Delta M}^B = [CPM_{B,B}^S]_{M+\Delta M} \{S_B^S\}_{M+\Delta M} \quad (3.4-227)$$

where the elements of $\{S_B^S\}_{M+\Delta M}$ are computed from equation (3.4-77) using

$$[BSC_J^S]_{M+\Delta M} \quad (3.4-228)$$

From equations (3.4-225) through (3.4-227) it follows that the partitions of $\{\partial C_P^S / \partial M\}^{ISO}$ are given by

$$\left\{ \frac{\partial C_{PW}^S}{\partial M} \right\}^{ISO} \equiv \frac{1}{\Delta M} [\{C_{PW}^S\}_{M+\Delta M}^{ISO} - \{C_{PW}^S\}_M^{ISO}] \quad (3.4-229)$$

and

$$\left\{ \frac{\partial C_P^S}{\partial M} \right\}_B^{ISO} \equiv \frac{1}{\Delta M} [\{C_P^S\}_{M+\Delta M}^{ISO} - \{C_P^S\}_M^{ISO}] \quad (3.4-230)$$

Also, from the thickness interference relation, equation (3.4-175), the increment to the interference flow incidence is found as

$$\{\psi^S\}_{M+\Delta M}^{int} = [TD]_{M+\Delta M} \{S^S\}_{M+\Delta M} \quad (3.4-231)$$

In applying the Mach number variation formula, i.e., equation (2.3-74), to the combined steady lifting problem and to the computation of thickness interference pressures, section 3.4.7, the Mach number variations arising from pitch rate and yaw rate must be ignored. These computation cases involve influence coefficients which are derived assuming the free stream to be uniform, section 3.2.2.1. In this respect they are unlike the isolated thickness pressure which arises from local perturbations to the flow and which may be computed on the basis of a local Mach number. The Mach number variation leads to the following steady lifting pressure increment:

$$\Delta \{C_P\} = \left[\frac{\partial LSC}{\partial M} \right] \{\Psi'\} \frac{\Delta U}{M} \quad (3.4-232)$$

where $\{\Psi'\}$ is defined by equation (3.4-168) while

$$\left[\frac{\partial LSC}{\partial M} \right] \equiv \frac{1}{\Delta M} [[LSC]_{M+\Delta M} - [LSC]_M]$$

and

$$[LSC]_{M+\Delta M} = [CPM]_{M+\Delta M} [AIC]_{M+\Delta M}^{-1}$$

The increment in thickness interference pressure is

$$\Delta \{C_{PW}^v\}_{int} = \left\{ \frac{\partial C_P^v}{\partial M} \right\}_{int} \frac{\Delta u}{M} \quad (3.4-233)$$

where

$$\left\{ \frac{\partial C_P^v}{\partial M} \right\}_{int} \equiv \frac{1}{\Delta M} [\{C_{PW}^v\}_{M+\Delta M}^{int} - \{C_{PW}^v\}_M^{int}]$$

and $\{C_{PBW}^V\}_{M+\Delta M}^{int}$ is computed on the basis of the interference flow incidence of equation (3.4-231).

The leading edge correction, section 3.4.12, is also a function of Mach number through terms involving the integrated flow incidence, equations (3.4-222) and (3.4-223). These two terms are evaluated at the incremented Mach number, $M + \Delta M$, leading to

$$[IDM]_{M+\Delta M} \quad \text{and} \quad [ISC_\theta]_{M+\Delta M} \quad (3.4-234)$$

From the second of these the increment in leading edge correction is found from equation (3.4-224) as

$$\begin{aligned} \frac{1}{q} \Delta\{D/b\} = \frac{M}{U} \left[\left(\left[\frac{\partial ISC_\theta}{\partial M} \right] \{\Psi\} \right) \otimes \{C_P\} \right. \\ \left. + \{w_I\} \otimes \left\{ \frac{\partial C_P}{\partial M} \right\} + \{\Delta w_I\} \otimes \left\{ \frac{\partial C_P}{\partial M} \right\} \right] \Delta u \end{aligned} \quad (3.4-235)$$

where

$$\left[\frac{\partial ISC_\theta}{\partial M} \right] \equiv \frac{1}{\Delta M} \left[[ISC_\theta]_{M+\Delta M} - [ISC_\theta]_M \right] \quad (3.4-236)$$

3.4.14 Empirical Corrections

From the second of these the increment in leading edge correction is found from equation (3.4-224) as

Empirical corrections may be imposed on the steady lifting part of the solution to the aerodynamic problem given in section 3.4.7.1. The empirical corrections are of three types. One introduces modifications to the steady aerodynamic influence coefficients; the second introduces changes to the flow incidence distribution on the aircraft; the third introduces direct changes to the lifting pressure.

Two sets of steady aerodynamic influence coefficients, viz., those defined by equation (3.4-169) and those defined by equation (3.4-171), are used in the empirical correction methods. The influence coefficients [LSC] are included to permit corrections to the flow incidence at the mean surfaces of slender bodies; thus, empirical corrections are made by making corrections to the following equation:

$$\{C_P\} = [LSC]\{\Psi'\} + [A]\{\Psi\} \quad (3.4-237)$$

where the incidence matrix $\{\Psi'\}$ is defined by equation (3.4-168) and includes $\{\Psi_B^V\}$ - the flow incidence at slender body mean surfaces.

The empirical corrections are applied to equation (3.4-237) as follows:

- (1) The flow incidence distribution $\{\Psi'\}$ may be modified by multiplying the value at each control point by a constant, c_1 . Thus, a modified flow incidence distribution is obtained as

$$\{C_P\} = [LSC] [c_1] \{\Psi'\} \quad (3.4-238)$$

where $[c_1]$ is a diagonal matrix of correction constants.

- (2) The lifting pressure distribution may be corrected by multiplying the aerodynamic influence coefficients by correction constants as follows:

$$\{C_P\} = [c_2] [LSC] \{\Psi'\} \quad (3.4-239)$$

where $[c_2]$ is a diagonal matrix of correction constants.

- (3) Any or all elements of the steady aerodynamic influence coefficient matrix $[LSC]$ may be replaced by an empirical value.
- (4) The flow incidence distribution $\{\Psi'\}$ may be arbitrarily prescribed as a linear function of some motion parameter such as angle of attack, viz.

$$\{\Psi'\} = \{\Psi'_\alpha\} \alpha$$

and an incremental lifting pressure coefficient may be added as

$$\{\Delta C_P\} = \{\Delta C_{P_o}\} + \{\Delta C_{P_\alpha}\} \alpha + \{\Delta C_{P_\beta}\} \beta \quad (3.4-240)$$

The lifting pressure due to this flow incidence and the incremental pressure is then superimposed on the lifting pressure computed by equation (3.4-218) to correct the lift pressure as follows:

$$\begin{aligned} \{C_P\} = & [A] \{\Psi\} + [LSC] \{\Psi'\} + \frac{1}{U} [\delta A] \{\dot{\Psi}\} \\ & + \{\Delta C_{P_o}\} + \{\Delta C_{P_\alpha}\} \alpha + \{\Delta C_{P_\beta}\} \beta \end{aligned} \quad (3.4-241)$$

where the matrices $[A]$ and $[LSC]$ may be subjected to the corrections of (1) through (3) above.

A sample empirical correction using method (1) in conjunction with wind tunnel pressure model data is presented in volume IV. An example involving methods (3) and (4) is as follows. Assume that wind tunnel testing or some other source provides the flow incidence distribution on a conventional aft-mounted horizontal tail and that the flow incidence is given as a function of angle of attack. Calling this flow incidence distribution the measured distribution, the empirical flow incidence distribution $\{\Psi'_\alpha\}$ of method (4) is introduced as the difference between the measured and theoretical distributions at the horizontal tail panel control points. Assuming the horizontal tail to be the 1th thin body, the theoretical distribution of flow incidence is found from equation (3.4-168) as

$$\{\Psi_{WI_\alpha}\} = [AIC_{WI}][AIC]^{-1}\{\Psi_\alpha\}$$

where

$$\equiv \left[[a_{WI,B}^D] \begin{vmatrix} \\ \\ \end{vmatrix} [a_{WI,B}^V] \begin{vmatrix} \\ \\ \end{vmatrix} [a_{WI,W1}^V] \cdots [a_{WI,WI}^V] \cdots [a_{WI,WN}^V] \right]$$

contains the rows of the matrix [AIC] describing flow incidence at the control points of the horizontal tail with that partition describing the influence of the horizontal tail set to zero.

3.4.15 Near Field-Far Field Approximation

The FLEXSTAB system contains a near field-far field approximation in the thin body lifting aerodynamic solution. A portion of the aerodynamic surface, e.g., a wing tip or a control surface, may be represented by a very dense paneling and solved as an isolated flow problem. This solution is then averaged, in the manner described below, and patched into the aerodynamic solution for a complete configuration. The result is a flow solution for the complete configuration—the far field—based on the detailed solution to the isolated portion of the aerodynamic surface—the near field.

3.4.15.1 Aerodynamic matrices involved in the approximation.—The aerodynamic matrix equations which are generated using the near field-far field approximation are given by equations (3.4-62) and (3.4-157), viz.,

$$\{\Psi_{BW}^V\} = [a_{BW,W}^V] \{S_W^V\}$$

and

$$\{\Psi_{BW}^V\} = [a_{BW,BW}^V] \{S_{BW}^V\}$$

wherein the matrix $[a_{WB,W}^V]$ is a partition of the matrix $[a_{WB,WB}^V]$. These equations, it may be recalled, are the relations describing flow incidence at the thin body vortex panel control points, the flow incidence resulting from the strengths of the vorticity distributions on these panels.

3.4.15.2 Near field panel arrangement.—Two vortex paneling arrangements are associated with a near field region, figure 3.4-26. Taking a wing for an example and choosing the tip region as a near field, the wing is paneled without considering the large vorticity distribution gradients in the tip region, figure 3.4-26. The panel size at the tip is deliberately chosen to be too large to describe the detailed pressure distribution but small enough to accurately yield the aerodynamic forces, assuming that the lifting pressure on each panel is an accurate average value for the lifting pressure acting on the aerodynamic surface represented by the panel. The accurate average values of lifting pressures are obtained from a near field solution to the flow problem in the tip region.

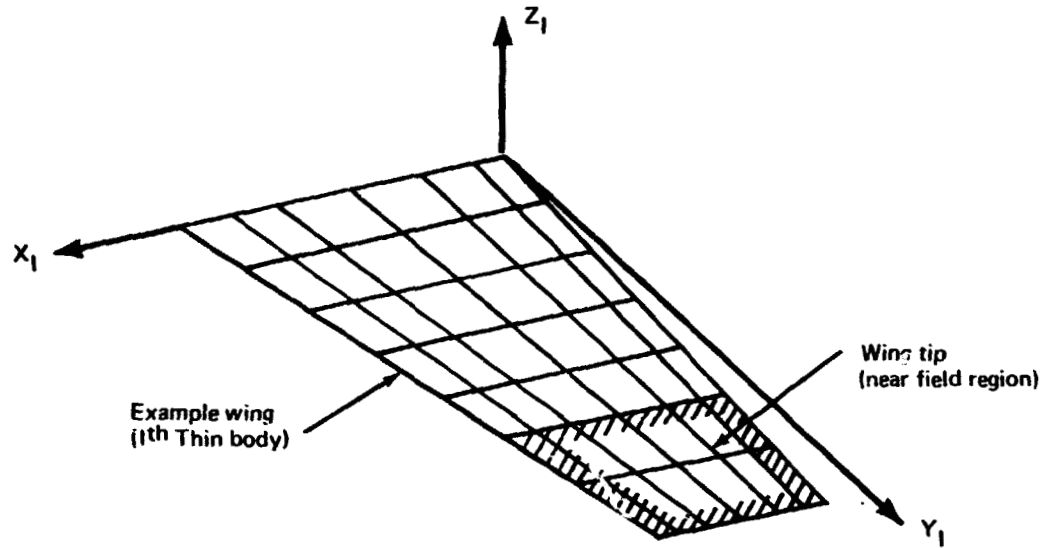


FIGURE 3.4-26.—EXAMPLE OF NEAR FIELD—FAR FIELD APPROXIMATION

The vortex panels of the near field region are subdivided into smaller panels, figure 3.4-27. A number n of chordwise subdivisions and a number m of spanwise subdivisions are specified and each near field vortex panel is subdivided as shown by figure 3.4-27. If b_{Wli} is the span of a panel in the near field region, the subpanel has the span b_{Wli}/m ; if C_{WliL} and C_{WliR} are the left- and right-hand chords of i th panel, then the subpanel chords at left- and right-hand edges are C_{WliL}/n and C_{WliR}/n , respectively.

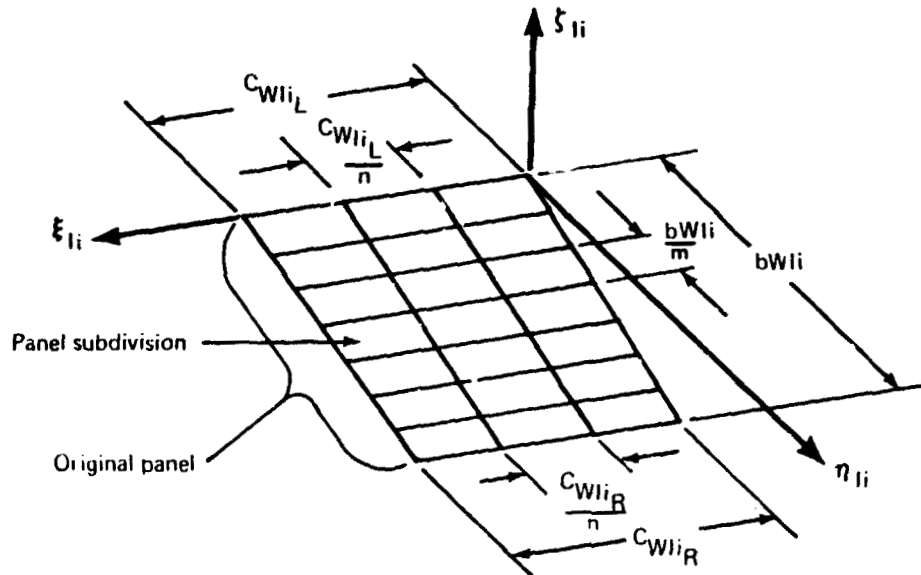


FIGURE 3.4-27.—NEAR FIELD VORTEX PANEL SUBDIVISION

3.4.15.3 Modifications of the aerodynamic equations.—An aerodynamic equation, analogous to equation (3.4-157), is generated for the near field region as follows:

$$\{\Psi_n^V\} = [a_{n,n}^V] \{S_n^V\} \quad (3.4-242)$$

where $\{\Psi_n^V\}$ is the flow incidence at the near field panel subdivision control points induced by the near field vorticity strengths $\{S_n^V\}$ — the strengths of the panel subdivisions. This equation is solved to find the vorticity strengths of the panel subdivisions as

$$\{S_n^V\} = [a_{n,n}^V]^{-1} \{\Psi_n^V\} \quad (3.4-243)$$

A single control point at the geometric centroid of each of the original panels is introduced. Considering the i^{th} panel of the original panels of the near field region, the flow incidences at control points of the panel subdivisions of the i^{th} panel are set equal to the flow incidence at the i^{th} panel geometric centroid control point. This operation is accomplished by the matrix operation

$$\{\Psi_n^V\}_i = \{1\}_i \Psi_i^V \quad (3.4-244)$$

where $\{\Psi_n^V\}_i$ and $\{1\}_i$ have m times n elements— $\{1\}_i$ being simply a column matrix of ones. Extending this operation to all the panels of the near field region leads to

$$\{\Psi_n^V\} = [T_n] \{\tilde{\Psi}_n^V\} \quad (3.4-245)$$

where

$$[T_n] \equiv \begin{bmatrix} \{1\}_1 & \text{zeros} & & \\ & \{1\}_2 & & \\ \text{zeros} & & \ddots & \\ & & & \ddots \end{bmatrix}$$

and $\{\tilde{\Psi}_n^V\}$ is the matrix of flow incidences at the geometric centroid control points of the original panels in the near field region.

An average vortex panel strength is also computed for each of the original panels. This is a weighted average based on the panel subdivision areas. The weighted average strength of the i^{th} original panel is expressed as

$$S_{WIi}^V = [S_i]_i \{S_n^V\}_i \quad (3.4-246)$$

where

$$[S]_i \equiv \frac{1}{S_{WIi}} [S_1, S_2, \dots, S_{(n \times m)}]$$

and S_i is the area of i^{th} panel subdivision while S_{WIi} is the area of the i^{th} original panel. Extending this result to all panels and panel subdivisions leads to the expression

$$\{\bar{S}_n^V\} = [S_n] \{S_n^V\} \quad (3.4-247)$$

where

$$[S_n] \equiv \begin{bmatrix} [S]_1 & \text{zeros} & & \\ & [S]_2 & & \\ & & \ddots & \\ \text{zeros} & & & \ddots \end{bmatrix}$$

Substituting the transformations, equations (3.4-245) and (3.4-247), into the near field solution, equation (3.4-243), leads to

$$\{\bar{S}_n^V\} = [A_{n,n}] \{\bar{\Psi}_n^V\} \quad (3.4-248)$$

where

$$[A_{n,n}] \equiv [S_n] [a_{n,n}^V]^{-1} [T_N]$$

This expression is now inverted to obtain

$$\{\bar{\Psi}_n^V\} = [A_{n,n}]^{-1} \{\bar{S}_n^V\} \quad (3.4-249)$$

The elements of the matrix $[A_{n,n}]^{-1}$ are inserted into the matrices $[a_{WB,W}^V]$ and $[a_{WB,WB}^V]$, replacing the elements corresponding to the original panels of the near field region. The matrices $[a_{WB,W}^V]$ and $[a_{WB,WB}^V]$, in this modified form, are then used in the solutions to the combined steady aerodynamic problem, section 3.4.7, as well as in the combined unsteady aerodynamic lifting problem, section 3.4.11.

3.4.15.4 Application of the near field-far field approximation. – As noted above, the near field-far field approximation is used in constructing the solution to that part of the aerodynamic problem which incorporates the vortex panels, i.e., the lifting part. The approximation has a close resemblance to Saint-Venant's principle, reference 2-1, pp 89-90, viz., if the boundary condition at a portion of the surface is replaced by a different boundary condition on the same portion of the surface, then the effects of the two different boundary conditions sufficiently far removed are essentially the same, provided that the force distributions are statically equivalent.

The near field-far field approximation may be applied in several ways. The near field may be confined to a portion of a single thin body, as in the example above, or it may encompass the entire body or several bodies. The near field may also include the interference surface of a slender body. This capability allows a wing-body intersection to be paneled densely in a near field, thereby increasing the accuracy of the solution in this region of complex vorticity distribution.

3.5 AERODYNAMIC FORCE DERIVATIVES

In this section the results derived in the preceding sections are combined into a set of matrix equations describing the aerodynamic forces acting on an aircraft arising from changes in the aircraft's motion, control surface settings, and elastic deformation. These matrix equations are used in the FLEXSTAB system analysis to generate the aerodynamic force derivatives and, subsequently, in sections 5 and 6, to generate the stability derivatives for a flexible aircraft. In section 3.5.1 transformation matrices are derived which transform the aerodynamic pressure coefficients of section 3.4 into a system of aerodynamic forces acting on an aircraft. In section 3.5.2 matrix expressions are derived which relate the aerodynamic pressure coefficients to an aircraft's motion, control surface settings, and elastic deformation. The results of sections 3.5.1 and 3.5.2 are then combined in a first-order perturbation expansion in section 3.5.3. This expansion yields equations for formulating the aerodynamic force derivatives.

3.5.1 Aerodynamic Forces

The objective of this section is to derive equations which resolve the aerodynamic surface pressure into a force and couple at the center of mass of an aircraft. These equations are derived from the following integrals:

$$\vec{F}_C^A = - \bar{q} \iint_S C_p \vec{n} ds \quad (3.5-1)$$

and

$$\vec{M}_C^A = - \bar{q} \iint_S C_p \vec{r}_x \vec{n} ds \quad (3.5-2)$$

where C_p is the aerodynamic surface pressure coefficient governed by the equations of section 3.3.3, \hat{n} is the unit vector normal to the aerodynamic surfaces defined analytically by the equations in sections 3.2.3 and 3.2.4, and \vec{r} is the position vector shown by figure 2.3-3 from the center of mass to a point on the aerodynamic surface. The derived equations incorporate the matrices of pressure coefficients, derived in sections 3.4.2 through 3.4.11, into a matrix analogue to the integral equations given by equations (3.5-1) and (3.5-2) above. These matrix equations for the total aerodynamic force and couple are derived as first-order approximations consistent with the aerodynamic theory developed in section 3.2 and are based on the numerical method of solution developed in section 3.4.

3.5.1.1 Paneling scheme expansion of the aerodynamic force and couple.—The matrix equations for the aerodynamic force and couple are derived starting from an expansion of equations (3.5-1) and (3.5-2). This expansion is in terms of aerodynamic forces acting at the centers of pressure of the surface segments introduced by the paneling scheme of section 3.4.1. As such, the aerodynamic force and couple at the aircraft center of mass appear as follows:

$$\vec{F}_C^A = \sum_{I=1}^N \sum_{i=1}^{nI} \vec{f}_{WIi}^A + \sum_{J=1}^M \sum_{j=1}^{mJ} \vec{f}_{BJj}^A + \sum_{J=1}^M \sum_{k=1}^{lJ} \vec{f}_{BJk}^a$$

and

$$\begin{aligned} \vec{M}_C^A = & \sum_{I=1}^N \sum_{i=1}^{nI} \vec{r}_{Ii} \times \vec{f}_{WIi}^A + \sum_{J=1}^M \sum_{j=1}^{mJ} \vec{r}_{Jj} \times \vec{f}_{BJj}^A + \\ & + \sum_{J=1}^M \sum_{k=1}^{lJ} \vec{r}_{Jk} \times \vec{f}_{BJk}^a \end{aligned} \quad (3.5-3)$$

where \vec{f}_{WIi}^A is the force at the i^{th} panel of the I^{th} thin body, \vec{f}_{BJj}^A is the force at the j^{th} panel on the mean interference surface of the J^{th} slender body, and \vec{f}_{BJk}^a is the force at the k^{th} segment of the J^{th} slender body, figures 3.4-1 and 3.4-2. Letting each of these forces be expanded on the Reference Axis System, the components of the i^{th} force are expressed as

$$\{f_i^A\} \equiv \begin{bmatrix} f_{X_i}^A \\ f_{Y_i}^A \\ f_{Z_i}^a \end{bmatrix} \quad (3.5-4)$$

and the components of force and couple at the center of mass are formed as

$$\{F_C^A(i)\} = [\phi_i^*]^T \{f_i^A\} \quad (3.5-5)$$

where

$$\{F_C^A(i)\} \equiv \begin{bmatrix} F_X^A(i) \\ F_Z^A(i) \\ M_Y^A(i) \\ F_Y^A(i) \\ M_X^A(i) \\ M_Z^A(i) \end{bmatrix}$$

and

$$[\bar{\phi}_i^*]^T \equiv \begin{bmatrix} 1 & 0 & 0 \\ 0 & 0 & 1 \\ \bar{Z}_i & 0 & -\bar{X}_i \\ 0 & 1 & 0 \\ 0 & -\bar{Z}_i & \bar{Y}_i \\ -\bar{Y}_i & \bar{X}_i & 0 \end{bmatrix}$$

The coordinates \bar{X}_i , \bar{Y}_i , \bar{Z}_i are the coordinates of the center of pressure at the i^{th} panel or slender body segment relative to the center of mass and expanded on the Reference Axis System. The total force and couple at the center of mass due to the aerodynamic forces at n panels and segments is expressed as

$$\{F_C^A\} = [\bar{\phi}^*]^T \{F^A\} \quad (3.5-6)$$

where

$$[\bar{\phi}^*] \equiv \begin{bmatrix} [\bar{\phi}_1^*] \\ \vdots \\ [\bar{\phi}_i^*] \\ \vdots \\ [\bar{\phi}_n^*] \end{bmatrix}$$

and

$$\{f^A\} \equiv \begin{bmatrix} \{f_1^A\} \\ \vdots \\ \{f_{\frac{n}{2}}^A\} \\ \vdots \\ \{f_n^A\} \end{bmatrix}$$

The matrix $[\bar{\phi}^*]$ is termed the rigid body mode shape matrix for reasons made apparent in section 4.

3.5.1.2 Aerodynamic force at a thin body panel.—The aerodynamic force at the center of pressure of a thin body panel, \vec{F}_{WII}^A , is expressed as an integral of quantities which may be defined in terms of the (ξ, η) local panel coordinates shown by figure 3.4-3. The aerodynamic force therefore appears as follows:

$$\vec{F}_{WII}^A = - \bar{q} \iint_{S_{WII}} (C_{P_u} \vec{n}_u + C_{P_l} \vec{n}_l) ds \quad (3.5-7)$$

where the subscripts u and l, respectively, refer to evaluation at points on the upper and lower aerodynamic surfaces.

The unit surface normals, \vec{n}_u and \vec{n}_l , are described analytically by equation (3.2-14). To first order in the aerodynamic perturbation parameters they are expressed as

$$\begin{aligned} \vec{n}_u \approx & - \frac{\partial}{\partial X_I} \left(\tau_I F_I(X_I, Y_I) + H_I H_I(X_I, Y_I) \right) \hat{i} \\ & - \sin \theta_I \hat{j} + \cos \theta_I \hat{k} \end{aligned}$$

and

$$\begin{aligned} \vec{n}_l \approx & \frac{\partial}{\partial X_I} \left(\tau_I F_I(X_I, Y_I) - H_I H_I(X_I, Y_I) \right) \hat{i} \\ & + \sin \theta_I \hat{j} - \cos \theta_I \hat{k}. \end{aligned} \quad (3.5-8)$$

The aerodynamic pressure distribution is assumed to be the sum of two parts, one part a symmetric function of the local thin body coordinate Z_I and the second part an antisymmetric function of Z_I . First-order approximations to these pressure distributions based on the thin wing theory of reference 2-3 are used in the derivation. The antisymmetric part, therefore, is governed by

$$\Delta C_P^V \equiv C_{P_l}^V - C_{P_u}^V = 2\gamma(X_I, Y_I) \quad (3.5-9)$$

and

$$C_{P_l}^V = - C_{P_u}^V$$

where $\gamma(X_I, Y_I)$ is the vorticity distribution at the mean surface,

$$C_{P_u}^V \equiv C_P^V|_{Z_I} = 0^+$$

and

$$C_{P_l}^V \equiv C_P^V|_{Z_I} = 0^-$$

The symmetric part of the pressure distribution is approximated as

$$C_{P_u}^S \approx C_P^S(Z_I = \tau_I F_I(X_I, Y_I))$$

and

(3.5-10)

$$C_{P_l}^S \approx C_P^S(Z_I = -\tau_I F_I(X_I, Y_I))$$

where $Z_I = \pm \tau_I F_I(X_I, Y_I)$ is the thin body thickness shape.

Introducing the approximations to the normal to the aerodynamic surfaces given by equations (3.5-8) and (3.5-10), the aerodynamic panel force, \vec{f}_{WIi}^A , is found from equation (3.5-7) as follows:

$$\begin{aligned} \vec{f}_{WIi}^A = \bar{q} \iint_{S_{WIi}} \Delta C_P^V \left\{ -\hat{i} \frac{\partial H_I}{\partial X_I} - \sin \theta_I \hat{j} + \cos \theta_I \hat{k} \right\} dS \\ - 2\bar{q} \iint_{S_{WIi}} C_{P_l}^S \tau_I \frac{\partial F_I}{\partial X_I} \hat{i} dS \end{aligned} \quad (3.5-11)$$

Since the vorticity is uniform on each panel, sections 3.4.3 and 3.4.8, equation (3.5-11) immediately reduces to

$$\begin{aligned} \vec{f}_{WII}^A = \bar{q} \Delta C_{PWII}^V \left\{ -H_I \iint_{S_{WII}} \frac{\partial H_I}{\partial X_I} d\vec{S} - S_{WII} (\sin \theta_I \hat{j} - \cos \theta_I \hat{k}) \right\} \\ - 2\bar{q} \iint_{S_{WII}} C_{P_I}^S \tau_I \frac{\partial F_I}{\partial X_I} d\vec{S} \end{aligned} \quad (3.5-12)$$

where ΔC_{PWII}^V is the lifting pressure coefficient defined by equation (3.4-66) for the i^{th} panel. Several approximations are made in evaluating this expression in the FLEXSTAB system. These are as follows:

$$\begin{aligned} \iint_{S_{WII}} \frac{\partial H_I}{\partial X_I} d\vec{S} &\approx \left(\frac{\partial H_I}{\partial X_I} \right)_i S_{WII} \\ \iint_{S_{WII}} C_{P_I}^S \frac{\partial F_I}{\partial X_I} d\vec{S} &\approx C_{PWII}^S \left(\frac{\partial F_I}{\partial X_I} \right)_i S_{WII} \end{aligned} \quad (3.5-13)$$

where $(\partial H_I / \partial X_I)_i$, $(\partial F_I / \partial X_I)_i$ and C_{PWII}^S are the values of the functions at the geometric centroid of the panel. Introducing the approximations into equation (3.5-12) results in

$$\begin{aligned} \vec{f}_{WII}^A = \bar{q} \Delta C_{PWII}^V S_{WII} \left\{ -H_I \left(\frac{\partial H_I}{\partial X_I} \right)_i \hat{i} - \sin \theta_I \hat{j} + \cos \theta_I \hat{k} \right\} \\ - 2\bar{q} C_{PWII}^S S_{WII} \tau_I \left(\frac{\partial F_I}{\partial X_I} \right)_i \end{aligned} \quad (3.5-14)$$

Introducing the definition

$$\{f_{WII}^A\} \equiv \begin{bmatrix} f_{X_{WII}}^A \\ f_{Y_{WII}}^A \\ f_{Z_{WII}}^A \end{bmatrix} \quad (3.5-15)$$

which corresponds with the definition of equation (3.5-14), the components of aerodynamic panel force are expressed as follows:

$$\{\vec{f}_{WII}^A\} = \bar{q} \begin{bmatrix} 1 & 0 \\ 0 & -\sin\theta_I \\ 0 & \cos\theta_I \end{bmatrix} \begin{bmatrix} -H(\frac{\partial H_I}{\partial X_I})_i \\ 1 \end{bmatrix} S_{WII} \Delta C_{P_{WII}}^V - \begin{bmatrix} 2S_{WII} \tau_I (\frac{\partial F_I}{\partial X_I})_i \\ 0 \end{bmatrix} C_{P_{WII}}^S \quad (3.5-16)$$

3.5.1.3 Aerodynamic force at a mean interference surface panel of a slender body.—The aerodynamic force at the center of pressure of a mean interference surface panel, \vec{f}_{BJj}^A , is developed following the approach of section 3.5.1.2 above. As shown by figures 3.4-1 and 3.4-7, the mean interference surface is a cylinder with a polygon cross section, and a unit vector normal to the surface of the j^{th} panel is given by

$$\vec{n}_{BJj} = \sin\theta_{BJj} \hat{j} + \cos\theta_{BJj} \hat{k} \quad (3.5-17)$$

where θ_{BJj} is the angle shown by figure 3.5-1. The normal to the slender body surface at the geometric centroid of the j^{th} panel is obtained from the analytical description of the slender body surface normal, equation (3.2-20). To a first-order approximation in the perturbation aerodynamic parameters this vector is given by

$$\vec{n}_{BJj} = \left\{ -\left[a_J \left(\frac{dR_J}{dX_J} \right)_j + b_J \left(\frac{\partial G_J}{\partial X_J} \right)_j \cos\mu_{BJj} + c_J \left(\frac{\partial I_J}{\partial X_J} \right)_j \sin\mu_{BJj} \right] \hat{i} + \cos\mu_{BJj} \hat{j} + \sin\mu_{BJj} \hat{k} \right\} \quad (3.5-18)$$

where the angles θ_{BJj} and μ_{BJj} are related as

$$\theta_{BJj} = \pi/2 - \mu_{BJj} \quad (3.5-19)$$

The panel force is expressed as

$$\vec{f}_{BJj}^A = -\bar{q} \iint_{S_{BJj}} C_{P_{BJj}}^V \vec{n}_{BJj} dS,$$

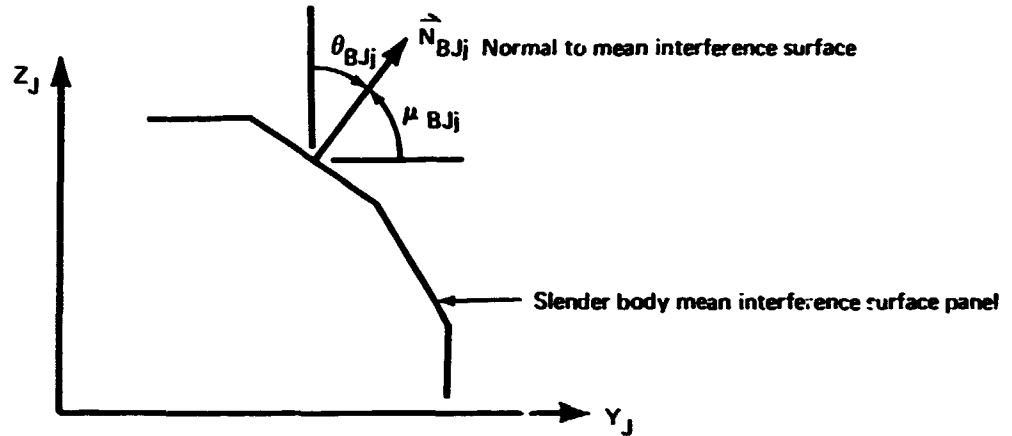


FIGURE 3.5-1.—SLENDER BODY MEAN INTERFERENCE SURFACE UNIT NORMAL VECTOR

but on assuming that equation (3.5-18) holds for all points on the panel and on recognizing that the pressure is uniform this expression reduces to

$$\begin{aligned} \hat{f}_{BJj}^A = & -qC_{p_{BJj}}^V S_{BJj} \left\{ -\left[a_J \left(\frac{dR_J}{dX_J} \right)_j + b_J \left(\frac{\partial G_J}{\partial X_J} \right) \cos \mu_{BJj} \right. \right. \\ & \left. \left. + c_J \left(\frac{\partial I_J}{\partial X_J} \right)_j \sin \mu_{BJj} \right] \hat{i} + \cos \mu_{BJj} \hat{j} + \sin \mu_{BJj} \hat{k} \right\} \end{aligned} \quad (3.5-20)$$

The matrix expression for the components of force, similar to equation (3.5-16), appears as

$$\begin{aligned} \{f_{BJj}^A\} = & \\ = \bar{q} \begin{bmatrix} +\left[a_J \left(\frac{dR_J}{dX_J} \right)_j + b_J \left(\frac{\partial G_J}{\partial X_J} \right)_j \cos \mu_{BJj} + c_J \left(\frac{\partial I_J}{\partial X_J} \right)_j \sin \mu_{BJj} \right] S_{BJj} \\ - \cos \mu_{BJj} S_{BJj} \\ - \sin \mu_{BJj} S_{BJj} \end{bmatrix} C_{F_{BJj}}^V \end{aligned} \quad (3.5-21)$$

3.5.1.4 Aerodynamic force at a slender body segment.—The aerodynamic force at the center of pressure of the k^{th} slender body segment, \vec{F}_{BJk}^A , is approximated as

$$\vec{F}_{BJk}^A = -\bar{q} \int_0^{2\pi} \int_{L_{BJk}} C_P \vec{n} r_J(\xi) d\xi d\mu \quad (3.5-22)$$

where the approximations arise by taking $r_J(X_J)$ to be the radius of an equivalent body of revolution, section 3.2.4. A further approximation is introduced by letting the unit normal vector \vec{n} be the first-order approximation from equation (3.4-20), i.e.,

$$\vec{n} = \left\{ -\left[a_J \frac{dR_J}{dX_J} + b_J \frac{\partial G_J}{\partial X_J} \cos \mu + c_J \frac{\partial I_J}{\partial X_J} \sin \mu \right] \hat{i} + \cos \mu \hat{j} + \sin \mu \hat{k} \right\}; \quad (3.5-23)$$

The pressure coefficient C_P is due to the isolated slender body thickness and lift, sections 3.4.4, 3.4.5, and 3.4.9. The surface pressure distribution, expressed in terms of the coordinate θ shown by figure 3.4-20, is given by

$$C_P(X_J, \theta) = C_P^S(X_J) + C_P^{ZD}(X_J) \sin \theta - C_P^{YD}(X_J) \cos \theta \quad (3.5-24)$$

where $C_P^S(X_J)$ is the pressure induced by line sources, while $C_P^{ZD}(X_J) \sin \theta$ and $C_P^{YD}(X_J) \cos \theta$ are, respectively, the pressures induced by the z and y line doublets, equations (3.4-129), (3.4-130), and (3.4-137).

Substituting the above expressions for the unit normal vector and the pressure into equation (3.5-22) and carrying out the integration with respect to μ noting that $\mu \equiv \theta$ yields

$$\begin{aligned} \vec{F}_{BJk}^A = -\bar{q} \int_{L_{BJk}} \{ & -\pi \left[2a_J \frac{dR_J}{dX_J} C_P^S - b_J \frac{\partial G_J}{\partial X_J} C_P^{YD} + \right. \\ & \left. + c_J \frac{\partial I_J}{\partial X_J} C_P^{ZD} \right] \hat{i} - \pi C_P^{YD} \hat{j} + \pi C_P^{ZD} \hat{k} \} r_J d\xi \end{aligned} \quad (3.5-25)$$

The integration with respect to X_J is carried out introducing the following approximations

$$\begin{aligned} \int_{L_{BJk}} \frac{dR_J}{dX_J}(\xi) C_P^S(\xi) r_J(\xi) d\xi &\approx \left(\frac{dR_J}{dX_J} \right)_k C_{P_{BJk}}^S r_{Jk} L_{BJk} \\ \int_{L_{BJk}} \frac{\partial G_J}{\partial X_J}(\xi) C_P^{YD}(\xi) r_J(\xi) d\xi &\approx \left(\frac{\partial G_J}{\partial X_J} \right)_k C_{P_{BJk}}^{YD} r_{Jk} L_{BJk} \\ \int_{L_{BJk}} \frac{\partial I_J}{\partial X_J}(\xi) C_P^{ZD}(\xi) r_J(\xi) d\xi &\approx \left(\frac{\partial I_J}{\partial X_J} \right)_k C_{P_{BJk}}^{ZD} r_{Jk} L_{BJk} \end{aligned} \quad (3.5-26)$$

$$\int_{L_{BJk}} C_P^{YD}(\xi) r_J(\xi) d\xi \approx C_{P_{BJk}}^{YD} r_{Jk} L_{BJk}$$

$$\int_{L_{BJk}} C_P^{ZD}(\xi) r_J(\xi) d\xi \approx C_{P_{BJk}}^{ZD} r_{Jk} L_{BJk}$$

where the subscript k denotes evaluation at the midpoint of the slender body segment. From equations (3.5-25) and (3.5-26) the matrix expression for the components of force at the center of pressure is deduced as

$$\begin{aligned} \{f_{BJk}^A\} &= \bar{q} \begin{bmatrix} 2\pi r_{Jk} a_J \left(\frac{dR_J}{dX_J} \right)_k L_{BJk} \\ 0 \\ 0 \end{bmatrix} C_{P_{BJk}}^S \\ &+ \bar{q} \begin{bmatrix} -\pi r_{Jk} b_J \left(\frac{\partial G_J}{\partial X_J} \right)_k L_{BJk} & \pi C_J \left(\frac{\partial I_J}{\partial X_J} \right)_k L_{BJk} \\ \pi r_{Jk} L_{BJk} & 0 \\ 0 & -\pi r_{Jk} L_{BJk} \end{bmatrix} \begin{bmatrix} C_{P_{BJk}}^{YD} \\ C_{P_{BJk}}^{ZD} \end{bmatrix} \end{aligned} \quad (3.5-27)$$

3.5.1.5 Combined aerodynamic panel and slender body segment forces.—The matrix expressions given by equations (3.5-16), (3.5-21), and (3.5-24) describing the aerodynamic forces at panels and slender body segments are combined into a single matrix expression as follows: (3.5-28)

$$\{f^A\} = \bar{q}[T_{fT}][TRANS_t]\{C_P^S\}^{iso} + \bar{q}[T_{fT}][T_{TF}][T_{FP}]\{C_P\}$$

where $\{C_P^S\}^{iso}$ is the matrix of isolated thickness induced pressure coefficients defined by equation (3.4-173), $\{C_P\}$ is the matrix of lifting pressure coefficients defined by equation (3.4-166), and contains $\{C_P^V\}^{int}$ —the thickness interference pressure defined by equation (3.4-174), while

$$\{f^A\} \equiv \begin{bmatrix} \vdots \\ f_{X_{BJj}}^A \\ f_{Y_{BJj}}^A \\ f_{Z_{BJj}}^A \\ \vdots \\ \hline f_{X_{WII}}^A \\ f_{Y_{WII}}^A \\ f_{Z_{WII}}^A \\ \vdots \end{bmatrix} \quad \begin{array}{c} \uparrow \\ \text{forces at slender body} \\ \text{segments} \\ \downarrow \\ \text{forces at thin body} \\ \text{panels} \\ \downarrow \end{array} \quad (3.5-29)$$

The matrix $\{f^A\}$ defined by equation (3.5-29) is identical to that appearing in equation (3.5-6); therefore, the total aerodynamic force and couple at the aircraft's center of mass can be computed from equation (3.5-28) by the operations indicated by equation (3.5-6).

The transformation matrices appearing in equation (3.5-28) which resolve the aerodynamic pressure coefficients, $\{C_P\}^{iso}$ and $\{C_P\}$, into thin body panel and slender body segment forces are as follows. The matrix $[T_{fT}]$ transforms the components of force from the local thin and slender body axis systems to the Reference Axis System; therefore,

$$[T_{fT}] \equiv \begin{bmatrix} [I] & \text{zeros} \\ \vdots & \ddots \\ \text{zeros} & \begin{bmatrix} \text{zeros} \\ 1 & 0 \\ 0 & -\sin \theta_I \\ 0 & \cos \theta_I \end{bmatrix} \\ \vdots & \ddots \end{bmatrix} \quad (3.5-30)$$

The matrix $[TRANS_t]$ transforms isolated thickness induced pressure, i.e., $\bar{q}\{C_p^S\}^{ISO}$, to components of force in the local thin and slender body axis systems; therefore, it follows from equations (3.5-16) and (3.5-27) that

$$[TRANS_t] \equiv \begin{bmatrix} \ddots & \begin{bmatrix} 2\pi r_{Jk} \left(\frac{dr_J}{dX_J}\right)_k L_{BJk} \\ 0 \\ 0 \end{bmatrix} & \vdots \\ \vdots & \text{zeros} & \ddots \\ \text{zeros} & \vdots & \begin{bmatrix} 2S_{wIi} \left(\frac{\partial Z_I}{\partial X_I}\right)_i \\ 0 \\ \text{zeros} \end{bmatrix} \end{bmatrix} \quad (3.5-31)$$

where

$$\left(\frac{dr_J}{dX_J}\right)_k \equiv c_{Jk} \left(\frac{dR_J}{dX_J}\right)_k \quad \left(\frac{\partial Z_I}{\partial X_I}\right)_i \equiv \tau_{Ii} \left(\frac{\partial F_I}{\partial X_I}\right)_i$$

The matrix $[T_{TF}]$ transforms forces at thin body panels from components normal to the mean camber surface to components expanded on the local thin body axis systems; therefore, it follows from equations (3.5-16) and (3.5-27) that

$$[T_{TF}] \equiv \left[\begin{array}{c|ccc} [I] & & & \text{zeros} \\ \hline & \ddots & & \\ & & \text{zeros} & \\ & & \begin{bmatrix} \frac{\partial Z_I}{\partial X_I} \\ -(\frac{\partial Z_I}{\partial X_I})_i \\ 1 \end{bmatrix} & \\ \hline \text{zeros} & & & \text{zeros} \end{array} \right] \quad (3.5-32)$$

where

$$\left(\frac{\partial Z_I}{\partial X_I}\right)_i \equiv \theta_{YIi} \left(\frac{\partial H_I}{\partial X_I}\right)_i$$

and θ_{YIi} is the local camber angle.

The matrix $[T_{FP}]$ transforms lifting pressures $\bar{q}\{C_i\}$ to components of force $\{FA\}$, equation (3.5-38), and is expressed in partitioned form as

$$[T_{FP}] = \left[\begin{array}{c|c|c} [DBL] & [INT] & \text{zeros} \\ \hline \text{zeros} & \text{zeros} & [A_W] \end{array} \right] \quad (3.5-33)$$

where

$$[A_W] \equiv \left[\begin{array}{ccc} \cdot & \text{zeros} & \\ \cdot & & \\ \cdot & & \\ & S_{WIi} & \\ \text{zeros} & & \cdot \\ & & \cdot \end{array} \right] \quad (3.5-34)$$

The partition $[A_W]$ transforms the lifting pressure on thin body panels, equation (3.5-16), into lifting force components normal to the mean camber surfaces.

The partition $[INT]$ yields the aerodynamic forces at slender body centerlines as a result of aerodynamic pressure on the slender body mean interference surfaces, figure 3.5-2. The aerodynamic pressure on each panel of the interference surface is resolved into three components of force acting at the panel centroid, as shown by equation (3.5-21). Expressed in terms of the θ_{Jj} coordinate shown by figure 3.5-2 these components are given by

$$f_{X_{BJj}}^A = \bar{q} \left[a_J \left(\frac{dR_J}{dX} \right)_j + b_J \left(\frac{\partial G_J}{\partial X} \right)_j \sin \theta_{Jj} + c_J \left(\frac{\partial I_J}{\partial X} \right)_j \cos \theta_{Jj} \right] S_{BJj} C_{P_{BJj}}^V$$

$$f_{Y_{BJj}}^A = -\bar{q} \sin \theta_{Jj} S_{BJj} C_{P_{BJj}}^V$$

$$f_{Z_{BJj}}^A = -\bar{q} \cos \theta_{Jj} S_{BJj} C_{P_{BJj}}^V$$

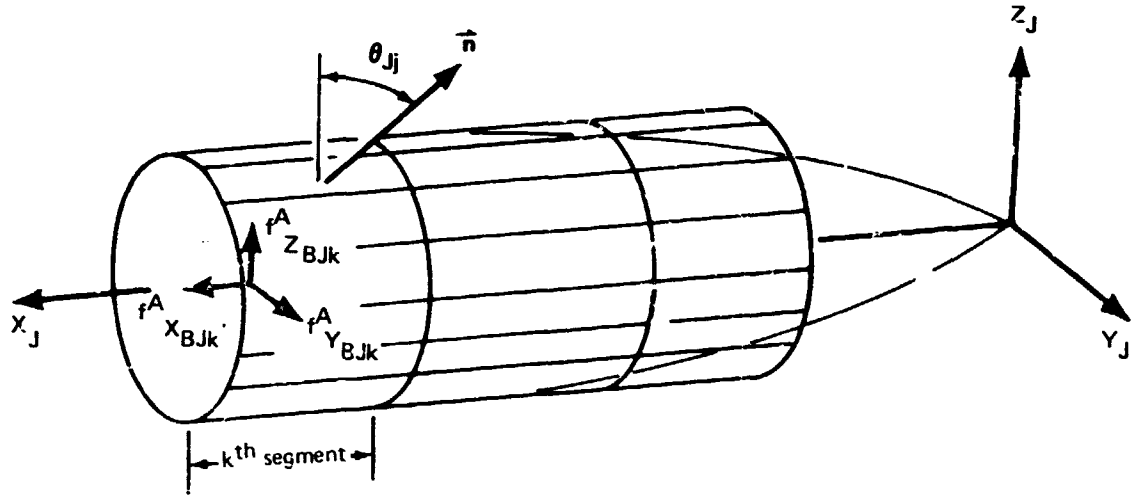


FIGURE 3.5-2.—AERODYNAMIC FORCES FROM INTERFERENCE PRESSURE ON A SLENDER BODY

where $(dR_J/dX)_j$ is the slope of the thickness shape of the body at the j^{th} panel centroid and θ_{Jj} is the angular orientation of the j^{th} panel, figure 3.5-2. The components of force at the panel centroids are applied directly to the centerline of the slender body at the centroid of the interference surface centroid as follows:

$$f_{X_{Jj}}^A = \bar{q} \sum_{j=1}^n \left[\left(\frac{dR_J}{dX} \right)_j + b_J \left(\frac{\partial G_J}{\partial X} \right)_j \sin \theta_{Jj} + c_J \left(\frac{\partial I_J}{\partial X} \right)_j \cos \theta_{Jj} \right] S_{BJj} C_{P_{BJj}}^V$$

$$f_{Y_{Jj}}^A = -\bar{q} \sum_{j=1}^n \sin \theta_{Jj} S_{BJj} C_{P_{BJj}}^V$$

$$f_{Z_{Jj}}^A = -\bar{q} \sum_{j=1}^n \cos \theta_{Jj} S_{BJj} C_{P_{BJj}}^V$$

where the sum is over the n panels forming the k^{th} segment of the interference surface. The partition [INT] is therefore given by (3.5-35)

$$[\text{INT}] \equiv \begin{bmatrix} \ddots & & & & \text{zeros} \\ & \left[\begin{array}{c} \left(\frac{dr_J}{dX_J} \right)_j + b_J \left(\frac{\partial G_J}{\partial X_J} \right)_j \sin \theta_{Jj} + c_J \left(\frac{\partial I_J}{\partial X_J} \right)_j \cos \theta_{Jj} \end{array} \right] S_{BJj} \cdots \\ & & - \sin \theta_{Jj} S_{BJj} & \cdots \\ & & - \cos \theta_{Jj} S_{BJj} & \cdots \\ & & & & \ddots \end{bmatrix}$$

zeros

The partition [DBL] yields the aerodynamic forces due to line doublet induced pressures; and, although the aerodynamic surface pressure induced by the line doublets varies in the X -direction, the nonlinear portion of the variation in the pressure is ignored and the pressure at each slender body segment centroid is taken to be the average of the pressure over the entire segment length. The aerodynamic forces at the segment centroids are found from equation (3.5-25) to have the following components:

$$\begin{aligned} f_{X_{Jj}}^A &= -q\pi L_{BJj} \left[b_J \left(\frac{\partial G_J}{\partial X_J} \right) C_{P_{BJj}}^{YD} - c_J \left(\frac{\partial I_J}{\partial X_J} \right) C_{P_{BJj}}^{ZD} \right] r_{Jj} \quad (3.5-36) \\ f_{Y_{Jj}}^A &= \bar{q}\pi r_{Jj} L_{BJj} C_{P_{BJj}}^{YD} \\ f_{Z_{Jj}}^A &= -\bar{q}\pi r_{Jj} L_{BJj} C_{P_{BJj}}^{ZD} \end{aligned}$$

The elements of the partition [DBL] are constructed from equation (3.5-36) with $\{C_P\}$ arranged so that all Y -doublet induced-pressure coefficients occur first, followed by all Z -doublet induced-pressure coefficients. Thus, (3.5-37)

$$[\text{DBL}] \equiv \left[\begin{array}{c} \ddots \\ \text{zeros} \\ \left[\begin{array}{c} -\pi C_J \left(\frac{\partial I_J}{\partial X_J} \right) L_{BJj} r_{Jj} \\ \pi r_{Jj} L_{BJj} \\ 0 \end{array} \right]_{YD} \\ \text{zeros} \\ \ddots \end{array} \right] \left[\begin{array}{c} \ddots \\ \text{zeros} \\ \left[\begin{array}{c} \pi b_J \left(\frac{\partial G_J}{\partial X_J} \right) L_{BJj} r_{Jj} \\ 0 \\ -\pi r_{Jj} L_{BJj} \end{array} \right]_{ZD} \\ \text{zeros} \\ \ddots \end{array} \right]$$

Matrices containing components of force computed by the above transformations are as follows:

$$\{F^A\} = \bar{q}[T_{FP}]\{C_P\}$$

and

$$\{f_T^A\} = \bar{q}[T_{TF}][T_{FP}]\{C_P\}$$

The elements of these two aerodynamic force (or airload) matrices are

$$\{F^A\} \equiv \begin{bmatrix} \vdots \\ f_{X_{BJj}}^A \\ f_{Y_{BJj}}^A \\ f_{Z_{BJj}}^A \\ \vdots \\ - \frac{\vdots}{\vdots} - \\ f_{Z_{WIi}}^A \\ \vdots \end{bmatrix} \quad (3.5-38)$$

and

$$\{f_T^A\} \equiv \begin{bmatrix} \vdots \\ f_{X_{BJj}}^A \\ f_{Y_{BJj}}^A \\ f_{Z_{BJj}}^A \\ \vdots \\ - \frac{\vdots}{\vdots} - \\ f_{X_{WIi}}^A \\ f_{Z_{WIi}}^A \\ \vdots \end{bmatrix} \quad (3.5-39)$$

3.5.1.6 Aerodynamic panel forces from leading edge correction.—The leading edge thrust correction, equation (3.4-224), for each thin body aerodynamic panel, where multiplied by the panel span b_i , yields an aerodynamic force in the X-direction. These airloads are incorporated into the system of airloads $\{f_T^A\}$, equation (3.5-39), by the following transformation

$$\{f_T^A\}_{ID} = [TRANS_{ID}]\{D\} \quad (3.5-40)$$

where the transformation matrix has the following partitions

$$[TRANS_{ID}] \equiv \begin{bmatrix} [0] \\ \text{---} \\ [ID] \end{bmatrix}$$

The zero partition causes the components of force at slender body segments to be unchanged by the leading edge correction. The non-zero partition contains the following elements along the diagonal:

$$\begin{bmatrix} b_i \\ 0 \end{bmatrix}$$

The transformation, equation (3.5-40), therefore leads to the force components

$$f_{ZIi}^A = 0 \quad f_{XIi}^A = \frac{D_i b_i}{b_I} = D_i$$

at each of the thin body vortex panel centroids.

3.5.2 Lifting Pressure Coefficients in Terms of Flow Incidence

The total lifting pressure distribution is found in coefficient form by combining the lifting pressure coefficients due to unsteady incidence, equation (3.4-218), with the thickness induced lifting pressure, equation (3.4-174). The result of this linear sum is expressed as

$$\{C_p\} = [A_{p\theta}]\{\psi\} + \frac{1}{U}[\delta A_{p\theta}]\{\dot{\psi}\} + \{C_p\}^{int} \quad (3.5-41)$$

where the interference pressure given by equation (3.4-174) must be written as

$$\{C_p\}^{int} \equiv \begin{bmatrix} \{0\} \\ \text{---} \\ \{C_{F_{BW}}^v\}^{int} \end{bmatrix}$$

the partition of zeros corresponding to line doublet induced pressures. This expression is further expanded by evaluating the flow incidence given by equation (2.3-69) at the aerodynamic control points. This operation is done in terms of the elastic deformation, the aircraft velocity components, and the control surface deflections as well as a reference camber shape, equation (2.3-69).

In carrying out the above operations the aerodynamic influence coefficient matrices, and $[A]$ and $[\delta A]$, are reorganized in that the columns of these matrices are ordered differently from those shown in section 3.4.7 and 3.4.11. This reordering is indicated in equation (3.5-41) by the following changes in notation introduced when constructing equation (3.5-41) from equation (3.4-218): $[A]$ is replaced by $[A_{p\theta}]$ and $[\delta A]$ is replaced by $[\delta A_{p\theta}]$. Similarly, these changes must appear in equation (3.4-240). The reordering is related entirely to the line doublets and leads to a flow incidence matrix having the following form:

$$[A] \longrightarrow [A_{p\theta}] \quad [\delta A] \longrightarrow [\delta A_{p\theta}]$$

For the symmetric case (sec. 3.4.1.5):

$$\{\Psi^S\} \equiv \begin{bmatrix} \Psi_1^{ZD} \\ \vdots \\ \Psi_r^{ZD} \\ \hline \Psi_{n+1}^{YD} \\ \Psi_{n+1}^{ZD} \\ \vdots \\ \Psi_{n+m}^{YD} \\ \Psi_{n+m}^{ZD} \\ \hline \{\Psi_W^V\} \end{bmatrix} \quad \begin{array}{l} \uparrow \\ \text{Z- doublets of slender} \\ \text{bodies on the plane} \\ \text{of symmetry, } n \equiv \ell_s^{on}, \\ \downarrow \\ \uparrow \\ \text{Y- and Z- doublets of slender} \\ \text{bodies off the plane of} \\ \text{symmetry, } m \equiv \ell_s^{off}, \\ \downarrow \\ \uparrow \\ \text{vorticity panels of thin bodies} \\ \text{off the plane of symmetry, } \ell_T^{off}. \end{array} \quad (3.5-42)$$

where Ψ_i^{YD} and Ψ_i^{ZD} denotes flow incidence at the i^{th} Y-doublet and i^{th} Z-doublet control points and ℓ_s^{on} , ℓ_s^{off} and ℓ_T^{off} are numbers defined in appendix B of volume III.

For the antisymmetric case (sec. 3.4.1.5):

(3.5-43)

$$\{\Psi^A\} \equiv \begin{bmatrix} \Psi_1^{YD} \\ \vdots \\ \Psi_n^{YD} \\ \hline \Psi_{n+1}^{YD} \\ \Psi_{n+1}^{ZD} \\ \vdots \\ \Psi_{n+m}^{YD} \\ \Psi_{n+m}^{ZD} \\ \hline \{\Psi_W^V\} \end{bmatrix}$$

Y- doublets of slender bodies
on the plane of symmetry,
 $n \equiv \ell_S^{\text{on}}$

Y- and Z- doublets of slender
bodies off the plane of
symmetry, $m \equiv 2\ell_S^{\text{off}}$,

vorticity panels of thin bodies
both on and off the plane of
symmetry, $\ell_T^{\text{on}} + \ell_T^{\text{off}}$.

where ℓ_T^{on} is a number defined in appendix B of volume III.

3.5.2.1 *Expansion of the flow incidence matrix.*—Based on equation (3.4-218) the flow incidence matrix may be expressed as

where $\{\Psi\} = \{\Psi_C\} + \{\dot{\theta}^*\} + \{\Psi_M\}$

$\{\Psi_C\} \equiv \{\Psi_0\}$ (3.5-44)

and

$$\{\dot{\Psi}\} = \{\dot{\theta}^*\} + \{\dot{\Psi}_M\}$$

The incidence $\{\Psi_C\}$ is based on the camber shape of the undeformed aircraft and is identified with $\{\Psi_0\}$ - the incidence in the absence of motion and elastic deformation, case (1) of section 2.3.3.1; $\{\dot{\theta}^*\}$ is the elastic deformation of the camber shape; and $\{\Psi_M\}$ is the flow incidence due to aircraft motion (viz., motion of the Body Axis System relative to the Fluid Axis System, section 2.2.3) and control surface deflections. Referring to equation (2.3-69), the flow incidence is expressed as

$$\begin{aligned}
\{\Psi_M\} = & \{\Psi_{\delta_e}\} \delta_e + \{\Psi_{\delta_a}\} \delta_a + \{\Psi_{\delta_r}\} \delta_r + \{\Psi_\alpha\} \alpha + \{\Psi_\beta\} \beta + \\
& + \{\Psi_P\} \frac{2\hat{P}}{\bar{b}} + \{\Psi_Q\} \frac{2\hat{Q}}{\bar{c}} + \{\Psi_R\} \frac{2\hat{R}}{\bar{b}} + \\
& + [\Psi_\theta] \{u\} + [\Psi_d] \{\hat{u}\}
\end{aligned} \tag{3.5-45}$$

where

$$\hat{P} \equiv \frac{b}{2U_1} P, \quad \hat{Q} \equiv \frac{\bar{c}}{2U_1} Q, \quad \hat{R} \equiv \frac{b}{2U_1} R$$

and

$$\hat{u}_i \equiv \frac{1}{U_1} \dot{u}_i$$

The elements of the coefficient column matrices are as follows:

Elevator:

$$\{\Psi_{\delta_e}\} \equiv \begin{bmatrix} \vdots \\ \Psi_{j\delta_e}^{ZD} \\ \vdots \\ \vdots \\ \Psi_{j\delta_e}^{YD} \\ \Psi_{j\delta_e}^{ZD} \\ \vdots \\ \vdots \\ \vdots \\ \Psi_{\delta_e}^V \end{bmatrix} \begin{array}{l} \uparrow \\ \text{Z- doublets slender bodies on the} \\ \text{plane of symmetry, } \ell_s^{\text{on}}, \\ \downarrow \\ \downarrow \\ \text{Y- and Z- doublets of slender bodies} \\ \text{off the plane of symmetry, } 2\ell_s^{\text{off}}, \\ \downarrow \\ \downarrow \\ \text{vorticity panels of thin bodies off} \\ \text{the plane of symmetry, } \ell_T^{\text{off}} \end{array} \tag{3.5-46}$$

where the elements may have any value representing surface camber change due to elevator control deflection δ_e .

The elements of the control incidence vectors, e.g., $\{\Psi_{\delta e}\}$, introduce the effects of arbitrary gearing of the control surface rotations. The change in incidence at each aerodynamic control point, e.g., $\Psi_{\delta e}^V$, is related to the control rotation δ_e by a gear ratio $(k\delta_e)_i$, which can have any specified value, either positive or negative. Further, the control surface hinge line for a thin body control surface (fig. 3.5-3) can have any angle of sweep, $\Gamma_{\delta e}^{WI}$. The hinge line sweep angle is measured in the local thin body axis system, section 3.2.4; thus, referring to equation (2.3-53), incidence at the i th panel centroid on the l th thin body is given by

$$\psi_i^{WI} = (n_{X_{\delta e}})_i^{WI} \delta_e$$

where

$$(n_{X_{\delta e}})_i^{WI} \equiv (K\delta_e)_i \cos \Gamma_{\delta e}^{WI}$$

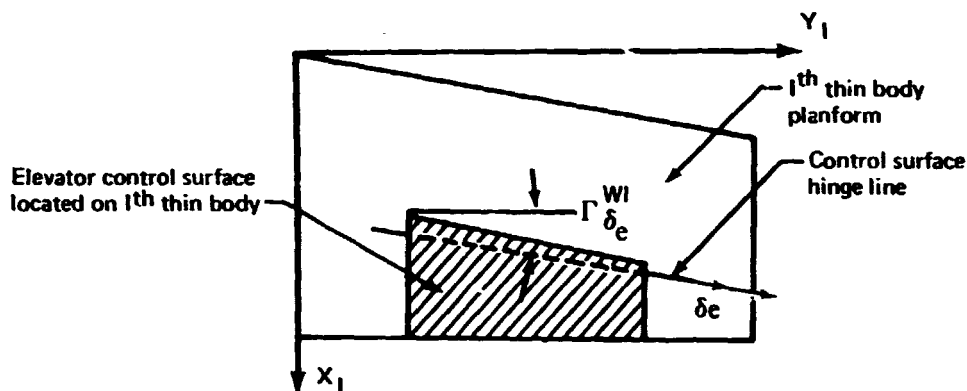


FIGURE 3.5-3.—CONTROL SURFACE HINGE LINE

The quantities $(n_{X_{\delta e}})_i$ are given the symbol S in sections 9.2.1 and 9.2.2 of Volume II—CONTROL SURFACE DATA.

Aileron:

$$\{\Psi_{\delta a}\} \equiv \begin{bmatrix} \vdots \\ \Psi_{i\delta a}^{YD} \\ \vdots \\ \vdots \\ \Psi_{i\delta a}^{YD} \\ \Psi_{i\delta a}^{ZD} \\ \vdots \\ \vdots \\ \{\Psi_{\delta a}^V\} \end{bmatrix} \begin{array}{c} \uparrow \\ l_S^{on} \\ \downarrow \\ \uparrow \\ 2l_S^{off} \\ \uparrow \\ \downarrow \\ l_T^{on} + l_T^{cff} \end{array} \quad (3.5-47)$$

where the elements may have any value representing camber surface change due to aileron control surface deflection, δ_a .

Rudder:

$$\{\Psi_{\delta r}\} \equiv \begin{bmatrix} \vdots \\ \Psi_{i\delta r}^{YD} \\ \vdots \\ \vdots \\ \Psi_{i\delta r}^{YD} \\ \Psi_{i\delta r}^{ZD} \\ \vdots \\ \vdots \\ \{\Psi_{\delta r}^V\} \end{bmatrix} \begin{array}{c} \uparrow \\ l_S^{on} \\ \downarrow \\ \uparrow \\ 2l_S^{off} \\ \uparrow \\ \downarrow \\ l_T^{on} + l_T^{off} \end{array} \quad (3.5-48)$$

where the elements may have any value representing camber surface change due to rudder control surface deflection δ_r .

Angle of attack:

$$\{\psi_\alpha\} \equiv \begin{bmatrix} \{1\} \\ \vdots \\ \begin{bmatrix} 0 \\ 1 \end{bmatrix}_i \\ \vdots \\ \cos\theta_I \{1\}_{WI} \\ \vdots \end{bmatrix} \begin{array}{c} \overline{\lambda}_s^{\text{on}} \\ \updownarrow \\ 2\lambda_s^{\text{off}} \\ \updownarrow \\ \lambda_T^{\text{off}} \\ \updownarrow \end{array} \quad (3.5-49)$$

where θ_I is the dihedral angle of the I^{th} thin body and $\{1\}_{WI}$ has as many elements as there are vorticity panels on the I^{th} thin body.

Angle of sideslip:

$$\{\psi_\beta\} \equiv \begin{bmatrix} \{1\} \\ \vdots \\ \begin{bmatrix} 1 \\ 0 \end{bmatrix}_i \\ \vdots \\ \sin\theta_I \{1\}_{WI} \\ \vdots \end{bmatrix} \begin{array}{c} \overline{\lambda}_s^{\text{on}} \\ \updownarrow \\ 2\lambda_s^{\text{off}} \\ \updownarrow \\ \lambda_T^{\text{on}} + \lambda_T^{\text{off}} \\ \updownarrow \end{array} \quad (3.5-50)$$

where θ_I is the dihedral angle of the I^{th} thin body and $\{1\}_{WI}$ has as many elements as there are vorticity panels on the I^{th} thin body.

Roll rate:

$$\{\Psi_P\} \equiv \begin{bmatrix} \{\bar{Z}\} \\ \vdots \\ \begin{bmatrix} \bar{Z}_i \\ -\bar{Y}_i \end{bmatrix} \\ \vdots \\ \{\bar{Z}\}_{WI} \sin \theta_I - \{\bar{Y}\}_{WI} \cos \theta_I \\ \vdots \end{bmatrix} \begin{matrix} \uparrow \\ \downarrow \end{matrix} \begin{matrix} \ell_s^{\text{on}} \\ 2\ell_s^{\text{off}} \\ \ell_T^{\text{on}} + \ell_T^{\text{off}} \end{matrix} \quad (3.5-51)$$

where θ_I is the dihedral angle of the I^{th} thin body and $\{\bar{Y}\}_{WI}, \{\bar{Z}\}_{WI}$ have the Reference Axis System coordinates of the vorticity panel centroids on the I^{th} thin body measured relative to the center of mass.

Pitch rate:

$$\{\Psi_Q\} \equiv \begin{bmatrix} \{\bar{X}\} \\ \vdots \\ \begin{bmatrix} 0 \\ \bar{X}_i \end{bmatrix} \\ \vdots \\ \{\bar{X}\}_{WI} \cos \theta_I \\ \vdots \end{bmatrix} \begin{matrix} \uparrow \\ \downarrow \end{matrix} \begin{matrix} \ell_s^{\text{cn}} \\ 2\ell_s^{\text{off}} \\ \ell_T^{\text{off}} \end{matrix} \quad (3.5-52)$$

where θ_I is the dihedral angle of the I^{th} thin body and $\{\bar{X}\}_{WI}$ contains the X-Reference Axis System coordinates of the vorticity panel centroids on the I^{th} thin body measured relative to the center of mass.

Yaw rate:

$$\{\Psi_R\} \equiv \begin{bmatrix} \{\bar{X}\} \\ \vdots \\ \begin{bmatrix} \bar{X}_i \\ 0 \end{bmatrix} \\ \vdots \\ \{\bar{X}\}_{WI} \sin \theta_I \\ \vdots \end{bmatrix} \begin{matrix} \uparrow \ell_s^{\text{on}} \\ \uparrow \\ 2\ell_s^{\text{off}} \\ \downarrow \\ \uparrow \\ \ell_T^{\text{on}} + \ell_T^{\text{off}} \\ \downarrow \end{matrix} \quad (3.5-53)$$

where θ_I is the dihedral angle of the I^{th} thin body and $\{\bar{X}\}_{WI}$ contains the X-Reference Axis System coordinates of the vorticity panel centroids on the I^{th} thin body measure relative to the center of mass.

3.5.2.2 Effects of dynamic pressure and Mach number variations. – Motion of the aircraft relative to the Fluid Axis System, section 2.2.3, introduces a variation in the dynamic pressure and Mach number at the aircraft surface, i.e., a variation in these quantities from their values apparent to an observer fixed relative to the Fluid Axis System. These variations are described by equations (2.3-76) and (2.3-77) of the kinematic description.

In the FLEXSTAB system the dynamic pressure and Mach number variations are simplified by assuming that the dimensions of an aircraft in the z-direction are always small—at least an order of magnitude less than either the span or the length. Variations in the dynamic pressure and Mach number along the z-direction therefore are neglected and equations (2.3-76) and (2.3-77) are approximated as

$$\bar{q}(\bar{Y}) = \bar{q}_\infty + 2\bar{q}_\infty \frac{R}{U} \bar{Y}$$

and

$$M(\bar{Y}) = M_\infty + M_\infty \frac{R}{U} \bar{Y}$$

The dynamic pressure is evaluated at the aerodynamic centroids of all aerodynamic segments (i.e., slender body centerline segments, slender body mean interference surface panels, and thin body mean surface panels, figures 3.4-1 and 3.4-2). The values obtained are arranged in matrix form to conform with the matrix $[CPM]$ defined by equation (3.4-167). The result is expressed as

$$\bar{q}_\infty [\bar{q}_c] = \bar{q}_\infty ([I_c] + \frac{2}{U_1} [\bar{Y}_c] R) \quad (3.5-54)$$

where $[I_c]$ is an identity matrix and

$$[\bar{Y}_c] \equiv \begin{bmatrix} \ddots & & & & & \\ & \ddots & & & & \\ & & \ddots & & & \\ & & & \ddots & & \\ & & & & \ddots & \\ & & & & & \ddots \end{bmatrix}$$

The matrix is partitioned into four quadrants by dashed lines. The top-left quadrant contains a diagonal sequence of dots labeled $\bar{Y}(i)$. The top-right quadrant is labeled "zeros". The bottom-left quadrant is labeled "zeros". The bottom-right quadrant contains a diagonal sequence of dots labeled $\bar{Y}(j)$, $\bar{Y}(k)$, and so on.

The quantities $\bar{Y}(i)$, $\bar{Y}(j)$, $\bar{Y}(k)$ are the coordinates of the segment aerodynamic centroids relative to the aircraft center of mass expanded on the Reference Axis System.

A matrix expression similar to equation (3.5-54) is constructed to account for the effect of dynamic pressure variations on the pressure generated by the isolated thickness, i.e., the source distributions of sections 3.4.3 and 3.4.4; hence, the matrix is constructed to conform to the matrix $\{C_P^S\}^{iso}$ defined by equation (3.4-173). The result is expressed as

$$[\bar{q}]_t = \bar{q}_\infty [\bar{q}_t] \quad (3.5-55)$$

where

$$[\bar{q}_t] \equiv ([I_t] + \frac{2}{U} [\bar{Y}_t] R)$$

and $[\bar{Y}_t]$ is formed like $[\bar{Y}_c]$ but does not include the coordinates of the slender body mean interference surface panels.

The effects of Mach number variations are applied only to the source distributions of the isolated thickness problems of sections 3.4.2 and 3.4.4. The matrix form, therefore, is given by

$$[M]_t = M_\infty [I_t] + [\Delta M_t] \quad (3.5-56)$$

where

$$[\Delta M_t] \equiv \frac{M_\infty}{U} [\tilde{Y}_t] R$$

Introducing the dynamic pressure and Mach number corrections given by equations (3.5-54) through (3.5-56) into the pressure transformation equation, i.e., equation (3.5-28), leads to

$$\begin{aligned} \{f^A\} = & \bar{q}_\infty [T_{fT}] [TRANS_t] [q_t] \left(\{C_P^{S, iso}\} + [\Delta M_t] \left\{ \frac{\partial C_P^S}{\partial M} \right\}^{iso} \right) \\ & + \bar{q}_\infty [T_{fT}] [T_{TF}] [T_{FP}] [q_c] \{C_P\} + \\ & + \bar{q}_\infty [T_{fT}] [TRANS_{ID}] [\bar{q}_c] \{D\} \end{aligned} \quad (3.5-57)$$

where $\left\{ \frac{\partial C_P^S}{\partial M} \right\}^{ISO}$ is the effect of speed variations on the isolated thickness pressure coefficients given by equation (3.4-229).

3.5.3 Aerodynamic Force Derivative Formulation

The aerodynamic forces are found by substituting the pressure coefficients, equation (3.4-217), into the pressure transformation given by equation (3.5-57) and constructing a first-order perturbation expansion. The coefficients of the perturbation motion variables are the desired aerodynamic force derivatives.

3.5.3.1 Reference State.—In the FLEXSTAB system the aerodynamic force derivatives are found from perturbations about a reference state which consists of steady motion. In the reference state the pressure transformation is given by

$$\begin{aligned} \{f^A\}_1 = & \bar{q}_1 [T_{fT}] [TRANS_t] [\bar{q}_t]_1 \left(\{C_P^S\}^{iso}_1 + [\Delta M_t]_1 \left\{ \frac{\partial C_P^S}{\partial M} \right\}_1^{iso} \right) \\ & + \bar{q}_1 [T_{fT}] [T_{TF}] [T_{FP}] [\bar{q}_c]_1 \{C_P\}_1 + \bar{q}_1 [T_{fT}] [TRANS_{ID}] [\bar{q}_c]_1 \{D\}_1 \end{aligned} \quad (3.5-58)$$

and the lifting pressure coefficients are

$$\{C_P\}_1 = [A_{p\theta}]_1 \{ \{\Psi_C\}_1 + \{\Psi^*\}_1 + \{\Psi_M\}_1 \} + \{C_P\}_1^{int} \quad (3.5-59)$$

where the subscript 1 denotes evaluation in the reference state and as noted in section 3.5.2

$$\{C_P\}^{int} \equiv \begin{bmatrix} \{0\} \\ \{C_{P_{WB}}^V\}^{int} \end{bmatrix}$$

3.5.3.2 Perturbation expansion.—The perturbation expansion is an expansion about the reference state described in the preceding section and is obtained by evaluating equation (3.5-57) for a state of unsteady motion consisting of a small perturbation from the steady, reference state of motion. The translational and rotational velocities of the aircraft, equation (2.2-3), are expressed as

$$\vec{V}_c = \vec{V}_c + \vec{V}_{cp}$$

and

$$\vec{\omega} = \vec{\omega}_1 + \vec{\omega}_p$$

where

$$\vec{V}_{cp} = u\hat{i}_B + v\hat{j}_B + w\hat{k}_B$$

and

$$\vec{\omega}_p = p\hat{i}_B + q\hat{j}_B + r\hat{k}_B$$

perturbation velocities. As a result of the unsteady perturbation motion there is a perturbation, to the dynamic pressure, equations (3.5-54) and 3.5-55).

$$(\bar{q}_\infty [\bar{q}_c])_p = \bar{q}_1 (2[\bar{q}_c]_1 \frac{u}{U_1} + 2[\bar{q}_c]_1 \frac{r}{U_1}) \quad (3.5-60)$$

and

$$(\bar{q}_\infty [\bar{q}_t])_p = \bar{q}_1 (2[\bar{q}_t]_1 \frac{u}{U_1} + 2[\bar{q}_t]_1 \frac{r}{U_1})$$

The Mach number of the oncoming stream, equation (3.5-53), is perturbed as

$$[M_t]_P = M_1 ([I_t] \frac{u}{U_1} + [Y_t] \frac{r}{U_1})$$

Finally, perturbations to the flow incidence occur and are obtained from equations (3.5-41) as

$$\{\psi\}_P = \{\theta^*\}_P + \{\psi_M\}_P$$

$$\{\dot{\psi}\}_P = \{\dot{\theta}^*\}_P + \{\dot{\psi}_M\}_P$$

Substituting the above first-order expansions into equation (3.5-57), neglecting terms which are of second and higher order in the perturbation quantities as well as a term involving a second-order derivative of the isolated thickness induced pressure coefficients, $\{C_P^S\}_{ISO}$, with respect to Mach number, leads to the following first-order perturbation expansion of the aerodynamic forces:

$$\begin{aligned} \{\dot{F}_T^A\}_P = \bar{q}_1 [TRANS_t] & \left[(2[\bar{q}_t] \frac{u}{U_1} + 2[\bar{Y}_t] \frac{r}{U_1}) (\{C_P^S\}_1^{iso} + \right. \\ & \left. + [\Delta M_t]_1 \{ \frac{\partial C_P^S}{\partial M} \}_1^{iso}) + [\bar{q}_t]_1 (\{C_P^S\}_P^{iso} + \right. \\ & \left. + \frac{M_1}{U_1} [\bar{v}_t] \{ \frac{\partial C_P^S}{\partial M} \}_1^{iso}) \right] + \bar{q}_1 [T_{TF}] [T_{FP}] \left[(2[\bar{q}_c] \frac{u}{U_1} + \right. \\ & \left. + 2[\bar{Y}_c] \frac{r}{U_1}) (\{C_P\}_1 + [\bar{q}_c]_1 \{C_P\}_P) + \right. \\ & \left. + [TRANS_{ID}] \left[(2[\bar{q}_c] \frac{u}{U_1} + 2[\bar{Y}_c] \frac{r}{U_1}) (\{D\}_1 + \right. \right. \\ & \left. \left. + [\bar{q}_c]_1 \{D\}_P) \right] \right] \end{aligned} \quad (3.5-63)$$

where the principal quantities appearing in this equation are listed as follows.

Reference flight condition lifting pressure coefficients:

$$\{C_F^A\}_1 \equiv [A_{F\theta}]_1 (\{C_F\}_1 + \{\theta^*\}_1 + \{\psi_M\}_1) + \{C_F\}_1^{int}$$

Reference flight condition flow incidence:

$$\{\Psi\}_1 = \{\Psi_c\} + \{\theta^*\}_1 + \{\Psi_M\}_1 \quad (3.5-64)$$

Perturbation isolated thickness pressure:

$$\{C_P^S\}_P^{iso} = M_1 \left\{ \frac{\partial C_P^S}{\partial M} \right\}_1 \frac{u}{U_1} \quad (3.5-65)$$

Perturbation lifting pressure coefficients:

$$\begin{aligned} \{C_P\}_P = [A_{P\theta}]_1 (\{\theta^*\}_P + \{\Psi_M\}_P) + \frac{1}{U_1} [\delta A_{P\theta}]_1 (\{\dot{\theta}^*\}_P \\ + \{\dot{\Psi}_M\}_P) + M_1 \left[\frac{\partial A_{P\theta}}{\partial M} \right]_1 \{\Psi\}_1 \frac{u}{U_1} + \{C_P\}_P^{int} \end{aligned} \quad (3.5-66)$$

Leading edge correction terms, $\{D\}_1$ and $\{D\}_P$, are expanded in the following.

3.5.3.3 Expansion of leading edge correction terms.—The expansion of the leading edge correction terms is developed from the results of section 3.4.12. The integrated incidence

$$\{w_I\} = [ISC_\theta] \{\Psi\}$$

contains the integrated incidence due to rigid body motion of the aircraft. This incidence is given by

$$\{\Delta w_{I_\alpha}\} \equiv \{LEC\} \otimes \{\Psi_\alpha\}$$

$$\{\Delta w_{I_\beta}\} \equiv \{LEC\} \otimes \{\Psi_\beta\}$$

$$\{\Delta w_{I_Q}\} \equiv \{LEC\} \otimes \{\Psi_Q\} \frac{1}{U_1} \quad (3.5-67)$$

$$\{\Delta w_{I_P}\} \equiv \{LEC\} \otimes \{\Psi_P\} \frac{1}{U_1}$$

and

$$\{\Delta w_{I_R}\} \equiv \{LEC\} \otimes \{\Psi_R\} \frac{1}{U_1}$$

where the column matrix $\{LEC\}$ contains the chord lengths of the leading edge panels of thin bodies, i.e.,

$$\{LEC\} \equiv \begin{bmatrix} \{0\} \\ \text{---} \\ \{C_1\} \\ \vdots \\ \{C_n\} \end{bmatrix} \quad (3.5-68)$$

and

$$\{C_i\} = \begin{bmatrix} C_i \\ 0 \\ \vdots \\ 0 \end{bmatrix} \quad \begin{array}{c} \text{---} \\ \uparrow \\ \text{number of panels in } i^{\text{th}} \text{ panel row} \\ \downarrow \\ \text{---} \end{array}$$

where C_i is the chord length of i^{th} leading edge panel while the incidence matrices are those given by equations (3.5-46) through (3.5-53).

For the reference flight condition the integrated incidence is given by

$$\{w_I\}_1 = [ISC_\theta] \{\gamma\}_1 - \{\Delta w_I\}_1 \quad (3.5-69)$$

where

$$\{\Delta w_I\}_1 \equiv \{\Delta w_I^T\} \alpha_1 + \{\Delta w_I^B\} \beta_1 + \{\Delta w_I^F\} \gamma_1$$

The leading edge correction for the reference flight condition is therefore given by

$$\{D\}_1 = \{w_I\}_1 \otimes \{C_F\}_1 - \{LD\}_1 \text{ and } \{D_{ref}\} \equiv [TRANS_{10}] \{D\}_1$$

$$\{LD\}_1 = \{\Delta w_I\}_1 \otimes \{C_F\}_1 \quad (3.5-70)$$

where

$$\{C_F\}_1 \equiv [A_{FE}] \{c\}_1$$

$$\{c\}_1 = \{w_I\}_0 \otimes \{D_F\}_0 \text{ and } \{D\}_1 \equiv [TRANS_{10}] \{D\}_0$$

$$\{w_I\}_0 \equiv [ISC_0] \{c\}_0 \text{ and } \{C_F\}_0 \equiv [A_{FE}] \{c\}_0$$

The perturbation leading edge correction appears as

$$\{D\}_P = [D_{P\theta}]\{\Psi\}_P - ([A_{P\theta}]\{\Psi\}_1) \alpha (\{LEC\} \alpha \{\Psi\}_P) + \{\frac{\partial D}{\partial M}\}_u \quad (3.5-71)$$

where $[D_{P\theta}] \equiv \{C_P\}_1 \alpha [ISC_\theta] + \{w_I\}_1 \alpha [A_{P\theta}]$

wherein $\{C_P\}_1 \equiv [A_{P\theta}]\{\Psi\}_1$ and $\{w_I\}_1 \equiv [ISC_\theta]\{\Psi\}_1$

and $\{\frac{\partial D}{\partial M}\} = \{w_{IP_u}\} \alpha ([A_{P\theta}]\{\Psi\}_1) + ([ISC_\theta]\{\Psi\}_1) \alpha \{C_{P_u}\}$

wherein $\{w_{IP_u}\} \equiv \frac{M_1}{U_1} [\frac{\partial ISC_\theta}{\partial M}]\{\Psi\}_1$, $\{C_{P_u}\} \equiv \frac{M_1}{U_1} [\frac{\partial A_{P\theta}}{\partial M}]\{\Psi\}_1$

The term $([A_{P\theta}]\{\Psi\}) \alpha (\{LEC\} \alpha \{\Psi\}_P)$ contributing to the perturbation leading edge thrust correction, equation (3.5-71), is expressed as a sum based on the expansion of the flow incidence matrix given by equation (3.5-67); this sum is given by

$$\{D\}_P = [D_{P\theta}]\{\Psi\}_P + \{\frac{\partial D}{\partial M}\}_u - \{\Delta D\}_P \quad (3.5-72)$$

where

$$\{\Delta D\}_P \equiv \{\Delta D_\alpha\} \alpha + \{\Delta D_\beta\} \beta + \{\Delta D_P\} p + \{\Delta D_Q\} q + \{\Delta D_R\} r$$

and $\{\Delta D_\alpha\} \equiv ([A_{P\theta}]\{\Psi\}_1) \alpha \{\Delta w_{I_\alpha}\}$

also $[D_{P\theta}] \equiv [TRANS_{ID}][D_{P\theta}]$

3.5.3.4 Formulation of the aerodynamic force derivatives.—The aerodynamic force derivatives are found by combining equations (3.5-61), (3.5-62), and (3.5-63), expanding $\{\Psi_M\}_P$ and $\{\dot{\Psi}_M\}_P$ by substituting from equation (3.5-42). The coefficients of the perturbation motion variables in the resulting expression are the aerodynamic force derivatives relating perturbation aerodynamic segment forces to the perturbation motion variables. Perturbations to the total aerodynamic force and couple at the aircraft center of mass are found by operating on $\{F^A\}_P$ using the rigid body mode shape matrix as in equation (3.5-6), i.e.,

$$\{F_C^A\}_P = 2[\bar{\phi}^*]^T \{F^A\}_P \quad (3.5-73)$$

Finally, $\{F_C^A\}_P$ is transformed to components in the Body Axis System in the transformation

$$\{F_B^A\}_P = 2[\mathcal{J}][\bar{\phi}^*]^T \{f^A\}_P \quad (3.5-74)$$

where

$$[\mathcal{J}] \equiv \left[\begin{array}{ccc|ccc} -1 & 0 & 0 & & & \\ 0 & -1 & 0 & & \text{zeros} & \\ 0 & 0 & 1 & & & \\ \hline & & & 1 & 0 & 0 \\ \text{zeros} & & & 0 & -1 & 0 \\ & & & 0 & 0 & -1 \end{array} \right]$$

The resulting expressions, however, are not immediately useful because the elastic deformation $\{\theta^*\}$ appears explicitly. Explicit dependence on the elastic deformation is eliminated using equations derived in section 4. Final expressions for the aerodynamic force derivatives are derived in sections 5 and 6.

Moments about the origin of the Reference Axis System are obtained by writing $\{\bar{\phi}_i^*\}$ of equation (3.5-5) in terms of the coordinates X_i, Y_i, Z_i . This results in

$$\{F_R^A\} = 2[\bar{\phi}_R^*]^T \{f^A\} \quad (3.5-76)$$

where $\{F_R^A\}$ contains the required aerodynamic moments about the origin of the Reference Axis System.

4.0 STRUCTURES

4.1 INTRODUCTION

The structural equations used in formulating the FLEXSTAB system are derived from the classical, linear theory of elasticity, reference 2-1. The derivation, based on the finite element method, leads to structural equations of motion expressed in terms of matrices relating structural motions to the applied aerodynamic, inertial, and propulsion system forces.

The structural motion was introduced in section 2.3 as a time-varying displacement field,* viz.,

$$\vec{d} = \vec{d}(X, Y, Z, t) \quad (4.1-1)$$

This equation represents the motion of the structure of an aircraft relative to the body-fixed axis systems (mean reference frames) introduced by section 2.2. In the finite element method, the structure is subdivided into elements, and the displacement field is described over each element by two sets of quantities: (1) simple functions of the Reference Axis System coordinates and (2) the values of the displacement components at a small number of element boundary points called nodes. The method yields equations which are an approximation to the partial differential equations which govern the components of \vec{d} in the theoretical elasticity problem. The approximate equations from the finite element method are a set of second-order, linear, ordinary differential equations governing the values of time-varying displacement components at the nodes. These equations, formulated in terms of matrices, are the structural equations of motion used in FLEXSTAB.

The equations of motion are derived in section 4.2 starting from Hamilton's principle, reference 4-1; this approach focuses the derivation on the kinematics of the problem. This starting point is chosen because the theory of elasticity used in the derivation introduces unusual constraints on the motion. The constraints are limitations on the magnitude of rotations of the structure relative to the coordinate system used in the analytical description of the elastic theory. The derivation proceeding from Hamilton's principle clarifies this important point. The reader who is not concerned with these details may ignore the contents of sections 4.2.1, 4.2.2.3, 4.2.2.4, and 4.2.2.5. The remainder of section 4.2 is sufficient for a description of the FLEXSTAB system formulation.

Much of the remainder of section 4.2 is aimed at deriving transformations related to the finite element method. Distributed applied forces, viz., the aerodynamic surface pressure and the inertial forces, are transformed to equivalent concentrated forces applied at the nodes; displacements at the nodes are transformed to describe deformation of the aerodynamic surfaces and displacement of the distributed mass. General methods for deriving these transformations are developed in section 4.2 from the basic concepts underlying the

*The notation for Lagrangian coordinates \tilde{X} , \tilde{Y} , \tilde{Z} is deleted.

finite element method. These methods are applied in sections 4.3 and 4.4 to derive the transformations for the specific finite element methods used in FLEXSTAB.

The FLEXSTAB system is formulated to function using finite element data from either of two sources. One source, a part of the FLEXSTAB system called the Internal Structural Influence Coefficient Method (ISIC), is derived in section 4.3. The finite element data from this source is based on the structure's being represented entirely as a collection of beams. The second source may be any method which generates finite element data satisfying certain requirements of the FLEXSTAB system. The requirements on the finite element data are delineated in section 4.4.

4.2 STRUCTURAL EQUATIONS OF MOTION

4.2.1 Hamilton's Principle

The equations of motion for a flexible aircraft are derived in this section from Hamilton's principle, section 2-4 of reference 4-1. For a flexible aircraft, Hamilton's principle appears as follows:

$$\delta \int_{t_1}^{t_2} (K - U') dt + \int_{t_1}^{t_2} \delta W dt = \quad (4.2-1)$$

where K is the kinetic energy defined as

$$K \equiv \frac{1}{2} \int_V \frac{d\vec{r}'}{dt} \cdot \frac{d\vec{r}'}{dt} \rho_A dV$$

U' is the strain energy, and δW is the virtual work of the applied surface stress, \vec{P} , and of the gravity forces, $\vec{g} \rho_A dV$, i.e.,

$$\delta W \equiv \int_S \vec{P} \cdot \delta \vec{r}' dS - \int_V \rho_A \vec{g} \cdot \delta \vec{r}' dV \quad (4.2-2)$$

The variation $\delta \vec{r}'$ is the first variation of the coordinates of the aircraft, i.e.,

$$\vec{r}' = \vec{r}'(x; y; z; t), \quad (2.3-1)$$

and the variation is required to vanish at times t_1 and t_2 . An important feature of this formulation is that all quantities appearing in equation (4.2-1), including the strain energy, are expressed in terms of the coordinates given by equation (2.3-1), i.e., position relative to the Inertial Axis System, figure 2.3-1.

In the FLEXSTAB system the structural theory (and, therefore, the strain energy) is expressed in a body-fixed axis system and not the Inertial Axis System as required by equation (4.2-1). The strain energy is expressed in a body-fixed axis system because the structural theory is based on the well-known approximations of the "classical" theory of elasticity, pp. 53-56 and 84-86 of reference 4-2. In part, these approximations relate to rotations of the structure relative to the coordinate system in which the structural theory is expressed, and for the approximations to be valid these rotations must be small. As shown by reference 4-2, when a structure is massive (i.e., having dimensions of the same order of magnitude in all directions) its rotations are described accurately by the theory only when they have the same small order of magnitude as the elastic elongations and shears—0.005 radians for typical aircraft materials. Following the classification of reference 4-2, when an aircraft structural component is flexible (i.e., having dimensions in one or two directions which are small by comparison with the dimensions in the remaining directions such as wings, tail surfaces, and slender fuselages) sections of the structure in directions of the small dimensions may undergo rotations accurately described by the theory when the rotations satisfy the less stringent requirement: small by comparison to unity. In either case, however, whether the structure is massive or flexible, the coordinate system used in expressing the strain energy cannot be the Inertial Axis System as required by equation (4.2-1). This conclusion follows because rotations of the structure relative to the Inertial Axis System must be permitted to have arbitrarily large magnitudes in a dynamic analysis such as that performed by FLEXSTAB.

Letting the coordinate system for the structural theory be the Reference Axis System, table 2.1-1, the coordinates appearing in Hamilton's principle are those introduced in section 2.3 as

$$\vec{r}'(X,Y,Z,t) = \vec{r}'_0(t) + \vec{r}(X,Y,Z) + \vec{d}(X,Y,Z,t) \quad (2.3-14)$$

where the coordinates $\vec{d}(X,Y,Z,t)$ depend on the quantities $\vec{r}'_0(t)$ and $\vec{\omega}(t)$ — $\vec{r}'_0(t)$ being the position of the center of mass relative to the Inertial Axis System and $\vec{\omega}(t)$ being the rotation rate of the Reference Axis System relative to the Inertial Axis System. The coordinates $\vec{d}(X,Y,Z,t)$, therefore, must be subject to constraint conditions related to the quantities $\vec{r}'_0(t)$ and $\vec{\omega}(t)$; and the constraint conditions related to $\vec{\omega}(t)$ must be such that rotations of the structure relative to the Reference Axis System have the degree of smallness described in the preceding paragraph. The choice of constraint conditions is arbitrary provided that they satisfy this requirement of small relative rotations. The mean reference frame constraint conditions, equations (2.3-18), are chosen for the FLEXSTAB system, and with this choice Hamilton's principle is expressed as follows:

$$\delta \int_{t_1}^{t_2} [K-U + \vec{\lambda}_1 \cdot \left(\int_V \vec{\partial} \rho_A dV \right) + \vec{\lambda}_2 \cdot \left(\int_V \vec{r} \times \vec{\partial} \rho_A dV \right)] dt + \int_{t_1}^{t_2} \delta W dt = 0 \quad (4.1-3)$$

*The notation for Lagrangian coordinates \tilde{X} , \tilde{Y} , \tilde{Z} is deleted.

where the components of $\vec{\lambda}_1$ and $\vec{\lambda}_2$ are six undetermined Lagrange multipliers, section 2-4 of reference 4-1, and the first variation of the coordinates is given by

$$\delta \vec{r}' = \delta \vec{r}'_0 + \delta \vec{\Omega} \times \vec{r}' + \delta \vec{d} \quad (4.2-4)$$

wherein the variation $\delta \vec{\Omega}$ is the variation in rotation obtained as $\delta \vec{\Omega} = \int \delta \vec{\omega} dt$ and $\delta \vec{d}$ is the variation in elastic deformation required to satisfy the mean reference frame constraint conditions.

The variational problem posed by equation (4.2-3) yields structural equations of motion which, for a complex structure like that of an aircraft, cannot be evaluated numerically. To obtain equations which can be evaluated, Hamilton's principle is expressed in the form used in the finite element method of structural analysis.

4.2.2 Finite Element Method

The objective of the finite element method is to reduce the equations governing the motions of a continuous, flexible aircraft to an approximate but accurate set of equations involving a finite number of degrees of freedom. The approximations used in doing this are consistent with those introduced for the aerodynamics problem of section 3. The finite element method of structural analysis is, in certain respects, similar to the surface segmenting scheme used in generating the aerodynamic influence coefficients developed in section 3.4.

4.2.2.1 Finite element concepts.—The concepts used in reducing the continuous problem to the approximate, finite element problem are introduced by reference 4-3 as follows:

- a) The continuous structure is separated by imaginary lines or surfaces into a finite set of "finite elements."
- b) The finite elements are assumed to be interconnected at a number of discrete nodal points situated on their boundaries. The displacements of these nodal points are the basic unknown quantities to be determined.
- c) For each finite element a function, $N^a(X,Y,Z)$ (or functions $N_{ij}^a(X,Y,Z)$), is chosen to define uniquely the state of displacement within the element in terms of its nodal displacements, $\{\delta^a\}$, as follows:

$$\{d^a\} = [N^a]\{\delta^a\} \quad (4.2-5)$$

where the elements of $\{d^a\}$ describe the state of displacement interior to the a^{th} finite element. Equation (4.2-5) is termed the displacement relation for the a^{th} finite element

Structural motion was introduced into the kinematic description by equation (2.3-14) as a time-varying displacement field relative to the body fixed axis systems, viz.,

$$\vec{d} = \vec{d}(X, Y, Z, t).$$

The components of this vector field are expanded on the Reference Axis System, section 2.2, as follows:

$$\begin{aligned} d_X &= d_X(X, Y, Z, t), \\ d_Y &= d_Y(X, Y, Z, t), \quad d_Z = d_Z(X, Y, Z, t). \end{aligned}$$

The displacement relations, equation (4.2-5), describe these components for each finite element in terms of displacement functions which are independent of time as follows:

$$d_X^a(X, Y, Z, t) = \sum_i N_{Xi}^a(X, Y, Z) \delta_i^a(t) \quad (4.2-6)$$

$$d_Y^a(X, Y, Z, t) = \sum_i N_{Yi}^a(X, Y, Z) \delta_i^a(t)$$

$$d_Z^a(X, Y, Z, t) = \sum_i N_{Zi}^a(X, Y, Z) \delta_i^a(t)$$

where the displacement functions $N_{Xi}^a(X, Y, Z)$, $N_{Yi}^a(X, Y, Z)$, $N_{Zi}^a(X, Y, Z)$ are continuous functions of the coordinates for points interior to the boundaries of the a^{th} finite element and $\delta_i^a(t)$ is the i^{th} nodal displacement component for the a^{th} finite element. Equations (4.2-6) are formulated in terms of matrices as follows:

$$\{d^a(X, Y, Z, t)\} = [N^a(X, Y, Z)]\{\delta^a(t)\} \quad (4.2-7)$$

where

$$\{d^a\} \equiv \begin{bmatrix} d_X^a \\ d_Y^a \\ d_Z^a \end{bmatrix}, \quad [N^a] \equiv \begin{bmatrix} N_{X1}^a & N_{X2}^a & \cdots & N_{Xi}^a & \cdots \\ N_{Y1}^a & N_{Y2}^a & \cdots & N_{Yi}^a & \cdots \\ N_{Z1}^a & N_{Z2}^a & \cdots & N_{Zi}^a & \cdots \end{bmatrix}$$

and

$$\{\delta^a\} \equiv \begin{bmatrix} \delta_1^a \\ \delta_2^a \\ \vdots \\ \delta_i^a \\ \vdots \end{bmatrix}$$

- d) The displacement functions (item c) define uniquely the state of strain within the element in terms of its nodal displacements. The strains, thus determined, together with the elastic properties of the material of the element, define the state of stress throughout the element and at its boundaries.
- e) The forces applied to the structure are replaced with an equivalent set of concentrated forces acting at the nodes. For the a^{th} finite element these nodal forces are denoted as $\{Q^a\}$, and equivalence with the external forces is established by the following virtual work relation:

$$\begin{aligned} \delta \bar{w} &= \delta \{\delta^a\}^T \{Q^a\} \\ &= \delta \{\delta^a\}^T \left(\int_{V^a} [N^a]^T \{R^a\} dV + \int_{S^a} [N^a]^T \{P^a\} dS \right) \end{aligned}$$

where $\delta \{\delta^a\}$ are virtual nodal displacements and the elements of $\{R^a\}$ and $\{P^a\}$ are the components of body forces and surface tractions applied to the a^{th} finite element of volume V^a and surface area S^a . Assuming the virtual displacements to be arbitrary, the equivalent nodal forces are found as follows:

$$\{Q^a\} = \int_{V^a} [N^a]^T \{R^a\} dV + \int_{S^a} [N^a]^T \{P^a\} dS \quad (4.2-8)$$

- f) The total forces concentrated at the nodes $\{T^a\}$ must be in equilibrium with the applied loads and the stresses at the element boundaries. Equilibrium of the a^{th} finite element therefore is expressed as follows:

$$\{T^a\} = [K^a] \{\delta^a\} - \{Q^a\} \quad (4.2-9)$$

where $\{\delta^a\}$ are the nodal displacements and $[K^a]$ (a square, symmetric matrix) is the stiffness matrix of the a^{th} finite element, cf., section 4.3.1.5.

- g) A structure is represented by a number of finite elements, and a stiffness relation for the structure is assembled by combining the element stiffness relations, i.e., equation (4.2-9). The element stiffness relations are combined by imposing two requirements: (1) that the nodal forces be in equilibrium and (2) that the nodal displacements be continuous. The resulting stiffness matrix is called the composite stiffness matrix.

The operations leading to assembly of the composite stiffness relation are made systematic by introducing the following notation. At the i^{th} node of the structure

$\{T_i\} \equiv$ components of total nodal force

$\{Q_i\} \equiv$ components of applied nodal force

$\{\delta_i\} \equiv$ components of nodal displacement

At the node of the a^{th} finite element joined to the i^{th} structural node

$\{T_i^a\} \equiv$ components of total nodal force*

$\{Q_i^a\} \equiv$ components of applied nodal forces*

$\{\delta_i^a\} \equiv$ components of nodal displacement

The nodal force quantities are set into correspondence by letting

$$\begin{aligned} \{T_i\} &= \sum_a \{T_i^a\} \\ \{Q_i\} &= \sum_a \{Q_i^a\} \end{aligned} \quad (4.2-10)$$

where the sum is over all elements joined to the i^{th} structural node. The nodal displacement quantities are set into correspondence by letting

$$\{\delta_i\} = \{\delta_i^a\} \quad (4.2-11)$$

where the equality is imposed for all elements joined to the i^{th} structural node. Equations (4.2-10) make the nodal forces at the structural nodes the resultants of the nodal forces acting on the elements joined to each structural node, while equation (4.2-11) imposes continuity at the structural nodes.

*Correspondence with the notation of reference 4-1 is given by

$$\{Q^a\} \equiv \{F\}_F^a + \{F\}_B^a \text{ and } \{T^a\} = \{F\}$$

The set of nodal displacement components for a structure with n nodes is contained in the matrix

$$\{\delta\} \equiv \begin{bmatrix} \{\delta_1\} \\ \{\delta_2\} \\ \vdots \\ \{\delta_n\} \end{bmatrix} \quad (4.2-12)$$

while the sets of total and applied nodal forces for the structure are contained in the matrices

$$\{\mathbf{T}\} \equiv \begin{bmatrix} \{\mathbf{T}_1\} \\ \{\mathbf{T}_2\} \\ \vdots \\ \{\mathbf{T}_n\} \end{bmatrix} \quad \{\mathbf{Q}\} \equiv \begin{bmatrix} \{\mathbf{Q}_1\} \\ \{\mathbf{Q}_2\} \\ \vdots \\ \{\mathbf{Q}_n\} \end{bmatrix} \quad (4.2-13)$$

Applying the operations shown by equations (4.2-10) and (4.2-11), the finite element stiffness relations, equation (4.2-9), are combined into a stiffness relation for the entire structure as

$$\{\mathbf{T}\} = [\mathbf{K}]\{\delta\} - \{\mathbf{Q}\}$$

where the matrix $[\mathbf{K}]$ —called the composite stiffness matrix—has elements consisting of sums of the elements of the finite element stiffness matrices $[\mathbf{K}^a]$.

Equilibrium is imposed on the structure by requiring the components of total nodal force to vanish at each node, i.e.,

$$\{\mathbf{T}_i\} = \{0\}.$$

The composite stiffness relation for the structure follows as

$$\{\mathbf{Q}\} = [\mathbf{K}]\{\delta\} \quad (4.2-14)$$

where the set of nodal forces $\{\mathbf{Q}\}$ are the forces which must be applied to the structure to maintain the deformed shape. When the structure is a free body, these nodal forces must be self-equilibrating, i.e., the total force and couple acting on the structure must vanish.

- h) The strain energy stored in the structure as a result of the elastic deformation $\{\delta\}$ is given by

$$U = \frac{1}{2} \{\delta\}^T [K] \{\delta\}. \quad (4.2-15)$$

- i) For each structural node (e.g., the i^{th} structural node) a rigid body mode shape matrix $[\bar{\phi}_i]$ describes the nodal displacement rate $\{\dot{\delta}_{iR}\}$ due to rigid body motion of the node relative to any chosen point as follows:

$$\{\dot{\delta}_{iR}\} = [\bar{\phi}_i] \{\dot{B}^i\} \quad (4.2-16)$$

where

$$\{B^i\} \equiv \begin{bmatrix} d'_{X0} \\ d'_{Z0} \\ \theta'_{Y0} \\ d'_{Y0} \\ \theta'_{X0} \\ \theta'_{Z0} \end{bmatrix}$$

and, if

$$\{\delta_i\} = \begin{bmatrix} d_{Xi} \\ d_{Yi} \\ d_{Zi} \end{bmatrix},$$

then

$$[\bar{\phi}_i] \equiv \begin{bmatrix} 1 & 0 & \bar{Z}_i & 0 & 0 & -\bar{Y}_i \\ 0 & 0 & 0 & 1 & -\bar{Z}_i & \bar{X}_i \\ 0 & 1 & -\bar{X}_i & 0 & \bar{Y}_i & 0 \end{bmatrix}$$

and $d'_{X0}, d'_{Y0}, d'_{Z0}$ are the components of position and $\theta'_{X0}, \theta'_{Y0}, \theta'_{Z0}$ are the components of rotation at the point relative to the Inertial Axis System. The velocity of a point interior to the finite element—*analogous to that of equation (2.3-16)*—is found from the displacement relation (item c) as follows:

$$\{V^a\} = [N^a] (\{\dot{\delta}^a\} + [\bar{\phi}_\delta^a] \{\dot{B}^i\}) \quad (4.2-17)$$

where

$$[\bar{\phi}_\delta^a] \equiv \begin{bmatrix} [\bar{\phi}_{i+1}^a] \\ [\bar{\phi}_{i+2}^a] \\ \vdots \\ [\bar{\phi}_{i+m}^a] \end{bmatrix}$$

wherein m is the number of nodes on the a^{th} finite element and the nodes are numbered sequentially starting with 1

- j) The mass matrix describing the inertia properties of the a^{th} finite element, equation 11.7 of refere. ex 4-3, is called herein the nodal mass matrix and is defined as

$$[m_\delta^a] \equiv \int_{V^a} [N^a]^T [\rho_A^a] [N^a] dV \quad (4.2-18)$$

where

$$[\rho_A^a] \equiv \begin{bmatrix} \rho_A^a(X,Y,Z) & & \text{zeros} \\ & \rho_A^a(X,Y,Z) & \\ \text{zeros} & & \rho_A^a(X,Y,Z) \end{bmatrix}$$

describes the mass density distribution of the element. It should be noted that the nodal mass matrix need not be a diagonal matrix.

- k) The kinetic energy of the a^{th} finite element, since $\{\dot{B}'\}$ is the velocity relative to the Inertial Axis System in item (i), is given by

$$K^a = \frac{1}{2} \int_{V^a} \{\dot{V}^a\}^T [\rho_A^a] \{\dot{V}^a\} dV \quad (4.2-19)$$

Hence, substituting equation (4.2-17), it follows that

$$\begin{aligned} K^a = & \frac{1}{2} \{\dot{B}'\}^T [\bar{\phi}_\delta^a]^T [m_\delta^a] [\bar{\phi}_\delta^a] \{\dot{B}'\} + \frac{1}{2} \{\dot{\delta}^a\}^T [m_\delta^a] \{\dot{\delta}^a\} \\ & + \frac{1}{2} \{\dot{B}'\}^T [\bar{\phi}_\delta^a]^T [m_\delta^a] \{\dot{\delta}^a\} + \frac{1}{2} \{\dot{\delta}^a\}^T [m_\delta^a] [\bar{\phi}_\delta^a] \{\dot{B}'\} \end{aligned}$$

The total kinetic energy of the structure is the sum of the element kinetic energies; hence,

$$\begin{aligned} K = & \frac{1}{2} \{\dot{B}'\}^T [\bar{\phi}_\delta]^T [m_\delta] [\bar{\phi}_\delta] \{\dot{B}'\} + \frac{1}{2} \{\dot{\delta}\}^T [m_\delta] \{\dot{\delta}\} \\ & + \frac{1}{2} \{\dot{B}'\}^T [\bar{\phi}_\delta]^T [m_\delta] \{\dot{\delta}\} + \frac{1}{2} \{\dot{\delta}\}^T [m_\delta] [\bar{\phi}_\delta] \{\dot{B}'\} \end{aligned} \quad (4.2-20)$$

where $[m_\delta]$ is the nodal mass matrix for the entire structure and for the i^{th} node

$$[m_\delta]_i \equiv \sum [m_\delta^a]_i$$

where the sum is over elements connected to the i^{th} node. Also,

$$[\bar{\phi}_\delta] \equiv \begin{bmatrix} [\bar{\phi}_1] \\ \vdots \\ [\bar{\phi}_n] \end{bmatrix} \quad (4.2-21)$$

is the rigid body mode shape matrix for the entire structure having n nodes.

- 1) The final three terms of equation (4.2-20) represent the relative kinetic energy of the aircraft, a quantity also described by equation (2.3-8). This quantity is minimized as in section 2.3.2 to determine \bar{V}_C and $\bar{\omega}$ —the velocity of the Body Axis System relative to the Inertial Axis System, figure 2.3-2. The components of \bar{V}_C and $\bar{\omega}$ are contained in the elements of $\{\dot{B}\}$; hence, letting $[\bar{\phi}_\delta]$ be expressed for rigid body motion about the center of mass, the relative kinetic energy is a minimum with respect to the elements of $\{\dot{B}\}$ if

$$[\bar{\phi}_\delta]^T [m_\delta] \{\dot{B}\} = \{0\} \quad (4.2-22)$$

This result is the finite element analogue of the exact mean reference frame constraint conditions, i.e., equations (2.3-17). Introducing the approximation of section 2.3.2.4, the mean reference frame constraint conditions, equations (2.3-18), are expressed as

$$[\bar{\phi}_\delta]^T [m_\delta] \{\delta\} = \{0\} \quad (4.2-23)$$

and the rigid body mode shape matrix is taken to be independent of time (i.e., the coordinates $\bar{X}_i, \bar{Y}_i, \bar{Z}_i$, equation (4.2-16), are constants) so that equation (4.2-22) follows from equation (4.2-23) by differentiation with respect to time.

When the mean reference frame constraint conditions are satisfied, the kinetic energy, equation (4.2-20), reduces to

$$K = \frac{1}{2} \{\dot{B}\}^T [M] \{\dot{B}\} + \frac{1}{2} \{\dot{\delta}\}^T [m_\delta] \{\dot{\delta}\} \quad (4.2-24)$$

where

$$[M] \equiv [\bar{\phi}_\delta]^T [m_\delta] [\bar{\phi}_\delta] \quad (4.2-25)$$

is the total mass-inertia matrix for the aircraft, viz.,

$$[M] = \begin{bmatrix} M & & & & & \\ & M & & & & \\ & & I_{YY} & & & \\ & & & M & & \\ & & & & I_{YX} & -I_{XZ} \\ & & & & -I_{ZX} & I_{ZZ} \end{bmatrix} \quad (4.2-26)$$

In developing equation (4.2-23) from equation (4.2-22), the rigid body mode shape matrix is treated as being independent of time. This assumption is identical with the assumptions made in obtaining equations (2.3-18) from equations (2.3-17). Here the assumption is seen to lead to moments and products of inertia which are treated as independent of time—a result which was evaluated in section 2.3.2.5 for the case when rigid body modes are evaluated in the two cases: (1) a steady reference flight condition and (2) an unsteady perturbation about the reference flight condition.

4.2.2.2 Finite element approximations and structural reference frame.—Two approximations are introduced when the finite element method is applied to the FLEXSTAB system. The first is inherent in the finite element method and stems from item (c) of section 4.2.2.1. When a structure is continuous, the displacement field which describes its deformed shape is continuous and has continuous partial derivatives with respect to spatial coordinates. When the structure is represented by finite elements, the continuous displacement field is approximated and replaced by one which, in general, will have discontinuous spatial derivatives at the boundaries of the finite elements.

The second approximation is not inherent in the finite element method but is introduced when the method is applied to FLEXSTAB. This second approximation is introduced when the operations of item (d) of section 4.2.2.1 are carried out. When the state of strain is computed from the displacement functions and when the state of stress is computed, these computations are based on the well-known approximations of the classical theory of elasticity. As noted in section 4.2.1, these approximations require that rotations of the structure (measured relative to the coordinate system used in describing the structural theory—the structural reference frame) must be very small. Motions of the structural reference frame relative to the structure, however, are arbitrary provided the relative rotations have the required degree of smallness.

The arbitrary rigid body displacement of the structural reference frame relative to the structure may be expressed as follows:

$$\vec{r}_p = \vec{r}_0 + \vec{\theta}_0 \times \vec{r} \quad (4.2-27)$$

where \vec{d}_0 is an arbitrary rigid body translation, $\vec{\theta}_0$ is a rotation having the required degree of smallness, and \vec{r} is the position of a point in the structure relative to the point of rotation. Equation (4.2-27) is expressed in terms of nodal displacement components by letting

$$\{B\} \equiv \begin{bmatrix} d_{X_0} \\ d_{Z_0} \\ \theta_{Y_0} \\ d_{Y_0} \\ \theta_{X_0} \\ \theta_{Z_0} \end{bmatrix} \quad (4.2-28)$$

where d_{X_0} , d_{Y_0} , d_{Z_0} are the components of translation and θ_{X_0} , θ_{Y_0} , θ_{Z_0} are the components of rotation of the structure relative to the structural reference frame. The rigid body nodal displacement components, equivalent to equation (4.2-27), are described by

$$\{\delta(R)\} = [\bar{\phi}_\delta]\{B\} \quad (4.2-29)$$

where matrix $[\bar{\phi}_\delta]$ is the rigid body mode shape matrix for the structure defined by equation (4.2-21).

The significance of the rigid body displacement, equation (4.2-29), can now be described formally by considering two sets of nodal displacement components, $\{\delta\}$ and $\{\delta'\}$, related as follows:

$$\{\delta\} = [\bar{\phi}_\delta]\{B\} + \{\delta'\} \quad (4.2-30)$$

The quantities $\{\delta\}$ and $\{\delta'\}$ are the result of two different deformations differing by the rigid body displacement described by equation (4.2-29). The rigid body displacement, however, is taken to be that of the undeformed reference shape of the aircraft relative to which the components of $\{\delta\}$ and $\{\delta'\}$ are measured, figure 4.2-1. This deformation is illustrated in figure 4.2-1 assuming that the elements of $\{\delta\}$ and $\{\delta'\}$ contain only translation components of displacement at the nodes. The two sets of nodal displacements are, therefore, given by

$$\{\delta\} = \{x'\} - \{x\}$$

and

$$\{\delta'\} = \{x'\} - \{x_0\}$$

where $\{x'\}$ contains the coordinates of the nodes in the deformed structure while $\{X\}$ and $\{X'\}$ are the coordinates of the nodes in the two undeformed shapes of the structure, C and C', differing only by the rigid body displacement. Under these assumptions, regarding the components of $\{\delta\}$ and $\{\delta'\}$ and the interpretation of equation (4.2-29), equation (4.3-29) becomes

$$\{X'\} - \{X\} = [\bar{\phi}_\xi] \{B\}. \quad (4.2-31)$$

Equation (4.2-30) is generated by subtracting equation (4.2-31) from the identity

$$\{x'\} \equiv \{x'\}$$

This operation demonstrates that equation (4.2-30) can be interpreted as relating two sets of nodal displacement components differing by rigid body displacement of the undeformed shape of the structure relative to which $\{\delta\}$ and $\{\delta'\}$ are measured.

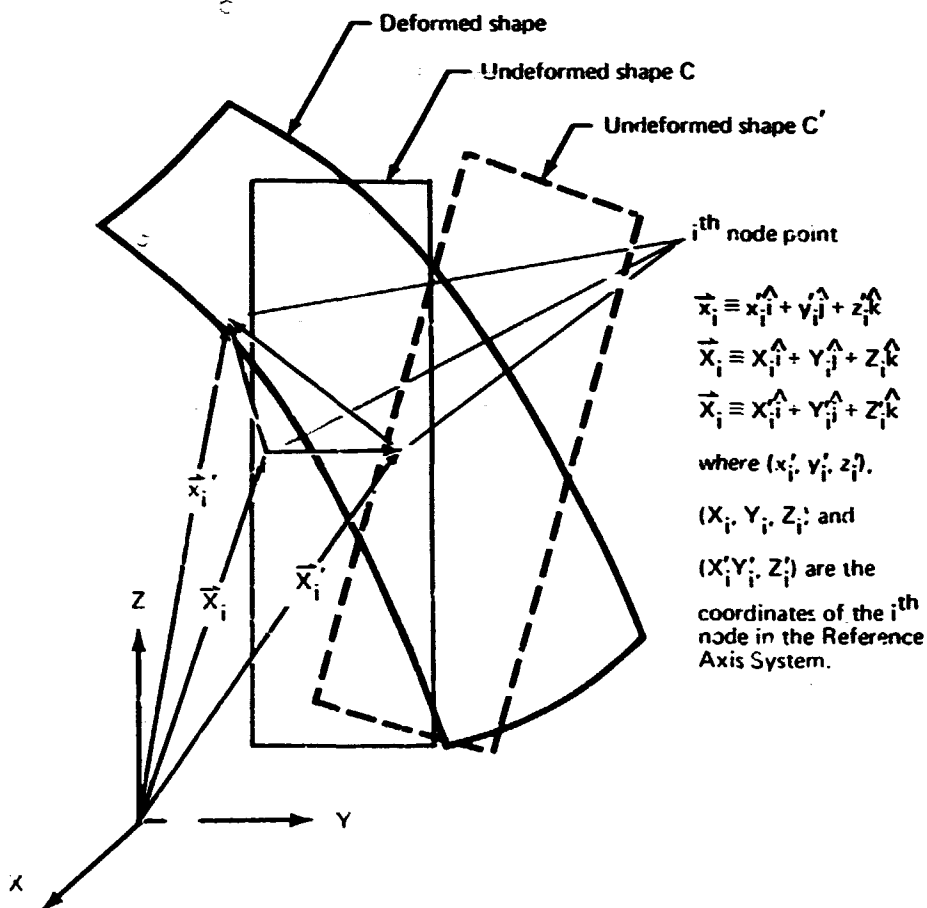


FIGURE 4.2-1. — RIGID BODY DISPLACEMENT OF THE UNDEFORMED REFERENCE SHAPE OF A STRUCTURE

The small rotation approximation is shown to be contained in equation (4.2-30) by considering the orthogonal coordinate transformation involving infinitesimal rotations, section 4-7 of reference 4-1, viz.,

$$\{X'\} = ([\epsilon] + [I]) (\{X\} + \{d_0\})$$

where $\{X\}$ and $\{X'\}$ contain the coordinates of one set of node points but in two different axis systems (viz., X,Y,Z and X',Y',Z') and $\{d_0\}$, containing three constants for each node point, represents translation of the origin of the X',Y',Z' system relative to the X,Y,Z system. Letting $[\epsilon]$ and $\{d_0\}$ be such that the coordinates $\{X'\}$ in the X',Y',Z' system are identical with the coordinates $\{X\}$ in the X,Y,Z system, the X',Y',Z' system is made to be fixed to the undeformed shape C' . The result is an expression that can be made identical with equation (4.2-31). Equations (4.2-31) and (4.2-30), therefore, contain the same order of approximation as the coordinate transformation; namely, the angles of rotation are infinitesimals.

An important observation to be made in the above is the following: In equation (4.2-31) both $\{X\}$ and $\{X'\}$ are expanded on the X,Y,Z system; while, when equation (4.2-31) is constructed using the coordinate transformation, $\{X'\}$ is in the X',Y',Z' system fixed to the undeformed shape C' while $\{X\}$ is in the X,Y,Z system fixed to the undeformed shape C . That this difference in coordinate systems produces no change in the expression for equation (4.2-29) follows from the analysis of section 4-7 of reference 4-1. This analysis shows that if the coordinate transformation of section 4-7 of reference 4-1 is applied to either equation (4.2-29) or equation (4.2-30), the forms of these equations are unchanged. The elements of $\{\delta'\}$ and $\{\delta\}$, therefore, can be regarded as expanded on either coordinate axis system with no change in the form of equation (4.2-30). This equivalence is used in the following where the X,Y,Z system is taken to be a mean reference frame while the X',Y',Z' system is taken to be a structural reference frame. The structural reference frame is used as a coordinate system in describing the elastic properties of a structure.

Throughout the remainder of section 4, the Reference Axis System is used interchangeably as a mean reference frame and as a structural reference frame but only when using it as a basis for expanding the components of nodal forces and nodal displacements. This interchangeability is valid because of the observation in the preceding paragraph. A separate coordinate system, identified as a structural reference frame, is not required and is never introduced. Nodal components of force and displacement will be expanded using the Reference Axis System as a basis; at times the Reference Axis System will be a mean reference frame, while at other times it will be a structural reference frame.

In section 4.2.2.5, the elements of $\{B\}$ are expressed as a linear combination of the elements of $\{\delta'\}$. Equation (4.2-30) is then expressed as

$$\{\delta\} = [T]\{\delta'\}$$

where the transformation involves orthogonal transformations introducing arbitrary translations but only infinitesimal rotations. Using the concept of virtual work, the applied nodal forces are found to be transformed as

$$\{Q'\} = [T]^T \{Q\} \quad (4.2-32)$$

The two preceding equations may appear to be only coordinate transformations; but, from the above, it is clear that $\{\delta'\}$ and $\{\delta\}$ are the results of two physically different displacements. In the following $\{Q'\}$ and $\{Q\}$ will be shown to represent two physically different sets of nodal forces. This physical difference depends on the particular linear relationship chosen to relate the elements of $\{B\}$ to the elements of $\{\delta'\}$. There are any number of choices for this linear relationship—three of them being shown on pages 4-6 of reference 2-4.

If equation (4.2-30) is substituted into the composite stiffness relation, equation (4.2-14), it follows that

$$\begin{aligned}\{Q\} &= [K]([\bar{\phi}_\delta]\{B\} + \{\delta'\}) \\ &= [K]\{\delta'\}\end{aligned}\quad (4.2-33)$$

The product of the stiffness matrix onto the rigid body mode shape matrix vanishes because a rigid body displacement of a structure, when it is a free body, requires no change in the applied nodal forces, i.e.,

$$\{C\} = [K][\bar{\phi}_\delta]\{B\}$$

Also, because the stiffness matrix is symmetric, the transpose of the above equation leads to the following expression:

$$\{B\}^T[\bar{\phi}_\delta]^T[K] = \{0\}^T \quad (4.2-34)$$

Introducing the transformation of the nodal forces, equation (4.2-32), into equation (4.2-33), it follows that:

$$\{Q'\} = [T]^T[K][T]\{\delta'\} \quad (4.2-35)$$

This equation, because the product $[K][\bar{\phi}_\delta]$ vanishes, immediately reduces to

$$\{Q'\} = [K]\{\delta'\}$$

This result shows that the composite stiffness matrix is invariant under transformations of the type under consideration. As a result, the elements of the matrix $\{B\}$ may be arbitrarily chosen provided the components of rotation θ_{X_0} , θ_{Y_0} , θ_{Z_0} , equation (4.2-23), have the required degree of smallness described in section 4.2.1. The elements of $\{B\}$ are determined in the following using the concept developed in section 2.3.2.

4.2.2.3 Hamilton's principle in finite element form. Each of the quantities appearing in Hamilton's principle, equation (4.2-3), including the constraint conditions, are derived in the following in terms of the finite element concepts introduced in section 4.2.2.1.

Consider first the kinetic energy, K , with the velocity expressed for an observer in the body fixed axis systems, equation (2.3-16), i.e.,

$$K = \frac{1}{2} \int_V \left(\frac{d\vec{r}_0'}{dt} + \vec{\omega} \times \vec{r} + \frac{\delta \vec{d}}{\delta t} \right) \cdot \left(\frac{d\vec{r}_0'}{dt} + \vec{\omega} \times \vec{r} + \frac{\delta \vec{d}}{\delta t} \right) \rho_A dV. \quad (4.2-36)$$

When $d\vec{r}_0'/dt$ and $\vec{\omega}$ are taken so that they minimize the relative kinetic energy, this expression becomes

$$K = \frac{1}{2} \int_V \left(\frac{d\vec{r}_0'}{dt} + \vec{\omega} \times \vec{r} \right) \cdot \left(\frac{d\vec{r}_0'}{dt} + \vec{\omega} \times \vec{r} \right) \rho_A dV + \frac{1}{2} \int_V \frac{\delta \vec{d}}{\delta t} \cdot \frac{\delta \vec{d}}{\delta t} \rho_A dV. \quad (4.2-37)$$

The final term of this expression may be replaced by its finite element analogue, item (k) of section 4.2.2.1, to obtain the following form for the kinetic energy:

$$K = \frac{1}{2} \int_V \left(\frac{d\vec{r}_0'}{dt} + \vec{\omega} \times \vec{r} \right) \cdot \left(\frac{d\vec{r}_0'}{dt} + \vec{\omega} \times \vec{r} \right) \rho_A dV + \frac{1}{2} \{\dot{d}\}^T [m_\delta] \{\dot{d}\} \quad (4.2-38)$$

Consider, now, the virtual work of the applied forces—equation (4.2-2). This quantity is expressed in terms of finite elements using item (e) of section 4.2.2.1. The virtual displacement of a point in the structure is given by equation (4.2-4), i.e.,

$$\delta \vec{r} = \delta \vec{r}_0' + \delta \vec{\Omega} \times \vec{r} + \delta \vec{d} \quad (4.2-39)$$

where

$$\delta \vec{\Omega} \equiv \int \delta \vec{\omega} dt$$

is a virtual rotation. The virtual work of the applied forces is now expressed as follows using equations (4.2-2) and (4.2-39):

$$\delta W = (\vec{F}_C - M\vec{g}) \cdot \delta \vec{r}_0' + \vec{M}_C \cdot \delta \vec{\Omega} + \int_S \vec{P} \cdot \delta \vec{d} ds \quad (4.2-40)$$

where

$$\vec{F}_C \equiv \int_S \vec{P} ds$$

is a resultant force at the center of mass and

$$\vec{M}_c \equiv \int_S \vec{r} \times \vec{P} dS$$

is a resultant couple at the center of mass. Introducing the displacement relations, equation (4.2-5), the virtual work is obtained in terms of applied nodal forces, equation (4.2-13), as follows:

$$\delta W = (\vec{F}_c - M\vec{g}) \cdot \delta \vec{r}_0 + \vec{M}_c \cdot \delta \vec{\Omega} + \{Q^S\}^T \delta \{\delta\} \quad (4.2-41)$$

where the elements of $\{Q^S\}$ are the nodal forces due to surface tractions, viz.,

$$\{Q_i^S\} \equiv \sum_a \int_{S^a} [N_i^a]^T \{P^a\} dS$$

with the sum over all elements having nodes at the i^{th} structural node.

Hamilton's principle in the form given by equation (4.2-3) is now expressed in terms of the finite element method as follows:

$$\begin{aligned} & \delta \int_{t_1}^{t_2} \frac{1}{2} \left[\int_V \left(\frac{d\vec{r}_0}{dt} + \vec{\omega} \times \vec{r} \right) \cdot \left(\frac{d\vec{r}_0}{dt} + \vec{\omega} \times \vec{r} \right) \rho_A dV + \{\delta\}^T [m_\delta] \{\delta\} - \right. \\ & \quad \left. - \{\delta\}^T [K] \{\delta\} \right] dt + \int_{t_1}^{t_2} [(\vec{F}_c - M\vec{g}) \cdot \delta \vec{r}_0 + \vec{M}_c \cdot \delta \vec{\Omega} + \\ & \quad + \{Q^S\}^T \delta \{\delta\}] dt + \int_{t_1}^{t_2} \{\lambda\}^T [\Phi_\delta]^T [m_\delta] \delta \{\delta\} dt = 0 \end{aligned}$$

where $\{\lambda\}$ is a matrix of six Lagrange multipliers replacing the vectors $\vec{\lambda}_1$ and $\vec{\lambda}_2$ in equation (4.2-3) and multiplying the constraint conditions in the finite element form given by equation (4.2-23).

4.2.2.4 Derivation of the equations of motion. Carrying out the variation of the kinetic and strain energies and integrating by parts, equation (4.2-42) leads to the following variational equation:

$$\begin{aligned}
\int_{t_1}^{t_2} \left\{ \left[M \frac{d^2 \vec{r}_0}{dt^2} + M \vec{g} - \vec{F}_c \right] \cdot \delta \vec{r}_0 - \int_V (\vec{\omega} \times \vec{r}) \cdot \delta (\vec{\omega} \times \vec{r}) \rho_A dV \right. \\
- \vec{M}_c \cdot \delta \vec{\Omega} + [\{\ddot{\delta}\}]^T [m_\delta] + \{\delta\}^T [K] - \{Q^S\}^T \{\delta\} - \\
\left. - \{\lambda\}^T [\bar{\phi}_\delta]^T [m_\delta] \delta \{\delta\} \right\} dt = 0
\end{aligned} \quad (4.2-43)$$

The Lagrange multipliers may be so chosen that equation (4.2-43) can be expressed as a set of equations, viz.,

$$M \frac{d^2 \vec{r}_0}{dt^2} + M \vec{g} = \vec{F}_c, \quad (4.2-44)$$

$$\int_{t_1}^{t_2} \left[\int_V (\vec{\omega} \times \vec{r}) \cdot \delta (\vec{\omega} \times \vec{r}) \rho_A dV + \vec{M}_c \cdot \delta \vec{\Omega} \right] dt = 0, \quad (4.2-45)$$

and

$$[m_\delta] \{\ddot{\delta}\} + [K] \{\delta\} = \{Q^S\} + [m_\delta] [\bar{\phi}_\delta] \{\lambda\} \quad (4.2-46)$$

Introducing the kinematic approximation of section 2.3.2.4, i.e., ignoring variations in the moments and products of inertia, the variational quantity

$$\int_{t_1}^{t_2} \int_V (\vec{\omega} \times \vec{r}) \cdot (\vec{\omega} \times \delta \vec{r}) \rho_A dV dt$$

is ignored in equation (4.2-45). As a result the first term of this equation may be integrated by parts with respect to time to obtain

$$\begin{aligned}
\int_{t_1}^{t_2} (\vec{\omega} \times \vec{r}) \cdot \delta (\vec{\omega} \times \vec{r}) dt &= [\vec{r} \times (\vec{\omega} \times \vec{r})] \cdot \delta \vec{\Omega} \Big|_{t_1}^{t_2} \\
&- \int_{t_1}^{t_2} \left[\vec{r} \times \frac{d}{dt} (\vec{\omega} \times \vec{r}) \right] \cdot \delta \vec{\Omega} dt
\end{aligned}$$

The variation $\delta\vec{\Omega}$ vanishes at the instants of time, t_1 and t_2 ; hence, this result is used to write equation (4.2-44) as follows:

$$\int_{t_1}^{t_2} \left[\int_V \vec{r} \times \frac{d}{dt} (\vec{\omega} \times \vec{r}) \rho_A dV - \vec{M}_C \right] \cdot \delta \vec{r} dt = 0$$

Now, because the components of $\delta\vec{\Omega}$ can now be chosen arbitrarily, it follows that

$$\int_V \vec{r} \times \frac{d}{dt} (\vec{\omega} \times \vec{r}) \rho_A dV = \vec{M}_C \quad (4.2-47)$$

The kinematic approximation of section 2.3.2.4 is seen to eliminate the mechanical coupling between the elastic deformation and the rotational motion of the aircraft. This conclusion follows from the fact that equation (4.2-47) is simply the vector form of Euler's equations of motion for a rotating rigid body, equations (5-34) of reference 4-1.

4.2.2.5 Evaluation of the Lagrange multipliers. -- As pointed out in section 2-4 of reference 4-1, the Lagrange multipliers have a physical significance. The term containing the Lagrange multipliers in equation (4.2-46) can be identified with forces of constraint. If equation (4.2-46) is premultiplied by the transpose of the rigid body mode shape matrix, equation (4.2-21), the terms on the left vanish by virtue of equations (4.2-23) and (4.2-34) yielding

$$[\bar{\phi}_\delta]^T \{Q^S\} = - [M] \{\lambda\} \quad (4.2-48)$$

where $[M]$ is the total mass-inertia matrix of equation (4.2-26) and the operation on the left yields the resultants of the applied surface forces at the center of mass of the aircraft, i.e.,

$$\{F_C\} = [\bar{\phi}_\delta]^T \{Q^S\} \quad (4.2-49)$$

where, for the choice of $[\phi_\delta]$ shown in equation (4.2-16),

$$\{F_C\} = \begin{bmatrix} F_X \\ F_Z \\ M_Y \\ F_Y \\ M_X \\ M_Z \end{bmatrix}$$

The Lagrange multipliers are found from equation (4.2-48) as

$$\{\lambda\} = - [M]^{-1} \{F_c\} \quad (4.2-50)$$

Equation (4.2-50) can be interpreted as showing that the Lagrange multipliers represent components of rigid body acceleration relative to an inertial reference frame. If the inertial reference frame is taken to be the Inertial Axis System, then

$$\{\lambda\} = - \{\ddot{B}'\} \quad (4.2-51)$$

where $\{\ddot{B}'\}$ is the matrix defined by equation (4.2-16). This is a correct interpretation, however, only at the instant of time when the Inertial and Body Axis Systems are coincident. The Lagrange multipliers, therefore, must be interpreted as representing components of rigid body acceleration relative to a portable axis system of the type introduced by section 2.3.2; specifically, the inertial reference frame is taken to be a nonaccelerating and non-rotating axis system coincident with the Body Axis System at any instant of time under consideration. This interpretation of the Lagrange multipliers leads to equation (4.2-48) being viewed as rigid body equations of motion based on a kinematical description consistent with that of section 2.3.2.

Combining equations (4.2-49) and (4.2-50) with equation (4.2-46), the structural deformation of the aircraft is found to be governed by the following expression:

$$[K]\{\delta\} = [P]\{Q^S\} - [m_\delta]\{\ddot{\delta}\} \quad (4.2-52a)$$

where

$$[P] \equiv [[I] - [m_\delta][\bar{\phi}_\delta][M]^{-1}[\bar{\phi}_\delta]^T] \quad (4.2-53)$$

The matrix $[P]$, a singular matrix, is seen to incorporate the inertial forces (including the gravity force). This matrix incorporates into equation (4.2-52) the forces of constraint, i.e., the final term of equation (4.2-46). This term is now written as

$$\{0^I\} = - [m_\delta][\bar{\phi}_\delta][M]^{-1}[\bar{\phi}_\delta]^T\{Q^S\}$$

and represents forces usually interpreted as "inertial relief" forces. Also, equation (4.2-52a) can be written as

$$[K]\{\delta\} = [P](\{Q^S\} - [m_\delta]\{\ddot{\delta}\}) \quad (4.2-52b)$$

because

$$[P][m_\delta]\{\ddot{\delta}\} = [m_\delta]\{\ddot{\delta}\}.$$

The comments following equation (4.2-32) in section 4.2.2.2 are borne out by the above results. The two sets of nodal force components $\{Q\}$ and $\{Q^S\}$ are related in the above as in equation (4.2-32) with the transformation matrix $[T]^T$ replaced by the transformation matrix defined by equation (4.2-53), i.e.,

$$\{Q\} = [P]\{Q^S\}.$$

Also, there is a physical difference between the forces $\{Q^S\}$ and the forces $\{Q\}$. They differ by the inertial relief forces, i.e.,

$$\{Q\} - \{Q^S\} = -[m_\delta][\bar{\phi}_\delta][M]^{-1}[\bar{\Gamma}_\delta]^T\{Q^S\} - [m_\delta]\{\ddot{\delta}\}$$

where the first term on the right describes the inertial nodal forces arising from rigid body acceleration. This physical difference is the result of having chosen the mean reference frame constraint conditions, equation (4.2-23), as the constraint conditions to be used in expressing Hamilton's principle in the form shown by equation (4.2-42).

Referring, again, to the comments appearing in section 4.2.2.2, the elements of the matrix $\{B\}$, appearing in the nodal displacement component relation given by equation (4.2-30), are linearly related by the constraint conditions to the nodal displacement components $\{\delta'\}$. This linear relationship is found by premultiplying the matrix $[\bar{\phi}_\delta]^T[m_\delta]$ onto equation (4.2-30) and by employing the mean reference frame constraint conditions, equation (4.2-23). The result is given by

$$\{B\} = -[M]^{-1}[\bar{\phi}_\delta]^T[m_\delta]\{\delta'\};$$

and, on substituting this result into equation (4.2-30), the two sets of nodal displacement components are related as

$$\{\delta\} = [P]^T\{\delta'\}.$$

This result ensures that the undeformed shape C, shown by figure 4.2-1, viz., the reference shape relative to which the displacement components of $\{\delta\}$ are measured, is a mean frame of reference. The undeformed shape C', viz., the reference shape relative to which the displacement components of $\{\delta'\}$ are measured, is, as yet, undetermined outside of the requirement that C and C' differ at most by an arbitrary, but infinitesimally small, rotation.

In using Hamilton's principle to derive the equations of motion in the form given by equations (4.2-44), (4.2-47), and (4.2-52), the form of the derived equations of motion is seen to depend on the choice of the constraint conditions. The derivation makes it clear that the form of the equations of motion is not arbitrary once the conditions are chosen for determining the elements of $\{B\}$ in equation (4.2-30). If, for example, the elements of $\{B\}$ are set to zero and the undeformed shape C' is constrained to selected nodes of the structure (the Attached Axes of section 2.1.4 of reference 2-4), then the form of the equations of motion will be similar to those above but the physical significance of the matrices, particularly that of the motion variables, will be changed.

The only arbitrariness remaining in the formulation, after having chosen the mean reference frame constraint conditions to be the conditions for determining the elements of $\{B\}$, is the undeformed configuration C' , figure 4.2-1, relative to which the nodal displacement components $\{\delta'\}$ are measured. In the FLEXSTAB system, the undeformed shape C' is determined by choosing six nodal degrees of freedom, represented as the elements of $\{\delta_R\}$, which, if set to zero, constrain the structure from rigid body motions. The undeformed shape C' is fixed relative to these nodal degrees of freedom; thus, because C' is arbitrary, the particular choice of the six constraining nodal degrees of freedom $\{\delta_R\}$ is arbitrary. These operations are described in section 4.2.3.1.

4.2.3 Equations of Motion for the Steady Reference Flight Condition

Under the assumption of steady motion, all time dependence apparent to an observer in a body-fixed axis system vanishes. The equations of motion (equations (4.2-44), (4.2-47) and 4.2-52)) then reduce to the following:

$$M\vec{\omega}_1 \times \vec{V}_{C_1} + M\vec{g}_1 = \vec{F}_{C_1}, \quad (4.2-54)$$

$$\int_{V_1} \vec{r}_1 \times [\vec{\omega}_1 \times (\vec{\omega}_1 \times \vec{r}_1)] \rho_A dV = \vec{M}_{C_1}, \quad (4.2-55)$$

and

$$[K]\{\delta\}_1 = [P]_1\{Q^S\}_1 \quad (4.2-56)$$

or

$$[K]\{\delta\}_1 = \{Q\}_1$$

since

$$[P]_1\{Q^S\}_1 = \{Q\}_1$$

where, as pointed out by the discussion concerning equation (4.2-53), the matrix $[P]_1$ introduces the effects of inertia. Equations (4.2-54) and (4.2-55) govern the steady motion of the aircraft moving as a rigid body, while equation (4.2-56) governs the steady elastic deformation of the aircraft. Equations (4.2-54) and (4.2-55) are expressed in the Body Axis System, figure 2.2-1; while the structural equations, equation (4.2-56), are expressed in the Reference Axis System, figure 2.2-2. The components of a force and couple, \vec{F}_{C_1} and \vec{M}_{C_1} , are computed from forces at the structural nodes by the operation shown by equation (4.2-49):

$$\{\vec{F}_{C_1}\}_1 = [\vec{\phi}_\delta]_1^T \{Q^S\}_1 \quad (4.2-57)$$

where $[\bar{\phi}_\delta]_1$ is the rigid body mode shape matrix evaluated for the reference flight condition and

$$\{F_C\}_1 \equiv \begin{bmatrix} F_X \\ F_Z \\ M_Y \\ F_Y \\ M_X \\ M_Z \end{bmatrix}_1$$

are the components of the force and moments acting at the center of mass—the right hand members of equations (4.2-54) and (4.2-55).

4.2.3.1 Structural equations in terms of flexibility.—In the analysis to follow, the deformation of the structure $\{\delta\}$ must be expressed as an explicit function of the applied loads. The structural equations, equation (4.2-56), wherein the deformed shape $\{\delta\}$ is an unknown quantity, therefore, are solved in the following to yield the deformed shape in terms of the applied loads and the flexibility matrix.

The structural equations are solved by assuming that the stiffness matrix $[K]$ is the result of having performed a reduction on another stiffness matrix removing six rows and columns. The stiffness matrix $[K]$, therefore, is defined as

$$[K] \equiv \left[[K_{\delta\delta}] - [K_{\delta R}][K_{RR}]^{-1}[K_{R\delta}] \right] \quad (4.2-58)$$

where the matrices appearing on the right are partitions of the stiffness matrix appearing in the following stiffness relation:

$$\begin{bmatrix} \{Q\} \\ \{Q_R\} \end{bmatrix} = \begin{bmatrix} [K_{\delta\delta}] & [K_{\delta R}] \\ [K_{R\delta}] & [K_{RR}] \end{bmatrix} \begin{bmatrix} \{\delta\} \\ \{\delta_R\} \end{bmatrix} \quad (4.2-59)$$

The elements of the nodal displacement matrix $\{\delta_R\}$ are six in number and represent six degrees of freedom which, if constrained, constrain the structure against all rigid body motion except that which gives rise to structural strain. The nodal forces $\{Q_R\}$ are the forces at the constrained nodes, and these forces vanish if the structure is a free body. In the case of an aircraft in flight—a free body so that $\{Q\}$ equals $[P]\{Q^S\}$ —equation (4.2-59) is reduced to equation (4.2-56) with the stiffness matrix given by equation (4.2-58).

The stiffness matrix $[K_{\delta\delta}]$ is nonsingular and may be inverted to obtain the flexibility of the constrained structure as follows:

$$\{\delta'\} = [C]\{Q\} \quad (4.2-60)$$

where

$$[C] \equiv [K_{\delta\delta}]^{-1}$$

and $\{\delta'\}$ are the nodal displacement components measured relative to a structural reference frame fixed to the structural constraints. Introducing the coordinate transformation given by equation (4.2-30), equation (4.2-60) is expressed as

$$\{\delta\} - [\bar{\Phi}_\delta]\{B\} = [C]\{Q\} \quad (4.2-61)$$

where the elements of $\{B\}$ may be arbitrarily specified provided the requirements of section 4.2.2.2 are satisfied. Using the approximate form of the mean reference frame constraint conditions, equation (4.2-23), i.e.,

$$[\bar{\Phi}_\delta]^T [m_\delta] \{\delta\} = \{0\},$$

the elements of $\{B\}$ are determined, as in section 4.2.2.5, using equations (4.2-23) and (4.2-25), to find

$$\{B\} = - [M]^{-1} [\bar{\Phi}_\delta]^T [m_\delta] [C] \{Q\}. \quad (4.2-62)$$

Substituting this result into equation (4.2-61) leads to

$$\{\delta\} = [P]^T [C] \{Q\} \quad (4.2-63)$$

where the transformation matrix $[P]$ is that given by equation (4.2-53).

4.2.2.2 Virtual relief.—When the operations leading to equation (4.2-63) are applied to the structural equations for an aircraft in flight, i.e., equation (4.2-56), they are found to yield the following:

$$\{\delta\}_i = [\tilde{C}]_i \{Q^S\}_i \quad (4.2-64)$$

where

$$[\tilde{C}]_i = [P]_i^T [C] [P]_i.$$

The matrix $[\tilde{C}]_1$ is termed the "free-body flexibility" matrix and, like the stiffness matrix $[K]$ for the structure as a free body, is singular. The post multiply by $[P]_1$ introduces the inertial forces. As previously noted, this is termed inertial relief.

4.2.4 Equations of Motion for the Unsteady Perturbation Flight Condition

Equations (4.2-44), (4.2-47), and (4.2-52) will now be specialized for the case of unsteady perturbation motion relative to the steady reference motion of section 4.2.3.

Letting

$$\frac{d\vec{r}'_0}{dt} = \vec{v}_{c1} + \vec{v}_{cp}, \quad (4.2-65)$$

$$\vec{\omega} = \vec{\omega}_1 + \vec{\omega}_p,$$

and

$$\{\delta\} = \{\delta\}_1 + \{\delta\}_p,$$

leads to the following perturbation equations of motion:

$$M\left(\frac{\delta\vec{v}_{cp}}{\delta t} + \vec{\omega}_p \times \vec{v}_{c1} + \vec{\omega}_1 \times \vec{v}_{cp} + \vec{\omega}_p \times \vec{v}_{cp} + \vec{g}_p\right) = \vec{F}_{cp}, \quad (4.2-66)$$

$$\int_V \vec{r}_1 \times \left[\frac{\delta\vec{\omega}_p}{\delta t} \times \vec{r}_1 + \vec{\omega}_1 \times (\vec{\omega}_p \times \vec{r}_1) + \vec{\omega}_p \times (\vec{\omega}_1 \times \vec{r}_1) + \right. \\ \left. + \vec{\omega}_p \times (\vec{\omega}_p \times \vec{r}_1) \right] \rho_A dV = \vec{M}_{cp} \quad (4.2-67)$$

and

$$[m_s][\ddot{\delta}]_p + [K]\{\delta\}_p = [F]_1\{Q^S\}_p. \quad (4.2-68)$$

Equations (4.2-66) and (4.2-67) are the perturbation equations of motion for the aircraft moving as a rigid body while equation (4.2-68) governs the unsteady perturbation motion of the structure.

4.2.4.1 Free vibration mode shapes In the dynamic analyses performed by the FLEXSTAB system the nodal displacements $\{\delta\}$ are transformed as follows:

$$\{\delta\} = [\phi_s]\{u\} \quad (4.2-69)$$

where the columns of the transformation matrix $[\phi_\delta]$ are the free vibration mode shapes for the structure and the degrees of freedom $\{u\}$ are the amplitudes of the mode shape deflections. The free vibration mode shapes are solutions to the eigenvalue problem posed by the structural equations of motion, equation (4.2-68), when the applied nodal forces $\{Q^S\}_p$ are set to zero and when the structural motion is assumed to be harmonic, i.e.,

$$([K] - \omega^2[m_\delta])\{\delta_o\} = 0 \quad (4.2-70)$$

where ω is the frequency of the harmonic motion, equation (11.11) of reference 4-3. The transformation matrix, equation (4.2-69), therefore, is given by

$$[\phi_\delta] = [\{\delta_o\}_1, \{\delta_o\}_2, \dots] \quad (4.2-71)$$

where $\{\delta_o\}_j$ is the j^{th} eigenvector (or free vibration mode shape) having the natural frequency ω_j .

The free vibration mode shapes are found to have the following properties:

$$\begin{aligned} \{\delta_o\}_r^T [m_\delta] \{\delta_o\}_s &= m_r \quad \text{when } r=s \\ &= 0 \quad \text{when } r \neq s \end{aligned} \quad (4.2-72)$$

$$\{\delta_o\}_r^T [m_\delta] [\bar{\phi}_\delta] = 0 \quad \text{for all } r \quad (4.2-73)$$

$$\begin{aligned} \{\delta_o\}_r^T [K] \{\delta_o\}_s &= K_j \quad \text{when } r=s=j \\ &= 0 \quad \text{when } r \neq s \end{aligned} \quad (4.2-74)$$

$$\{\delta_o\}_r^T [K] [\bar{\phi}_\delta] = 0 \quad \text{for all } r \quad (4.2-75)$$

where equations (4.2-73) and (4.2-75) follow from equations (4.2-23) and (4.2-34). When the transformation, equation (4.2-69), is substituted into the structural equations of motion, equation (4.2-68), and the result is multiplied by the transpose of the mode shapes, the above properties lead to the following:

$$\begin{aligned} [m] \{\ddot{u}\}_p + [K] \{u\}_p &= [\phi_\delta]^T [F]_1 \{Q^S\}_p \\ &= [\phi_\delta]^T [\{Q^S\}]_p \end{aligned} \quad (4.2-76)$$

Equation (4.2-76) governs the structural motion described in terms of the generalized coordinates $\{u\}_p$; and, when the motion is transformed to the coordinates $\{\delta\}_p$ by equation (4.2-69), the motions represented by equation (4.2-76) are identical to those represented by equation (4.2-68)—nothing is lost by the transformation of coordinates introduced by equation (4.2-69) provided $[\phi_\delta]$ contains the complete set of modes.

4.2.4.2 Structural equations of motion in terms of flexibility.—When the structural equations of motion as given by equation (4.2-68) are multiplied by the flexibility matrix $[C]$, equation (4.2-60), these equations become as follows:

$$\{\delta\}_p = [C][P]_1 (\{Q^S\}_p - [m_\delta] \{\ddot{\delta}\}_p). \quad (4.2-77)$$

Introducing the coordinate transformation, equation (4.2-30), determining the components of $\{B\}$ using the approximate mean axis system constraint conditions, equation (4.2-23), leads to structural perturbation equations of motion expressed in the following form:

$$\{\delta\}_p = [\tilde{C}]_1 (\{Q^S\}_p - [m_\delta] \{\ddot{\delta}\}_p) \quad (4.2-78)$$

where the flexibility matrix, $[\tilde{C}]_1$, is the free-body flexibility matrix appearing in equation (4.2-64).

4.2.4.3 Residual flexibility formulation.—If the structural equations of motion given by equation (4.2-76) were used in the FLEXSTAB system analysis without modification, then little or no advantage would accrue from having introduced the transformation to free-vibration modal coordinates. The number of elements contained in $\{u\}$ (i.e., the number of dynamic structural degrees of freedom) is only six less than the number of elements contained in $\{\delta\}$; having transformed the problem to the generalized coordinates $\{u\}$, the only simplification achieved is the elimination of six rigid-body degrees of freedom. The primary reason for expressing the problem in terms of free-vibration modal coordinates is to allow an analyst to compare the orders of magnitude of the terms in the equations of motion and simplify them by eliminating negligibly small terms.

FLEXSTAB analysis is aimed primarily at evaluating the stability characteristics of large aircraft. The motions under evaluation, therefore, are generally low frequency motions. If a large aircraft is subjected to high frequency, unsteady aerodynamic or propulsion system loads, the rigid-body motion is virtually unaffected. The dominant response of an aircraft to high frequency unsteady loads occurs in the structural free-vibration modal degrees of freedom having natural frequencies nearly equal to those of the high frequency applied loads. Since the FLEXSTAB analysis is aimed at evaluating only low frequency response, high frequency unsteady loads are completely eliminated from the analytical representation. Because high frequency motions are eliminated, equations (4.2-76) are divided into two parts as follows:

$$[m_1]\{\ddot{u}_1\}_p + [K_1]\{u_1\}_p = [\phi_{\delta_1}]^T\{Q^S\}_p \quad (4.2-79)$$

and

$$[m_2]\{\ddot{u}_2\}_p + [K_2]\{u_2\}_p = [\phi_{\delta_2}]^T\{Q^S\}_p$$

where $\{u_1\}$ are the modal degrees of freedom whose natural frequencies are small and $\{u_2\}$ are the modal degrees of freedom whose natural frequencies are large.

The dynamic (or modal inertia) terms $\{\ddot{u}_2\}$ may be neglected as negligibly small: even so, the modal degrees of freedom $\{u_2\}$ may have pronounced effects on the characteristics of low frequency rigid-body and structural motions. The second of equations (4.2-79), neglecting $\{\ddot{u}_2\}$, describes the following quasi-static elastic deflections:

$$\{\delta_2\}_p = [\phi_{\delta_2}][K_2]^{-1}[\phi_{\delta_2}]^T\{Q^S\}_p. \quad (4.2-80)$$

The deflections $\{\delta_2\}_p$ are a consequence of the applied loads $\{Q^S\}_p$ and the flexibility of the structure associated with the high frequency modes, viz.,

$$[\tilde{C}_R] \equiv [\phi_{\delta_2}][K_2]^{-1}[\phi_{\delta_2}]^T. \quad (4.2-81)$$

The influence of the deflections $\{\delta_2\}$ on low frequency aerodynamic forces is readily illustrated by the aeroelastic characteristics of a typical aircraft stabilizing surface, e.g., a conventional horizontal tail surface, figure 4.2-2. The section center of mass of such a surface often lies very close to the elastic axis. The inertial couple producing torsion about the elastic axis is small for these surfaces, and the twisting motion of the surface is contained in a free-vibration mode shape having a large natural frequency even though the torsional stiffness of the surface may be only moderate. Low frequency motions such as plunge or pitch of an aircraft or motions in the low frequency free-vibration modes cause unsteady angle of attack changes at the horizontal tail surface and, therefore, low frequency unsteady pressure distributions which may produce large torsional couples about the elastic axis. Since the inertial couple arising from a rotational acceleration of the surface is small, the twist of the surface is very nearly in phase with and proportional to the low frequency unsteady aerodynamic pressure distribution, i.e., the aeroelastic twisting occurs quasi-statically. Quasi-static deformation of this type can have a drastic influence on aircraft stability and control and may greatly alter the flutter and response characteristics of the low frequency structural mode shapes. The aeroelastic effects introduced by equations (4.2-80) are retained in the FLEXFAB system analysis.

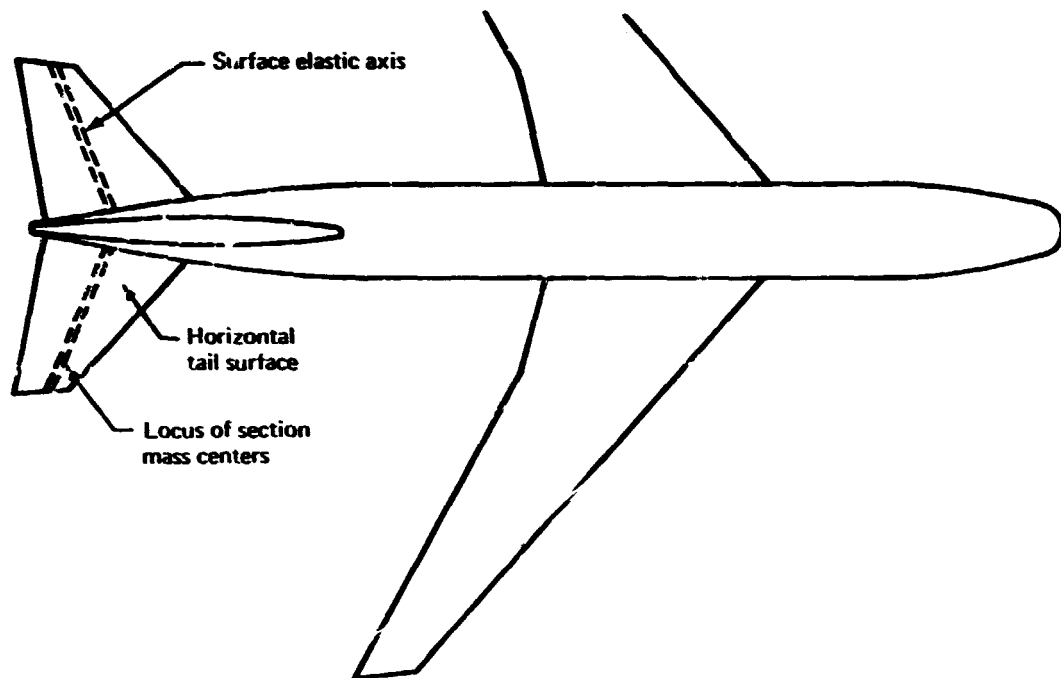


FIGURE 4.2-2.—ELASTIC AXIS AND LOCUS OF SECTION MASS CENTERS OF A TYPICAL HORIZONTAL TAIL

Assuming that a low frequency unsteady loading is characterized by a frequency ω , the equations of motion for the high frequency modal coordinates, viz.,

$$\{\ddot{u}_2\}_p + [\omega_2^2]\{u_2\}_p = [m_2]^{-1}[\phi_{\delta_2}]^T\{Q^S\}_p$$

where

$$[\omega_2^2] \equiv [m_2]^{-1}[K_2] \quad (4.2-82)$$

are closely approximated by the following:

$$(-\omega^2[I] + [\omega_2^2])\{u_2\}_p = [m_2]^{-1}[\phi_{\delta_2}]^T\{Q^S\}_p.$$

This approximation is valid if the elastic deformation, represented by $\{\delta_2\}$ has the characteristics described in the preceding example. The value of ω is small and ω^2 is negligible compared with the diagonal elements of $[\omega_2^2]$. Equation (4.2-82), therefore, reduces to the following approximate expression used to form equation (4.2-80):

$$[\omega_2^2]\{u_2\}_p = [m_2]^{-1}[\phi_{\delta_2}]^T\{Q^S\}_p.$$

The flexibility associated with the high frequency modes, equation (4.2-81), may be computed as a residual. The total flexibility of the structure as a free body, viz., $[\tilde{C}]$, defined by equation (4.2-64), is equal to the flexibility represented by the complete set of free-vibration modes, i.e.,

$$[\tilde{C}] = [\phi_{\delta}] [K]^{-1} [\phi_{\delta}]^T.$$

When the modes are separated into two sets $[\phi_{\delta_1}]$ and $[\phi_{\delta_2}]$, the expression is given by the following:

$$[\tilde{C}] = [\phi_{\delta_1}] [K_1]^{-1} [\phi_{\delta_1}]^T + [\phi_{\delta_2}] [K_2]^{-1} [\phi_{\delta_2}]^T.$$

The flexibility of the structure represented by equation (4.2-81) is computed as the following residual:

$$[\tilde{C}_R] = [\tilde{C}] - [\phi_{\delta_1}] [K_1]^{-1} [\phi_{\delta_1}]^T. \quad (4.2-83)$$

The structural equations of motion, therefore, are expressed as

$$[m_1] \{\ddot{u}_1\}_P + [K_1] \{u_1\}_P = [\phi_{\delta_1}]^T \{Q^S\}_P \quad (4.2-84)$$

and

$$\{\delta_2\}_P = [\tilde{C}_R] \{Q^S\}_P$$

where the residual flexibility $[\tilde{C}_R]$ is computed using equation (4.2-83). The total perturbation deformation is now expressed as

$$\{\delta\}_P = [\tilde{C}_P] \{Q^S\}_P + [\phi_{\delta_1}] \{u_1\}_P \quad (4.2-85)$$

or, equivalently,*

$$\{\delta\}_P = [\tilde{C}_R] \left(-[m_{\delta}] [\phi_{\delta_1}] \{\ddot{u}_1\}_P + \{Q^S\}_P \right) + [\phi_{\delta_1}] \{u_1\}_P.$$

In the development leading to equation (4.2-84), no consideration has been given to aerodynamic inertial, damping and stiffness forces. Those quantities are introduced in section 6. The order of magnitude comparisons which lead to equations (4.2-84) tacitly assume negligible influence from aerodynamic forces on the low frequency response of the structure in the $\{u_1\}$ modal degrees of freedom. The aerodynamic damping and inertial forces induced by high frequency variations of the modal coordinates $\{u_2\}$ are assumed to be negligibly small by comparison with the aerodynamic and structural stiffness forces related to the $\{u_2\}$ coordinates.

* The inertial forces of mode acceleration are retained in volume I even though they do not contribute to $\{\delta\}_P$ in equation (4.2-85).

4.2.5 Simplification Using the Symmetry of an Aircraft

Using the geometric, structural, and inertial symmetry of an aircraft, the structural equations of motion are separated into symmetric and antisymmetric forms. The stiffness relation, equation (4.2-14), is expressed as follows:

$$\text{symmetric form: } \{Q\}^S = [K]^S \{\delta\}^S \quad (4.2-86)$$

$$\text{antisymmetric form: } \{Q\}^A = [K]^A \{\delta\}^A$$

The nodal displacements ($\{\delta\}^S$ and $\{\delta\}^A$) and the applied nodal forces ($\{Q\}^S$ and $\{Q\}^A$) are expressed for node points on the plane of symmetry and on the right-hand side of the structure only, figure 4.2-3.

For the symmetric form, the nodal displacements and forces are assumed to be symmetric functions of the Y-coordinate. At node points on the plane of symmetry, nodal displacement components corresponding to d_Y , θ_X , θ_Z are zero and do not appear in $\{\delta\}^S$. Under deformation the plane of symmetry may stretch, but it remains a plane. The components of nodal force corresponding to F_Y , M_X , M_Z are set to zero at the plane of symmetry and are removed from $\{Q\}$ in forming $\{Q\}^S$. At node points off the plane of symmetry the following relations are assumed satisfied:

$$\begin{bmatrix} d_X \\ d_Y \\ d_Z \\ \theta_{F_X} \\ \theta_{F_Y} \\ \theta_{F_Z} \end{bmatrix}_R = \begin{bmatrix} d_X \\ -d_Y \\ d_Z \\ -\theta_{F_X} \\ \theta_{F_Y} \\ -\theta_{F_Z} \end{bmatrix}_L \quad \text{and} \quad \begin{bmatrix} F_X \\ F_Y \\ F_Z \\ M_X \\ M_Y \\ M_Z \end{bmatrix}_R = \begin{bmatrix} F_X \\ -F_Y \\ F_Z \\ -M_X \\ M_Y \\ -M_Z \end{bmatrix}_L \quad (4.2-87)$$

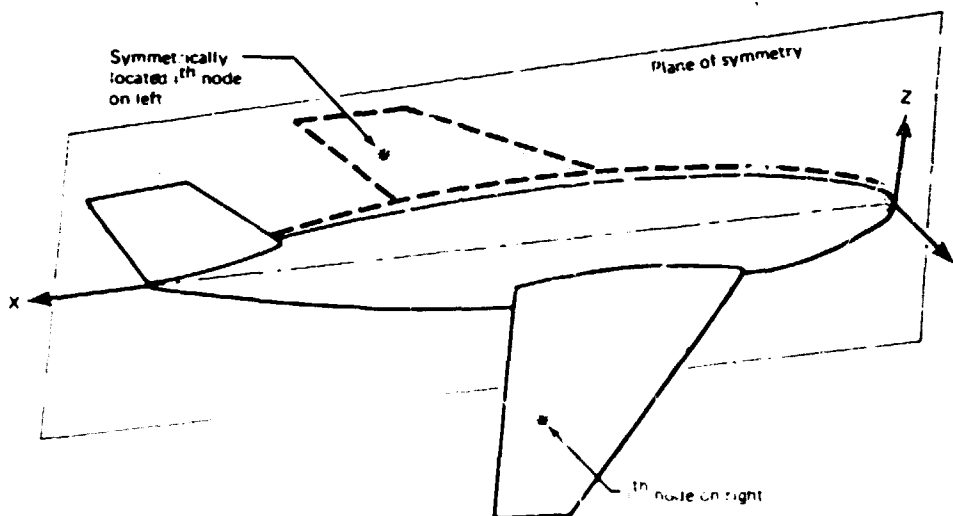


FIGURE 4.2-3.—PLANE OF STRUCTURAL SYMMETRY

where the subscripts R and L denote evaluation at the i^{th} node on the right and the symmetrically located node on the left, figure 4.2-3. The aircraft structure takes on a symmetrically deformed shape, the net force on the aircraft in Y-direction is zero, and net moments about X- and Z-axes vanish.

For the antisymmetric form, the components of nodal displacement d_X , d_Z and θ_Y and components of nodal force F_X , F_Z and M_Y are set to zero at nodes on the plane of symmetry and do not appear in $\{\delta\}^A$ and $\{Q\}^A$. Under antisymmetric deformation, the plane of symmetry warps but does not stretch. At nodes off the plane of symmetry the following relations are satisfied:

(4.2-88)

$$\begin{bmatrix} d_X \\ d_Y \\ d_Z \\ \theta_{E_X} \\ \theta_{E_Y} \\ \theta_{E_Z} \end{bmatrix}_R = \begin{bmatrix} -d_X \\ d_Y \\ -d_Z \\ \theta_{E_X} \\ -\theta_{E_Y} \\ \theta_{E_Z} \end{bmatrix}_L \quad \text{and} \quad \begin{bmatrix} F_X \\ F_Y \\ F_Z \\ M_X \\ M_Y \\ M_Z \end{bmatrix}_R = \begin{bmatrix} -F_X \\ F_Y \\ -F_Z \\ M_X \\ -M_Y \\ M_Z \end{bmatrix}_L$$

The structure takes on an antisymmetric shape, the net forces in the X- and Z-directions vanish and the net moment about the Y-axis is zero.

Using the above arrangement, the equations of motion in sections 4.2.3 and 4.2.4 are separated into symmetric and antisymmetric forms. In lieu of a single set of equations expressed in terms of nodal displacement and force components at nodes on both sides of an aircraft, two sets of the structural equations of motion are obtained in terms of the nodal quantities on the plane of symmetry and on the right hand side of the aircraft only.

4.2.6 Deformation of the Aerodynamic Surfaces

The boundary conditions for the aerodynamic problem, derived in terms of flow incidence in section 2.3.3, contain terms related to elastic deformation of the structure. These boundary conditions were linearized in section 2.3.3.2, where it was shown that the flow incidence due to elastic deformation must satisfy the following relations at the mean aerodynamic surfaces:

$$\psi_\theta = \hat{i} \cdot (\vec{\theta}_E \times \vec{n}_1)$$

and

$$\psi_d = -\frac{1}{U_1} \frac{\delta \vec{d}}{\delta t} \cdot \vec{n}_1$$

(4.2-89)

At the mean surfaces of thin bodies, equations (4.2-89) are expressed in terms of the local thin body coordinate systems, and at slender body surfaces equations (4.2-89) are expressed in terms of the Reference Axis System, figure 4.2-4. The linearized boundary conditions have the following forms:

$$\text{and} \quad \left. \begin{aligned} \psi_{\theta} &= \theta_{E_{Y_N}} \\ \psi_{\dot{d}} &= -\frac{1}{U_1} \dot{d}_{Z_N} \end{aligned} \right\} \quad \text{thin bodies} \quad (4.2-90)$$

$$\text{and} \quad \left. \begin{aligned} \psi_{\theta_Y} &= \theta_{E_Y} \\ \psi_{\theta_Z} &= \theta_{E_Z} \\ \psi_{\dot{d}_Y} &= -\frac{1}{U_1} \dot{d}_Y \\ \psi_{\dot{d}_Z} &= -\frac{1}{U_1} \dot{d}_Z \end{aligned} \right\} \quad \text{slender bodies} \quad (4.2-91)$$

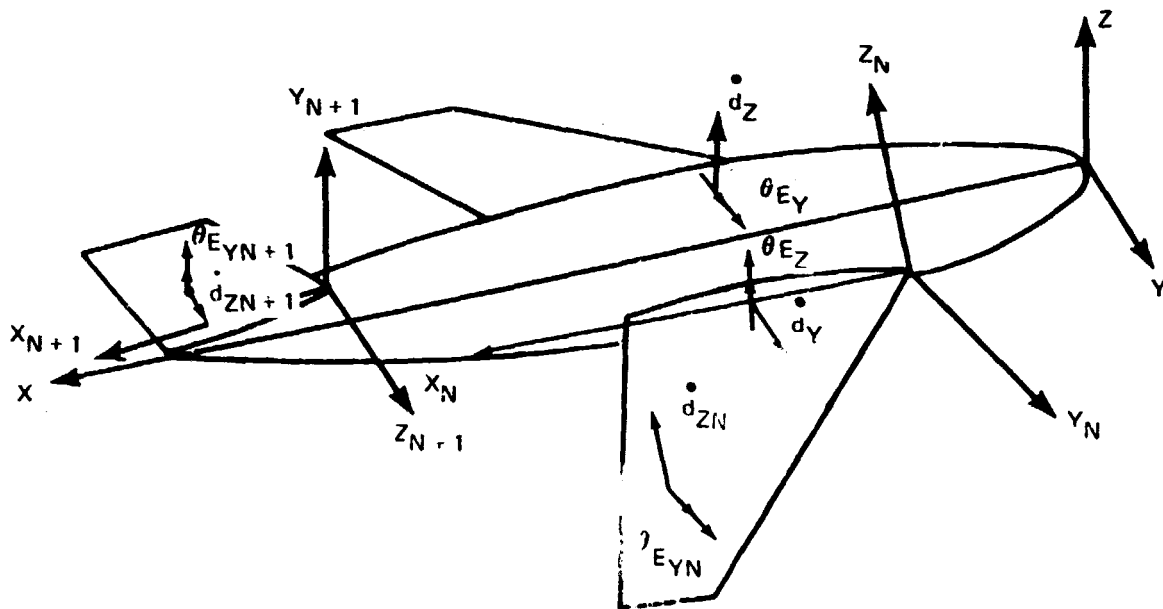


FIGURE 4.2-4. ELASTIC DEFORMATION OF AERODYNAMIC SURFACES

In the FLEXSTAB system, elastic deformation of the thickness shapes of thin and slender bodies is ignored. The elastic deformation contained in equations (4.2-90) or (4.2-91), therefore, is solely a consequence of deformation to the camber shapes. As a result, the elastic deformation of slender bodies may be evaluated at the slender body centerline in lieu of the slender body surface as shown by figure 4.2-4; thus, the elastic deformation of slender bodies is represented as shown by figure 4.2-5.

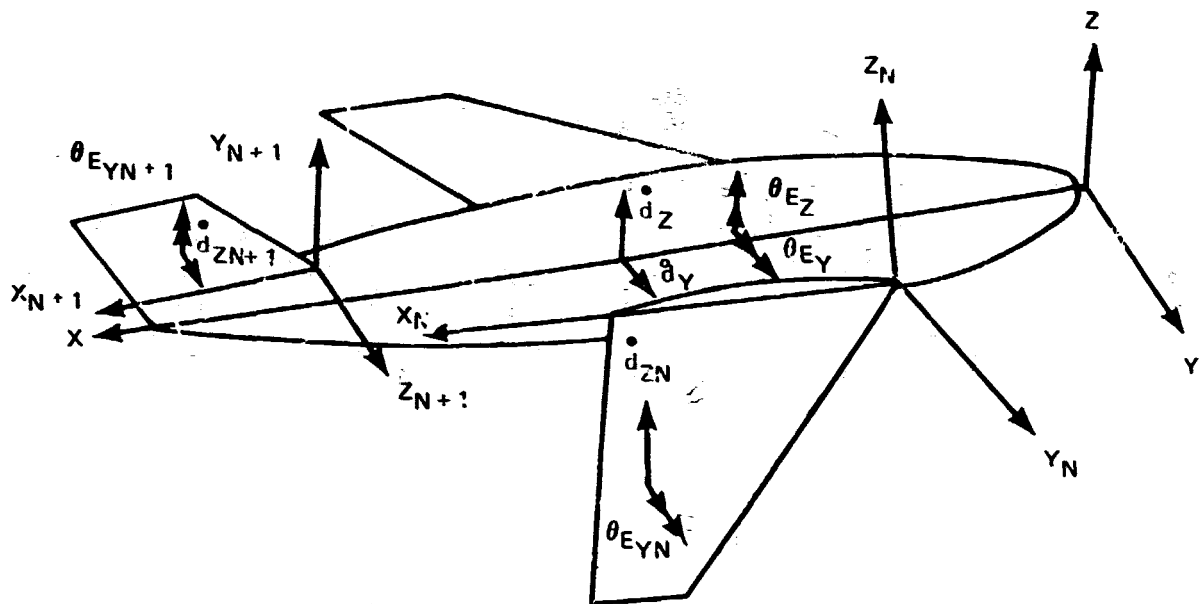


FIGURE 4.2-5.—ELASTIC DEFORMATION OF SLENDER BODY CENTERLINE

4.2.6.1 *Rotational deformation.*—The components of the elastic rotation appearing in equations (4.2-90) and (4.2-91) are computed from the displacement field \vec{d} using the matrix equivalent of $\vec{\theta}_E = 1/2 \nabla \times \vec{d}$, i.e.,

$$\begin{bmatrix} \theta_{E_X} \\ \theta_{E_Y} \\ \theta_{E_Z} \end{bmatrix} = \frac{1}{2} \begin{bmatrix} 0 & -\frac{\partial}{\partial Z} & \frac{\partial}{\partial Y} \\ \frac{\partial}{\partial Z} & 0 & -\frac{\partial}{\partial X} \\ -\frac{\partial}{\partial Y} & \frac{\partial}{\partial X} & 0 \end{bmatrix} \begin{bmatrix} d_X \\ d_Y \\ d_Z \end{bmatrix}. \quad (4.2-92)$$

For thin structural bodies, which deform in a platelike manner, the transverse shear strains γ_{XZ} and γ_{YZ} (reference 2-1, page 25) are assumed to be zero; hence

$$\frac{\partial d_{ZN}}{\partial Y_N} = -\frac{\partial d_{YN}}{\partial Z_N} \quad \text{and} \quad \frac{\partial d_{ZN}}{\partial X_N} = -\frac{\partial d_{XN}}{\partial Z_N}. \quad (4.2-93)$$

Under these conditions the rotation at a point is equal to the deformation gradient in the X-direction; thus, the surface rotation at the a^{th} element is

$$\{\epsilon_E^a\} = [N_\theta^a(X_N, Y_N)]\{\delta^a(t)\} \quad (4.2-94)$$

where

$$\{\theta_E^a\} \equiv \theta_{E,YN}^a$$

and

$$[N_\theta^a] \equiv \left[-\frac{\partial N_{ZN_1}}{\partial X_N}, -\frac{\partial N_{ZN_2}}{\partial X_N}, \dots, -\frac{\partial N_{ZN_n}}{\partial X_N} \right]_{Z_N} = 0.$$

For slender structural bodies, which deform in a beamlike manner, the shear strains γ_{XZ} and γ_{XY} are assumed to be zero so that

$$\frac{\partial d_X}{\partial X} = -\frac{\partial d_Z}{\partial Z} \quad \text{and} \quad \frac{\partial d_Y}{\partial X} = -\frac{\partial d_X}{\partial Y}.$$

Thus, the centerline rotation at a point on the a^{th} element is

$$\{\theta_E^a\} = [N_\theta^a(X_M)]\{\delta^a(t)\} \quad (4.2-95)$$

where

$$\{\theta_E^a\} \equiv \begin{bmatrix} \theta_{EY}^a \\ \theta_{EZ}^a \end{bmatrix}$$

and

$$[N_\theta^a] \equiv \begin{bmatrix} -\frac{\partial N_{Z_1}}{\partial X} & -\frac{\partial N_{Z_2}}{\partial X} & \dots & -\frac{\partial N_{Z_m}}{\partial X} \\ \frac{\partial N_{Y_1}}{\partial X} & \frac{\partial N_{Y_2}}{\partial X} & \dots & \frac{\partial N_{Y_m}}{\partial X} \end{bmatrix}.$$

4.2.6.2 Translational deformation rate.—The elastic displacement rates contained in equations (4.2-90) and (4.2-91) are found directly from the displacement relations for slender bodies the elastic displacement rates are as follows:

$$\{\dot{d}^a\} = [N_d^a(X_M)]\{\dot{\delta}^a(t)\} \quad (4.2-96)$$

where

$$\{\dot{d}^a\} \equiv \begin{bmatrix} \dot{d}_Y^a \\ \dot{d}_Z^a \end{bmatrix}$$

$$[N_d^a(X_M)] = \begin{bmatrix} N_{Y1}^a & N_{Y2}^a & \cdots & N_{Yn}^a \\ N_{Z1}^a & N_{Z2}^a & \cdots & N_{Zn}^a \end{bmatrix} \quad \begin{matrix} Y_M = 0 \\ Z_M = 0 \end{matrix};$$

while for thin bodies they are

(4.2-97)

$$\{\dot{d}^a\} = [N_d^a(X_N, Y_N)]\{\dot{\delta}^a(t)\}$$

where

$$\{\dot{d}^a\} \equiv \dot{d}_{ZN}^a$$

$$[N_d^a(X_N, Y_N)] \equiv [N_{ZN1}^a \quad N_{ZN2}^a \quad \cdots \quad N_{ZNn}^a] \quad Z_N = 0.$$

4.2.6.3 Surface deformation at aerodynamic control points.—The aerodynamic control points were introduced in section 3.4 as the aerodynamic surface points where the flow incidence induced by the flow singularities are evaluated. These are points at the surfaces of slender bodies shown by figure 3.4-15 and at panels on the mean surfaces of thin bodies shown by figure 3.4-13. The elastic deformation quantities for thin bodies contained in equation (4.2-94) and (4.2-97) are evaluated at the geometric centroids of aerodynamic thin body panels and combined into matrices to conform with the requirements of equations (3.4-172), viz., the flow incidence matrices for the steady and unsteady combined lifting aerodynamic problem solutions. Even though the aerodynamic control points are not at the geometric centroids, the matrices describing elastic deformation participation in the aerodynamic boundary conditions are expressed in terms of deformation at the geometric centroids to obtain an improved approximation, cf., the discussion following equation (3.4-172). These matrices appear as follows:

$$\{d^*\} \equiv \begin{bmatrix} \vdots \\ d_Y(X_M(j)) \\ d_Z(X_M(j)) \\ \vdots \\ \hline d_{ZN}(X_N(i), Y_N(i)) \\ \vdots \end{bmatrix} \begin{array}{l} \text{slender bodies} \\ \\ \text{thin bodies} \end{array} \quad (4.2-98)$$

$$\{\theta^*\} \equiv \begin{bmatrix} \vdots \\ \theta_Y(X_M(j)) \\ \theta_Z(X_M(j)) \\ \vdots \\ \hline \theta_{YN}(X_N(i), Y_N(i)) \\ \vdots \end{bmatrix} \begin{array}{l} \text{slender bodies} \\ \\ \text{thin bodies} \end{array} \quad (4.2-99)$$

where $X_M(j)$ is the coordinate of the j^{th} control point on the M^{th} slender body and $X_N(i)$, $Y_N(i)$ are the coordinates of the i^{th} panel centroids on the N^{th} thin body.

The relations which yield the quantities $\{d^*\}$ and $\{\theta^*\}$ as a result of nodal displacements at all of the structural nodes $\{\delta\}$, equation (4.2-12), are obtained by combining equations (4.2-94) through (4.2-97) expressed for all the finite elements of a structure. The resulting expressions are denoted as follows:

$$\{d^*\} = [P_d]\{\delta\} \quad (4.2-100)$$

and

$$\{\theta^*\} = [P_\theta]\{\delta\}. \quad (4.2-101)$$

Equations (4.2-90), (4.2-91), (4.2-100) and (4.2-101) allow the flow incidence at the aerodynamic panel centroids to be related to the values of $\{d^*\}$ and $\{\theta^*\}$ at the panel centroids and to be expressed as follows:

$$\{\psi_c\}_E = [P_\theta]\{\delta\} - \frac{1}{U_1} [P_d]\{\dot{\delta}\} \quad (4.2-102)$$

The rate of change of flow incidence is given by

$$\{\dot{\Psi}_c\}_E = [P_\theta]\{\dot{\delta}\} - \frac{1}{U_1} [P_d]\{\dot{\delta}\} \quad (4.2-103)$$

4.2.7 Forces at the Structural Nodes due to Aerodynamic Surface Pressure

The nodal forces arising from aerodynamic surface pressure are derived by considering the work done by the aerodynamic surface pressure in deforming the aircraft structure, viz.,

$$W = \frac{1}{2} \iint_S \{d\}^T \{P\} dS \quad (4.2-104)$$

where S is the total aerodynamic surface. $\{P\}$ is a pressure matrix with components of pressure expanded on the Reference Axis System, viz.,

$$\{P\} \equiv \begin{bmatrix} P_X(X,Y,Z,t) \\ P_Y(X,Y,Z,t) \\ P_Z(X,Y,Z,t) \end{bmatrix} ;$$

and $\{d\}$ is the displacement matrix, viz.,

$$\{d\} \equiv \begin{bmatrix} d_X(X,Y,Z,t) \\ d_Y(X,Y,Z,t) \\ d_Z(X,Y,Z,t) \end{bmatrix} .$$

As noted above, the effects of elastic deformation on the thickness shape of an aircraft are ignored. Equation (4.2-104), therefore, may be expressed in terms of airload, viz., the lifting pressure distribution on thin bodies,

$$\Delta P \equiv P_t - P_u,$$

and the aerodynamic load \bar{P} on the centerline of a slender body. When these quantities are expressed in terms of components expanded on the local thin and slender body axis systems of sections 3.2.3 and 3.2.4, equation (4.2-104) becomes as follows:

$$W = \frac{1}{2} \sum_{I=1}^N \iint_{S_{WI}} \{d_T\}^T \{\Delta P\} dS + \sum_{J=1}^M \frac{1}{2} \int_{L_{BJ}} \{d_T\}^T \{\bar{p}\} d\xi \quad (4.2-105)$$

where the notation of section 3.3 has been introduced and at thin body mean surfaces

$$\{\Delta P\} \equiv \begin{bmatrix} \Delta P_{XN}(X_N, Y_N, t) \\ \Delta P_{ZN}(X_N, Y_N, t) \end{bmatrix} \quad \begin{array}{l} \text{at thin body} \\ \text{mean surfaces} \end{array}$$

and

$$\{d_T\} \equiv \begin{bmatrix} d_{XN}(X_N, Y_N, t) \\ d_{ZN}(X_N, Y_N, t) \end{bmatrix} \quad \begin{array}{l} \text{at thin body} \\ \text{mean surfaces} \end{array} ;$$

while at slender body surfaces

$$\{\bar{p}\} \equiv \begin{bmatrix} \bar{p}_X(X_M, t) \\ \bar{p}_Y(X_M, t) \\ \bar{p}_Z(X_M, t) \end{bmatrix} \quad \begin{array}{l} \text{at slender} \\ \text{body surfaces} \end{array}$$

and

$$\{d_T\} \equiv \begin{bmatrix} d_X(X_M, t) \\ d_Y(X_M, t) \\ d_Z(X_M, t) \end{bmatrix} \quad \begin{array}{l} \text{at slender} \\ \text{body surfaces} \end{array}$$

The displacement relations, equations (4.2-7), are readily used to construct the elements of the displacement matrix $\{d_T\}$ as follows:

$$\{d_T^a\} = [N_T^a] \{\delta^a\} \quad (4.2-106)$$

where at thin bodies

$$[N_T^a] \equiv \begin{bmatrix} N_{XN_1}^a & N_{ZN_2}^a & \cdots & N_{XN_n}^a \\ N_{ZN_1}^a & N_{ZN_2}^a & \cdots & N_{ZN_n}^a \end{bmatrix} \quad Z_N = 0$$

and at slender bodies

$$[N_T^a] \equiv \begin{bmatrix} N_{X_1}^a & N_{X_2}^a & \cdots & N_{X_n}^a \\ N_{Y_1}^a & N_{Y_2}^a & \cdots & N_{Y_n}^a \\ N_{Z_1}^a & N_{Z_2}^a & \cdots & N_{Z_n}^a \end{bmatrix} \quad \begin{aligned} Y_M &= 0 \\ Z_M &= 0 \end{aligned}$$

Letting the aerodynamic surface of the a^{th} structural finite element be given by S^a , the portion of the work represented by equation (4.2-105) which is done on the a^{th} finite element, at a thin body finite element, is

$$W^a = \frac{1}{2} \{\delta^a\}^T \iint_{S^a} [N_T^a]^T \{\Delta P\} dS \quad (4.2-107a)$$

and, at a slender body finite element, is

$$W^a = \frac{1}{2} \{\delta^a\}^T \int_{L_{BJ}^a} [N_T^a]^T \{\bar{P}\} d\xi \quad (4.2-107b)$$

where L_{BJ}^a is the centerline segment related to the a^{th} finite element.

As previously noted, the solution to the aerodynamic problem, section 3.4, is expressed in terms of airloads at aerodynamic panels on thin bodies and on segments of the slender body centerlines. These panels and centerline segments, however, need not coincide with the finite element surface areas S^a . Equations (4.2-107) must, therefore, be expressed as follows:

$$W^a = \frac{1}{2} \{\delta^a\}^T \sum_i^a \iint_{S_{Wi}} [N_T^a]^T \{\Delta P\} dS \quad (4.2-108)$$

where S_{Wi} is the surface of the i^{th} aerodynamic panel and the sum is over the aerodynamic panels on the a^{th} finite element surface, S^a , and

$$W^a = \frac{1}{2} \{\delta^a\}^T \sum_j^a \int_{L_{BJj}} [N_T^a]^T \{\bar{P}\} d\xi \quad (4.2-109)$$

where L_{BJj} is the length of the j^{th} aerodynamic centerline segment and the sum is over the aerodynamic centerline segments on L_{BJ}^a . These expressions are greatly simplified in the FLEXSTAB system. The airloads are either uniform or nearly uniform on each small aerodynamic panel and centerline segment and are thus resolved into aerodynamic forces applied at aerodynamic centroids of each panel and centerline segment, figure 4.2-6. They are computed as follows:

$$\iint_{S_{Wi}} \{\Delta P\} dS \equiv \{F_i^A\}_W \quad (4.2-110)$$

and

$$\int_{L_{BJj}} \{\bar{P}\} d\xi \equiv \{F_j^A\}_B$$

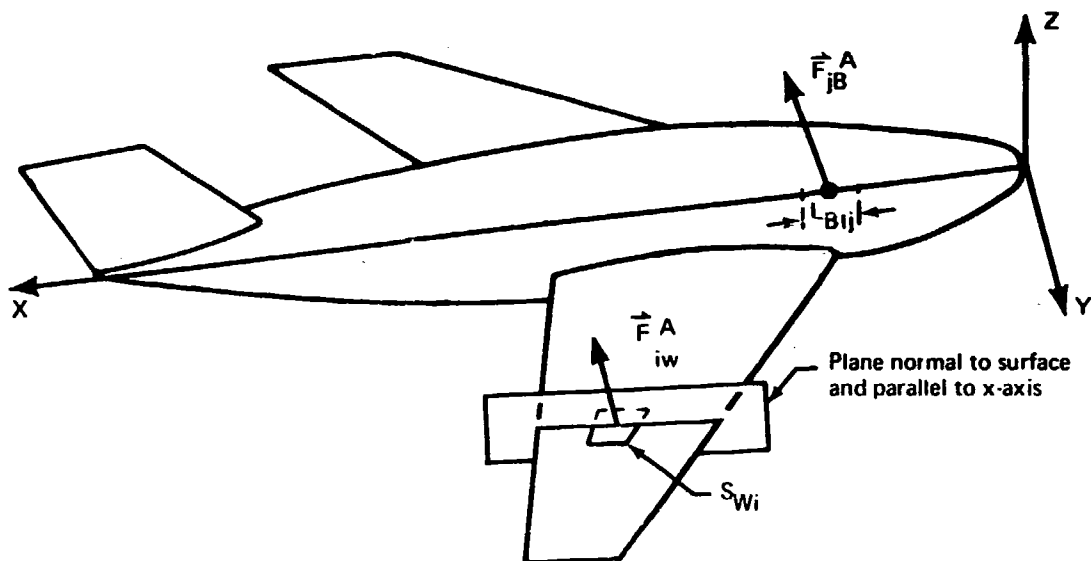


FIGURE 4.2-6.—AERODYNAMIC FORCES ACTING ON AERODYNAMIC PANELS AND SLENDER BODY CENTERLINE SEGMENTS

where at thin bodies

$$\{F_i^A\}_W \equiv \begin{bmatrix} F_{XN_i}^A \\ F_{ZN_i}^A \end{bmatrix}$$

and at slender bodies

$$\{F_j^A\}_B \equiv \begin{bmatrix} F_{X_i}^A \\ F_{Y_i}^A \\ F_{Z_i}^A \end{bmatrix}$$

The variation in the displacement components over each aerodynamic panel and centerline segment is ignored as small and equations (4.2-108) are expressed at thin bodies as

$$W^a = \frac{1}{2} \{\delta^a\}^T \sum_i^a [N_T^a(i)]^T \{F_i^A\}_W \quad (4.2-111)$$

and at slender bodies as

$$W^a = \frac{1}{2} \{\delta^a\}^T \sum_j^a [N_T^a(j)]^T \{F_j^A\}_B \quad (4.2-112)$$

where $[N_T^a(i)]$ and $[N_T^a(j)]$ denote evaluation of the displacement functions, equations (4.2-106), at the aerodynamic centroid of the j^{th} thin body panel or j^{th} slender body centerline segment. The steps leading from equations (4.2-108 and (4.2-109) to equations (4.2-111) and (4.2-112) involve approximations for the two finite element methods used in FLEXSTAB and described in sections 4.3 and 4.4.

Equation (4.2-105) is the sum of the work done by the airloads at all of the finite elements on aerodynamic surfaces. Equation (4.2-105), therefore, may be expressed in matrix form in terms of equations (4.2-111) and (4.2-112) as follows:

$$W = \frac{1}{2} \{\delta\}^T [P_T]^T \{f_T^A\} \quad (4.2-113)$$

where

$$\{f_T^A\} \equiv \begin{bmatrix} \vdots \\ F_Y^A(j) \\ F_Y^A(j) \\ F_Z^A(j) \\ \vdots \\ \vdots \\ F_{XN}^A(i) \\ F_{ZN}^A(i) \\ \vdots \end{bmatrix}$$

slender bodies

thin bodies

The matrix $[P_T]$ is obtained simply by evaluating the displacement relations given by equations (4.2-106) at the aerodynamic centroids and arranging the matrices $[N_T^a(j)]$ to obtain the following relation:

$$\{d_T\} = [P_T]\{\delta\} \quad (4.2-114)$$

where

$$\{d_T\} \equiv \begin{bmatrix} \vdots \\ d_X(j) \\ d_Y(j) \\ d_Z(j) \\ \vdots \\ \vdots \\ d_{XN}(i) \\ d_{ZN}(i) \\ \vdots \end{bmatrix}$$

slender bodies

thin bodies

Letting $\{Q^A\}$ represent a set of nodal forces, the following expression represents the work done by these nodal forces in deforming the structure:

$$W = \frac{1}{2}\{\delta\}^T\{Q^A\}. \quad (4.2-115)$$

This work is equated with that done by the airloads, equation (4.2-113), i.e.,

$$\frac{1}{2}\{\delta\}^T\{Q^A\} = \frac{1}{2}\{\delta\}^T[P_T]^T\{f_T^A\}.$$

The nodal displacement components are independent quantities. It follows, therefore, that the nodal forces $\{Q^A\}$ are equivalent to the airloads $\{f_T^A\}$ if

$$\{Q^A\} = [P_T]^T\{f_T^A\} \quad (4.2-116)$$

This expression is the desired result; it relates the airloads at the aerodynamic panels and centerline segments to the forces at the structural nodes in the finite element method.

4.2.8 Propulsion System Forces and Motions

Two additional transformations relate concentrated loads and motions at the mounting points of the propulsion system to the nodal forces $\{Q\}$ and nodal displacements $\{\delta\}$. In the FLEXSTAB system, the propulsion system consists of up to ten engines supplying thrust and having rotating parts. The mounting points are assumed to be at the centers of mass of the engines. A gyroscopic couple M_i^G is assumed to act at each mounting point, but the thrust vectors T_i may be distributed along a slender structural body representing an engine. Translational displacements at the points of applied thrust are expressed as

$$\{d_T^T\} = [NAF]^T[P_T]\{\delta\}. \quad (4.2-117)$$

This expression is obtained by evaluating equation (4.2-114) at the thrust application point. The rotational displacements at the mounting points are expressed as

$$\{\theta^G\} = [\Delta_G]^T\{\delta\} \quad (4.2-118)$$

and this result follows by applying the operation $\vec{\theta} = 1/2 (\vec{\nabla} \times \vec{d})$ to the displacement components of equation (4.2-6) as in the case of equation (4.2-92). When the result is evaluated at the engine mounting points, equation (4.2-118) is obtained. The work done at the structural nodes is equated to the work done at the thrust application points to obtain

$$\{\delta\}^T\{Q^T\} = \{\delta\}^T[P_T]^T[NAF]\{T\}$$

where $\{T\}$ is a column matrix of thrust components expanded on the Reference Axis System and

$$\{\delta\}^T\{Q^G\} = \{\delta\}^T[\Delta_G]\{M^G\}$$

where $\{M^G\}$ is a column matrix of gyroscopic couple components expanded on the Reference Axis System. The nodal forces are now found as follows:

$$\begin{aligned}\{Q^T\} &= [P_T]^T [NAF] \{T\} \\ \{Q^G\} &= [\Delta_G] \{M^G\}.\end{aligned}\tag{4.2-119}$$

A detailed description of the transformation matrix $[NAF]$ is contained in sections 4.3.6 and 4.4.4 and the matrix $\{M^G\}$ is derived in section 6.2.1.

4.3 INTERNAL STRUCTURAL INFLUENCE COEFFICIENTS

The structural matrices used in formulating the structural equations of motion in section 4.2 are derived in this section assuming that an aircraft structure may be represented as a collection of beams. The components of an aircraft configuration are classed as thin bodies and slender bodies using the classification introduced in section 3 and the structural behavior of each body is approximated assuming it to behave as a beam. Each body has an elastic axis, figure 4.3-1, which is assumed to deform by bending and twisting. The derivation of the structural matrices is based on the finite element method introduced in section 4.2. The elastic axes of the bodies are divided into finite elements, and the derivation follows the approach of section 4.2 leading to the flexibility matrix, the mass matrix, the free vibration mode shape matrices, and the transformation matrices required to formulate the structural equations of motion.

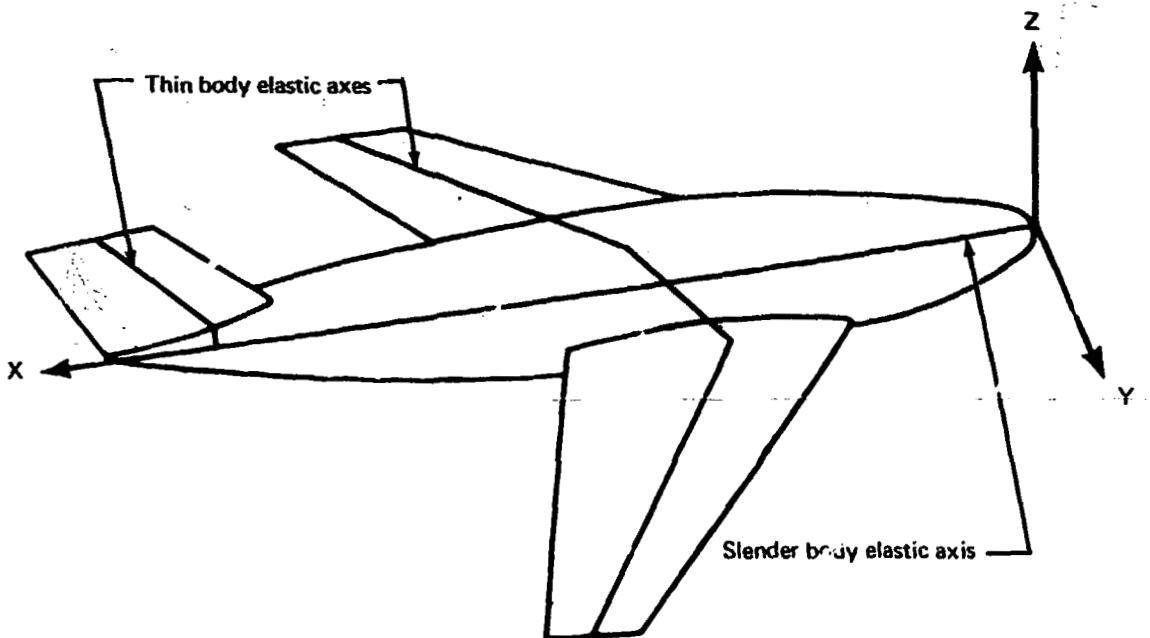


FIGURE 4.3-1.—ELASTIC AXES OF A TYPICAL CONFIGURATION

The derivation of the structural matrices is based on the usual beam theory approximation, which assumes that plane sections of the structure initially perpendicular to the elastic axis remain plane and perpendicular to the elastic axis after structural deformation, reference 2-1, pp. 106-109. The consequence of this approximation on the deformation of the structure is illustrated by letting \vec{r} be the position (relative to the elastic axis) of point P in a plane section, figure 4.3-2. Consider the point O on the elastic axis where the plane section and the elastic axis intersect. If the point O undergoes the small rotation $\vec{\theta}_O$ and the small translation \vec{d}_O , then the point P rotates through the angle $\vec{\theta}_O$ and translates through the distance $\vec{d} = \vec{d}_O + \vec{\theta}_O \times \vec{r}$. Under this approximation the deformed shape of a structure is seen to be completely determined by the deformation of its elastic axis.

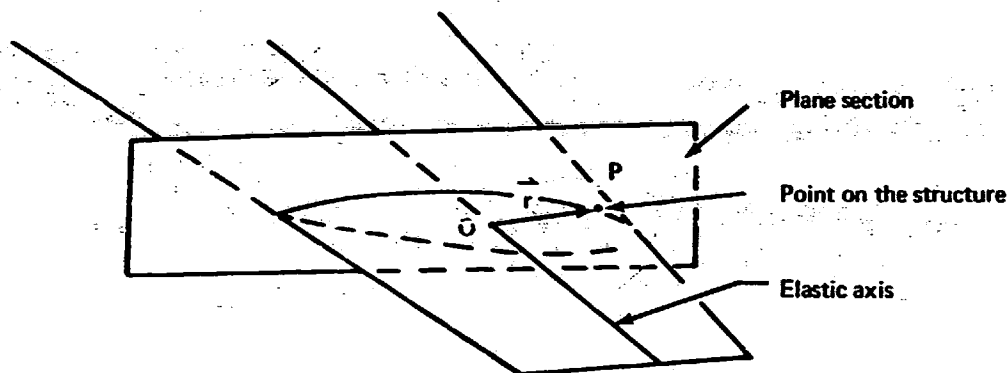


FIGURE 4.3-2.—TYPICAL PLANE SECTION OF A STRUCTURAL BODY

Beam theory yields a valid approximation to the true structural behavior if the structure has appropriate geometry. For beam theory to be valid the dimensions of the structure in the directions in which its elastic axis is assumed to bend must be small by comparison with the length of the elastic axis of the structure. In the FLEXSTAB system the elastic axis of a slender body may undergo beam bending in any direction; therefore, slender bodies are assumed to have small slenderness ratios. Thin bodies are assumed to bend out of plane but are assumed to be rigid for in-plane bending. Thin bodies, therefore, must be thin and must have aspect ratios which are an order of magnitude greater than their thickness ratios. Experience has shown that the beam theory approximation is sufficiently accurate for aeroelastic predictions if slender bodies have slenderness ratios less than 0.15 and if thin bodies have average thickness ratios less than 0.10 and aspect ratios greater than six and less than twenty (i.e., $0 < AR < 20$ assuming AR is based on span).

The derivation of the required structural matrices begins in section 4.3.1 with a description of the elastic axis followed by a description of the beam finite elements. The derivation then leads to stiffness matrices for the individual finite elements, equation (4.2-9). These matrices are combined following the method outlined in section 4.2.2.1 (item (g)) to form a composite stiffness matrix for the structure of an entire aircraft, equation (4.2-14). Section 4.3.1 ends with a reduction of the composite stiffness matrix eliminating nodal force and displacement components which are not relevant to the development following section 4.3.1.

Most of section 4.3.2 is aimed at deriving the beam theory forms of the transformations introduced in sections 4.2.6 and 4.2.7, viz.,

$$\{d^*\} = [P_d]\{\delta\} \quad (4.2-100)$$

$$\{\theta^*\} = [P_\theta]\{\delta\} \quad (4.2-101)$$

and

$$\{Q^A\} = [P_T]^T \{f_T^A\}. \quad (4.2-116)$$

These transformations, termed the aerodynamic panel transformations, are derived from formulas developed in sections 4.2.6 and 4.2.7 using the displacement relations for the beam theory finite elements, viz.,

$$\{d^a\} = [N^a]\{\delta^a\} \quad (4.2-5)$$

where the displacement functions contained in $[N^a]$ describe the beam theory deformation shown by figure 4.3-2.

The propulsion system forces are related to the nodal forces of the beam finite element method in section 4.3.3. This section, therefore, contains a derivation of the transformations developed for a general finite element method in section 4.2.8, viz.,

$$\{Q^T\} = [NAF]\{T\} \quad (4.2-119)$$

and

$$\{Q^G\} = [\Delta_G]\{M^G\}.$$

The nodal mass matrix $[m_\delta^a]$ is derived in section 4.3.7. This derivation is based on equation (4.2-18), viz.,

$$[m_\delta^a] \equiv \int_{V^a} [N^a]^T [\rho_A] [N^a] dV, \quad (4.2-18)$$

again, using the beam theory displacement relations. When the beam theory displacement relations are introduced into equation (4.2-18), the distributed mass interior to the finite elements is equivalent to a system of lumped masses. Formulas for the equivalent lumped masses are derived in section 4.3.7 along with formulas for computing the elements of the nodal mass matrix from the system of equivalent lumped masses.

4.3.1 Description of the Elastic Axis and Beam Finite Elements

As noted in the preceding an aircraft configuration is idealized as an assemblage of thin and slender bodies and in this section each thin and slender body has the structural characteristics of a beam. Each thin and slender body, therefore, has an elastic axis; and, as shown by figure 4.3-3, the elastic axes of these configuration components are joined at points termed "junction points." The elastic axis of a slender body coincides with its aerodynamic mean centerline, figures 3.2-2 and 3.2-5, while the elastic axis of a thin body lies in its aerodynamic mean surface, figures 3.2-2 and 3.2-4. The classification of configuration components as thin and slender structural bodies follows the aerodynamic classification of section 3 but aerodynamic thin and slender bodies may be subdivided by any number of junction points along their elastic axes.

4.3.1.1 Thin body elastic axis.—As noted, the elastic axis of a thin body is assumed to lie in the aerodynamic mean surface. It is approximated by a sequence of straight line segments in figure 4.3-4. The points of connection are termed "segment nodes" and the elastic axis extends from the "reference junction point node" at one end to the "outboard junction point node," as shown by figure 4.3-4. The length of the i^{th} segment of elastic axis on the N^{th} thin body is denoted as $L(Ni)$; and additional nodes, termed "interior nodes," may be evenly spaced between segment nodes with the spacing

$$\Delta L(Ni) \equiv \frac{L(Ni)}{\alpha(Ni)+1} \quad 4.3-1)$$

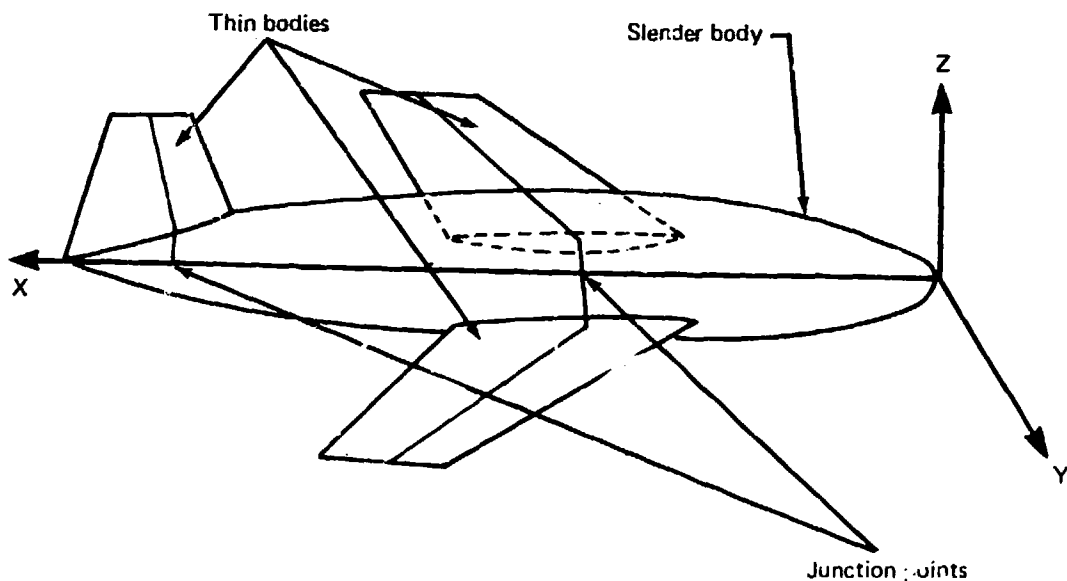


FIGURE 4.3-3.—GENERAL ARRANGEMENT OF ELASTIC AXIS

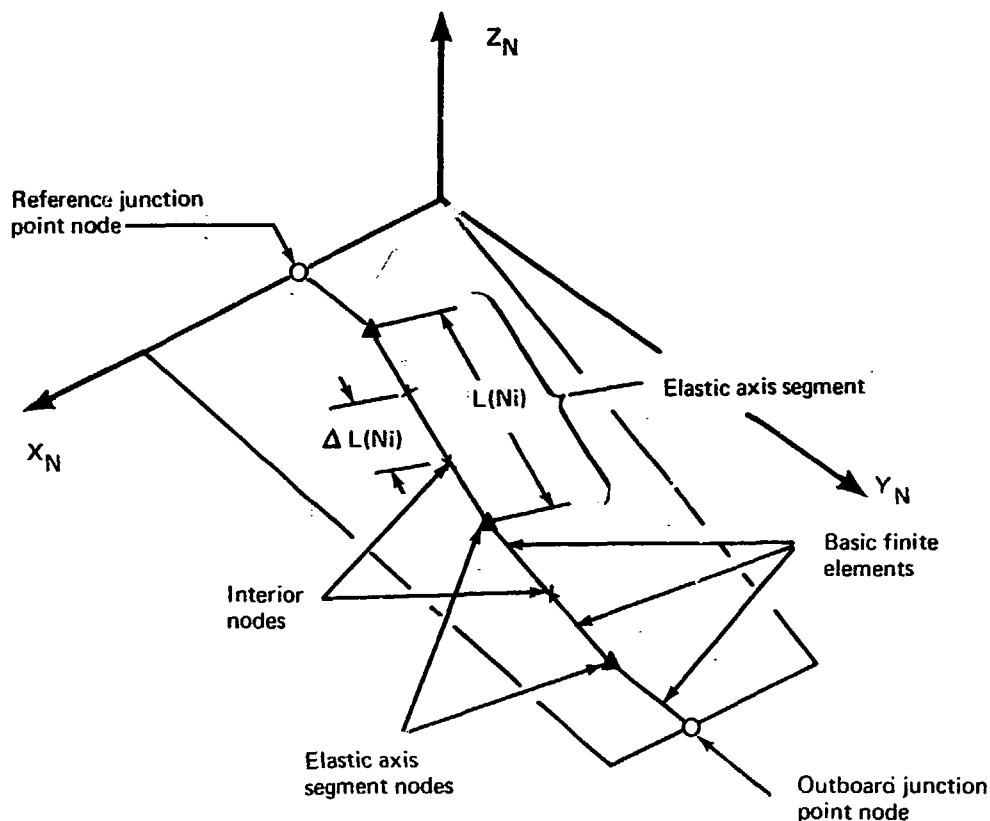


FIGURE 4.3-4.—THIN BODY ELASTIC AXIS NODES

where $\alpha(N_i)$ is the number of interior nodes on the i th segment. Thin bodies are seen to have four types of nodes: reference junction point nodes, outboard junction point nodes, elastic axis segment nodes, and interior nodes. The segment nodes are points on the elastic axis where it changes direction and where its stiffness changes. In all other respects the segment nodes are treated in the same way as interior nodes, and the portion of the elastic axis between any two adjacent nodes is called a finite element. The nodes between the reference and outboard junction point nodes are numbered in sequence increasing from one at the node adjacent to the reference junction point node to p at the node adjacent to the outboard junction point node. This numbering scheme is used to systemize the operations of equations (4.2-10) and (4.2-11) to form a composite stiffness matrix for each portion of a thin body between adjacent reference and outboard junction point nodes.

The stiffness characteristics of a thin body elastic axis finite element (i.e., the elements of the element stiffness matrix, equation (4.2-9)) are expressed in local elastic axis coordinate systems (x_{N_i} , y_{N_i} , z_{N_i}), figure 4.3-5. The x_{N_i} and y_{N_i} axes lie in the aerodynamic mean surface with the y_{N_i} axis aligned with the i th elastic axis segment; hence, the local elastic axis system is oriented relative to the local thin body axis system, sections 3.2.2 and 3.2.3, by an orthogonal coordinate transformation producing a rotation about the Z_{N_i} axis through the elastic axis sweep angle, figure 4.3-5, as follows:

$$x_{Ni} = X_N \cos \Gamma_{Ni} + Y_N \sin \Gamma_{Ni} \quad (4.3-2)$$

$$y_{Ni} = -X_N \sin \Gamma_{Ni} + Y_N \cos \Gamma_{Ni}$$

$$z_{Ni} = Z_N$$

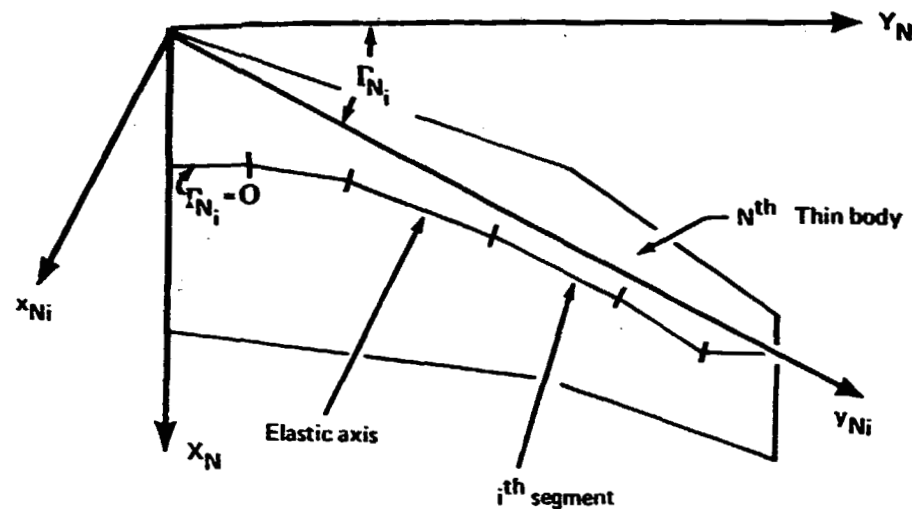


FIGURE 4.3-5.—ELASTIC AXIS OF THE N^{TH} THIN BODY

The reference and outboard junction point nodes are points where the structural thin bodies may be joined to other components of a configuration. At junction points where the elastic axis of a structural thin body is joined to the elastic axis of a structural slender body or another structural thin body having a different dihedral angle, the structure is assumed to contain a very stiff member aligned with the X-axis of the Reference Axis System (e.g., a closeout rib, a nacelle support rib, or a keel beam), figure 4.3-6. The assumed large stiffness of this fore and aft member tends to cause one of the directions of principal stress, section 17 of reference 2-i, at the elastic axis to be aligned with the stiff structural member. The elastic axis always lies in the direction of one of the two mutually perpendicular principal stress directions; hence, the elastic axis must turn at a junction point of this type to become nearly perpendicular to the X-direction as shown by figures 4.3-5 and 4.3-6.

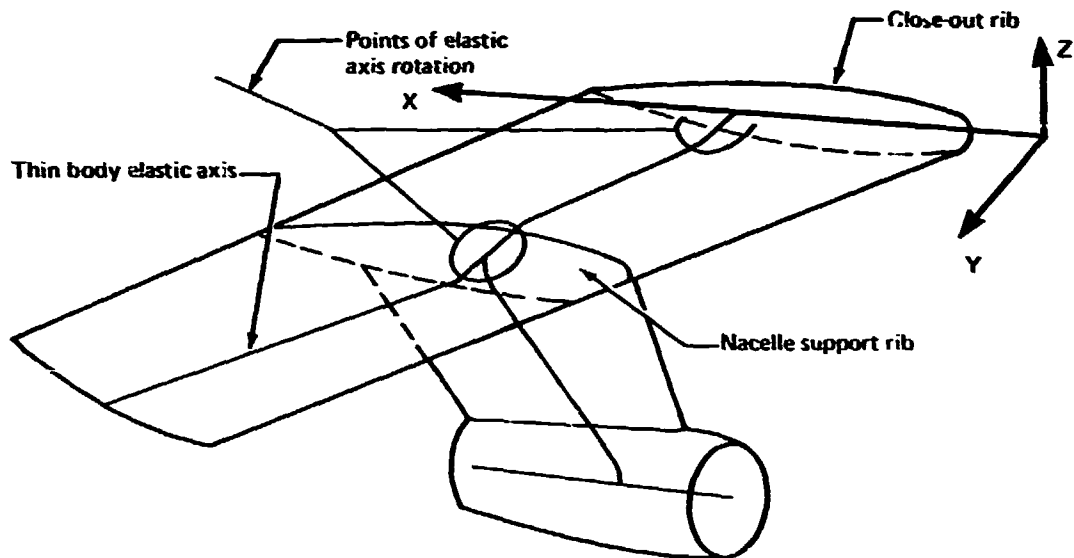


FIGURE 4.3-6.—THIN BODY ELASTIC AXIS AT A JUNCTION POINT

In the FLEXSTAB system, the stiff fore and aft members at junction points are assumed to be perfectly rigid. The segment of the elastic axis forming the terminus of a structural thin body at a junction point, therefore, must be perpendicular to the X-direction. If this restriction were not imposed, the stiffness matrix representing the structure would be singular.

At a junction point node located between the inboard (i.e., reference) and outboard junction points of a structural thin body, where there is no change in the dihedral angle, the elastic axis sweep angle need not be zero. These junction point nodes are given the special designation "coplanar thin body junction point nodes," section 4.3.1.13.

4.3.1.2 Slender body elastic axis. The elastic axis of a slender body is assumed to coincide with the aerodynamic mean centerline, figure 3.2-2; therefore, it is a straight line. Nodes on the elastic axis are arranged and designated in the same manner as for thin bodies, figure 4.3-7. One end terminates at a reference junction point node, the other at an

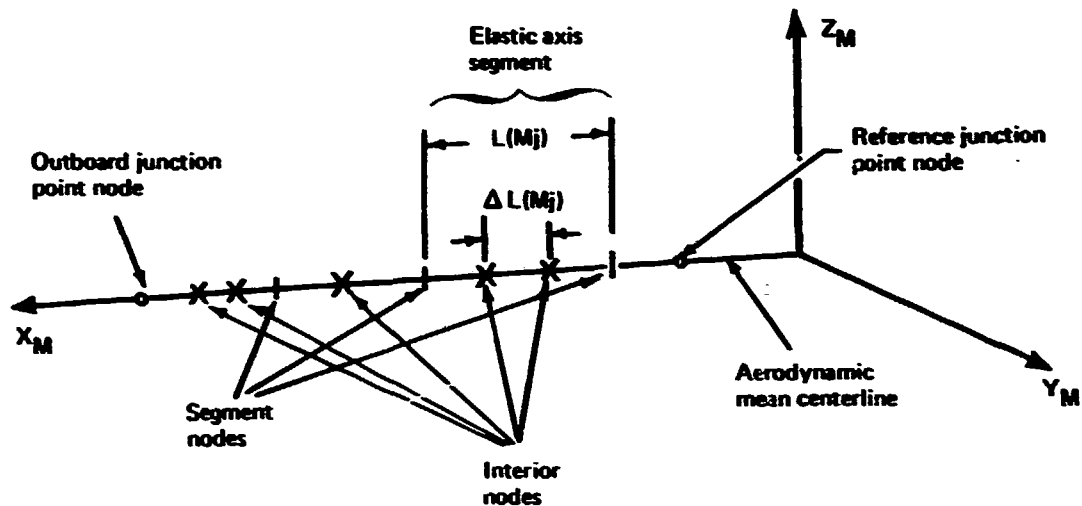


FIGURE 4.3-7.—SLENDER BODY ELASTIC AXIS NODES

outboard junction point node. Segment nodes are used but, as noted in the following, they are used only to separate segments of the elastic axis having different stiffnesses and do not introduce a change in the direction of the elastic axis as in section 4.3.1.3. The elastic axis segment lengths are denoted as $L(M_j)$ and have interior nodes spaced evenly between segment nodes with the spacing

$$\Delta L(M_j) \equiv \frac{L(M_j)}{[\alpha(M_j) + 1]} \quad (4.3-3)$$

where $\alpha(M_j)$ is the number of interior nodes on the j^{th} segment of the M^{th} slender body. Again, as in the case of a thin body, there are four types of nodes on each slender body elastic axis: reference junction point nodes, outboard junction point nodes, elastic axis segment nodes, and interior nodes. Also, the portion of elastic axis between any two adjacent nodes is termed a finite element. Numbering of the nodes is identical to that for thin bodies, section 4.3.1.1. This numbering scheme is used to systemize the operations of equations (4.2-10) and (4.2-11) to assemble a composite stiffness matrix for each portion of a slender body between adjacent reference and outboard junction points.

4.3.1.3 Assembly of thin and slender structural bodies to form a configuration. — As already noted, the thin and slender bodies are structural components of a configuration assembled by joining the elastic axis of the thin and slender bodies at their reference and outboard junction points. The junction points for the thin and slender structural components on the right hand side of a configuration are numbered as shown by figure 4.3-8. The operations, equations (4.2-10) and (4.2-11), which assemble the composite stiffness matrix

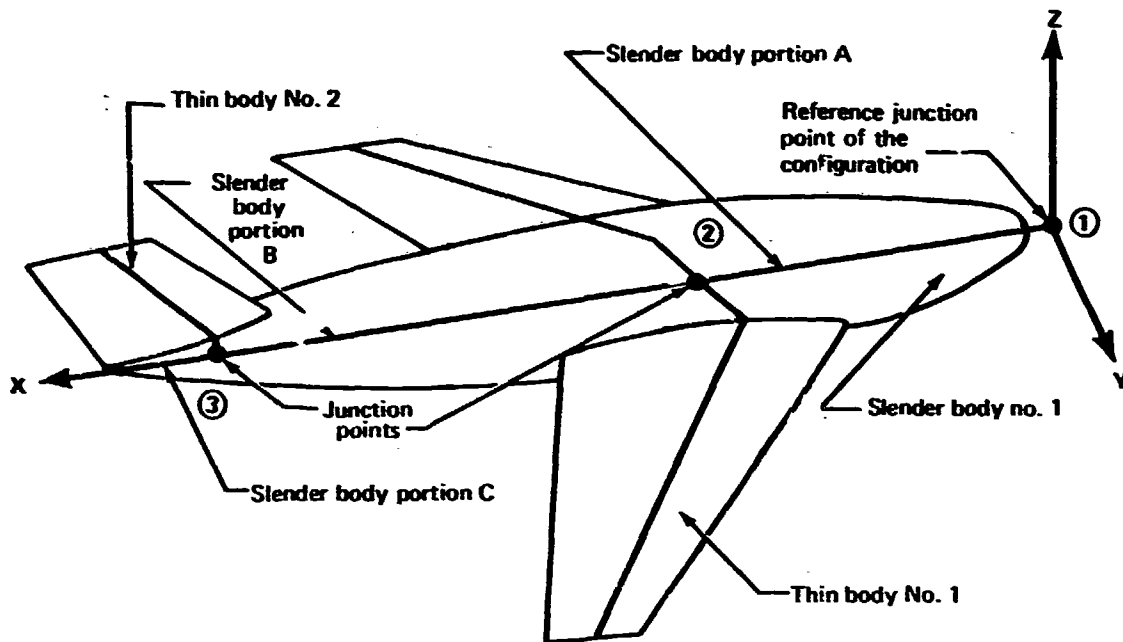


FIGURE 4.3-8.—STRUCTURAL BODY AND JUNCTION POINT DESIGNATION

for the configuration from the composite stiffness matrices of the thin and slender body components, are systemized by assigning the appropriate structural node numbers to the reference and outboard junction points of the components, figures 4.3-4 and 4.3-7. In the example shown by figure 4.3-8, the slender body is separated into three portions by junction points with the portions denoted A, B, and C while each thin body has only a single reference and outboard junction point. The configuration therefore requires for its representation three slender body composite stiffness matrices and two thin body composite stiffness matrices.

The junction point number assignment is shown by figure 4.3-9. The reference junction point of thin body No. 1 is assigned the structural junction point node number (2) while its outboard junction point is designated a free end and assigned a node number in the numbering sequence for segment and interior nodes. The portion of the slender body denoted as portion B is assigned the structural junction point node number (2) at its reference junction point and the structural junction point node number (3) at its outboard junction point. One reference junction point—that of a slender body on the plane of symmetry—is designated the reference junction point of the configuration and is shown as structural junction point node number (1).

4.3.1.4 Elastic axis element stiffnesses.—The stiffness of the elastic axis is specified in terms of the following relations:

$$\frac{1}{R} = \frac{M}{EI} \quad (4.3-4)$$

and

$$\Theta = \frac{T}{GJ}$$

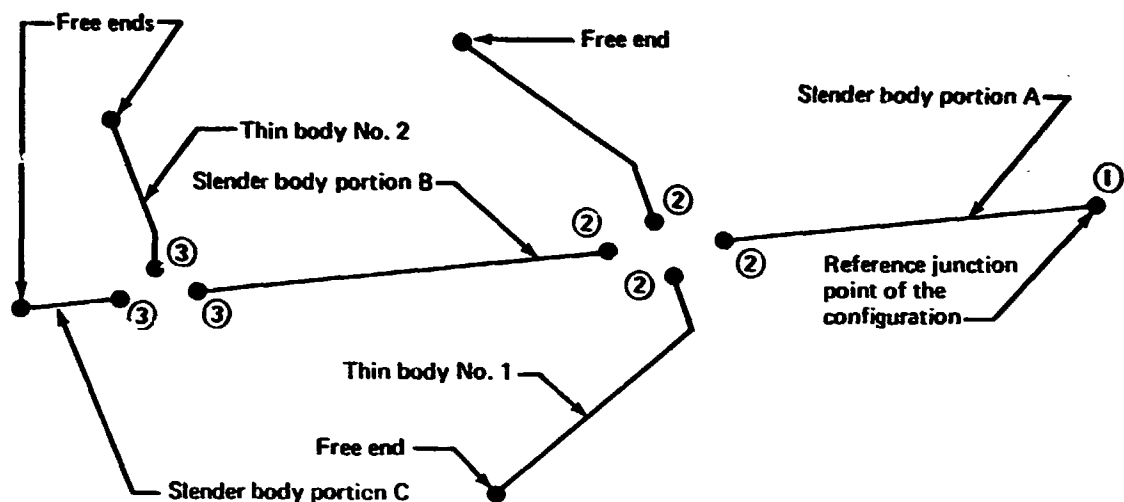


FIGURE 4.3-9.—THIN AND SLENDER STRUCTURAL BODY JUNCTION POINT NUMBERING

where M is a bending moment, R is the radius of curvature of an initially straight elastic axis, EI is the flexural rigidity, T is a torsional couple, θ is the angle of twist per unit of length, and GJ is the torsional rigidity. The first of these formulas expresses the Bernoulli-Euler law, reference 2-1, p. 106, and the second expresses the law derived by Navier for torsion of a cylindrical shaft, reference 2-1, equation 34.11. The factor J in the torsional rigidity may be derived from equation 35.10 of reference 2-1, or, for thin-walled structures, from a simplification of that formula given by reference 2-1, section 47.

4.3.1.5 Elastic axis element stiffness matrices.—An element of the elastic axis is the section between two adjacent nodes. The nodes are numbered sequentially; thus, there is an element of elastic axis from node α to node $(\alpha + 1)$. The stiffness relation, equation (4.2-9), for this element is expressed as follows:

$$\begin{bmatrix} \{T_{\alpha}\} \\ \{T_{\alpha+1}\} \end{bmatrix} = \begin{bmatrix} [K_{\alpha\alpha}] & [K_{\alpha \alpha+1}] \\ [K_{\alpha+1}] & [K_{\alpha+1 \alpha+1}] \end{bmatrix} \begin{bmatrix} \{\delta_{\alpha}\} \\ \{\delta_{\alpha+1}\} \end{bmatrix} - \begin{bmatrix} \{Q_{\alpha}\} \\ \{Q_{\alpha+1}\} \end{bmatrix} \quad (4.3-5)$$

where $\{\delta_{\alpha}\}$ contains the nodal displacement components at node α , $\{T_{\alpha}\}$ contains the total force components from the element at node α , $\{Q_{\alpha}\}$ contains the applied force components at node α , $[K_{\alpha\alpha}]$ is the linear relationship relating nodal forces at node α to nodal displacements at node α and $[K_{\alpha\alpha+1}]$ is the linear relationship relating nodal forces at node α to nodal displacements at node $(\alpha + 1)$.

Consider, now, the stiffness relation for the element from node $(\alpha - 1)$ to node α . This stiffness relation is expressed as

$$\begin{bmatrix} \{T_{\alpha-1}\} \\ \{T_{\alpha}\} \end{bmatrix} = \begin{bmatrix} [K_{\alpha-1 \ \alpha-1}] & [K_{\alpha-1 \ \alpha}] \\ [K_{\alpha \ \alpha-1}] & [K'_{\alpha\alpha}] \end{bmatrix} \begin{bmatrix} \{\delta_{\alpha-1}\} \\ \{\delta_{\alpha}\} \end{bmatrix} - \begin{bmatrix} \{Q_{\alpha-1}\} \\ \{Q_{\alpha}\} \end{bmatrix} \quad (4.3-6)$$

where the prime indicates that the stiffness matrix $[K'_{\alpha\alpha}]$ relates to the elastic axis element from node $(\alpha - 1)$ to node α . The prime is necessary to distinguish this partition of the element stiffness matrix from $[K_{\alpha\alpha}]$ appearing in equation (4.3-5). The two element stiffness relations are combined as in equation (4.2-10) as follows:

$$\begin{bmatrix} \{T_{\alpha-1}\} \\ \{0\} \\ \{T_{\alpha+1}\} \end{bmatrix} = \begin{bmatrix} [K_{\alpha-1 \ \alpha-1}] & [K_{\alpha-1 \ \alpha}] & [0] \\ [K_{\alpha \ \alpha-1}] & [K'_{\alpha\alpha} + K_{\alpha\alpha}] & [K_{\alpha \ \alpha+1}] \\ [0] & [K_{\alpha+1 \ \alpha}] & [K_{\alpha+1 \ \alpha+1}] \end{bmatrix} \begin{bmatrix} \{\delta_{\alpha-1}\} \\ \{\delta_{\alpha}\} \\ \{\delta_{\alpha+1}\} \end{bmatrix} - \begin{bmatrix} \{Q_{\alpha-1}\} \\ \{Q_{\alpha}\} \\ \{Q_{\alpha+1}\} \end{bmatrix} \quad (4.3-7)$$

Equation (4.3-7) illustrates the operations involved in forming the composite stiffness relation from the element stiffness relations. The total forces at nodes, i.e., $\{T_{\alpha}\}$, are required to vanish for equilibrium at the nodes, and the nodal displacements, $\{\delta_{\alpha}\}$, of elements joining a structural node are required to be identical for continuity of the elastic axis at the nodes. $\{Q_{\alpha}\}$ appearing in equation (4.3-7) is the sum of $\{Q_{\alpha}\}$ from equations (4.3-5) and (4.3-6). When the operations leading to equation (4.3-7) are carried out for all structural nodes, the composite stiffness relation is generated.

In section 4.2 the composite stiffness relation for a complete structure, equation (4.2-14), infers that the structure is unconstrained. The beam theory of this section does not lead to completely unconstrained composite stiffness relation because the slender body joined to the reference junction point of the structure is assumed to be infinitely stiff for axial extension. The composite stiffness relation for the structure is expressed as

$$\{Q\} = [K]\{\delta\} \quad (4.3-8)$$

but the components of displacement and force at the reference junction point node are given by

$$\{\delta_R^*\} \equiv \begin{bmatrix} d_{YR} \\ d_{ZR} \\ \theta_{XR} \\ \theta_{YR} \\ \theta_{ZR} \end{bmatrix} \quad \text{and} \quad \{Q_R^*\} \equiv \begin{bmatrix} F_{YR} \\ F_{ZR} \\ M_{XR} \\ M_{YR} \\ M_{ZR} \end{bmatrix}$$

The components of force and displacement F_{XR} and d_{XR} at the reference junction point do not appear in the composite stiffness relation.

4.3.1.6 Composite stiffness matrix.—The composite stiffness matrix is obtained, as noted above, by assembling the element stiffness relations for all elements of a configuration's elastic axis. In the FLEXSTAB system, the structural nodes are numbered in the specific order introduced in sections 4.3.1.1, 4.3.1.2, and 4.3.1.3, thereby leading to a specific arrangement of the composite stiffness matrix. Nodes at junction points are considered first taking in order the reference junction point of the configuration, the general junction points (i.e., those junction points having no special characteristics), and then the coplanar thin body junction points. Nodes on slender bodies occur next, followed by nodes on thin bodies. The matrix is partitioned in terms of this nodal designation arrangement as follows:

$$[K] \equiv \begin{bmatrix} \text{Reference} & & & & \\ \text{Junction} & & & & \\ \text{Point} & & & & \\ \hline [0] & [0] & [0] & \text{Coupling} & [0] \\ \hline [0] & \text{General} & [0] & \text{Coupling} & \text{Coupling} \\ & \text{Junction} & & & \\ & \text{Points} & & & \\ \hline [0] & [0] & \text{Coplanar} & [0] & \text{Coupling} \\ & & \text{Thin body} & & \\ & & \text{Junction} & & \\ & & \text{Points} & & \\ \hline \text{Coupling} & \text{Coupling} & [0] & \text{Slender} & [0] \\ & & & \text{Bodies} & \\ \hline [0] & \text{Coupling} & \text{Coupling} & [0] & \text{Thin} \\ & & & & \text{Bodies} \end{bmatrix} \quad (4.3-9)$$

where the coupling partitions contain the stiffness coefficients which relate nodal forces at the junction points to nodal displacements at nodes on the thin and slender bodies and vice versa. Each of the partitions of equation (4.3-9) are derived in the following as separate composite stiffness matrices for the thin bodies, slender bodies, and junction points. Assembly of the composite stiffness matrix for the complete structure is carried out by assigning structural junction point numbers to each of the reference and outboard junction points of the thin and slender bodies as described in section 4.3.1.3.

4.3.1.7 Thin body finite element stiffness matrices.—Consider the partition of the composite stiffness matrix, equation (4.3-9), related to thin bodies.

As noted previously, the elastic axis of a thin body lies in its mean aerodynamic surface and consists of straight line segments, figure 4.3-4. The stiffness properties of the elastic axis elements are expressed in terms of local elastic axis coordinate systems (x_{Nj} , y_{Nj} , z_{Nj}), figure 4.3-5, which are obtained by transformation of coordinates from the local thin body coordinate system, equation (4.3-2). The axis is aligned with the elastic axis segments by a rotation of the coordinates through the elastic axis angle of sweep Γ_{Nj} .

The segments of elastic axis on thin bodies have finite torsional stiffness and finite out-of-plane bending stiffness, i.e., for bending out of the plane of the thin body. Thin bodies, however, are assumed to be infinitely stiff for in-plane bending and extension in their planes. The components of elastic nodal displacement at a node on the i^{th} elastic axis segment of the N^{th} thin body, therefore, are given as follows (figure 4.3-10):

$$\{\delta_{\alpha}(i)\} \equiv \begin{bmatrix} d_{zNi} \\ \theta_{xNi} \\ \theta_{yNi} \end{bmatrix}_{\alpha} \quad (4.3-10)$$

where d_{zNi} is a translation normal to the thin body's mean surface and θ_{xNi} and θ_{yNi} denote elastic rotations about the x_{Ni} and y_{Ni} axes. The components of nodal force at the same node are given by

$$\{Q_{\alpha}(i)\} \equiv \begin{bmatrix} F_{zNi} \\ M_{xNi} \\ M_{yNi} \end{bmatrix}_{\alpha} \quad (4.3-11)$$

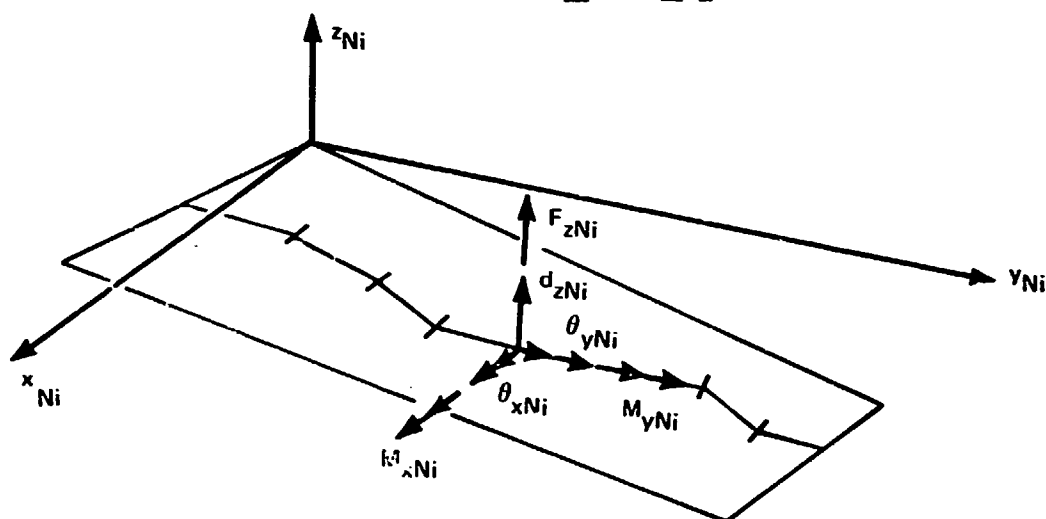


FIGURE 4.3-10.—NODAL FORCES AND DISPLACEMENTS AT A NODE ON THE N^{TH} THIN BODY

where F_{zN_i} is a force normal to the thin body mean surface, M_{yN_i} is a torsional couple, and M_{xN_i} is a bending moment, figure 4.3-10.

The stiffness matrix for the elastic axis element between nodes α and $\alpha + 1$ on the i^{th} segment of the N^{th} thin body is found from equation (4.3-4) as follows:

$$\begin{bmatrix} [K_{\alpha\alpha}] & [K_{\alpha \alpha+1}] \\ [K_{\alpha+1 \alpha}] & [K_{\alpha+1 \alpha+1}] \end{bmatrix} = \begin{bmatrix} \frac{12EI}{(\Delta L)^3} & & & & & \\ & \frac{6EI}{(\Delta L)^2} & \frac{4EI}{\Delta L} & & & \\ & 0 & 0 & \frac{GJ}{\Delta L} & & \\ & -\frac{12EI}{(\Delta L)^3} & -\frac{6EI}{(\Delta L)^2} & 0 & & \\ & \frac{6EI}{(\Delta L)^2} & \frac{2EI}{\Delta L} & 0 & & \\ & 0 & 0 & -\frac{GJ}{\Delta L} & & \\ & & & & \text{SYM.} & \\ & & & & & \frac{12EI}{(\Delta L)^3} \\ & & & & & -\frac{6EI}{(\Delta L)^2} & \frac{4EI}{\Delta L} \\ & & & & & 0 & 0 & \frac{GJ}{\Delta L} \end{bmatrix} \quad (4.3-12)$$

where $EI \equiv EI(N_i)$ is the bending stiffness of the segment, $GJ \equiv GJ(N_i)$ is the torsional stiffness of the segment, and

$$\Delta L \equiv L(N_i)/[\alpha(N_i)+1]$$

is the length of the elastic axis element.

4.3.1.8 Thin body composite stiffness matrix. - Thin body composite stiffness matrices are formed from the element stiffness matrices following the operations described in section 4.3.1.6, but at nodes where the elements of the elastic axis are not colinear, joining elements are expressed in different coordinate systems. Before the two elements may be assembled at this node by the operation of equation (4.3-7), the nodal forces and displacements at the segment node must be transformed to a common coordinate system. The adjoining segments are denoted as $(i-1)$ and i , figure 4.3-11, and the nodal forces and displacements on the i^{th} segment, i.e., the segment farthest from the reference junction point of the thin body, are transformed to the coordinate system of the $(i-1)^{\text{th}}$ segment as follows:

$$\begin{aligned} \{\delta_{\alpha}(i-1)\} &= [\lambda(i-1, i)]\{\delta_{\alpha}(i)\} \\ \{Q_{\gamma}(i-1)\} &= [\lambda(i-1, i)]\{Q_{\alpha}(i)\} \end{aligned} \quad (4.3-13)$$

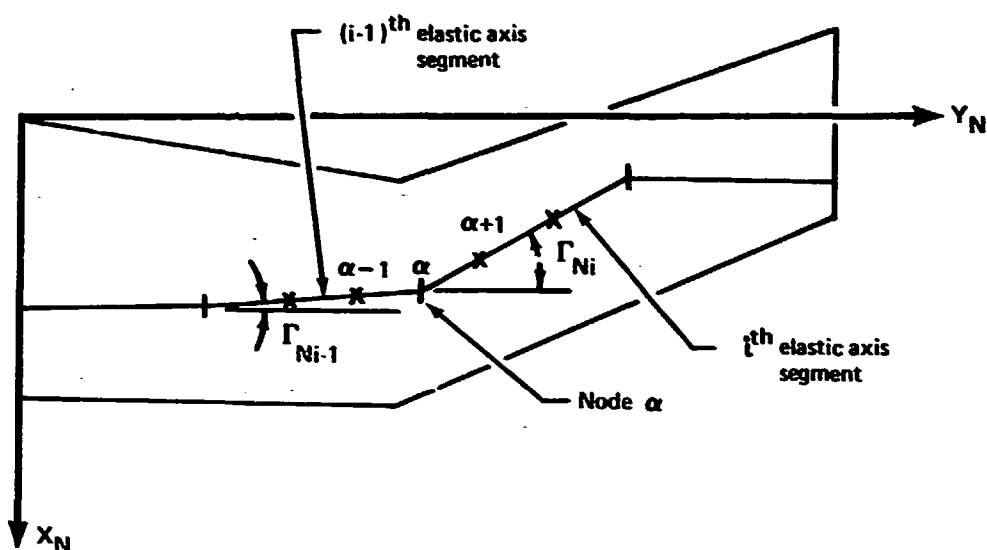


FIGURE 4.3-11.—ADJOINING FINITE ELEMENTS ON THE ELASTIC AXIS OF A THIN BODY

where the transformation matrix is a partition of an orthogonal transformation matrix of size 6×6 for rotation about the Z_N -axis and is given by

$$[\lambda(i-1, i)] \equiv \begin{bmatrix} 1 & 0 & 0 \\ 0 & \cos(\Gamma_{Ni} - \Gamma_{Ni-1}) & -\sin(\Gamma_{Ni} - \Gamma_{Ni-1}) \\ 0 & \sin(\Gamma_{Ni} - \Gamma_{Ni-1}) & \cos(\Gamma_{Ni} - \Gamma_{Ni-1}) \end{bmatrix}$$

The transformation, equation (4.3-13), is applied to the partitions of the element stiffness matrix, equation (4.3-12), for the element from node α to node $(\alpha + 1)$ as follows:

$$\begin{bmatrix} [\lambda(i-1, i)] \{T_{\alpha}(i)\} \\ \hline \{T_{\alpha+1}\} \end{bmatrix} = \begin{bmatrix} [\lambda(i-1, i)] [K_{\alpha\alpha}] [\lambda(i-1, i)]^T & | & [\lambda(i-1, i)] [K_{\alpha\alpha+1}] \\ \hline [K_{\alpha+1\alpha}] [\lambda(i-1, i)]^T & | & [K_{\alpha+1\alpha+1}] \end{bmatrix} \times \begin{bmatrix} [\lambda(i-1, i)] \{\delta_{\alpha}(i)\} \\ \hline \{\delta_{\alpha}(i)\} \end{bmatrix} - \begin{bmatrix} [\lambda(i-1, i)] \{Q_{\alpha}(i)\} \\ \hline \{Q_{\alpha+1}\} \end{bmatrix}$$

where $[\lambda(i-1, i)]^T$ is a partition of the transposed orthogonal transformation matrix. It follows therefore that

$$\begin{bmatrix} \{T_{\alpha}(i-1)\} \\ \{T_{\alpha+1}(i)\} \end{bmatrix} = \begin{bmatrix} [\lambda(i-1, i)][K_{\alpha\alpha}][\lambda(i-1, i)]^T & [\lambda(i-1, i)][K_{\alpha\alpha+1}] \\ [K_{\alpha+1\alpha}][\lambda(i-1, i)]^T & [K_{\alpha+1\alpha+1}] \end{bmatrix} \begin{bmatrix} \{\delta_{\alpha}(i-1)\} \\ \{\delta_{\alpha+1}(i)\} \end{bmatrix} - \begin{bmatrix} \{Q_{\alpha}(i-1)\} \\ \{Q_{\alpha+1}(i)\} \end{bmatrix} \quad (4.3-14)$$

Equation (4.3-14) defines a new element stiffness matrix in which the nodal forces and displacements at node α are expressed in the local coordinate system of the $(i-1)^{th}$ elastic axis segment. This stiffness matrix can now be combined with the stiffness matrix for the element from node $(\alpha-1)$ to node α . The resulting composite stiffness matrix for the two element is as follows:

$$\begin{bmatrix} \{T_{\alpha-1}(i-1)\} \\ \{0\} \\ \{T_{\alpha+1}(i)\} \end{bmatrix} = \begin{bmatrix} [K'_{\alpha-1\alpha-1}] & [K'_{\alpha-1\alpha}] & [0] \\ [K'_{\alpha\alpha-1}] & [K'_{\alpha\alpha}] + [\lambda(i-1, i)][K_{\alpha\alpha}][\lambda(i-1, i)]^T & [\lambda(i-1, i)][K_{\alpha\alpha+1}] \\ [0] & [K_{\alpha+1\alpha}][\lambda(i-1, i)]^T & [K_{\alpha+1\alpha+1}] \end{bmatrix} \times \begin{bmatrix} \{\delta_{\alpha-1}(i-1)\} \\ \{\delta_{\alpha}(i-1)\} \\ \{\delta_{\alpha+1}(i)\} \end{bmatrix} - \begin{bmatrix} \{Q_{\alpha-1}(i-1)\} \\ \{Q_{\alpha}(i-1)\} \\ \{Q_{\alpha+1}(i)\} \end{bmatrix} \quad (4.3-15)$$

The operations leading to the composite stiffness matrix given by equation (4.3-15) are repeated for all of the nodes on the N^{th} thin body. Assuming the reference junction point of the body is the Q^{th} junction point while the outboard junction point is the P^{th} junction point, the composite stiffness matrix for the N^{th} thin body is expressed as follows:

$$\begin{bmatrix} \{T_Q\} \\ \{0\} \\ \{T_P\} \end{bmatrix} = \begin{bmatrix} [K_{QQ}] & [K_{QN}] & [0] \\ [K_{NQ}] & [K_{NN}] & [K_{NP}] \\ [0] & [K_{PN}] & [K_{PP}] \end{bmatrix} \begin{bmatrix} \{\delta_Q\} \\ \{\delta_N\} \\ \{\delta_P\} \end{bmatrix} - \begin{bmatrix} \{Q_Q\} \\ \{Q_N\} \\ \{Q_P\} \end{bmatrix} \quad (4.3-16)$$

where $[K_{QQ}]$ and $[K_{PP}]$ are the stiffnesses for nodal forces and displacements at the junction points; $[K_{NN}]$ is the composite stiffness matrix for all nodes on the N^{th} thin body (exclusive of junction point nodes); and $[K_{QN}]$, $[K_{NQ}]$, $[K_{PN}]$, and $[K_{NP}]$ represent coupling of nodal forces and displacements at the junction points with the nodal forces $\{Q_N\}$ and nodal displacements $\{\delta_N\}$ at nodes on the thin body.

The composite stiffness matrix $[K_{NN}]$ represents the structure of the N^{th} thin body as if it were clamped at its junction points, figure 4.3-12. Matrices of this form are generated for each thin body; and, the thin body partition of equation (4.3-9) contains these matrices arranged on the diagonal as follows:

$$\begin{bmatrix} \text{thin body partition} \\ \text{of Equ. (4.3-9)} \end{bmatrix} \equiv \begin{bmatrix} [K_{11}] & & & \text{zeros} \\ & [K_{22}] & & \\ & & \ddots & \\ \text{zeros} & & & [K_{NN}] \end{bmatrix} \quad (4.3-17)$$

where the partition is expressed for N thin bodies.

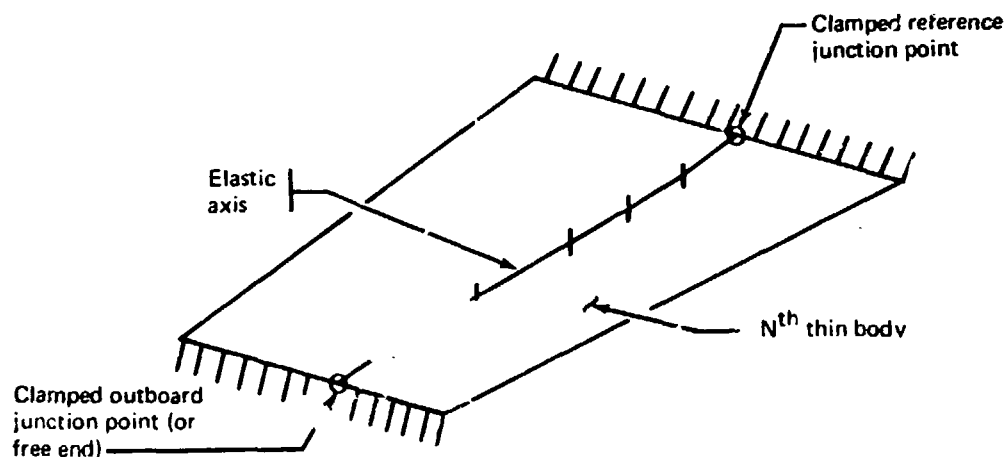


FIGURE 4.3-12.—THIN BODY CLAMPED AT ITS JUNCTION POINTS

4.3.1.9 Slender body finite element stiffness matrices.—The partition of the composite stiffness matrix, equation (4.3-9), for slender bodies is derived as follows: The elastic axes of slender bodies are made up of elastic axis segments which lie along the centerlines of the slender bodies, figure 4.3-7. The stiffness characteristics of all elastic axis elements are therefore described in the Reference Axis System.

The elastic axis segments of slender bodies have finite torsional stiffness and finite bending stiffness for bending in any direction. Slender bodies, however, are assumed to be infinitely rigid for extension of the centerline. The components of nodal displacements at the α^{th} , typical, node on the body, figure 4.3-13, are as follows:

$$\{\delta_{\alpha}\} \equiv \begin{bmatrix} d_Y \\ d_Z \\ \theta_X \\ \theta_Y \\ \theta_Z \end{bmatrix}_{\alpha} \quad (4.3-18)$$

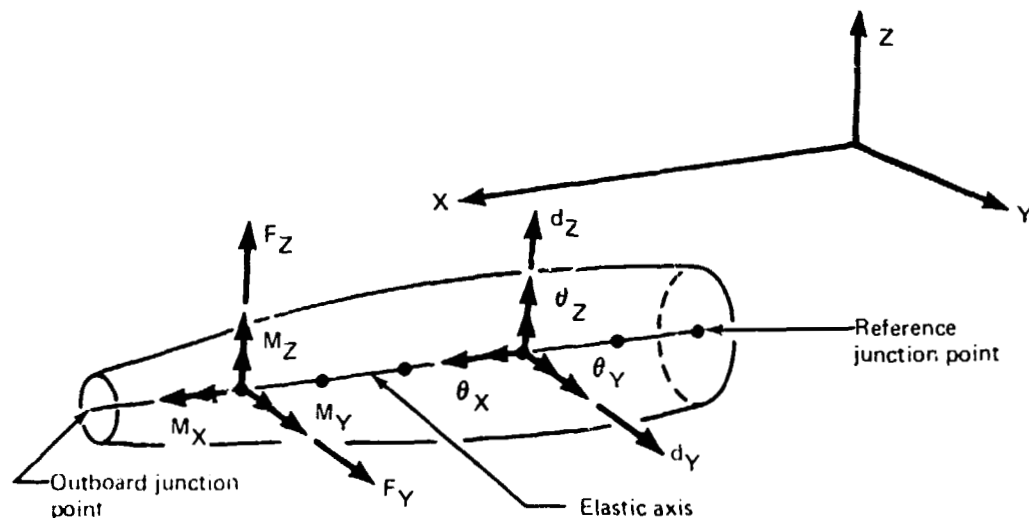


FIGURE 4.3-13. —NODAL FORCES AND DISPLACEMENTS AT NODES ON SLENDER BODIES

while the components of nodal force at the α^{th} node are given by

$$\{Q_\alpha\} \equiv \begin{bmatrix} F_Y \\ F_Z \\ M_X \\ M_Y \\ M_Z \end{bmatrix}_\alpha \quad (4.3-19)$$

The stiffness matrix for the elastic axis element between nodes α and $(\alpha + 1)$ on the j^{th} segment of the M^{th} slender body is given by the following:

$$\begin{bmatrix} [K_{\alpha\alpha}] & [K_{\alpha\ \alpha+1}] \\ [K_{\alpha+1\ \alpha}] & [K_{\alpha+1\ \alpha+1}] \end{bmatrix} \equiv \quad (4.3-20)$$

$\frac{12EI_Z}{(\Delta L)^3}$							
0	$\frac{12EI_Y}{(\Delta L)^3}$						
0	0	$\frac{GJ}{\Delta L}$			Sym.		
0	$-\frac{6EI_Y}{(\Delta L)^2}$	0	$\frac{4FI_Y}{\Delta L}$				
$\frac{6EI_Z}{(\Delta L)^2}$	0	0	0	$-\frac{4EI_Z}{\Delta L}$			
$-\frac{12EI_Z}{(\Delta L)^3}$	0	0	0	$-\frac{6EI_Z}{(\Delta L)^2}$	$\frac{12EI_Z}{(\Delta L)^3}$		
0	$-\frac{12EI_Y}{(\Delta L)^3}$	0	$\frac{6EI_Y}{(\Delta L)^2}$	0	0	$\frac{12FI_Y}{(\Delta L)^3}$	
0	0	$-\frac{GJ}{\Delta L}$	0	0	0	0	$\frac{GJ}{\Delta L}$
0	$-\frac{6EI_Y}{(\Delta L)^2}$	0	$\frac{2EI_Y}{\Delta L}$	0	0	$-\frac{6EI_Y}{(\Delta L)^2}$	$\frac{4EI_Y}{\Delta L}$
$\frac{6EI_Z}{(\Delta L)^2}$	0	0	0	$\frac{2EI_Z}{\Delta L}$	$-\frac{6EI_Z}{(\Delta L)^2}$	0	0
						0	$\frac{4EI_Z}{\Delta L}$

where for the M_j^{th} elastic axis element $EI_Y \equiv EI_Y(M_j)$ is the bending stiffness about the Y-axis, $EI_Z \equiv EI_Z(M_j)$ is the bending stiffness about the Z-axis, $GJ \equiv GJ(M_j)$ is the torsional stiffness, and

$$\Delta L \equiv \frac{L(M_j)}{\alpha(M_j) + 1} \quad (4.3-3)$$

is the length of the elastic axis element.

4.3.1.10 Slender body composite stiffness matrix.—Since all elements of elastic axis lie on the mean centerline of the slender body and are colinear, the composite stiffness matrix for two adjacent elements is found by a direct application of the operations leading to equation (4.2-7). Repetition of the operations for all elements of the M^{th} slender body, with the reference junction point numbered R and the outboard junction point numbered S, leads to the following composite stiffness relationship:

$$\begin{bmatrix} \{T_R\} \\ \{0\} \\ \{T_S\} \end{bmatrix} = \begin{bmatrix} [K_{RR}] & [K_{RM}] & [0] \\ [K_{MR}] & [K_{MM}] & [K_{MS}] \\ [0] & [K_{SM}] & [K_{SS}] \end{bmatrix} \begin{bmatrix} \{\delta_R\} \\ \{\delta_M\} \\ \{\delta_S\} \end{bmatrix} - \begin{bmatrix} \{Q_R\} \\ \{Q_M\} \\ \{Q_S\} \end{bmatrix} \quad (4.3-21)$$

where $[K_{RR}]$ and $[K_{SS}]$ are the stiffnesses for nodal forces and displacements at the junction points; $[K_{MM}]$ is the composite stiffness matrix for all nodes on the M^{th} slender body (exclusive of the junction point nodes); and $[K_{RM}]$, $[K_{MR}]$, $[K_{SM}]$, and $[K_{MS}]$ are coupling of nodal forces and displacements at the junction points with the nodal forces $\{Q_M\}$ and displacements $\{\delta_M\}$ at nodes on the slender body.

The composite stiffness matrix $[K_{MM}]$ represents the structure of the M^{th} slender body as if it were clamped at its junction points, figure 4.3-14. Matrices of this form are generated, and the slender body partition of composite stiffness matrix for the complete structure, equation (4.3-9), contains these matrices arranged on the diagonal as follows:

(4.3-22)

$$\begin{bmatrix} \text{Slender Body} \\ \text{Partition of} \\ \text{Eqn. (4.3-9)} \end{bmatrix} \equiv \begin{bmatrix} [K_{11}] & & & \text{Zeros} \\ & [K_{22}] & & \\ & & \ddots & \\ \text{Zeros} & & & [K_{MM}] \end{bmatrix}$$

when the partition is expressed for M slender bodies.

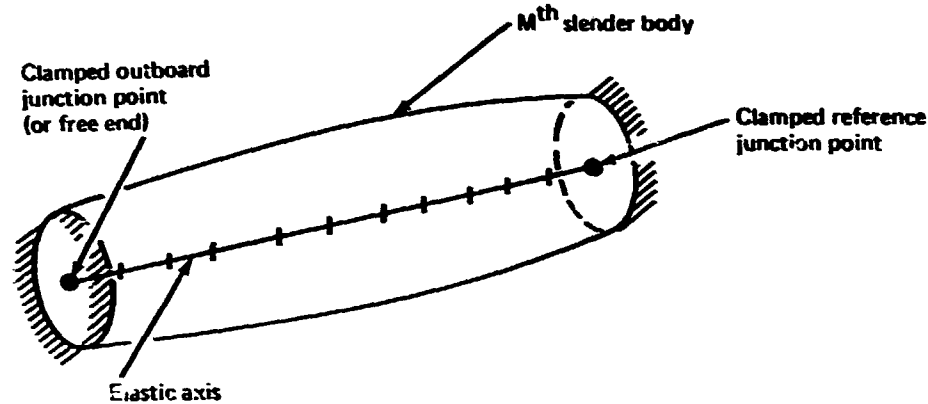


FIGURE 4.3-14.—SLENDER BODY CLAMPED AT ITS JUNCTION POINTS

4.3.1.11 Junction point stiffness matrices.—The elements of the composite stiffness matrix, equation (4.3-9), related to the junction points of the structure are developed in this section. From the partitions identified in equation (4.3-9) it will be recalled that the junction points are separated into three types: the reference junction point of the structure, general junction points, and coplanar thin body junction points. In deriving the junction point stiffness matrices a further separation is introduced. General junction points joining only thin bodies must be treated separately from those which join at least one slender body.

Consider a junction point where only thin bodies are joined, such as the example shown in figure 4.3-15. Only one of the thin body junction points is an outboard junction point at the Q^{th} structural junction point node: that of the N^{th} thin body. From section 4.3.1.1 it will be recalled that the elastic axis segments of all of the joining thin bodies lie in the same plane parallel to the Y,Z plane of the Reference Axis System. As a result, the components of nodal force and displacement at

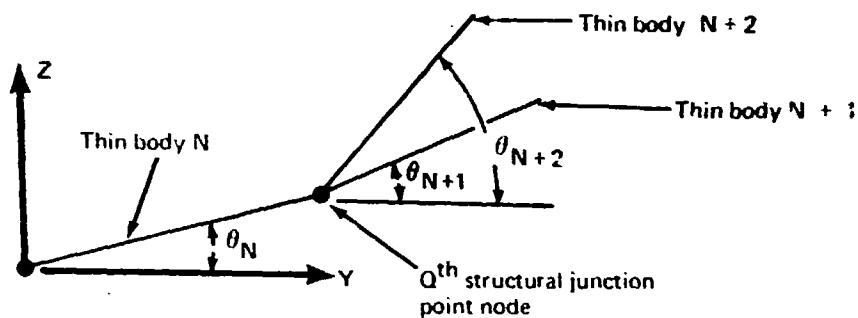


FIGURE 4.3-15.—JUNCTION POINT NODE JOINING THIN BODIES

the outboard junction point node of the N^{th} thin body and at the reference junction point node of the other joining thin bodies are expanded on the local thin body coordinate systems. To make them consistent, all components are transformed to the local thin body coordinate system of the thin body, which is joined by its outboard junction point, the N^{th} thin body in the example.

The components of nodal forces and displacement at the outboard junction point of the N^{th} thin body are given as

$$\{\delta_Q(N)\} \equiv \begin{bmatrix} d_{ZN} \\ e_{XN} \\ \theta_{YN} \end{bmatrix}_Q \quad (4.3-23)$$

and

$$\{Q_Q(N)\} \equiv \begin{bmatrix} F_{ZN} \\ M_{XN} \\ M_{YN} \end{bmatrix}_Q \quad (4.3-24)$$

The components of nodal forces and displacements at the reference junction point of thin body $N+1$ are transformed to the local thin body axis system of the thin body N as follows:

$$\{\delta_Q(N)\} = [\gamma(N+1, N)] \{\delta_Q(N+1)\} \quad (4.3-25)$$

and

$$\{Q_Q(N)\} = [\gamma(N+1, N)] \{Q_Q(N+1)\}$$

where the transformation matrix is a partition of the orthogonal transformation matrix for rotation about the X-axis and is given by

$$[\gamma(N+1, N)] \equiv \begin{bmatrix} \cos(\theta_{N+1} - \theta_N) & 0 & 0 \\ 0 & 1 & 0 \\ 0 & 0 & \cos(\theta_{N+1} - \theta_N) \end{bmatrix}$$

The element stiffness relation for the elastic axis finite element on thin body N+1 which connects the reference junction point node to node Q on the elastic axis has the following form: (4.3-26)

$$\begin{bmatrix} \{T_Q(N+1)\} \\ \{T_1(N+1)\} \end{bmatrix} = \begin{bmatrix} [K_{QQ}^{N+1}] & [K_{Q1}^{N+1}] \\ [K_{1Q}^{N+1}] & [K_{11}^{N+1}] \end{bmatrix} \begin{bmatrix} \{\delta_Q(N+1)\} \\ \{\delta_1(N+1)\} \end{bmatrix} - \begin{bmatrix} \{Q_Q(N+1)\} \\ \{Q_1(N+1)\} \end{bmatrix}$$

The transformation, equation (4.3-25), is applied to this expression to find

$$\begin{bmatrix} [\gamma(N+1,N)]\{T_Q(N+1)\} \\ \{T_1(N+1)\} \end{bmatrix} = \quad (4.3-27)$$

$$\begin{bmatrix} [\gamma(N+1,N)][K_{QQ}^{N+1}][\gamma(N+1,N)]^T & [\gamma(N+1,N)][K_{Q1}^{N+1}] \\ [K_{1Q}^{N+1}][\gamma(N+1,N)]^T & [K_{11}^{N+1}] \end{bmatrix} \times \begin{bmatrix} [\gamma(N+1,N)]\{\delta_Q(N+1)\} \\ \{\delta_1(N+1)\} \end{bmatrix} - \begin{bmatrix} [\gamma(N+1,N)]\{Q_Q(N+1)\} \\ \{Q_1(N+1)\} \end{bmatrix}$$

as a consequence of equation (4.3-25). (4.3-28)

$$\begin{bmatrix} \{T_Q(N)\} \\ \{T_1(N+1)\} \end{bmatrix} = \begin{bmatrix} [\gamma(N+1,N)][K_{QQ}^{N+1}][\gamma(N+1,N)]^T & [\gamma(N+1,N)][K_{Q1}^{N+1}] \\ [K_{1Q}^{N+1}][\gamma(N+1,N)]^T & [K_{11}^{N+1}] \end{bmatrix} \times \begin{bmatrix} \{\delta_Q(N)\} \\ \{\delta_1(N+1)\} \end{bmatrix} - \begin{bmatrix} \{Q_Q(N)\} \\ \{Q_1(N+1)\} \end{bmatrix}$$

When the three thin bodies shown by figure 4.3-15 are assembled at the junction point, the following stiffness relation describes the stiffness at the junction point:

$$\{Q_Q\} = [K_{QQ}]\{\delta_Q\} \quad (4.3-29)$$

where

$$[K_{QQ}] = [K_{QQ}^N] + [\gamma(N+1,N)][K_{QQ}^{N+1}][\gamma(N+1,N)]^T + [\gamma(N+2,N)][K_{QQ}^{N+2}][\gamma(N+2,N)]^T$$

$$\begin{array}{c|c|c|c}
 & [K_{QP}^N][\gamma(N+1, N)] & [K_{Qi}^{N+1}] & [\gamma(N+2, N)][K_{Qj}^{N+2}] \\
 \hline
 [K_{PQ}^{N+1}] & & & \\
 \hline
 [K_{iQ}^{N+1}][\gamma(N+1, N)]^T & & & \\
 \hline
 [K_{jQ}^{N+2}][\gamma(N+2, N)]^T & & & \\
 \hline
 & & & (4.3-30)
 \end{array}$$

At general junction points where at least one slender body is joined, the nodal forces and displacements are transformed to the Reference Axis System. The components at all nodes on slender bodies are expressed in the Reference Axis System, section 2.2.4 hence, only nodal force and displacement components at the reference and outboard junction point nodes of thin bodies are derived in the local thin body axis systems and require transformation. They are transformed to the Reference Axis System as follows:

and

where the transformation matrix is a partition of the orthogonal transformation matrix for rotation about the X-axis and is given by

4-69

Consider the example of the N^{th} thin body joined at its reference junction point to the outboard junction point of the M^{th} slender body at structural junction point node P, figure 4.3-16. The composite stiffness relation for the node is found as

$$\{Q_P\} = [K_{PP}]\{\delta_P\} \quad (4.3-34)$$

where

$$[K_{PP}] = [K_{PP}^M] + [\gamma_N][K_{PP}^N][\gamma_N]^T. \quad (4.3-35)$$

The stiffness matrix $[K_{PP}]$ appears in the general junction point partition of equation (4.3-9) and the following stiffness matrices are introduced into the coupling partitions:

$$\begin{array}{c|c} [K_{PP}^M] & [\gamma_N][K_{PP}^N] \\ \hline [K_{nP}] & | \\ \hline [K_{nP}^N][\gamma_N]^T & | \end{array} \quad (4.3-36)$$

where n is the number of the node nearest the outboard junction point node of the slender body.

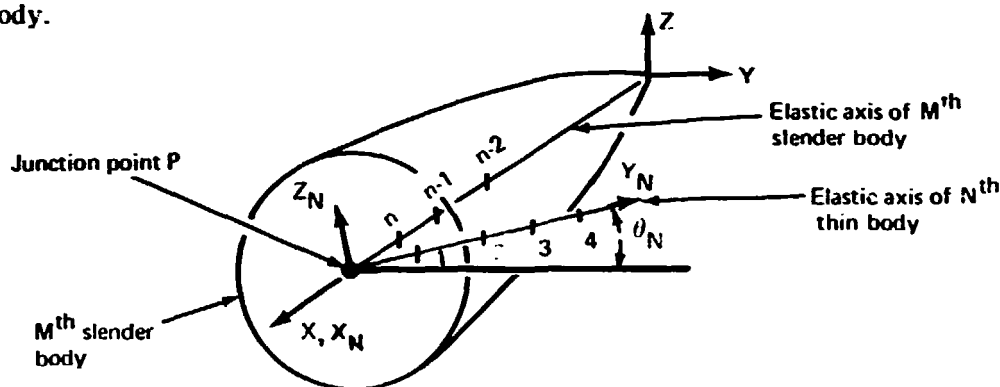


FIGURE 4.3-16.—JUNCTION POINT JOINING A SLENDER BODY

4.3.1.12 Reference junction point for the structure. As noted in section 4.3.1.3, the reference junction point for the entire aircraft structure is the reference junction point of a single slender body, figure 4.3-9. The junction points of no other thin or slender bodies may be joined to this structural junction point. Even if a configuration consists of a wing alone, figure 4.3-17, a slender body on the plane of symmetry must be appended to the structure in order that a reference junction point for the entire structure may be included in the formulation.

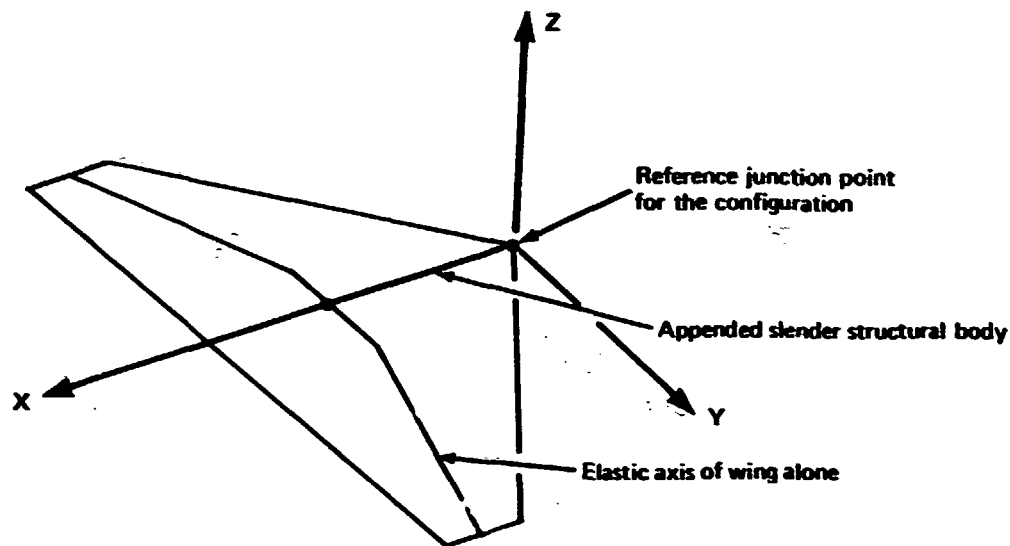


FIGURE 4.3-17.—STRUCTURAL REPRESENTATION OF A WING ALONE

4.3.1.13 Coplanar thin body junction points.—The composite stiffness relation for the nodal forces and displacements at a coplanar thin body junction point is of the same form as that given by equation (4.3-15). These junction point nodes are treated nearly like an elastic axis segment node. The sole difference is that the nodes at the ends of two thin body elastic axes meeting at a coplanar thin body junction point are designated the outboard junction point of one thin structural body and the reference junction point of the other thin structural body, figure 4.3-18. Recalling equation (4.3-15), designating the two joining thin structural bodies as N and $N + 1$ and the coplanar thin body junction point as P results in

$$\begin{bmatrix} \{T_n(i-1)\} \\ \{0\} \\ \{T_1(i)\} \end{bmatrix} = \begin{bmatrix} [K'_{nn}] & [K'_{np}] & [0] \\ [K'_{pn}] & [K'_{pp}] + [\lambda(i-1,i)][K_{pp}][\lambda(i-1,i)]^T & [\lambda(i-1,i)][K_{p1}] \\ 0 & [K_{1p}][\lambda(i-1,i)]^T & [K_{11}] \end{bmatrix} \times \begin{bmatrix} \{\delta_n(i-1)\} \\ \{\delta_p(i-1)\} \\ \{\delta_1(i)\} \end{bmatrix} - \begin{bmatrix} \{Q_n(i-1)\} \\ \{Q_p(i-1)\} \\ \{Q_1(i)\} \end{bmatrix} \quad (4.3-37)$$

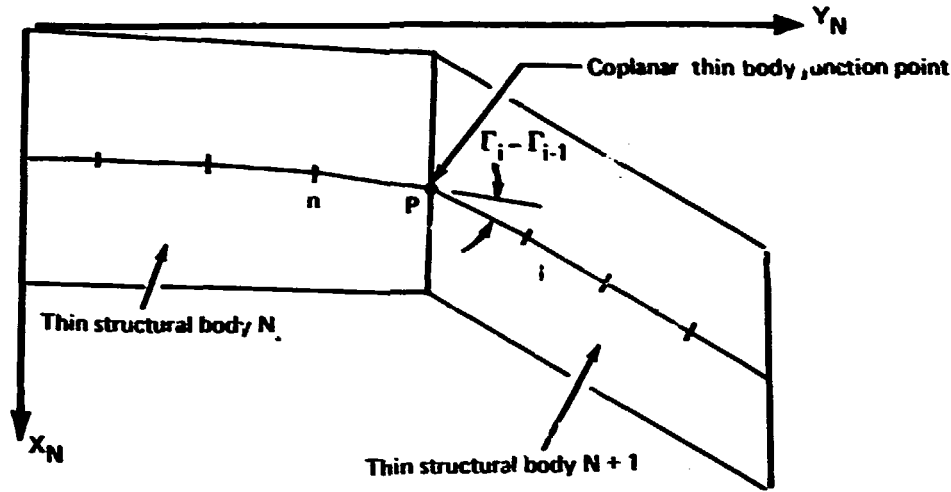


FIGURE 4.3-18.—COPLANAR THIN BODY JUNCTION POINT CONNECTING TWO THIN STRUCTURAL BODIES BELONGING TO THE SAME THIN AERODYNAMIC BODY

where

$$[\lambda(i, i-1)] \equiv \begin{bmatrix} 1 & 0 & 0 \\ 0 & \cos(\Gamma_i - \Gamma_{i-1}) & -\sin(\Gamma_i - \Gamma_{i-1}) \\ 0 & \sin(\Gamma_i - \Gamma_{i-1}) & \cos(\Gamma_i - \Gamma_{i-1}) \end{bmatrix}$$

and Γ_{i-1} and Γ_i are the sweep angles of the elastic axis segments adjacent to the junction point, figure 4.3-18.

The partitions of the composite stiffness matrix, equation (4.3-37), which enters the coplanar thin body junction point partition and corresponding coupling partitions of equation (4.3-9), are as follows:

$$[K_{pp}] \equiv [K'_{pp}] + [\lambda(i, i-1)][K_{pp}][\lambda(i, i-1)]^T \quad (4.3-38)$$

appears on the diagonal of the coplanar thin body junction point partition.

$[K'_{np}]$ represents coupling with the M^{th} slender body, and

$[K_{1p}]$ represents coupling with the N^{th} thin body.

The remaining elements of the composite stiffness matrix of equation (4.3-37) are members of the partitions for thin bodies in equation (4.3-9).

4.3.1.14 Plane of structural symmetry. -- All configurations which are analyzed by the FLEXSTAB system must have a plane of geometric, structural, and inertial symmetry. The composite stiffness relation for the structure, i.e.,

$$\{Q\} = [K]\{\delta\}, \quad (4.2-14)$$

and the composite stiffness matrix, equation (4.3-9), are expressed in terms of nodal forces and displacements at nodes on the plane of symmetry and on the right-hand side of the aircraft. Two composite stiffness relations are developed as noted in section 4.2.5. One assumes that the nodal forces and displacements are symmetric functions of the Y-coordinate. The other assumes that the nodal forces and displacements are antisymmetric functions of the Y-coordinate, and the two composite stiffness relations are denoted as follows:

$$\{Q\}^S = [K]^S \{\delta\}^S \quad \text{symmetric} \quad (4.3-39)$$

and

$$\{Q\}^A = [K]^A \{\delta\}^A \quad \text{anti-symmetric} \quad (4.3-40)$$

4.3.1.15 Special consideration for nodes on the plane of symmetry. --

- The stiffnesses of elastic axes of bodies lying on the plane of symmetry are reduced by one-half when the composite stiffness matrix is formulated.*
- In the symmetric case the components of nodal displacement d_Y , θ_X , and θ_Z are set to zero for nodes on the plane of symmetry.
- In the antisymmetric case the components of nodal displacement d_Z and θ_Y are set to zero for nodes on the plane of symmetry.

As a consequence of the above, nodal forces and displacements at nodes on thin bodies lying on the plane of symmetry, e.g., a conventional vertical tail, do not appear in the symmetric form of the composite stiffness relation, equation (4.3-39).

4.3.2 Reduction of the Composite Stiffness Matrix

4.3.2.1 Composite stiffness matrix partitions. -- Certain nodal components of force contained in $\{Q\}$, i.e., the nodal forces generated by the composite stiffness matrix, equation (4.3-8), are always set to zero. This is the case with the nodal forces at coplanar thin body junction points. The objective here is to remove these nodal forces from the stiffness relation. To accomplish this objective the composite stiffness relation for the structure is partitioned according to equation (4.3-9) as follows:

*Stiffnesses of elastic axes on the plane of symmetry are input as full valued

$$\begin{bmatrix} \{Q_R^*\} \\ \{Q_J^*\} \\ \{Q_C\} \\ \{Q_B^*\} \\ \{Q_W^*\} \end{bmatrix} = \begin{bmatrix} [K_{RR}] [K_{RJ}] [K_{RC}] [K_{RB}] [K_{RW}] \\ [K_{JR}] [K_{JJ}] [K_{JC}] [K_{JB}] [K_{JW}] \\ [K_{CR}] [K_{CJ}] [K_{CC}] [K_{CB}] [K_{CW}] \\ [K_{BR}] [K_{BJ}] [K_{BC}] [K_{BB}] [K_{BW}] \\ [K_{WR}] [K_{WJ}] [K_{WC}] [K_{WB}] [K_{WW}] \end{bmatrix} \begin{bmatrix} \{\delta_R^*\} \\ \{\delta_J^*\} \\ \{\delta_C\} \\ \{\delta_B^*\} \\ \{\delta_W^*\} \end{bmatrix} \quad (4.3-41)$$

where $\{Q_C\}$ are the nodal forces at the coplanar junction points. Letting these nodal forces vanish, i.e.,

$$\{Q_C\} = \{0\}.$$

Equation (4.3-41) reduces to the following

$$\{Q^*\} = [\bar{K}]\{\delta^*\} \quad (4.3-42)$$

where

$$\{Q^*\} \equiv \begin{bmatrix} \{Q_R^*\} \\ \{Q_J^*\} \\ \{Q_B^*\} \\ \{Q_W^*\} \end{bmatrix} \quad (4.3-43)$$

and

$$\{\delta^*\} \equiv \begin{bmatrix} \{\delta_R^*\} \\ \{\delta_J^*\} \\ \{\delta_B^*\} \\ \{\delta_W^*\} \end{bmatrix}. \quad (4.3-44)$$

Note that the superscript asterisk is not used to indicate a relationship with the quantities appearing on equations (4.2-100) and (4.2-101).

The asterisk is used in the partitions of equations (4.3-43) and (4.3-44) to indicate that these quantities are generated by the composite stiffness matrix as given by equation (4.3-42) rather than those generated by equation (4.3-8). Equation (4.3-42) represents the stiffness matrix for the structure in terms of independent nodal displacement components and in terms of applied nodal force components which are non-zero. It is formulated for the symmetric and antisymmetric cases described by sections 4.2.5 and 4.3.1.14 so that forms corresponding to equations (4.3-39) and (4.3-40) are obtained. In either case, however, the stiffness matrix is square and singular.

4.3.2.2 Structural node point degrees of freedom.—The structural node point degrees of freedom represented by $\{\delta^*\}$ in equation (4.3-44), i.e., the components of nodal displacement contained in this matrix, are independent elastic degrees of freedom, and an element of $\{\delta^*\}$ may be assigned any value independent of the values assigned to the other elements. This linear independence is achieved as a result of the special choice of coordinate systems at the various types of structural nodes introduced in the preceding. Table 4.3-1 summarizes the coordinate systems used in expanding the nodal displacement and force components, the independent elastic degrees of freedom, and the constrained degrees of freedom at junction points listing this information for each type of node identified by its location. This separation of nodal degrees of freedom at junction point nodes into independent elastic and constrained degrees of freedom is introduced into the notation by letting all six degrees of freedom at a junction point, e.g., the p^{th} junction point, be expressed as

$$\{\delta_p\} \equiv \begin{bmatrix} d_{X_p} \\ \{\delta_p^*\} \end{bmatrix} \quad (4.3-45)$$

where the elements of $\{\delta_p^*\}$ are the independent elastic degrees of freedom and d_{X_p} is a constrained degree of freedom.

4.3.3 Displacement Relations for Beam Finite Elements

In this section the displacement relations, equation (4.2-7), are derived for the beam theory used in FLEXSTAB. They are required to evaluate the nodal mass matrix, equation (4.2-18), as well as the transformations appearing in sections 4.2.6 through 4.2.8 as equations (4.2-100), (4.2-101), (4.2-116), (4.2-119), and (4.2-120).

The derivation of the displacement relations for the beam theory finite elements is complicated by the assumed partial rigidities of the thin and slender structural bodies. In item (c), section 4.2.2.1, it was assumed that the displacement relations could be expressed for each finite element of the structure as

$$\{d^a\} = [r^a]\{\delta^a\} \quad (4.2-5)$$

TABLE 4.3.1.—SUMMARY OF STRUCTURAL NODE POINT DEGREES OF FREEDOM

Node location	Independent elastic degrees of freedom	Constrained degrees of freedom	Coordinate system
N th thin body elastic axis, node on i th segment of elastic axis	$d_{zNi}, \theta_{xNi}, \theta_{yNi}$	$d_{xNi}, d_{yNi}, \theta_{zNi}$	Local elastic axis segment system, figures 4.3.4 and 4.3.6
M th slender body elastic axis, node on elastic axis	$d_Y, d_Z, \theta_X, \theta_Y, \theta_Z$	d_X	Reference axis system, figure 2.2.2
Junction point node which is the outboard junction point of a thin body—the N th thin body	$d_{ZN}, \theta_{xN}, \theta_{yN}$	$d_{xN}, d_{yN}, \theta_{zN}$	n th thin body local axis system, figures 4.3.4 and 4.3.6
Junction point node which is the outboard junction point of a slender body—the M th slender body	$d_Y, d_Z, \theta_X, \theta_Y, \theta_Z$	d_X	Reference axis system, figures 4.3.13 and 4.3.16
Reference junction point for the entire structure	$d_Y, d_Z, \theta_X, \theta_Y, \theta_Z$	d_X	Reference axis system, figures 4.3.13 and 4.3.17

where $\{d^a\}$ represents three components of elastic deformation, equation (4.2-6), at points interior to the a^{th} finite element. The finite elements of the beam theory are sections of the thin and slender bodies between node points, figure 4.3-19. Because of the assumed rigidities, however, displacement relations in terms of the nodal displacements at the nodes of the beam finite elements cannot provide a complete description of the finite element displacement. The displacement relations for the beam finite elements are expressed as

(4.3-46)

$$\{d_e^a\} = [N_e^a]\{\delta_e^{*a}\}$$

where elements of $\{\delta_e^{*a}\}$ represent the independent elastic degrees of freedom, table 4.3-1, at the nodes of the a^{th} beam finite element expressed in the local axis system of the elastic axis, figure 4.3-5. The total displacement of the a^{th} finite element is, however, the sum of the displacement given by equation (4.3-46) and a constrained displacement relative to the reference junction point of the body on which the a^{th} element is located, i.e.,

(4.3-47)

$$\{d^N\}_C = [N_C^N]\{\delta_P\}$$

The total displacement of the a^{th} finite element on the N^{th} structural body is, therefore, given by the following:

(4.3-48)

$$\{d^a\} = [N_e^a]\{\delta_e^{*a}\} + [N_C^N]\{\delta_P\}$$

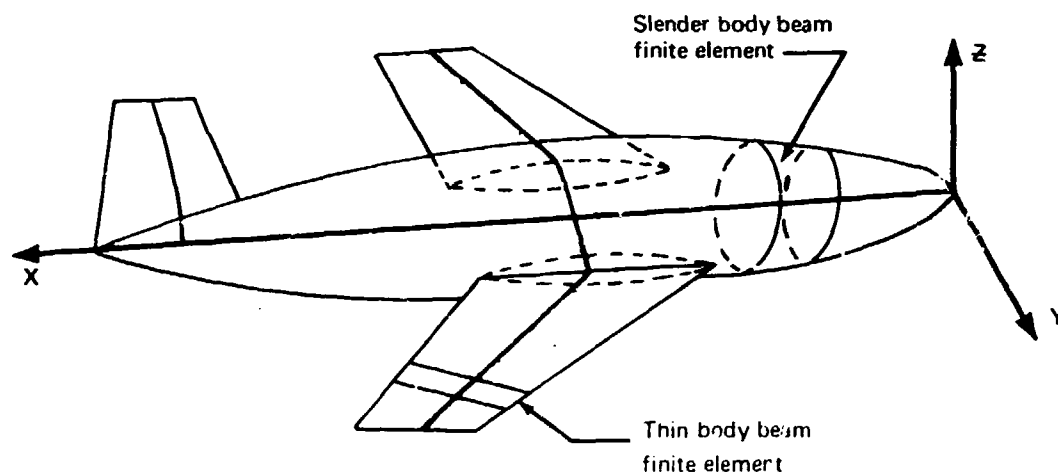


FIGURE 4.3-19. —THIN AND SLENDER BODY BEAM FINITE ELEMENTS

when the reference junction point of the body is at the P^{th} junction point node of the structure.

4.3.3.1 Constrained displacement relations.—The constrained displacements denoted by equation (4.3-47) for thin and slender structural bodies are shown by figures 4.3-20 and 4.3-21. The constrained degrees of freedom for thin structural bodies, e.g., the N^{th} thin body, are d_{X_N} , d_{Y_N} , θ_{Z_N} , and the points i with the coordinates $X_N(i)$, $Y_N(i)$ relative to the reference junction point of the body undergo the following constrained displacements:

$$d_{X_N}(i) = d_{X_{N_P}} - Y_N(i)\theta_{Z_{N_P}} \quad (4.3-49)$$

$$d_{Y_N}(i) = d_{Y_{N_P}} + X_N(i)\theta_{Z_{N_P}}.$$

The only constrained degree of freedom for the slender structural bodies, e.g., the M^{th} slender body, is d_X , and all points such as the j^{th} point of a slender body undergo the following constrained displacement:

$$d_X(j) = d_{X_P} \quad (4.3-50)$$

where the reference junction point of the body is assumed to be the P^{th} junction point node of the structure.

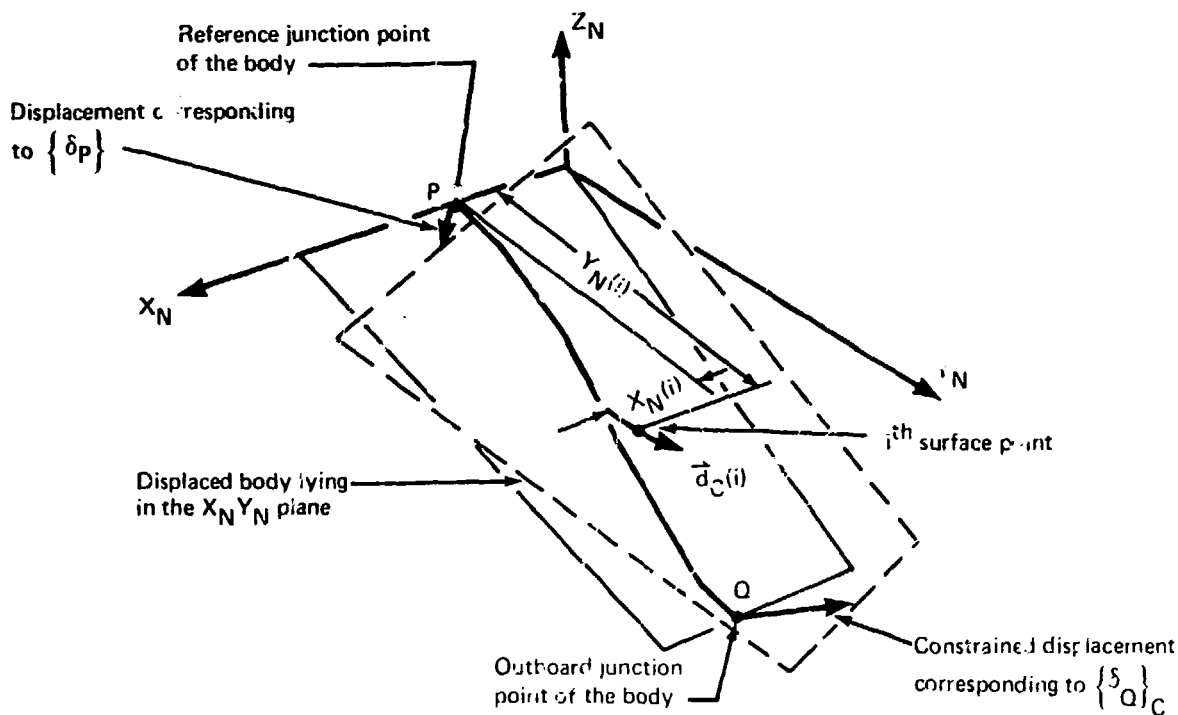


FIGURE 4.3-20.—CONSTRAINED DISPLACEMENT OF A THIN BODY

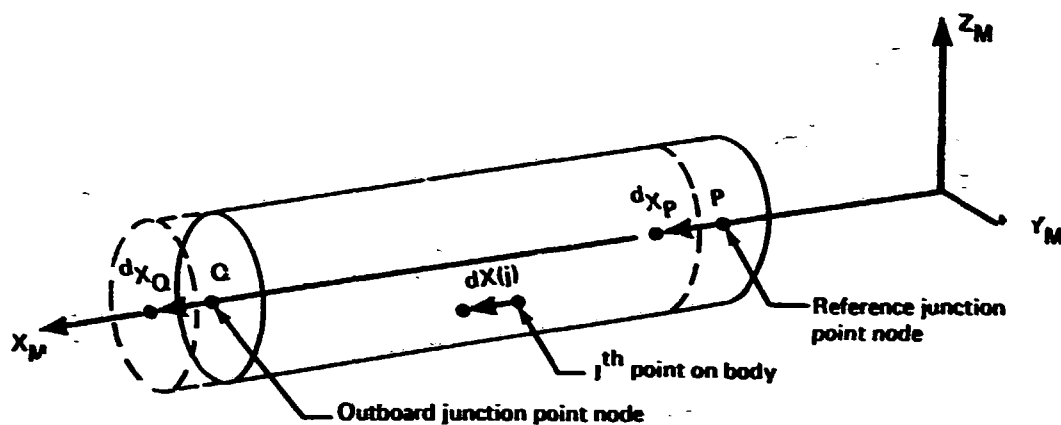


FIGURE 4.3-21.—CONSTRAINED DISPLACEMENT OF A SLENDER BODY

The constrained displacement relations for thin and slender structural bodies are derived from equations (4.3-49) and (4.3-50), respectively. In either case, the reference junction point node of the body has six degrees of freedom expanded on the Reference Axis System, i.e.,

$$\{\delta_P\}^T \equiv [d_{X_P}, d_{Y_P}, d_{Z_P}, \theta_{X_P}, \theta_{Y_P}, \theta_{Z_P}] \quad (4.3-51)$$

For the N^{th} thin structural body having dihedral angle θ_N the matrix $[N_C^N]$ evaluated at the i^{th} surface point, figure 4.3-20, has the following elements:

$$[N_C^N] = \begin{bmatrix} 1 & 0 & 0 & 0 & Y_N(i)\sin\theta_N & -Y_N(i)\cos\theta_N \\ 0 & \cos\theta_N & \sin\theta_N & 0 & -X_N(i)\sin\theta_N & X_N(i)\cos\theta_N \\ 0 & 0 & 0 & 0 & 0 & 0 \end{bmatrix} \quad (4.3-52)$$

For the M^{th} slender structural body the matrix $[N_C^M]$ is given simply as

$$[N_C^M] = \begin{bmatrix} 1 & 0 & 0 & 0 & 0 & 0 \\ 0 & 0 & 0 & 0 & 0 & 0 \\ 0 & 0 & 0 & 0 & 0 & 0 \end{bmatrix} \quad (4.3-53)$$

The components of displacement contained in $\{\delta_P\}$ represent a combination of independent elastic degrees of freedom and constrained degrees of freedom at the structural junction point node. As shown in table 4.3-1, the independent elastic and constrained degrees of freedom at the structural junction point node are those of the body whose outboard junction point is at the node. Constrained motion of the outboard junction point $\{\delta_Q\}_C$ is the result of a rigid connection with the reference junction point of the body. The displacement of the Q^{th} junction point node may therefore be expressed as follows:

$$\{\delta_Q\} = [T_{QQ}^*]\{\delta_Q^*\} + [T_{QP}^*]\{\delta_P\} \quad (4.3-54)$$

where the matrix $[T_{QQ}^*]$ transforms the independent degrees of freedom at the Q^{th} junction point node to the Reference Axis System and introduces zeros for the constrained degrees of freedom while the matrix $[T_{QP}^*]$ is obtained from equations (4.3-52) and (4.3-53) evaluated at the coordinates of the outboard junction point, viz.,

$$\{\delta_Q\}_C = [T_{QP}^*]\{\delta_P\}. \quad (4.3-55)$$

Assume that the structural body providing the outboard junction point at the Q^{th} structural junction point node is the $(N-1)^{\text{th}}$ thin body having dihedral angle θ_{N-1} . The independent elastic degrees of freedom at the junction point node are d_{ZN-1} , θ_{XN-1} , θ_{YN-1} (table 4.3-1), and the elements of $[T_{QQ}^*]$ are as follows:

$$[T_{QQ}^*] = \begin{bmatrix} 0 & 0 & 0 \\ -\sin\theta_{N-1} & 0 & 0 \\ \cos\theta_{N-1} & 0 & 0 \\ 0 & 1 & 0 \\ 0 & 0 & \cos\theta_{N-1} \\ 0 & 0 & \sin\theta_{N-1} \end{bmatrix} \quad (4.3-56)$$

For the same arrangement, the elements of $[T_{QP}^*]$ are

$$[T_{QP}^*] = \begin{bmatrix} 1 & 0 & 0 & Y_{N-1}(PQ)\sin\theta_{N-1} & -Y_{N-1}(PQ)\cos\theta_{N-1} \\ 0 & \cos^2\theta_{N-1} & \cos\theta_{N-1} & -X_{N-1}(PQ)\cos\theta_{N-1} & X_{N-1}(PQ)\cos^2\theta_{N-1} \\ & & \times \sin\theta_{N-1} & \times \sin\theta_{N-1} & \\ 0 & \cos\theta_{N-1} & \sin^2\theta_{N-1} & -X_{N-1}\sin^2\theta_{N-1} & X_{N-1}\cos\theta_{N-1} \\ & \times \sin\theta_{N-1} & & & \times \sin\theta_{N-1} \\ 0 & 0 & 0 & 0 & 0 \\ 0 & 0 & 0 & \sin^2\theta_{N-1} & -\sin\theta_{N-1} \\ & & & & \times \cos\theta_{N-1} \\ 0 & 0 & 0 & -\sin\theta_{N-1} & \cos^2\theta_{N-1} \\ & & & \times \cos\theta_{N-1} & \end{bmatrix} \quad (4.3-57)$$

where $X_{N-1}(PQ)$ and $Y_{N-1}(PQ)$ are the coordinates of node point Q relative to node point P in the local body axis system of the $(N-1)^{\text{th}}$ thin structural body.

If the structural body providing the outboard junction point at the Q^{th} structural junction point node is the M^{th} slender body, then

$$[T_{QQ}^*] = \begin{bmatrix} 0 & 0 & 0 & 0 & 0 \\ 1 & 0 & 0 & 0 & 0 \\ 0 & 1 & 0 & 0 & 0 \\ 0 & 0 & 1 & 0 & 0 \\ 0 & 0 & 0 & 1 & 0 \\ 0 & 0 & 0 & 0 & 1 \end{bmatrix} \quad (4.3-58)$$

and

$$[T_{QP}^*] = \begin{bmatrix} 1 & 0 & 0 & 0 & 0 & 0 \\ 0 & 0 & 0 & 0 & 0 & 0 \\ 0 & 0 & 0 & 0 & 0 & 0 \\ 0 & 0 & 0 & 0 & 0 & 0 \\ 0 & 0 & 0 & 0 & 0 & 0 \\ 0 & 0 & 0 & 0 & 0 & 0 \end{bmatrix} \quad (4.3-59)$$

4.3.3.2 Example of combined constraint relations.—Consider a configuration consisting of four structural bodies, figure 4.3-22. The reference junction point of the configuration is junction point node R, and the reference and outboard junction point nodes of the bodies are denoted as follows:

<u>Body Number</u>	<u>Reference Junction Point Node</u>	<u>Outboard Junction Point Node</u>
1	R	P
2	P	S
3	S	Q
4	Q	T (Free End)

The nodal displacements at junction point node Q are given by

$$\{\delta_Q\} = [T_{QQ}^*]\{\delta_{eQ}^*\} + [T_{QS}^*]\{\delta_S\}, \quad (4.3-60)$$

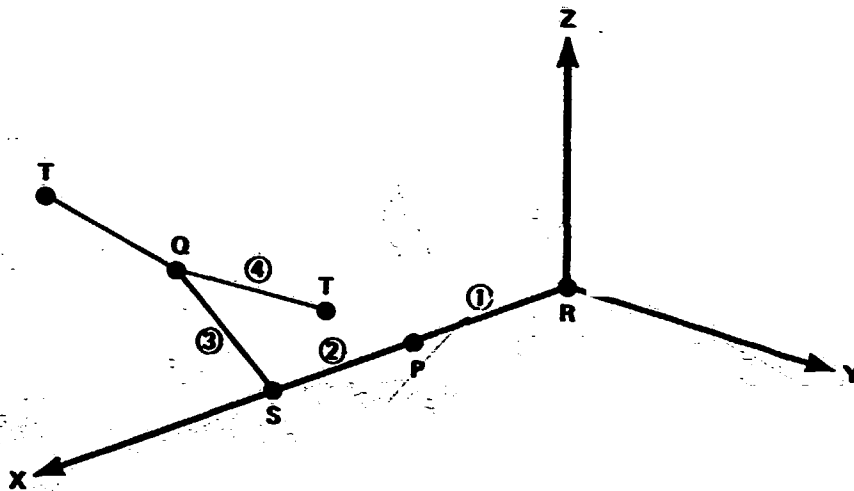


FIGURE 4.3-22—EXAMPLE STRUCTUR. CONFIGURATION

i.e., the nodal displacements due to elastic deformation at junction point node Q superimposed on the constrained displacements arising from nodal displacements at S. Similar relations are expressed for junction point nodes S and P as

$$\{\delta_S\} = [T_{SS}^*]\{\delta_{eS}^*\} + [T_{SP}^*]\{\delta_P\} \quad (4.3-61)$$

and

$$\{\delta_P\} = [T_{PP}^*]\{\delta_{eP}^*\} + [T_{PR}^*]\{\delta_R\}. \quad (4.3-62)$$

These three equations are combined to describe the junction point nodal displacements at Q, S, and P in terms of d_{xR} (viz., the reference junction point of the structure) and the elastic nodal displacements at the junction point nodes Q, S, and P as follows:

$$\begin{aligned} \{\delta_Q\} &= [T_{QQ}^*]\{\delta_{eQ}^*\} + [T_{QS}^*][T_{SS}^*]\{\delta_{eS}^*\} \\ &\quad + [T_{QS}^*][T_{SP}^*][T_{PP}^*]\{\delta_{eP}^*\} \\ &\quad + [T_{QS}^*][T_{SP}^*][T_{PR}^*]\{\delta_R\} \end{aligned} \quad (4.3-63)$$

$$\{\delta_S\} = [T_{SS}^*]\{\delta_{eS}^*\} + [T_{SP}^*][T_{PP}^*]\{\delta_{eP}^*\} + [T_{SP}^*][T_{PR}^*]\{\delta_R\} \quad (4.3-64)$$

$$\{\delta_P\} = [T_{PP}^*]\{\delta_{eP}^*\} + [T_{PR}^*]\{\delta_R\} \quad (4.3-65)$$

For an arbitrary number of bodies the nodal displacements at the Qth junction point node are given as (4.3-66)

$$\{\delta_Q\} = [T_{QQ}^*]\{\delta_{eQ}^*\} + \sum_L^{Q-1} ([T_{QP}^*][T_{P-}^*] \cdots [T_{-S}^*][T_{SL}^*][T_{LL}^*]\{\delta_{eL}^*\}) + ([T_{QP}^*][T_{P-}^*] \cdots [T_{-S}^*][T_{SL}^*][T_{LR}^*])\{\delta_R\}$$

where the sum on L is over all junction point nodes which link Q to the reference junction point node of the aircraft.

Equation (4.3-66) is used to generate the following transformation:

$$\{\delta_J\} = [T_{JJ}^*]\{\delta_{eJ}^*\} + [T_{JR}^*]\{\delta_R\} \quad (4.3-67)$$

where the matrices are given by the following for the example structure shown by figure 4.3-22:

$$\{\delta_J\} \equiv \begin{bmatrix} \{\delta_Q\} \\ \{\delta_S\} \\ \{\delta_P\} \end{bmatrix} \quad \{\delta_{eJ}^*\} \equiv \begin{bmatrix} \{\delta_{eP}^*\} \\ \{\delta_{eS}^*\} \\ \{\delta_{eP}^*\} \end{bmatrix} \quad (4.3-68)$$

$$[T_{JJ}^*] \equiv \begin{bmatrix} [T_{QQ}^*] & [T_{QS}^*][T_{SS}^*] & [T_{QS}^*][T_{SP}^*][T_{PP}^*] \\ \text{---} & \text{---} & \text{---} \\ [0] & [T_{SS}^*] & [T_{SP}^*][T_{PP}^*] \\ \text{---} & \text{---} & \text{---} \\ [0] & [0] & [T_{PP}^*] \end{bmatrix} \quad (4.3-69)$$

$$[T_{JR}^*] \equiv \begin{bmatrix} [T_{QS}^*] & [T_{SP}^*] & [T_{PR}^*] \\ \hline & [T_{SP}^*][T_{PR}^*] & \\ \hline & & [T_{PR}^*] \end{bmatrix} \quad (4.3-70)$$

4.3.3.3 Constrained displacement relation for combined structure.—The matrices for the constrained displacement of thin and slender structural bodies are combined into a single matrix to conform with the column matrix of independent elastic degrees of freedom at the structural junction point nodes, i.e., $\{\delta_e^*\}$ of equation (4.3-68). For the example structure of figure 4.3-22,

$$[N_c] \equiv \begin{bmatrix} [N_c^4] & & & \text{zeros} \\ & [N_c^3] & & \\ & & [N_c^2] & \\ \text{zeros} & & & [N_c^1] \end{bmatrix} \quad (4.3-71)$$

Using the notation of equation (4.3-67), the constrained displacement relation for the structure is given by the following expression:

$$\{d\}_c = [N_c]([T_{JJ}^*]\{\delta_J^*\} + [T_{JR}^*]\{\delta_R\}). \quad (4.3-72)$$

Equation (4.3-72) is actually a function of the local coordinate systems which may be evaluated at any point on the mean aerodynamic surface of a thin body or on the centerline of a slender body. The result is two components of constrained displacement at the thin bodies, viz., d_{XN} and d_{YN} , as well as a single component of constrained displacement at slender bodies, d_{ZN} . The component d_{ZN} at a thin body and the components d_Y and d_Z at a slender body are independent elastic components of displacement.

4.3.3.4 Independent elastic displacement relations.—The displacement relations for the independent elastic degrees of freedom, $\{\delta_e^{*a}\}$, remain to be derived, i.e.,

$$\{d^a\} = [N_e^a]\{\delta_e^{*a}\} \quad (4.3-46)$$

The derivation is carried out in the following, first for thin structural bodies and then for slender structural bodies.

4.3.3.5 Thin structural bodies—displacement relations.—Thin structural bodies are initially planar and are subjected to bending and torsion along the elastic axis. As shown by figure 4.3-3, the elastic axis is made up of straight segments and the distance between nodes is denoted as $\Delta L(N_i)$. A finite element, shown by figure 4.3-23, is the portion of the body between two plane sections normal to the elastic. The plane sections pass through adjacent nodes, α and $\alpha + 1$.

The deformed shape of the finite element is described in terms of the elastic axis coordinate system, figure 4.3-4. Let ξ, η represent coordinates relative to the α^{th} node in the elastic axis system, figure 4.3-24, and, to simplify notation, let L replace $\Delta L(N_j)$ as the distance from the α^{th} node to the $(\alpha + 1)^{\text{th}}$ node.

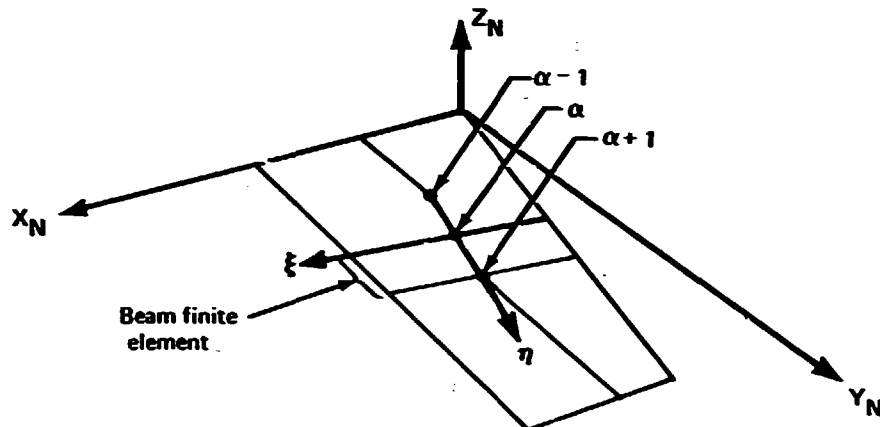


FIGURE 4.3-23.—FINITE ELEMENT OF A THIN STRUCTURAL BODY

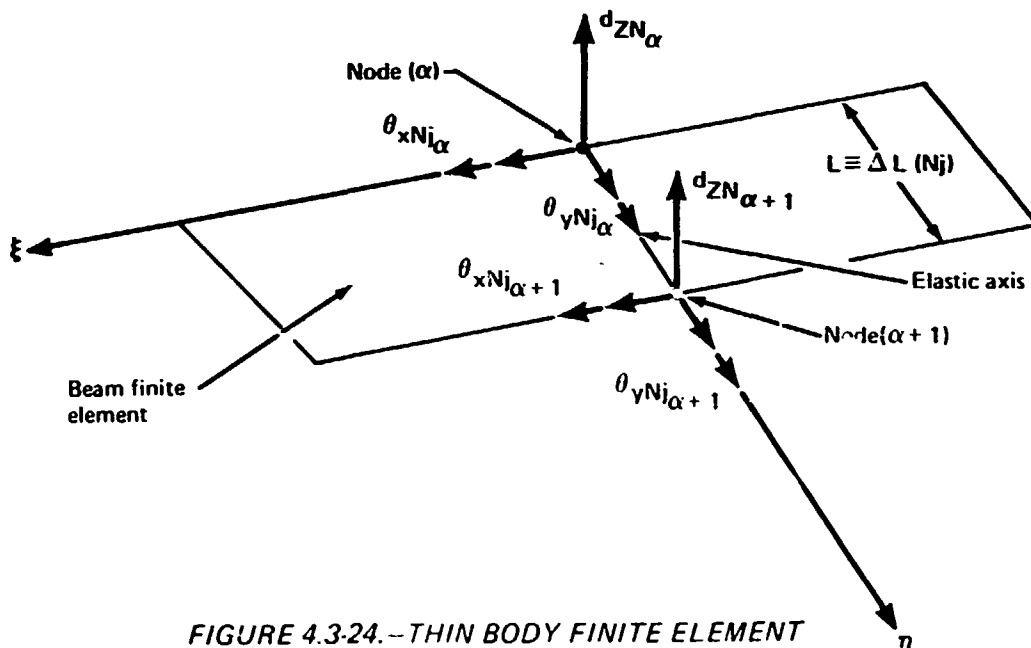


FIGURE 4.3-24.—THIN BODY FINITE ELEMENT

From the Bernoulli-Euler law, equation (32.1) of reference 2-1, the flexure of the elastic axis is given by the following differential equation:

$$\frac{d^4(d_{ZN})}{d\eta^4} = 0. \quad (4.3-73)$$

Integrating and evaluating the constants of integration using the nodal displacement components at the α^{th} and $(\alpha + 1)^{\text{th}}$ nodes, figure 4.3-24, leads to a description of the elastic axis deformation—the following beam spline expression:

$$d_{ZN} = (1 - 3\eta^2/L^2 + 2\eta^3/L^3)d_{ZN\alpha} + (\eta - 2\eta^2/L + \eta^3/L^2)\theta_{xNj\alpha} - (3\eta^2/L^2 - 2\eta^3/L^3)d_{ZN\alpha+1} + (\eta^3/L^2 - \eta^2/L)\theta_{xNj\alpha+1}. \quad (4.3-74)$$

This result describes the deformation of the finite element arising from bending. Torsion deforms the finite element into a helix, i.e.,

$$d_{ZN} = -\xi\theta_{yNj\alpha} - \frac{\eta\xi}{L}(\theta_{yNj\alpha+1} - \theta_{yNj\alpha}). \quad (4.3-75)$$

Combining equations (4.3-74) and (4.3-75), the displacement relation for the beam finite element is found as follows:

$$\begin{bmatrix} d_{xNj} \\ d_{yNj} \\ d_{ZN} \end{bmatrix} = [N_d^a] \begin{bmatrix} \{\delta^*\}_\alpha \\ \{\delta^*\}_{\alpha+1} \end{bmatrix} \quad (4.3-76)$$

where

$$\{\delta^*\}_\alpha \equiv \begin{bmatrix} d_{ZN\alpha} \\ \theta_{xNj\alpha} \\ \theta_{yNj\alpha} \end{bmatrix}, \quad \{\delta^*\}_{\alpha+1} \equiv \begin{bmatrix} d_{ZN\alpha+1} \\ \theta_{xNj\alpha+1} \\ \theta_{yNj\alpha+1} \end{bmatrix} \quad (4.3-77)$$

and

$$\begin{aligned} [N_{ZN\alpha}^a] &= \left[\frac{1}{L^3} (L^3 - 3\eta^2 L + 2\eta^3), \frac{1}{L^2} (L^2 \eta - 2\eta^2 L + \eta^3), (-\xi + \frac{\eta}{L} \xi) \right] \\ [N_{ZN\alpha+1}^a] &= \left[-\frac{1}{L^3} (3\eta^2 L + 2\eta^3), \frac{1}{L^2} (-\eta^2 L + \eta^3), -\frac{\eta}{L} \xi \right]. \end{aligned} \quad (4.3-78)$$

4.3.3.6 Slender structural bodies—displacement relations.—For the analysis performed in the FLEXSTAB system, the deformed shape of a slender structural body may be entirely in terms of its centerline—the elastic axis, figure 4.3-7. Letting ξ represent position relative to the α^{th} node on the elastic axis, figure 4.3-25, flexure of the elastic axis is governed by two differential equations analogous to equation (4.3-73), viz.,

$$\frac{d^4(d_z)}{d\xi^4} = 0$$

and

$$\frac{d^4(d_y)}{d\xi^4} = 0.$$

(4.3-79)

Integrating and evaluating the constants of integration using the nodal displacement components at nodes α and $\alpha + 1$ leads to beam spline relations identical in form with equation (4.3-74). The displacement relation for the slender body finite element follows directly as

$$\begin{bmatrix} d_x \\ d_y \\ d_z \end{bmatrix} = [N_d^a] \begin{bmatrix} \{\delta^*\}_\alpha \\ \{\delta^*\}_{\alpha+1} \end{bmatrix} \quad (4.3-80)$$

where

$$\{\delta^*\}_\alpha \equiv \begin{bmatrix} d_y \\ d_z \\ \theta_{x\alpha} \\ \theta_{y\alpha} \\ \theta_{z\alpha} \end{bmatrix}, \quad \{\delta^*\}_{\alpha+1} \equiv \begin{bmatrix} d_{y\alpha+1} \\ d_{z\alpha+1} \\ \theta_{x\alpha+1} \\ \theta_{y\alpha+1} \\ \theta_{z\alpha+1} \end{bmatrix} \quad (4.3-81)$$

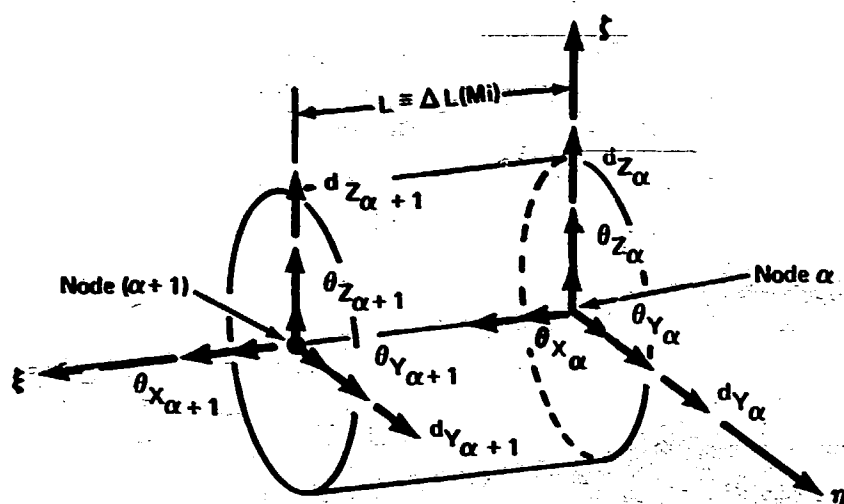


FIGURE 4 3-25.—SLENDER BODY BEAM FINITE ELEMENT

and

$$\begin{aligned}
 [N_Y]_{\alpha} &\equiv \left[\frac{1}{L^3} (L^3 - 3\xi^2 L + 2\xi^3), 0, 0, 0, \frac{1}{L^2} (L^2 \xi - 2\xi^2 L + \xi^3) \right] \\
 [N_Y]_{\alpha+1} &\equiv \left[-\frac{1}{L^3} (3\xi^2 L + 2\xi^3), 0, 0, 0, \frac{1}{L^2} (-\xi^2 L + \xi^3) \right] \\
 [N_Z]_{\alpha} &\equiv \left[0, \frac{1}{L^3} (L^3 - 3\xi^2 L + 2\xi^3), 0, \frac{1}{L^2} (L^2 \xi - 2\xi^2 L + \xi^3), 0 \right] \\
 [N_Z]_{\alpha+1} &\equiv \left[0, -\frac{1}{L^3} (3\xi^2 L + 2\xi^3), 0, \frac{1}{L^2} (-\xi^2 L + \xi^3), 0 \right]
 \end{aligned} \tag{4.3-82}$$

4.3.4 Deformation of the Aerodynamic Surfaces

Aerodynamic surface deformation arising from deformation at the elastic axis nodes, i.e., the matrix relations given by equations (4.2-95) and (4.2-96), are now derived from the preceding. That representing flow incidence arising from a displacement rate normal to the aerodynamic surface, i.e., equation (4.2-96), follows directly from equations (4.3-76) and (4.3-80). Rotations of the aerodynamic surfaces are computed from the preceding displacement relations using the operations of equation (4.2-92).

4.3.4.1 Constrained rotations at aerodynamic surfaces. —The constrained rotations at thin bodies $\{\theta_C^N\}$ are found by substituting the Z_N components of $[N_C^N]$, equation (4.3-52), into equation (4.2-95). The Z_N components are all zeros; therefore, there is no constrained rotational contribution at thin bodies.

The constrained rotations at slender bodies are found by substituting the Y and Z components of $[N_C^N]$, equation (4.3-52), into equation (4.2-95). As in the case of thin bodies, these components are all zeros, thereby leading to zero constrained rotation at slender bodies.

4.3.4.2 Independent elastic rotations at aerodynamic surfaces. – The independent elastic rotations are found by substituting the displacement functions given by equations (4.3-78) and (4.3-81) into equation (4.2-95).

Thin bodies: The thin body displacement functions, equations (4.3-78), are expressed in terms of the elastic axis coordinate system; therefore, the surface rotation is first found in the elastic axis system and then transformed to the local thin body coordinate system to find θ_{EYN} .

The components of the surface rotation in the elastic axis system are found as

$$\begin{bmatrix} \theta_{xNj} \\ \theta_{yNj} \\ \theta_{zN} \end{bmatrix} = \left[\frac{1}{2} \text{curl} \right] \begin{bmatrix} d_{xNj} \\ d_{yNj} \\ d_{zN} \end{bmatrix} \quad (4.3-83)$$

where in a manner analogous to equation (4.2-92)

$$\left[\frac{1}{2} \text{curl} \right] \equiv \frac{1}{2} \begin{bmatrix} 0 & -\frac{\partial}{\partial z_N} & \frac{\partial}{\partial \eta} \\ \frac{\partial}{\partial z_N} & 0 & -\frac{\partial}{\partial \xi} \\ -\frac{\partial}{\partial \eta} & \frac{\partial}{\partial \xi} & 0 \end{bmatrix}$$

Because of the platelike behavior of the thin bodies, the displacement components are related as

$$\frac{\partial d_{zN}}{\partial \eta} = -\frac{\partial d_{yNj}}{\partial z_N} \quad \text{and} \quad \frac{\partial d_{zN}}{\partial \xi} = -\frac{\partial d_{xNj}}{\partial z_N};$$

and it follows that

$$\begin{bmatrix} \theta_{xNj} \\ \theta_{yNj} \\ \theta_{zN} \end{bmatrix} = [N_{\theta j}^a] \begin{bmatrix} \{\delta^*\}_\alpha \\ \{\delta^*\}_{\alpha+1} \end{bmatrix} \quad (4.3-84)$$

where

$$[N_{\theta j}^a] \equiv [\frac{1}{2} \text{curl}] [N^a]$$

and

$$[N_{\theta j}^a] \equiv \begin{bmatrix} 6(-\frac{\eta}{L^2} + \frac{\eta^2}{L^3}), & (1 - \frac{4\eta}{L} + \frac{3\eta^2}{L^2}), & \frac{\xi}{L}, & -6(\frac{\eta}{L^2} + \frac{\eta^2}{L^3}), & (-\frac{2\eta}{L} + \frac{3\eta^2}{L^2}), & -\frac{\xi}{L} \\ 0 & 0 & (1 - \eta/L) & 0 & 0 & \eta/L \\ 0 & 0 & 0 & 0 & 0 & 0 \end{bmatrix}$$

Transforming to the local thin body axis system, figure 4.3-5, the rotation θ_{EYN} is found as

$$\theta_{EYN}^a = [N_{\theta}^a] \{\delta^a\} \quad (4.3-85)$$

where

$$[N_{\theta}^a]_{\alpha} = [6 \sin \Gamma_{Nj} (-\frac{\eta}{L^2} + \frac{\eta^2}{L^3}), \sin \Gamma_{Nj} (1 - \frac{4\eta}{L} + \frac{3\eta^2}{L^2}), \\ \sin \Gamma_{Nj} \frac{\xi}{L} - \cos \Gamma_{Nj} (1 - \eta/L)]$$

$$[N_{\theta}^a]_{\alpha+1} = [-6 \sin \Gamma_{Nj} (\frac{\eta}{L^2} + \frac{\eta^2}{L^3}), \sin \Gamma_{Nj} (-\frac{2\eta}{L} + \frac{3\eta^2}{L^2}), \\ - \sin \Gamma_{Nj} \frac{\xi}{L} - \cos \Gamma_{Nj} \eta/L]$$

Slender bodies: Independent elastic rotations at the centerlines of slender bodies are found by substituting the displacement functions for slender bodies, equations (4.3-82), into equation (4.2-95). The result of this operation is

$$\begin{bmatrix} \theta_{EZ}^a \\ \theta_{EY}^a \end{bmatrix} = [N_{\theta}^a] \begin{bmatrix} \{\delta^*\}_{\alpha} \\ \{\delta^*\}_{\alpha+1} \end{bmatrix} \quad (4.3-86)$$

where

$$[N_{\theta}^a]_{\alpha} \equiv \begin{bmatrix} \frac{6}{L^3}(-\xi L + \xi^2), 0, 0, 0, \frac{1}{L^2}(L^2 - 4\xi L + 3\xi^2) \\ 0, \frac{6}{L^3}(-\xi L + \xi^2), 0, \frac{1}{L^2}(L^2 - 4\xi L + 3\xi^2), 0 \end{bmatrix}$$

$$[N_{\theta}^a]_{\alpha+1} \equiv \begin{bmatrix} -\frac{6}{L^3}(\xi L + \xi^2), 0, 0, 0, \frac{1}{L^2}(-2\xi L + 3\xi^2) \\ 0, -\frac{6}{L^3}(\xi L + \xi^2), 0, \frac{1}{L^2}(-2\xi L + 3\xi^2), 0 \end{bmatrix}$$

4.3.4.3 Evaluation of the aerodynamic surface deformation on thin bodies.—In the FLEXSTAB system, the displacement relations for thin bodies are always evaluated on beam sections which pass through a node at the elastic axis. Referring to equations (4.3-76) and (4.3-85), the displacement functions contained in the matrices of the displacement relations are evaluated with the coordinate η (or Y_{Nj}) set to zero. The displacement relations are thus greatly simplified, but this has been achieved by introducing an approximation.

To illustrate the approximation, consider the general arrangement of the aerodynamic paneling, figure 4.3-26. The airload on each panel, being the result of a uniform pressure, is represented by a concentrated force at the geometric centroid of the panel. Also, as noted in section 4.2.6.3, aerodynamic control points are located at the geometric centroids of the panel.

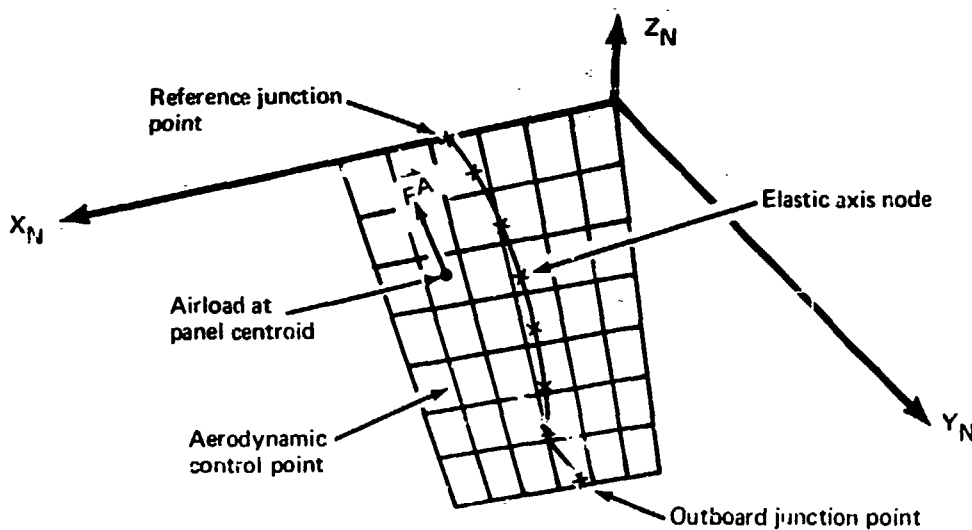


FIGURE 4.3-26.—AERODYNAMIC PANELING OF A THIN BODY

The coordinates of the panel geometric centroids are used in evaluating the displacement relations. In the FLEXSTAB system, these coordinates are approximated by requiring them to describe a point on a beam section passing through a node.

A typical thin body aerodynamic panel is shown by figure 4.3-27. The node which is nearest to the point where a line from the geometric centroid intersects the elastic axis at a right angle is assigned to the panel. The geometric centroid of the panel is treated as if it were located on the beam section through that node. This is an approximation because the effect of the eccentricity, Δy_{Nj} , shown by figure 4.3-27, is ignored. The approximation can be avoided if the nodes are chosen to be located at the intersection points.

Using the approximation regarding the geometry of the panels, the displacement relations given by equations (4.3-76) and (4.3-85) are simplified and lead to the translation and rotation of the panel being described in terms of the nodal displacement components at the node assigned to the panel. The translation displacement components are given by

$$\{d^a\} = [N_d^a]_{\alpha} \{\delta^e\}_{\alpha} \quad (4.3-87)$$

where

$$[N_d^a]_{\alpha} = \begin{bmatrix} 0 & 0 & 0 \\ 0 & 0 & 0 \\ 1 & 0 & -x_{Nj} \end{bmatrix};$$

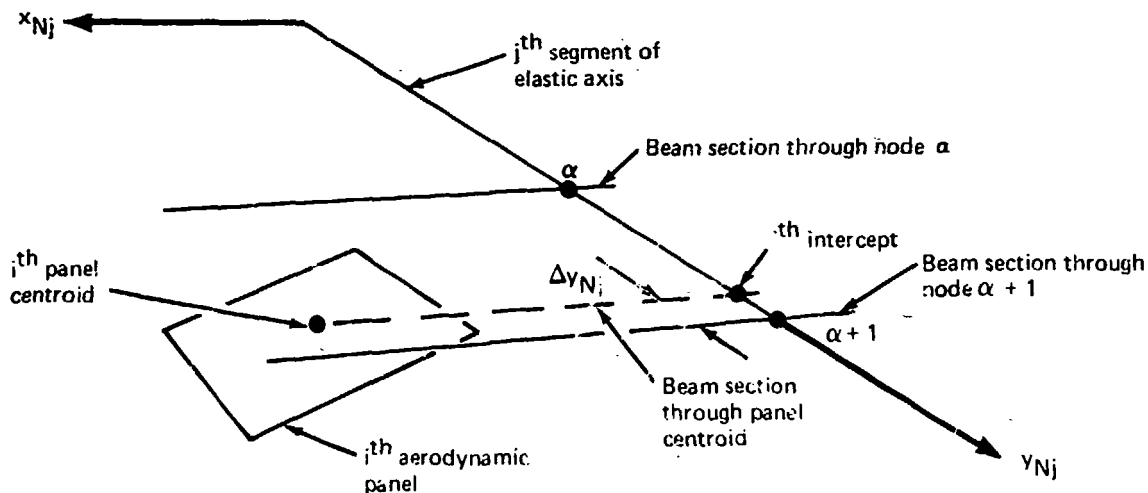


FIGURE 4.3-27.—BEAM SECTION AT AN AERODYNAMIC PANEL CENTROID

while the rotation is given by

$$\theta_{E_{YN}}^a = [N_{\theta}^a]_{\alpha} \{\delta\}_{\alpha} + [N_{\theta T}^a]_{\alpha} \theta'_{YNj\alpha} \quad (4.3.88)$$

where

$$[N_{\theta}^a]_{\alpha} \equiv [0, \sin \Gamma_{Nj}, -\cos \Gamma_{Nj}]$$

$$[N_{\theta T}^a]_{\alpha} \equiv -x_{Nj}(i) \sin \Gamma_{Nj}$$

$$\theta'_{YNj\alpha} \equiv \frac{\theta_{YNj\alpha+1} - \theta_{YNj\alpha}}{L}$$

The quantity $\theta'_{YNj\alpha}$ is the rate of elastic axis twist at the α^{th} node.

4.3.4.4 Evaluation of the aerodynamic surface deformation on slender bodies.--At slender bodies the aerodynamic pressure acting at the surfaces is resolved into point forces \vec{F}_j^A acting at the slender body centerlines, figure 4.3-28. The aerodynamic control points for line doublets, figure 3.4-18, are also located at the surfaces of the slender bodies, but the contribution to the boundary value arising from elastic deformation is evaluated at the elastic axis, figure 4.3-28.

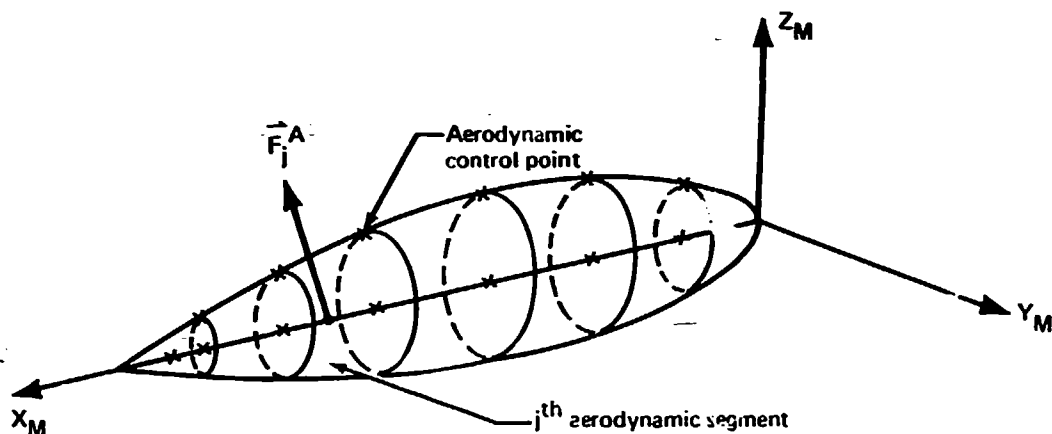


FIGURE 4.3-28.—AERODYNAMIC SEGMENTS OF A SLENDER BODY

In the FLEXSTAB system an approximation is introduced for the positions of the aerodynamic forces and control points relative to the elastic axis nodes. The aerodynamic forces and control points are made to coincide with the nodes nearest their true locations. Again, as in the case of thin bodies, the approximation simplifies the displacement relations and allows them to be expressed in terms of nodal displacement components at a single node. Evaluating equations (4.3-82) at $\xi = 0$ leads to

$$\begin{bmatrix} d_X^a \\ d_Y^a \\ d_Z^a \end{bmatrix} = [N_d^a]_{\alpha} \{\delta^*\}_{\alpha} \quad (4.3-89)$$

where

$$[N_d^a]_{\alpha} \equiv \begin{bmatrix} 0 & 0 & 0 & 0 & 0 \\ 1 & 0 & 0 & 0 & 0 \\ 0 & 1 & 0 & 0 & 0 \end{bmatrix}.$$

while evaluating equation (4.3-85) at $\xi = 0$ leads to

$$\begin{bmatrix} \theta_{E_Z}^a \\ \theta_{E_Y}^a \end{bmatrix} = [N_{\theta}^a]_{\alpha} \{\delta^*\}_{\alpha} \quad (4.3-90)$$

where

$$[N_{\theta}^a]_{\alpha} \equiv \begin{bmatrix} 0 & 0 & 0 & 0 & 1 \\ 0 & 0 & 0 & 1 & 0 \end{bmatrix}.$$

4.3.4.5 Elastic axis rate of twist - The rate of twist $\theta'_{YNj\alpha}$, introduced by equation (4.3-88), is expressed for all thin body elastic axis nodes as

$$\{\delta_T\} \equiv \begin{bmatrix} \vdots \\ \theta'_{YNj\alpha} \\ \vdots \end{bmatrix} \quad (4.3-91)$$

This deformation is related to forces applied at the elastic axis nodes $\{Q_e^*\}$, equation (4.3-43), as follows:

$$\{\delta_T\} = [C_e^*] \{Q_e^*\} \quad (4.3-92)$$

where the subscript e indicates that the forces $\{Q_R^*\}$ are excluded

The rate of twist at the α^{th} node is given by

$$\dot{\theta}_{YNj\alpha} = \frac{M_{YNj\alpha}}{GJ_i} \quad (4.3-93)$$

where GJ_i is the torsional stiffness of the i^{th} elastic axis segment containing the node α . The partitions of the flexibility matrix $[C_e^*]$ corresponding to those introduced by equation (4.3-44) appear as

$$[C_e^*] = \begin{bmatrix} [C_{WJ}^*] & [C_{WB}^*] & [C_{WW}^*] \end{bmatrix}. \quad (4.3-94)$$

The partitions are all null except $[C_{WW}^*]$ and this partition has the elements made up of the following matrices

$$[C_{WWNj\alpha}^*] \equiv \left[\frac{1}{GJ_j}, 0, 0 \right] \quad (4.3-95)$$

such that

$$[C_{WW}^*] = \begin{bmatrix} \ddots & & \text{zeros} \\ & [C_{WWNj\alpha}^*] & \\ \text{zeros} & & \ddots \end{bmatrix}. \quad (4.3-96)$$

4.3.5 Summary of Aerodynamic Surface Deformation Transformation:

The displacement relations of the preceding permit evaluation of the aerodynamic surface deformation, viz., $\{d^*\}$ of equation (4.2-100), $\{\theta^*\}$ of equation (4.2-101), and $\{d_T\}$ of equation (4.2-114). The transformations obtained from the displacement relations and used in evaluating aerodynamic surface deformation are expressed in terms of subsets of the set of elastic axis nodal displacement components $\{\delta\}$.

4.3.5.1 Subsets of elastic axis nodal displacement components.—The subsets of elastic axis nodal displacement components are as follows:

$$\begin{array}{l} \uparrow \\ \{\delta_R\} \\ \uparrow \\ \{\delta_R^*\} \\ \uparrow \quad \uparrow \\ \{\delta_e^*\} \quad \{\delta^*\} \quad \{\delta\} \\ \uparrow \\ \{\delta_T\} \end{array} \quad (4.3-97)$$

where the subsets are as follows:

d_{xR} : X-translation of aircraft reference junction point;

$\{\delta_R^*\}$: elastic nodal displacement components at aircraft reference junction point, equation (4.3-18);

$\{\delta_T\}$: rate of twist components, equation (4.3-91)

The subsets $\{\delta_R^*\}$ and $\{\delta_e^*\}$ are obtained from the transformations

$$\begin{aligned}\{\delta_R^*\} &= [T_R^{**}]\{\delta^*\} \\ \{\delta_e^*\} &= [T_{**}^R]\{\delta^*\}\end{aligned}\quad (4.3-98)$$

where the matrices $[T_R^{**}]$ and $[T_{**}^R]$, when combined, produce the identity matrix of size equal to $\{\delta^*\}$, i.e.,

$$\begin{bmatrix} [T_R^{**}] \\ [T_{**}^R] \end{bmatrix} = [I].$$

4.3.5.2 Partitioned deformation transformations.—The deformation of the aerodynamic surfaces is related to elastic axis nodal displacement components as follows:

- Aerodynamic surface normal translation:

$$\{d^*\} = [P_d]\{\delta\} \quad (4.2-100)$$

where

$$[P_d] \equiv \begin{bmatrix} \{0\} & | & \{0\} & | & [T_{de}^*] \end{bmatrix}$$

and can be written as

$$\{d^*\} = [T_{de}^*]\{\delta_e^*\} \quad (4.3-99)$$

- Aerodynamic surface rotation:

$$\{\theta^*\} = [P_\theta]\{\delta\} \quad (4.2-101)$$

where

$$[P_\theta] \equiv \begin{bmatrix} [T_{\theta R}^*] & | & [T_{\theta e}^*] & | & [T_{\theta T}] \end{bmatrix}$$

and can be written as

$$\{\theta^*\} = [T_{\theta R}^*]\{\delta_R^*\} + [T_{\theta e}^*]\{\delta_e^*\} + [T_{\theta T}]\{\delta_T\} \quad (4.3-100)$$

- Aerodynamic surface translation:

$$\{d_T\} = [P_T]\{\delta\} \quad (4.2-141)$$

where

$$[P_T] = \begin{bmatrix} \{T_R^*\} & | & [0] & | & \{T_{Te}^*\} \end{bmatrix}$$

and can be written as

$$\{d_T\} = \{T_R^*\}d_{X_R} + [T_{Te}^*]\{\delta_e^*\} \quad (4.3-101)$$

The T transformations appearing in equations (4.3-99), (4.3-100), and (4.3-101) are derived, in the following, in terms of three partitions related to junction points, slender bodies, and thin bodies, e.g.,

$$[T] = \begin{bmatrix} [T]_J & | & [T]_B & | & [T]_W \end{bmatrix} \quad (4.3-102)$$

where $[T]_J$, $[T]_B$, and $[T]_W$ are, respectively, the junction point partition, the slender body partition, and the thin body partition. These partitions correspond to the following subsets of $\{\delta_e^*\}$:

$$\{\delta_e^*\} = \begin{bmatrix} \{\delta_e^*\}_J \\ \{\delta_e^*\}_B \\ \{\delta_e^*\}_W \end{bmatrix} \quad (4.3-103)$$

4.3.5.3 Junction point partitions. --The junction point partitions involve the transformations given by equation (4.3-67), viz.,

$$\{\delta\}_J = [T_{JJ}^*]\{\delta_e^*\}_J + [T_{JR}^*]\{\delta_K\}. \quad (4.3-67)$$

For the Q^{th} junction point, $\{\delta_Q^*\}$ --a subset of $\{\delta_e^*\}_J$ --the displacement relations given by equations (4.3-52) and (4.3-53) are evaluated for points on thin bodies and slender bodies to construct $[T]_J$ in the form given by equation (4.3-73) to find the junction point partitions of equation (4.3-101) as

$$[T_{\theta R}^*] \equiv [N_C][T_{JR}^*]$$

and

$$[T_{Te}^*]_J \equiv [N_C][T_{JJ}^*]\{\delta_e^*\}_J. \quad (4.3-104)$$

The partition $[T_{\theta R}^*]$ of equation (4.3-100) is replaced by a rigid body mode shape matrix expanded about the aircraft reference junction point, i.e.,

$$[\bar{\phi}_{\theta}^*] \equiv [T_{\theta R}^*], \quad (4.3-105)$$

and the J partitions of $[T_{\theta e}^*]$, $[T_{de}^*]$ and $[T_{\theta T}^*]$ are null.

4.3.5.4 Slender body partitions.—The slender body partitions follow from the displacement relations given by equations (4.3-80) and (4.3-86) evaluated in the manner described in section 4.3.4.3. Thus, for the j^{th} aerodynamic centroid on the J^{th} slender body and the α^{th} node on the J^{th} slender body, the partitions are as follows:

$$[T_{Te}^*]_B \equiv \begin{bmatrix} \cdot & \cdot & \cdot & \text{zeros} \\ & [T_{T_{Jj\alpha}}^*] & & \\ \text{zeros} & & \cdot & \cdot & \cdot \end{bmatrix} \quad (4.3-106)$$

where

$$[T_{T_{Jj\alpha}}^*] \equiv \begin{bmatrix} 0 & 0 & 0 & 0 & 0 \\ 1 & 0 & 0 & 0 & 0 \\ 0 & 1 & 0 & 0 & 0 \end{bmatrix}$$

$$[T_{de}^*]_B = \begin{bmatrix} \cdot & \cdot & \cdot & \text{zeros} \\ & [T_{d_{Jj\alpha}}^*] & & \\ \text{zeros} & & \cdot & \cdot & \cdot \end{bmatrix} \quad (4.3-107)$$

where

$$[T_{d_{Jj\alpha}}^*] \equiv \begin{bmatrix} 1 & 0 & 0 & 0 & 0 \\ 0 & 1 & 0 & 0 & 0 \end{bmatrix}$$

$$[T_{\theta e}^*]_B = \begin{bmatrix} \cdot & \cdot & \cdot & & \\ & [T_{\theta_{Jj\alpha}}^*] & & & \\ & & \cdot & \cdot & \cdot \end{bmatrix} \quad (4.3-108)$$

$$[T_{\theta_{Jj\alpha}}^*] \equiv \begin{bmatrix} 0 & 0 & 0 & 1 & 0 \\ 0 & 0 & 0 & 0 & 1 \end{bmatrix}$$

while $[T_{\theta T}]_B$ is null.

For the i^{th} aerodynamic centroid on the l^{th} thin body and the α^{th} node on a slender body, the partitions are all null.

4.3.5.5 Thin body partitions.—The thin body partitions follow from the displacement relations given by equations (4.3-76) and (4.3-84) evaluated in the manner described in section 4.3.4.3. Thus, for the j^{th} aerodynamic centroid on the j^{th} slender body and the α^{th} node on a thin body, the partitions are all null. For the i^{th} aerodynamic centroid on the l^{th} thin body and the α^{th} node on the l^{th} thin body, the partitions are as follows:

$$[T_{Te}^*]_W \equiv \begin{bmatrix} \ddots & & & \\ & [T_{T_{Ii\alpha}}^*] & & \\ & & \ddots & \end{bmatrix} \quad (4.3-109)$$

where

$$[T_{T_{Ii\alpha}}^*] \equiv \begin{bmatrix} 0 & 0 & 0 \\ 1 & 0 & -x_{Ij}(i) \end{bmatrix}$$

for node α on the j^{th} elastic axis segment, figure 4.3-27.

$$[T_{de}^*]_W \equiv \begin{bmatrix} \ddots & & \text{zeros} \\ & [T_{d_{Ii\alpha}}^*] & \\ \text{zeros} & & \ddots \end{bmatrix} \quad (4.3-110)$$

where

$$[T_{d_{Ii\alpha}}^*] \equiv [1, 0, -x_{Ij}(i)]$$

for node α on the j^{th} elastic axis segment.

$$[T_{\theta e}^*]_W \equiv \begin{bmatrix} \ddots & & \text{zeros} \\ & [T_{\theta_{Ii\alpha}}^*] & \\ \text{zeros} & & \ddots \end{bmatrix} \quad (4.3-111)$$

where

$$[T_{\theta_{Ii\alpha}}^*] \equiv [0, \sin \Gamma_{Ij}, -\cos \Gamma_{Ij}]$$

for node α on the j^{th} elastic axis segment, figure 4.3-11,

$$[T_{\theta T}]_W \equiv \begin{bmatrix} \ddots & & & \text{zeros} \\ & -x_{Ij}(i)\sin\Gamma_{Ij} & & \\ & \text{zeros} & \ddots & \end{bmatrix} \quad (4.3-112)$$

for node α on the j^{th} elastic axis segment.

4.3.6 Propulsion System Forces and Motions

In the FLEXSTAB system, the propulsion system consists of up to ten engines which generate thrust forces and gyroscopic couples. The objective of this section is to derive transformations which relate these forces and couples to the nodal forces of the special beam theory of the system. The forms of the transformations were introduced in section 4.2.8 as follows:

$$\{\dot{Q}^T\} = [NAF]\{T\} \quad (4.3-113)$$

and

$$\{\dot{Q}^G\} = [\Delta_G^*]\{M^G\} \quad (4.3-114)$$

where * denotes the reduced set of nodal forces (i.e., equation (4.3-14)).

The FLEXSTAB system requires that the engine be represented as slender bodies. The thrust forces are applied to the nodes on the slender bodies, while the gyroscopic couples are applied to the junction point nodes of the slender bodies. A typical engine installation is shown by figure 4.3-29, indicating a distribution of thrust force and the location of the gyroscopic couple.

In the example, the nacelle is considered to contain the A^{th} engine, and the thrust force is divided into two components acting at the α^{th} and β^{th} slender body nodes. The column matrix $\{T\}$ of equation (4.3-120) contains only the amplitude of the thrust for each engine, i.e.,

$$\{T\} \equiv \begin{bmatrix} \vdots \\ T(A) \\ \vdots \end{bmatrix} \quad (4.3-115)$$

and the matrix $[NAF]$ contains the direction cosines for the thrust vectors describing their orientation with respect to the Reference Axis System (e.g., $nX_\alpha(A)$, $nY_\alpha(A)$, $nZ_\alpha(A)$) and scaling factors (e.g., $K(A)$) which specify the portion of the total thrust to be applied at each node. For each slender body node, therefore, the matrix operation of equation (4.3-120) leads to the following nodal forces:

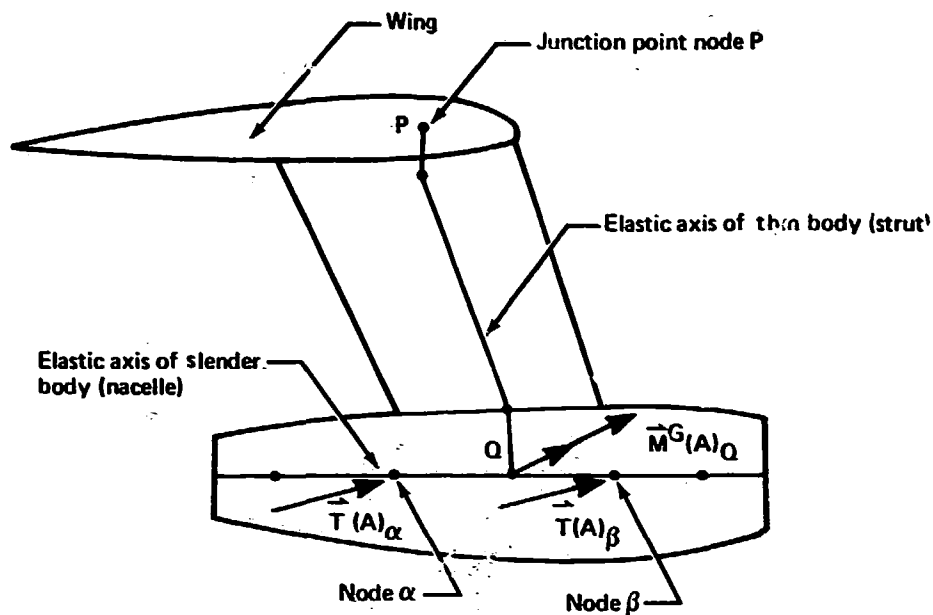


FIGURE 4.3-29.—TYPICAL ENGINE INSTALLATION

$$\{Q^*\}_\alpha = K(A)_\alpha \begin{bmatrix} \eta_{X_\alpha}(A) \\ \eta_{Y_\alpha}(A) \\ \eta_{Z_\alpha}(A) \end{bmatrix} T(A). \quad (4.3-116)$$

The matrix $[NAF]$ contains the elements

$$\begin{bmatrix} K(A)_\alpha \eta_{X_\alpha}(A) \\ K(A)_\alpha \eta_{Y_\alpha}(A) \\ K(A)_\alpha \eta_{Z_\alpha}(A) \end{bmatrix},$$

which distribute the thrust forces to specified slender body nodes, but all other elements are zeros. The matrix operation of equation (4.3-120) yields $\{Q^*T\}$, with zero components of nodal force everywhere except at the selected slender body nodes where thrust forces are assumed to act.

As noted above, the gyroscopic couples act at junction point nodes. These couples are expanded in terms of components on the Reference Axis System, and the column matrix $\{M^G\}$ contains the following elements:

$$\{M^G\} \equiv \begin{bmatrix} \vdots \\ M_{XQ}^G \\ M_{YQ}^G \\ M_{ZQ}^G \\ \vdots \end{bmatrix} \quad (4.3-117)$$

where $M_{XQ}^G, M_{YQ}^G, M_{ZQ}^G$ are the components of the gyroscopic couple at the Q^{th} junction point node.

Consider the deformation at the junction point node where the gyroscopic couple is applied in the example shown by figure 4.3-29, i.e., at the outboard junction point of a thin body. This deformation is given by equation (4.3-51) as

$$\{\delta_Q\} \equiv \begin{bmatrix} d_{XQ} \\ d_{YQ} \\ d_{ZQ} \\ \theta_{XQ} \\ \theta_{YQ} \\ \theta_{ZQ} \end{bmatrix}$$

and is a consequence of the elastic deformation at the node point, i.e., the deformation transferred to the Q^{th} junction point node by the constraints in all of the structural bodies between the Q^{th} junction point node and the reference junction point of the entire structure. The deformations at all junction point nodes of a structural configuration were deduced from equation (4.3-66) and given by equation (4.3-67) as follows:

$$\{\delta_J\} = [T_{JJ}^*]\{\delta_{e_J}^*\} + [T_{JR}^*]\{\delta_R\}. \quad (4.3-118)$$

Let $[T_G]$ be a matrix which yields the components of nodal force at all junction point nodes as a consequence of gyroscopic couples, i.e.,

$$\{Q_J\} = [T_G^*]\{M^G\} \quad (4.3-119)$$

The partition of $[T_G]$ corresponding to the Q^{th} node is given by

$$[T_{G_{QQ}}^*] \equiv \begin{bmatrix} 0 & 0 & 0 \\ 0 & 0 & 0 \\ 0 & 0 & 0 \\ 1 & 0 & 0 \\ 0 & 1 & 0 \\ 0 & 0 & 1 \end{bmatrix} \quad (4.3-120)$$

If there is only one engine, then $[T_G^*]$ is of the form

$$[T_G^*] = \begin{bmatrix} \text{zeros} \\ [T_{G_{QQ}}^*] \\ \text{zeros} \end{bmatrix}$$

and the junction point nodal forces are zero except for the Q^{th} junction point node.

Combining equations (4.3-67) and (4.3-119), the work done by the gyroscopic couples in deforming the structure is given by

$$\begin{aligned} \{\delta_J\}^T \{Q\} = & \{\delta_{e_J}^*\}^T [T_{JJ}^*]^T [T_G^*] \{M^G\} \\ & + \{\delta_R\} [T_{JR}^*]^T [T_G^*] \{M^G\} \end{aligned} \quad (4.3-121)$$

The nodal forces at the reference junction point of the configuration, viz.,

$$[T_{JR}^*]^T [T_G^*] \{M^G\},$$

must vanish; equation (4.3-121) therefore reduces to

$$\{\delta_{e_J}^*\}^T (\{Q_{e_J}^*\} - [T_{JJ}^*]^T [T_G^*] \{M^G\}) = 0$$

and the forces acting on the junction point nodes are given as

$$\{Q_{e_J}^*\} = [T_{JJ}^*]^T [T_G^*] \{M^G\} \quad (4.3-122)$$

The transformation, equation (4.3-114), is now expressed as

$$\{Q_{e_J}^*\} = [T_G^*] \{M^G\} \quad (4.3-123)$$

by letting

$$[\Delta_G] = [T_{**}^R]^T [T_G]$$

and

$$[T_G] \equiv \begin{bmatrix} [T_{JJ}^*]^T [T_G] \\ - \quad - \quad - \\ [0] \end{bmatrix} \quad (4.3-124)$$

so that the nodal forces at all structural nodes vanish except at junction point nodes affected by the gyroscopic couples.

4.3.7 Mass Matrix

The objective of this section is to derive the form of the nodal mass matrix (termed the element mass matrix by reference 4-3, equation (11.7)) when the finite elements of the structure are those of the preceding beam theory. The nodal mass matrix for the a th finite element is given by equation (4.2-18), i.e.,

$$[m_\delta^a] = \int_{V^a} [N^a]^T [\rho_A^a] [N^a] dV \quad (4.2-18)$$

where the matrix $[N^a]$ contains the displacement functions, equation (4.2-6), used in formulating the finite element displacement relations of equation (4.2-7),

$$\{d^a\} = [N^a] \{\delta^a\}. \quad (4.2-7)$$

The nodal mass matrix for the beam theory is obtained by substituting into equation (4.2-18) the displacement relations developed in section 4.3.3 and carrying out the indicated integration.

Because the displacement relations for the beam theory are separated into constrained and independent elastic displacement relations in sections 4.3.3.1 and 4.3.3.4, the nodal mass matrix is formed in two parts:

- Junction point nodal mass matrix, related to the constrained displacements shown by figure 4.3-20 and 4.3-21,

$$[m_\delta^Q] = \int_{V^Q} [N_C^Q]^T [\rho_A] [N_C^Q] dV \quad (4.3-125)$$

where V^Q is the volume of the thin or slender body from the Q^{th} reference junction point to the adjacent outboard junction point

- Elastic axis nodal mass matrix,

$$[m_{\delta}^a] = \int_{V^a} [N_e^a]^T [\rho_A] [N_e^a] dV \quad (4.3-126)$$

where V^a is the volume of the a^{th} finite element, figure 4.3-19.

These two nodal mass matrices are derived separately in the following.

The nodal mass matrices are generated for the FLEXSTAB system in two steps. In the first step the distributed mass of the aircraft is replaced by an inertially equivalent system of point masses termed "lumped masses"; this step is performed exterior to the FLEXSTAB system. In the second step the nodal mass matrices are generated from lumped parameter forms of equation (4.3-125) and (4.3-126); this step is performed by the FLEXSTAB system. The lumped parameter forms of equations (4.3-125) and (4.3-126) follow directly from having replaced the distributed mass by a system of point masses. Letting the i^{th} lumped mass be denoted as m_i , the lumped parameter forms for the nodal mass matrices are given by

$$[m_{\delta i}^Q] = [N_c^Q(i)]^T \begin{bmatrix} m_i & 0 & 0 \\ 0 & m_i & 0 \\ 0 & 0 & m_i \end{bmatrix} [N_c^Q(i)] \quad (4.3-127)$$

and

$$[m_{\delta i}^a] = [N_e^a(i)]^T \begin{bmatrix} m_i & 0 & 0 \\ 0 & m_i & 0 \\ 0 & 0 & m_i \end{bmatrix} [N_e^a(i)]$$

where the matrices $[N_c^Q(i)]$ and $[N_e^a(i)]$ contain the values of the displacement functions obtained by evaluating them at the coordinates of the i^{th} lumped mass. Formulas for obtaining the values and coordinates of the lumped masses to achieve inertial equivalence with the distributed are developed in the following.

4.3.7.1 Inertially equivalent lumped masses.—The beam finite elements subdivide the thin and slender bodies of a configuration as shown in figure 4.3-30. The motion of each subdivision relative to the elastic axis is governed entirely by the elastic degrees of freedom at the elastic axes shown by figures 4.3-24 and 4.3-25, and this motion is described by the displacement functions developed in sections 4.3.3.5 and 4.3.3.6.

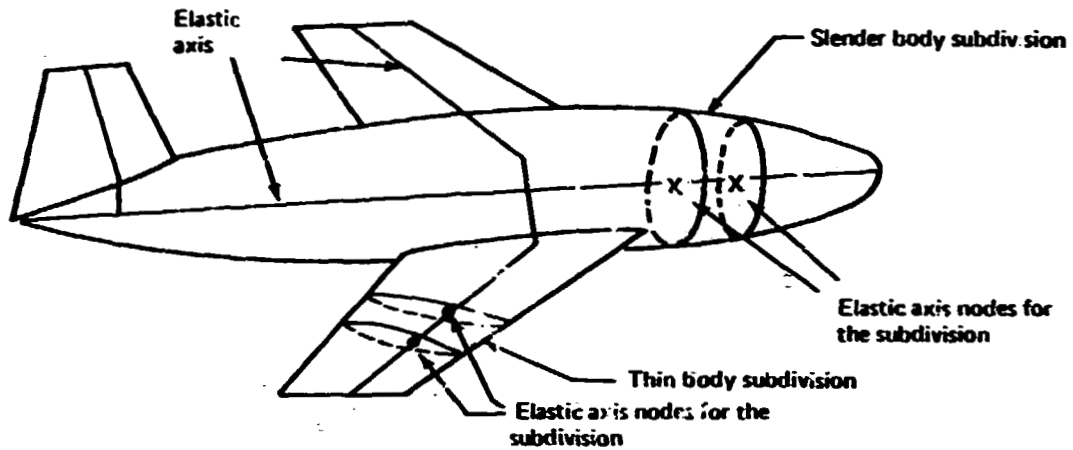


FIGURE 4.3-31.—FINITE ELEMENT SUBDIVISION OF THE STRUCTURAL MASS

Accelerations relative to the elastic axes of the distributed mass contained in each thin and slender subdivision give rise to inertial forces and couples at the nodes having the components shown by figures 4.3-10 and 4.3-13. A system of point masses may be rigidly connected to the nodes which, when accelerations occur in the nodal degrees of freedom, give rise to inertial nodal forces identical to those due to the distributed mass. These lumped masses are inertially equivalent to the distributed mass.

4.3.7.2 Lumped masses on a thin body.—Consider the thin structural body shown by figure 4.3-31. The lumped masses are assumed to be located on sections of the thin body which are normal to the elastic axis and pass through the nodes on the elastic axis. A lumped mass at the point P on the section through the α^{th} node therefore moves relative to the node as follows:

$$d_{ZN}^{(P)} = d_{ZN\alpha} - x_{Nj}^{(P)} \theta_{YNj\alpha} \quad (4-3.128)$$

A matrix expression for the three components of relative displacement expanded on the Reference Axis System appears as

$$\{d\} = [N_e] \{\delta_{\alpha}^*\} \quad (4-3.129)$$

where

$$\{d\} = \begin{bmatrix} d_X \\ d_Y \\ d_Z \end{bmatrix}$$

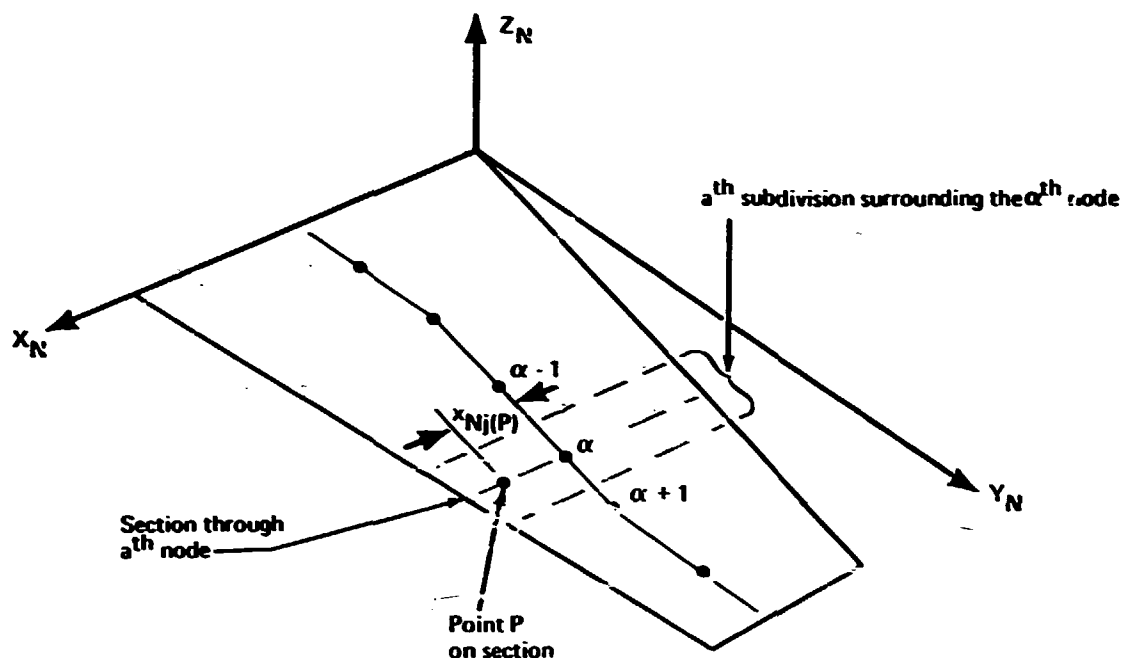


FIGURE 4.3-31.—SECTION OF A THIN BODY PASSING THROUGH AN ELASTIC AXIS NODE

and

$$[N_e] \equiv \begin{bmatrix} 0 & 0 & 0 \\ -\sin\theta_N & 0 & x_{Nj}\sin\theta_N \\ \cos\theta_N & 0 & -x_{Nj}\cos\theta_N \end{bmatrix}$$

A simple approximation for the motion of the distributed mass of the thin body assumes that a subdivision of the thin body surrounding the α^{th} node, figure 4.3-31, moves with the node in the manner given by equation (4.3-128). The nodal mass matrix of the α^{th} node is then approximated as

$$[m_{\delta\alpha}^a] = \begin{bmatrix} M_\alpha & 0 & -\bar{x}_{Nj}M_\alpha \\ 0 & 0 & 0 \\ -\bar{x}_{Nj}M_\alpha & 0 & I_{YNj\alpha} \end{bmatrix} \quad (4.3-130)$$

where

$$M_\alpha \equiv \int_{V_a} \rho_A dV, \quad \bar{x}_{Nj} \equiv \frac{1}{M_\alpha} \int_{V_a} x_{Nj} \rho_A dV, \quad I_{YNj\alpha} \equiv \int_{V_a} (x_{Nj})^2 \rho_A dV,$$

The elements of the nodal mass matrix, equation (4.3-130), are inertially equivalent to two lumped masses, figure 4.3-32. Letting the two lumped masses be denoted as m_i and m_{i+1} , they are inertially equivalent to the distributed mass of the subdivision if

$$m_i = m_{i+1} = M\alpha/2 \quad (4.3-131)$$

$$x_{Nj}(i) + x_{Nj}(i+1) = 2\bar{x}_{Nj}(\alpha)$$

and

$$[x_{Nj}(i)] + [x_{Nj}(i+1)] = I_{YNj\alpha}/m_i$$

The operations given by equations (4.3-131) constitute the first step in generating the nodal mass matrix for a thin body finite element. These equations ignore the moment of inertia of the finite element about the beam section through the node; therefore, there is no inertial force arising from the rotational acceleration $\ddot{\theta}_{yNj\alpha}$, figure 4.3-24, at the node. This constitutes an approximation, but the approximation is warranted because it greatly simplifies the computations for the lumped masses and because it is readily compensated for. In practice the inertia associated with the θ_{yNj} degree of freedom is difficult to compute and the error in having neglected this inertia can be readily reduced by simply decreasing the distance between nodes along the elastic axis.

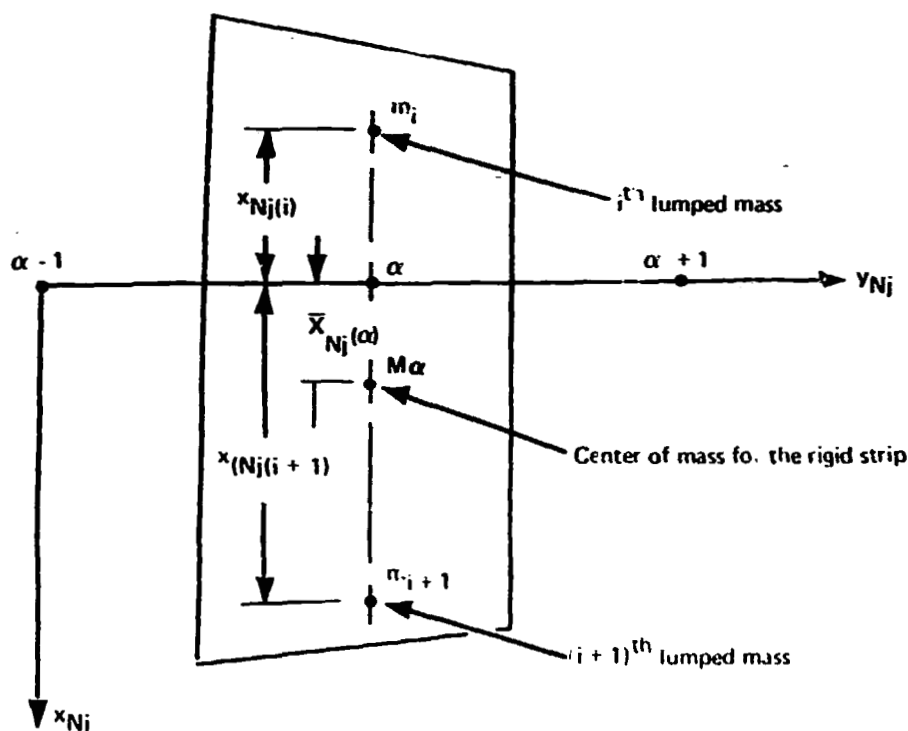


FIGURE 4.3-32. - LUMPED MASSES ON A THIN BODY SUBDIVISION

4.3.7.3 Nodal mass matrix for a thin body node.—The second step in generating the nodal mass matrix for an element of a thin body is facilitated by defining a lumped mass matrix of the form appearing in equation (4.3-127), viz.,

$$[m_i] = \begin{bmatrix} m_i & 0 & 0 \\ 0 & m_i & 0 \\ 0 & 0 & m_i \end{bmatrix}. \quad (4.3-132)$$

Evaluating the displacement functions, equation (4.3-128), at the coordinates of the i^{th} lumped mass, i.e.,

$$[N_e^a(i)] = \begin{bmatrix} 0 & 0 & 0 \\ -\sin\theta_N & 0 & x_{Nj}(i)\sin\theta_N \\ \cos\theta_N & 0 & -x_{Nj}(i)\cos\theta_N \end{bmatrix}, \quad (4.3-133)$$

the inertia at the α^{th} node due to the i^{th} lumped mass is given by the following

$$[m_{\delta}^a(i)_{\alpha}] = [\bar{n}_e^a(i)]^T [m_i] [\bar{N}_e^a(i)]. \quad (4.3-134)$$

The total inertia at this node is a consequence of the two masses m_i and m_{i+1} ; thus, the inertia given by equation (4.3-130) is found as

$$[m_{\delta\alpha}^a] = \left[[N_e^a(i)]^T [N_e^a(i+1)]^T \right] \begin{bmatrix} [m_i] & [0] \\ [0] & [m_{i+1}] \end{bmatrix} \begin{bmatrix} [N_e^a(i)] \\ [N_e^a(i+1)] \end{bmatrix}. \quad (4.3-135)$$

4.3.7.4 Lumped masses on a slender body.—Introducing approximations analogous to those adopted in section 4.3.7.2, the lumped masses on a slender body are point masses located at the slender body elastic axis nodes. The values of these lumped masses are equal to the mass of the slender body contained in the subdivisions shown by figures 4.3-33. In this case, in contrast to the approximation for thin bodies, increasing the number of subdivisions does not compensate entirely for the approximation introduced by replacing the distributed mass by point masses. Regardless of the number of lumped masses, the accelerations $\ddot{\theta}\chi_{\alpha}$, figure 4.3-25, fail to give rise to an inertial torsional couple about the elastic axis.

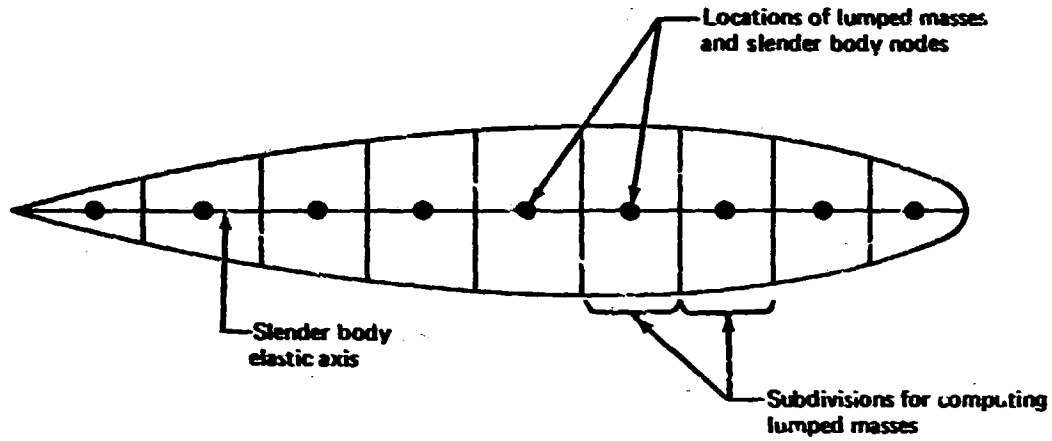


FIGURE 4.3-33.—LUMPED MASSES ON A SLENDER BODY SUBDIVISION

4.3.7.5 Nodal mass matrix for a slender body node.—The displacement relations for slender structural bodies, equation (4.3-80), when evaluated at the lumped mass, take on the following simple form

$$[N^a(i)] \equiv \begin{bmatrix} 0 & 0 & 0 & 0 & 0 \\ 1 & 0 & 0 & 0 & 0 \\ 0 & 1 & 0 & 0 & 0 \end{bmatrix} \quad (4.3-136)$$

The inertia at the α^{th} slender body node is found from equation (4.3-125) as

$$[m_\delta^a(i)_\alpha] = [N^a(i)]^T [m_i] [N^a(i)] \quad (4.3-137)$$

where $[m_i]$ is a diagonal mass matrix of the form given by equation (4.3-132). Carrying out the operations of equation (4.3-137), the inertia at the node is found as follows:

$$[m_\delta^a(i)_\alpha] = \begin{bmatrix} m_i & 0 & 0 & 0 & 0 \\ 0 & m_i & 0 & 0 & 0 \\ 0 & 0 & 0 & 0 & 0 \\ 0 & 0 & 0 & 0 & 0 \\ 0 & 0 & 0 & 0 & 0 \end{bmatrix} \quad (4.3-138)$$

4.3.7.6 Nodal mass matrices for junction point nodes.—The inertia of the structural components relative to the junction point nodes is obtained from equation (4.3-125). The i^{th} lumped mass on the N^{th} structural body with reference junction point at the Q^{th} node contributes the following inertia:

$$[m_\delta^N(i)_Q] = [N_C^N(i)]^T [m_i] [N_C^N(i)] \quad (4.3-139)$$

where $[N_C^N(i)]$ is the value of the constrained displacement relation, equation (4.3-52) or (4.3-53), at the location of the i^{th} lumped mass and $[m_i]$ is, again, given by equation (4.3-135).

The nodal inertia at the junction point node due to the i^{th} lumped mass on the m^{th} slender structural body is found to be

$$[m_{\delta}^M(i)_Q] = \begin{bmatrix} m_i & 0 & 0 & 0 & 0 & 0 \\ 0 & & & & & \\ 0 & & & & & \\ 0 & & \text{zeros} & & & \\ 0 & & & & & \\ 0 & & & & & \end{bmatrix} \quad (4.3-140)$$

while if the lumped mass is on the N^{th} thin body the contribution to the nodal mass matrix is given by

$$[m_{iQ}^N] \equiv \quad (4.3-141)$$

$$\begin{bmatrix} 1 & 0 & 0 & 0 & Y_N(i) & -Y_N(i) \\ & & & & \times \mu_N & \times \lambda_N \\ 0 & \lambda_N^2 & \lambda_N \mu_N & 0 & -X_N(i) & X_N(i) \\ & & & & \times \lambda_N \mu_N & \times \lambda_N^2 \\ 0 & \lambda_N \mu_N & \mu_N^2 & 0 & -X_N(i) & X_N(i) \\ & & & & \times \mu_N^2 & \times \lambda_N \mu_N \\ 0 & 0 & 0 & 0 & 0 & 0 \\ Y_N(i) & -X_N(i) & -X_N(i) & 0 & (Y_N(i)^2 + X_N(i)^2) & (X_N(i)^2 + Y_N(i)^2) \\ \times \mu_N & \times \lambda_N \mu_N & \times \mu_N^2 & & \times \mu_N^2 & \times (-\lambda_N \mu_N) \\ -Y_N(i) & X_N(i) & X_N(i) & 0 & (Y_N(i)^2 + X_N(i)^2) & (X_N(i)^2 + Y_N(i)^2) \\ \times \lambda_N & \times \lambda_N^2 & \times \lambda_N \mu_N & 0 & \times (-\lambda_N \mu_N) & \times \lambda_N^2 \end{bmatrix}$$

where $\cos \theta_N \equiv \lambda_N$ and $\sin \theta_N \equiv \mu_N$

4.3.7.7 Nodal mass matrix for a complete structure. - The operations leading to each of the element nodal mass matrices in the preceding involved evaluating the displacement relations, section 4.2.2.1, at the lumped masses. These displacement relations were combined into a single matrix, $[P_T]$, in section 4.2.7. Evaluating this matrix at the coordinates of the lumped masses, the resulting transformation is denoted as

$$\{d_m\} = [P_m]\{\delta\} \quad (4.3-142)$$

where $\{d_m\}$ describes the translational displacement of the lumped masses.

The lumped masses are combined into a single lumped mass matrix as follows:

$$[m] \equiv \begin{bmatrix} & & & & & \\ & & & & & \\ & & m_i & & & \\ & & & m_i & & \\ & & & & m_i & \\ & & & & & \\ \text{zeros} & & & & & \end{bmatrix} \quad (4.3-143)$$

where, as in equation (4.3-132), each lumped mass is repeated on the diagonal. The nodal mass matrix of a complete structure is now obtained as

$$[m_\delta] \equiv [P_m]^T [m] [P_m]. \quad (4.3-144)$$

This matrix appears in the equations of motion described in section 4.2.4—equations (4.2-68) and (4.2-78).

4.3.8 Reduction of the Nodal Mass Matrix

The nodal mass matrix, as given by equation (4.3-144), is singular and must be reduced to a nonsingular matrix to satisfy the requirements of the free-vibration problem introduced in section 4.2.4.1. The singularity of the nodal mass matrix is a consequence of the rows and columns of zeros appearing in the element nodal mass matrices—equations (4.3-130), (4.3-138), (4.3-140), and (4.3-141). The lumped mass matrix, $[m]$, which appears in the expression for the nodal mass matrix, is nonsingular; hence, the singularity stems from the transformation matrix $[P_m]$, equation (4.3-145), from nodal degrees of freedom to the degrees of freedom of the masses. A nonsingular nodal mass matrix therefore is obtained by carrying out a reduction of this transformation matrix.

4.3.8.1 Reduction of the mass transformation matrix $[P_m]$.—The basis for reducing the $[P_m]$ transformation matrix follows from a consideration of the following inertial forces acting at the lumped masses:

$$[m]\{\ddot{d}_m\} = [m][P_m]\{\ddot{\delta}\}. \quad (4.3-145)$$

Certain degrees of freedom contained in $\{\delta\}$ do not contribute to the inertial forces.

The massless degrees of freedom are removed from the set of nodal displacement components $\{\delta\}$ by a matrix operation. In the FLEXSTAB system, a mass is never located at the reference junction point of an aircraft, figure 4.3-7; therefore, the degrees of freedom at the reference junction point must be removed from $\{\delta\}$ along with the massless degrees of freedom listed in table 4.3-2. Since

$$\{\delta\} \equiv \begin{bmatrix} d_{X_R} \\ \{\delta_R^*\} \\ \{\delta_e^*\} \end{bmatrix} \quad (4.3-146)$$

the desired reduction is given by

$$\{\delta_{es}\} = [T_S^{**}] \{\delta_e^*\} \quad (4.3-147)$$

where $[T_S^{**}]$ is formed from an identity matrix by deleting the columns corresponding to the massless degrees of freedom contained in $\{\delta_e^*\}$. The columns deleted from the identity matrix in forming $[T_S^{**}]$ are formed into a second matrix $[T_{**}^S]$ so that

$$\{\delta_\theta\} = [T_{**}^S] \{\delta_e^*\} \quad (4.3-148)$$

where $\{\delta_\theta\}$ are the massless degrees of freedom listed in table 4.3-2.

TABLE 4.3-2.—MASSLESS INDEPENDENT DEGREES OF FREEDOM

Node location	Massless independent elastic degrees of freedom
Nth thin body elastic axis, node on the i^{th} elastic axis segment	θ_{xNi}
M^{th} slender body elastic axis, node on the elastic axis	$\theta_X, \theta_Y, \theta_Z$
Junction point node, outboard junction point of Nth thin body	
Joined to a thin body	θ_{XN}
Joined only to a slender body	$d_{ZN}, \theta_{XN}, \theta_{YN}$
Junction point node, outboard junction point of a slender body	
Joined to a thin body	θ_X
Joined only to a slender body	$d_Y, d_Z, \theta_X, \theta_Y, \theta_Z$

The transformation matrix $[P_m]$ must be partitioned to yield the following expression

$$\{d_m\} = [\{T_R\} \quad [T_R^*] \quad [T_e^*]] \begin{bmatrix} d_{xR} \\ \{\delta_R^*\} \\ \{\delta_e^*\} \end{bmatrix} \quad (4.3-149)$$

Letting

$$[T_e] \equiv [T_e^*][T_S^{**}]^T, \quad (4.3-150)$$

the reduced transformation is found as follows:

$$\{d_m\} = \{T_R\}d_{xR} + [T_e]\{\delta_{es}\} \quad (4.3-151)$$

where $\{d_m\}$ is unchanged from that given by equation (4.3-142).

4.3.8.2 Equilibrium of the inertial forces.—The inertial forces acting at the lumped masses, as a consequence of nodal accelerations, must be in self-equilibrium for the structure to be a free body. The inertial forces are given by

$$[m]\{\ddot{d}_m\} = [m]\{T_R\}\ddot{d}_{xR} + [m][T_e]\{\ddot{\delta}_{es}\} \quad (4.3-152)$$

and the inertial force at the structural reference point node must vanish for equilibrium:

$$Q_{X_R}^I = \{T_R\}^T [m]\{T_R\}\ddot{d}_{xR} + \{T_R\}^T [m][T_e]\{\ddot{\delta}_{es}\} = 0.$$

Introducing the mass definition

$$m_R = \{T_R\}^T [m]\{T_R\}, \quad (4.3-153)$$

the acceleration of the reference junction point node is found as

$$\ddot{d}_{xR} = -\frac{1}{m_R} \{T_R\}^T [m][T_e]\{\ddot{\delta}_{es}\}.$$

Substituting this expression for \ddot{d}_{xR} into equation (4.3-153), the following expression describes the accelerations of the lumped masses:

$$\{\ddot{d}_m\} = \left[[I] - \frac{1}{m_R} \{T_R\}\{T_R\}^T [m] \right] [T_e]\{\ddot{\delta}_{es}\}.$$

The reduced nodal mass matrix follows as

$$\begin{aligned} [m_{es}] &= [P_{em}]^T [m] [P_{em}] \\ &= [T_e]^T [m] [P_{em}] \end{aligned} \quad (4.3-154)$$

where

$$[P_{em}] \equiv \left[[I] - \frac{1}{m_R} \{T_R\}^T [m] \right] [T_e].$$

Equation (4.3-154) yields a nonsingular nodal mass matrix provided that lumped masses are placed at all nodes on the elastic axes of the thin and slender structural bodies. In the FLEXSTAB system, lumped masses need not be placed at all nodes; hence, a further reduction is required. A transformation matrix $[T_{es}^{**}]$ is formed in the manner of that appearing in equation (4.3-147) to eliminate elastic degrees of freedom of nodes which are not associated with lumped masses. The reduced nodal mass matrix is found using this transformation matrix as follows:

$$[m_e] \equiv [T_{es}^{**}] [m_{es}] [T_{es}^{**}]^T. \quad (4.3-155)$$

This nodal mass matrix has the desired nonsingular character and corresponds to the nodal mass matrix appearing in equation (4.2-70) - the eigenvalue problem for free vibration. A combined reduction transformation is obtained by combining equations (4.3-147) and the transformation $[T_{es}^{**}]$ and appears

$$[T_e^{**}] \equiv [T_{es}^{**}] [T_s^{**}] \quad (4.3-156)$$

and yields the following result

$$\{\delta_e^*\} = [T_e^{**}]^T \{\delta_e\}$$

where, in this case, the elements of $\{\delta_e^*\}$ corresponding to $\{\delta_m\}$ and $\{\delta_\theta\}$ have the value 0.

4.3.9 Free Vibrations

The structural equations of motion for the structure undergoing free vibrations are given by equation (4.2-70), i.e.,

$$\left[[K] - \omega^2 [m_\delta] \right] \{\delta_0\} = \{0\}. \quad (4.3-157)$$

As noted in section 4.2.4.1, this expression poses an eigenvalue problem which must be solved to find the free-vibration frequencies and mode shapes used in formulating the structural equations of motion in terms of the modal amplitudes $\{u_1\}$ and the residual flexibility in section 4.2.4.2.

The eigenvalue problem, equation (4.2-70), is not of standard form. Equation (4.2-70) represents a generalized eigenvalue problem. In the following, equation (4.2-70) is reduced to the form:

$$[A] - \omega^2[I]\{\xi\} = \{0\}, \quad (4.3-158)$$

i.e., the eigenvalue problem of standard form solved in the FLEXSTAB system. The reduction involves two steps.

4.3.9.1 Reduction to a standard eigenvalue problem.—The first step of the reduction eliminates the nodal components of acceleration contained in $\{\ddot{\xi}\}$ which do not give rise to nodal inertial forces. The nodal masses associated with these nodal components of acceleration are zero, and the mass matrix $[m_\delta]$ is rearranged and partitioned to give the following result:

$$\begin{bmatrix} \{Q_e^I\} \\ \{0\} \end{bmatrix} = \begin{bmatrix} [m_e] & [0] \\ [0] & [0] \end{bmatrix} \begin{bmatrix} \{\ddot{\delta}_e\} \\ \{\ddot{\delta}_m\} \end{bmatrix} \quad (4.3-159)$$

where the elements of $\{Q_e^I\}$ are all non-zero and the mass matrix $[m_e]$ is nonsingular.

The stiffness matrix $[K]$ is rearranged and partitioned to conform with equation (4.3-158) so that equation (4.2-70) is expressed as two matrix relations as follows:

$$[K_e]\{\delta_e\} + [K_{em}]\{\delta_m\} - \omega^2[m_e]\{\delta_e\} = \{0\}$$

and

$$[K_{me}]\{\delta_e\} + [K_m]\{\delta_m\} = \{0\}.$$

The second equation is solved for $\{\delta_m\}$, and the result is substituted into the first equation to obtain

$$[\bar{K}_e]\{\delta_e\} - \omega^2[m_e]\{\delta_e\} = \{0\} \quad (4.3-160)$$

where

$$[\bar{K}_e] \equiv [K_e] - [K_{em}][K_m]^{-1}[K_{me}]$$

Having reduced the problem so that it is expressed in terms of a nonsingular mass matrix, the second step makes use of the following transformation:

$$\{\xi\} = [L]^T \{\delta_e\} \quad (4.3-161)$$

where the transformation matrix $[L]$ is related to the mass matrix as follows:

$$[L][L]^T = [m_e]. \quad (4.3-162)$$

The transformation matrix $[L]$ is nonsingular by virtue of the nonsingular nature of $[m_e]$. Introducing the inverse transformation, viz.,

$$\{\delta_e\} = ([L]^T)^{-1} \{\xi\}, \quad (4.3-163)$$

and equation (4.3-162) into equation (4.3-160) and premultiplying the resulting expression by $[L]^{-1}$, it follows that

$$[A] - \omega^2 [I] \{\xi\} = \{0\} \quad (4.3-164)$$

where

$$[a] \equiv [L]^{-1} [\bar{K}_e] ([L]^T)^{-1}.$$

The mass matrix no longer appears since, by equation (4.3-162),

$$[L]^{-1} [m_e] ([L]^T)^{-1} = [I].$$

4.3.9.2 Solution to the free vibration problem. Equation (4.3-164) represents the standard form eigenvalue problem which is solved by the FLEXSTAB system. The eigenvalues are denoted as ω_i^2 and the eigenvectors as $\{\xi\}_i$. These quantities are formed into matrices as follows:

$$[\phi_\xi] \equiv [\{\xi\}_1 \{\xi\}_2 \cdots \{\xi\}_P] \quad (4.3-165)$$

and

$$[\omega^2] \equiv \begin{bmatrix} \omega_1^2 & & & \text{zeros} \\ & \omega_2^2 & & \\ & & \ddots & \\ \text{zeros} & & & \omega_P^2 \end{bmatrix}. \quad (4.3-166)$$

Equation (4.3-165) is referred to as a mode shape matrix because each column corresponds to a deformed shape for the aircraft, i.e., a mode of deformation. The mode shapes are transformed to the nodal displacement components by applying the inverse transformation given by equation (4.3-163), i.e.,

$$[\phi_e] = ([L]^T)^{-1}[\phi_\xi] \quad (4.3-167)$$

4.3.9.3 Construction of the transformation matrix.—The transformation matrix $[L]$ is a nonsingular, lower-triangular matrix, i.e.,

$$[L] = \begin{bmatrix} L_{11} & & & \\ L_{12} & L_{22} & \text{zeros} & \\ \vdots & \vdots & \vdots & \\ L_{n1} & L_{n2} & \dots & L_{nn} \end{bmatrix} \quad (4.3-168)$$

having elements computed as follows:

$$L_{11} = \sqrt{m_{e_{11}}}$$

$$L_{i1} = m_{e_{i1}} / L_{11} \quad \text{for } i=2,3,\dots,n$$

$$L_{ii} = \sqrt{m_{e_{ii}} - \sum_{K=1}^{i-1} L_{iK}^2} \quad \text{for } i>1 \quad (4.3-169)$$

$$L_{ij} = m_{e_{ij}} - \sum_{K=1}^{j-1} L_{iK} L_{jK} \quad \text{for } j<i \text{ and } j>1$$

$$L_{ij} = 0 \quad \text{for } i<j.$$

4.3.9.4 Nodal displacements in terms of generalized coordinates. If the nodal components of displacement $\{\delta_e\}$ are regarded as generalized coordinates, reference 4-1, pp. 11-12, then the free-vibration mode shape matrix is a transformation matrix, i.e.,

$$\{\delta_e\} = [\phi_e]\{u\} \quad (4.3-170)$$

where $\{u\}$ are amplitudes of mode shape deflections—modal amplitudes—and are new generalized coordinates which determine the elastic deformation of the structure.

The free-vibration mode shapes have the following orthogonality properties:

$$[\phi_e]^T [m_e] [\phi_e] = [\phi_\xi]^T [\phi_\xi] = [I], \quad (4.3-171)$$

i.e., $[\phi_\xi]$ is an orthogonal matrix.

$$[\phi_e]^T [\bar{K}_e] [\phi_e] = [\omega^2]$$

where $[\omega^2]$ is the diagonal matrix of eigenvalues.

It is necessary to have free-vibration mode shapes expressed in terms of the nodal displacements $\{\delta\}$. This is accomplished by a computation involving the stiffness matrix $[\bar{K}_e]$, equation (4.3-160); the flexibility matrix $[\tilde{C}]$, equation (4.2-64); and the special transformation matrix $[T_{es}^{**}]$, equation (4.3-155). The operation is as follows:

$$\{\delta\} = [\tilde{C}] [T_{es}^{**}]^T [\bar{K}_e] [\phi_e] \quad (4.3-172)$$

where, as noted in section 4.3.9.1, $[T_{es}^{**}]$ is constructed by deleting rows from an identity matrix $[I]$ initially equal in size to the flexibility matrix $[\tilde{C}]$. The rows deleted correspond to the rows deleted from the column matrix $\{\delta_{es}\}$ in the reduction to $\{\delta_e\}$, equation (4.3-159). The appropriateness of equation (4.3-172) may be seen by considering the following operation:

$$\{Q_e\}_i = [\bar{K}_e] \{\phi_e\}_i \quad (4.3-173)$$

The nodal forces $\{Q_e\}_i$ are the forces which must be applied to the structure to deform it into the shape of the i^{th} node. The nodal forces corresponding to the nodal displacement components $\{\delta_m\}$, equation (4.3-159), are all zero. Thus, the non-zero elements of

$$\{Q_{es}\}_i = [T_{es}^{**}] \{Q_e\}_i$$

are the nodal forces contained in $\{Q_{es}\}_i$, and it follows that

$$\{\phi_\delta\}_i = [C] [T_{es}^{**}]^T [\bar{K}_e] \{\phi_e\}_i \quad (4.3-174)$$

where, again, $[\tilde{C}]$ is the flexibility matrix defined by equation (4.2-84).

4.3.10 Combined Structural Relations

The structural relations derived in the preceding portions of section 4.3 are combined to produce the structural equations of motion for the steady reference flight condition, equation (4.2-64), and the unsteady perturbation flight condition, equation (4.2-78) or equations (4.2-84). These equations of motion contain the flexibility matrix $[\tilde{C}]$ and the residual flexibility matrix $[\tilde{C}_R]$; and, as shown by sections 4.2.6 through 4.2.8, these flexibility matrices are transformed to relate deformation of the aerodynamic surfaces to the applied aerodynamic and propulsion system forces. In the case of the elastic axis (i.e., beam theory) representation of the structure these transformations are identical to those of section 4.2; but, here, the transformations are formed in a manner differing computationally from that of section 4.2.

In the theoretical development of section 4.2, the nonsingular (i.e., clamped) flexibility matrix, C , is transformed to the free aircraft flexibility matrix, \tilde{C} , section 4.2.3.1, using the transformation matrix $[P]$, equation (4.2-53). The free aircraft flexibility matrix is then transformed using the transformations of sections 4.2.6 through 4.2.8. In the elastic axis representation of this section, i.e., section 4.2, the use of subsets of nodal displacement components, tables 4.3-1 and 4.3-2, allows special arrangements of the transformations $[P]$, $[P_\theta]$, $[P_d]$, $[P_T]$ and $[\Delta_G]$ to reduce the computational task involved in generating the structural equations of motion. These special forms are the subject of this section.

The combined structural relations developed herein are as follows:

$$\{d^*\} = [\tilde{C}_{dT}]\{f_T\} \quad (4.3-175)$$

$$\{\theta^*\} = [\tilde{C}_{\theta T}]\{f_T\} \quad (4.3-176)$$

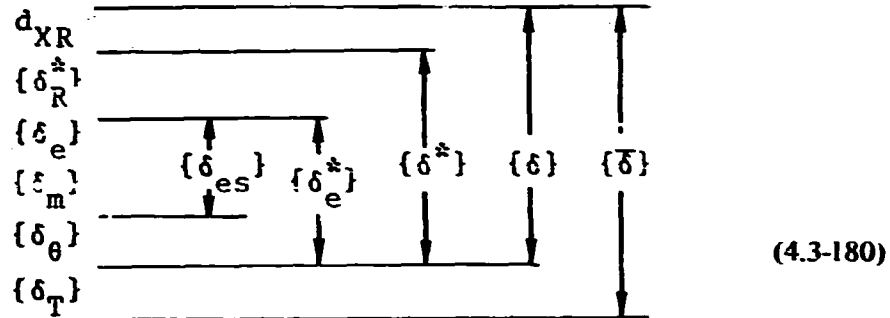
$$\{d^*\} = [\tilde{C}_{dG}]\{M^G\} \quad (4.3-177)$$

$$\{\theta^*\} = [\tilde{C}_{\theta G}]\{M^G\} \quad (4.3-178)$$

$$\begin{aligned} \{\phi_d^*\}_i &= [\tilde{C}_{dQ}][T_e^{**}]^T[\bar{K}_e]\{\phi_e\}_i \\ \{\phi_\theta^*\}_i &= [\tilde{C}_{\theta Q}][T_e^{**}]^T[\bar{K}_e]\{\phi_e\}_i \end{aligned} \quad (4.3-179)$$

Equations (4.3-175) and (4.3-176) relate the aerodynamic surface deformation to the set of aerodynamic forces, $\{f_T\}$, introduced by equation (3.5-39). Equations (4.3-177) and (4.3-178) relate aerodynamic surface deformation to the propulsion system gyroscopic couples, $\{M^G\}$, defined by equation (4.3-117). Finally, equations (4.3-179) yield aerodynamic surface translations and rotations related to free vibration mode shapes in the manner of equation (4.3-174). These relations are developed also for the case of residual flexibility.

The subsets of nodal displacement components related to the development are summarized as follows:



where the quantities on the left are defined as follows:

- d_{xR} : X-translation of reference junction point,
- $\{\delta_R^*\}$: elastic displacement of reference junction point, equation (4.3-18);
- $\{\delta_e\}$: node point displacement components producing displacement of point masses having finite masses;
- $\{\delta_m\}$: node point displacement components producing displacement of point masses having zero values;
- $\{\delta_\theta\}$: node point displacement components producing no displacement of point masses (having either zero or finite value);
- $\{\delta_T\}$: rate of twist components, equation (4.3-91).

These subsets are related by the following transformation matrices:

$$\begin{aligned}
 \{\delta_{es}\} &= [T_S^{**}]\{\delta_e^*\} \\
 \{\delta_\theta\} &= [T_{**}^S]\{\delta_e^*\} \\
 \{\delta_e\} &= [T_{es}^{**}]\{\delta_{es}\} \\
 \{\delta_m\} &= [T_{**}^{es}]\{\delta_{es}\} \\
 \{\delta_e\} &= [T_e^{**}]\{\delta_e^*\} \\
 \begin{bmatrix} \{\delta_m\} \\ \{\delta_e\} \end{bmatrix} &= [T_{**}^e]\{\delta_e^*\}
 \end{aligned}
 \tag{4.3-181}$$

$$\{\delta_R^*\} = [T_R^{**}]\{\delta^*\}$$

$$\{\delta_e^*\} = [T_{**}^P]\{\delta^*\}$$

$$\{\delta_{es}\} = [T^{**}]\{\delta^*\}$$

$$\{\delta_\theta\} = [T_{**}]\{\delta^*\}$$

Conjugate to the nodal displacement subsets are the following subsets of nodal forces:

$$\begin{array}{c} F_{XR} \\ \hline \{Q_R^*\} \\ \{Q_e\} \\ \{Q_m\} \\ \{Q_\theta\} \end{array} \quad \begin{array}{c} \xrightarrow{\quad} \\ \xrightarrow{\quad} \\ \xrightarrow{\quad} \\ \xrightarrow{\quad} \\ \xrightarrow{\quad} \end{array} \quad \begin{array}{c} \{Q^*\} \\ \{Q_e^*\} \\ \{Q_\theta^*\} \\ \{Q\} \end{array} \quad (4.3-182)$$

where it may be noted that the set of forces $\{Q\}$ contains no elements conjugate to the displacement set $\{\delta_T\}$, i.e., the twist rates introduced by section 4.3.4.5.

4.3.10.1 *Stiffness matrices.*—Recall the composite stiffness relation given by equation (4.3-42), i.e.,

$$\{Q^*\} = [\bar{K}]\{\varepsilon^*\}. \quad (4.3-42)$$

This expression is written as follows using the transformation described by equation (4.3-181):

$$\begin{bmatrix} \{Q_R^*\} \\ \{Q_{es}\} \\ \{Q_\theta\} \end{bmatrix} = \begin{bmatrix} [K_{RR}] & [K_{RS}] & [K_{R\theta}] \\ & [K_{SS}] & [K_{S\theta}] \\ \text{SYM.} & & [K_{\theta\theta}] \end{bmatrix} \begin{bmatrix} \{\delta_R^*\} \\ \{\delta_{es}\} \\ \{\delta_\theta\} \end{bmatrix} \quad (4.3-183)$$

where, for example,

$$[K_{RR}] \equiv [T_R^{**}]^T [K] [T_R^{**}]$$

This stiffness relation is reduced assuming the forces $\{Q_R^*\}$ and $\{Q_\theta\}$ to be zero. The reduced relation is

$$\{Q_{es}\} = [\tilde{K}]\{\delta_{es}\} \quad (4.3-184)$$

where

$$\begin{aligned} [\tilde{K}] = & ([K_{ss}] - [K_{s\theta}][K_{\theta\theta}]^{-1}[K_{s\theta}]^T) \\ & - ([K_{Rs}]^T - [K_{s\theta}][K_{\theta\theta}]^{-1}[K_{R\theta}]^T) \\ & \times ([K_{RR}] - [K_{R\theta}][K_{\theta\theta}]^{-1}[K_{R\theta}]^T)^{-1} \\ & \times ([K_{Rs}] - [K_{R\theta}][K_{\theta\theta}]^{-1}[K_{s\theta}]^T). \end{aligned}$$

A second reduction is performed as

$$[\bar{K}_e] = [\tilde{K}_{ee}] - [\tilde{K}_{em}][\tilde{K}_{mm}]^{-1}[\tilde{K}_{me}] \quad (4.3-155)$$

where

$$[\tilde{K}_{em}] \equiv [T_{es}^{**}][\tilde{K}][T_{**}^{es}]^T$$

$$[\tilde{K}_{mm}] \equiv [T_{**}^{es}][\tilde{K}][T_{**}^{es}]^T$$

$$[\tilde{K}_{ee}] \equiv [T_{es}^{**}][\tilde{K}][T_{es}^{**}]^T.$$

This is the stiffness matrix appearing in the free vibration problem, equation (4.3-160).

4.3.10.2. Flexibility.—The flexibility matrix is found from the stiffness relation

$$\begin{bmatrix} \{Q_R^*\} \\ \{Q_e^*\} \end{bmatrix} = \begin{bmatrix} [K_{RR}] & [K_{Re}] \\ [K_{eR}] & [K_{ee}] \end{bmatrix} \begin{bmatrix} \{\delta_R^*\} \\ \{\delta_e^*\} \end{bmatrix}$$

obtained from equation (4.3-43) and is given by

$$[C_e^*] = [K_{ee}]^{-1} \quad (4.3-186)$$

The flexibility relation is then written as

$$\{\delta_e^*\}' = [C_e^*]\{Q_e^*\} \quad (4.3-187)$$

where the prime indicates nodal displacement components measured relative to a reference frame fixed to the node at the reference junction point of the assembled configuration

Recall the transformation given by equation (4.3-149) from which translation of the point masses, equation (4.3-142), relative to the reference frame fixed to the aircraft reference junction point, are given by

$$\{d'_m\} = [T_e] \{\delta'_{es}\} \quad (4.3-188)$$

Introducing the reference frame transformation given by equation (4.2-30) yields

$$\{d_m\} = \{d'_m\} + [\bar{\phi}_R] \{\delta_R\} \quad (4.3-189)$$

The mean reference frame constraint conditions, equation (4.2-62), are now introduced to determine the elements of $\{\delta_R\}$ as

$$\{\delta_R\} = -[M_R]^{-1} [\bar{\phi}_R]^T [f_m] [T_e] [C_e] \{C_{es}\} \quad (4.3-190)$$

where

$$[C_e] \equiv [T_s^{**}] [C_e^*] [T_s^{**}]^T$$

and

$$[M_R] \equiv [\bar{\phi}_R]^T [f_m] [\bar{\phi}_R]$$

Deformation of the aerodynamic surfaces $\{d^*\}$ does not involve the nodal displacement components $\{\delta_p\}$ defined by equation (4.3-180); thus,

$$\{d^*\} = [T_{de}^{**}] \{\delta'_{es}\} \quad (4.3-191)$$

where

$$[T_{de}^{**}] \equiv [T_{de}^*] [T_s^{**}]^T,$$

i.e., a combination of the transformation matrices introduced by equations (4.3-99) and (4.3-181). The deformation $\{d^*\}$ is subjected to the structural reference frame transformation, equation (4.3-189), to obtain

$$\{d^*\} = [\bar{\phi}_R^*] \{\delta_R\} + [T_{de}^{**}] \{\delta'_{es}\} \quad (4.3-192)$$

A similar result is obtained for the surface deformation $\{\theta^*\}$. Recalling equation (4.3-100), this deformation is transformed as

$$\{\theta^*\} = [\bar{\phi}_\theta^*] \{\delta_R\} + [T_{de}^*] \{\delta'_{es}\} + [T_{\theta T}^*] \{\delta_T\} \quad (4.3-193)$$

where $[\bar{\phi}_\theta^*]$ describes aerodynamic surface rotation due to rigid body motion about the aircraft reference junction point. Introducing the reference junction point components of nodal displacement from equation (4.3-190), the aerodynamic surface deformation relative to a mean reference frame is found as

$$\{d^*\} = [T_{de}^*] \{\delta'_{es}\} \quad (4.3-194)$$

where

$$[T_{de}^*] \equiv [T_{de}^{**}] - [\bar{\phi}_R^*] [M_R]^{-1} [\bar{\phi}_R]^T [f_m] [T_e]$$

and

$$\{\theta^*\} = [P_{\theta e}^*]\{\delta_e^*\} + [P_{\theta T}^*]\{\delta_T\} \quad (4.3-195)$$

where

$$[P_{\theta e}^*] \equiv [T_{\theta e}^*] - [\bar{\phi}_{\theta}^*][M_R]^{-1}[\bar{\phi}_R]^T[m][T_e][T_S^{**}].$$

The results obtained above lead to the following flexibility relations:

$$\{d^*\} = [\bar{C}_{dQ}]\{Q_{es}\} \quad (4.3-196)$$

where

$$[\bar{C}_{dQ}] \equiv [P_{de}][C_e]$$

and

$$\{\theta^*\} = [\bar{C}_{\theta Q}]\{Q_{es}\} \quad (4.3-197)$$

where

$$[\bar{C}_{\theta Q}] \equiv [P_{\theta e}][T_S^{**}]^T + [T_{\theta T}^*][C_e^*],$$

$$[P_{\theta e}] \equiv [P_{\theta e}^*][C_e^*],$$

and

$$[C_e^*] \equiv [C_e^{**}][T_S^{**}]^T.$$

These flexibility relations are related to the point mass inertial forces $\{F^I\}$ by introducing the transformation matrix $[T_e]$, equation (4.3-150), thereby yielding

$$\{d^*\} = [\bar{C}_{de}]\{F^I\} \quad (4.3-198)$$

where

$$[\bar{C}_{de}] \equiv [\bar{C}_{dQ}][T_e]^T$$

and

$$\{\theta^*\} = [\bar{C}_{\theta e}]\{F^I\} \quad (4.3-199)$$

where

$$[\bar{C}_{\theta e}] \equiv [\bar{C}_{\theta Q}][T_e]^T$$

Following the development of section 4.2.2.5, the forces acting on the aircraft structure are given by

$$\{Q\} = \{Q^S\} = [m_\delta][\bar{\phi}_\delta][M]^{-1}[\bar{\phi}_\delta]^T\{Q^S\} - [m_\delta]\{\ddot{\delta}\}. \quad (4.3-200)$$

The inertial forces, i.e., the second and third terms on the right of equation 4.3-200, are expressed in terms of the point masses, $[m]$ of equation (4.3-144), as

$$\{F^I\} = - \left([m][\bar{\phi}_m]\{\ddot{B}\} + [m]\{\ddot{d}_m\} \right) \quad (4.3-201)$$

where $[\bar{\phi}_m]$ is the rigid body mode shape matrix for the point mass locations expressed relative to the aircraft center of mass. The applied forces in the form $\{f_T\}$, equation 3.5-39, are transformed to the elastic axis nodes using equation (4.2-116), i.e.,

$$\{Q^A\} = [P_T]^T\{f_T\},$$

and equation (4.3-101) as

$$\{Q_{es}^A\} = [T_{Te}^{**}]^T\{f_T^A\} \quad (4.3-202)$$

and

$$F_{XR}^A = [T_R^*]^T\{f_T^A\}$$

where

$$[T_{Te}^{**}] = [T_{Te}^*][T_S^{**}]^T$$

The inertial forces at the elastic axis nodes follow from equation (4.3-151) as

$$\{Q_{es}^I\} = - [T_e]^T \left([m][\bar{\phi}_m]\{\ddot{B}\} + [m]\{\ddot{d}_m\} \right) \quad (4.3-203)$$

and

$$F_{XR}^I = -[T_R]^T \left([m][\bar{\phi}_m]\{\ddot{B}\} + [m]\{\ddot{d}_m\} \right).$$

Combining the first of equations (4.3-202) with the first of equations (4.3-203) leads to the equivalent of equation (4.3-200), viz.,

$$\{Q_{es}\} = [T_{Te}^{**}]^T\{f_T\} - [T_e]^T \left([m][\bar{\phi}_m]\{\ddot{B}\} + [m]\{\ddot{d}\} \right). \quad (4.3-204)$$

Also, from the second of equations (4.3-202) and 4.3-203) and from the fact that, at the aircraft reference junction point, the total force must vanish, i.e.,

$$F_{XR} + F_{XR}^I = 0,$$

it follows that

$$\{T_R^*\}^T \{f_T\} = \{T_R\}^T \left([m][\ddot{\phi}_m] \{B\} + [m][\ddot{d}_m] \right). \quad (4.3-205)$$

But, from equation (4.3-152)

$$\{\ddot{d}_m\} = \{T_R\} \ddot{d}_{XR} + [T_e] \{\ddot{\delta}_{es}\}, \quad (4.3-206)$$

it follows from equations (4.3-205) and (4.3-206) that

$$\ddot{d}_{XR} = - \frac{1}{m_R} \{T_R\}^T [m] [T_e] \{\ddot{\delta}_{es}\} \quad (4.3-207)$$

where

$$m_R \equiv \{T_R\}^T [m] \{T_R\}.$$

Substituting equation (4.3-207) into (4.3-206) and, in turn, substituting the result into equation (4.3-204), leads to the total forces at the elastic axis nodes expressed as

$$\{Q_{es}\} = [P_e]^T \{f_T\} - [m_{es}] \{\ddot{\delta}_{es}\} \quad (4.3-208)$$

where

$$[P_e]^T \equiv [T_{Te}^{**}]^T - 2[T_e]^T [m] [\ddot{\phi}_m] [M]^{-1} [\ddot{\phi}^*]^T$$

and the mass matrix, identical with equation (4.3-154), is expressed as

$$[m_{es}] \equiv [T_e]^T [m] \left([I] - \frac{1}{m_R} \{T_R\} \{T_R\}^T [m] \right) [T_e].$$

The desired flexibility relations, equations (4.3-175) through (4.3-179), are now found as follows:

Equation (4.3-175) follows from equations (4.3-196) and (4.3-208) as

$$\{d^*\} = [\tilde{C}_{dT}] \{f_T\} \quad (4.3-209)$$

where

$$[\tilde{C}_{dT}] \equiv [\tilde{C}_{dq}] [P_e]^T$$

Equation (4.3-176) follows from equations (4.3-197) and (4.3-208) as

$$\{\theta^*\} = [\tilde{C}_{\theta T}]\{f_T\} \quad (4.3-210)$$

where

$$[\tilde{C}_{\theta T}] \equiv [\bar{C}_{\theta T}][P_e]^T$$

Equation (4.3-177) follows from equation (4.3-196) and (4.3-123) as

$$\{d^*\} = [\tilde{C}_{dG}]\{M^G\} \quad (4.3-211)$$

where

$$[\tilde{C}_{dG}] \equiv [P_{de}][T_e^{**}][C_e^*][T_G]$$

Equation (4.3-178) follows from equation (4.3-197) and (4.3-123) as

$$\{\theta^*\} = [\tilde{C}_{\theta G}]\{M^G\} \quad (4.3-212)$$

where

$$[\tilde{C}_{\theta G}] \equiv ([P_{\theta e}] + [T_{\theta T}][C_e^*])[T_G]$$

Equations (4.3-179) follow directly by combining equations (4.3-185), (4.3-196), and (4.3-197).

4.3.10.3 Residual flexibility matrices.—The structural equations of motion in the case of residual flexibility, section 4.2.4.2, are derived from the stiffness relation given by equation (4.3-184) expressed in terms of the partitions defined by equation (4.3-185), viz.,

$$\begin{bmatrix} [\tilde{K}_{ee}] & [\tilde{K}_{em}] \\ [\tilde{K}_{me}] & [\tilde{K}_{mm}] \end{bmatrix} \begin{bmatrix} \{\delta_e\} \\ \{\delta_m\} \end{bmatrix} = \begin{bmatrix} [T_{es}^{**}] \\ [T_{ms}^{es}] \end{bmatrix} [P_e]^T \{f_T\}$$

$$= - \begin{bmatrix} [m_e] \{\ddot{\delta}_e\} \\ \{0\} \end{bmatrix} \quad (4.3-213)$$

where the nodal forces are those given by equation (4.3-208) and

$$[m_e] \equiv [T_{es}^{**}][m_{es}][T_{es}^{**}]^T \quad (4.3-214)$$

The mass matrix $[m_e]$ is the nonsingular mass matrix appearing in the free vibration problem equation (4.3-158).

Treating equation (4.3-213) as two matrix equations, one may be solved for the nodal displacement components $\{\delta_m\}$ as

$$\{\delta_m\} = [\tilde{K}_{mm}]^{-1} \left([T_{**}^{es}] [P_e]^T \{f_T\} - [\tilde{K}_{me}] \{\delta_e\} \right)$$

and substituted into the other to obtain

$$[\bar{K}_e] \{\delta_e\} = [P_e^*]^T \{f_T\} - [m_e] \{\ddot{\delta}_e\} \quad (4.3-215)$$

where $[\bar{K}_e]$ is the stiffness matrix defined by equation (4.3-185) and

$$[P_e^*]^T \equiv \left([T_{es}^{**}] - [\tilde{K}_{em}] [\tilde{K}_{mm}]^{-1} [T_{**}^{es}] \right) [P_e]^T$$

The physical significance of the operation

$$[P_e^*]^T \{f_T\}$$

is as follows:

$$[T_{**}^{es}] [P_e]^T \{f_T\} = \text{net forces acting at nodes having no mass (i.e., massless nodes);}$$

$$[\tilde{K}_{mm}]^{-1} [P_e]^T \{f_T\} = \text{deflections at massless nodes due to net forces at massless nodes;}$$

$$[\tilde{K}_{em}] [\tilde{K}_{mm}]^{-1} [P_e]^T \{f_T\} = \text{net forces of constraint at nodes having mass due to net forces at massless nodes;}$$

$$[T_{es}^{**}] [P_e]^T \{f_T\} = \text{net forces acting directly on nodes having mass; and}$$

finally,

$$[P_e^*]^T \{f_T\} = \text{net forces acting on nodes having mass due to direct net forces plus the net forces acting at massless nodes.}$$

Introducing the free vibration mode shapes of section 4.2.9 by substituting

$$\{\delta_e\} = [\phi_e] \{u\} \quad (4.3-170)$$

and by applying the orthogonality conditions of equation (4.3-171), the structural equations of motion, equation (4.3-215), become

$$\{u\} = [\omega^2] [\phi_\xi]^T \left\{ [I]^{-1} [P_e^*]^T \{f_T\} - [\phi_\xi] \{\ddot{u}\} \right\} \quad (4.3-216)$$

The residual flexibility form of the equations of motion, corresponding to equations (4.2-84), are obtained by partitioning equation (4.3-216),

The appropriate partitioned form of equation (4.3-216) is that corresponding to equation (4.2-79) and is obtained by letting

$$\{u\} = \begin{bmatrix} \{u_1\} \\ \{u_2\} \end{bmatrix} \quad (4.3-217)$$

Assuming that the term $\{\ddot{u}_2\}$ is negligible and following the development of section 4.3.9, the structural equations of motion are found as

$$\{\ddot{u}_1\} + [\omega_1^2]\{u_1\} = [\phi_{e1}]^T [P_e^*]^T \{f_T\} \quad (4.3-218)$$

and

$$\{d_2^*\} = [\tilde{C}_{RdQ}][P_e^*]^T \{f_T\} \quad (4.3-219)$$

$$\{\theta_2^*\} = [\tilde{C}_{R\theta Q}][P_e^*]^T \{f_T\} \quad (4.3-220)$$

where

$$[\tilde{C}_{RdQ}] \equiv [\bar{C}_{dQ}][T_{es}^{**}]^T - [\phi_{d1}][\omega_1^2]^{-1}[\phi_{e1}]^T$$

$$[\tilde{C}_{R\theta Q}] \equiv [\bar{C}_{\theta Q}][T_{es}^{**}]^T - [\phi_{\theta 1}][\omega_1^2]^{-1}[\phi_{e1}]^T$$

and

$$[\phi_{d1}] \equiv [\bar{C}_{dQ}][T_e^{**}]^T [\bar{k}_e][\phi_{e1}]$$

$$[\phi_{\theta 1}] \equiv [\bar{C}_{\theta Q}][T_e^{**}]^T [\bar{k}_e][\phi_{e1}]$$

The residual flexibility matrices corresponding to equations (4.3-175) and (4.3-176) are seen to be as follows:

$$[\tilde{C}_{RdT}] \equiv [\tilde{C}_{RdQ}][P_e^*]^T \quad (4.3-221)$$

$$[\tilde{C}_{R\theta T}] \equiv [\tilde{C}_{R\theta Q}][P_e^*]^T \quad (4.3-222)$$

4.4 EXTERNAL STRUCTURAL INFLUENCE COEFFICIENTS

In this section the following matrices are assumed to be generated by a finite element structural analysis computer program which is external to the FLEXSTAB system:

$[C]$, flexibility matrix for a constrained structure, equation (4.2-60);

$[m_\delta]$, nodal mass matrix, equation (4.2-18);

$[M]$, total mass-inertia matrix, equation (4.2-26);

$[\bar{\phi}_\delta]$, rigid body mode shape matrix, equation (4.2-21);

$[\phi_\delta]$, free vibration mode shape matrix, equation (4.2-69);

$[k_1]$, $[m_1]$, generalized stiffness and mass matrices, equation (4.2-76);

$[\Delta_G]$, gyroscopic transformation matrix, equation (4.2-118).

These matrices provide all the data required to formulate the structural equations of motion in terms of nodal displacements and forces. For the steady reference flight condition, section 4.2.3, the equations of motion are given by

$$\{\delta\}_1 = [\tilde{C}]_1 \{Q^S\}_1 \quad (4.2-64)$$

and for the unsteady perturbation flight condition, section 4.2.4, the equations of motion are given by

$$[m_1] \{\ddot{u}_1\}_p + [k_1] \{u_1\}_p = [\phi_{\delta 1}]^T \{Q^S\}_p + [k_1] \{u_1\}_p$$

and

$$\{\delta_2\}_p = [\tilde{C}_R]_1 \{Q^S\}_p. \quad (4.2-84)$$

The supplied matrices, listed above, must be such that they can be related to the structural idealization incorporated into the FLEXSTAB system. Also, the elements of the supplied matrices are required to have a specific arrangement. The objective of this section is to derive the equations relating the supplied matrices to the structural idealization and to delineate the requirements that the supplied matrices must satisfy.

The structural idealization is described in sections 4.2.6 and 4.2.7, where it is deduced from the boundary conditions for the linear, first order aerodynamic theory derived in section 3.2. Using the finite element concept of a displacement function, item (c) of section 4.2.2.1, the structural idealization was related to nodal force and displacement components (i.e., $\{Q\}$ and $\{\delta\}$) by the following matrix relations:

$$\{d^*\} = [P_\delta] \{\delta\} \quad (4.2-100)$$

$$\{q^*\} = [I_\delta] \{Q\} \quad (4.2-101)$$

$$\{Q^A\} = [P_T]^T \{f_T^A\} \quad (4.2-116)$$

$$\{g^G\} = [\Delta_G]^T \{\delta\} \quad (4.2-118)$$

$$\{Q^T\} = [P_T]^T [NAF] \{T\} \quad (4.2-119)$$

and

$$[P] = \left[[I] - [m_\delta] [\tilde{\phi}_\delta] [M]^{-1} [\tilde{\phi}_\delta]^T \right] \quad (4.2-53)$$

where the matrix operator $[P]$ is used to perform the following transformations of section 4.2.2.5 related to structural inertia:

$$\{\delta\} = [P]^T \{\delta^*\}$$

and

$$\{Q\} = [P]\{Q^S\}.$$

In section 4.2 no particular form was chosen for the displacement relations used in generating these formulas; hence, the nodal force and displacement components were left unspecified in section 4.2. In the following a particular choice of the displacement relations is made. This choice places specific requirements on nodal displacement components and on the locations of the node points; and, through the virtual work relationship of item (c) of section 4.2.2.1, the choice of displacement relations also determines the nodal force components that are admissible. These requirements are imposed on the supplied matrices.

The matrix operators $[P_d]$, $[P_\theta]$, $[P_T]$, $[\Delta_G]$, and $[P]$ are derived in the following, and this derivation delineates the requirements that must be satisfied by the supplied matrices. The derivation of the matrix operators $[P_d]$, $[P_\theta]$, and $[P_T]$ is based on the FLEXTAB system idealization of the structure. This derivation is carried out in section 4.4.1 and is based on the assumption that the supplied structural matrices are expressed in terms of the coordinate systems used in formulating the aerodynamic theory, i.e., the Reference Axis System, section 2.2.4, and the local thin body axis systems, section 3.2.4. The supplied matrices, however, can be described in alternate coordinate systems introduced by section 4.4.2, but there can be no coordinate transformation producing a change in the nodal components. The contents of section 4.4.2, therefore, hold in the alternate coordinate systems. The matrix operator $[\Delta_G]$ is described in section 4.4.3, and special forms of the matrix operator $[P]$ are developed in section 4.4.4. Finally, the requirements that must be satisfied by the supplied matrices are summarized in section 4.4.5.

4.4.1 Structural Idealization

As shown in sections 4.2.6 and 4.2.7, the structure is idealized as a collection of thin and slender structural bodies set into correspondence with the thin and slender bodies introduced

by the aerodynamic idealization of section 4. The elastic deformation, which has a first order effect on the aerodynamic surface pressure, cf., section 3.2, is that which appears as a platelike deformation at the aerodynamic mean surfaces of thin bodies and as a beamlike deformation at the aerodynamic mean centerlines of slender bodies. (See figure 4.2-5.) Further, as shown in sections 3.5 and 4.2.7, the aerodynamic surface pressure distribution is resolved into airloads acting at the mean surfaces of thin bodies and at the mean centerlines of slender bodies.

The finite element representation of the structure is required to incorporate nodal displacement components $\{\delta\}$. These govern displacement relations which, in turn, will describe the platelike and beamlike elastic deformation of the structural bodies. The nodal displacement components and their work-conjugate nodal force components employed in the FLEX-STAB system, are described in the sections immediately following. The displacement relations chosen for the thin and slender structural bodies are then introduced and are used in a derivation of the matrix operators $[P_d]$, $[P_\theta]$, and $[P_T]$.

4.4.1.1 Components of nodal displacement.—The structural node points are assumed to be located on the mean aerodynamic surfaces of thin bodies and on the mean aerodynamic centerlines of slender bodies, sections 3.2.3 and 3.2.4. Up to three mutually perpendicular components of translation are permitted at each node, figure 4.4-1. For the α^{th} node on a thin body mean surface, the components are expanded on the local thin body axis system, figures 3.2-3 and 3.2-4, as follows:

$$\{\delta_\alpha\}_W \equiv \begin{bmatrix} d_{XN\alpha} \\ d_{YN\alpha} \\ d_{ZN\alpha} \end{bmatrix}_W \quad (4.4-1)$$

For the α^{th} node on a slender body mean centerline, the components are expanded on the Reference Axis System,* section 2.2.4, as follows:

$$\{\delta_\alpha\}_B \equiv \begin{bmatrix} d_{X\alpha} \\ d_{Y\alpha} \\ d_{Z\alpha} \end{bmatrix}_B \quad (4.4-2)$$

*Note, from the contents of section 2.2.2, that these axis systems can be either mean or structural reference frames.

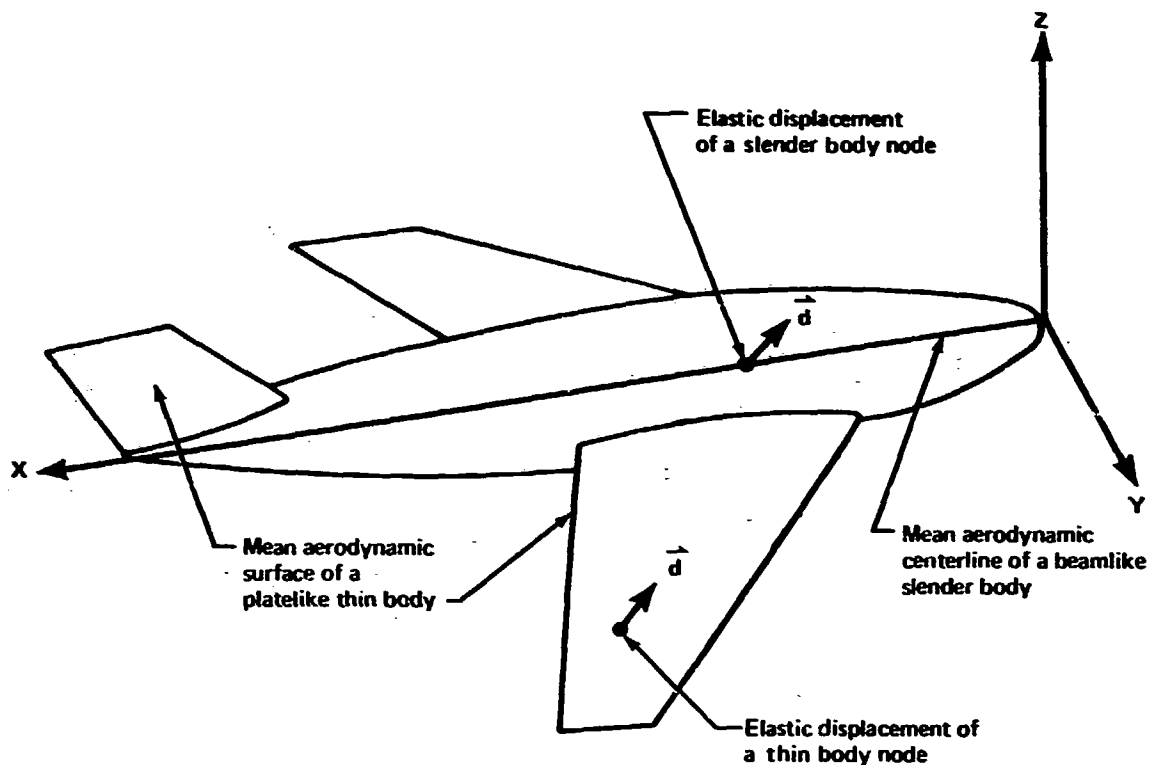


FIGURE 4.4-1.—DEFORMATION OF A CONFIGURATION

The entire nodal displacement matrix $\{\delta\}$ has elements arranged as follows:

$$\{\delta\} \equiv \begin{bmatrix} \vdots \\ \{\delta_{\alpha}\}_B \\ \vdots \\ \vdots \\ \{\delta_{\alpha}\}_w \\ \vdots \end{bmatrix} \begin{matrix} \uparrow \\ \text{nodes on slender bodies} \\ \uparrow \\ \downarrow \\ \text{nodes on thin bodies} \\ \downarrow \end{matrix} \quad (4.4-3)$$

In the analysis of many aircraft configurations, certain of the components contained in the nodal displacement matrix, equation (4.4-3), have negligible effect on the aeroelasticity. For conventional aircraft configurations the nodal displacement components dX_{α} and $dY_{N_{\alpha}}$ may usually be deleted at thin body nodes while dX_{α} may usually be deleted at slender body nodes. The set of nodal displacement components retained in equation (4.4-3) is optional; but

considerable care must be exercised in the selection of the displacement components to be deleted to avoid elimination of significant aeroelastic effects in the FLEXSTAB system analysis because, as shown below, the work-conjugate aerodynamic forces are also eliminated.

4.4.1.2 Components of nodal forces.—The nodal force components used in formulating the externally generated structural matrices are required to be conjugate with nodal displacement components in a computation of the work done by the applied forces in deforming the structure:

$$W = \frac{1}{2} \{\delta\}^T \{Q\} \equiv \frac{1}{2} \begin{bmatrix} \{\delta\}_B \\ \{\delta\}_W \end{bmatrix}^T \begin{bmatrix} \{Q\}_B \\ \{Q\}_W \end{bmatrix} \quad (4.4-4)$$

The nodal force at the α^{th} node of a thin body may, therefore, have the following components expanded on the local thin body axis system:

$$\{Q_\alpha\}_W \equiv \begin{bmatrix} F_{XNa} \\ F_{YNa} \\ F_{ZNa} \end{bmatrix}_W \quad (4.4-5)$$

At the α^{th} node of a slender body the components of nodal force are expanded on the Reference Axis System:

$$\{Q_\alpha\}_B \equiv \begin{bmatrix} F_{Xa} \\ F_{Ya} \\ F_{Za} \end{bmatrix}_B \quad (4.4-6)$$

The entire nodal force matrix $\{Q\}$ has elements arranged as follows:

$$\{Q\} = \begin{bmatrix} \vdots \\ \{Q_\alpha\}_B \\ \vdots \\ \hline \vdots \\ \{Q_\alpha\}_W \end{bmatrix} \quad \begin{array}{l} \text{nodes on slender bodies} \\ \\ \text{nodes on thin bodies} \end{array} \quad (4.4-7)$$

4.4.1.3 Symmetric and antisymmetric forms.—To be consistent with the FLEXSTAB system, the externally generated structural matrices must be expressed only in terms of nodes located on and to the right of the plane of symmetry of a configuration, section 4.2.5. The nodal force and displacement matrices are assumed to express symmetry or antisymmetry with respect to the plane of symmetry in the manner of equations (4.2-86) through (4.2-88). For the symmetric case the nodal force and displacement matrices, $\{Q\}^S$ and $\{\delta\}^S$, contain only X and Z components at nodes on the plane of symmetry, while for the antisymmetric case, $\{Q\}^A$ and $\{\delta\}^A$ contain only Y components at nodes on the plane of symmetry.

4.4.1.4 Displacement relations.—The objective of the following is to develop the forms of the displacement relations used in deriving the matrix operators $[P_d]$, $[P_\theta]$, and $[P_T]$.

4.4.1.5 Thin body displacement relations.—The structure of a thin body is assumed to consist of a rib-spar-cover plate arrangement typical of aircraft lifting surface structures, figure 4.4-2. Node points are assumed to be located along the line of intersection of rib and spar structural components. The assumption is also made that the change in nodal displacement along this line through the thickness of the thin body is negligible and that the node may be placed at any point between the two cover plates.

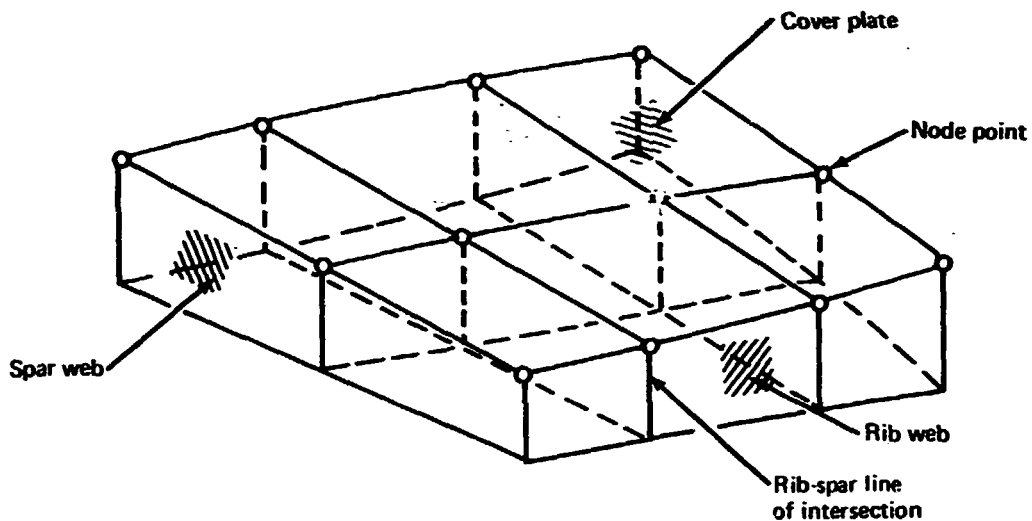


FIGURE 4.4-2.—TYPICAL THIN BODY STRUCTURE

Local bending deflections of the cover plates are ignored in computing deformation of the camber shape of a thin body. The camber shape between nodes is assumed to deform as a membrane. The quadrilateral sections of the thin body mean surface cut out by the spars and ribs are subdivided, as in section 5.8 3.1 of reference 1-2, into the four triangular regions shown by figure 4.4-3. Each triangular region is a structural finite element having simple support at its vertices (i.e., at the nodes of the structure) and having infinite stiffness for out-of-plane bending and zero stiffness for in-plane stretching.

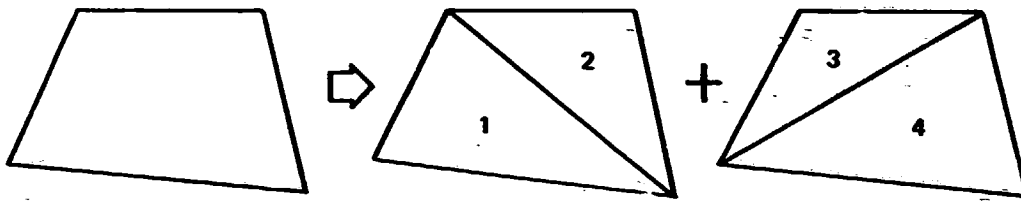


FIGURE 4.4-3.—QUADRILATERAL MEMBRANE FINITE ELEMENT

The displacement relation for the triangular element, figure 4.4-4, is the following linear function of the local thin body coordinates (X_N, Y_N):

$$\begin{aligned} d_{XN}(X_N, Y_N) &= a_1 X_N + b_1 Y_N + c_1 \\ d_{YN}(X_N, Y_N) &= a_2 X_N + b_2 Y_N + c_2 \\ d_{ZN}(X_N, Y_N) &= a_3 X_N + b_3 Y_N + c_3 \end{aligned} \quad (4.4-8)$$

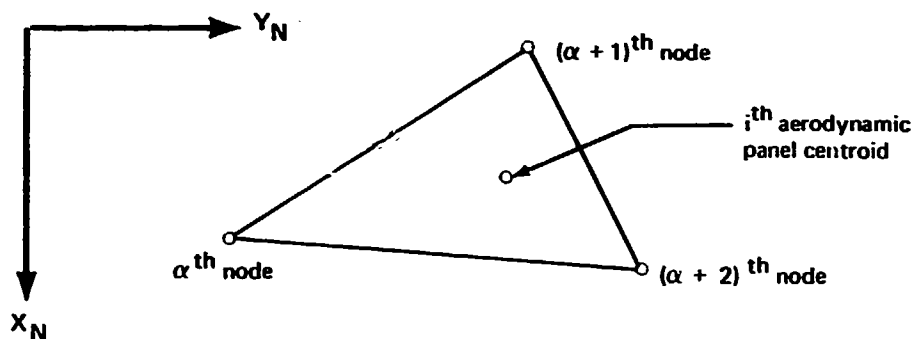


FIGURE 4.4-4.—TRIANGULAR FINITE ELEMENT

The nine coefficients a , b , and c are determined from the system of nine equations obtained by evaluating equation (4.4-8) at the nodes of the triangular element, e.g.,

$$\begin{aligned} d_{XN_\alpha} &= a_1 X_{N_\alpha} + b_1 Y_{N_\alpha} + c_1 \\ d_{XN_{\alpha+1}} &= a_1 X_{N_{\alpha+1}} + b_1 Y_{N_{\alpha+1}} + c_1 \\ d_{XN_{\alpha+2}} &= a_1 X_{N_{\alpha+2}} + b_1 Y_{N_{\alpha+2}} + c_1 \end{aligned}$$

The resulting displacement relation is found as follows:

$$\begin{bmatrix} d_{XN} \\ d_{YN} \\ d_{ZN} \end{bmatrix} = \begin{bmatrix} N_{XN_\alpha} & 0 & 0 & N_{XN_{\alpha+1}} & 0 & 0 & N_{XN_{\alpha+2}} & 0 & 0 \\ 0 & N_{YN_\alpha} & 0 & 0 & N_{YN_{\alpha+1}} & 0 & 0 & N_{YN_{\alpha+2}} & 0 \\ 0 & 0 & N_{ZN_\alpha} & 0 & 0 & N_{ZN_{\alpha+1}} & 0 & 0 & N_{ZN_{\alpha+2}} \end{bmatrix} \begin{bmatrix} d_{XN_\alpha} \\ d_{YN_\alpha} \\ d_{ZN_\alpha} \\ d_{XN_{\alpha+1}} \\ d_{YN_{\alpha+1}} \\ d_{ZN_{\alpha+1}} \\ d_{XN_{\alpha+2}} \\ d_{YN_{\alpha+2}} \\ d_{ZN_{\alpha+2}} \end{bmatrix} \quad (4.4-9)$$

where the non-zero displacement functions are given by

$$\begin{aligned} N_{XN_\alpha} &= N_{YN_\alpha} = N_{ZN_\alpha} \equiv \frac{1}{2A} \left[(Y_{N_{\alpha+1}} - Y_{N_{\alpha+2}})X_N + (X_{N_{\alpha+2}} - X_{N_{\alpha+1}})Y_N \right. \\ &\quad \left. + (X_{N_{\alpha+1}}Y_{N_{\alpha+2}} - X_{N_{\alpha+2}}Y_{N_{\alpha+1}}) \right] \\ N_{XN_{\alpha+1}} &= N_{YN_{\alpha+1}} = N_{ZN_{\alpha+1}} \equiv \frac{1}{2A} \left[(Y_{N_{\alpha+2}} - Y_{N_\alpha})X_N + (X_{N_\alpha} - X_{N_{\alpha+2}})Y_N \right. \\ &\quad \left. + (Y_{N_\alpha}X_{N_{\alpha+2}} - X_{N_\alpha}Y_{N_{\alpha+2}}) \right] \\ N_{XN_{\alpha+2}} &= N_{YN_{\alpha+2}} = N_{ZN_{\alpha+2}} \equiv \frac{1}{2A} \left[(Y_{N_\alpha} - Y_{N_{\alpha+1}})X_N + (X_{N_{\alpha+1}} - X_{N_\alpha})Y_N \right. \\ &\quad \left. + (X_{N_\alpha}Y_{N_{\alpha+1}} - X_{N_{\alpha+1}}Y_{N_\alpha}) \right] \end{aligned}$$

and A is the area of the triangular element:

$$A \equiv \frac{1}{2} \left[(X_{N_\alpha} - Y_{N_{\alpha+1}})(Y_{N_\alpha} - Y_{N_{\alpha+2}}) - (X_{N_\alpha} - X_{N_{\alpha+2}})(Y_{N_\alpha} - Y_{N_{\alpha+1}}) \right]$$

The displacement relation for a point in the quadrilateral region is found by averaging the values obtained in evaluating the triangular element displacement functions for the four triangular elements of figure 4.4-3. Letting the four triangular elements be denoted as j, k, l, and m, the displacement functions, as expressed by equation (4.4-10), for these triangular elements are denoted by a superscript, i.e., N_{XN}^j , N_{XN}^k , N_{XN}^l , etc. This leads to a set of 48 displacement functions related to a single quadrilateral region. Letting the quadrilateral region be denoted as the i th finite element, the 48 displacement functions are averaged to form 12 displacement functions typified by

$$\begin{aligned}\bar{N}_{XN_\alpha}^i &\equiv \frac{1}{4} \left[N_{XN_\alpha}^j + N_{XN_\alpha}^k + N_{XN_\alpha}^l + N_{XN_\alpha}^m \right] \\ \bar{N}_{YN_\alpha}^i &\equiv \frac{1}{4} \left[N_{YN_\alpha}^j + N_{YN_\alpha}^k + N_{YN_\alpha}^l + N_{YN_\alpha}^m \right] \\ \bar{N}_{ZN_\alpha}^i &\equiv \frac{1}{4} \left[N_{ZN_\alpha}^j + N_{ZN_\alpha}^k + N_{ZN_\alpha}^l + N_{ZN_\alpha}^m \right]\end{aligned}\quad (4.4-11)$$

These displacement functions are incorporated into the displacement relation for the quadrilateral element having the four nodes α , $\alpha + 1$, $\alpha + 2$, and $\alpha + 3$, viz.,

$$\begin{bmatrix} d_{XN}(X_N, Y_N) \\ d_{YN}(X_N, Y_N) \\ d_{ZN}(X_N, Y_N) \end{bmatrix} = \left[\bar{N}^i(X_N, Y_N) \right] \begin{bmatrix} d_{XN_\alpha} \\ d_{YN_\alpha} \\ d_{ZN_\alpha} \\ d_{XN_{\alpha+1}} \\ d_{YN_{\alpha+1}} \\ d_{ZN_{\alpha+1}} \\ d_{XN_{\alpha+2}} \\ d_{YN_{\alpha+2}} \\ d_{ZN_{\alpha+2}} \\ d_{XN_{\alpha+3}} \\ d_{YN_{\alpha+3}} \\ d_{ZN_{\alpha+3}} \end{bmatrix}\quad (4.4-12)$$

where

$$[\bar{N}^i(X_N, Y_N)] = \left[[\bar{N}_\alpha^i] \mid [\bar{N}_{\alpha+1}^i] \mid [\bar{N}_{\alpha+2}^i] \mid [\bar{N}_{\alpha+3}^i] \right]$$

and

$$[\bar{N}_\alpha^i] \equiv \begin{bmatrix} \bar{N}_{XN_\alpha}^i(X_N, Y_N) & 0 & 0 \\ 0 & \bar{N}_{YN_\alpha}^i(X_N, Y_N) & 0 \\ 0 & 0 & \bar{N}_{ZN_\alpha}^i(X_N, Y_N) \end{bmatrix}$$

4.4.1.6 Slender body displacement relations.—The structure of a slender body is assumed to consist of a semimonocoque arrangement typical of aircraft fuselage structures, figure 4.4-5. Deformation of the cross-sectional shape is assumed to be negligible, and the slender body structure is taken to have a beamlike behavior. Nodes are assumed to be located along a line corresponding to the aerodynamic mean centerline shown by figure 3.2-2. These nodes may be introduced into the finite element model by rigidly constraining the node on the centerline to nodes on the periphery, eliminating the peripheral nodes (e.g., the multipoint constraint of section 3.5.1 of reference 1-2), by modeling the body initially as a beam, or by some alternate but equivalent device.

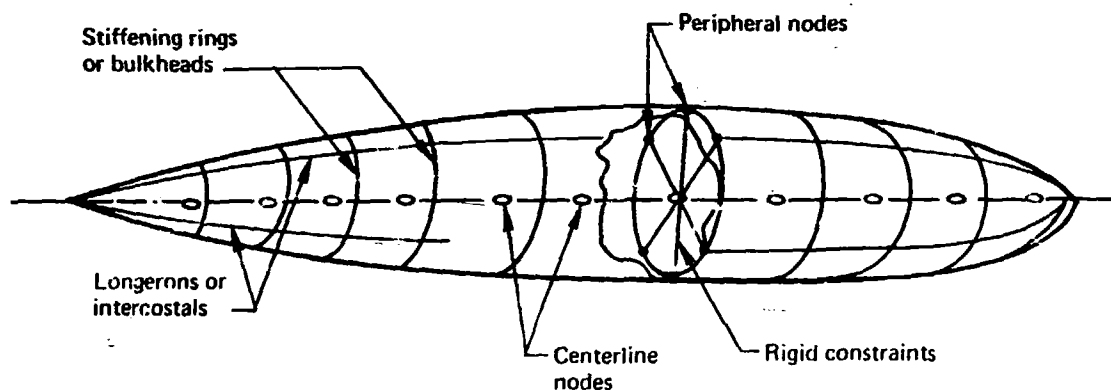


FIGURE 4.4-5.—TYPICAL SLENDER BODY STRUCTURE

Consider the segment of slender body centerline between the nodes α and $\alpha + 1$, figure 4.4-6. The Z-component of displacement is assumed to vary linearly between the nodes as follows:

$$d_Z(X) = [N_{Z_\alpha}(X)]d_{Z_\alpha} + [N_{Z_{\alpha+1}}(X)]d_{Z_{\alpha+1}} \quad \text{for } X_\alpha \leq X \leq X_{\alpha+1} \quad (4.4-13)$$

where

$$N_{Z_\alpha}(X) \equiv \frac{X_{\alpha+1} - X}{X_{\alpha+1} - X_\alpha} \quad (4.4-14)$$

and

$$N_{Z_{\alpha+1}}(X) \equiv \frac{X - X_\alpha}{X_{\alpha+1} - X_\alpha}.$$

The X- and Y-components of displacement are given by

$$d_X(X) = [N_{X_\alpha}(X)]d_{X_\alpha} + [N_{X_{\alpha+1}}(X)]d_{X_{\alpha+1}} \quad \text{for } X_\alpha \leq X \leq X_{\alpha+1}$$

and

$$d_Y(X) = [N_{Y_\alpha}(X)]d_{Y_\alpha} + [N_{Y_{\alpha+1}}(X)]d_{Y_{\alpha+1}} \quad \text{for } X_\alpha \leq X \leq X_{\alpha+1}$$

where the displacement functions are all given by equation (4.4-14), i.e.,

$$N_{X_\alpha}(X) = N_{Y_\alpha}(X) = N_{Z_\alpha}(X)$$

and

$$N_{X_{\alpha+1}}(X) = N_{Y_{\alpha+1}}(X) = N_{Z_{\alpha+1}}(X).$$

The displacement relation for the segment of centerline is expressed in the form of equation (4.2-7) as follows:

$$\begin{bmatrix} d_X(X) \\ d_Y(X) \\ d_Z(X) \end{bmatrix} = \begin{bmatrix} N_{X_\alpha}(X) & 0 & 0 & N_{X_{\alpha+1}}(X) & 0 & 0 \\ 0 & N_{Y_\alpha}(X) & 0 & 0 & N_{Y_{\alpha+1}}(X) & 0 \\ 0 & 0 & N_{Z_\alpha}(X) & 0 & 0 & N_{Z_{\alpha+1}}(X) \end{bmatrix} \begin{bmatrix} d_{X_\alpha} \\ d_{Y_\alpha} \\ d_{Z_\alpha} \\ d_{X_{\alpha+1}} \\ d_{Y_{\alpha+1}} \\ d_{Z_{\alpha+1}} \end{bmatrix} \quad (4.4-15)$$

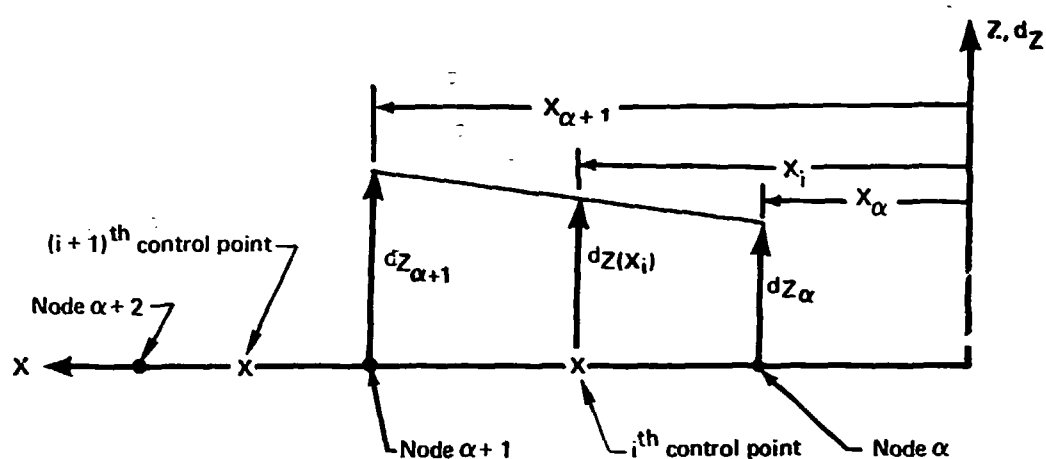


FIGURE 4.4-6.—DISPLACEMENT FUNCTION FOR A SLENDER BODY

Except for changes in the coordinates of the nodes, i.e., X_α and $X_{\alpha+1}$, equation (4.4-10) represents the displacement relation between any two slender body structural nodes.

4.4.1.7 Aerodynamic surface deformation transformations.—The nodal displacements $\{\delta\}$ are transformed to translational and rotation deformations at the aerodynamic panel centroids and slender body line doublet control points by the matrices $[P_d]$ and $[P_\theta]$, respectively, as developed in section 4.2.6.3, equations (4.2-100) and (4.2-101). The forms of these transformations appropriate for transforming the structural equations of motion described in section 4.4 are found by substituting the displacement relations of sections 4.4.1.5 and 4.4.1.6 into equations (4.2-100) and (4.2-101). In carrying out this substitution, the operations are more clearly described if the transformations are expressed in partitioned form.

The deformed shapes of the structure at the aerodynamic panel centroids and slender body line doublet control points, i.e., $\{d^*\}$ and $\{\theta^*\}$, are expressed in terms of partitions related to thin and slender bodies—equations (4.2-98) and 4.2-99)—denoted as follows:

$$\{d^*\} \equiv \begin{bmatrix} \{d^*\}_B \\ \{d^*\}_W \end{bmatrix} \quad \text{and} \quad \{\theta^*\} \equiv \begin{bmatrix} \{\theta^*\}_B \\ \{\theta^*\}_W \end{bmatrix}.$$

The nodal displacement components of equation (4.4-3) are similarly partitioned; hence, convenient forms for the aerodynamic surface transformations are given by

$$\{d^*\} = [P_d]\{\delta\} = \begin{bmatrix} [P_{d_{B,B}}] & [P_{d_{B,W}}] \\ [P_{d_{W,B}}] & [P_{d_{W,W}}] \end{bmatrix} \begin{bmatrix} \{\delta\}_B \\ \{\delta\}_W \end{bmatrix} \quad (4.4-16)$$

and

$$[P_\theta]\{\delta\} = \left[\begin{array}{c|c} [P_{\theta_{B,B}}] & [P_{\theta_{B,W}}] \\ \hline [P_{\theta_{W,B}}] & [P_{\theta_{W,W}}] \end{array} \right] \left[\begin{array}{c} \{\delta\}_B \\ \hline \{\delta\}_W \end{array} \right] \quad (4.4-17)$$

The partitions of the transformation matrices are derived in the following:

(1) $[P_{dB,B}]$

Consider the i^{th} aerodynamic control point on a slender body between the nodes α and $\alpha+1$, figure 4.4-6. The elements of the transformation matrices which relate deflections at this aerodynamic control point to components of nodal displacement at nodes α and $\alpha+1$ are as follows:

From the displacement relation of equation (4.4-15)

$$\left[\begin{array}{c|c} [P_{d_{i,\alpha}}] & [P'_{d_{i,\alpha+1}}] \end{array} \right] = \quad (4.4-18)$$

$$\left[\begin{array}{ccc|ccc} 0 & \frac{X_{\alpha+1}-X_i}{X_{\alpha+1}-X_\alpha} & 0 & 0 & \frac{X_i-X_\alpha}{X_{\alpha+1}-X_\alpha} & 0 \\ 0 & 0 & \frac{X_{\alpha+1}-X_i}{X_{\alpha+1}-X_\alpha} & 0 & 0 & \frac{X_i-X_\alpha}{X_{\alpha+1}-X_\alpha} \end{array} \right]$$

where X_i is the coordinate of the i^{th} control point.

For the two-segment example shown by figure 4.4-6, the partition $[P_{dB,B}]$ is given by

$$[P_{dB,B}] = \left[\begin{array}{c|c|c} [P_{d_{i,\alpha}}] & [P'_{d_{i,\alpha+1}}] & [0] \\ \hline [0] & [P_{d_{i+1,\alpha+1}}] & [P'_{d_{i+1,\alpha+2}}] \end{array} \right] \quad (4.4-19)$$

(2) $[P_{dW,W}]$

Consider now the i^{th} aerodynamic panel centroid on a thin body located at the j^{th} triangular element with the nodes α , $\alpha + 1$, and $\alpha + 2$, figure 4.4-4. The elements of the transformation matrices which relate deflections at this aerodynamic centroid to components of nodal displacement at the node α are as follows:

From the displacement relation of equation (4.4-9),

$$[P_{d_i, \alpha}^j] = \begin{bmatrix} 0 & 0 & \bar{N}_{ZN_{i\alpha}}^j \end{bmatrix} \quad (4.4-20)$$

where

$$\begin{aligned} \bar{N}_{ZN_{i\alpha}}^j = \frac{1}{2A} [& (Y_{N_{\alpha+1}} - Y_{N_{\alpha+2}}) X_{N_i} + (X_{N_{\alpha+2}} - X_{N_{\alpha+1}}) Y_{N_i} \\ & + (X_{N_{\alpha+1}} Y_{N_{\alpha+2}} - X_{N_{\alpha+2}} Y_{N_{\alpha+1}})] \end{aligned}$$

and X_{N_i} , Y_{N_i} are the coordinates of the aerodynamic centroids in the local thin body axis system.

For the i^{th} centroid on the j^{th} quadrilateral finite element, equation (4.4-20) is replaced by

$$[P_{d_i, \alpha}^j] = \begin{bmatrix} 0 & 0 & \bar{N}_{ZN_{i\alpha}}^j \end{bmatrix} \quad (4.4-21)$$

where the element $\bar{N}_{ZN_{i\alpha}}$ is obtained by evaluating the corresponding element of equation (4.4-16). In the case of a thin body having two quadrilateral finite elements, six nodes, and three panel centroids, figure 4.4-7, the thin body partition of equation (4.4-16) appears as

$$[P_{dW,W}] = \quad (4.4-22)$$

$$\begin{bmatrix} [P_{d_i, \alpha}^j] & [P_{d_i, \alpha+1}^j] & [0] & [0] & [P_{d_i, \alpha+4}^j] & [P_{d_i, \alpha+5}^j] \\ [P_{d_{i+1}, \alpha}^j] & [P_{d_{i+1}, \alpha+1}^j] & [0] & [0] & [P_{d_{i+1}, \alpha+4}^j] & [P_{d_{i+1}, \alpha+5}^j] \\ [0] & [P_{d_{i+2}, \alpha+1}^{j+1}] & [P_{d_{i+2}, \alpha+2}^{j+1}] & [P_{d_{i+2}, \alpha+3}^{j+1}] & [P_{d_{i+2}, \alpha+4}^{j+1}] & [0] \end{bmatrix}$$

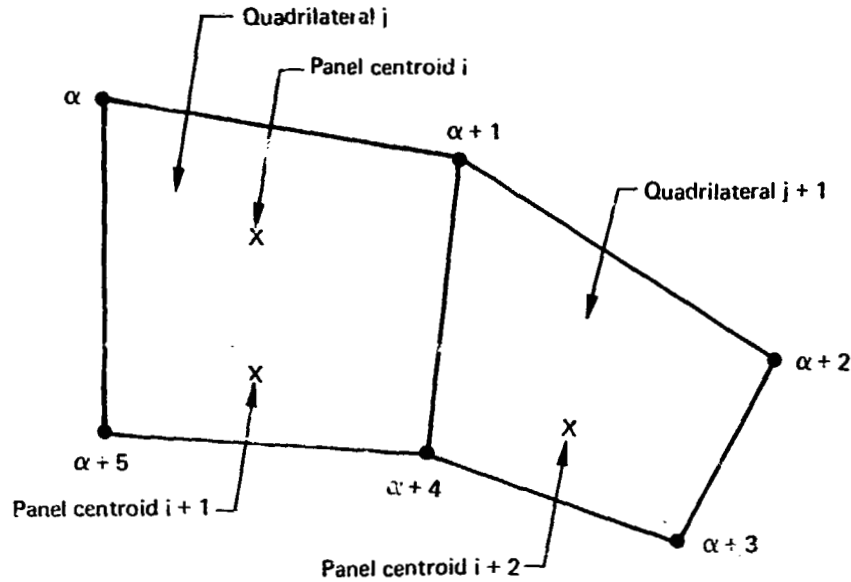


FIGURE 4.4-7.—THIN BODY HAVING TWO QUADRILATERAL FINITE ELEMENTS

Coupling between slender bodies and thin bodies given by the partition $[P_{dB}]$ is always zero, but the partition $[P_{dWB}]$ can be non-zero when nodes on slender bodies are simultaneously designated to be nodes on thin bodies. For example, if the two nodes α and $\alpha+5$ in figure 4.4-7 were nodes on a slender body as well as nodes on the thin body, the non-zero coupling partition would be given as

$$[P_{dWB}] = \begin{bmatrix} [P_{di,\alpha}^j] & | & [P_{di,\alpha+5}^j] \\ \hline [P_{di+1,\alpha}^j] & | & [P_{di+1,\alpha+5}^j] \\ \hline [0] & | & [0] \end{bmatrix} \quad (4.4-23)$$

and the matrices appearing in equation (4.4-23) would be deleted from the thin body partition shown by equation (4.4-22) so that there is consistency with the definitions of $\{d^*\}$ and $\{\delta\}$, cf., equations (4.2-98) and (4.4-3).

(3) $[P_{\theta_{B,B}}]$

The aerodynamic surface rotation at a control point of a slender body is found by substituting into equation (4.2-92) the displacement relation given by equation (4.4-15). The result of that operation evaluated at a control point located anywhere between the nodes α and $\alpha + 1$ is given by

$$\begin{bmatrix} [P_{\theta_{i,\alpha}}] & \vdots & [P_{\theta_{i,\alpha+1}}] \end{bmatrix} = \quad (4.4-24)$$

$$\frac{1}{2} \begin{bmatrix} 0 & 0 & \frac{1}{X_{\alpha+1} - X_{\alpha}} & 0 & 0 & -\frac{1}{X_{\alpha+1} - X_{\alpha}} \\ 0 & -\frac{1}{X_{\alpha+1} - X_{\alpha}} & 0 & 0 & \frac{1}{X_{\alpha+1} - X_{\alpha}} & 0 \end{bmatrix}$$

The partition $[P_{\theta_{B,B}}]$ is an array of the matrices described by equation (4.4-24), which are assembled in the same manner as $[P_{d_{B,B}}]$.

(4) $[P_{\theta_{W,W}}]$

The surface rotation due to displacement of a triangular thin body mean surface element is found by substituting equation (4.4-9) into equation (4.2-92) as

$$\begin{bmatrix} [P_{\theta_{i,\alpha}}] & \vdots & [P_{\theta_{i,\alpha+1}}] & \vdots & [P_{\theta_{i,\alpha+2}}] \end{bmatrix} = \quad (4.4-25)$$

$$\frac{1}{2} \begin{bmatrix} \frac{\partial N_{ZN}^j}{\partial X_N} & \frac{\partial N_{ZN}^j}{\partial X_N} & \frac{\partial N_{ZN}^j}{\partial X_N} \\ [0 \ 0 \ \frac{\partial N_{ZN}^j}{\partial X_N}] & [0 \ 0 \ \frac{\partial N_{ZN}^j}{\partial X_N}] & [0 \ 0 \ \frac{\partial N_{ZN}^j}{\partial X_N}] \end{bmatrix}$$

where

$$\frac{\partial N_{ZN}^j}{\partial X_N} = \frac{1}{2A}(Y_{N_{\alpha+1}} - Y_{N_{\alpha+2}}), \quad \frac{\partial N_{ZN}^j}{\partial X_N} = \frac{1}{2A}(Y_{N_{\alpha+2}} - Y_{N_{\alpha}}),$$

$$\frac{\partial N_{ZN}^j}{\partial X_N} = \frac{1}{2A}(Y_{N_{\alpha}} - Y_{N_{\alpha+1}})$$

The surface rotation at a quadrilateral surface element is found by superposition to find the average rotation in a process identical to that leading to equation (4.4-20). The partition $[P_{\theta W, W}]$ is an array of the matrices described by equation (4.4-25).

The coupling between slender and thin bodies, i.e., $[P_{\theta B, W}]$ and $[P_{\theta W, B}]$, is like that appearing as $[P_{dB, W}]$ and $[P_{dW, B}]$. The partition $[P_{\theta B, W}]$ is always zero and the partition $[P_{\theta W, B}]$ is non-zero only when nodes on thin bodies are, at the same time, nodes on slender bodies.

4.4.1.8 Forces at the structural nodes due to aerodynamic surface pressure.—The nodal forces due to aerodynamic surface pressure are derived in section 4.2.7 and are given by the matrix transformation

$$\{Q^A\} = [P_T]^T \{f_T^A\} \quad (4.2-116)$$

The transformation matrix $[P_T]$ is shown in section 4.2.7 to be derived from the displacement relations, and this derivation leads to

$$\{d_T\} = [P_T]\{\delta\} \quad (4.2-114)$$

The components of displacement $\{d_T\}$ differ from those contained in $\{d^*\}$ in that $\{d_T\}$ contains X-components of displacements at thin body nodes.

The transformation matrix is developed in terms of thin and slender body partitions in the manner of the preceding, i.e.,

$$\{d_T\} = [P_T]\{\delta\} = \begin{bmatrix} [P_{TB, B}] & | & [P_{TB, W}] \\ \hline [P_{TW, B}] & | & [P_{TW, W}] \end{bmatrix} \begin{bmatrix} \{\delta\}_B \\ \hline \{\delta\}_W \end{bmatrix} \quad (4.4-26)$$

The partitions of this matrix are derived in a manner closely analogous to the partitions of $[P_d]$. The derivation is as follows:

(1) $[P_{TB, B}]$

This partition is very similar to $[P_{dB, B}]$ appearing in section 4.4.1.7 and is constructed of the following partitions:

$$\begin{bmatrix} [P_{Ti, \alpha}] & | & [P_{Ti, \alpha+1}] \end{bmatrix} =$$

$$\left[\begin{array}{ccc|ccc} \frac{X_{\alpha+1}-X_i}{X_{\alpha+1}-X_\alpha} & 0 & 0 & \frac{X_i-X_\alpha}{X_{\alpha+1}-X_\alpha} & 0 & 0 \\ 0 & \frac{X_{\alpha+1}-X_i}{X_{\alpha+1}-X_\alpha} & 0 & 0 & \frac{X_i-X_\alpha}{X_{\alpha+1}-X_\alpha} & 0 \\ 0 & 0 & \frac{X_{\alpha+1}-X_i}{X_{\alpha+1}-X_\alpha} & 0 & 0 & \frac{X_i-X_\alpha}{X_{\alpha+1}-X_\alpha} \end{array} \right]$$

(2) $[P_{TW,W}]$

Consider the i^{th} aerodynamic control point located on the j^{th} triangular element with nodes α , $\alpha + 1$, and $\alpha + 2$, figure 4.4-4. The elements of the transformation matrix that relate deflections $\{d_T\}$ at this aerodynamic panel centroid to components of nodal displacement at node α are as follows:

From the displacement relation (4.4-9),

$$[P_{T,i,\alpha}^j] = \begin{bmatrix} N_{XN_{i\alpha}}^j & 0 & 0 \\ 0 & 0 & N_{ZN_{i\alpha}}^j \end{bmatrix} \quad (4.4-27)$$

For the i^{th} control point on the j^{th} quadrilateral finite element, equation (4.4-27) is replaced by

$$[P_{T,i,\alpha}^j] = \begin{bmatrix} \bar{N}_{XN_{i\alpha}}^j & 0 & 0 \\ 0 & 0 & \bar{N}_{ZN_{i\alpha}}^j \end{bmatrix} \quad (4.4-28)$$

where the elements $\bar{N}_{XN_{i\alpha}}^j$ and $\bar{N}_{ZN_{i\alpha}}^j$ are obtained by evaluating equation (4.4-12). In the case of the thin body example shown by figure 4.4-7, the thin body partition of equation (4.4-26) is given by

$$[P_{TW,W}] = \begin{bmatrix} [P_{T,i,\alpha}^j] & [P_{T,i,\alpha+1}^j] & [0] & [0] & [P_{T,i,\alpha+4}^j] & [P_{T,i,\alpha+5}^j] \\ \hline [P_{T,i+1,\alpha}^j] & [P_{T,i+1,\alpha+1}^j] & [0] & [0] & [P_{T,i+1,\alpha+4}^j] & [P_{T,i+2,\alpha+5}^j] \\ \hline [0] & [P_{T,i+2,\alpha+1}^{j+1}] & [P_{T,i+2,\alpha+2}^{j+1}] & [P_{T,i+2,\alpha+3}^{j+1}] & [P_{T,i+2,\alpha+4}^{j+1}] & [0] \end{bmatrix} \quad (4.4-29)$$

Coupling between slender and thin bodies given by the partition $[P_{TB,W}]$ is always zero, but the partition $[P_{TW,B}]$ can be non-zero when nodes on slender bodies are simultaneously designated as nodes on thin bodies. For example, if the nodes α and $\alpha + 5$ in figure 4.4-7 were nodes on slender bodies as well as nodes on the thin body, the non-zero coupling partition would be given by

$$[P_{TW,B}] = \begin{bmatrix} [F_{Ti,\alpha}^j] & | & [P_{Ti,\alpha+5}] \\ \hline [F_{Ti+1,\alpha}] & | & [P_{Ti+1,\alpha+5}] \\ \hline [0] & | & [0] \end{bmatrix} \quad (4.4-30)$$

and the matrices appearing in equation (4.4-30) would be deleted from the thin body partition shown by equation (4.4-29).

4.4.1.9 Reduction of the structural degrees of freedom.—The supplied structural matrices are assumed to be expressed in terms of three translational degrees of freedom at each node or in terms of specific subsets of these degrees of freedom. The subsets are restricted in that every node on one thin or slender body must have the same degrees of freedom. The choice, however, may differ for different bodies, e.g., the nodes on the i^{th} thin body may have d_{Zi} degrees of freedom while nodes on the j^{th} thin body may have d_{Xj}, d_{Yj}, d_{Zj} degrees of freedom.

When the degrees of freedom are deleted from $\{\delta\}$, their work-conjugate nodal force components must also be deleted in $\{Q\}$; thus, if the flexibility matrix $[C]$ is supplied with the rows corresponding to d_{Xi} degrees of freedom deleted for the i^{th} thin body, then the columns corresponding to F_{Xi} components of force must also be deleted for the i^{th} thin body. The F_{Xi} components of inertial force for the thin body, however, may be retained in the analysis using the methods described in section 4.4.4.

4.4.1.10 Approximations in the pressure-force transformation matrix.—The transformation expressed by equation (4.2.116), relating the aerodynamic surface pressure to components of force at the structural nodes, contains approximations implied by the derivation of section 4.2.7. The nature of these approximations, when the method of section 4.2.7 is applied, is described in the following, first, for the slender body partition and, second, for the thin body partition.

4.4.1.11 Slender body application.—As shown by sections 3.5.1.3 and 3.5.1.4, the aerodynamic surface pressure acting on the surfaces of slender bodies is resolved into three components of force. These components of force are expanded on the Reference Axis System and are assumed to act at the aerodynamic centroids of the slender body aerodynamic segments. The components of displacement in the directions of the resolved force components are evaluated by the equation (4.2-20), and the nodal force components are computed by the work relations of section 4.2.7.

The preceding operations introduce several approximations. One of these approximations ignores the effect of the variation of surface pressure in the X-direction. This approximation is identical with that introduced in section 3.5, where the total aerodynamic forces acting on the aircraft are derived. In addition to this approximation, the integrals appearing in equations (4.2-108) and (4.2-109) are carried out assuming that every aerodynamic surface segment lies entirely interior to the nodes of a single structural finite element. In practice, one aerodynamic surface segment may span one or more structural finite elements. The approximation, in these cases, places the airload of the entire aerodynamic segment on that structural finite element that contains the aerodynamic centroid of the aerodynamic surface segment. The validity of this approximation degenerates as the lengths of the aerodynamic surface segments in the X-direction are increased in relation to the lengths of the structural finite elements.

4.4.1.12 Thin body application.—In applying the transformation to thin bodies, the approximations are less severe than in the slender body approximation. The reduced severity stems from the fact that the lifting pressure is uniform on the aerodynamic surface segments (i.e., the panels). Because the pressure is uniform and the displacement relations are linear functions of the local axis system coordinates, the integral appearing in the work relationship given by equation (4.2-108) contains no approximation, provided that the aerodynamic panel is entirely interior to a structural finite element.

Approximations are introduced by the fact that the edges of aerodynamic panels fail to coincide with the edges of structural finite elements, figure 4.4-8. The aerodynamic panel is treated as if it were entirely interior to the structural finite element containing the geometric centroid of the panel. In effect, this approximation replaces the boundaries of the structural finite elements with the boundaries of the aerodynamic panels, figure 4.4-8.

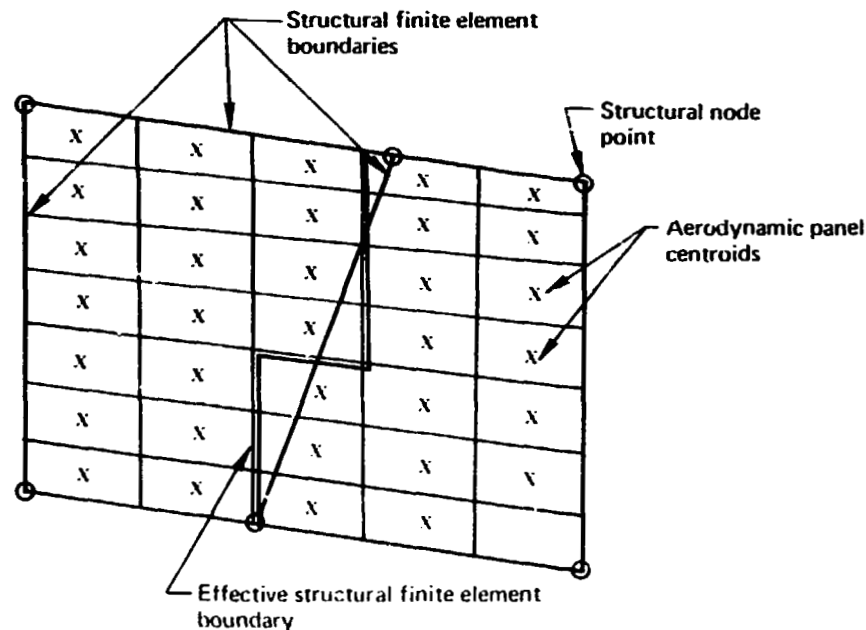


FIGURE 4.4-8.—APPROXIMATE STRUCTURAL FINITE ELEMENT BOUNDARIES ON THIN BODIES

Often the structural finite elements do not extend to the edges of the thin body planform, figure 4.4-9. This situation usually occurs because the leading edge, trailing edge, or tip structure is treated as secondary structure in constructing the finite element model. In these cases the distances from the structural finite element geometric centroids to the panel geometric centroids, figure 4.4-8, are used as a basis for choosing the structural finite element to be related to a panel outside the structural planform. The structural finite element, whose geometric centroid is nearest to the geometric centroid of the panel, is related to the panel. The displacement relation for the so-related structural finite element is extended, in analytic definition, to the coordinates of the panel geometric centroid and evaluated there. This value is then used in the construction of the transformation matrices $[P_d]$, $[P_\theta]$, and $[P_T]$, as in sections 4.4.1.7 and 4.4.1.8.

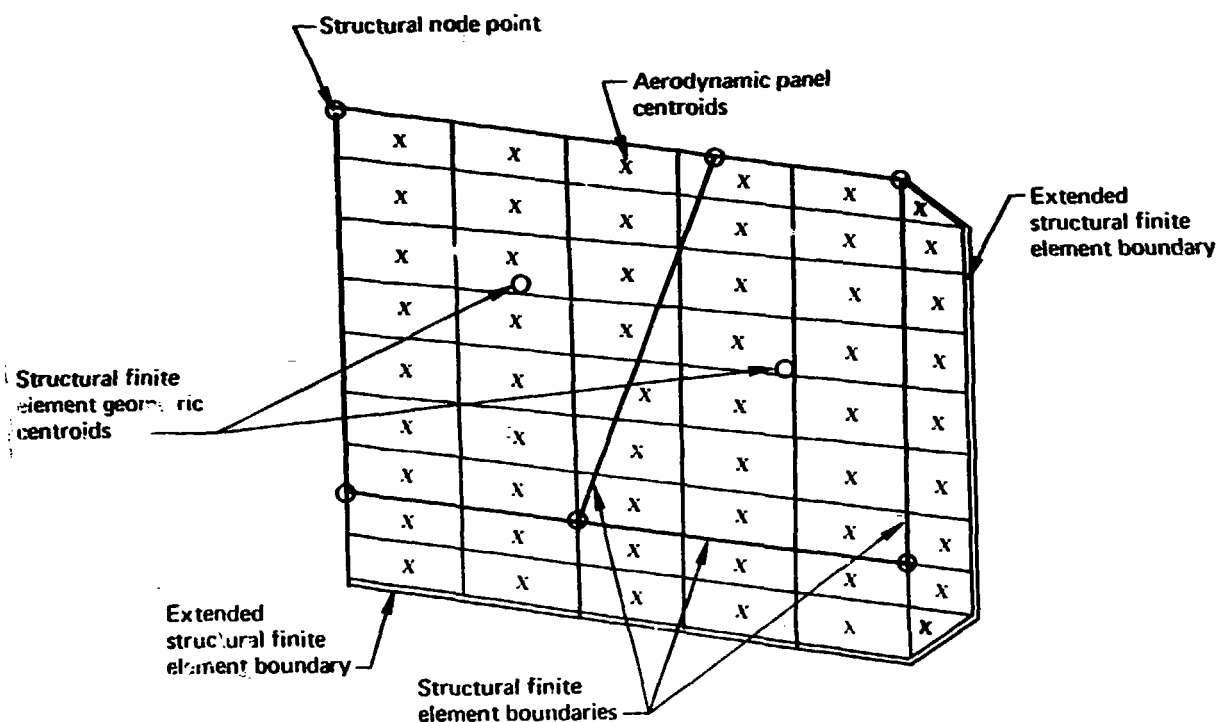


FIGURE 4.4-9.—EXTENDED STRUCTURAL FINITE ELEMENT BOUNDARIES

4.4.2 ESIC Coordinate Systems

As noted in sections 2 and 4, the FLEXSTAB system computations, related to the structural equations, are expressed in the same coordinate systems used in the aerodynamic computations, viz., the Reference Axis System introduced by section 2.2.4 and the local thin body aerodynamic axis systems introduced by section 3.2.4. As seen in section 4.4.1, the components of nodal force and displacement (i.e., $\{Q\}$ and $\{\delta\}$) are expanded on these coordinate systems; therefore, the supplied matrices, listed at the beginning of section 4.4, are assumed to be expanded on the same coordinate systems.

In practice, the supplied matrices are usually expressed in terms of coordinate systems differing from those used in the aerodynamic computations. Recalling the discussion of sections 2.3.23 and 4.2.2.4, the coordinate systems used in describing the structural behavior are seen to be fixed to a geometric shape (or configuration) of the aircraft that is regarded as undeformed; this is also true of the coordinate systems used in describing the aerodynamics. The undeformed shape used in the aerodynamic idealization, however, may differ from that used in the structural idealization, thereby leading to differences between the structural and aerodynamic coordinate systems.

Differences between the structural and aerodynamic coordinate systems have two sources. The first source is the overall rotation and translation, described in section 4.2.2.2, of the aerodynamic coordinate systems relative to the structural coordinate systems. This difference arises because the defining coordinate systems for the supplied structural matrices are structural reference frames while the coordinate systems used in describing the aerodynamics are mean reference frames. As noted in section 4.2.2.2, this difference is ignored and the Reference Axis System is used as the fundamental coordinate system in both cases. The second source is an effect of structural deformation on the local thin body aerodynamic axis systems that causes the local thin body axis systems of the aerodynamic idealization to be different from those of the structural idealization.

The structural finite element model is usually formulated using the geometry of the aircraft in its design-point flight condition. The mean surfaces of thin bodies, containing the structural node points of thin bodies, section 4.4.1.1, therefore have the locations appropriate to the design-point shape. The thin body mean surfaces used in the aerodynamic computations, however, may be chosen to be located in positions appropriate to an off-design-point flight condition being analyzed for stability. Relative translations between these two sets of thin body mean surfaces are of no first-order consequence to the analysis, but relative rotations lead to nodal force and displacement components in the two idealizations expanded on two different sets of coordinate systems. As noted in sections 2.3.3.3 and 2.3.3.4, equations (2.3-52) and (2.3-57), as well as in section 4.2.1, these rotations must be very small, and their effect on the nodal components is negligible.

The nodal force and displacement components related to the supplied matrices are treated as if they were expanded on the Reference Axis System and the local thin body aerodynamic axis systems of the aerodynamic computations. The effects of elastic rotations on the local thin body axis systems are ignored for the same reasons that relative rotations between mean and structural reference frames are ignored, cf., section 4.2.2.2. It should be noted from section 2.3.3.3, however, that relative rotations about the Y and Z axes are included in the aerodynamic boundary conditions; the effects of changes in dihedral angle (i.e., relative rotations about the X axis) that significantly affect lateral-directional stability predictions are deleted from the aerodynamic boundary conditions to obtain linearity. The effect of dihedral angle deformation must be introduced into the analysis as suggested above, viz., the local thin body axis systems for the aerodynamic idealization are chosen to be those appropriate to the shape of the aircraft in the reference flight condition being analyzed for stability.

An ESIC Reference Axis System and ESIC local thin body axis systems, figure 4.4-10, are introduced as a convenience for the FLEXSTAB system user. The origin of the ESIC Reference Axis System can be arbitrarily located, but the axes of this system must be parallel with the axes of the Reference Axis System. The origin of an ESIC local thin body axis system is located in the mean surface of the thin body in the geometry of the structural idealization, and the x_{E_n}, y_{E_n} plane must coincide with the mean surface. The dihedral angle θ_n , however, as noted in the preceding, may differ from the dihedral angle θ_N in the aerodynamic idealization, but this difference is used only to effect node point geometry—section 4.4.2.2.

4.4.2.1 Arrangement of the ESIC coordinate systems.—The ESIC Reference Axis System is introduced with the origin having coordinates $\Delta X_{REF}, \Delta Y_{REF}, \Delta Z_{REF}$ in the Reference Axis System; the coordinate lines (X_E, Y_E, Z_E) are parallel to the X, Y, Z coordinate lines of the Reference Axis System. The origin of an ESIC local axis system is located by its coordinates $(X_{E_0}, Y_{E_0}, Z_{E_0})$ in the ESIC Reference Axis System; x_{E_n} is parallel to the X_E axis, and y_{E_n}, z_{E_n} are oriented by a positive rotation θ_n about the x_{E_n} axis. The x_{E_n}, y_{E_n} plane coincides with the mean surface of the thin body in the geometry of the structural idealization.

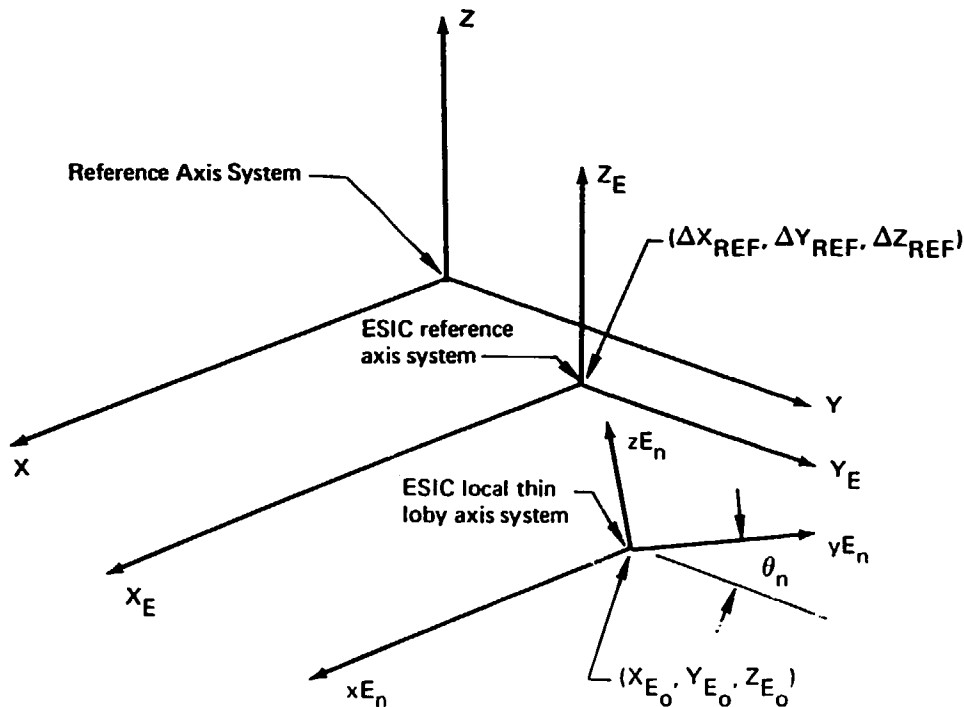


FIGURE 4.4-10.—ESIC COORDINATE SYSTEMS

4.4.2.2 Transformation of node point geometry.—The FLEXSTAB system is capable of generating the rigid body mode shape matrix, $[\bar{\phi}_\delta]$, based on the arrangement shown by equations (4.2-16) and (4.2-21). This computation utilizes the geometric locations of the structural node points described to the FLEXSTAB system in the ESIC coordinate systems. The coordinates of these points must, therefore, be transformed to the Reference Axis System.

The coordinates of nodes on slender bodies (e.g., the α^{th} node) are expressed in the ESIC Reference Axis System as

$$X_E(\alpha), Y_E(\alpha), Z_E(\alpha)$$

The locations of these points are expressed in the Reference Axis System as

$$\begin{aligned} X(\alpha) &= X_E(\alpha) + \Delta X_{\text{REF}} \\ Y(\alpha) &= Y_E(\alpha) + \Delta Y_{\text{REF}} \\ Z(\alpha) &= Z_E(\alpha) + \Delta Z_{\text{REF}} \end{aligned} \quad (4.4-31)$$

The coordinates of nodes on thin bodies (e.g., the α^{th} node on the N^{th} thin body) are expressed in the ESIC local thin body axis system as

$$x_{E_n}(\alpha), y_{E_n}(\alpha)$$

the z_{E_n} coordinate being zero. The locations of these points are expressed in the ESIC Reference Axis System as

$$\begin{aligned} X_E(\alpha) &= x_{E_n}(\alpha) + X_{E_0} \\ Y_E(\alpha) &= y_{E_n}(\alpha) \cos \theta_n + Y_{E_0} \\ Z_E(\alpha) &= z_{E_n}(\alpha) \sin \theta_n + Z_{E_0} \end{aligned} \quad (4.4-32)$$

The locations in the Reference Axis System are then obtained by substituting equations (4.4-32) into equations (4.4-31).

4.4.3 Construction of the Gyroscopic Couple Transformation Matrix

The gyroscopic couple transformation matrix describes rotation, $\{\theta^G\}$, at the center of the masses of the engines. These rotations arise from the nodal displacement components $\{\delta\}$, equation (4.2-118), i.e.,

$$\{\theta^G\} = [\Delta_G]^T \{\delta\} \quad (4.2-118)$$

The rotations at the engines are expressed as

$$\{\theta^G\} = \begin{bmatrix} \cdot \\ \cdot \\ \cdot \\ \{\theta_i^G\} \\ \cdot \\ \cdot \\ \cdot \end{bmatrix} \quad (4.4-33)$$

where

$$\{\theta_i^G\} \equiv \begin{bmatrix} \theta_{X_i}^G \\ \theta_{Y_i}^G \\ \theta_{Z_i}^G \end{bmatrix}$$

The components of $\{\theta_i^G\}$, expanded on the Reference Axis System, are assumed to be the result of a rigid connection of the i^{th} engine to a subset of the nodal displacement components, $\{\delta\}$. Equation (4.2-118) can then be expressed in terms of partitions of the following form:

$$\{\theta_i^G\} \equiv [\Delta_{Gi}]^T \{\delta_i^G\} \quad (4.4-34)$$

where $\{\delta_i^G\}$ is the subset of $\{\delta\}$ for the i^{th} engine.

Engine supports are almost always chosen to be statically determinant as in the following example. As a result, if the subset $\{\delta_i^G\}$ is taken to contain the three components of translational displacement at nodes representing the engine support points and in the directions of engine loads, then the degrees of freedom $\{\delta_i^G\}$ uniquely determine the rigid body rotation at the engine center of mass. Assuming this to be the case, the elements of $[\Delta_{Gi}]$ are readily computed from the components of the vector product

$$\vec{d}_i = \vec{r}_i^e \times \vec{\theta}_i^G$$

where \vec{r}_i^e is the position vector from the engine center of mass to an engine support node. Alternately, the elements of $[\Delta_{Gi}]$ can be found from the expressions describing the moments at the engine center of mass arising from unit values of the engine loads at the engine support nodes.

Consider the example shown by figure 4.4-11, wherein the engine has statically determinate support provided by forces at three nodes. The components of force that provide reactions to the engine loads at these nodes are shown by figure 4.4-11. The components of moment at the engine center of mass arising from node force reactions are given by

$$M_X^G = F_{Z_\alpha} y^e(\alpha+2) + F_{Z_{\alpha+2}} y^e(\alpha+2) - F_{Z_{\alpha+1}} y^e(\alpha+1)$$

$$M_Y^G = -F_{Z_\alpha} x^e(\alpha)$$

$$M_Z^G = -F_{X_{\alpha+1}} y^e(\alpha+2) + F_{Y_\alpha} x^e(\alpha)$$

where $x^e(\alpha)$, $y^e(\alpha)$, etc. are the components of the position vector \vec{r}^e evaluated at the support nodes. These three relations plus three relations relating engine thrust and weight to the supporting nodal forces, i.e.,

$$F_X^T = F_{X_{\alpha+2}}$$

$$F_Y^T = F_{Y_\alpha} + F_{Y_{\alpha+2}}$$

$$F_Z^T = F_{Z_\alpha} + F_{Z_{\alpha+1}} + F_{Z_{\alpha+2}},$$

are solved for the six force components at the support nodes. The partition of the resulting coefficient matrix multiplying the components M_X^G , M_Y^G , M_Z^G yields the desired gyroscopic couple transformation matrix partition. Assuming that the engine is the i^{th} engine, this partition is given by

$$[\Delta_{Gi}] = \begin{bmatrix} 0 & 0 & 0 \\ 0 & 0 & 0 \\ 0 & 0 & 0 \\ 0 & 0 & \frac{1}{x^e(\alpha)} \\ 0 & 0 & 0 \\ 0 & 0 & \frac{-1}{x^e(\alpha)} \\ 0 & \frac{1}{y^e(\alpha+2)} & 0 \\ \frac{1}{y^e(\alpha+1)+y^e(\alpha+2)} & 0 & 0 \\ \frac{-1}{y^e(\alpha+1)+y^e(\alpha+2)} & \frac{1}{y^e(\alpha+2)} & 0 \end{bmatrix}$$

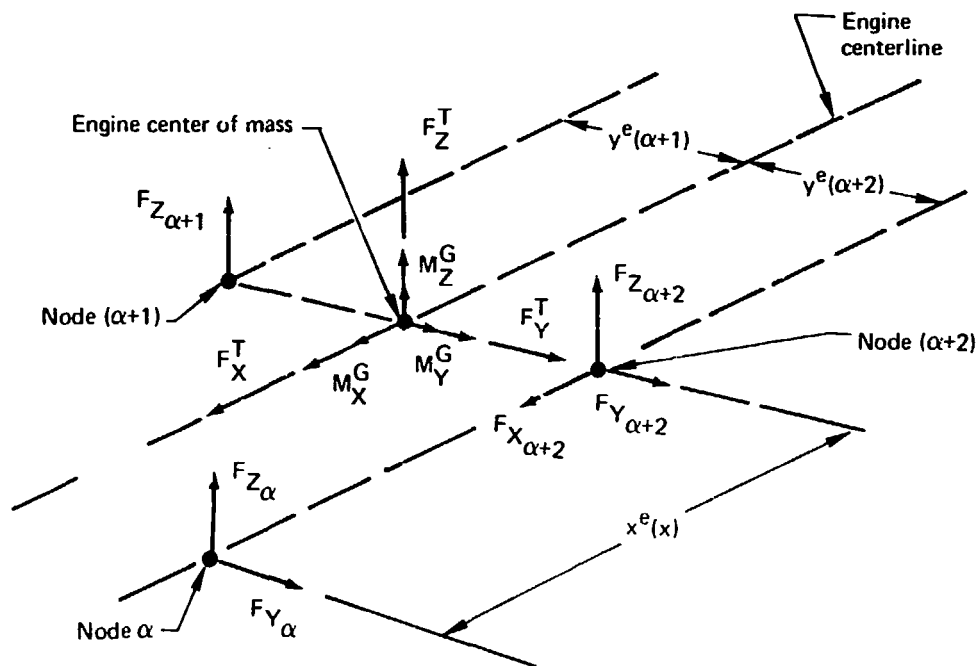


FIGURE 4.4-11.—ENGINE STRUCTURAL SUPPORT LOADS

4.4.4 Matrix Operators Involving Nodal Inertial Forces

The objective of this section is to describe, in detail, the construction of the matrix $[P]$ defined by equation (4.2-53). As shown in section 4.2.2.5, this transformation matrix is used in the following operations involving inertial forces at the structural nodes:

$$\{\delta\} = [P]^T \{\delta'\} \quad (4.4-35)$$

and

$$\{Q\} = [P]\{Q^S\}. \quad (4.4-36)$$

As seen by equation (4.2-53), i.e.,

$$[P] \equiv \left[[I] - [m_\delta][\bar{\phi}_\delta][M]^{-1}[\bar{\phi}_\delta]^T \right], \quad (4.2-53)$$

the transformation matrix is constructed from the rigid body mode shape matrix, the nodal mass matrix, and the total mass-inertia matrix; however, this form of the transformation matrix is not actually used in the FLEXSTAB system in the computation shown by equation (4.4-35). Equation (4.4-35) is replaced in the FLEXSTAB system by the expression

$$\{\delta\} = [P']^T \{\delta'\} \quad (4.4-37)$$

where

$$[P'] \equiv \left[[I] - [m_\delta][\bar{\phi}_\delta]([\bar{\phi}_\delta]^T[m_\delta][\bar{\phi}_\delta]^T)^{-1}[\bar{\phi}_\delta]^T \right]. \quad (4.4-38)$$

Equation (4.4-37) is introduced in lieu of equation (4.4-35) because the operation

$$[\bar{\phi}_\delta]^T[m_\delta][\bar{\phi}_\delta]$$

appearing in equation (4.4-38) may fail to yield the total mass-inertia of the aircraft as shown by equation (4.2-26). This failure occurs when approximations, described in the following, are introduced into the nodal mass and rigid body mode shape matrices; when these matrices contain approximations, equations (4.4-36) and (4.4-37) yield results that only approximate the desired results, viz., in the case of equation (4.4-36)—the incorporation of nodal inertial forces—and in the case of equation (4.4-37)—the incorporation of a mean reference frame. The reasons for choosing equations (4.4-36) and (4.4-37), as the best approximations, are explained in the following.

4.4.4.1 Reduction of the nodal degrees of freedom.—As noted in section 4.4.1, the finite element model of the structure is nearly always described initially in terms of a set of degrees of freedom that contain the set $\{\delta\}$ as a subset. The structural matrices supplied to the FLEXSTAB system and listed at the beginning of this section are the result of a reduction process. The choice of the particular reduction process used is at the discretion of the FLEXSTAB system user, but special attention must be given to the reduction process chosen for obtaining the nodal mass matrix, $[m_\delta]$.

Using the notation of table 2a of reference 1-2, the nodal degrees of freedom $\{\delta\}$ correspond to those denoted as $\{u_l\}$. These degrees of freedom are a subset of $\{u_g\}$, whose members are the set of all possible physical components used in modeling the structure. The reduction to $\{u_l\}$ involves three operations: (1) elimination of $\{u_m\}$ by multipoint constraints; (2) elimination of $\{u_s\}$ by single-point constraints; and (3) elimination of $\{u_o\}$ and $\{u_r\}$ by structural partitioning. Letting, as in section 3.3 of reference 2-1,

$$\{u_g\} \equiv \begin{bmatrix} \{u_m\} \\ \{u_s\} \\ \{u_o\} \\ \{u_r\} \\ \{u_l\} \end{bmatrix}$$

the stiffness and mass matrices for the structure corresponding to these degrees of freedom are denoted as $[K_{gg}]$ and $[M_{gg}]$, respectively. The contents of section 3.5 of reference 1-2 describe methods for reducing the stiffness and mass matrices to those given as $[K_{aa}]$ and $[M_{aa}]$ in terms of the degrees of freedom defined as

$$\{u_a\} \equiv \begin{bmatrix} \{u_l\} \\ \{u_r\} \end{bmatrix}$$

and a further reduction to $[K_{ll}]$ and $[M_{ll}]$ is an obvious extension of the contents of section 3.5 of reference 1-2.

4.4.4.2 Approximate mass matrix.—If the reduction methods of section 3.5 of reference 1-2 are used in obtaining the matrices supplied to the FLEXSTAB system, then the operations shown by equation (4.4-36) and by either equation (4.4-35) or (4.4-37) lead to a correct mean reference frame and correct inertial forces at the nodes. In practice, however, the nodal mass matrix is not always the result of the reduction processes of the cited reference; the mass matrix may be the result of an ad hoc lumping of the masses at the nodes—the lumping process being based on engineering judgment. Mass matrices generated in this manner are considered approximate because the operations $[\bar{\phi}_\delta]^T [m_\delta] [\bar{\phi}_\delta]$ may not lead to the total mass-inertia matrix shown by equation (4.2-26).

4.4.4.3 Computation of the mean reference frame.—Nodal displacement relative to a mean reference frame is described in section 4.2 as

$$\{\delta\} = \{\delta'\} - [\bar{\phi}_\delta][M]^{-1}[\bar{\phi}_\delta]^T[m_\delta]\{\delta'\} \quad (4.4-39)$$

where

$$[M]^{-1}[\bar{\phi}_\delta]^T[m_\delta]\{\delta'\} = \{B\}, \quad (4.4-40)$$

cf., section 4.2.2.5; hence, as shown by equation (4.2-30),

$$\{\delta\} = \{\delta'\} - [\bar{\phi}_\delta]\{B\}$$

These expressions are valid if the nodal mass matrix contains no approximations; but if the nodal mass matrix is approximate and does not satisfy the relation

$$[\bar{\phi}_\delta]^T[m_\delta][\bar{\phi}_\delta] = [M],$$

with $[M]$ given by equation (4.2-26), then the values of the matrix $\{B\}$ fail to yield nodal displacement components $\{\delta\}$ measured relative to a mean reference frame.

In the FLEXSTAB system analysis, the nodal displacement components $\{\delta\}$ must satisfy the mean reference frame constraint conditions shown by equation (4.2-23); thus, when equation (4.4-39) is substituted into equation (4.2-23), there results the following matrix expression which must vanish:

$$\begin{aligned} & [\bar{\phi}_\delta]^T[m_\delta]\{\delta\} = \\ & = [\bar{\phi}_\delta]^T[m_\delta]\{\delta'\} - [\bar{\phi}_\delta]^T[m_\delta][\bar{\phi}_\delta][M]^{-1}[\bar{\phi}_\delta]^T[m_\delta]\{\delta'\}. \end{aligned} \quad (4.4-41)$$

If the total mass-inertia matrix, $[M]$, is replaced by $[\bar{\phi}_\delta]^T[m_\delta][\bar{\phi}_\delta]$ as in equation (4.4-37), then the right-hand member of equation (4.4-41) vanishes, showing that equation (4.4-37) describes nodal displacement relative to a mean reference frame as required.

4.4.4.4 Computation of the nodal inertial forces.—The inertial forces at the nodes, related to rigid body acceleration, are given by

$$\{Q^I\} = \{Q\} - \{Q^S\}; \quad (4.4-42)$$

and, from equations (4.4-36) and (4.2-53),

$$\{Q^I\} = -[m_\delta][\bar{\phi}_\delta][M]^{-1}[\bar{\phi}_\delta]^T\{Q^S\} \quad (4.4-43)$$

where, as shown in section 4.2.2.5,

$$[M]^{-1}[\bar{\phi}_\delta]^T\{Q^S\} = \{\ddot{B}'\} \quad (4.4-44)$$

represents rigid body acceleration. Equation (4.4-43), therefore, may be expressed as

$$\{Q^I\} = - [m_\delta][\bar{\phi}_\delta](\ddot{B}) \quad (4.4-45)$$

and the right-hand member of equation (4.4-43) is seen to describe the inertial forces at the nodes arising from rigid body acceleration.

4.4.4.5 Deletion of aerodynamic forces resulting from reduced degrees of freedom.—The degrees of freedom at thin and slender body nodes can be reduced such that

$$\{\delta_\alpha\}_W = \begin{bmatrix} d_{XN_\alpha} \\ d_{ZN_\alpha} \end{bmatrix}_W \quad \text{and} \quad \{\delta_\alpha\}_B = \begin{bmatrix} d_{X_\alpha} \\ d_{Y_\alpha} \\ d_{Z_\alpha} \end{bmatrix}_B, \quad (4.4-46)$$

without deleting aerodynamic forces, cf., section 3.5.1.2 and equation (3.5-39). If they are further reduced, then the resultant aerodynamic forces computed from equation (4.2-49), viz.,

$$\{F_C^A\} = [\bar{\phi}_\delta]^T \{Q^A\},$$

will not be equal to the values of these forces given by equation (3.5-6). This defect arises from the fact that

$$[\bar{\phi}_\delta]^T [P_T]^T \{f_T^A\} \neq [\bar{\phi}_\delta]^T [T_{fT}] \{f_T^A\}$$

when $[P_T]$ fails to relate to at least the degrees of freedom shown by equation (4.4-46). The defect leads to rigid body accelerations $\{\ddot{B}\}$, which are in error. In this case, the inertial forces described by equation (4.4-45) and introduced into the FLEXSTAB system analysis by equation (4.4-36) are also in error.

The error in the inertial forces is unavoidable when the degrees of freedom are less than those shown by equation (4.4-46); but in most cases of practical interest, the error has an insignificant effect on the stability analysis performed by the FLEXSTAB system. Usually, aircraft slender body structural components are very stiff in the X-direction compared with stiffnesses in the Y- and Z-directions, and thin body structural components are usually very stiff in the X and Y_N directions. It is the X and Y_N components of displacement at the nodes that are usually deleted, i.e., reduced from flexibility matrix and either deleted or reduced from the mass matrix. The X and Y_N components of the inertial forces at the nodes are then in error, but the large stiffnesses of the structural components in the X-direction lead to negligible deformation influencing the stability derivatives.

4.4.5 Requirements That Supplied Structural Matrices Must Satisfy

4.4.5.1 Coordinate systems. – The supplied matrices must be expressed for nodal components of force and displacement expanded on the ESIC coordinate systems described in section 4.4.2. Geometric locations of structural node points must be expressed in the ESIC coordinate systems.

4.4.5.2 Symmetric and antisymmetric forms. – The supplied matrices must be expressed using the simplification offered by having required the aircraft to have a plane of symmetry, section 4.2.5. They are expressed, therefore, in terms of nodes located only on and to the right of the plane of symmetry, and they are generated in two parts—symmetric and antisymmetric—corresponding to two sets of boundary conditions applied to nodal force and displacement components at the nodes on the plane of symmetry. See section 4.4.1.4.

4.4.5.3 Admissible nodal degrees of freedom. – The supplied matrices are assumed to be in terms of three translational degrees of freedom at each node or in terms of the specific subsets of these degrees of freedom. See sections 4.4.1.1, 4.4.1.2, and 4.4.1.9.

4.4.5.4 Flexibility matrix requirements. – The supplied flexibility matrix $[C]$ is assumed to be nonsingular, i.e., it is assumed to describe the flexibility of the structure relative to nodal constraints that constrain the structure against rigid body motion. As noted in sections 4.2.2.5 and 4.2.3.1, the choice of constraining nodal degrees of freedom, viz., $\{\delta_R\}$ of equation (4.2-59), is of no consequence provided that the symmetry requirements of section 4.2.5 are satisfied.

4.4.5.5 Free vibration mode shapes. – The free vibration mode shapes $\{\phi_\delta\}$ are assumed to be generated for the unconstrained structure. See section 4.2.4.1.

4.4.5.6 Constraining degrees of freedom. – None of the supplied matrices is assumed to contain the constraining degrees of freedom $\{\delta_R\}$. See section 4.2.3.1.

4.4.5.7 Nodal mass matrix. – The nodal mass matrix $[m_\delta]$ is unrestricted in that it may contain off-diagonal masses representing inertial coupling between nodes. Nodal masses at nodes on the plane of symmetry are assumed to have values appropriate to the simplification of section 4.2.5; i.e., the values for masses at nodes on the plane of symmetry are assumed to be one-half the values of these masses when both halves of the aircraft are included in the computation. The total, equivalent point mass represented by $[m_\delta]$, therefore, is expected to be one-half the total aircraft mass. Also, the nodal masses associated with the $\{\delta_R\}$ degrees of freedom must be distributed to the translational degrees of freedom of $\{\delta\}$, or this mass will be neglected in the analysis. When there are less than three degrees of freedom at each node, the inertial forces may be in error. See section 4.4.4.

4.4.5.8 Rigid body mode shape matrix. – The rigid body mode shape matrix $\{\bar{\phi}_\delta\}$ may be generated either internally or externally to the FLEXSTAB system. Internal generation is based on the geometric locations of the nodes of the structure, and the resulting rigid body mode matrix is of the form given by equation (4.2-16). The method for external generation is obviously at the discretion of the user; however, because of the form of equation (4.2-53), the externally generated rigid body modes must describe rigid body motion about the aircraft center of mass.

4.4.5.9 Total mass-inertia matrix.—The elements of the total mass-inertia matrix, equation (4.2-26), are assumed to describe the rigid body inertial characteristics of the entire aircraft (i.e., of both the right- and left-hand sides) for rigid body motion about the center of mass.

5.0 STEADY, REFERENCE FLIGHT CONDITION

5.1 INTRODUCTION

The objective of this section is to derive the method used in the FLEXSTAB system to evaluate static stability and trim characteristics. Throughout section 5 the aircraft is assumed to be in a state of steady flight, i.e., a state of motion such that

$$\dot{U} = \dot{V} = \dot{W} = \dot{P} = \dot{Q} = \dot{R} = 0 \quad (5.1-1)$$

where U, V, W, P, Q, R are the translational and rotational components of velocity in the Body Axis System, equation (2.2-3). This steady state of flight is termed the reference flight condition, and may consist of any steady or quasi-steady maneuver chosen by the FLEXSTAB system user. Examples of the reference flight condition are truly steady maneuvers such as rectilinear flight, steady sideslip, level turns, and helical turns. In addition, the reference flight condition may consist of a quasi-steady maneuver for which the restrictions imposed by equations (5.1-1) are only approximately satisfied, e.g., a steady pull-up.

The equations of motion for the steady, reference flight condition are introduced in section 5.2. The equations of motion expanded on the Body Axis System, section 2.2.2, are six in number and contain 12 trim parameters. As shown in section 5.2.1, the reference flight condition is specified by specifying the values of six of the trim parameters. The remaining six trim parameters—termed the trim variables—are determined by solving the equations of motion. This operation consists of solving the trim problem formulated in section 5.2.2.

The aerodynamic derivatives* and the corresponding forces acting on the aircraft in the steady reference flight condition are derived in sections 5.3 through 5.3.4. This derivation is based on the linear aerodynamic and structural theories of sections 3 and 4, but section 5.3.5 describes a method used in the FLEXSTAB system for introducing the effects of nonlinear aerodynamics. Section 5.4 contains a derivation of the equations which introduce the effects of the propulsion system on the reference flight condition. Sections 5.1 through 5.4 contain all of the results needed to express the equations of motion in the form which poses the trim problem.

Two methods for solving the trim problem are derived in section 5.5. One is a straightforward algebraic solution used when the equations of motion are linear functions of the trim variables. The second is used when the equations of motion are nonlinear functions of the trim variables. This latter method is based on a Newton iteration formula, reference 5-1, taking into account nonlinear rigid body aircraft dynamics as well as nonlinear aerodynamics. The nonlinear aerodynamics are introduced into the equations of motion using a tabular scheme described in section 5.5.4. Finally, sections 5.6 and 5.7 contain the derivation of the formulas which describe the following static stability and trim characteristic:

The static stability derivatives* (expanded on the Stability Axis System, section 2.2.5):

*The distinction between aerodynamic derivatives and stability derivatives is explained in section 5.2.2.4.

$$\begin{array}{ccc}
C_{D_0}, & C_{D_\alpha}, & C_{D_Q} \\
L_0, & C_{L_\alpha}, & C_{L_Q} \\
C_{m_0}, & C_{m_\alpha}, & C_{m_Q} \\
C_{Y_\beta}, & C_{Y_P}, & C_{Y_R} \\
C_{l_\beta}, & C_{l_P}, & C_{l_R} \\
C_{n_\beta}, & C_{n_P}, & C_{n_R}
\end{array}$$

The control effectivenesses:

$$\begin{array}{ccc}
C_{L_{\delta_e}}, & C_{D_{\delta_e}}, & C_{m_{\delta_e}} \\
C_{Y_{\delta_a}}, & C_{l_{\delta_a}}, & C_{n_{\delta_a}} \\
C_{Y_{\delta_r}}, & C_{l_{\delta_r}}, & C_{n_{\delta_r}}
\end{array}$$

The following static stability parameters:

- static margin,
- maneuver margin,
- neutral point,
- maneuver point,
- load factor,
- stick-speed stability, and
- elevator angle per g.

In addition, section 5.7 contains a derivation of the formulas determining the static elastic deformation, static loads, and static lifting surface pressure distribution.

None of the derivations contained in this section are complete in themselves; they make extensive use of quantities derived in sections 2, 3, and 4.

5.2 EQUATIONS OF MOTION FOR THE STEADY, REFERENCE FLIGHT CONDITION

The equations of motion for an aircraft in steady flight are given in vector form by equations (4.2-54) and (4.2-55). Expanded in scalar form on the Body Axis System, section 2.2.2, these equations appear as follows:

$$\begin{aligned}
M(Q_1 W_1 - R_1 V_1) + Mg \sin \theta_1 &= F_{XB_1} \\
M(R_1 U_1 - P_1 W_1) - Mg \cos \theta_1 \sin \phi_1 &= F_{YB_1} \\
M(P_1 M_1 - Q_1 U_1) - Mg \cos \theta_1 \cos \phi_1 &= F_{ZB_1}
\end{aligned} \tag{5.2-1}$$

$$(I_{ZZ_1} - I_{YY_1})Q_1 R_1 - I_{XZ_1} P_1 Q_1 = M_{XB_1}$$

$$(I_{XX_1} - I_{ZZ_1})R_1 P_1 + I_{XZ_1} (P_1^2 - R_1^2) = M_{YB_1}$$

$$(I_{YY_1} - I_{XX_1})P_1 Q_1 + I_{XZ_1} Q_1 R_1 = M_{ZB_1}$$

The subscript 1 denotes evaluation in the reference flight condition, and the right-hand members are components of force and moment arising from the aerodynamics and the propulsion system; these components are dependent on the elastic deformation.

Equations (5.2-1) are functions of the six velocity components, equations (2.2-3) and, in addition, the right-hand members are functions of a thrust amplitude setting T_1 and the following aerodynamic control surface settings:

δe_1 — pitch control

δa_1 — roll control

δr_1 — yaw control

Assuming that the inertial and aerodynamic characteristics of the aircraft are specified, the equations of motion may be regarded as containing 12 parameters— U_1 , V_1 , W_1 , P_1 , Q_1 , R_1 , ϕ_1 , θ_1 , T_1 , δe_1 , δa_1 , and δr_1 . The reference flight condition is chosen by the FLEXSTAB system user by specifying the values of six of these parameters; and the equations of motion, equations (5.2-1), then consist of six equations in terms of the remaining six unspecified parameters. Aircraft trim is computed by solving the six equations for the six unspecified parameters.

5.2.1 Specification of the Reference Flight Condition

The FLEXSTAB system user is required to specify the following parameters:

- 1) U_1 — forward velocity
- 2) P_1 — roll rate
- 3) Q_1 — pitch rate (or, alternately, load factor, cf., section 5.7.1)
- 4) R_1 — yaw rate
- 5) ϕ_1 — angle of bank
- 6) Either T_1 — thrust amplitude setting or $\gamma_1 = \theta_1 - \tan W_1/U_1$ — flight path angle, figure 5.2-1.

The system computes the following trim parameters: the control surface settings (δe_1 , δa_1 , δr_1), the angle of attack ($\alpha_1 = \tan^{-1} (W_1/U_1)$), the angle of sideslip ($\beta_1^* = \tan^{-1} (V_1/U_1)$), and either the flight path angle γ_1 or the thrust amplitude setting T_1 .

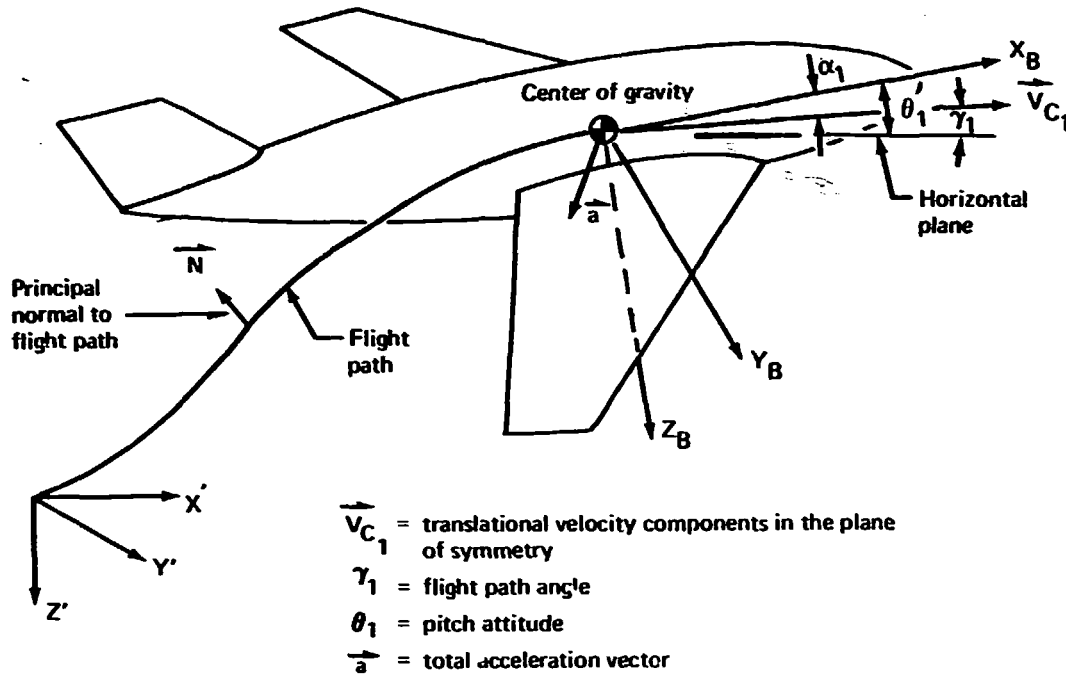


FIGURE 5.2-1.—FLIGHT PATH OF AN AIRCRAFT

5.2.1.1 Coordinated maneuvers.—Selection of the reference flight condition as a coordinated maneuver requires special consideration. A coordinated maneuver is one in which the total acceleration of the aircraft is a vector lying in the plane of symmetry of the aircraft. The total acceleration is the vector sum of the gravitational acceleration and the acceleration due to flight path curvature, figure 5.2-1, where the acceleration due to flight path curvature is given by the following expression:

$$\vec{a}_n = \frac{\vec{V}_c \cdot \vec{V}_c}{\rho} \vec{N} \quad (5.2-2)$$

where \vec{V}_c is the velocity of the aircraft along the flight path, ρ is the radius of flight path curvature, and \vec{N} is the principal normal to the flight path, reference 5-1, p. 294. The gravitational acceleration \vec{g} is given by

$$\vec{g} = g \vec{E}' \quad (5.2-3)$$

*Note that this is not the usual definition of β , cf., page 11 of reference 2-2.

The total acceleration \vec{a} , therefore is the following vector sum:

$$\vec{a} = g\vec{k} + \frac{V^2}{\rho} \vec{N} \quad (5.2-4)$$

Following the usual practice of trimming an aircraft for a coordinated maneuver, the bank angle ϕ_1 for the reference flight condition is selected so that the vector \vec{a} lies in the plane of symmetry of the aircraft.

When an aircraft is undergoing a maneuver which involves a change in heading, the bank angle required to have the total acceleration vector lie in the plane of symmetry must be found by iteration. Even for a reference flight condition consisting of a steady level turn, choice of the appropriate bank angle is complicated by the fact that the equations of motion are expressed in terms of the Body Axis System. The bank angle ϕ is a rotation about the X_B axis, equation (2.1-1), and the orientation of the X_B axis relative to the plane of the turn is governed by θ —one of the unspecified parameters in the trim problem. The appropriate bank angle is therefore not known a priori.

For the case of a steady, level turn the flight path angle is zero ($\gamma_1 = 0$); hence, θ_1 is equal to the angle of attack, $\alpha_1 = \tan^{-1} W_1/U_1$. The FLEXSTAB system user may estimate the value for α_1 and compute the input bank angle and the rotation rates P_1, Q_1, R_1 from the following formulas;

$$\tan \phi_1 = \frac{U_1^2 (1 + \alpha_1^2)}{\rho g} \sin \alpha_1$$

or

$$(5.2-5)$$

$$\tan \phi_1 \approx \frac{U_1 (1 + \alpha_1)}{g} \sin \alpha_1 \dot{\psi}$$

(where ρ is the turn radius and $\dot{\psi}$ is rate of change of heading angle) and

$$\begin{aligned} P_1 &= \dot{\psi} \sin \alpha_1 \\ Q_1 &= \dot{\psi} \sin \phi_1 \cos \alpha_1 \\ R_1 &= \dot{\psi} \cos \phi_1 \cos \alpha_1 \end{aligned} \quad (5.2-6)$$

The values of $U_1, P_1, Q_1, R_1, \phi_1$, and γ_1 obtained from these formulas lead to values of $V_1, W_1, \delta e_1, \delta a_1, \delta r_1$, and T_1 which produce a steady, reference flight condition; but, unless the estimated value of α_1 is exactly equal to that computed in the trim problem, the computed reference flight condition will be a steady turn which takes place with a change in altitude. The values of the velocity components V_1 and W_1 will, in general, lead to a helical flight path.

even though the flight path angle is set to zero, and the total acceleration vector will not lie in the plane of symmetry. Trim for the resulting reference flight condition, therefore, requires a lateral control deflection to produce a force contributing to the lateral acceleration of the turn.

The steady, level turn may be more closely approximated by recomputing the input data. The angular rates and the bank angle are computed a second time using equations (5.2-5) and (5.2-6) and a new estimate for the value of angle of attack. This process may be repeated until the desired reference flight condition is approximated with the desired degree of accuracy and the trim problem is regarded as solved for the steady, level turn.

5.2.1.2 Quasi-steady maneuvers.—The equations of steady motion, equations (5.2-1), are used as approximations for evaluating static stability and trim of an aircraft in a reference flight condition when the pitch attitude θ_1 and/or bank angle ϕ_1 change with time. The maneuvers represented by these reference flight conditions, e.g., pull-ups and rolling flight, involve motions which violate the assertions of equations (5.1-1) because the rotation rates P_1 , Q_1 , R_1 fail to satisfy the following relations:

$$\begin{aligned}\dot{\theta}_1 &= Q_1 \cos \phi_1 - R_1 \sin \phi_1 = 0 \\ \dot{\phi}_1 &= P_1 + (Q_1 \sin \phi_1 + R_1 \cos \phi_1) \tan \theta_1 = 0\end{aligned}\tag{5.2-7}$$

These equations are satisfied by the rotation rates of steady turning flight, equations (5.2-6), but they yield non-zero values for steady rolling flight and steady pull-ups. Even though equations (5.2-7) are not satisfied, trim and static stability are computed on the basis of equations (5.2-1) and the reference flight condition is considered to be quasi-steady.

Consider a typical example—a steady symmetric pull-up with pitch rate Q_1 . The pitch attitude angular rate is given by the first of equations (5.2-7) as

$$\dot{\theta}_1 = Q_1$$

The equations of steady motion, equations (5.2-1), evaluated for the pull-up yield the following:

$$\begin{aligned}MQ_1 W_1 + Mg \sin \theta_1 &= F_{XB_1} \\ 0 &= F_{YB_1} \\ -MQ_1 U_1 - Mg \cos \theta_1 &= F_{ZB_1} \\ 0 &= M_{XB_1} \\ 0 &= M_{YB_1} \\ 0 &= M_{ZB_1}\end{aligned}\tag{5.2-8}$$

The gravitational terms in these equations are varying with time; therefore, the velocity components U_1 and W_1 must also be functions of time, contrary to the assertion of Equations (5.1-1). This contradiction is ignored and equations (5.2-8) are used as a basis for evaluating the static stability and trim characteristics. Inertial force components $M\dot{U}_1$ and $M\dot{W}_1$ and corresponding unsteady aerodynamic force components are neglected as small, thereby leading to the quasi-steady approximation.

5.2.2 Formulation of the Trim Problem

The equations of steady motion, equations (5.2-1), are rearranged in this section to formulate the trim problems solved by the FLEXSTAB system. The FLEXSTAB system user has the option of specifying either the flight path angle or the thrust amplitude of the reference flight condition, and may also solve either a nonlinear or a linear trim problem. These options require four distinct forms of the equations of steady motion.

5.2.2.1 Nonlinear trim problems.—The nonlinear forms are as follows:

(1) Specified flight path angle γ_1 ,

$$\begin{aligned}
 MU_1(Q_1 \tan \alpha_1 - R_1 \tan \beta_1) + Mg \sin(\gamma_1 + \alpha_1) &= F_{XB_1}^T + F_{XB_1}^A \\
 MU_1(R_1 - P_1 \tan \alpha_1) - Mg \cos(\gamma_1 + \alpha_1) \sin \phi_1 &= F_{YB_1}^T + F_{YB_1}^A \\
 MU_1(P_1 \tan \beta_1 - Q_1) - Mg \cos(\gamma_1 + \alpha_1) \cos \phi_1 &= F_{ZB_1}^T + F_{ZB_1}^A \\
 (I_{ZZ_1} - I_{YY_1})Q_1 R_1 - I_{XZ_1} P_1 Q_1 &= M_{XB_1}^T + M_{XB_1}^A \\
 (I_{XX_1} - I_{ZZ_1})P_1 R_1 + I_{XZ_1} (P_1^2 - R_1^2) &= M_{YB_1}^T + M_{YB_1}^A \\
 (I_{YY_1} - I_{XX_1})P_1 Q_1 + I_{XZ_1} R_1 Q_1 &= M_{ZB_1}^T + M_{ZB_1}^A
 \end{aligned} \tag{5.2-9}$$

where $\alpha_1 \equiv \tan^{-1} W_1/U_1$ and $\beta_1 \equiv \tan^{-1} V_1/U_1$.*

(2) Specified thrust amplitude setting T_1 ,

$$\begin{aligned}
 MU_1(Q_1 \tan \alpha_1 - R_1 \tan \beta_1) + Mg \sin \theta_1 &= F_{XB_1}^T + F_{XB_1}^A \\
 MU_1(R_1 - P_1 \tan \alpha_1) - Mg \cos \theta_1 \sin \phi_1 &= F_{YB_1}^T + F_{YB_1}^A \\
 MU_1(R_1 \tan \beta_1 - Q_1) - Mg \cos \theta_1 \cos \phi_1 &= F_{ZB_1}^T + F_{ZB_1}^A \\
 (I_{ZZ_1} - I_{YY_1})R_1 Q_1 - I_{XZ_1} P_1 Q_1 &= M_{XB_1}^T + M_{XB_1}^A \\
 (I_{XX_1} - I_{ZZ_1})P_1 R_1 + I_{XZ_1} (P_1^2 - R_1^2) &= M_{YB_1}^T + M_{YB_1}^A \\
 (I_{YY_1} - I_{XX_1})P_1 Q_1 + I_{XZ_1} R_1 Q_1 &= M_{ZB_1}^T + M_{ZB_1}^A
 \end{aligned} \tag{5.2-10}$$

*Note that this is not the usual definition of β , cf., page 11 of reference 2-2.

Equations (5.2-9) and (5.2-10) are clearly nonlinear from the trigonometric functional dependence on α and β . Additional nonlinearity may arise in the components of force and couple which are thrust dependent and appear on the right of equations (5.2-9) and (5.2-10). These terms may be nonlinear functions of the thrust amplitude as a consequence of the gyroscopic couples from rotating engine parts.

5.2.2.2 Nonlinear aerodynamic forces.—The components of force and couple arising from the aerodynamics may also be nonlinear functions with the following dependence:

$$\begin{aligned}
 F_{XB_1}^A &= F_{XB_0}^A + F_{XB}^A(\alpha_1, Q_1, \delta_{e_1}, \beta_1, P_1, R_1, \delta_{a_1}, \delta_{r_1}) \\
 F_{YB_1}^A &= F_{YB}^A(\alpha_1, Q_1, \delta_{e_1}, \beta_1, P_1, R_1, \delta_{a_1}, \delta_{r_1}) \\
 F_{ZB_1}^A &= F_{ZB_0}^A + F_{ZB}^A(\alpha_1, Q_1, \delta_{e_1}, \beta_1, P_1, R_1, \delta_{a_1}, \delta_{r_1}) \\
 M_{XB_1}^A &= M_{XB}^A(\alpha_1, Q_1, \delta_{e_1}, \beta_1, P_1, R_1, \delta_{a_1}, \delta_{r_1}) \\
 M_{YB_1}^A &= M_{YB_0}^A + M_{YB}^A(\alpha_1, Q_1, \delta_{e_1}, \beta_1, P_1, R_1, \delta_{a_1}, \delta_{r_1}) \\
 M_{ZB_1}^A &= M_{ZB}^A(\alpha_1, Q_1, \delta_{e_1}, \beta_1, P_1, R_1, \delta_{a_1}, \delta_{r_1})
 \end{aligned} \tag{5.2-11}$$

where $F_{XB_0}^A, F_{ZB_0}^A, M_{YB_0}^A$ are force and moment components acting on the aircraft when all motion variables and control surface settings except U_1 are set at zero.

5.2.2.3 Linear trim problem.—The linear trim problem corresponds to the linear, first-order aerodynamic theory developed in section 3. As such, the angles of attack and sideslip (α, β) and the pitch attitude (θ) must be so small that their products with one another are negligible. With these approximations the equations of steady motion, given by equations (5.2-9) and (5.2-10), reduce to the following approximations:

(1) Specified flight path angle γ_1 ,

$$\begin{aligned}
 MU_1(Q_1\alpha_1 - R_1\beta_1) + Mg(\sin\gamma_1 + \alpha_1\cos\gamma_1) &= F_{XB_1}^T + F_{XB_1}^A \\
 MU_1(R_1 - P_1\alpha_1) - Mg\sin\phi_1(\cos\gamma_1 - \alpha_1\sin\gamma_1) &= F_{YB_1}^T + F_{YB_1}^A \\
 MU_1(P_1\beta_1 - Q_1) - Mg\cos\phi_1(\cos\gamma_1 - \alpha_1\sin\gamma_1) &= F_{ZB_1}^T + F_{ZB_1}^A
 \end{aligned} \tag{5.2-12}$$

$$(I_{ZZ_1} - I_{YY_1})Q_1 R_1 - I_{XZ_1} P_1 Q_1 = M_{XB_1}^T + M_{XB_1}^A$$

$$(I_{XX_1} - I_{ZZ_1})P_1 R_1 + I_{XZ_1} (P_1^2 - R_1^2) = M_{YB_1}^T + M_{YB_1}^A$$

$$(I_{YY_1} - I_{XX_1})P_1 Q_1 + I_{XZ_1} R_1 Q_1 = M_{ZB_1}^T + M_{ZB_1}^A$$

where

$$\alpha_1 \approx \frac{W_1}{U_1}$$

$$\beta_1 \approx \frac{V_1}{U_1}$$

(2) specified thrust amplitude setting T_1 ,

$$MU_1(Q_1 \alpha_1 - R_1 \beta_1) + Mg \theta_1 = F_{XB_1}^T + F_{XB_1}^A$$

$$MU_1(R_1 - P_1 \alpha_1) - Mg \sin \phi_1 = F_{YB_1}^T + F_{YB_1}^A$$

$$MU_1(R_1 \beta_1 - Q_1) - Mg \cos \phi_1 = F_{ZB_1}^T + F_{ZB_1}^A$$

$$(I_{ZZ_1} - I_{YY_1})Q_1 R_1 - I_{XZ_1} P_1 Q_1 = M_{XB_1}^T + M_{XB_1}^A \quad (5.2-13)$$

$$(I_{XX_1} - I_{ZZ_1})P_1 R_1 + I_{XZ_1} (P_1^2 - R_1^2) = M_{YB_1}^T + M_{YB_1}^A$$

$$(I_{YY_1} - I_{XX_1})P_1 Q_1 + I_{XZ_1} R_1 Q_1 = M_{ZB_1}^T + M_{ZB_1}^A$$

For the case of specified flight path angle the gyroscopic couples due to rotating engine parts can no longer be nonlinear functions of the thrust amplitude T_1 . The components of force and couple produced by the propulsion system therefore become linear functions of T_1 , e.g.,

$$M_{YB_1}^T = M_{YB_1}^T \delta T_1$$

5.2.2.4 Linear aerodynamic forces.—As already noted, the linear aerodynamic theory requires that the components of aerodynamic force and couple be linear functions of the aircraft's motion and the control surface settings. Also, motions of control surface settings which are symmetric with respect to the plane of symmetry of the aircraft can give rise only to symmetric distributions of aerodynamic pressure, while antisymmetric motions and control surface settings produce only antisymmetric aerodynamic pressure distributions. The non-linear aerodynamic terms of equations (5.2-11), therefore, reduce to the following linear forms:

$$\begin{aligned}
 F_{XB_1}^A &= F_{XB_0}^A + F_{XB_\alpha}^A \alpha_1 + F_{XB_Q}^A Q_1 + F_{XB_{\delta e}}^A \delta e_1 \\
 F_{YB_1}^A &= F_{YB_\beta}^A \beta_1 + F_{YB_P}^A P_1 + F_{YB_R}^A R_1 + F_{YB_{\delta a}}^A \delta a_1 + F_{YB_{\delta r}}^A \delta r_1 \\
 F_{ZB_1}^A &= F_{ZB_0}^A + F_{ZB_\alpha}^A \alpha_1 + F_{ZB_Q}^A Q_1 + F_{ZB_{\delta e}}^A \delta e_1 \\
 M_{XB_1}^A &= M_{XB_\beta}^A \beta_1 + M_{XB_P}^A P_1 + M_{XB_R}^A R_1 + M_{XB_{\delta a}}^A \delta a_1 + M_{XB_{\delta r}}^A \delta r_1 \\
 M_{YB_1}^A &= M_{YB_0}^A + M_{YB_\alpha}^A \alpha_1 + M_{YB_Q}^A Q_1 + M_{YB_{\delta e}}^A \delta e_1 \\
 M_{ZB_1}^A &= M_{ZB_\beta}^A \beta_1 + M_{ZB_P}^A P_1 + M_{ZB_R}^A R_1 + M_{ZB_{\delta a}}^A \delta a_1 + M_{ZB_{\delta r}}^A \delta r_1
 \end{aligned} \tag{5.2-14}$$

where the coefficients of the motion variables and control surface settings are all constants. These coefficients constitute the aerodynamic derivatives of an aircraft and as indicated in equation (5.2-14), the aerodynamic derivatives are coefficients in a truncated Taylor series expansion about the flight condition wherein all trim parameters are set to zero except U_1 . The aerodynamic derivatives are, therefore, distinct from the stability derivatives because the latter are the result of perturbations about the reference flight condition wherein all of the trim parameters may be different from zero.

5.2.2.5 Aerodynamic derivatives.—The aerodynamic derivatives appearing as coefficients of the motion variables and control surface settings in equations (5.2-14) are separated into two classes as follows:

Longitudinal aerodynamic derivatives:

$$\begin{array}{cccc}
 F_{XB_0}^A & F_{XB_\alpha}^A & F_{XB_Q}^A & F_{XB_{\delta e}}^A \\
 F_{ZB_0}^A & F_{ZB_\alpha}^A & F_{ZB_Q}^A & F_{ZB_{\delta e}}^A \\
 M_{YB_0}^A & M_{YB_\alpha}^A & M_{YB_Q}^A & M_{YB_{\delta e}}^A
 \end{array} \tag{5.2-15}$$

Lateral-directional aerodynamic derivatives:

$$\begin{aligned}
 &F_{YB\beta}^A \quad F_{YB_P}^A \quad F_{YB_R}^A \quad F_{YB\delta a}^A \quad F_{YB\delta r}^A \\
 &M_{XB\beta}^A \quad M_{XB_P}^A \quad M_{XB_R}^A \quad M_{XB\delta a}^A \quad M_{XB\delta r}^A \\
 &M_{ZB\beta}^A \quad M_{ZB_P}^A \quad M_{ZB_R}^A \quad M_{ZB\delta a}^A \quad M_{ZB\delta r}^A
 \end{aligned} \quad (5.2-16)$$

Longitudinal and lateral-directional classifications denote uncoupling of the aerodynamics as a result of linear theory and the assumed symmetry of the aircraft configuration—sections 3.4.1.5 and 4.2.5. The following section, section 5.3, presents a derivation of these aerodynamic derivatives from the results of sections 3 and 4. This section also presents the methods used in the FLEXSTAB system to extend equations (5.2-14) to the nonlinear case, equations (5.2-10), by the incorporation of empirical data.

5.3 AERODYNAMICS OF THE REFERENCE FLIGHT CONDITION—AERODYNAMIC DERIVATIVES

The reference flight condition aerodynamic forces on the thin body mean surface panels and at the slender body segments of a configuration are developed in section 3.5. In the present section these aerodynamic forces are resolved into the components of aerodynamic force and couple appearing in equations (5.2-11) and (5.2-14)—the aerodynamic forces acting on an aircraft undergoing the steady motion of the reference flight condition.

5.3.1 Summary of Linear Aerodynamic and Structural Theories

The aerodynamic equations which determine the aerodynamic forces in the steady, reference flight condition are obtained from equations developed in section 3.5; namely, the following:

The aerodynamic pressure transformation:

$$\begin{aligned}
 \{f^A\}_1 &= \bar{q}_1 [T_{fT}] [TRANS_t] \left([\bar{q}_t]_1 \{C_P^S\}^{iso} + [\Delta M_t]_1 \left\{ \frac{\partial C_P^S}{\partial M} \right\}_1^{iso} \right) + \\
 &+ \bar{q}_1 [T_{fT}] [T_{TF}] [T_{FP}] [q_C]_1 \{C_P\}_1 + \\
 &+ \bar{q}_1 [T_{fT}] [TRANS_{ID}] [q_C]_1 \{D\}_1,
 \end{aligned} \quad (3.5-58)$$

the lifting pressure coefficients:

$$\{C_P\}_1 = [A_{P\theta}]_1 (\{\psi_C\}_1 + \{\theta^*\}_1 + \{\psi_M\}_1) + \{C_P^v\}_1^{int} \quad (3.5-59)$$

and the steady flow incidence:

$$\begin{aligned} \{\psi_M\}_1 = & \{\psi_{\delta_e}\}_1 \delta_{e1} + \{\psi_{\delta_a}\}_1 \delta_{a1} + \{\psi_{\delta_r}\}_1 \delta_{r1} + \{\psi_{\alpha}\}_1 \alpha_1 \\ & + \{\psi_{\beta}\}_1 \beta_1 + \{\psi_P\}_1 \frac{\hat{z}}{b} P_1 + \{\psi_Q\}_1 \frac{\hat{z}}{c} Q_1 + \{\psi_R\}_1 \frac{\hat{z}}{b} R_1 \end{aligned} \quad (4.5-45)$$

The structural equations which determine the deformed shape of the aircraft in the steady, reference flight condition are given by equations (4.2-64), (4.2-101), and (4.2-116) and 4.2-119) of section 4.2, viz:

The structural equations for steady motion:

$$\{\delta\}_1 = [\tilde{C}]_1 \{Q^S\}_1, \quad (4.2-64)$$

where $\{Q^S\} \equiv \{Q^A\} + \{Q^T\} + \{Q^G\}$

the camber deformation transformation:

$$\{\theta^*\} = [P_\theta] \{\delta\}, \quad (4.2-101)$$

the airload transformation:

$$\{Q^A\} = [P_T]^T \{f_T^A\}, \quad (4.2-116)$$

and the propulsion system load transformations:

$$\begin{aligned} \{Q^T\} &= [NAF] \{T\} \\ \{Q^G\} &= [\Delta_G] \{M^G\} \end{aligned} \quad (4.2-119)$$

5.3.1.1 Linear structural equation.—The structural equations listed above are combined into a single expression describing the camber deformation arising from the aerodynamic and propulsion system forces of the reference flight condition:

$$\begin{aligned} \{\theta^*\}_1 = & [\tilde{C}_{\theta T}]_1 \{f_T^A\}_1 + [\tilde{C}_{\theta G}]_1 \{M^G\}_1 \\ & + [P_\theta][\tilde{C}][NAF]\{T\}_1 \end{aligned} \quad (5.3-1)$$

where:

$$[\tilde{C}_{\theta T}] \equiv [P_{\theta}][\tilde{C}][P_T]^T$$

$$[\tilde{C}_{\theta G}] \equiv [P_{\theta}][\tilde{C}][\Delta_G]$$

5.3.1.2 Linear aerodynamic equations.—A simplifying approximation is introduced in the aerodynamic pressure transformation to obtain an expression which is linear in the unspecified trim variables. This approximation consists of neglecting the leading edge correction to the aerodynamics (see section 3.4.12). Using this approximation, the terms multiplying the matrix $[T_{TF}]$ in equation (3.5-58) are denoted as $\{f_T^A\}_1$ and combined with equation (3.5-59). The result is expressed as follows:

$$\{f_T^A\}_1 = [T_{TF}]\{F^A\}_1' + \{f_T^A\}' \quad (5.3-2)$$

where

$$\{F^A\}_1' \equiv \bar{q}_1 [A_{F\theta}]_1 \{\theta^*\}_1, \quad (5.3-3)$$

$$[A_{F\theta}] \equiv [T_{FP}][\bar{q}_C]_1 [A_{P\theta}],$$

and $\{f_T^A\}_1' \equiv$ all remaining terms exclusive of the leading edge correction term containing $\{D\}_1$.

5.3.1.3 Combined aerodynamic and structural equations.—Introducing the transformation

$$\{f_T^A\} = [T_{TF}]\{F^A\}, \quad (3.5-32)$$

the structural equation, equation (5.3-1), is combined with equation (5.3-3) so as to eliminate $\{\theta^*\}_1$, and the resulting expression is solved for the aerodynamic forces $\{F^A\}_1$ to obtain

$$\begin{aligned} \{F^A\}_1' = \bar{q}_1 [\tilde{D}]_1^{-1} [A_{F\theta}]_1 \left([\tilde{C}_{\theta T}]_1 \{f_T^A\}_1' + [\tilde{C}_{\theta G}]_1 \{M_G\}_1 + \right. \\ \left. + [P_{\theta}][\tilde{C}][NAF]\{T\}_1 \right) \end{aligned} \quad (5.3-4)$$

where

$$[\tilde{D}]_1 \equiv [I] - \bar{q}_1 [A_{F\theta}]_1 [\tilde{C}_{\theta T}]_1 [T_{TF}] \quad (5.3-5)$$

is termed the "aeroelastic matrix" for the aircraft. Combining equation (5.3-4) with equation (5.3-2), the aerodynamic forces on the flexible aircraft in the steady, reference flight condition (including the aerodynamic forces resulting from propulsion system induced elastic deformation) are found as

$$\begin{aligned} \{f_T^A\}_1 = & \left([I] + \bar{q}_1 [T_{TF}] [\tilde{D}]^{-1} [A_{F\theta}]_1 [\tilde{C}_{\theta T}]_1 \right) \{f_T^A\}_1 + \\ & + \bar{q}_1 [T_{TF}] [\tilde{D}]^{-1} [A_{F\theta}]_1 \left([\tilde{C}_{\theta G}]_1 \{M^G\}_1 + \right. \\ & \left. + [\tilde{C}_{\theta T}] [NAF] \{T\}_1 \right) \end{aligned} \quad (5.3-6)$$

where

$$\{f_T^A\}_1 = \{f_T^A\}_1^t + \bar{q}_1 [T_{TF}] [A_{F\theta}]_1 \left(\{\psi_C\}_1 + \{\psi_M\}_1 \right) \quad (5.3-7)$$

and $\{f_T^A\}_1^t \equiv \{f_T^A\}_1^{iso} + \{f_T^A\}_1^{int}$

$$\{f_T^A\}_1^{iso} \equiv \bar{q}_1 [TRANS_t] \left([\tilde{q}_t]_1 \{C_P^S\}_1^{iso} + [\Delta M_t]_1 \left\{ \frac{\partial C_P^S}{\partial M} \right\}_1^{iso} \right) \quad (5.3-8)$$

$$\{f_T^A\}_1^{int} \equiv \bar{q}_1 [T_{TF}] [T_{FP}] [\tilde{q}_c]_1 \{C_P\}_1^{int}$$

5.3.2 Aerodynamic Derivatives for a Flexible Aircraft

The terms appearing in the linear aerodynamic equations, equation (5.2-14), follow directly from the linear theory represented by equations (5.3-6), (5.3-7), and (5.3-8) above. The components of total aerodynamic force and couple acting on the aircraft are generated from equation (5.3-6) using the rigid body mode shape matrix, equation (3.5-6), and the transformations given by equation (3.5-30) and (3.5-65). Equation (3.5-30) transforms the aerodynamic forces $\{f_T^A\}_1$ from the local body axis systems to the Reference Axis System, i.e.,

$$\{f^A\}_1 = 2 [T_{FT}] \{f_T^A\}_1 \quad (5.3-9)$$

These forces, exclusive of the aeroelastic effects of the propulsion system forces, are resolved into Reference Axis System components of total force and couple at the aircraft center of mass as

$$\{F_C^A\}_1 = 2 [\tilde{q}^*]^T [T_{FT}] \left(\{f_T^A\}_1 - \Delta \{f_T^T\}_1 \right) \quad (5.3-10)$$

where

$$\Delta \{f_T^T\}_1 \equiv \bar{q}_1 [T_{TF}] [\tilde{D}]^{-1} [A_{F\theta}]_1 \left([\tilde{C}_{\theta G}]_1 \{M^G\}_1 + [\tilde{C}_{\theta T}] [NAF] \{T\}_1 \right)$$

and these components are transformed to the Body Axis System as

$$\{F_B^A\}_1 = 2[\mathcal{J}][\bar{\phi}^*]^T [T_{FT}] (\{f_T^A\}_1 - \Delta\{f_T^T\}_1) \quad (5.3-11)$$

where

$$[\mathcal{J}] \equiv \begin{bmatrix} -1 & & & \text{zeros} \\ & -1 & & \\ & & 1 & \\ & & & 1 & - \\ \text{zeros} & & & & -1 & -1 \end{bmatrix}$$

The quantities appearing in equation (5.2-14) as coefficients of the velocity components and the control surface settings are constructed from the expansion of equation (5.3-11) obtained by introducing equations (5.3-6) through (5.3-8).

5.3.2.1 Longitudinal aerodynamic derivatives for flexible aircraft.—All of the structural, aerodynamic, and geometric characteristics are taken, in this section, to be for the symmetric aircraft case (see sections 3.4.1.5 and 4.2.5). As a result of this assumption, the only non-zero components of force and couple generated by equation (5.3-11) are F_{XB}^A , F_{ZB}^A , and M_{YB}^A . These are components related to the longitudinal aerodynamic derivatives listed in section 5.2.2.5. They are derived from equation (5.3-11) by expanding the aerodynamic forces $\{f_T^A\}_1$ through the introduction of equations (5.3-6), (5.3-7), and (3.4-45). The aerodynamic derivatives appear in the expanded equation as the coefficients of the trim parameters. The expansion is based on the following equation:

$$\{F_B^A\}_1 = ([G_T] + \bar{q}_1 [G_\theta] [\tilde{C}_{\theta T}]_1) \times \\ \times (\{f_T^A\}_1^{\text{iso}} + \{f_T^A\}_1^{\text{int}}) + \bar{q}_1 [G_\theta] (\{\psi_C\}_1 + \{\psi_M\}_1)$$

and uses the identity

$$[\tilde{D}]_1^{-1} \equiv ([I] + \bar{q}_1 [\tilde{D}]_1^{-1} [A_{F\theta}]_1 [\tilde{C}_{\theta T}]_1 [T_{TF}])$$

The resulting coefficient matrices are as follows:

$$\begin{bmatrix} F_{XB_0}^A \\ F_{ZB_0}^A \\ M_{YB_0}^A \end{bmatrix}_E = ([G_T] + \bar{q}_1 [G_\theta] [\tilde{C}_{\theta T}]) (\{f_T^A\}_0^{\text{iso}} + \{f_T^A\}_0^{\text{int}}) + \bar{q}_1 [G_\theta] \{\psi_C\}_1 \quad (5.3-12)$$

where

$$\begin{aligned}
 \{f_T^A\}_0^{iso} &\equiv \bar{q}_1 [TRANS_t] \{C_P^S\}_1^{iso} \\
 \{f_T^A\}_0^{int} &\equiv \bar{q}_1 [T_{TF}] [T_{FP}] \{C_P\}_1^{int} \\
 [G_T] &\equiv 2[\mathcal{J}][\bar{\Phi}^*]^T [T_{fT}] \\
 [G_F] &\equiv [G_T] [T_{TF}] \\
 [G_\theta] &\equiv [G_F] [\tilde{D}]^{-1} [A_{F\theta}]_1
 \end{aligned} \tag{5.3-13}$$

and

$$\begin{bmatrix} F_{XB_\alpha}^A \\ F_{ZB_\alpha}^A \\ M_{YB_\alpha}^A \end{bmatrix}_E = \bar{q}_1 [G_\theta] \{\psi_\alpha\} \tag{5.3-14}$$

$$\begin{bmatrix} F_{XB_Q}^A \\ F_{ZB_Q}^A \\ M_{YB_Q}^A \end{bmatrix}_E = \bar{q}_1 [G_\theta] \{\psi_Q\} \frac{1}{U_1} \tag{5.3-15}$$

$$\begin{bmatrix} F_{XB_{\delta_e}}^A \\ F_{ZB_{\delta_e}}^A \\ M_{YB_{\delta_e}}^A \end{bmatrix}_E = \bar{q}_1 [G_\theta] \{\psi_{\delta_e}\} \tag{5.3-16}$$

5.3.2.2 Lateral-directional aerodynamic derivatives for a flexible aircraft.—All of the structural, aerodynamic, and geometric characteristics are taken in this section to be for the antisymmetric aircraft case—sections 3.4.1.5 and 4.2.5. As a result of this assumption, the only non-zero components of force and couple generated by equation (5.3-11) are F_{YB}^A , M_{XB}^A , and M_{ZB}^A . Expanding equations (5.3-11) following the approach of section 5.3.2.1, the lateral-directional aerodynamic derivatives are found to be as follows:

$$\begin{bmatrix} F_{YB\beta}^A \\ M_{XB\beta}^A \\ M_{ZB\beta}^A \end{bmatrix}_E = \bar{q}_1 [G_\theta] \{\psi_\beta\} \quad (5.3.17)$$

$$\begin{bmatrix} F_{YB_P}^A \\ M_{XB_P}^A \\ M_{ZB_P}^A \end{bmatrix}_E = \bar{q}_1 [G_\theta] \{\psi_P\} \frac{1}{U_1} \quad (5.3.18)$$

$$\begin{bmatrix} F_{YB_R}^A \\ M_{XB_R}^A \\ M_{ZB_R}^A \end{bmatrix}_E = \bar{q}_1 [G_\theta] \{\psi_R\} \frac{1}{U_1} + \bar{q}_1 \left([G_T] + [G_\theta] [\tilde{C}_{\theta T}] \right) \times [TRANS_t] [\bar{Y}_t] \left(2 \{C_P\}_1^{iso} + M_1 \left\{ \frac{\partial C_P^{iso}}{\partial M} \right\}_1 \right) + 2 [\bar{T}_{TF}] [\bar{T}_{FP}] [\bar{Y}_c] \{C_P\}_1^{int} \frac{1}{U_1} \quad (5.3-19)$$

where the quantities containing $[\bar{Y}_t]$ and $[\bar{Y}_c]$ arise from equation (5.3-8).

$$\begin{bmatrix} F_{YB_{\delta a}}^A \\ M_{XB_{\delta a}}^A \\ M_{ZB_{\delta a}}^A \end{bmatrix}_E = \bar{q}_1 [G_\theta] \{\psi_{\delta a}\} \quad (5.3-20)$$

$$\begin{bmatrix} F_{YB\delta r}^A \\ M_{XB\delta r}^A \\ M_{ZB\delta r}^A \end{bmatrix}_E = \bar{q}_1 [G_\theta] \{\psi_{\delta r}\} \quad (5.3-21)$$

5.3.3 Linear Aerodynamic Forces for a Rigid Aircraft

For the case of a rigid aircraft the elastic deformation $\{\theta^*\}_1$ vanishes in the expression for the lifting pressure coefficients, equation (3.5-59). The appropriate linear relation for the aerodynamic forces is obtained from equations (3.5-58) and (3.5-59) by neglecting the leading edge correction to the aerodynamics and by setting $\{\theta^*\}_1$ to zero. The result is as follows:

$$\begin{aligned} \{f_B^A\}_1 = 2[\mathbf{J}][\bar{\phi}^*]^T [T_{fT}] & \left[\left(\{f_T^A\}_1^{iso} + \{f_T^A\}_1^{int} \right) \right. \\ & \left. + \bar{q}_1 [T_{TF}][A_{F\theta}]_1 \left(\{\psi_c\}_1 + \{\psi_M\}_1 \right) \right] \end{aligned} \quad (5.3-22)$$

where, as in equation (5.3-8), the aerodynamic forces due to isolated and interference aerodynamic thickness are given by

$$\{f_T^A\}_1^{iso} \equiv \bar{q}_1 [TRANS_t] \left([\bar{q}_t]_1 \{C_P^S\}_1^{iso} + [\Delta M_t]_1 \left\{ \frac{\partial C_P^S}{\partial M_1} \right\}^{iso} \right)$$

and

$$\{f_T^A\}_1^{int} \equiv \bar{q}_1 [T_{TF}][T_{FP}] [\bar{q}_c]_1 \{C_P\}_1^{int}$$

(5.3-8)

5.3.3.1 Longitudinal aerodynamic derivatives for a rigid aircraft.—The aerodynamic and geometric characteristics are taken in this section to be for the symmetric aircraft case (see section 3.4.1.5). As a result of this assumption, the only non-zero components of force and couple generated by equation (5.3-22) are F_{XB}^A , F_{ZB}^A , and M_{YB}^A . The longitudinal aerodynamic derivatives listed by equation (5.2-15) for the case of a rigid aircraft, therefore, follow from equation (5.3-22) by introducing the expanded form of the flow incidence matrix, equation (3.5-45), and taking the aerodynamic derivatives to be the coefficients of the motion variables and the control surface settings. The results are as follows:

$$\begin{bmatrix} F_{XB_0}^A \\ F_{ZB_0}^A \\ M_{YB_0}^A \end{bmatrix}_E = \bar{q}_1 [G_T] \left(\{f_T^A\}_0^{iso} + \{f_T^A\}_0^{int} \right) + [G_{\theta E}] \{\psi_c\} \quad (5.3-23)$$

where

$$[G_T] \equiv 2[\mathcal{J}][\phi^*]^T [T_{fT}]$$

$$[G_F] \equiv [G_T][T_{TF}]$$

$$[G_{\theta R}] \equiv [G_F][A_{F\theta}]$$

$$\begin{bmatrix} F_{XB\alpha}^A \\ F_{ZB\alpha}^A \\ M_{YB\alpha}^A \end{bmatrix}_R = \bar{q}_1 [G_{\theta R}] \{\psi_\alpha\} \quad (5.3-24)$$

$$\begin{bmatrix} F_{XBQ}^A \\ F_{ZBQ}^A \\ M_{YBQ}^A \end{bmatrix}_R = \bar{q}_1 [G_{\theta R}] \{\psi_Q\} \frac{1}{U_1} \quad (5.3-25)$$

$$\begin{bmatrix} F_{XB\delta e}^A \\ F_{ZB\delta e}^A \\ M_{YB\delta e}^A \end{bmatrix}_R = \bar{q}_1 [G_{\theta R}] \{\psi_{\delta e}\} \quad (5.3-26)$$

5.3.3.2 Lateral-directional aerodynamic derivatives for a rigid aircraft.—In this section the aerodynamic and geometric characteristics of the aircraft are taken to be for the antisymmetric case (see section 3.4.1.5). As a result, the non-zero components of force and couple generated by equation (5.3-22) are F_{YB}^A , M_{XB}^A , and M_{ZB}^A . The lateral-directional aerodynamic derivatives, listed by equation (5.2-16) for the case of a rigid aircraft, therefore, follow from equation (5.3-22) by introducing the expanded form of the flow incidence matrix, equation (3.5-45), and by identifying the aerodynamic derivatives as the coefficients of the motion variables and control surface settings. The results are as follows:

$$\begin{bmatrix} F_{YB\beta}^A \\ M_{XB\beta}^A \\ M_{ZB\beta}^A \end{bmatrix} = \bar{q}_1 [G_{\theta R}] \{\psi_\beta\} \quad (5.3-27)$$

where $[G_{\theta R}]$ is the matrix defined by equation (5.3-23).

$$\begin{bmatrix} F_{YB_P}^A \\ M_{XB_P}^A \\ M_{ZB_P}^A \end{bmatrix} = \bar{q}_1 [G_{\theta R}] \{\psi_P\} \frac{1}{U_1}$$

(5.3-28)

$$\begin{bmatrix} F_{YB_R}^A \\ M_{XB_R}^A \\ M_{ZB_R}^A \end{bmatrix} = \bar{q}_1 [G_{\theta R}] \{\psi_R\} \frac{1}{U_1} + \bar{q}_1 [G_T] \left[[TRANS_t] [\bar{Y}_t] \left(2 \{C_P^S\}_1^{iso} + M_1 \left\{ \frac{\partial C_P^S}{\partial M} \right\}_1^{iso} \right) + 2 [T_{TF}] [T_{FP}] [\bar{Y}_c] \{C_P\}_1^{int} \right] \frac{1}{U_1}$$

$$\begin{bmatrix} F_{YB_{\delta a}}^A \\ M_{XB_{\delta a}}^A \\ M_{ZB_{\delta a}}^A \end{bmatrix} = \bar{q}_1 [G_{\theta R}] \{n_{X_{\delta a}}\}$$

(5.3-29)

$$\begin{bmatrix} F_{YB_{\delta r}}^A \\ M_{XB_{\delta r}}^A \\ M_{ZB_{\delta r}}^A \end{bmatrix} = \bar{q}_1 [G_{\theta R}] \{n_{X_{\delta r}}\}$$

5.3.4 Aeroelastic Increment to the Aerodynamic Derivatives

The aerodynamic derivatives are derived in section 5.3.2 for a flexible aircraft and in section 5.3.3 for a rigid aircraft; in this section it is shown that the flexible aircraft aerodynamic derivatives are composed of the sums of two quantities—the rigid aircraft aerodynamic derivatives and an increment due to static aeroelasticity. This composition of the flexible aircraft aerodynamic derivatives is deduced from an expansion of the aeroelastic matrix given by equation (5.3-5).

5.3.4.1 Expansion of the aeroelastic matrix.—The matrix $[G_\theta]$, which appears in each of the formulas for the flexible aircraft aerodynamic derivatives, contains the inverse of the aeroelastic matrix, i.e.,

$$[G_\theta] = [G_F][\tilde{D}]_1^{-1}[A_{F\theta}]_1 \quad (5.3-13)$$

The inverse aeroelastic matrix is expanded as

$$[\tilde{D}]_1^{-1} \equiv [I] + \bar{q}_1 [A_{F\theta}]_1 [\tilde{C}_{\theta T}]_1 [T_{TF}][\tilde{D}]_1^{-1} \quad (5.3-30)$$

Hence, it follows that

$$[G_\theta] = [G_{\theta R}] + \bar{q}_1 [G_{\theta E}] \quad (5.3-31)$$

where $[G_{\theta R}]$ is the matrix operator appearing in each of the formulas for the rigid aircraft aerodynamic derivatives of section 5.3.3 and

$$[G_{\theta E}] \equiv [G_T][T_{TF}][A_{F\theta}]_1 [\tilde{C}_{\theta T}]_1 [T_{TF}][\tilde{D}]_1^{-1}[A_{F\theta}]_1$$

The expansion given by equation (5.3-31) leads to the desired result—an expansion of the flexible aircraft aerodynamic derivatives into a rigid component plus an aeroelastic increment.

Having demonstrated that the expansion of $[G_\theta]$ given by equation (5.3-31) is theoretically sound, the aeroelastic increment is obtained by a direct computation. Writing equation (5.3-31) as follows:

$$\bar{q}_1 [G_{\theta E}] = [G_\theta] - [G_{\theta R}] ,$$

reference to equation (5.3-13) and the definition of $[G_{\theta R}]$ following equation (5.3-23) shows that the aeroelastic increment can be computed as

$$[G_{\theta E}] = [G_T][T_{TF}][\tilde{AD}^{-1}]_1[A_{F\theta}]_1 \quad (5.3-32)$$

where

$$[\tilde{AD}^{-1}]_1 \equiv [\tilde{D}]_1^{-1} - [I]$$

This formulation of the matrix $[\Delta G_{\theta E}]$ poses a much smaller computational task than that posed by the preceding formula.

5.3.4.2 Expansion of the longitudinal aerodynamic derivatives for a flexible aircraft.—Substituting equation (5.3-31) into each of the formulas appearing in section 5.3.2.1 leads to the following expansion of the longitudinal aerodynamic derivatives for a flexible aircraft:

$$\begin{bmatrix} F_{XB_0}^A \\ F_{ZB_0}^A \\ M_{YB_0}^A \end{bmatrix}_E = \begin{bmatrix} F_{XB_0}^A \\ F_{ZB_0}^A \\ M_{YB_0}^A \end{bmatrix}_R + \begin{bmatrix} \Delta F_{XB_0}^A \\ \Delta F_{ZB_0}^A \\ \Delta M_{YB_0}^A \end{bmatrix}_E \quad (5.3-33)$$

where

$$\begin{bmatrix} \Delta F_{XB_0}^A \\ \Delta F_{ZB_0}^A \\ \Delta M_{YB_0}^A \end{bmatrix}_C \equiv \bar{q}_1 [G_{\theta}] [\tilde{C}_{\theta T}] \left(\{f_T^A\}_0^{iso} + \{f_T^A\}_0^{int} \right) + \bar{q}_1 [G_{\theta E}] \{\psi_c\} \quad (5.3-34)$$

$$\begin{bmatrix} F_{XB_\alpha}^A \\ F_{ZB_\alpha}^A \\ M_{YB_\alpha}^A \end{bmatrix}_F = \begin{bmatrix} F_{XB_\alpha}^A \\ F_{ZB_\alpha}^A \\ M_{YB_\alpha}^A \end{bmatrix}_R + \begin{bmatrix} \Delta F_{XB_\alpha}^A \\ \Delta F_{ZB_\alpha}^A \\ \Delta M_{YB_\alpha}^A \end{bmatrix}_F$$

where

$$\begin{bmatrix} \Delta F_{XB_\alpha}^A \\ \Delta F_{ZB_\alpha}^A \\ \Delta M_{YB_\alpha}^A \end{bmatrix}_E \equiv \bar{q}_1 [G_{\theta E}] \{\psi_\alpha\}$$

$$\begin{bmatrix} F_{XB_Q}^A \\ F_{ZB_Q}^A \\ M_{YB_Q}^A \end{bmatrix}_E = \begin{bmatrix} F_{XB_Q}^A \\ F_{ZB_Q}^A \\ M_{YB_Q}^A \end{bmatrix}_R + \begin{bmatrix} \Delta F_{XB_Q}^A \\ \Delta F_{ZB_Q}^A \\ \Delta M_{YB_Q}^A \end{bmatrix}_E \quad (5.3-35)$$

where,

$$\begin{bmatrix} \Delta F_{XB_Q}^A \\ \Delta F_{ZB_Q}^A \\ \Delta M_{YB_Q}^A \end{bmatrix}_E \equiv \bar{q}_1 [G_{\theta E}] \{\psi_Q\} \frac{1}{J_1}$$

$$\begin{bmatrix} F_{XB_{\delta e}}^A \\ F_{ZB_{\delta e}}^A \\ M_{YB_{\delta e}}^A \end{bmatrix}_E = \begin{bmatrix} F_{XB_{\delta e}}^A \\ F_{ZB_{\delta e}}^A \\ M_{YB_{\delta e}}^A \end{bmatrix}_R + \begin{bmatrix} \Delta F_{XB_{\delta e}}^A \\ \Delta F_{ZB_{\delta e}}^A \\ \Delta M_{YB_{\delta e}}^A \end{bmatrix}_E \quad (5.3-36)$$

where

$$\begin{bmatrix} \Delta F_{XB_{\delta e}} \\ \Delta F_{ZB_{\delta e}} \\ \Delta M_{YB_{\delta e}} \end{bmatrix}_E \equiv \bar{q}_1 [G_{\theta E}] \{\psi_{\delta e}\}$$

5.3.4.3 Expansion of the lateral-directional aerodynamic derivatives for a flexible aircraft.—Substituting equation (5.3-31) into each of the formulas appearing in section 5.3.2.2 leads to the following expansion of the lateral-directional aerodynamic derivatives for a flexible aircraft:

$$\begin{bmatrix} F_{YB_{\beta}}^A \\ M_{XB_{\beta}}^A \\ M_{ZB_{\beta}}^A \end{bmatrix}_E = \begin{bmatrix} F_{YB_{\beta}}^A \\ M_{XB_{\beta}}^A \\ M_{ZB_{\beta}}^A \end{bmatrix}_R + \begin{bmatrix} \Delta F_{YB_{\beta}}^A \\ \Delta M_{XB_{\beta}}^A \\ \Delta M_{ZB_{\beta}}^A \end{bmatrix}_E \quad (5.3-37)$$

where

$$\begin{bmatrix} \Delta F_{YB_{\beta}}^A \\ \Delta M_{XB_{\beta}}^A \\ \Delta M_{ZB_{\beta}}^A \end{bmatrix}_E \equiv \bar{q}_1 [G_{\theta E}] \{\psi_{\beta}\}$$

$$\begin{bmatrix} F_{YB_P}^A \\ M_{XB_P}^A \\ M_{ZB_P}^A \end{bmatrix}_E = \begin{bmatrix} F_{YB_P}^A \\ M_{XB_P}^A \\ M_{ZB_P}^A \end{bmatrix}_R + \begin{bmatrix} \Delta F_{YB_P}^A \\ \Delta M_{XB_P}^A \\ \Delta M_{ZB_P}^A \end{bmatrix}_E \quad (5.3-38)$$

where

$$\begin{bmatrix} \Delta F_{YB_P}^A \\ \Delta M_{XB_P}^A \\ \Delta M_{ZB_P}^A \end{bmatrix}_E \equiv \hat{q}_1 [G_{\theta E}] \{\psi_r\} \frac{1}{U_1}$$

$$\begin{bmatrix} F_{YB_R}^A \\ M_{XB_R}^A \\ M_{ZB_R}^A \end{bmatrix}_E = \begin{bmatrix} F_{YB_R}^A \\ M_{XB_R}^A \\ M_{ZB_R}^A \end{bmatrix}_R + \begin{bmatrix} \Delta F_{YB_R}^A \\ \Delta M_{XB_R}^A \\ \Delta M_{ZB_R}^A \end{bmatrix}_E \quad (5.3-39)$$

where

$$\begin{bmatrix} \Delta F_{YB_R}^A \\ \Delta M_{XB_R}^A \\ \Delta M_{ZB_R}^A \end{bmatrix}_E \equiv \bar{q}_1 [G_{\theta E}] \{\psi_r\} \frac{1}{U_1} + \bar{q}_1 [G_{\theta}] [\tilde{C}_{\theta T}] \left[[TRANS_t] [\bar{Y}_t] + \right. \\ \left. + (2\{C_P^S\}_1^{iso} + M_1 \{\frac{\partial C_P^S}{\partial M}\}_1^{iso}) + 2[T_{TF}] [T_{FP}] [\bar{Y}_t] \{C_P\}_1^{int} \right] \frac{1}{U_1}$$

$$\begin{bmatrix} F_{YB_{\delta a}}^A \\ M_{XB_{\delta a}}^A \\ M_{ZB_{\delta a}}^A \end{bmatrix}_E = \begin{bmatrix} F_{YB_{\delta a}}^A \\ M_{XB_{\delta a}}^A \\ M_{ZB_{\delta a}}^A \end{bmatrix}_R + \begin{bmatrix} \Delta F_{YB_{\delta a}}^A \\ \Delta M_{XB_{\delta a}}^A \\ \Delta M_{ZB_{\delta a}}^A \end{bmatrix}_E \quad (5.3-40)$$

where

$$\begin{bmatrix} \Delta F_{YB}^A \\ \Delta M_{XB}^A \\ \Delta M_{ZB}^A \end{bmatrix}_{\delta a} \equiv \bar{a}_1 [G_{\theta E}] \{\psi_{\delta a}\}$$

$$\begin{bmatrix} F_{YB}^A \\ M_{XB}^A \\ M_{ZB}^A \end{bmatrix}_E = \begin{bmatrix} F_{YB}^A \\ M_{XB}^A \\ M_{ZB}^A \end{bmatrix}_R + \begin{bmatrix} \Delta F_{YB}^A \\ \Delta M_{XB}^A \\ \Delta M_{ZB}^A \end{bmatrix}_E \quad (5.3.41)$$

$$\begin{bmatrix} \Delta F_{YB}^A \\ \Delta M_{XB}^A \\ \Delta M_{ZB}^A \end{bmatrix}_E \equiv \bar{a}_1 [G_{\theta E}] \{\psi_{\delta r}\}$$

5.3.5 NonLinear Aerodynamic Derivatives

The effects of nonlinear aerodynamic behavior on the aerodynamic derivatives are introduced in this section using the expansion of the derivatives appearing in section 5.3.4. The method for introducing the effects of nonlinear aerodynamics on flexible aircraft aerodynamic derivatives is based on the assumption that the aeroelastic component of the derivatives can be treated as a linear perturbation from rigid aircraft derivatives. Following this approach the rigid aircraft aerodynamic derivatives are supplied to the FLEXSTAB system as tabulated functions of the trim variables. The aeroelastic increments are then computed by the FLEXSTAB system using the formulas of section 5.3.4 and using the empirical correction methods of section 3.4.14 to impose the influence of nonlinear aerodynamic behavior on the aeroelastic increments. The empirical correction schemes of section 3.4.14, therefore, are used in an attempt to model the nonlinear aerodynamic behavior contributing to the aeroelasticity as a linear perturbation from the aerodynamics of a rigid aircraft. Caution must be exercised.

however, as this method has been given little theoretical foundation and predictions based on the method should be used with care and substantiated with extensive wind tunnel testing.

5.3.5.1 Aeroelastic effects.—The nonlinear aerodynamic terms appearing in equations (5.2-11) are expanded into two terms. One represents the aerodynamics of a rigid aircraft, the other an aeroelastic increment. This expansion is justified on the basis of section 5.3.4. Nonlinear dependence on the trim variables is assumed to be contained entirely in the rigid aircraft term, e.g., for the i^{th} set of values for the trim variables

$$\left(\frac{\partial F_{XB}^A}{\partial \alpha} \right)_E = \left(\frac{\partial F_{XB}^A}{\partial \alpha} \right)_R + \Delta \left(\frac{\partial F_{XB}^A}{\partial \alpha} \right)_E \quad (5.3-42)$$

where the second term on the right—the aeroelastic increment—is a constant coefficient based on the linear theory of section 5.3. The aeroelastic increment, however, may be corrected for nonlinear aerodynamics using the techniques of section 3.4.14, but the corrections are held constant in the trim problem.

5.3.5.2 Nonlinear, rigid aircraft aerodynamic derivatives.—The nonlinear aerodynamics of a rigid aircraft are represented in the FLEXSTAB system by tables of rigid aircraft force and moment data. The tabulated data are used to construct the components of aerodynamic force and moment as functions of the trim variables.* These functions appear as follows:

$$\begin{aligned} (F_{XB}^A)_R &= F_{XB}^A(\alpha_i, \delta_{ei}) + \Delta F_{XB}^A(\alpha_i, \delta_{ai}) + \Delta F_{XB}^A(\alpha_i, \delta_{ri}) + \Delta F_{XB}^A(\alpha_i, \beta_i) \\ (F_{ZB}^A)_R &= F_{ZB}^A(\alpha_i, \delta_{ei}) + \Delta F_{ZB}^A(\alpha_i, \delta_{ai}) + \Delta F_{ZB}^A(\alpha_i, \delta_{ri}) + \Delta F_{ZB}^A(\alpha_i, \beta_i) \\ (M_{YB}^A)_R &= M_{YB}^A(\alpha_i, \delta_{ei}) + \Delta M_{YB}^A(\alpha_i, \delta_{ai}) + \Delta M_{YB}^A(\alpha_i, \delta_{ri}) + \Delta M_{YB}^A(\alpha_i, \beta_i) \\ (F_{YB}^A)_R &= F_{YB}^A(\alpha_i, \beta_i) + \Delta F_{YB}^A(\alpha_i, \delta_{ai}) + \Delta F_{YB}^A(\alpha_i, \delta_{ri}) + \Delta F_{YB}^A(\delta_{ei}, \beta_i) \\ (M_{XB}^A)_R &= M_{XB}^A(\alpha_i, \beta_i) + \Delta M_{XB}^A(\alpha_i, \delta_{ai}) + \Delta M_{XB}^A(\alpha_i, \delta_{ri}) + \Delta M_{XB}^A(\delta_{ei}, \beta_i) \\ (M_{ZB}^A)_R &= M_{ZB}^A(\alpha_i, \beta_i) + \Delta M_{ZB}^A(\alpha_i, \delta_{ai}) + \Delta M_{ZB}^A(\alpha_i, \delta_{ri}) + \Delta M_{ZB}^A(\delta_{ei}, \beta_i) \end{aligned} \quad (5.3-43)$$

Although the formulas, equation (5.3-43), are expressed in the Body Axis System the tabulated data are supplied to the FLEXSTAB system expressed in terms of a Stability Axis System with origin at a reference point, figure 5.3-1, and in terms of lift and drag components of force—quantities expanded on coordinates fixed relative to the free stream.

*Note that α and β must be as defined in sections 5.2.1 and 5.2.2.

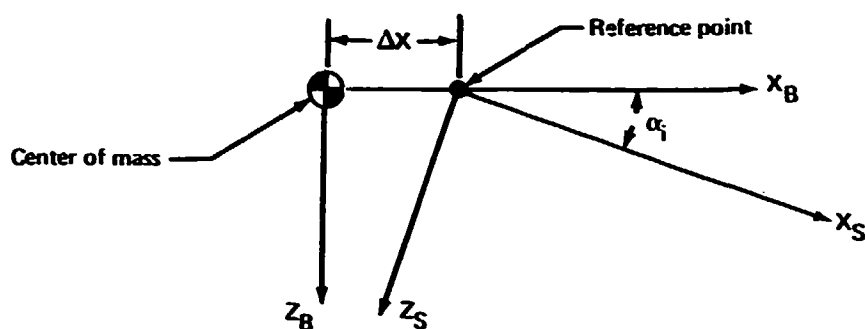


FIGURE 5.3-1.—STABILITY AXIS SYSTEM OF TABULATED DATA

The tabulated data are expressed in nondimensional form consistent with equations (5.3-3) and (5.3-4). The quantities appearing in Equations (5.3-43) are therefore obtained using the following transformations:

$$\begin{bmatrix} F_{XB}^A(i) \\ F_{ZB}^A(i) \\ M_{YB}^A(i) \end{bmatrix} = [SD^S] \begin{bmatrix} C_L(i) \\ C_D(i) \\ C_m(i) \end{bmatrix} \quad (5.3-44)$$

where

$$[SD^S] \equiv \bar{Q}_1 S_w \begin{bmatrix} \sin \alpha_i & -\cos \alpha_i & 0 \\ -\cos \alpha_i & -\sin \alpha_i & 0 \\ \Delta x \cos \alpha_i & \Delta x \sin \alpha_i & \bar{C} \end{bmatrix}$$

and

$$\begin{bmatrix} F_{YB}^A(i) \\ M_{XB}^A(i) \\ M_{ZB}^A(i) \end{bmatrix} = [C^A] \begin{bmatrix} C_Y(i) \\ C_l(i) \\ C_n(i) \end{bmatrix} \quad (5.3-45)$$

where

$$[SD^A] \equiv \bar{q}_1 S_w \begin{bmatrix} 1 & 0 & 0 \\ 0 & b \cos \alpha_i & -b \sin \alpha_i \\ \Delta X & b \sin \alpha_i & b \cos \alpha_i \end{bmatrix}$$

These formulas require the tabulated data to describe the graphs shown in figures 5.3-2 through 5.3-9.

In addition to the components of aerodynamic force and couple represented by equations (5.3-43), the FLEXSTAB system may be supplied with empirical values of the angular rate stability derivatives as tabulated functions of angle of attack. These tabulated data are also nondimensional and expressed in the Stability Axis System of figure 5.3-1. The components of aerodynamic force and couple arising from steady rotation of the aircraft are therefore found as follows:

$$\begin{aligned} \begin{bmatrix} F_{XB_Q}^A(i) \\ F_{ZB_Q}^A(i) \\ M_{YB_Q}^A(i) \end{bmatrix} &= \frac{\bar{c}}{2U_1} [SD^S] \begin{bmatrix} C_{L_Q}(i) \\ C_{D_Q}(i) \\ C_{m_Q}(i) \end{bmatrix} \\ \begin{bmatrix} F_{YB_P}^A(i) \\ M_{XB_P}^A(i) \\ M_{ZB_P}^A(i) \end{bmatrix} &= \frac{b}{2U_1} [SD^A] \begin{bmatrix} C_{Y_P}(i) \\ C_{\ell_P}(i) \\ C_{n_P}(i) \end{bmatrix} \\ \begin{bmatrix} F_{YB_R}^A(i) \\ M_{XB_R}^A(i) \\ M_{ZB_R}^A(i) \end{bmatrix} &= \frac{b}{2U_1} [SD^A] \begin{bmatrix} C_{Y_R}(i) \\ C_{\ell_R}(i) \\ C_{n_R}(i) \end{bmatrix} \end{aligned} \quad (5.3-46)$$

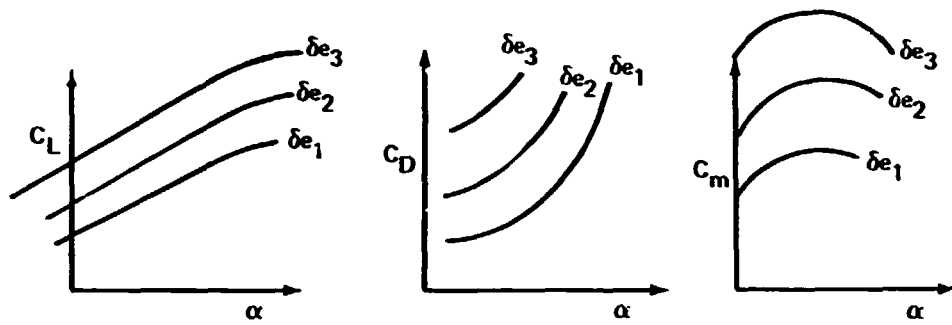


FIGURE 5.3-2.— C_L , C_D , AND C_m VERSUS α FOR VARIOUS LONGITUDINAL CONTROL SETTINGS WITH β , δa , δr SET TO ZERO

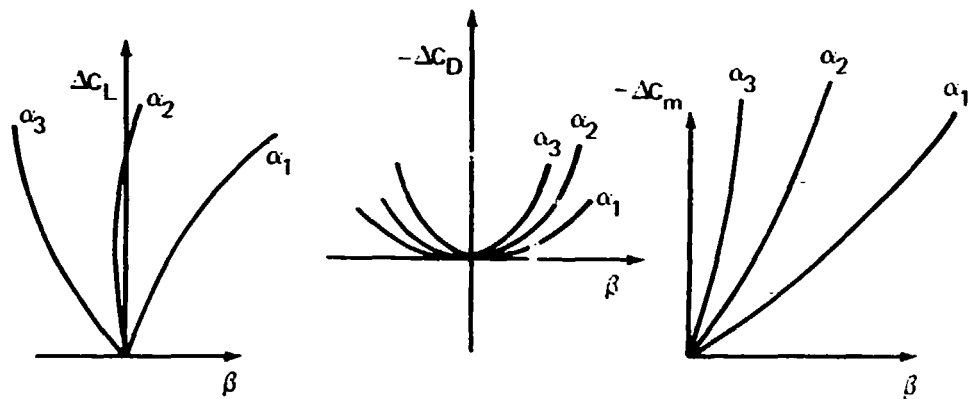


FIGURE 5.3-3.— C_L , C_D , AND C_m VERSUS β FOR VARIOUS ANGLES OF ATTACK WITH δe , δa , δr SET TO ZERO

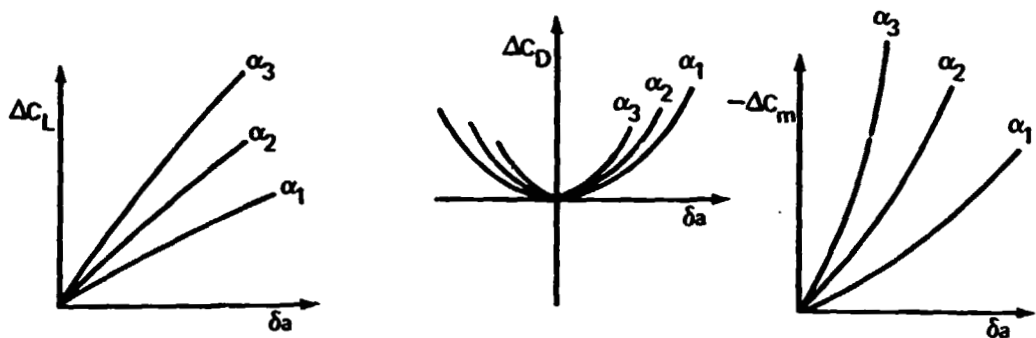


FIGURE 5.3-4.— C_L , C_D , AND C_m VERSUS δa FOR VARIOUS ANGLES OF ATTACK WITH δe , δr , β SET TO ZERO

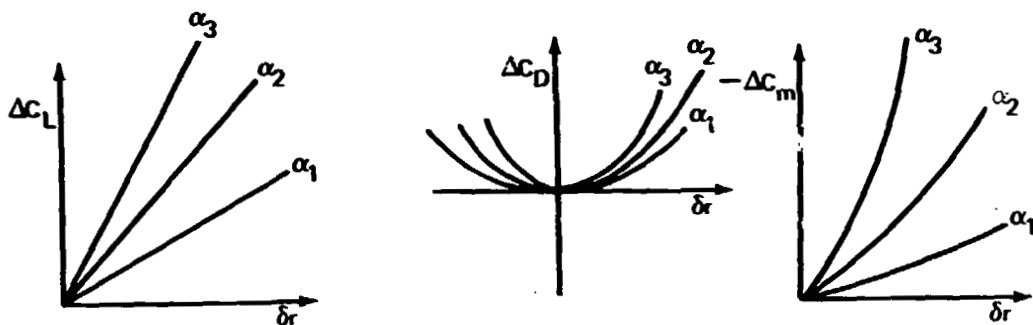


FIGURE 5.3-5.— C_L , C_D , AND C_m VERSUS δr FOR VARIOUS ANGLES OF ATTACK WITH δe , δa , β SET TO ZERO

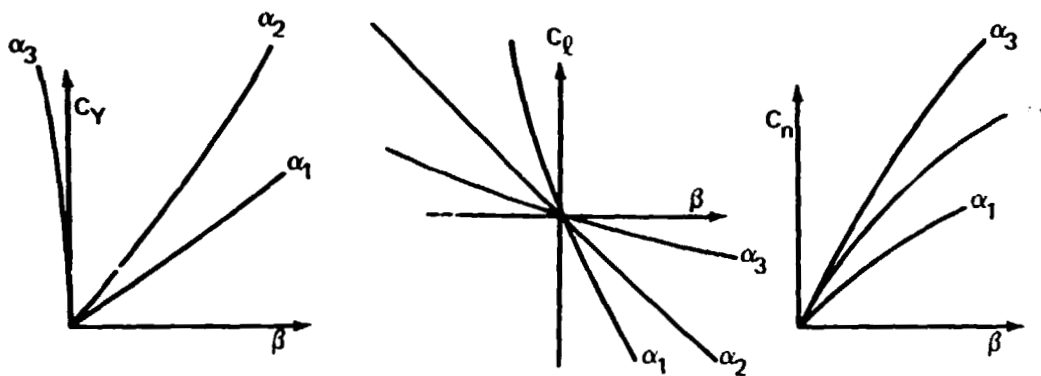


FIGURE 5.3-6.— C_Y , C_l AND C_n VERSUS β FOR VARIOUS ANGLES OF ATTACK WITH δe , δa , δr SET TO ZERO

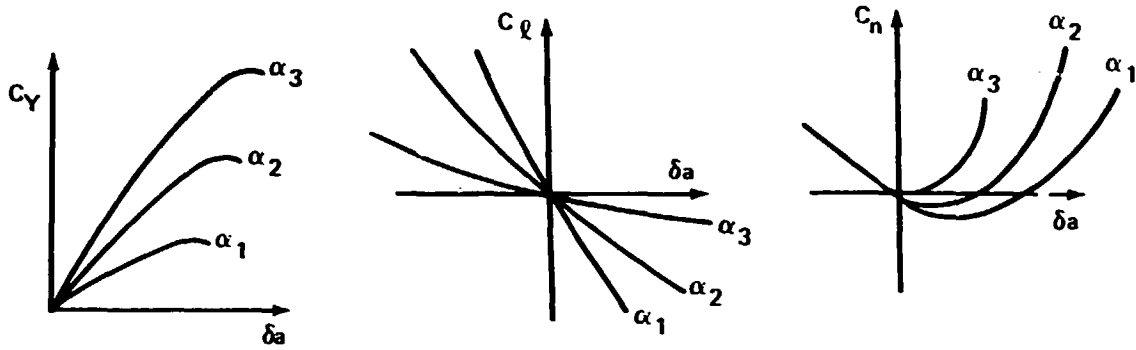


FIGURE 5.3-7.— C_Y , C_L , AND C_n VERSUS δa FOR VARIOUS ANGLES OF ATTACK WITH δe , δr , β SET TO ZERO

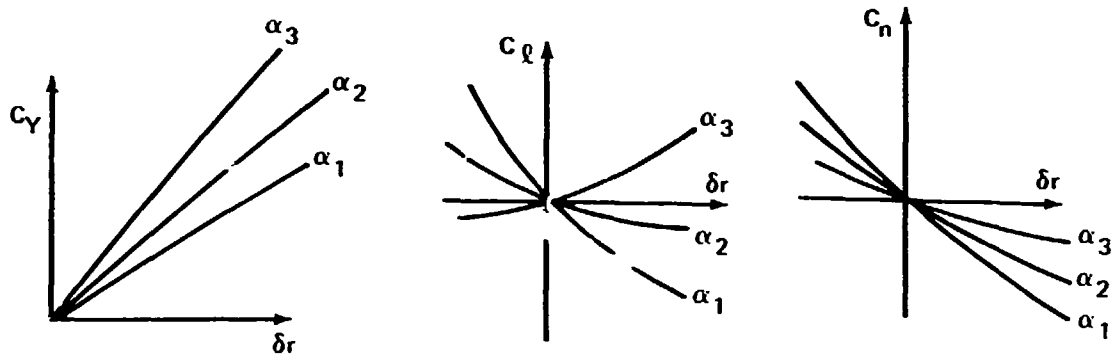


FIGURE 5.3-8.— C_Y , C_L , AND C_n VERSUS δr FOR VARIOUS ANGLES OF ATTACK WITH δe , δa , β SET TO ZERO

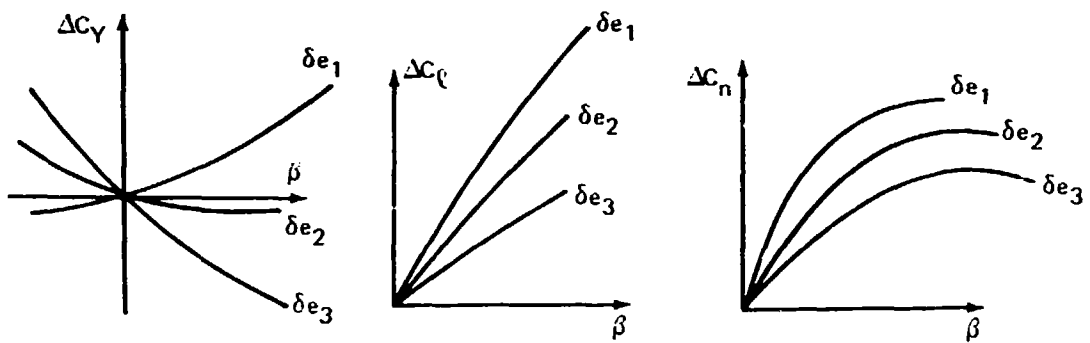


FIGURE 5.3-9.— C_Y , C_L , AND C_n VERSUS β FOR VARIOUS δe WITH α , δa , δr , δa SET TO ZERO

The aerodynamic terms appearing in equations (5.2-11) are expanded as follows:

$$\begin{aligned}
 F_{XB_1}^A(i) &= (F_{XB}^A(i))_R + F_{YB_Q}^A(i)Q_1 + \Delta(F_{XB_\alpha}^A)_E \alpha_i + \Delta(F_{XB_{\delta e}}^A)_E \delta_{ei} \\
 &\quad + \Delta(F_{XB_Q}^A)_E Q_1 \\
 F_{ZB_1}^A(i) &= (F_{ZB}^A(i))_R + F_{ZB_Q}^A(i)Q_1 + \Delta(F_{ZB_\alpha}^A)_E \alpha_i + \Delta(F_{ZB_{\delta e}}^A)_E \delta_{ei} \\
 &\quad + \Delta(F_{ZB_Q}^A)_E Q_1 \quad (5.3-47) \\
 M_{YB_1}^A(i) &= (M_{YB}^A(i))_R + M_{YB_Q}^A(i)Q_1 + \Delta(M_{YB_\alpha}^A)_E \alpha_i + \Delta(M_{YB_{\delta e}}^A)_E \delta_{ei} \\
 &\quad + \Delta(M_{YB_Q}^A)_E Q_1 \\
 F_{YB_1}^A(i) &= (F_{YB}^A(i))_R + F_{YB_P}^A(i)P_1 + F_{YB_R}^A(i)R_1 + \Delta(F_{YB_P}^A)_E P_1 \\
 &\quad + \Delta(F_{YB_R}^A)_E R_1 + \Delta(F_{YB_\beta}^A)_E \beta_i + \Delta(F_{YB_{\delta a}}^A)_E \delta_{ai} + \Delta(F_{YB_{\delta r}}^A)_E \delta_{ri} \\
 M_{XB_1}^A(i) &= (M_{XB}^A(i))_R + M_{XB_P}^A(i)P_1 + M_{XB_R}^A(i)R_1 + \Delta(M_{XB_P}^A)_E P_1 \\
 &\quad + \Delta(M_{XB_R}^A)_E R_1 + \Delta(M_{XB_\beta}^A)_E \beta_i + \Delta(M_{XB_{\delta a}}^A)_E \delta_{ai} + \Delta(M_{XB_{\delta r}}^A)_E \delta_{ri} \\
 M_{ZB_1}^A(i) &= (M_{ZB}^A(i))_R + M_{ZB_P}^A(i)P_1 + M_{ZB_R}^A(i)R_1 + \Delta(M_{ZB_P}^A)_E P_1 \\
 &\quad + \Delta(M_{ZB_R}^A)_E R_1 + \Delta(M_{ZB_\beta}^A)_E \beta_i + \Delta(M_{ZB_{\delta a}}^A)_E \delta_{ai} + \Delta(M_{ZB_{\delta r}}^A)_E \delta_{ri}
 \end{aligned}$$

If the tabulated data are not complete, the components of aerodynamic force and couple are replaced by empirical or computed stability derivatives for those trim variables not included in the trim data. For example, if $(F_{XB}^A)_R$ is given as a tabulated function of α_i , β_i , δ_{ai} , δ_{ri} , then

$$\begin{aligned}
 (F_{XB}^A(i))_R &= F_{XB}^A(\alpha_i) + (F_{XB_{\delta e}}^A)_R \delta_{ei} + \Delta F_{XB}^A(\alpha_i, \delta_{ai}) \\
 &\quad + \Delta F_{XB}^A(\alpha_i, \delta_{ri}) + \Delta F_{XB}^A(\alpha_i, \beta_i)
 \end{aligned} \quad (5.3-48)$$

where $(F_{XB_{\delta e}}^A)_R$ is a constant coefficient which is either supplied to the FLEXSTAB system as an empirical quantity or computed by the system using influence coefficients.

5.4 PROPULSION SYSTEM FORCES

The components of force and couple at the center of mass of the aircraft arising from the propulsion system are expressed as

$$\{F_B^T\} \equiv \begin{bmatrix} F_{XB}^T \\ F_{ZB}^T \\ M_{YB}^T \\ F_{YB}^T \\ M_{XB}^T \\ M_{ZB}^T \end{bmatrix} \quad (5.4-1)$$

The elements of this column matrix are the propulsion system terms appearing in the right-hand members of the equations of motion of section 5.2.2. These terms represent not only the direct effect of the thrust forces and gyroscopic couples of the propulsion system but also an indirect effect which is aeroelastic in origin. The direct effect is found from equations (4.2-57) and (4.2-119) as

$$\{F_B^T\}_R = [\mathcal{L}][\bar{\phi}_\delta]^T \left([NAF]\{T\} + [\Delta_G]\{M^G\} \right) \quad (5.4-2)$$

where $\{T\}$ contains the thrust forces and $\{M^G\}$ contains the gyroscopic couples from the propulsion system. The indirect, aeroelastic effect is contained in equation (5.3-6); and, using the transformations appearing in section 5.3.2, the aeroelastic effects from the propulsion system are found from the definition following equation (5.3-10) as

$$\begin{aligned} \{F_B^T\}_E &= \bar{q}_1 [\mathcal{L}][\bar{\phi}^*]^T [T_{FT}][T_{TF}][D]^{-1} [A_{F\theta}] \\ &\times \left([\tilde{C}_{\theta T}][NAF]\{T\} + [\tilde{C}_{\theta G}]\{M^G\} \right) \end{aligned} \quad (5.4-3)$$

5.4.1 Thrust Forces

The thrust forces are introduced in section 4.2.8 simply as a system of forces which are applied at the centerlines of slender bodies used in the aerodynamic and structural idealization of an aircraft. These slender bodies will usually be regarded as nacelles. The arrangement of

the transformation matrix $[NAF]$ is described in sections 4.3.6 and 4.4.4. This matrix describes the nacelle centerline forces arising from up to ten engines operating at the thrust levels contained in the matrix $\{T\}$.

A single thrust variable T_1 is introduced by letting

$$[NAF]\{T\} = \{NP\}T_1 \quad (5.4-4)$$

where

$$\{NP\} \equiv [NAF]\{\psi_{\delta T}\}$$

and

$$\{\psi_{\delta T}\} \equiv \begin{bmatrix} \vdots \\ k_i \\ \vdots \end{bmatrix}$$

with the quantities k_i ($0 \leq i \leq 10$) being the relative thrust levels of the individual engines. The thrust force and couple at the center of mass, expanded on the Reference Axis System, therefore, are given by

$$\{F_B^T\} = [S] \left([\bar{\phi}_\delta]^T + \bar{q}_1 [\bar{\phi}^*]^T [T_{fT}] [T_{TF}] [D]^{-1} [A_{F\theta}] [\tilde{C}_{\theta T}] \right) \{NP\} T_1 \quad (5.4-5)$$

5.4.2 Engine Gyroscopic Forces

A gyroscopic force term $\{F_{GYRO}^T\}$ describes the sum of the direct, inertial couple from rotating engine parts and the indirect, aeroelastic effects.

The contribution to the inertial couple from the i^{th} engine is given by

$$\vec{\omega}_1 \times \vec{h}_i^G$$

where, from equation (2.2-3),

$$\vec{\omega}_1 = P_1 \hat{i}_B + Q_1 \hat{j}_B + R_1 \hat{k}_B$$

is the steady rotation rate of the aircraft in the reference flight condition. The vector \vec{h}_i is expanded on the Reference Axis System as

$$\vec{h}_i^G = h_{Xi}^G \hat{i} + h_{Yi}^G \hat{j} + h_{Zi}^G \hat{k} \quad (5.4-6)$$

This equation describes the angular momentum of a rotating engine. The gyroscopic couple of the i^{th} engine is given by

$$\vec{M}_i^G = -\vec{\omega}_1 \times \vec{h}_i^G \quad (5.4-7)$$

and its components on the Reference Axis System are found as

$$\begin{aligned} M_{Xi}^G &= -Q_1 h_{Zi}^G - R_1 h_{Yi}^G \\ M_{Yi}^G &= R_1 h_{Xi}^G - P_1 h_{Zi}^G \\ M_{Zi}^G &= P_1 h_{Yi}^G + Q_1 h_{Xi}^G \end{aligned} \quad (5.4-8)$$

These components are formed into the matrix $\{M^G\}$, equation (4.2-119), and used as a basis for computing the aeroelastic effects of the gyroscopic couples in equation (5.3-6).

The inertial couples of the engines have components which are equal and opposite to the gyroscopic couples. The total inertial couple from the engines is therefore computed using equations (4.2-57) and (4.2-119) as

$$- [\bar{\phi}_\delta]^T [\Delta_G] \{M^G\}$$

The gyroscopic part of equation (5.4-1) may now be expressed in terms of the gyroscopic couples $\{M^G\}$ as follows:

$$\begin{aligned} \{F_B^G\} &= [J] \left(-[\bar{\phi}_\delta]^T + \bar{q}_1 [\bar{\phi}^*]^T [T_{fT}] [T_{TF}] [D]^{-1} [A_{F\theta}] [\tilde{C}_{\delta Q}] \right) \\ &\quad \times [\Delta_G] \{M^G\} \end{aligned} \quad (5.4-9)$$

where the second term interior to the bracket arises from the aeroelasticity, equation (5.3-6).

In the FLEXSTAB system, the engines at either side of a configuration must be symmetrically located relative to the X,Z plane, figure 5.4-1; but there are two possible choices for the direction of spin of the engines at either side—parallel or counter rotation. Letting ω denote

engine spin rate, the components of angular momentum of an engine located on the right side of the aircraft are related to those of the symmetrically located engine on the left as follows:

for parallel rotation, i.e., $\omega_R = \omega_L$,

$$h_{XR}^G = h_{XL}^G, \quad h_{YR}^G = -h_{YL}^G, \quad h_{ZR}^G = h_{ZL}^G$$

for counter rotation, i.e., $\omega_R = -\omega_L$,

$$h_{XR}^G = -h_{XL}^G, \quad h_{YR}^G = h_{YL}^G, \quad h_{ZR}^G = -h_{ZL}^G \quad (5.4-10)$$

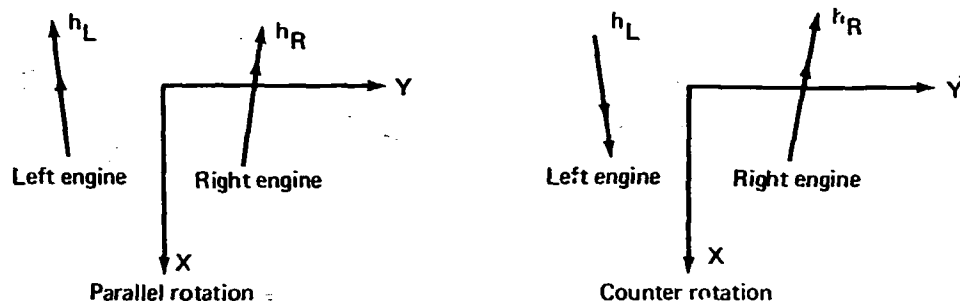


FIGURE 5.4-1.—ANGULAR MOMENTUM OF ROTATING ENGINES

For the two possible engine rotations the components of the gyroscopic couple at the right and left engines are given as follows:

parallel rotation,

$$M_{XR} = -Q_1 h_Z^G - R_1 h_Y^G$$

$$M_{XL} = -Q_1 h_Z^G + R_1 h_Y^G$$

$$M_{YR} = R_1 h_X^G - P_1 h_Z^G$$

$$M_{YL} = R_1 h_X^G - P_1 h_Z^G$$

$$M_{ZR} = P_1 h_Y^G + Q_1 h_X^G$$

$$M_{ZL} = P_1 h_Y^G + Q_1 h_X^G$$

(5.4-11)

counter rotation,

$$M_{XR} = -Q_1 h_Z^G - R_1 h_Y^G$$

$$M_{XL} = Q_1 h_Z^G - R_1 h_Y^G$$

$$M_{YR} = R_1 h_X^G - P_1 h_Z^G$$

$$M_{YL} = -R_1 h_X^G + P_1 h_Z^G$$

$$M_{ZR} = P_1 h_Y^G + Q_1 h_X^G$$

$$M_{ZL} = P_1 h_Y^G - Q_1 h_X^G$$

These components constitute a load distribution on the aircraft which is symmetric with respect to the X,Z plane when

$$M_{XR} = -M_{XL}, \quad M_{YR} = M_{YL}, \quad M_{ZR} = -M_{ZL} \quad (5.4-12)$$

and antisymmetric when

$$M_{XR} = M_{XL}, \quad M_{YR} = -M_{YL}, \quad M_{ZR} = M_{ZL} \quad (5.4-13)$$

The gyroscopic couples are expressed in matrix form by the expression

$$\{M^G\} = \left[\frac{\partial G}{\partial \omega} \right] \{V\} \omega(T) \quad (5.4-14)$$

where $\omega(T)$ is the engine spin rate as a function of thrust amplitude setting—supplied to the FLEXSTAB system as a table—and $\{V\}$ is the velocity vector partitioned into symmetric and antisymmetric parts, i.e.,

$$\{V\} = \begin{bmatrix} \{V^S\} \\ \{V^A\} \end{bmatrix} = \begin{bmatrix} U \\ W \\ Q \\ V \\ P \\ R \end{bmatrix} \quad (5.4-15)$$

The matrix $[\partial G/\partial \omega]$ is expressed in terms of symmetric and antisymmetric components, i.e.,

$$[\frac{\partial G}{\partial \omega}] = \begin{bmatrix} [\frac{\partial G}{\partial \omega}]^{SS} & [\frac{\partial G}{\partial \omega}]^{SA} \\ [\frac{\partial G}{\partial \omega}]^{AS} & [\frac{\partial G}{\partial \omega}]^{AA} \end{bmatrix} \quad (5.4-16)$$

and each partition of this matrix contains additional partitions, which are related to the individual engines, e.g.,

$$[\frac{\partial G}{\partial \omega}]^{SS} \equiv \begin{bmatrix} \vdots \\ [\frac{\partial G}{\partial \omega}]_i^{SS} \\ \vdots \end{bmatrix} \quad (5.4-17)$$

where $[\partial G^{SS}/\partial \omega]_i$ pertains to the i^{th} engine. Finally, the partitions of equation (5.4-14) for the i^{th} engine are as follows for the two possible cases of engine rotation directions:

parallel rotation:

$$\begin{aligned} [\frac{\partial G}{\partial \omega}]_i^{SS} &\equiv \begin{bmatrix} 0 & 0 & 0 \\ 0 & 0 & 0 \\ 0 & 0 & 0 \end{bmatrix} & [\frac{\partial G}{\partial \omega}]_i^{SA} &\equiv \begin{bmatrix} 0 & 0 & -\frac{\partial h_Y^G}{\partial \omega} \\ 0 & -\frac{\partial h_Z^G}{\partial \omega} & \frac{\partial h_X^G}{\partial \omega} \\ 0 & \frac{\partial h_Y^G}{\partial \omega} & 0 \end{bmatrix} \\ [\frac{\partial G}{\partial \omega}]_i^{AS} &\equiv \begin{bmatrix} 0 & 0 & -\frac{\partial h_Z^G}{\partial \omega} \\ 0 & 0 & \frac{\partial h_X^G}{\partial \omega} \\ 0 & 0 & \frac{\partial h_Y^G}{\partial \omega} \end{bmatrix} & [\frac{\partial G}{\partial \omega}]_i^{AA} &\equiv \begin{bmatrix} 0 & 0 & 0 \\ 0 & 0 & 0 \\ 0 & 0 & 0 \end{bmatrix} \end{aligned} \quad (5.4-18)$$

counter rotation:

$$\left[\frac{\partial G^{SS}}{\partial \omega} \right]_i = \begin{bmatrix} 0 & 0 & -\frac{\partial h_Z^G}{\partial \omega} \\ 0 & 0 & 0 \\ 0 & 0 & \frac{\partial h_X^G}{\partial \omega} \end{bmatrix} \quad \left[\frac{\partial G^{SA}}{\partial \omega} \right]_i = \begin{bmatrix} 0 & 0 & 0 \\ 0 & 0 & 0 \\ 0 & 0 & 0 \end{bmatrix} \quad (5.4-19)$$

$$\left[\frac{\partial G^{AS}}{\partial \omega} \right]_i = \begin{bmatrix} 0 & 0 & 0 \\ 0 & 0 & 0 \\ 0 & 0 & 0 \end{bmatrix} \quad \left[\frac{\partial G^{AA}}{\partial \omega} \right]_i = \begin{bmatrix} 0 & 0 & -\frac{\partial h_Y^G}{\partial \omega} \\ 0 & -\frac{\partial h_Z^G}{\partial \omega} & \frac{\partial h_X^G}{\partial \omega} \\ 0 & \frac{\partial h_Y^G}{\partial \omega} & 0 \end{bmatrix}$$

In the case of counter rotation the aircraft rotation rate Q_1 leads only to a couple M_{YB} tending to produce motion in the plane of symmetry, while the rotation rates P_1 and R_1 lead to gyroscopic couples which tend to produce motion which is out of the plane of symmetry. Counter rotating engines therefore eliminate gyroscopic coupling in the motion of an aircraft. If an aircraft is undergoing symmetric motion, e.g., a pull-up with wings level, counter rotating engines produce no net couple—either directly as an inertial couple or indirectly through aeroelasticity as in equation (5.3-6)—which tends to roll or yaw the aircraft.

The components of force and couple generated by the propulsion system, $\{F_B^T\}$ of equation (5.4-2), are expressed in terms of the thrust amplitude setting T_1 by letting the spin rate ω be expressed as

$$\omega(t) = \frac{\partial \omega}{\partial T}(T) T_1 \quad (5.4-20)$$

Introducing this expression into equation (5.4-14) and the resulting expression into (5.4-7), it follows that

$$\{F_B^T\} = \{F_{\delta T}^G\} T_1 \quad (5.4-21)$$

where

$$\{F_{\delta T}^G\} \equiv \left[-[\mathcal{M}][\bar{\phi}_\delta][\Delta_G] + [F_{GYRO}] \right] \left[\frac{\partial G}{\partial \omega} \right] \{V\} \frac{\partial \omega}{\partial T}$$

$$[F_{GYRO}] \equiv \bar{q}_1 [G_\theta] [\tilde{C}_{\theta G}]$$

Introducing equation (5.4-21) leads to the desired result--

$$\{F_B^T\} = (\{F_T^T\} + \{F_T^G\})_{T_1} \quad (5.4-22)$$

5.5 TRIM PROBLEM SOLUTION

As noted in section 5.2, the trim problem consists of the six equations of motion expressed in terms of a specified steady, reference flight condition and in terms of six unspecified trim variables. The methods for solving for the unspecified trim variables are described in the following.

5.5.1 Methods of Solution

The FLEXSTAB system utilizes two methods of solution for the trim problem—one is a direct solution for a linear trim problem and the second is a Newton iteration solution, reference 5-1, section 7.3a for a nonlinear trim problem. In the case of a linear trim problem the equations of motion are expressed in the following matrix form:

$$\{H_j\} = [F_{jk}]\{x_k\} \quad (5.5-1)$$

where the elements of x_k are the unknown trim variables.* The problem is solved by multiplying equation (5.5-1) with the inverse of the matrix $\{F_{jk}\}$, i.e.,

$$\{x_k\} = [F_{jk}]^{-1} \{H_j\} \quad (5.5-2)$$

In the case of a nonlinear trim problem the equations of motion are expressed in a homogeneous matrix form, viz.,

$$\{G_j\} = \{0\}, \quad (5.5-3)$$

and expanded in a truncated Taylor series about an assumed solution,

$$\{G_j(i)\} + \left[\frac{\partial G_j}{\partial x_k}(i) \right] \{\Delta x_k(i+1)\} = \{0\} \quad (5.5-4)$$

*For the case of coupled motion

$$\{x_k\} = [x_1, T_1 \text{ or } \theta_1, \delta_{\alpha_1}, \delta_1, \delta_{\alpha_1}, \delta_{\alpha_1}]^T$$

The solution is found as

$$\{x_k(N)\} = \{x_k(1)\} + \sum_{i=1}^n \{\Delta x_k(i+1)\} \quad (5.5-5)$$

where

$$\{\Delta x_k(i+1)\} = -\left[\frac{\partial G_j}{\partial x_k}(i)\right]^{-1} \{G_j(i)\} \quad (5.5-6)$$

and $\{x_k(1)\}$ is an initially assumed solution. The sum appearing in equation (5.5-5) is carried out until the increment of each unknown trim variable becomes less than a specified value.

5.5.2 Linear Trim Problem

The equations of motion for the linear trim problem are developed in section 5.2. They are given by Equations (5.2-12) and (5.2-13) when the propulsion system and aerodynamic terms are represented by the linear functions given by equations (5.2-14) and (5.2-15). The coefficients appearing in equations (5.2-14) and (5.2-15) are derived in sections 5.3 and 5.4.

For the two cases of specified reference flight condition—Case (1): specified flight path angle, and Case (2): specified thrust amplitude—the matrices of the linear trim problem, equation (5.5-1) are as follows:

5.5.2.1 Case (1), Specified flight path angle.—

$[F] \equiv$

$$\begin{bmatrix} (F_{XB_\alpha}^A - MU_1 Q_1) & F_{XB_{\delta e}}^A & F_{XB_{\delta T}}^T & MU_1 R_1 & 0 & 0 \\ -M_g \cos \gamma_1 & & & & & \\ (F_{ZB_\alpha}^A & F_{ZB_{\delta e}}^A & F_{ZB_{\delta T}}^T & -MU_1 P_1 & 0 & 0 \\ -M_g \cos \phi_1 \sin \gamma_1 & & & & & \\ M_{YB_\alpha}^A & M_{YB_{\delta e}}^A & M_{YB_{\delta T}}^T & 0 & 0 & 0 \\ -M_g \sin \phi_1 \sin \gamma_1 & 0 & 0 & F_{YB_\beta}^A & F_{YB_{\delta a}}^A & F_{YB_{\delta r}}^A \\ -MU_1 P_1 & & & M_{XB_\beta}^A & M_{XB_{\delta a}}^A & M_{XB_{\delta r}}^A \\ 0 & 0 & 0 & M_{ZB_\beta}^A & M_{ZB_{\delta a}}^A & M_{ZB_{\delta r}}^A \\ 0 & 0 & 0 & & & \end{bmatrix} \quad (5.5-7)$$

$$\{H\} \equiv \begin{bmatrix} M_g \sin \gamma_1 - F_{XB_{GYRO}}^T - F_{XB_0}^A - F_{XB_Q}^A Q_1 \\ -MU_1 Q_1 - Mg \cos \phi_1 \cos \gamma_1 - F_{ZB_{GYRO}}^T - F_{ZB_0}^A - F_{ZB_Q}^A Q_1 \\ (I_{XX_1} - I_{ZZ_1}) R_1 P_1 + I_{XZ_1} (P_1^2 - R_1^2) - M_{YB_{GYRO}}^T - M_{YB_0}^A - M_{YB_Q}^A Q_1 \\ \hline MU_1 R_1 - Mg \sin \theta_1 \cos \gamma_1 - F_{YB_{GYRO}}^T - F_{YB_P}^A P_1 - F_{YB_R}^A R_1 \\ (I_{ZZ_1} - I_{YY_1}) Q_1 R_1 - I_{XZ_1} P_1 Q_1 - M_{XB_{GYRO}}^T - M_{XB_P}^A P_1 - M_{XB_R}^A R_1 \\ (I_{YY_1} - I_{XX_1}) P_1 Q_1 + I_{XZ_1} R_1 Q_1 - M_{ZB_{GYRO}}^T - M_{ZB_P}^A P_1 - M_{ZB_R}^A R_1 \end{bmatrix}$$

5.5.2.2 Case (2), Specified thrust amplitude setting T_1 .--

$$[F] \equiv \begin{bmatrix} (-MU_1 Q_1 + F_{XB_\alpha}^A) & F_{XB_{\delta e}}^A & -Mg & MU_1 R_1 & 0 & 0 \\ F_{ZB_\alpha}^A & F_{ZB_{\delta e}}^A & 0 & -MU_1 R_1 & 0 & 0 \\ M_{YB_\alpha}^A & M_{YB_{\delta e}}^A & 0 & 0 & 0 & 0 \\ \hline MU_1 P_1 & 0 & 0 & F_{YB_\beta}^A & F_{YB_{\delta a}}^A & F_{YB_{\delta r}}^A \\ 0 & 0 & 0 & M_{XB_\beta}^A & M_{XB_{\delta a}}^A & M_{XB_{\delta r}}^A \\ 0 & 0 & 0 & M_{ZB_\beta}^A & M_{ZB_{\delta a}}^A & M_{ZB_{\delta r}}^A \end{bmatrix} \quad (5.5-8)$$

$$\{H\} \equiv \begin{bmatrix} -F_{XB_1}^T & -F_{XB_0}^A & -F_{XB_Q}^A & Q_1 \\ -MU_1 Q_1 & -Mg \cos \phi_1 & -F_{XB_1}^T & -F_{ZB_0}^A & -F_{ZB_Q}^A & Q_1 \\ (I_{XX_1} - I_{ZZ_1}) P_1 R_1 + I_{XZ} (P_1^2 - R_1^2) & -M_{YB_1}^T & -M_{YB_0}^A & -M_{YB_Q}^A & Q_1 \\ \hline MU_1 R_1 & -Mg \sin \phi_1 & -F_{YB_P}^A & -F_{YB_R}^A & -F_{YB_1}^T \\ (I_{ZZ_1} - I_{YY_1}) Q_1 R_1 - I_{XZ} P_1 Q_1 & -M_{XB_1}^T & -M_{XB_P}^A & -M_{XB_R}^A & R_1 \\ (I_{YY_1} - I_{XX_1}) P_1 Q_1 + I_{XZ} R_1 Q_1 & -M_{ZB_1}^T & -M_{ZB_P}^A & -M_{ZB_R}^A & R_1 \end{bmatrix}$$

5.5.2.3 Longitudinal motion.—The trim problem is represented by a reduced set of equations when two conditions are satisfied: (1) the reference flight condition is a symmetric motion

$$(i.e., \phi_1 = 0, \beta_1 = 0, P_1 = 0, R_1 = 0, \delta_{a_1} = 0, \delta_{r_1} = 0) \quad (5.5-9)$$

and (2) the gyroscopic couples from the propulsion system are zero or are the result of counter rotating engines, equations (5.4-12) through (5.4-17). Assuming these conditions to be satisfied, the trim variables reduce to

$$\{x_k\} \equiv \begin{bmatrix} \alpha_1 \\ \delta e_1 \\ \theta_1 (or T_1) \end{bmatrix} \quad (5.5-10)$$

and the matrices $[F]$ and $\{H\}$ reduce to the following:

Case (1) specified flight path angle

$$[F] \equiv \begin{bmatrix} F_{XB_\alpha}^A & -MU_1 C_1 - Mg \cos \gamma_1 & F_{XB_{\delta e}}^A & F_{XB_{\delta T}}^T \\ F_{ZB_\alpha}^A & -Mg \sin \gamma_1 & F_{ZB_{\delta e}}^A & F_{ZB_{\delta T}}^T \\ M_{YB_\alpha}^A & & M_{YB_{\delta e}}^A & M_{YB_{\delta T}}^T \end{bmatrix} \quad (5.5-11)$$

$$\{H\} \equiv \begin{bmatrix} Mg \sin \gamma_1 - F_{XB_{GYRO}}^T & -F_{XB_0}^A & -F_{XB_Q}^A Q_1 \\ -MU_1 Q_1 - F_{ZB_{GYRO}}^T & -F_{ZB_0}^A & -F_{ZB_Q}^A Q_1 \\ -M_{YB_{GYRO}}^T & -M_{YB_0}^A & -M_{YB_Q}^A Q_1 \end{bmatrix}$$

Case (2) specified thrust amplitude setting, T

$$[F] \equiv \begin{bmatrix} (-MU_1 Q_1 + F_{XB_\alpha}^A) & F_{XB_{\delta e}}^A & -Mg \\ F_{ZB_\alpha}^A & F_{ZB_{\delta e}}^A & 0 \\ M_{YB_\alpha}^A & M_{YB_{\delta e}}^A & 0 \end{bmatrix} \quad (5.5-12)$$

$$\{H\} \equiv \begin{bmatrix} -F_{XB_1}^T & -F_{XB_0}^A & -F_{XB_Q}^A Q_1 \\ -MU_1 Q_1 - Mg \cos \phi_1 - F_{ZB_1}^T & -F_{ZB_0}^A & -F_{ZB_Q}^A Q_1 \\ (I_{XX_1} - I_{ZZ_1}) R_1 P_1 + I_{XZ_1} (P_1^2 - P_2^2) & -M_{YB_1}^T & -M_{YB_0}^A & -M_{YB_Q}^A Q_1 \end{bmatrix}$$

5.5.3 Nonlinear Trim Problem

The equations of motion for the nonlinear trim problem are developed in section 5.2. They are given by equations (5.2-9) for case (1), specified flight path angle, and by equations (5.2-10) for case (2), specified thrust amplitude. The matrices for the solution to the problem appearing in the iterative formula, equations (5.5-5) and (5.5-6), are developed for the two cases as follows:

The matrix $\{G_j(i)\}$ is simply the left-hand members of the equations of motion written in homogeneous form and evaluated using the trim variable values at the i^{th} iteration, $x_k(i)$.

The elements of the matrix $\{\partial G_j(i)/\partial x_k\}$ are the derivatives of the elements of the matrix $\{G_j\}$ with respect to the trim variables x_k evaluated at the i^{th} iteration, i.e.,

$$\left[\frac{\partial G_j}{\partial x_k}(i) \right] \equiv \left[\left\{ \frac{\partial G_j}{\partial x_1} \right\}_i \quad \left\{ \frac{\partial G_j}{\partial x_2} \right\}_i \quad \cdots \quad \left\{ \frac{\partial G_j}{\partial x_6} \right\}_i \right]$$

The matrices for the two cases available in the FLEXSTAB system for specifying reference flight condition are as follows:

Case (1) specified flight path angle γ_1

$$\{G_j(i)\} \equiv$$

$$\begin{bmatrix} MU_1(Q_1 \tan \alpha_i - R_1 \tan \beta_i) + Mg \sin(\gamma_1 + \alpha_i) - F_{XB_1}^T(i) - F_{XB_1}^A(i) \\ MU_1(Q_1 \tan \beta_i - R_1) - Mg \cos(\gamma_1 + \alpha_i) \cos \phi_1 - F_{ZB_1}^T(i) - F_{ZB_1}^A(i) \\ (I_{XX_1} - I_{ZZ_1})P_1 R_1 + I_{XZ_1}(P_1^2 - R_1^2) - M_{YB_1}^T(i) - M_{YB_1}^A(i) \\ MU_1(R_1 - P_1 \tan \alpha_i) - Mg \cos(\gamma_1 + \alpha_i) \sin \phi_1 - F_{YB_1}^T(i) - F_{YB_1}^A(i) \\ (I_{ZZ_1} - I_{YY_1})Q_1 R_1 - I_{XZ_1}P_1 Q_1 - M_{XB_1}^T(i) - M_{XB_1}^A(i) \\ (I_{YY_1} - I_{XX_1})P_1 Q_1 + I_{XZ_1}R_1 Q_1 - M_{ZB_1}^T(i) - M_{ZB_1}^A(i) \end{bmatrix} \quad (5.5-13)$$

Case (2) specified thrust amplitude setting T_1

$$\{G_j(i)\} \equiv \begin{bmatrix} MU_1(Q_1 \tan \alpha_i - R_1 \tan \beta_i) + Mg \sin \theta_i - F_{XB_1}^T(i) - F_{XB_1}^A(i) \\ MU_1(Q_1 \tan \beta_i - R_1) - Mg \cos \theta_i \cos \phi_1 - F_{ZB_1}^T(i) - F_{ZB_1}^A(i) \\ (I_{XX_1} - I_{ZZ_1})P_1 R_1 + I_{XZ_1}(P_1^2 - R_1^2) - M_{YB_1}^T(i) - M_{YB_1}^A(i) \\ MU_1(R_1 - P_1 \tan \alpha_i) - Mg \cos \theta_i \sin \phi_1 - F_{YB_1}^T(i) - F_{YB_1}^A(i) \\ (I_{ZZ_1} - I_{YY_1})Q_1 R_1 - I_{XZ_1}P_1 Q_1 - M_{XB_1}^T(i) - M_{XB_1}^A(i) \\ (I_{YY_1} - I_{XX_1})P_1 Q_1 + I_{XZ_1}R_1 Q_1 - M_{ZB_1}^T(i) - M_{ZB_1}^A(i) \end{bmatrix} \quad (5.5-14)$$

Case (1) specified flight path angle

$$\left[\frac{\partial G_i}{\partial x_k}(i) \right] =$$

(5.5-15)

$$\begin{bmatrix} MU_1 \sec^2 \alpha_i + \frac{\partial F_{XB}^A}{\partial \delta_e} - \frac{\partial F_{XB}^T}{\partial T} - MU_1 R_1 \sec^2 \beta_i - \frac{\partial F_{XB}^A}{\partial \delta_a} - \frac{\partial F_{XB}^A}{\partial \delta_r} \\ + Mg \cos(\gamma_1 + \alpha_i) - \frac{\partial F_{XB}^A}{\partial \alpha} - \frac{\partial F_{XB}^A}{\partial \beta} \\ Mg \cos(\gamma_1 + \alpha_i) \times \frac{\partial F_{ZB}^A}{\partial \delta_e} - \frac{\partial F_{ZB}^T}{\partial T} - MU_1 P_1 \sec^2 \beta_i - \frac{\partial F_{ZB}^A}{\partial \delta_a} - \frac{\partial F_{ZB}^A}{\partial \delta_r} \\ \times \cos \phi_1 - \frac{\partial F_{ZB}^A}{\partial \alpha} - \frac{\partial F_{ZB}^A}{\partial \beta} \\ \frac{\partial M_{YB}^A}{\partial \alpha} - \frac{\partial M_{YB}^A}{\partial \delta_e} - \frac{\partial M_{YB}^T}{\partial T} - \frac{\partial M_{YB}^A}{\partial \beta} - \frac{\partial M_{YB}^A}{\partial \delta_a} - \frac{\partial M_{YB}^A}{\partial \delta_r} \\ - MU_1 P_1 \sec^2 \alpha_i + \frac{\partial F_{YB}^A}{\partial \delta_e} - \frac{\partial F_{YB}^T}{\partial T} - \frac{\partial F_{YB}^A}{\partial \beta} - \frac{\partial F_{YB}^A}{\partial \delta_a} - \frac{\partial F_{YB}^A}{\partial \delta_r} \\ \times \sin \phi_1 - \frac{\partial F_{YB}^A}{\partial \alpha} \\ \frac{\partial M_{XB}^A}{\partial \alpha} - \frac{\partial M_{XB}^A}{\partial \delta_e} - \frac{\partial M_{XB}^T}{\partial T} - \frac{\partial M_{XB}^A}{\partial \beta} - \frac{\partial M_{XB}^A}{\partial \delta_a} - \frac{\partial M_{XB}^A}{\partial \delta_r} \\ \frac{\partial M_{ZB}^A}{\partial \alpha} - \frac{\partial M_{ZB}^A}{\partial \delta_e} - \frac{\partial M_{ZB}^T}{\partial T} - \frac{\partial M_{ZB}^A}{\partial \beta} - \frac{\partial M_{ZB}^A}{\partial \delta_a} - \frac{\partial M_{ZB}^A}{\partial \delta_r} \end{bmatrix}$$

Case (2) specified thrust amplitude setting T_1

$$\left[\frac{\partial G_j}{\partial x_k}(i) \right] \equiv$$

(5.5-16)

$$\begin{bmatrix} MU_1 Q_1 \sec^2 \alpha_i & \frac{\partial F_{XB}^A}{\partial \delta_e} & Mg \cos \theta_i & \frac{\partial F_{XB}^A}{\partial \beta} & \frac{\partial F_{XB}^A}{\partial \delta_a} & \frac{\partial F_{XB}^A}{\partial \delta_r} \\ \frac{\partial F_{XB}^A}{\partial \alpha} & & & & & \\ \frac{\partial F_{ZB}^A}{\partial \alpha} & \frac{\partial F_{ZB}^A}{\partial \delta_e} & Mg \sin \theta_i \times \sin \phi_1 & \frac{\partial F_{ZB}^A}{\partial \beta} & \frac{\partial F_{ZB}^A}{\partial \delta_a} & \frac{\partial F_{ZB}^A}{\partial \delta_r} \\ \frac{\partial M_{YB}^A}{\partial \alpha} & \frac{\partial M_{YB}^A}{\partial \delta_e} & 0 & \frac{\partial M_{YB}^A}{\partial \beta} & \frac{\partial M_{YB}^A}{\partial \delta_a} & \frac{\partial M_{YB}^A}{\partial \delta_r} \\ -MU_1 P_1 \sec^2 \alpha_i & \frac{\partial F_{YB}^A}{\partial \delta_e} & Mg \sin \theta_i \times \sin \phi_1 & \frac{\partial F_{YB}^A}{\partial \beta} & \frac{\partial F_{YB}^A}{\partial \delta_a} & \frac{\partial F_{YB}^A}{\partial \delta_r} \\ \frac{\partial F_{YB}^A}{\partial \alpha} & & & & & \\ \frac{\partial M_{XB}^A}{\partial \alpha} & \frac{\partial M_{XB}^A}{\partial \delta_e} & 0 & \frac{\partial M_{XB}^A}{\partial \beta} & \frac{\partial M_{XB}^A}{\partial \delta_a} & \frac{\partial M_{XB}^A}{\partial \delta_r} \\ \frac{\partial M_{ZB}^A}{\partial \alpha} & \frac{\partial M_{ZB}^A}{\partial \delta_e} & 0 & \frac{\partial M_{ZB}^A}{\partial \beta} & \frac{\partial M_{ZB}^A}{\partial \delta_a} & \frac{\partial M_{ZB}^A}{\partial \delta_r} \end{bmatrix}$$

5.6 STATIC STABILITY DERIVATIVES

The static stability derivatives describe the aerodynamic force and couple generated by static perturbations of an aircraft about the reference flight condition, reference 2-2, chapter 2. This section contains a derivation of the static stability derivatives based on the linear aerodynamic and structural theories of sections 3 and 4. The derivation leads to matrix equations describing the static stability derivatives in terms of the aerodynamic matrices developed in section 3 and the structural matrices developed in section 4. The derivation proceeds from the steady form of the perturbation expansion of the aerodynamic forces given by equation (3.5-63) and the steady form of the perturbation structural equations of motion given by equation (4.2-78). This derivation is carried out assuming that the steady (or static) perturbations are relative to the reference flight condition.

5.6.1 Classification of Static Stability Derivatives

Following accepted practice, reference 2-2, the static stability derivatives are separated into two groups—longitudinal and lateral-directional—and are expressed in terms of the Body Axis System and in physical dimensions as follows:

5.6.1.1 Longitudinal static stability derivatives.—

$$\begin{aligned}
 &F_{XB_0}^A, \quad F_{XF_1}^A, \quad (F_{XB_u}^A)_1, \quad (F_{XB_w}^A)_1, \quad (F_{XB_Q}^A)_1, \quad (F_{XB_{\delta e}}^A)_1 \\
 &F_{ZB_0}^A, \quad F_{ZB_1}^A, \quad (F_{ZB_u}^A)_1, \quad (F_{ZB_w}^A)_1, \quad (F_{ZB_Q}^A)_1, \quad (F_{ZB_{\delta e}}^A)_1 \\
 &M_{YB_0}^A, \quad M_{YB_1}^A, \quad (M_{YB_u}^A)_1, \quad (M_{YB_w}^A)_1, \quad (M_{YB_Q}^A)_1, \quad (M_{YB_{\delta e}}^A)_1
 \end{aligned} \tag{5.6-1}$$

5.6.1.2 Lateral-directional static stability derivatives.—

$$\begin{aligned}
 &(F_{YB_v}^A)_1, \quad (F_{YB_p}^A)_1, \quad (F_{YB_r}^A)_1, \quad (F_{YB_{\delta a}}^A)_1, \quad (F_{YB_{\delta r}}^A)_1, \\
 &(M_{XB_v}^A)_1, \quad (M_{XB_p}^A)_1, \quad (M_{XB_r}^A)_1, \quad (M_{XB_{\delta a}}^A)_1, \quad (M_{XB_{\delta r}}^A)_1, \\
 &(M_{ZB_v}^A)_1, \quad (M_{ZB_p}^A)_1, \quad (M_{ZB_r}^A)_1, \quad (M_{ZB_{\delta a}}^A)_1, \quad (M_{ZB_{\delta r}}^A)_1,
 \end{aligned} \tag{5.6-2}$$

5.6.2 Nondimensional Form of the Static Stability Derivatives

In the FLEXSTAB system the static stability derivatives are transformed to the Stability Axis System, equation (2.2-8), and are nondimensionalized using the system summarized in Table 5.6-1.

TABLE 5.6-1.—NONDIMENSIONALIZATION OF QUANTITIES RELATED TO THE STABILITY DERIVATIVES

Dimensional quantity in the Body Axis System	Divisor	Nondimensional quantity in the Stability Axis System
F_{XB}^A F_{YB}^A F_{ZB}^A	$\bar{q}_1 S_W$	C_D C_L C_Y
M_{XB}^A M_{YB}^A M_{ZB}^A	$\bar{q}_1 S_W l$	C_l C_m C_n
$(U-U_1)$ V W	U_1	\hat{u} β α
P Q R	$2U_1/l$	\hat{p} \hat{q} \hat{r}
where S_W and l are characteristic surface area and length		

The nondimensional static stability derivatives, expressed in the Stability Axis System, are found from quantities shown by equations (5.6-1) and (5.6-2) as follows:

5.6.2.1 Nondimensional longitudinal static stability derivatives. —

$$C_{D_1} \equiv \frac{1}{\bar{q}_1 S_W} (F_{XB_1}^A \cos \alpha_1 + F_{ZB_1}^A \sin \alpha_1)$$

$$C_{L_1} \equiv \frac{1}{\bar{q}_1 S_W} (F_{XB_1}^A \sin \alpha_1 - F_{ZB_1}^A \cos \alpha_1)$$

$$C_{m_1} \equiv \frac{1}{\bar{q}_1 S_W \bar{C}} M_{YB_1}^A$$

$$C_{D_u} \equiv \frac{U_1}{\bar{q}_1 S_W} \left[(F_{XB_u}^A)_1 \cos \alpha_1 + (F_{ZB_u}^A)_1 \sin \alpha_1 \right]$$

$$C_{L_u} \equiv \frac{U_1}{\bar{q}_1 S_W} \left[(F_{XB_u}^A)_1 \sin \alpha_1 - (F_{ZB_u}^A)_1 \cos \alpha_1 \right]$$

$$C_{m_u} \equiv \frac{U_1}{\bar{q}_1 S_W \bar{C}} (M_{YB_u}^A)_1$$

$$C_{D_\alpha} \equiv -\frac{U_1}{\bar{q}_1 S_w} \left[(F_{XB_w}^A)_1 \cos \alpha_1 + (F_{ZB_w}^A)_1 \sin \alpha_1 \right] \sec^2 \alpha_1 + C_{L_1} \quad (5.6-3)$$

$$C_{L_\alpha} \equiv \frac{U_1}{\bar{q}_1 S_w} \left[(F_{XB_w}^A)_1 \sin \alpha_1 - (F_{ZB_w}^A)_1 \cos \alpha_1 \right] \sec^2 \alpha_1 - C_{D_1}$$

$$C_{m_\alpha} \equiv \frac{U_1}{\bar{q}_1 S_w \bar{c}} (M_{YB_w}^A)_1 \sec^2 \alpha_1$$

$$C_{D_Q} \equiv -\frac{2U_1}{\bar{q}_1 S_w \bar{c}} \left[(F_{XB_Q}^A)_1 \cos \alpha_1 + (F_{ZB_Q}^A)_1 \sin \alpha_1 \right]$$

$$C_{L_Q} \equiv \frac{2U_1}{\bar{q}_1 S_w \bar{c}} \left[(F_{XB_Q}^A)_1 \sin \alpha_1 - (F_{ZB_Q}^A)_1 \cos \alpha_1 \right]$$

$$C_{m_Q} \equiv \frac{2U_1}{\bar{q}_1 S_w \bar{c}^2} (M_{YB_Q}^A)_1$$

$$C_{D_{\delta e}} \equiv -\frac{1}{\bar{q}_1 S_w} \left[(F_{XB_{\delta e}}^A)_1 \cos \alpha_1 + (F_{ZB_{\delta e}}^A)_1 \sin \alpha_1 \right]$$

$$C_{L_{\delta e}} \equiv \frac{1}{\bar{q}_1 S_w} \left[(F_{XB_{\delta e}}^A)_1 \sin \alpha_1 - (F_{ZB_{\delta e}}^A)_1 \cos \alpha_1 \right]$$

$$C_{m_{\delta e}} \equiv \frac{1}{\bar{q}_1 S_w \bar{c}} (M_{YB_{\delta e}}^A)_1$$

5.6.2.2 Nondimensional lateral-directional static stability derivatives.—

$$C_{Y_\beta} \equiv \frac{U_1}{\bar{q}_1 S_w} (F_{YE_v}^A)_1$$

$$C_{l_\beta} \equiv \frac{U_1}{\bar{q}_1 S_w b} \left[(M_{XB_v}^A)_1 \cos \alpha_1 + (M_{ZB_v}^A)_1 \sin \alpha_1 \right]$$

$$C_{n_\beta} \equiv \frac{U_1}{\bar{q}_1 S_w b} \left[(M_{XB_v}^A)_1 \sin \alpha_1 + (M_{ZB_v}^A)_1 \cos \alpha_1 \right]$$

$$C_{Y_r} \equiv \frac{2U_1}{\bar{q}_1 S_w b} \left[(F_{YB_p}^A)_1 \cos \alpha_1 + (F_{ZB_p}^A)_1 \sin \alpha_1 \right]$$

$$C_{1P} \equiv \frac{2U_1}{\bar{q}_1 S_W b^2} \left\{ \left[(M_{XB_P}^A)_1 \cos \alpha_1 + (M_{ZB_P}^A)_1 \sin \alpha_1 \right] \cos \alpha_1 + \right. \\ \left. + \left[(M_{XB_R}^A)_1 \cos \alpha_1 + (M_{ZB_R}^A)_1 \sin \alpha_1 \right] \sin \alpha_1 \right\}$$

$$C_{n_P} \equiv \frac{2U_1}{\bar{q}_1 S_W b^2} \left\{ \left[-(M_{XB_P}^A)_1 \sin \alpha_1 + (M_{ZB_P}^A)_1 \cos \alpha_1 \right] \cos \alpha_1 + \right. \\ \left. + \left[-(M_{XB_R}^A)_1 \sin \alpha_1 + (M_{ZB_R}^A)_1 \cos \alpha_1 \right] \sin \alpha_1 \right\}$$

$$C_{Y_R} \equiv \frac{2U_1}{\bar{q}_1 S_W b} \left[-(F_{YB_P}^A)_1 \sin \alpha_1 + (F_{YB_R}^A)_1 \cos \alpha_1 \right]$$

$$C_{1_R} \equiv \frac{2U_1}{\bar{q}_1 S_W b^2} \left\{ - \left[(M_{XB_P}^A)_1 \cos \alpha_1 + (M_{ZB_P}^A)_1 \sin \alpha_1 \right] \sin \alpha_1 + \right. \\ \left. + \left[(M_{XB_R}^A)_1 \cos \alpha_1 + (M_{ZB_R}^A)_1 \sin \alpha_1 \right] \cos \alpha_1 \right\}$$

$$C_{n_R} \equiv \frac{2U_1}{\bar{q}_1 S_W b^2} \left\{ \left[(M_{XB_P}^A)_1 \sin \alpha_1 - (M_{ZB_P}^A)_1 \cos \alpha_1 \right] \sin \alpha_1 + \right. \\ \left. + \left[-(M_{XB_R}^A)_1 \sin \alpha_1 + (M_{ZB_R}^A)_1 \cos \alpha_1 \right] \cos \alpha_1 \right\}$$

$$C_{Y_{\delta a}} \equiv \frac{1}{\bar{q}_1 S_W} (F_{YB_{\delta a}}^A)_1 \quad (5.6-4)$$

$$C_{1_{\delta a}} \equiv \frac{1}{\bar{q}_1 S_W b} \left[(M_{XB_{\delta a}}^A)_1 \cos \alpha_1 + (M_{ZB_{\delta a}}^A)_1 \sin \alpha_1 \right]$$

$$C_{n_{\delta a}} \equiv \frac{1}{\bar{q}_1 S_W b} \left[-(M_{XB_{\delta a}}^A)_1 \sin \alpha_1 + (M_{ZB_{\delta a}}^A)_1 \cos \alpha_1 \right]$$

$$C_{Y_{\delta r}} \equiv \frac{1}{\bar{q}_1 S_W} (F_{YB_{\delta r}}^A)_1$$

$$C_{l\delta r} \equiv \frac{1}{\bar{q}_1 S_W b} \left[(M_{XB\delta r}^A)_1 \cos \alpha_1 + (M_{ZB\delta r}^A)_1 \sin \alpha_1 \right]$$

$$C_{n\delta r} \equiv \frac{1}{\bar{q}_1 S_W b} \left[- (M_{XB\delta r}^A)_1 \sin \alpha_1 + (M_{ZB\delta r}^A)_1 \cos \alpha_1 \right]$$

where

\bar{q}_1 = dynamic pressure of reference flight condition

S_W = wing reference area

\bar{c} = reference chord

b = wing span

5.6.3 Static Perturbation Aerodynamic Forces

5.6.3.1 Basic relations used in the formulation. -- The aerodynamic forces generated at the aerodynamic surface segments for steady (or quasi-static) perturbations about the reference flight condition are given by equation (3.5-66) with the perturbation lifting pressure expressed for steady flow, viz.,

$$\{C_P\}_P = [A_{P\theta}]_1 (\{\theta^*\}_P + \{\psi_M\}_P) + M_1 \left[\frac{\partial A_{P\theta}}{\partial M} \right]_1 \{\psi\}_1 \frac{u}{U_1} + \{C_P\}_P^{int} \quad (5.6-5)$$

and the perturbation structural equations of motion expressed for quasi-static perturbations, viz.,

$$\{\delta\}_P = [\tilde{C}]_1 \{Q^S\}_P \quad (5.6-6)$$

The structural deformation $\{\delta\}_P$ is transformed to describe perturbation camber deformation using equation (4.2-101), i.e.,

$$\{\theta^*\}_P = [P_\theta] \{\delta\}_P, \quad (5.6-7)$$

and the perturbation applied loads are expanded in terms of aerodynamic and propulsion system perturbation loads as

$$\{Q^S\}_P = \{Q^A\}_P + \{Q^T\}_P + \{Q^B\}_P \quad (5.6-8)$$

where the airloads at the structural nodes are obtained from airloads at the aerodynamic segments using the transformation given by equation (4.2-116), viz.,

$$\{Q^A\}_P = [P_T]^T \{f_T^A\}_P \quad (5.6-9)$$

The appropriate form for the structural equation, therefore, is

$$\{\theta^*\}_P = [\tilde{C}_{\theta T}]_1 \{f_T^A\}_P + [P_\theta][\tilde{C}]_1 (\{Q^T\}_P + \{Q^G\}_P) \quad (5.6-10)$$

where $[C_{\theta T}]_1$ is the flexibility matrix previously defined by equation (5.3-1).

Combining the structural equation, equation (5.6-10), with the perturbation lifting pressure, equation (5.6-5), and with the perturbation leading edge correction, i.e.,

$$\{D\}_P = [D_{P\theta}]_1 (\{V_M\}_P + \{\theta^*\}_P) + M_1 \left(\frac{\partial D}{\partial M} \right)_1 \bar{U}_1 - \{\Delta D\}_P \quad (5.6-11)$$

leads to equations which can be substituted into equation (3.5-63) to express the static perturbation aerodynamic forces in a form in which the deformation $\{\theta^*\}_P$ does not appear explicitly. The resulting formula may be solved for the aerodynamic forces $\{f_T^A\}_P$ by inverting the following matrix:

$$[\tilde{D}_T]_1 \equiv \left([I] - \bar{q}_1 [T_{TF}] [A_{F\theta}]_1 [\tilde{C}_{\theta T}]_1 - \bar{q}_1 [\text{TRANS}_{ID}] [\bar{q}_C]_1 [D_{P\theta}]_1 [\tilde{C}_{\theta T}]_1 \right) \quad (5.6-12)$$

In the FLEXSTAB system the numerical computations arising from this operation are greatly reduced by neglecting the contribution to the leading edge correction, equation (5.6-11), arising from the elastic deformation $\{\theta^*\}_P$. The matrix $[D_T]_1$ appears multiplying the matrix $[T_{TF}]$ and this matrix product is expressed in terms of the aeroclastic matrix, equation (5.3-5) as

$$[\tilde{D}_T]_1 [T_{TF}] = [T_{TF}] [\tilde{D}]_1 \quad (5.6-13)$$

5.6.3.2 Formulation of the static perturbation aerodynamic forces. - Consider the expression for the perturbation aerodynamic forces, equation (3.5-63), expressed as:

$$\{f_T^A\}_P = [T_{TF}] \{F^A\}_P + \{f_T^A\}_P \quad (5.6-14)$$

where

$$\{F^A\}_P \equiv \bar{q}_1 [A_{F\theta}]_1 \{\theta^*\}_P \quad (5.6-15)$$

and $\{f_T^A\}_P \equiv$ (all remaining terms appearing in equation (3.5-63)) but neglecting the term

$$\bar{q}_1 [\text{TRANS}_{ID}] [\bar{q}_C]_1 [D_{P\theta}]_1 \{\theta^*\}_P \quad (5.6-16)$$

Introducing the structural equation, equation (5.6-10), into equation (5.6-15) so as to eliminate $\{\theta^*\}_P$ and solving for the forces $\{F^A\}_P$, the resulting expression is substituted into equation (5.6-14) to obtain

$$\{f_T^A\}_P = ([I] + \bar{q}_1 [T_{TF}] [\tilde{D}]_1^{-1} [A_{F\theta}] [\tilde{C}_{\theta T}]_1) \{f_T^A\}_F + \bar{q}_1 [T_{TF}] [\tilde{D}]_1^{-1} [A_{F\theta}] [F_\theta] [\tilde{C}]_1 (\{Q^T\}_P + \{Q^G\}_F) \quad (5.6-17)$$

Making use of the following matrix identity:

$$[\tilde{D}]_1^{-1} \equiv [I] + \bar{q}_1 [\tilde{D}]_1^{-1} [A_{F\theta}]_1 [\tilde{C}_{\theta T}]_1 [T_{TF}], \quad (5.6-18)$$

and substituting for the aerodynamic forces $\{f_T^A\}_P$ from equation (3.5-63), the static perturbation aerodynamic forces are found as

$$\begin{aligned} \{f_T^A\}_P = & \bar{q}_1 ([I] + \bar{q}_1 [T_{TF}] [\tilde{D}]_1^{-1} [A_{F\theta}]_1 [\tilde{C}_{\theta T}]_1) \times \\ & \times \left\{ [TRANS_t] \left[2 ([\bar{q}_t]_1^u + [\bar{y}_t]_1^r) (\{C_F^S\}_1^{iso} + \right. \right. \\ & + [\Delta M_t]_1 \left\{ \frac{\partial C_P^S}{\partial M} \right\}_1^{iso} + [\bar{q}_t]_1 (M_1 \left\{ \frac{\partial C_P^S}{\partial M} \right\}_1^u + \\ & + M_1 [\bar{y}_t]_1 \left\{ \frac{\partial C_P^S}{\partial M} \right\}_1^r) \left. \right] + [TRANS_{ID}] \left[2 ([\bar{q}_c]_1^u + \right. \\ & + [\bar{y}_c]_1^r) (D)_1 + M_1 [\bar{q}_c]_1 \left\{ \frac{\partial D}{\partial M} \right\}_1^u + \\ & + [\bar{q}_c]_1 ([D_{P\theta}]_1 \{y_M\}_P - \{\Delta D\}_F) \left. \right] + \\ & + \bar{q}_1 [T_{TF}] [\tilde{D}]_1^{-1} \left\{ [T_{FP}] \left[2 ([\bar{q}_c]_1^u + \right. \right. \\ & + [\bar{y}_c]_1^r) (C_F)_1^{int} + M_1 [\bar{q}_c]_1 \left\{ \frac{\partial C_F}{\partial M} \right\}_1^{int} + \\ & + (2 [A_{F\theta}]_1 + M_1 \left\{ \frac{\partial A_{F\theta}}{\partial M} \right\}_1) \{y\}_1^u + \\ & + 2 [T_{FP}] [\bar{y}_c]_1 [A_{F\theta}]_1 \{y\}_1^r + \\ & + [A_{F\theta}]_1 \{y_M\}_F + [F_\theta] [\tilde{C}]_1 (\{Q^T\}_F + \\ & \left. \left. + \{Q^G\}_F) \right\} \right\} \end{aligned} \quad (5.6-19)$$

This analytical form for the static perturbation aerodynamic forces is used in the FLEXSTAB system as the basis for computing static stability derivatives

5.6.4 Static Stability Derivative Formulation

The formulas which determine the static stability derivatives follow from the perturbation expansion given by equation (5.6-19). In carrying out the derivation of these formulas an approximation is made regarding the aeroelastic effect from the aerodynamic leading edge correction. This approximation is in addition to that which neglects the term shown as equation (5.6-16). As shown by the development in section 3.4.12, the aerodynamic leading edge correction introduces aerodynamic forces in the direction of the free stream only—nearly in the X-direction of the Reference Axis System. The aerodynamic forces computed from the leading edge correction are neglected in the computation of elastic deformation. This approximation eliminates a large computational task—that of computing

$$\begin{aligned} & \bar{q} [T_{TF}] [D]^{-1} [A_{F\theta}]_1 [\tilde{C}_{\theta T}]_1 [TRANS_{ID}] \left[(2[\bar{q}_c]_1 \frac{u}{U_1} \right. \\ & \left. + 2[\bar{Y}_c]_1^T \frac{r}{U_1}) \{D\}_1 + [\bar{q}_c]_1 \{D\}_P \right] \end{aligned} \quad (5.6-20)$$

Since elastic deformation of practical aircraft configurations arising from forces in the X-direction is very small, neglect of the terms represented by equation (5.6-20) should have a negligibly small effect on the static stability derivatives by comparison with the lifting and thickness induced aerodynamic forces.

The static stability derivatives—both longitudinal and lateral-directional—are developed in the following for the case of a rigid aircraft. Aeroelastic increments to the stability derivatives are then developed using the expansion of the aeroelastic matrix appearing in section 5.3.4.1. The sum of the rigid aircraft static stability derivatives and the corresponding aeroelastic increments constitute the static stability derivatives of a flexible aircraft.

5.6.4.1 Rigid aircraft longitudinal stability derivatives.—In formulating the longitudinal static stability derivatives, the aerodynamics of the aircraft, equation (5.6-19), are assumed to be those for the symmetric case described in section 3.4.1.5. The static stability derivatives for the aircraft as a rigid body are found by setting to zero the flexibility matrices appearing in equation (5.6-19) and by introducing the following notation:

$$[G_\eta] \equiv 2[\mathcal{J}][\tilde{\phi}^*]^T [T_{FT}]$$

$$[G_F] \equiv [G_\eta][T_{TF}]$$

$$[G_{\theta P}] = [G_F][A_{F\theta}]_1$$

and

$$[\mathcal{G}_{\theta P}] = [G_\eta][TRANS_{ID}][D_{F\theta}]_1$$

where $\{D_o\}$ is given by equation (3.5-70)

$$[A] \equiv \begin{bmatrix} -1 & 0 & 0 \\ 0 & -1 & 0 \\ 0 & 0 & 1 \end{bmatrix} \quad (5.6-21)$$

and

$$[\bar{\phi}^*]^T \equiv [\bar{\phi}_\delta]^T [P_T]^T \quad (5.6-22)$$

The formulas for the rigid aircraft longitudinal static stability derivatives expanded on the Body Axis System are as follows:

$$\begin{bmatrix} F_{XB_o}^A \\ F_{ZB_o}^A \\ M_{YB_o}^A \end{bmatrix}_R = \bar{q}_1 [G_{\theta R}] \{\Psi_c\} + [G_T] (\{f_T^A\}_o^{iso} + \{f_T^A\}_o^{int}) + \bar{c}_1 [G_T] [TRANS_{ID}] \{D_o\} \quad (5.6-23)$$

where $\{D_o\}$ is given by equation (3.5-70)

$$\begin{bmatrix} F_{XB_1}^A \\ F_{ZB_1}^A \\ M_{YB_1}^A \end{bmatrix}_R = \bar{q}_1 [G_{\theta R}] \{\Psi_M\}_1 + \bar{q}_1 [G_T] (\{f_T^A\}_1^{iso} + \{f_T^A\}_1^{int}) + \bar{q}_1 [G_T] [TRANS_{ID}] (\{D\}_1 - \{\Delta\}_1) \quad (5.6-24)$$

$$\begin{bmatrix} F_{XB_u}^A \\ F_{ZB_u}^A \\ M_{YB_u}^A \end{bmatrix}_R = \bar{q}_1 [G_T] \left\{ [TRANS_t] \left[2\{C_P^S\}_1^{iso} + M_1 \left\{ \frac{\partial C_P^S}{\partial M} \right\}_1^{iso} \right] + \right. \\ \left. + [TRANS_{ID}] (2\{D\}_1 + M_1 \left\{ \frac{\partial D}{\partial M} \right\}_1) \right\} \frac{1}{U_1} + \\ + \bar{q}_1 [G_T] [T_{TF}] [T_{FP}] (2\{C_P\}_1^{int} + M_1 \left\{ \frac{\partial C_P}{\partial M} \right\}_1^{int}) + (2[A_{F\theta}]_1 + M_1 \left[\frac{\partial A_{F\theta}}{\partial M} \right]_1) \{\psi\}_1 \frac{1}{U_1}
 \quad (5.6-25)$$

$$\begin{bmatrix} F_{XB_w}^A \\ F_{ZB_w}^A \\ M_{YB_w}^A \end{bmatrix}_R = \bar{q}_1 ([G_{\theta R}] + [Y_{\theta R}]) \{\tau_\alpha\} \frac{1}{U_1} - \bar{q}_1 [G_T] [TRANS_{ID}] (\Delta D_\alpha) \frac{1}{U_1}
 \quad (5.6-26)$$

$$\begin{bmatrix} F_{XB_Q}^A \\ F_{ZB_Q}^A \\ M_{YB_Q}^A \end{bmatrix}_R = \bar{q}_1 ([G_{\theta R}] + [Y_{\theta R}]) \{\tau_Q\} \frac{1}{U_1} - \bar{q}_1 [G_T] [TRANS_{ID}] (\Delta D_Q) \frac{1}{U_1}
 \quad (5.6-27)$$

$$\begin{bmatrix} F_{XB\delta e}^A \\ F_{ZB\delta e}^A \\ M_{YB\delta e}^A \end{bmatrix}_R = \bar{q}_1 ([G_{\theta R}] + [\mathcal{J}_{\theta R}]) \{\Psi_{\delta e}\} \quad (5.6-28)$$

5.6.4.2 Rigid aircraft lateral-directional static stability derivatives.—In the formulation of the lateral-directional static stability, the aerodynamics of the aircraft, equation (5.6-19), are assumed to be expressed for the antisymmetric case described by section 3.4.1.5. Using the notation defined by equations (5.6-2), but replacing the transformation to the Body Axis System, equation (5.6-21), with the transformation

$$[\mathcal{J}] \equiv \begin{bmatrix} 1 & 0 & 0 \\ 0 & -1 & 0 \\ 0 & 0 & -1 \end{bmatrix} \quad (5.6-29)$$

the formulas for the lateral-directional static stability derivatives are found as follows:

$$\begin{bmatrix} F_{Y\beta}^A \\ M_{XB\beta}^A \\ M_{ZB\beta}^A \end{bmatrix}_R = \bar{q}_1 ([G_{\theta R}] + [\mathcal{J}_{\theta R}]) \{\Psi_{\beta}\} \frac{1}{U_1} - \bar{q}_1 [G_T] [\text{TRANS}_{ID}] \{\Delta D_{\beta}\} \frac{1}{U_1} \quad (5.6-30)$$

$$\begin{bmatrix} F_{YB_P}^A \\ M_{XB_P}^A \\ M_{ZB_P}^A \end{bmatrix}_R = \bar{q}_1 ([G_{\theta R}] + [\mathcal{J}_{\theta R}]) \{\Psi_P\} \frac{1}{U_1} - \bar{q}_1 [G_T] [\text{TRANS}_{ID}] \{\Delta D_P\} \frac{1}{U_1} \quad (5.6-31)$$

$$\begin{bmatrix} F_{YB_R}^A \\ M_{XB_R}^A \\ M_{ZB_R}^A \end{bmatrix}_R = \bar{q}_1 [G_T] \left[[\text{TRANS}_t] [\bar{Y}_t] \left(2\{C_F^S\}_1^{\text{iso}} + M_1 \left\{ \frac{\partial C_P^{\text{iso}}}{\partial M} \right\}_1 \right) + \right. \\
\left. + [\text{TRANS}_{ID}] [\bar{Y}_c] \{D\}_1 \right] \frac{1}{U_1} + \bar{q}_1 ([G_{\theta R}] + [\mathcal{G}_{\theta R}]) \{\psi_R\} \frac{1}{U_1} + \bar{q}_1 [G_F] [\tilde{D}_1]^{-1} [T_{FP}] \times \\
\times [\bar{Y}_c] \left(2\{C_P\}_1^{\text{int}} + 2[A_{P\theta}] \{\psi\}_1 \right) \frac{1}{U_1} - \bar{q}_1 [G_T] [\text{TRANS}_{ID}] \{\Delta D_R\} \frac{1}{U_1} \quad (5.6-32)$$

$$\begin{bmatrix} F_{YB_{\delta a}}^A \\ M_{XB_{\delta a}}^A \\ M_{ZB_{\delta a}}^A \end{bmatrix}_R = \bar{q}_1 ([G_{\theta R}] + [\mathcal{G}_{\theta R}]) \{\psi_{\delta a}\} \quad (5.6-33)$$

$$\begin{bmatrix} F_{YB_{\delta r}}^A \\ M_{XB_{\delta r}}^A \\ M_{ZB_{\delta r}}^A \end{bmatrix}_R = \bar{q}_1 ([G_{\theta R}] + [\mathcal{G}_{\theta R}]) \{\psi_{\delta r}\} \quad (5.6-34)$$

5.6.4.3 Aeroelastic increments to the longitudinal static stability derivatives. The aeroelastic increments to the static stability derivatives are derived by applying the expansion of the aeroelastic matrix, section 5.3.4, to the perturbation aerodynamic forces, equation (5.6-19). Using the notation of section 5.6.4.1 and section 5.3.4 and using the approximation

which neglects the leading edge correction term in equation (5.6-19) given by equation (5.6-20), the formulas governing the aeroelastic increments are found to be given by the following equations with all matrices expressed for the symmetric case described by sections 3.4.1.5 and 4.2.5:

$$\begin{bmatrix} \Delta F_{XB_0}^A \\ \Delta F_{ZB_0}^A \\ \Delta M_{YB_0}^A \end{bmatrix}_E = \bar{q}_1 [G_{\theta E}] \{\psi_C\} + \bar{q}_1 [G_\theta] [\tilde{C}_{\theta T}]_1 \left(\{f_T^A\}_0^{iso} + \{f_T^A\}_0^{int} \right) \quad (5.6-35)$$

$$\begin{bmatrix} \Delta F_{XB_1}^A \\ \Delta F_{ZB_1}^A \\ \Delta M_{YB_1}^A \end{bmatrix}_E = \begin{bmatrix} \Delta F_{XB_0}^A \\ \Delta F_{ZB_0}^A \\ \Delta M_{YB_0}^A \end{bmatrix}_E + \bar{q}_1 [G_{\theta E}] \{\psi_M\}_1 \quad (5.6-36)$$

$$\begin{bmatrix} \Delta F_{XB_u}^A \\ \Delta F_{ZB_u}^A \\ \Delta M_{YB_u}^A \end{bmatrix}_E = \bar{q}_1 [G_\theta] [\tilde{C}_{\theta T}]_1 [TRANS_t] \left(2\{C_P^S\}_1^{iso} + M_1 \left\{ \frac{\partial C_P^S}{\partial M} \right\}_1 \right) \frac{1}{U_1} + \bar{q}_1 [G_F] [\Delta \tilde{D}^{-1}] [T_{FP}] \left(2\{C_F\}_1^{int} + M_1 \left\{ \frac{\partial C_F}{\partial M} \right\}_1^{int} \right) + \left(2[A_{F\theta}]_1 + M_1 \left[\frac{\partial A_{F\theta}}{\partial M} \right]_1 \right) \{\psi\}_1 \frac{1}{U_1} \quad (5.6-37)$$

$$\begin{bmatrix} \Delta F_{XB_w}^A \\ \Delta F_{ZB_w}^A \\ \Delta M_{YB_w}^A \end{bmatrix}_E = \bar{q}_1 [G_{\theta E}] \{\psi_\alpha\} \frac{1}{U_1} \quad (5.6-38)$$

$$\begin{bmatrix} \Delta F_{XB_Q}^A \\ \Delta F_{ZB_Q}^A \\ \Delta M_{YB_Q}^A \end{bmatrix}_E = \bar{q}_1 [G_{\theta E}] \{\psi_Q\} \frac{1}{U_1} \quad (5.6-39)$$

$$\begin{bmatrix} \Delta F_{XB_{\delta e}}^A \\ \Delta F_{ZB_{\delta e}}^A \\ \Delta M_{YB_{\delta e}}^A \end{bmatrix}_E = \bar{q}_1 [G_{\theta E}] \{\psi_{\delta e}\} \quad (5.6-40)$$

5.6.4.4 Aeroelastic increments to the lateral-directional static stability derivatives. –

Following the same approach as in section 5.6.4.3 immediately above, the formulas governing the aeroelastic increment to the lateral-directional static stability derivatives are given by the following equations with all matrices expressed for the antisymmetric case described by sections 3.4.1.5 and 4.2.5:

$$\begin{bmatrix} \Delta F_{YB_V}^A \\ \Delta M_{XB_V}^A \\ \Delta M_{ZB_V}^A \end{bmatrix}_E = \bar{q}_1 [G_{\theta E}] \{\psi_\beta\} \frac{1}{U_1} \quad (5.6-41)$$

$$\begin{bmatrix} \Delta F_{YB_P}^A \\ \Delta M_{XB_P}^A \\ \Delta M_{ZB_P}^A \end{bmatrix}_E = \bar{q}_1 [G_{\theta E}] \{\psi_P\} \frac{1}{U_1} \quad (5.6-42)$$

$$\begin{bmatrix} \Delta F_{YB_R}^A \\ \Delta M_{XB_R}^A \\ \Delta M_{ZB_R}^A \end{bmatrix}_E = \bar{q}_1^2 [G_\theta] [TRANS_t] [\bar{Y}_T] \left(2 \{C_P^S\}_1^{iso} + M_1 \left\{ \frac{\partial C_P^S}{\partial M} \right\}_1^{iso} \right) \frac{1}{U_1} + \\
 + \bar{q}_1^2 [\Delta G_{\theta E}] \{\psi_R\} \frac{1}{U_1} + (5.6-43) \\
 + 2 \bar{q}_1 [G_T] [T_{TF}] [L^{-1}]_1 [T_{FP}] [\bar{Y}_C] \left(\{C_P\}_1^{int} + \right. \\
 \left. + [A_{P\theta}]_1 \{\psi\}_1 \right) \frac{1}{U_1}$$

$$\begin{bmatrix} \Delta F_{YB_{\delta a}}^A \\ \Delta M_{XB_{\delta a}}^A \\ \Delta M_{ZB_{\delta a}}^A \end{bmatrix}_E = \bar{q}_1 [G_{\theta E}] \{\psi_{\delta a}\} \quad (5.6-44)$$

$$\begin{bmatrix} \Delta F_{YB_{\delta r}}^A \\ \Delta M_{XB_{\delta r}}^A \\ \Delta M_{ZB_{\delta r}}^A \end{bmatrix}_E = \bar{q}_1 [G_{\theta E}] \{\psi_{\delta r}\} \quad (5.6-45)$$

5.7 STATIC STABILITY AND TRIM CHARACTERISTICS

The static stability and trim characteristics computed by the FLEXSTAB system consist of the static stability derivatives listed by equations (5.6-3) and (5.6-4), the values of the trim variables listed in section 5.2.1, the static stability parameters (viz., stick speed stability, elevator angle per g, neutral point, static margin, and maneuver margin), the static loads the static elastic deformation, and the static aerodynamic pressure distributions on lifting surfaces. Expressions for the static stability derivatives and for the values of the trim variables are derived in the preceding. This section is aimed at the derivation of the remaining static stability and trim characteristics.

5.7.1 Static Stability Parameters

The static stability parameters are computed by FLEXSTAB neglecting the effects of the propulsion system and, except for the elevator angle per g parameter, the static stability parameters are for a steady, reference flight condition consisting of symmetric rectilinear flight. The equations of motion are expressed as

$$0 = C_{m_0} + C_{m_\alpha} \alpha_1 + C_{m_{\delta e}} \delta e_1 + C_{m_{\dot{Q}}} \hat{Q}_1 \quad (5.7-1)$$

and

$$C_{L_1} = C_{L_0} + C_{L_\alpha} \alpha_1 + C_{L_{\delta e}} \delta e_1 + C_{L_{\dot{Q}}} \hat{Q}_1 \quad (5.7-2)$$

where

$$C_{L_1} \equiv \frac{nW}{\bar{q}_1 S_W}$$

and

$$\hat{Q}_1 \equiv \frac{\dot{Q}_1 \bar{c}}{2V_{C_1}}$$

The pitch rate \dot{Q}_1 is determined by specifying the load factor n for two cases—steady pull-up

$$\dot{Q}_1 = \frac{(n-1)g}{V_{C_1}} \quad (5.7-3)$$

and steady turn

$$\dot{Q}_1 = \frac{n}{V_{C_1}} \left(1 - \frac{1}{n^2} \right) \quad (5.7-4)$$

The pull-up pitch rate, equation (5.7-3), is based on the assumption that the aircraft is at that point of the flight path where the flight path angle is zero; while the turn pitch rate, equation (5.7-4), is based on the assumptions appearing in section 9.8 of reference 2-2 (i.e., zero side force, $F_{YB_1} = 0$, and small, steady values for angle of attack, α_1 , and pitch attitude, θ_1).

5.7.1.1 Stick speed stability. Stick speed stability is defined as the derivative of the trim setting of the longitudinal control surface taken with respect to speed, i.e.,

$$\frac{d\delta_{e_1}}{dV_{C_1}}$$

Setting the pitch rate to zero and combining equations (5.7-1) and (5.7-2) yields the trim control setting for rectilinear flight as

$$\delta_{e1} = \frac{C_{L\alpha} C_{m_0} + C_{m_\alpha} (C_{L1} - C_{L0})}{C_{m_\alpha} C_{L\delta e} - C_{m_{\delta e}} C_{L\alpha}} \quad (5.7-5)$$

Differentiating this expression with respect to speed, noting that

$$\frac{d}{dv_{C1}} (C_{L1}) = -2 \frac{C_{L1}}{v_{C1}},$$

the stick speed stability is found to be given by

$$\begin{aligned} \left(\frac{d\delta_{e1}}{dv_{C1}} \right)_E &= \frac{1}{C_{m_\alpha} C_{L\delta e} - C_{L\alpha} C_{m_{\delta e}}} \left\{ \rho U_1 \left[C_{L\alpha} \frac{\partial C_{m_0}}{\partial \bar{q}_1} + C_{m_0} \frac{\partial C_{L\alpha}}{\partial \bar{q}_1} - \right. \right. \\ &\quad \left. \left. - C_{m_\alpha} \left(\frac{C_{L1}}{\bar{q}_1} + \frac{\partial C_{L0}}{\partial \bar{q}_1} \right) + (C_{L1} - C_{L0}) \frac{\partial C_{m_\alpha}}{\partial \bar{q}_1} - \right. \right. \\ &\quad \left. \left. - \delta_{e1} \left(C_{m_\alpha} \frac{\partial C_{L\delta e}}{\partial \bar{q}_1} + C_{L\delta e} \frac{\partial C_{m_\alpha}}{\partial \bar{q}_1} - C_{m_{\delta e}} \frac{\partial C_{L\alpha}}{\partial \bar{q}_1} - \right. \right. \right. \\ &\quad \left. \left. \left. - C_{L\alpha} \frac{\partial C_{m_{\delta e}}}{\partial \bar{q}_1} \right) \right] + \frac{1}{a_1} \left[(C_{L1} - C_{L0}) \frac{\partial C_{m_\alpha}}{\partial M} - C_{m_\alpha} \frac{\partial C_{L0}}{\partial M} + \right. \right. \\ &\quad \left. \left. + C_{L\alpha} \frac{\partial C_{m_\alpha}}{\partial M} + C_{m_0} \frac{\partial C_{L\alpha}}{\partial M} - \delta_{e1} \left(\frac{\partial C_{m_\alpha}}{\partial M} C_{L\delta e} + \right. \right. \right. \\ &\quad \left. \left. \left. + C_{m_\alpha} \frac{\partial C_{L\delta e}}{\partial M} - C_{L\alpha} \frac{\partial C_{m_{\delta e}}}{\partial M} - C_{m_{\delta e}} \frac{\partial C_{L\alpha}}{\partial M} \right) \right] \right\} \end{aligned} \quad (5.7-6)$$

where a_1 denotes the freestream speed of sound.

5.7.1.2 *Neutral point.* - The pitching moment due to angle of attack is given by

$$C_{m_\alpha} = (h - h_n) C_{L\alpha} \quad (5.7-7)$$

where

$$h = \frac{\bar{x}}{c}$$

with ξ defined as the distance aft from the leading edge of the reference chordline defined to the FLEXSTAB system. The coordinate ξ extends to the point where the pitching moment is measured (i.e., the location of the center of mass). The quantity h_n indicates the point about which C_{m_α} vanishes. This point is termed the neutral point and is given

$$h_n = h = C_{m_\alpha} / C_{L_\alpha} \quad (5.7-8)$$

5.7.1.3 Static margin.—The static margin is obtained from equation (5.7-7) as

$$h_n = h = -C_{m_\alpha} / C_{L_\alpha} \quad (5.7-9)$$

5.7.1.4 Elevator angle per g (pull-up).—The expression for elevator angle per g for a pull-up maneuver is derived from equations (5.7-1), (5.7-2), and (5.7-3) as in section 3.1 of reference 2-2 and is given by

$$\frac{\Delta \delta e}{n-1} = \frac{C_{m_\alpha} C_{L_1} + \frac{C_{L_1}}{2\mu} (C_{L_\alpha} C_{m_Q} - C_{m_\alpha} C_{L_Q})}{C_{L_\alpha} C_{m_{\delta e}} - C_{m_\alpha} C_{L_{\delta e}}} \quad (5.7-10)$$

where $\mu \equiv zM/\rho S \bar{c}$ is the relative mass.

5.7.1.5 Elevator angle per g (turn).—The expression for elevator angle per g for a turning maneuver is derived from equations (5.7-1), (5.7-2), and (5.7-4) as in section 9.8 of reference 2-2 and is given by

$$\frac{d\delta e}{dn} = \frac{1}{C_{m_\alpha} C_{L_{\delta e}} - C_{L_\alpha} C_{m_{\delta e}}} [C_{L_1} C_{m_\alpha} + \frac{C_{L_1}}{2\mu} (1 + \frac{1}{n^2}) (C_{L_\alpha} C_{m_Q} - C_{m_\alpha} C_{L_Q})] \quad (5.7-11)$$

5.7.1.6 Maneuver point.—The maneuver point is the center of mass location for which elevator angle per g vanishes for the pull-up maneuver, equation (5.7-10). The value of elevator angle per g vanishes when

$$C_{m_\alpha} + \frac{1}{2\mu} (C_{L_\alpha} C_{m_Q} - C_{m_\alpha} C_{L_Q}) = 0$$

Introducing equation (5.7-9), the maneuver point is found as

$$h_m = h_n - \left(\frac{C_{mQ}}{2\mu - C_{LQ}} \right) \quad (5.7-12)$$

5.7.2 Elastic Deformation

The FLEXSTAB system computes the elastic deformation arising from the reference flight condition aerodynamic, inertial, and propulsion system loads. This deformation is given by the following operations involving the flexibility relations developed in section 4, viz. The deformed camber shape is given by

$$\{\Psi_{c_{out}}\} = \{\Psi_{c_{in}}\} + \{\theta_{out}^*\} \quad (5.7-13)$$

where

$$\{\theta_{out}^*\} = [\tilde{C}_{\theta T}]\{f_T^A\}_1 + [\tilde{C}_{\theta T}]\{NP\}_T + [\tilde{C}_{\theta G}]\{M^G\}_1$$

The matrix $\{\Psi_{c_{in}}\}$ contains the initial camber shape, i.e., $\{\Psi_c\}$ in equations (3.5-44).

Translational deformation of the camber shape is given by

$$\{d_{out}^*\} = [\tilde{C}_{dT}]\{f_T^A\}_1 + [\tilde{C}_{dT}]\{NP\}_T + [\tilde{C}_{dT}]\{M^G\}_1 + \{d_{in}^*\} \quad (5.7-14)$$

where $\{d_{in}^*\}$ is an initial shape deformation which can be arbitrarily specified and

$$[\tilde{C}_{dT}] \equiv [P_d][\tilde{C}][P_T]^T, \quad [\tilde{C}_{\theta T}] \equiv [P_\theta][\tilde{C}][P_T]^T,$$

$$[\tilde{C}_{dG}] \equiv [P_d][\tilde{C}][\Delta_G] \text{ and } [\tilde{C}_{\theta G}] \equiv [P_\theta][\tilde{C}][\Delta_G]$$

The aerodynamic loads $\{f_T^A\}$ are found by combining equations ((5.3-6) and (5.3-7) with equations (5.3-7) evaluated for the trim motion variables ($\alpha_1, \beta_1, P_1, Q_1, R_1$) and the trim control surface settings ($\delta e_1, \delta a_1, \delta r_1$).

5.7.2.1 Jig shape computation.—The jig shape is the geometry of an aircraft used in laying out the fabrication jigs; and, because the structure is in a stress-free condition when it is supported in the fabrication jigs, the jig shape corresponds to zero applied loads. Aircraft which are very flexible have a design shape selected for a particular design point flight condition. Letting the aerodynamic and propulsion system loads appearing in equations (5.7-13) and (5.7-14) be those of the design point flight condition, the deformation given by equations (5.7-13) and (5.7-14) then represents the difference between the design and jig shapes.

The jig shape is computed by solving the trim problem for the design point flight condition with the aircraft treated as a rigid body having the design shape. The resulting aerodynamic and propulsion system loads are then inserted into equations (5.7-13) and 5.7-14). The camber $\{\theta_{out}^*\}$ computed from equation (5.7-13) is subtracted from the design shape camber $\{\Psi_{c_{in}}\}$ and the displacements $\{d_{out}^*\}$ computed from equation (5.7-14) are subtracted from the design shape coordinates of the thin body mean surfaces and slender body mean centerlines. These operations establish the jig coordinates.

5.7.2.2 Off-design point flight condition shapes.—When the static stability characteristics of a flexible aircraft are evaluated for any flight condition, the camber shape $\{\psi_C\}_1$ appearing in equation (5.3-7) must be the jig shape camber. The elastic deformation of the camber shape $\{\theta^*\}$ appearing in equation (5.3-7) is then the elastic deformation corresponding to the aerodynamic and propulsion system loads of the selected reference flight condition. Except for approximations to the inertial loads corresponding to those discussed in section 2.3.1.4 and approximations in computing aerodynamic couples, the camber shape $\{\psi_C\}_1$ leads to the correct aerodynamic loading of the aircraft.

Approximations related to the inertial loads arise in the computation of the flexibility matrix transformation, i.e.,

$$[P] = [I] - [m_\delta][\bar{\phi}_\delta][M]^{-1}[\bar{\phi}_\delta]^T, \quad (4.2-53)$$

and the rigid body inertia matrix, i.e.,

$$[M] = [\bar{\phi}_\delta]^T [m_\delta] [\bar{\phi}_\delta]. \quad (4.2-25)$$

These approximations stem from having used the rigid body mode shape matrix $[\bar{\phi}_\delta]$ based on the geometry of the jig shape. A similar approximation occurs in the computation of the moment of the aerodynamic loads about the aircraft center of mass, i.e.,

$$\{F_C\} = 2[\bar{\phi}^*]^T \{f^A\}. \quad (4.2-57)$$

The error in the analysis introduced by this approximation tends to be small, however, because the elastic displacement tends to be in the direction of the applied loads. Letting the displacement of the point at \vec{r} relative to the center of mass be denoted as \vec{d} , figure 2.3-3, and letting the applied force at \vec{r} be denoted as \vec{F} , the couple about the center of mass \vec{M} is given by

$$\vec{M} = (\vec{r} + \vec{d}) \times \vec{F};$$

but, because

$$\vec{d} \times \vec{F} \approx 0, \quad \vec{M} \approx \vec{r} \times \vec{F}.$$

Thus, the moment of the applied loads about the center of mass tends to be accurately predicted when the computation is based on the undeformed geometry of the jig shape. Increased accuracy can only be achieved by an iterative solution of the trim problem in which the rigid body mode shape matrix is updated at each iteration.

5.7.3 Static Loads and Pressure Distribution

5.7.3.1 Static loads.—The FLEXSTAB system computes static loads which may occur in either of two forms. One form consists of the net loads at the $\{\delta_{es}\}$ degrees of freedom, equation (4.3-180), at the elastic axis described in section 4.3.1. The second form consists

of the nodal components of forces (applied, net, and inertia loads) described in section 4.4.1.

The distributed static airloads $\{f_T^A\}$ are given by equation (5.3-6). These loads are combined with the engine thrust forces to yield applied structural loads

$$\{L_2\} \equiv \{Q^S\}$$

using the relation

(5.7-15)

$$\{Q^S\} = [P_T]^T \{f_T\}$$

where

$$\{f_T\} = \{f_T^A\} + \{NP\} T_1$$

Note that the contribution of gyroscopic couples is not included in the load vector; however, its effect has been included in the aeroelastic solution.

The matrix $\{Q^S\}$ describes the applied loads at the elastic axis nodes and junction points in terms of the $\{\delta_{es}\}$ degrees of freedom when the transformation $[P_T]$ is generated as in section 4.3.5, or $\{Q^S\}$ describes the nodal forces at the structural nodes when $[P_T]$ is generated as in section 4.4.3. The inertial loads are introduced by the transformation shown by either equation (4.2-53) or equation (4.3-208) leading to net loads, section 4.2.2.5,

$$\{L_1\} \equiv \{Q\} \quad (5.7-16)$$

and the net loads are found as

$$\{Q\} = [P] [P_T]^T \{f_T\}$$

or

(5.7-17)

$$\{Q\} \equiv [P_e]^T \{f_T\}$$

The inertial loads are found from the difference

$$\{L_{12}\} \equiv \{L_1\} - \{L_2\}$$

As noted above, the net loads are in terms of $\{\delta_{es}\}$ degrees of freedom when the structure is defined as an elastic axis. When the structural properties are input to the FLEXSTAB system, section 4.4, the loads contain either one, two, or three components of force at each structural node point of the structural representation, cf., section 4.4.5. The contribution of thrust is found as

$$\begin{aligned}
\{L_1^T\} &= [P_e]^T \{NP\} T_1 \\
\{L_2^T\} &= [P_T]^T \{NP\} T_1 \\
\{L_{12}^T\} &= \{L_1^T\} - \{L_2^T\}
\end{aligned}
\tag{5.7-17a}$$

Only the actual net loads $\{L_1\}$ and $\{L_1^T\}$ are formed in FLEXSTAB when the elastic axis method is used.

In addition to the loads computed by equation (5.7-15), the airload shear, bending, and torsion can be computed at any selected point $(X(A), Y(A), Z(A))$ in the Reference Axis System when the structural properties are input to the FLEXSTAB system as in section 4.4. These loads are given by the formulas

$$\vec{F}(A) = \int_{S(A)} P \vec{n} dS$$

and

$$\vec{M}(A) = \int_{S(A)} P [\vec{r} - \vec{r}(A)] \times \vec{n} dS$$

(5.7-18)

where $S(A)$ is the aerodynamic surface of the aircraft participating in the computation. This is the aerodynamic surface contained in a rectangular parallelepiped volume of space defined in the Reference Axis System by the FLEXSTAB user. The position $\vec{r}(A)$ is the point, in the Reference Axis System, where the airload resultants, $\vec{F}(A)$ and $\vec{M}(A)$, are measured and \vec{r} is the point, in the Reference Axis System, where the pressure and surface normal are evaluated in the surface integration. The integration process, however, is simply a numerical summation over the airloads $\{f_t^A\}$ acting at the aerodynamic centroids of the aerodynamic segments contained in the rectangular parallelepiped volume.

5.7.3.2 Reference flight condition aerodynamic lifting pressure distribution.—The reference flight condition aerodynamic lifting pressure distribution is computed from the aerodynamic surface forces shown by equation (5.3-4) including the direct lifting pressure forces from thickness interference. The resulting lifting pressure forces are denoted as $\{\Delta \mathcal{F}_P\}$ and the lifting pressure is computed by the formula

$$\{\Delta C_P\} = [T_{\Delta P}]\{\Delta \mathcal{F}_P\} \quad (5.7-19)$$

where the aerodynamic forces coefficients are given by

$$\begin{aligned} \{\Delta \mathcal{F}_P\} = [\tilde{D}]^{-1} \{ & [A_{F\theta}] \left[\{\psi_C\}_1 + \{\psi_M\}_1 + [\tilde{C}_{\theta T}]\{NP\}T_1 \right. \\ & \left. + [\tilde{C}_{\theta G}]\{M^G\}_1 + [\tilde{C}_{\theta T}]\{f_t^A\}^{iso} \right] + \{\Delta \mathcal{F}_P^t\} \} \end{aligned} \quad (5.7-20)$$

wherein $\{\Delta \mathcal{F}_P^t\} \equiv [T_{FP}]\{C_P\}^{int}$
and $[T_{\Delta P}]$ is a matrix of surface area reciprocals, viz.,

$$[T_{\Delta P}] \equiv \left[\begin{array}{c|c} [1/A_B] & \text{zeros} \\ \hline \text{zeros} & [1/A_W] \end{array} \right] \quad (5.7-21)$$

where $[1/A_W]$ contains the surface areas of the thin body mean surface panels and $[1/A_B]$ contains the reciprocals of the areas as slender body segments projected on XZ and XY planes of the Reference Axis System. The matrix of pressure coefficients, $\{\Delta C_P\}$, therefore, contains the Y and Z components of average slender body segment lifting pressures and the thin body panel lifting pressures.

5.7.3.3 Airloads due to a vertical gust during 1-g level flight.—The objective of this section is to describe a method available in the FLEXSTAB system for determining the airloads resulting from a vertical gust neglecting the effects of gust penetration and neglecting the dynamic response of the aircraft to the gust airloads. The aircraft is initially trimmed in a state of steady level flight and is then instantaneously and completely immersed in a uniform gust velocity flow in the Z-direction of the Reference Axis System. This flow results in a change in angle of attack $\Delta\alpha$ leading to gust airloads which are evaluated at the instant of time when the aircraft is immersed in the gust. Structural deformation is assumed to occur quasistatically and the only inertial loads contributing to the deformation are the result of the rigid body acceleration arising from the gust airloads.

The incremental angle of attack is computed from the formula

$$\Delta\alpha = K_g \frac{U_{de}}{g V_{EAS}} MF \quad (5.7-22)$$

where K_g is the gust alleviation factor given by

$$K_g = \frac{.88\mu_g}{5.3 + \mu_g}$$

the quantity μ_g being the airplane mass ratio

$$\mu_g = \frac{2(M/S_W)}{\rho_1 \bar{c} (F_{ZB\alpha}^A)_E}$$

wherein $(F_{ZB\alpha}^A)_E$ is the aerodynamic derivative given by equation (5.3-14); the quantity V_{EAS} is the equivalent airspeed, viz.,

$$V_{EAS} = U_1 \sqrt{\frac{\rho_H}{\rho_0}}$$

the quantities ρ_H and ρ_0 being, respectively, the air densities at altitude and at sea level; the quantity U_{de} is the derived gust velocity in feet per second; and MF is a magnification factor. The values of U_{de} and MF may be arbitrarily selected provided $\Delta\alpha$ is sufficiently small for the linear aerodynamic theory of section 3 to be valid.

The airloads are computed by equation (5.7-20) but incorporating the flow incidence due to the gust flow field, i.e.,

$$\begin{aligned} \{F_g^A\} = & [\tilde{D}]^{-1} \left\{ [A_{F\theta}] [\{\psi_c\}_1 + \{\psi_M\}_1 + \{\psi_\alpha\} \Delta\alpha \right. \\ & \left. + [\tilde{C}_{\theta G}] \{M^G\}_1 + [\tilde{C}_{\theta T}] \{f_T^A\}_1^{iso} \right\} + \{\Delta F_P^t\} \end{aligned} \quad (5.7-23)$$

5.8 IMPLEMENTATION OF EMPIRICAL AERODYNAMIC CORRECTION METHODS

To avoid complicating the development in preceding portions of section 5, the effects of the empirical aerodynamic correction methods were not included. These effects are introduced in this section, and they lead to modifications to the equations governing the aerodynamic derivatives of section 5.3 and the static stability derivatives of section 5.6. The corrections are readily incorporated into the equations of sections 5.3 and 5.6 either by regarding certain matrices to be modified by the empirical corrections or by adjoining additional terms. Also, in most cases the development of the modified equations exactly parallels the development of the corresponding uncorrected equations appearing in the preceding. In these cases the appropriate sections and equations of the preceding are cited and the details of the development are not repeated in their entirety.

5.8.1 Correction of the Steady Aerodynamic Influence Coefficients

Methods for making corrections to the steady aerodynamic influence coefficients were introduced by items (1), (2), and (3) of section 3.4.14. These correction methods modify the values of the elements of the matrix denoted as $[LSC]$ and defined by equation (3.4-170); they correct (or change) the linear relationship

$$\{C_p\} = [LSC]\{\psi\} \quad (3.4-169)$$

The modified matrix is reduced, as described in section 3.5.2, and formed into the steady aerodynamic matrices $[A_{p\theta}]$ and $[A_{F\theta}]$ appearing in the preceding portions of section 5. Throughout the preceding portions of section 5 and in this section the matrices $[LSC]$, $[A_{p\theta}]$, and $[A_{F\theta}]$ may be corrected or uncorrected with no distinction in notation.

5.8.2 Aerodynamic Surface Area Corrections

The aerodynamic surface area corrections were not introduced by section 3.4.14; they modify the values of the elements of the surface pressure transformation matrices $[T_{FP}]$ and $[TRANS_t]$ introduced by section 3.5.

The purpose of the aerodynamic surface area corrections is to correct discrepancies between the surface areas of actual aircraft components and the surface areas made up by the aerodynamic panel areas, S_{Wij} and S_{BJj} , used in constructing solutions to the aerodynamic problems in section 3.4. The aerodynamic panels must lie in streamwise rows having streamwise edges. (See figures 3.4-1, 3.4-6, and 3.4-7.) This requirement leads to thin body mean surface planforms which cannot always precisely match the mean surface planforms of the thin bodies being represented, figure 5.8-1, thereby causing an area discrepancy. A second case of area discrepancy is illustrated by the wing-body-tail configuration shown by figure 3.4-8. In this case the surface areas of all three components—wing, body, and tail—are distorted by the requirement that the mean surface of the body must be a cylinder with generator parallel to the X-axis of the Reference Axis System.

In either of the preceding examples, the distorted geometry represented by the panels leads to an aerodynamic pressure prediction that is an adequate first-order approximation. The assumption that the predicted pressure acts on the panel areas, however, can lead to an

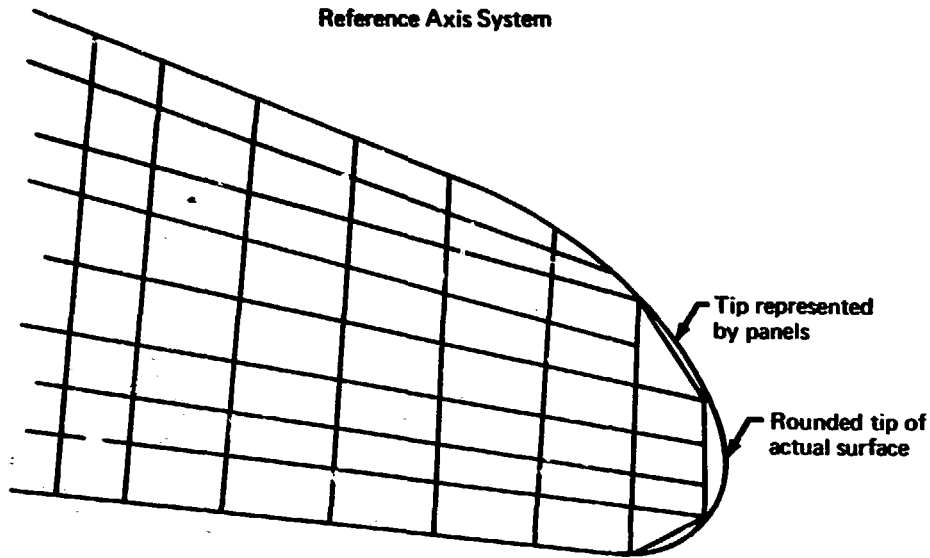


FIGURE 5.8-1.—PANELING OF A ROUNDED THIN BODY TIP

inadequate approximation to the aerodynamic forces. An improved approximation can be obtained by computing the aerodynamic forces arising from action of the aerodynamic surface pressure on the actual surface areas. This improved approximation is acquired by the FLEXSTAB system by scaling the panel areas, equations (3.4-1) and (3.4-2), so that their scaled areas sum to the actual surface areas of the thin and slender bodies.

The panel areas S_{WIi} and S_{BJj} are multiplied by area factors $(AF)_k$ before they are incorporated into the transformation matrices, $[T_{FP}]$ and $[TRANS_t]$, which transform the aerodynamic surface pressure into forces acting on the panels. A typical panel area correction is carried out as

$$S_{WIi} = (AF)_k S'_{WIi} \quad (5.8-1)$$

where S'_{WIi} denotes the area of a panel to be corrected. The values of the area factors can be greater or less than unity, thereby allowing the scaled areas to be greater or less than the areas of the original panels.

The area factors can be given any numerical values required to make the panel areas match, in value, the areas of regions of the actual surface. In general, however, the area factors should have numerical values that differ very little from the value unity; very large or very small values imply an inappropriate application of this correction method.

5.8.3 Corrections to Flow Incidence and Steady Lifting Pressure

Item (4) of section 3.4.14 introduces corrections to the flow incidence and steady lifting pressure by adding four terms to equation (3.4-218), leading to equation (3.4-241) viz.,

$$\{C_P\} = [A]\{\Psi\} + \frac{1}{U_1}[\delta A]\{\dot{\Psi}\} + \underline{[LSC]}\{\Psi'\} + \underline{\{\Delta C_{P_o}\} + \{\Delta C_{P_\alpha}\}_\alpha + \{\Delta C_{P_\beta}\}_\beta} \quad (5.8-2)$$

where the added terms are underlined. The flow incidence matrix $\{\Psi'\}$ is supplied to the FLEXSTAB system by supplying the column matrices appearing in the following flow incidence expression:

$$\{\Psi'\} = \{\Psi'_0\} + \{\Psi'_M\} \quad (5.8-3)$$

where

$$\begin{aligned} \{\Psi'_M\} \equiv & \{\Psi'_\alpha\}_\alpha + \{\Psi'_\beta\}_\beta + \{\Psi'_P\}\frac{P}{U_1} + \{\Psi'_Q\}\frac{q}{U_1} \\ & + \{\Psi'_R\}\frac{r}{U_1} + \{\Psi'_{\delta e}\}_{\delta e} + \{\Psi'_{\delta a}\}_{\delta a} + \{\Psi'_{\delta r}\}_{\delta r} \end{aligned}$$

Equation (5.8-2), combined with equation (5.8-3), is used to play the role of equation (3.4-218) in the derivation of the expression for the reference flight condition aerodynamic forces, equation (3.5-58). The development then parallels that of sections 5.3.3 and 5.3.4, resulting in corrections to the aerodynamic derivatives. Corrections to the static stability derivatives are found by using equation (5.8-2) in lieu of equation (3.4-218) in the derivation of equation (5.6-19), i.e., the expression governing the aerodynamic forces generated by static perturbations about the reference flight condition. This development parallels that of section 5.6.4.

5.8.3.1 Corrected reference flight condition aerodynamic forces.—The empirically corrected reference flight condition aerodynamic forces for a rigid aircraft are derived, as noted earlier, by replacing equation (3.4-218) with equation (5.8-2) in the derivation leading to equation (5.3-22). This derivation leads to the following result:

$$\begin{aligned}
\{F_B^A\}_R &= [G_T] \left(\{f_T^A\}_1^{iso} + \{f_T^A\}_1^{int} \right) + \bar{q}_1 [G_{\theta R}] (\{\psi_c\} \\
&+ \{\psi_M\}_1 + \bar{q}_1 [G_{\psi R}] (\{\psi_o'\}_1 + \{\psi_M'\}_1) \\
&+ \bar{q}_1 [G_F] [T_{FP}] [\bar{q}_c]_1 (\{\Delta C_{P_o}\} + \{\Delta C_{P_\alpha}\} \alpha_1 + \{\Delta C_{P_\beta}\} \beta_1)
\end{aligned} \tag{5.8-4}$$

where

The empirically corrected reference flight condition aerodynamic forces for a flexible aircraft are obtained by expressing equation (5.3-7) using equation (5.8-2) and by carrying out the development leading to equation (5.3-11). The expansion of the aeroelastic matrix, section 5.3.4.1, is then introduced to find the corrected expression for the aeroelastic increment to the reference flight condition aerodynamic forces. The result is as follows:

$$[G_{\psi R}] \equiv [G_F] [T_{FP}] [\bar{q}_c]_1 [LSC]$$

$$\begin{aligned}
\{\Delta F_B^A\}_E &= \bar{q}_1 [G_\theta] [\tilde{C}_{\theta T}] \left(\{f_T^A\}_1^{iso} + \{f_T^A\}_1^{int} \right) + \\
&+ \bar{q}_1 [G_{\theta E}] (\{\psi_c\} + \{\psi_M\}_1) + \\
&+ \bar{q}_1 [G_{\psi E}] (\{\psi_o'\}_1 + \{\psi_M'\}_1) + \\
&+ \bar{q}_1 [G_F] [\tilde{\Delta D}^{-1}]_1 [T_{FP}] [\bar{q}_c]_1 (\{\Delta C_{P_o}\} + \\
&+ \{\Delta C_{P_\alpha}\} \alpha_1 + \{\Delta C_{P_\beta}\} \beta_1)
\end{aligned} \tag{5.8-5}$$

where

$$[G_{\psi E}] \equiv [G_\psi] - [G_{\psi R}]$$

and

$$[G_\psi] \equiv [G_F] [\tilde{D}]_1^{-1} [T_{FP}] [\bar{q}_c]_1 [LSC]$$

The equations governing the empirically corrected aerodynamic derivatives and their aeroelastic increments are deduced directly from equations (5.8-4) and (5.8-5). The desired results

are of two types: (1) the coefficients of the quantities α_1 , β_1 , P_1 , Q_1 , R_1 , u_{e1} , δa_1 , and δr_1 , and (2) the values of equations (5.8-4) and (5.8-5) when these quantities are all set to zero.

5.8.3.2 Corrected longitudinal aerodynamic derivatives for a rigid aircraft.—Letting the matrices in equation (5.8-4) be expressed for the symmetric aircraft case (see sections 3.4.1.5 and 4.2.5), the longitudinal aerodynamic derivatives are found to be as follows.

$$\begin{bmatrix} F_{XB_0}^A \\ F_{ZB_0}^A \\ M_{YB_0}^A \end{bmatrix}_R = [G_T] \left(\{f_T^A\}_1^{iso} + \{f_T^A\}_1^{int} \right) + \bar{q}_1 [G_{\theta R}] \{\psi_c\} + \bar{q}_1 \left([G_{\theta R}] \{\psi_o'\} + [G_F] [T_{FP}] \{\Delta C_{P_o}\} \right) \quad (5.8-6)$$

$$\begin{bmatrix} F_{XB_\alpha}^A \\ F_{ZB_\alpha}^A \\ M_{YB_\alpha}^A \end{bmatrix}_R = \bar{q}_1 [G_{\theta R}] \{\psi_\alpha\} + \bar{q}_1 \left([G_{\psi R}] \{\psi_\alpha'\} + [G_F] [T_{FP}] \{\Delta C_{P_\alpha}\} \right) \quad (5.8-7)$$

$$\begin{bmatrix} F_{XB_Q}^A \\ F_{ZB_Q}^A \\ M_{YB_Q}^A \end{bmatrix}_R = \bar{q}_1 [G_{\theta R}] \{\psi_Q\} \frac{1}{U_1} + \bar{q}_1 [G_{\psi R}] \{\psi_Q'\} \frac{1}{U_1} \quad (5.8-8)$$

$$\begin{bmatrix} F_{XB\delta e}^A \\ F_{ZB\delta e}^A \\ M_{YB\delta e}^A \end{bmatrix}_R = \bar{q}_1 [G_{\theta R}] \{\psi_{\delta c}\} + \bar{q}_1 [G_{\psi R}] \{\psi'_{\delta e}\} \quad (5.8-9)$$

5.8.3.3 Corrected lateral-directional aerodynamic derivatives for a rigid aircraft.—Letting all of the matrices in equation (5.8-4) be expressed for the antisymmetric aircraft case (see sections 3.4.1.5 and 4.2.5), the lateral-directional aerodynamic derivatives are found to be as follows:

$$\begin{bmatrix} F_{YB\beta}^A \\ M_{XB\beta}^A \\ M_{ZB\beta}^A \end{bmatrix}_R = \bar{q}_1 [G_{\theta R}] \{\psi_{\beta}\} + \bar{q}_1 ([G_{\psi R}] \{\psi'_{\beta}\} + [G_F] [T_{FP}] \{\Delta C_{P_{\beta}}\}) \quad (5.8-10)$$

$$\begin{bmatrix} F_{YB_P}^A \\ M_{XB_P}^A \\ M_{ZB_P}^A \end{bmatrix}_R = \bar{q}_1 [G_{\theta R}] \{\psi_P\} \frac{1}{U_1} + \bar{q}_1 [G_{\psi R}] \{\psi'_P\} \frac{1}{U_1} \quad (5.8-11)$$

$$\begin{bmatrix} F_{YB_R}^A \\ M_{XB_R}^A \\ M_{ZB_R}^A \end{bmatrix}_R = \bar{q}_1 [G_{\theta R}] \{\psi_R\} \frac{1}{U_1} + \bar{q}_1 [G_{\psi R}] \{\psi'_R\} \frac{1}{U_1} + \quad (5.8-12) \\
 + \bar{q}_1 [G_T] [TRANS_t] [\bar{Y}_t] \left(2 \{C_P^S\}_1^{iso} + \right. \\
 \left. + M_1 \left\{ \frac{\partial C_P^S}{\partial \beta} \right\}_1^{iso} \right) + 2 [T_{TF}] [T_{FP}] [\bar{Y}_c] \{C_P\}_1^{int} \frac{1}{U_1}$$

$$\begin{bmatrix} F_{YB_{\delta a}}^A \\ M_{XB_{\delta a}}^A \\ M_{ZB_{\delta a}}^A \end{bmatrix}_R = \bar{q}_1 [G_{\theta R}] \{\psi_{\delta a}\} + \bar{q}_1 [G_{\psi R}] \{\psi'_{\delta a}\}$$

$$\begin{bmatrix} F_{YB_{\delta r}}^A \\ M_{XB_{\delta r}}^A \\ M_{ZB_{\delta r}}^A \end{bmatrix}_R = \bar{q}_1 [G_{\theta R}] \{\psi_{\delta r}\} + \bar{q}_1 [G_{\psi R}] \{\psi'_{\delta r}\} \quad (5.8-14)$$

5.8.3.4 *Corrected aeroelastic increments to the longitudinal aerodynamic derivatives.*--
 Letting all of the matrices in equation (5.8-5) be expressed for the symmetric aircraft case (see sections 3.4.1.5 and 4.2.5), the aeroelastic increments to the longitudinal aerodynamic derivatives are found to be as follows:

$$\begin{bmatrix} \Delta F_{XB_0}^A \\ \Delta F_{ZB_0}^A \\ \Delta M_{YB_0}^A \end{bmatrix}_E = \bar{q}_1 [G_\theta] [\tilde{C}_{\theta T}] (\{f_T^A\}_1^{iso} + \{f_T^A\}_1^{int}) + \quad (5.8-15) \\
 + \bar{q}_1 [G_{\theta E}] \{\psi_\theta\} + \bar{q}_1 [G_{\psi E}] \{\psi_\theta'\} + \\
 + \bar{q}_1 [G_F] [\Delta D^{-1}]_1 [T_{FP}] \{\Delta C_{P_0}\}$$

$$\begin{bmatrix} \Delta F_{XB_\alpha}^A \\ \Delta F_{ZB_\alpha}^A \\ \Delta M_{YB_\alpha}^A \end{bmatrix}_E = \bar{q}_1 [G_{\theta E}] \{\psi_\alpha\} + \bar{q}_1 [G_{\psi E}] \{\psi_\alpha'\} + \quad (5.8-16) \\
 + \bar{q}_1 [G_F] [\Delta D^{-1}]_1 [T_{FP}] \{\Delta C_{P_\alpha}\}$$

$$\begin{bmatrix} \Delta F_{XB_Q}^A \\ \Delta F_{ZB_Q}^A \\ \Delta M_{YB_Q}^A \end{bmatrix}_E = \bar{q}_1 [G_{\theta E}] \{\psi_Q\} \frac{1}{U_1} + \bar{q}_1 [G_{\psi E}] \{\psi_Q'\} \frac{1}{U_1} \quad (5.8-17)$$

$$\begin{bmatrix} \Delta F_{XB_{\delta e}}^A \\ \Delta F_{ZB_{\delta e}}^A \\ \Delta M_{YB_{\delta e}}^A \end{bmatrix}_E = \bar{q}_1 [G_{\theta E}] \{\psi_{\delta e}\} + \bar{q}_1 [G_{\psi E}] \{\psi_{\delta e}'\}$$

5.8.3.5 Corrected aeroelastic increments to the lateral-directional aerodynamic derivatives.—Letting all of the matrices in equation (5.8-5) be expressed for the antisymmetric aircraft case (see sections 3.4.1.5 and 4.2.5), the aeroelastic increments to the lateral-directional aerodynamic derivatives are found to be as follows:

$$\begin{bmatrix} \Delta F_{YB_\beta}^A \\ \Delta M_{XB_\beta}^A \\ \Delta M_{ZB_\beta}^A \end{bmatrix}_E = \bar{q}_1 [G_{\theta E}] \{\psi_\beta\} + \bar{q}_1 \left([G_{\psi E}] \{\psi'_\beta\} + [G_F] [\Delta \tilde{D}^{-1}]_1 [T_{FP}] [\bar{q}_c]_1 \{\Delta C_{P_\beta}\} \right) \quad (5.8-19)$$

$$\begin{bmatrix} \Delta F_{YB_P}^A \\ \Delta M_{XB_P}^A \\ \Delta M_{ZB_P}^A \end{bmatrix}_E = \bar{q}_1 [G_{\theta E}] \{\psi_P\} \frac{1}{U_1} + \bar{q}_1 [G_{\psi E}] \{\psi'_P\} \frac{1}{U_1} \quad (5.8-20)$$

$$\begin{bmatrix} \Delta F_{YB_R}^A \\ \Delta M_{XB_R}^A \\ \Delta M_{ZB_R}^A \end{bmatrix}_E = \bar{q}_1 [G_{\theta E}] \{\psi_R\} \frac{1}{U_1} + \bar{q}_1 [G_{\psi E}] \{\psi'_R\} \frac{1}{U_1} + 2\bar{q}_1 [G_F] [\Delta \tilde{D}^{-1}]_1 [T_{FP}] [\bar{q}_c]_1 \left(\{C_P\}_1^{int} + \{C_P\}_1 \right) \frac{1}{U_1} + \bar{q}_1 [G_\theta] [\tilde{C}_{\theta T}] [TRANS_t] [\bar{q}_t]_1 \left(2 \{C_P\}_1^{iso} + M_1 \left\{ \frac{\partial C_P^S}{\partial M} \right\}_1^{iso} \right) \frac{1}{U_1} \quad (5.8-21)$$

$$\begin{bmatrix} \Delta F_{YB}^A \\ \Delta M_{XB}^A \\ \Delta M_{ZB}^A \end{bmatrix}_{\delta a} = \bar{q}_1 [G_{\theta E}] \{\psi_{\delta a}\} + \bar{q}_1 [G_{\psi E}] \{\psi'_{\delta a}\} \quad (5.8-22)$$

$$\begin{bmatrix} \Delta F_{YB}^A \\ \Delta M_{XB}^A \\ \Delta M_{ZB}^A \end{bmatrix}_{\delta r} = \bar{q}_1 [G_{\theta E}] \{\psi_{\delta r}\} + \bar{q}_1 [G_{\psi E}] \{\psi'_{\delta r}\} \quad (5.8-23)$$

5.8.3.6 Corrected static perturbation aerodynamic force.—The corrected aerodynamic forces resulting from static perturbations about the reference flight condition are found by introducing the underlined terms appearing in equation (5.8-2) into the development leading to equation (5.6-19), neglecting the terms identified by equation (5.6-20). This development leads to modified matrix expressions for the leading edge thrust correction, section 3.4.12, and to the following terms which must be added to equation (5.6-20):

$$\begin{aligned} \Delta \{f_T^A\}_P = & \bar{q}_1 [T_{TF}] [\tilde{D}]_1^{-1} \left\{ \left[\left(2[A_{F\psi}]_1 + M_1 \left[\frac{\partial A_{F\psi}}{\partial M} \right]_1 \right) \{\psi'\}_1 + \right. \right. \\ & + 2[T_{FP}] [\bar{q}_c]_1 \left(\{\Delta C_{P_o}\} + \{\Delta C_{P_\alpha}\} \alpha_1 + \{\Delta C_{P_\beta}\} \beta_1 \right) \left. \right] \frac{u}{U_1} + \\ & + 2[T_{FP}] [\bar{Y}_c] \left([LSC] \{\psi'\}_1 + \{\Delta C_{P_o}\} + \{\Delta C_{P_\alpha}\} \alpha_1 + \right. \\ & + \{\Delta C_{P_\beta}\} \beta_1 \left. \right) \frac{r}{U_1} + [A_{F\psi}] \{\psi'_M\}_P + [T_{FP}] [\bar{q}_c]_1 \left(\{\Delta C_{P_\alpha}\} \alpha + \right. \\ & + \left. \{\Delta C_{P_\beta}\} \beta \right) \left. \right\} + \bar{q}_1 [TRANS_{ID}] [\bar{q}_c]_1 [D_{P\psi}] \{\psi'_M\}_1 \end{aligned} \quad (5.8-24)$$

where

$$[A_{F\Psi}] \equiv [T_{FP}][\bar{q}_c]_1 [LSC] \quad (5.8-25)$$

and

$$[D_{P\Psi}] \equiv \{w_I\}_1 \otimes [LSC] + \{C_P\}_1 \otimes [ISC_\Psi] \quad (5.8-26)$$

where

$$\begin{aligned} \{w_I\}_1 &\equiv [ISC_\theta]\{\Psi\}_1 + [ISC_\Psi]\{\Psi'\}_1 - \alpha_1 \left[\frac{\{Q\}}{\{LEC\} \otimes \{\Psi_\alpha\}} \right] \\ &\quad - \frac{Q_1}{U_1} \left[\frac{\{Q\}}{\{LEC\} \otimes \{\Psi_Q\}} \right] \end{aligned} \quad (5.8-27)$$

and

$$\begin{aligned} \{C_P\}_1 &\equiv [A_{P\theta}]\{\Psi\}_1 + [LSC]\{\Psi'\}_1 + \{\Delta C_{P_0}\} \\ &\quad + \{\Delta C_{P_\alpha}\}\alpha_1 + \{\Delta C_{P_\beta}\}\beta_1 \end{aligned} \quad (5.8-28)$$

The modified leading edge thrust correction terms are given by the following equations using the two matrices defined by equations (5.8-27) and (5.8-28):

$$\{D\}_1 = \{w_I\}_1 \otimes \{C_P\}_1, \quad (5.8-29)$$

$$\begin{aligned} \left\{ \frac{\partial D}{\partial M} \right\}_1 &= \{w_I\}_1 \otimes \left(\left[\frac{\partial A_{P\theta}}{\partial M} \right] \{\Psi\}_1 + \left[\frac{\partial LSC}{\partial M} \right] \{\Psi'\}_1 \right) + \\ &\quad + \{C_P\}_1 \otimes \left(\left[\frac{\partial ISC_\theta}{\partial M} \right] \{\Psi\}_1 + \left[\frac{\partial ISC_\Psi}{\partial M} \right] \{\Psi'\}_1 \right) \end{aligned} \quad (5.8-30)$$

and

$$\begin{aligned} \{\Delta D\}_P &= \{\Delta D_\alpha\}\alpha + \{\Delta D_\beta\}\beta + \{\Delta D_P\}p + \{\Delta D_Q\}q \\ &+ \{\Delta D_R\}r \end{aligned} \quad (5.8-31)$$

where

$$\begin{aligned} \{\Delta D_\alpha\} &\equiv ([A_{P\theta}]\{\psi\}_1 + [LSC]\{\psi'\}_1 + \{C_{P_0}\} + \\ &+ \{C_{P_\alpha}\}\alpha_1 + \{C_{P_\beta}\}\beta_1) \equiv \{\Delta w_{I_\alpha}\} \end{aligned} \quad (5.8-32)$$

and the remaining column matrices in the left-hand member of equation (5.8-31) are similarly defined, cf., equation (3.5-72).

5.8.3.7 Corrected longitudinal static stability derivatives for a rigid aircraft.—Setting the structural flexibility to zero and assuming that all of the matrices in equation (5.8-24) are expressed for the symmetric aircraft case (see section 3.4.1.5), the empirically corrected forms of the equations in section 5.6.4.1 are found to be as follows:

$$\begin{bmatrix} \dot{r} \\ X_{B_0} \\ F_{ZB_0}^A \\ M_{\dot{v}B_0}^A \end{bmatrix}_R = \bar{q}_1 [G_{\theta R}]\{\psi_c\} + \bar{q}_1 [G_T] \left(\{f_T^A\}_1^{iso} + \{f_T^A\}_1^{int} \right) + (5.8-33) \\ + \bar{q}_1 [G_T][TRANS_{ID}]\{D_0\} + \bar{q}_1 [G_F][T_{FP}]\{\Delta C_{P_0}\}$$

where

$$\begin{aligned} \{D_0\} &\equiv ([ISC_\theta]\{\psi_c\} + [ISC_\psi]\{\psi'_0\}) \equiv ([A_{P\theta}]\{\psi_c\} \\ &+ [LSC]\{\psi'_0\} + \{\Delta C_{P_0}\}) \end{aligned}$$

$$\begin{bmatrix} F_{XB_1}^A \\ F_{ZB_1}^A \\ F_{YB_1}^A \end{bmatrix}_R = \bar{q}_1 [G_{\theta R}] \{\Psi\}_1 + \bar{q}_1 [G_T] \left(\{f_T^A\}_1^{iso} + \{f_T^A\}_1^{int} \right) + \bar{q}_1 [G_T] [TRANS_{ID}] \left(\{D\}_1 - \{\Delta D\}_1 \right) + \bar{q}_1 [G_T] [T_{FP}] \left(\{\Delta C_{P_o}\} + \{\Delta C_{P_\alpha}\} \alpha_1 + \{\Delta C_{P_\beta}\} \beta_1 \right) \quad (5.8-34)$$

where

$$\{\Delta D\}_1 = \{\Delta D_\alpha\} \alpha_1 + \{\Delta D_\beta\} \beta_1 + \{\Delta D_P\} P_1 + \{\Delta D_Q\} Q_1 + \{\Delta D_R\} R_1$$

$$\begin{bmatrix} F_{XB_u}^A \\ F_{ZB_u}^A \\ M_{YB_u}^A \end{bmatrix}_R = \bar{q}_1 [G_T] \left\{ [TRANS_t] \left(2\{C_P^S\}_1^{iso} + M_1 \left\{ \frac{\partial C_P^S}{\partial M} \right\}_1^{iso} \frac{1}{U_1} \right) + [TRANS_{ID}] \left[2\left(\{D\}_1 - \{\Delta D\}_1 \right) + M_1 \left\{ \frac{\partial D}{\partial M} \right\}_1 \right] \right\} \frac{1}{U_1} + \bar{q}_1 [G_T] [T_{TF}] \left[[T_{FP}] \left(2\{C_P\}_1^{int} + M_1 \left\{ \frac{\partial C_P}{\partial M} \right\}_1^{int} \right) + \left(2[A_{F\theta}] + M_1 \left[\frac{\partial A_{F\theta}}{\partial M} \right]_1 \right) \{\Psi\}_1 + \left(2[A_{F\Psi}] + M_1 \left[\frac{\partial A_{F\Psi}}{\partial M} \right]_1 \right) \{\Psi'\}_1 + 2[T_{FP}] \left(\{\Delta C_{P_o}\} + \{\Delta C_{P_\alpha}\} \alpha_1 + \{\Delta C_{P_\beta}\} \beta_1 \right) \right] \frac{1}{U_1} \quad (5.8-35)$$

$$\begin{bmatrix} F_{XB_w}^A \\ F_{ZB_w}^A \\ M_{YB_w}^A \end{bmatrix}_R = \bar{q}_1 \left([G_{\theta R}] + [J_{\theta R}] \right) \{ \psi_\alpha \} \frac{1}{U_1} - \bar{q}_1 [G_T] [\text{TRANS}_{ID}] \{ \Delta D_\alpha \} \frac{1}{U_1} + \\
+ \bar{q}_1 \left([G_{\psi R}] + [J_{\psi R}] \right) \{ \psi'_\alpha \} \frac{1}{U_1} + \quad (5.8-36) \\
+ \bar{q}_1 [G_F] [T_{FP}] \{ \Delta C_{p_\alpha} \} \frac{1}{U_1}$$

where

$$[G_{\psi R}] \equiv [G_F] [A_{F\psi}]$$

and

$$[J_{\psi R}] \equiv [G_T] [\text{TRANS}_{ID}] [D_{P\psi}]$$

$$\begin{bmatrix} F_{XB_Q}^A \\ F_{ZB_Q}^A \\ M_{YB_Q}^A \end{bmatrix}_R = \bar{q}_1 \left([G_{\theta R}] + [J_{\theta R}] \right) \{ \psi_Q \} \frac{1}{U_1} - \bar{q}_1 [G_T] [\text{TRANS}_{ID}] \{ \Delta D_Q \} \frac{1}{U_1} + \\
+ \bar{q}_1 \left([G_{\psi R}] + [J_{\psi R}] \right) \{ \psi'_Q \} \frac{1}{U_1} \quad (5.8-37)$$

$$\begin{bmatrix} F_{XB_{\delta e}}^A \\ F_{ZB_{\delta e}}^A \\ M_{YB_{\delta e}}^A \end{bmatrix}_R = \bar{q}_1 \left([G_{\theta R}] + [J_{\theta R}] \right) \{ \psi_{\delta e} \} \\
+ \bar{q}_1 \left([G_{\psi R}] + [J_{\psi R}] \right) \{ \psi'_{\delta e} \} \quad (5.8-38)$$

5.8.3.8 Corrected lateral-directional static stability derivatives for a rigid aircraft.—Setting the structural flexibility to zero and assuming that all of the matrices in equation (5.8-24) are expressed for the antisymmetric aircraft case (see section 3.4.1.5), the empirically corrected forms of the equations in section 5.6.4.1 are found to be as follows:

$$\begin{bmatrix} F_{YB}^A \\ M_{XB}^A \\ M_{ZB}^A \end{bmatrix}_R = \bar{q}_1 \left([G_{\theta R}] + [J_{\theta R}] \right) \{ \psi_B \} \frac{1}{U_1} - \bar{q}_1 [G_T] [TRANS_{ID}] \{ \Delta D_B \} \frac{1}{U_1} + \\ + \bar{q}_1 \left([G_{\psi R}] + [J_{\psi R}] \right) \{ \psi'_B \} \frac{1}{U_1} + \\ + \bar{q}_1 [G_F] [T_{FP}] \{ C_{P_B} \} \frac{1}{U_1} \quad (5.8-39)$$

$$\begin{bmatrix} F_{YP}^A \\ M_{XP}^A \\ M_{ZP}^A \end{bmatrix}_R = \bar{q}_1 \left([G_{\theta R}] + [J_{\theta R}] \right) \{ \psi_P \} \frac{1}{U_1} - \bar{q}_1 [G_T] [TRANS_{ID}] \{ \Delta D_P \} \frac{1}{U_1} \\ + \bar{q}_1 \left([G_{\psi R}] + [J_{\psi R}] \right) \{ \psi'_P \} \frac{1}{U_1} \quad (5.8-40)$$

$$\begin{bmatrix} F_{YB_R}^A \\ M_{XB_R}^A \\ M_{ZB_R}^A \end{bmatrix}_R = \bar{q}_1 [G_T] \left[[TRANS_t] [\bar{Y}_t] \left(2 \{ C_F^S \}_1^{iso} + M_1 \left\{ \frac{\partial C_P^S}{\partial M} \right\}_1 \right) + \right. \\ \left. + [TRANS_{ID}] [\bar{Y}_c] \{ D \} \right] \frac{1}{U_1} + \\ + \bar{q}_1 \left([G_{\theta R}] + [J_{\theta R}] \right) \{ \psi_R \} \frac{1}{U_1} + \\ + 2 \bar{q}_1 [G_F] [T_{FP}] [\bar{Y}_c] \left(\{ C_P \}_1^{int} + \{ C_P \}_1 \right) \frac{1}{U_1} - \\ - \bar{q}_1 [G_T] [TRANS_{ID}] \{ \Delta D_R \} \frac{1}{U_1} \quad (5.8-41)$$

$$\begin{bmatrix} F_{YB}^A \delta a \\ M_{XB}^A \delta a \\ M_{ZB}^A \delta a \end{bmatrix}_R = \bar{q}_1 ([G_{\theta R}] + [J_{\theta R}]) \{\psi_{\delta a}\} + \bar{q}_1 ([G_{\psi R}] + [J_{\psi R}]) \{\psi'_{\delta a}\} \quad (5.8-42)$$

$$\begin{bmatrix} F_{YB}^A \delta r \\ M_{XB}^A \delta r \\ M_{ZB}^A \delta r \end{bmatrix}_R = \bar{q}_1 ([G_{\theta R}] + [J_{\theta R}]) \{\psi_{\delta r}\} + \bar{q}_1 ([G_{\psi R}] + [J_{\psi R}]) \{\psi'_{\delta r}\} \quad (5.8-43)$$

5.8.3.9 Corrected aeroelastic increments to the longitudinal static stability derivatives.—

The corrections to the aeroelastic increments are obtained by applying the expansion of the aeroelastic matrix, section 5.3.4, to the perturbation aerodynamic forces given by equation (5.8-24). All matrices are assumed to be expressed for the symmetric aircraft case (see sections 3.4.1.5 and 4.2.5), and the development, paralleling that of section 5.6, leads to the empirically corrected forms of the equations in section 5.6.4.3. The results are as follows:

$$\begin{bmatrix} \Delta F_{XB}^A \\ \Delta F_{ZB}^A \\ \Delta M_{YB}^A \end{bmatrix}_E = \bar{q}_1 [G_{\theta E}] \{\psi_c\} + \bar{q}_1 [G_{\theta}] [\tilde{C}_{\theta T}] \left(\{f_T^A\}_1^{iso} + \{f_T^A\}_1^{int} \right) + \bar{q}_1 \left([G_{\psi E}] \{\psi'_0\} + [G_F] [\tilde{\Delta D}^{-1}]_1 [T_{FP}] \{\Delta C_{P_0}\} \right) \quad (5.8-44)$$

$$\begin{bmatrix} \Delta F_{XB}^A \\ \Delta F_{ZB_1}^A \\ \Delta M_{YB_1}^A \end{bmatrix}_E = \begin{bmatrix} \Delta F_{XB}^A \\ \Delta F_{ZB_0}^A \\ \Delta M_{YB_0}^A \end{bmatrix}_E + \bar{q}_1 [G_{\theta E}] \{\psi_M\}_1 + \quad (5.8-45)$$

$$+ \bar{q}_1 \left[[G_{\psi E}] \{\psi_M'\} + [G_F] [\Delta \tilde{D}^{-1}]_1 [T_{FP}] (\{\Delta C_{P_0}\} + \{\Delta C_{P_\alpha}\} \alpha_1 + \{\Delta C_{P_\beta}\} \beta_1) \right]$$

$$\begin{bmatrix} \Delta F_{XB_u}^A \\ \Delta F_{ZB_u}^A \\ \Delta M_{YB_u}^A \end{bmatrix}_E = \bar{q}_1 [G_\theta] [\tilde{C}_{\theta T}] [TRANS_t] \left(2\{C_P^S\}^{iso} + M_1 \left\{ \frac{\partial C_P^S}{\partial M} \right\}^{iso} \right) \frac{1}{U_1} + \quad (5.8-46)$$

$$+ \bar{q}_1 [G_F] [\Delta \tilde{D}^{-1}]_1 [T_{FP}] \left(2\{C_P\}_1^{int} + M_1 \left\{ \frac{\partial C_P}{\partial M} \right\}^{int} \right) + \left(2[A_{F\theta}]_1 + M_1 \left[\frac{\partial A_{F\theta}}{\partial M} \right]_1 \right) \{\psi\}_1 +$$

$$+ \left(2[A_{F\psi}]_1 + M_1 \left[\frac{\partial A_{F\psi}}{\partial M} \right]_1 \right) \{\psi'\}_1 + \{\Delta C_{P_0}\} +$$

$$+ \{\Delta C_{P_\alpha}\} \alpha_1 + \{\Delta C_{P_\beta}\} \beta_1 \left] \frac{1}{U_1}$$

$$\begin{bmatrix} \Delta F_{XB_w}^A \\ \Delta F_{ZB_w}^A \\ \Delta M_{YB_w}^A \end{bmatrix}_E = \bar{q}_1 [G_{\theta E}] \{\psi_\alpha\} \frac{1}{U_1} + \bar{q}_1 [G_{\psi E}] \{\psi_\alpha'\} \frac{1}{U_1} + \quad (5.8-47)$$

$$+ \bar{q}_1 [G_F] [\Delta \tilde{D}^{-1}]_1 [T_{FP}] \{\Delta C_{P_\alpha}\} \frac{1}{U_1}$$

$$\begin{bmatrix} \Delta F_{XB_Q}^A \\ \Delta F_{ZB_Q}^A \\ \Delta M_{YB_Q}^A \end{bmatrix}_E = \bar{q}_1 [G_{\theta E}] \{\psi_Q\} \frac{1}{U_1} + \bar{q}_1 [G_{\psi E}] \{\psi_Q'\} \frac{1}{U_1} \quad (5.8-48)$$

$$\begin{bmatrix} \Delta F_{XB_{\delta e}}^A \\ \Delta F_{ZB_{\delta e}}^A \\ \Delta M_{YB_{\delta e}}^A \end{bmatrix}_E = \bar{q}_1 [G_{\theta E}] \{\psi_{\delta e}\} + \bar{q}_1 [G_{\psi E}] \{\psi_{\delta e}'\} \quad (5.8-49)$$

5.8.3.10 Corrected aeroelastic increments to the lateral-directional static stability derivatives.—Following the development of section 5.8.3.9 but assuming all matrices to be expressed for the antisymmetric aircraft case (see sections 3.4.1.5 and 4.2.5) leads to the following:

$$\begin{bmatrix} \Delta F_{YB_V}^A \\ \Delta M_{XB_V}^A \\ \Delta M_{ZB_V}^A \end{bmatrix}_E = \bar{q}_1 [G_{\theta E}] \{\psi_\beta\} \frac{1}{U_1} + \bar{q}_1 ([G_{\psi E}] \{\psi_\beta'\} + [G_F] [\Delta D^{-1}]_1 [T_{FP}] [\bar{q}_c]_1 \{\Delta C_{P_\beta}\} \frac{1}{U_1} \quad (5.8-50)$$

$$\begin{bmatrix} \Delta F_{YB_P}^A \\ \Delta M_{XB_P}^A \\ \Delta M_{ZB_P}^A \end{bmatrix}_E = \bar{q}_1 [G_{\theta E}] \{\psi_P\} \frac{1}{U_1} + \bar{q}_1 [G_{\psi E}] \{\psi_P'\} \frac{1}{U_1} \quad (5.8-51)$$

$$\begin{bmatrix} \Delta F_{YB_R}^A \\ \Delta M_{XB_R}^A \\ \Delta M_{ZB_R}^A \end{bmatrix}_E = \bar{q}_1 [G_\theta] [\tilde{C}_{\theta T}] [\text{TRANS}_t] [\tilde{Y}_t] \left(2 \{C_P^S\}_1^{\text{iso}} + \right. \quad (5.8-52) \\
\left. + M_1 \left\{ \frac{\partial C_P^S}{\partial M} \right\}_1^{\text{iso}} \right) \frac{1}{U_1} + \bar{q}_1 [G_{\theta E}] \{\psi_R\} \frac{1}{U_1} + \\
+ 2 \bar{q}_1 [G_F] [\Delta \tilde{D}^{-1}]_1 [T_{FP}] [\tilde{Y}_c] \left(\{C_P\}_1^{\text{int}} + \{C_P\}_1 \right) \frac{1}{U_1} + \\
+ \bar{q}_1 [G_{\psi E}] \{\psi_R'\} \frac{1}{U_1}$$

$$\begin{bmatrix} \Delta F_{YB_{\delta a}}^A \\ \Delta M_{XB_{\delta a}}^A \\ \Delta M_{ZB_{\delta a}}^A \end{bmatrix}_E = \bar{q}_1 [G_{\theta E}] \{\psi_{\delta a}\} + \bar{q}_1 [G_{\psi E}] \{\psi_{\delta a}'\} \quad (5.8-53)$$

$$\begin{bmatrix} \Delta F_{YB_{\delta r}}^A \\ \Delta M_{XB_{\delta r}}^A \\ \Delta M_{ZB_{\delta r}}^A \end{bmatrix}_E = \bar{q}_1 [G_{\theta E}] \{\psi_{\delta r}\} + \bar{q}_1 [G_{\psi E}] \{\psi_{\delta r}'\} \quad (5.8-54)$$

6.0 UNSTEADY PERTURBATION FLIGHT CONDITION

6.1 INTRODUCTION

The equations of motion for unsteady perturbation flight conditions are examined by the FLEXSTAB system to evaluate the dynamic characteristics of an aircraft. The characteristics evaluated are the dynamic stability (i.e., the characteristic modes of motion, their frequencies, and damping), dynamic stability derivatives and control effectivenesses, dynamic structural load coefficients for shear, bending and torsion at an elastic axis, and unsteady lifting pressure distributions. The bases for the dynamic stability evaluation are two methods for integrating the unsteady perturbation equations of motion: one is an eigenvalue problem solution method and the other is a numerical integration method. The remaining dynamic characteristics are evaluated by formulas derived from quantities appearing in the equations of motion.

The unsteady perturbation equations of motion are derived, in section 6.1, in a mixed vector and matrix form. In section 6.2, these equations are converted so that they are entirely in matrix form—the form appropriate to the FLEXSTAB system analysis. In this section the applied forces (i.e., the forces arising from the propulsion system and aerodynamics) are partially developed. The dependence of gyroscopic couples on the perturbation motion is developed to its final form, but the dependence of the aerodynamics—a more involved development—is treated in a separate section, viz. section 6.3.

The unsteady perturbation aerodynamic forces are developed from basic aerodynamic and structural relations derived previously in sections 3 and 4. The development leads to aerodynamic force coefficient matrices listed in section 6.3.2. These matrices are incorporated into the FLEXSTAB system in two ways: One, they are transformed to produce formulas for the dynamic stability derivatives—an end product of the FLEXSTAB system dynamic evaluation. Two, they are used to formulate combined aerodynamic matrices—quantities appearing in the equations of motion. In section 6.3.4, variant forms of the aerodynamic force coefficient matrices are used to express dynamic structural load coefficients and unsteady pressure distributions.

The dynamic stability evaluation method based on the solution of an eigenvalue problem—a linear dynamic analysis—is developed in section 6.4. The linear, unsteady perturbation equations of motion, including the effects of unsteady aerodynamics, are expressed as a system of first-order differential equations with constant coefficients. This system of equations, having constant coefficients because of the low frequency aerodynamic approximation of section 3.2.6, poses the eigenvalue problem, section 6.4.1. The solution—eigenvalues and eigenvectors—forms the basis for expressing an integral for the equations of motion; hence, the eigenvalues and eigenvectors contain the information required to compute a first-order approximation of the dynamic stability characteristic of an aircraft. The formulas for these computations appear in section 6.4.2.

The dynamic stability evaluation method based on numerical integration is developed in section 6.5. In this evaluation the equations of motion may be nonlinear and the nonlinear functionality may appear in either of two sets of terms: One set is the rigid-body inertial terms and the other set is the aerodynamic force terms. Nonlinear aerodynamics are introduced by tabular data in a form similar to that used in the nonlinear trim problem of section 5.

The perturbation motion may be initiated either by specifying initial values for the perturbation motion variables, or by subjecting the aircraft to a discrete gust, or by a combination of these two methods.

Excitation of the perturbation motion by penetration of a discrete gust flow field is described in section 5.3. The gust flow field has a one-dimensional spatial variation—in a direction arbitrarily oriented relative to the direction of aircraft motion—and the spatial variation may be that of either a sine wave, a one-minus-cosine wave, or a modified square wave. Although the spatial variation may be assigned any wave length, care must be exercised in choosing the wave length relative to the velocity of the aircraft. The reduced frequency of the gust flow incidence at the aircraft surface must be small by comparison with unity or the unsteady aerodynamic forces will not be accurately predicted, section 3.2.8. The unsteady aerodynamic forces computed by the FLEXSTAB system are linear functions of the frequency of the unsteady flow. A very high frequency gust flow incidence will result in very large, erroneous unsteady aerodynamic forces.

6.2 UNSTEADY PERTURBATION EQUATIONS OF MOTION

In the preceding, viz., section 4.2, the unsteady perturbation equations of motion are derived as the following system of equations: Two vector equations governing the dynamics of perturbation rigid body motion, i.e.,

$$M \left(\frac{\delta \vec{V}}{\delta t} + \vec{\omega}_P \times \vec{V}_{CP} + \vec{\omega}_1 \times \vec{V}_{CP} + \vec{\omega}_P \times \vec{V}_{CP} + \vec{g}_P \right) = \vec{F}_{CP} \quad (4.2-66)$$

$$\int_V \vec{r}_1 \times \left[\frac{\delta \vec{\omega}_P}{\delta t} \times \vec{r}_1 + \vec{\omega}_1 \times (\vec{\omega}_P \times \vec{r}_1) + \vec{\omega}_P \times (\vec{\omega}_1 \times \vec{r}_1) + \vec{\omega}_1 \times (\vec{\omega}_P \times \vec{r}_1) \right] \rho_A dV = \vec{M}_{CP}, \quad (4.2-67)$$

and two matrix equations governing the dynamics of perturbation structural motions, i.e.,

$$[m_1] \ddot{\{u\}}_P + [K_1] \{u_1\}_P = [\phi_{\delta_1}]^T \{Q^S\}_P \quad (4.2-84)$$

$$\{\delta\}_P = [\tilde{C}_R] \left(\{Q^S\}_P - [m_\delta] [\phi_{\delta_1}] \{\ddot{u}_1\}_P \right) + [\phi_{\delta_1}] \{u_1\}_P \quad (4.2-85)$$

where

$$\{Q^S\}_P = \{Q^A\}_P + \{Q^T\}_P + \{Q^G\}_P$$

These equations of motion govern the dynamic characteristics of a flexible aircraft when perturbed from the reference flight condition described in section 5; they are expanded in this

section and are developed into equations entirely in terms of matrices—the form required for the FLEXSTAB system method of dynamic analysis.

6.2.1 Applied Forces

The right-hand members of the equations of motion appearing in section 6.2, above, contain the perturbation aerodynamic and propulsion system forces. These perturbation forces are the consequence of perturbations to the applied surface tractions (i.e., $\{P^a\}$ in equation (4.2-8) and \vec{P} in equation (4.2-40)), and they are expanded in terms of the contributing effects of the aerodynamics and propulsion system as follows:

$$\vec{F}_{cp} = \vec{F}_{cp}^A + \vec{F}_{cp}^T, \quad (6.2-1)$$

$$\vec{M}_{cp} = \vec{M}_{cp}^A + \vec{M}_{cp}^T + \vec{M}_{cp}^G, \text{ and} \quad (6.2-2)$$

$$\{Q^S\}_P = \{Q^A\}_P + \{Q^T\}_P + \{Q^G\}_P \quad (6.2-3)$$

The superscripts (A, T, and G) denote the physical origin of the terms in the expansion, viz.,

- A—surface tractions arising from aerodynamics
- T—surface tractions arising from thrust of the propulsion system
- G—surface tractions arising from gyroscopic stiffness of the propulsion system

This notation is consistent with that used in describing the aerodynamic forces in sections 3.5.1 and 4.2.7 and in describing the propulsion system forces in section 4.2.8. The perturbation forces applied at the structural nodes $\{Q^S\}_P$ are simply the sum of the applied aerodynamic loads given by equation (4.2-116) and the applied propulsion system loads given by equation (4.2-119).

6.2.1.1 Perturbation aerodynamic forces.—Further expansion of the applied aerodynamic forces follows from the contents of section 3.5 and leads to matrix expressions of the following form:

$$\begin{aligned} \{F_B^A\}_P = & [A_1^A]\{V\}_P + [A_2^A]\{\dot{V}\}_P + [A_3^A]\{u_1\}_P + \\ & + [A_4^A]\{\dot{u}_1\}_P + [A_5^A]\{\ddot{u}_1\}_P \end{aligned} \quad (6.2-4)$$

and

$$\{\bar{Q}_1^A\}_P = [a_1^A]\{V\}_P + [a_2^A]\{\dot{V}\}_P + [a_3^A]\{u_1\}_P + [a_4^A]\{\dot{u}_1\}_P + [a_5^A]\{\ddot{u}_1\}_P \quad (6.2-5)$$

where

$$\{\bar{Q}_1^A\}_P \equiv [\phi_{\delta_1}]^T \{Q^A\}_P$$

is the matrix of generalized aerodynamic forces conjugate with the free vibration modal amplitudes $\{u_1\}$.

The matrix $\{F_B^A\}_P$ contains the components of \vec{F}_{CP}^A and \vec{M}_{CP}^A expanded on the Body Axis System, section 2.2.2, while the matrix $\{u_1\}_P$ contains the modal degrees of freedom of the structure appearing in equation (4.2-84) listed in section 6.2. The matrix $\{V\}_P$ contains perturbations to the rigid body velocities \vec{V}_{CP} and $\vec{\omega}_P$ arranged in the following matrix array:

$$\{V\}_P \equiv \begin{bmatrix} u \\ w \\ q \\ \hline v \\ p \\ r \end{bmatrix} \quad (6.2-6)$$

where

$$\vec{\omega}_P \equiv u\hat{i}_B + v\hat{j}_B + w\hat{k}_B$$

and

$$\omega_P \equiv p\hat{i}_B + q\hat{j}_B + r\hat{k}_B.$$

The derivation of the matrices $[A_i]$ and $[a_i]$ appears in the following in section 6.3.3.

6.2.1.2 Perturbation thrust forces.—The terms of equations (6.2-1), (6.2-2), and (6.2-3), arising from perturbations to the thrust of the propulsion system, follow directly from the contents of section 4.2.8 and from the expression for the rigid body mode shape matrix—equation (4.2-21). The perturbation loads at the structural nodes are found from equation (4.2-119) as

$$\{Q^T\}_P = [NAF]\{T\}_P \quad (6.2-8)$$

Premultiplication of this result by the transpose of the rigid body mode shape matrix yields

$$\{F_C^T\}_P = 2[\bar{\phi}_0]^T[NAF]\{T\}_P \quad (6.2-9)$$

where

$$\{F_C^T\}_P \equiv \begin{bmatrix} F_X^T \\ F_Z^T \\ M_Y^T \\ F_Y^T \\ M_X^T \\ M_Z^T \end{bmatrix} \quad (6.2-10)$$

The elements of $\{F_C^T\}_P$ are the components of \vec{F}_{CP}^T and \vec{M}_{CP}^T expanded on the Reference Axis System—the axis system in which the rigid body mode shapes are expressed. These components are transformed to the Body Axis System as follows:

$$\{F_B^T\}_P = 2[\mathcal{J}]\{F_C^T\}_P \quad (6.2-11)$$

where

$$[\mathcal{J}] \equiv \begin{bmatrix} -1 & & & & & \\ & -1 & & & & \\ & & 1 & & & \\ & & & 1 & & \\ & & & & -1 & \\ & & & & & -1 \end{bmatrix} \quad (6.2-12)$$

6.2.1.3 Perturbation gyroscopic forces.—The propulsion system gyroscopic terms appearing in equations (6.2-2) and (6.2-3) are the result of perturbations to the angular momentum of rotating engine parts. These rotating parts are denoted by the term “rotor” in the following.

Assuming that the center of mass of a rotor is on the axis of rotor spin, figure 6.2-1, and assuming that the rotor is a rigid body, the angular momentum of the i^{th} rotor about its center of mass, when the aircraft is perturbed from the reference flight condition, is given by

$$\vec{h}_i^e = \int_{V_i^e} \vec{r}_i^e \times [(\vec{\omega}_i + \vec{\omega}_p + \vec{\theta}_{iP}^G + \vec{\omega}_i^e) \times \vec{r}_i^e] \rho_A dV.$$

In this expression, V_i^e is the rotor volume, $\vec{\omega}_i$ and $\vec{\omega}_p$ are the reference and perturbation rigid body rotation rates of the aircraft, $\vec{\theta}_{iP}^G$ is the elastic rotation rate, and $\vec{\omega}_i^e$ is the rate of rotor spin. Gyroscopic stiffness of the i^{th} rotor is identified with the angular momentum due to spin, viz.,

$$\vec{h}_i^G = \int_{V_i^e} \vec{r}_i^e \times (\vec{\omega}_i^e \times \vec{r}_i^e) \rho_A dV \quad (6.2-13)$$

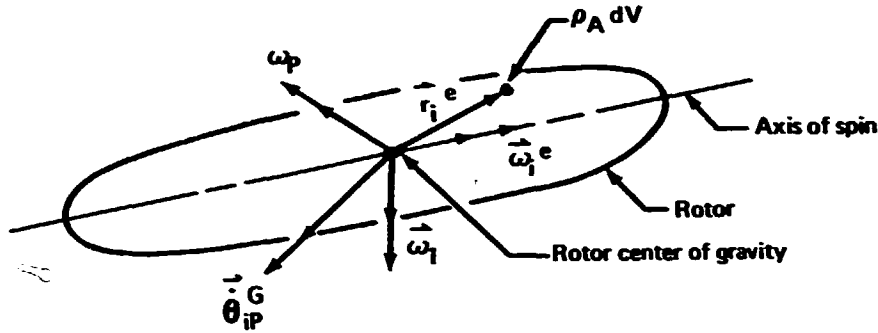


FIGURE 6.2-1.—PROPULSION SYSTEM ROTOR

The gyroscopic couple of the rotor about the engine center of mass—the reaction to the couple causing a change in the angular momentum \vec{h}_i^G —is expressed as

$$\vec{M}_i^G = -\left[\frac{\delta \vec{h}_i^G}{\delta t} + (\vec{\omega}_i + \vec{\omega}_p + \vec{\theta}_{iP}^G) \times \vec{h}_i^G\right] \quad (6.2-14)$$

where $\delta/\delta t$ is the time rate of change apparent to an observer in an axis system fixed to the axis of spin. The angular momentum of the rotor, \vec{h}_i^G , appears time invariant to this observer; hence, the perturbation gyroscopic couple is given by

$$\vec{M}_{iP}^G = -(\vec{\omega}_p + \vec{\theta}_{iP}^G) \times \vec{h}_i^G \quad (6.2-15)$$

The total gyroscopic couple from n rotors is expressed by the sum

$$\vec{M}_P^G = \sum_{i=1}^n \vec{M}_{iP}^G \quad (6.2-16)$$

6.2.1.4 Matrix formulation of perturbation gyroscopic couples.—The vector expression appearing above as equation (6.2-15) must be expressed in matrix form consistent with the structural node point forces, $\{Q^G\}_P$ appearing in equation (6.2-3). This expression is obtained from the propulsion system transformation equations developed section 4.2.8, i.e.,

$$\{Q^G\} = [\Delta_G]\{M^G\} \quad (4.2-119)$$

and

$$\{\theta^G\} = [\Delta_G]^T\{\delta\}. \quad (4.2-118)$$

These equations are in terms of the components of the vectors \vec{M}_i^G and $\vec{\theta}_i^G$ expanded on the Reference Axis System and written in matrix form as follows:

$$\{M^G\} \equiv \begin{bmatrix} \vdots \\ \{M_i^G\} \\ \vdots \end{bmatrix} \quad \text{where } \{M_i^G\} \equiv \begin{bmatrix} M_{X_i}^G \\ M_{Y_i}^G \\ M_{Z_i}^G \end{bmatrix} \quad (6.2-17)$$

and

$$\{\theta^G\} \equiv \begin{bmatrix} \vdots \\ \{\theta_i^G\} \\ \vdots \end{bmatrix} \quad \text{where } \{\theta_i^G\} \equiv \begin{bmatrix} \theta_{X_i}^G \\ \theta_{Y_i}^G \\ \theta_{Z_i}^G \end{bmatrix} \quad (6.2-18)$$

The matrix equivalent of the vector expression for a perturbation gyroscopic couple, equation (6.2-15), is expressed as

$$\{M_i^G\}_P = -[G_i]\{V\}_P - [\bar{G}_i]\{\dot{\theta}_i^G\}_P \quad (6.2-19)$$

where

$$[G_i] \equiv \begin{bmatrix} 0 & 0 & h_{Z_i}^G & | & 0 & 0 & -h_{Y_i}^G \\ 0 & 0 & 0 & | & 0 & -h_{Z_i}^G & h_{X_i}^G \\ 0 & 0 & -h_{X_i}^G & | & 0 & h_{Y_i}^G & 0 \end{bmatrix} \text{ or } [G_i] \equiv \left[\frac{\partial G_i}{\partial \omega} \right] \omega(T) \quad (6.2-20)$$

wherein $[\partial G_i / \partial \omega]$ is the matrix defined in section 5.4.2, and

$$[\bar{G}_i] \equiv \begin{bmatrix} 0 & h_{Z_i}^G & -h_{Y_i}^G \\ -h_{Z_i}^G & 0 & h_{X_i}^G \\ h_{Y_i}^G & -h_{X_i}^G & 0 \end{bmatrix} \text{ or } [\bar{G}_i] \equiv \left[\frac{\partial G_i}{\partial \omega} \right] \omega(T)_1 \quad (6.2-21)$$

A combined equation containing the gyroscopic couples of all engines is based on the matrices $\{M^G\}$, equation (6.2-17), and $\{\theta^G\}$, equation (6.2-18), and is given by

$$\{M^G\}_P = -[G]\{V\}_P - [\bar{G}]\{\dot{\theta}^G\} \quad (6.2-22)$$

where

$$[G] \equiv \begin{bmatrix} \vdots \\ [G_i] \\ \vdots \end{bmatrix} \quad (6.2-23)$$

and has partitions as defined in section 5.4.2 while

$$[\bar{G}] \equiv \begin{bmatrix} \cdot & & & \text{zeros} \\ & \cdot & & \\ & & \cdot & \\ & & & [\bar{G}_i] & \cdot \\ \text{zeros} & & & & \cdot & \cdot \end{bmatrix} \quad (6.2-24)$$

Finally, the structural node point forces arising from gyroscopic couples, $\{Q^G\}_P$, are found from equations (4.2-119) and (6.2-22) as follows*:

$$\{Q^G\}_P = -[\Delta_G] ([G]\{V\}_P + [\bar{G}]\{\dot{\theta}^G\}_P) \quad (6.2-25)$$

The perturbation effects of the gyroscopic couples acting on the aircraft as a rigid body are found using the rigid body mode shape matrix, equation (4.2-49). The result* is as follows:

$$\{F_C^G\} = -2[\bar{\phi}_\delta]^T[\Delta_G] \left([G]\{V\}_P + [\bar{G}]\{\dot{u}_1\}_P \right) \quad (6.2-26)$$

The first term of this result is also expressed as

$$[\bar{\phi}_\delta]^T[\Delta_G][G]\{V\}_P = - \begin{bmatrix} 0 & 0 & 0 & | & 0 & 0 & 0 \\ 0 & 0 & 0 & | & 0 & 0 & 0 \\ 0 & 0 & 0 & | & 0 & -h_Z^G & h_X^G \\ \hline 0 & 0 & 0 & | & 0 & 0 & 0 \\ 0 & 0 & h_Z^G & | & 0 & 0 & -h_Y^G \\ 0 & 0 & -h_X^G & | & 0 & h_Y^G & 0 \end{bmatrix} \begin{bmatrix} u \\ w \\ q \\ \hline v \\ p \\ r \end{bmatrix}$$

where the elements h_X^G , h_Y^G and h_Z^G are the components of the angular momentum of all rotating engine parts. The second term of equation (6.2-26) is expressed in terms of structural node point displacement rates by introducing equation (4.2-118). The result is

$$[\bar{\phi}_\delta]^T[\Delta_G][\bar{G}]\{\dot{\theta}^G\}_P = [\bar{\phi}]^T[\Delta_G][\bar{G}]\{\Delta_G\}^T\{\dot{\delta}\}_P;$$

and, in terms of the residual flexibility decomposition of the elastic deformation, equation (4.2-85), this expression becomes

$$[\bar{\phi}_\delta]^T[\Delta_G][\bar{G}]\{\dot{\theta}^G\}_P = [\bar{\phi}_\delta]^T[\Delta_G][\bar{G}\phi]\{\dot{u}_1\}_P \quad (6.2-28)$$

where

$$[\bar{G}\phi] \equiv [\bar{G}][\phi_{G_1}] \quad , \quad [\phi_{G_1}] \equiv [\Delta_G]^T[\phi_{\delta_1}]$$

6.2.2 Matrix Formulation of the Perturbation Equations of Motion

In formulating the perturbation equations of motion in terms of matrices, the equations are maintained as two separate sets—rigid body equations of motion and structural equations of motion. The rigid body equations of motion contain the nonlinearities shown by the vector formulation, equations (4.2-66) and (4.2-67), while the structural equations of motion are linear by virtue of the approximations introduced by section 4. In the following a nonlinear matrix formulation is deduced from equations (4.2-66) and (4.2-67) and then reduced to a system of linear equations. The reduction is accomplished, simply, by deleting products of perturbation variables in the nonlinear rigid body equations of motion.

*Separation into symmetric and antisymmetric systems of forces, section 4.2.5, follows from use of symmetric and antisymmetric forms for the matrix $[\Delta_G]$.

6.2.2.1 Nonlinear rigid body perturbation equations of motion.—The rigid body equations of motion are obtained in matrix form by writing a matrix equivalent to equations (4.2-66) and (4.2-67). In writing this equation the gyroscopic forces, developed in matrix form in the preceding section, are treated as terms separate from the thrust force terms. The matrices, developed in the preceding and used in writing the rigid body equations of motion, are: the total mass-inertia matrix, $[M]$, equation (4.2-26); the perturbation velocity matrix, $\{\dot{V}\}_P$, equation (6.2-6); and the matrices of applied forces expanded on the Body Axis System, $\{F_B^A\}_P + \{F_B^T\}_P$, equation (6.2-11). The matrix equivalent of equations (4.2-66) and (4.2-67)—the nonlinear, rigid-body, perturbation equations of motion—are as follows:

$$\begin{aligned} [M]\{\dot{V}\}_P + [MM_1]\{V\}_P + [MM_2]\{r_o\}_P = \\ = - [\bar{G}_R]\{u_1\}_P + \{F_B^A\}_P + \{F_B^T\}_P \end{aligned} \quad (6.2-29)$$

where

$$\{r_o\}_P \equiv \begin{bmatrix} \theta_P \\ \phi_P \\ \psi_P \end{bmatrix}$$

The matrices $[MM_1]$, $[MM_2]$, and $[\bar{G}_R]$ appearing in this equation are given by:

$$[MM_1] \equiv \left[\begin{array}{ccc|ccc} 0 & M(Q_1+q) & MW_1 & -M(R_1+r) & 0 & -MV_1 \\ -M(Q_1+q) & 0 & -MU_1 & M(P_1+p) & MV & 0 \\ 0 & 0 & 0 & 0 & A & B \\ \hline -M(R_1+r) & -M(P_1+p) & 0 & 0 & -MW_1 & MU_1 \\ 0 & 0 & C & 0 & D & E \\ 0 & 0 & F & 0 & G & H \end{array} \right] \quad (6.2-30)$$

where

$$\begin{aligned} A &= (2P_1+p)I_{XZ} + R_1(I_{XX}-I_{ZZ}) + h_Z^G \\ B &= -(2R_1+r)I_{XZ} + (P_1+p)(I_{XX}-I_{ZZ}) - h_X^G \\ C &= -P_1I_{XZ} + (R_1+r)(I_{ZZ}-I_{YY}) - h_Z^G \\ D &= -(Q_1+q)I_{XZ} \\ E &= Q_1(I_{ZZ}-I_{YY}) - h_Y^G \\ F &= (R_1+r)I_{XZ} + P_1(I_{YY}-I_{XX}) + h_X^G \\ G &= (Q_1+q)(I_{YY}-I_{XX}) + h_Y^G \\ H &= Q_1I_{XZ} \end{aligned} \quad (6.2-31)$$

$$[MM_2] \equiv Mg \begin{bmatrix} \cos\theta_1 & 0 & 0 \\ \sin\theta_1 \cos\phi_1 & \cos\theta_1 \sin\phi_1 & 0 \\ 0 & 0 & 0 \\ \hline \sin\theta_1 \sin\phi_1 & -\cos\theta_1 \cos\phi_1 & 0 \\ 0 & 0 & 0 \\ 0 & 0 & 0 \end{bmatrix} \quad (6.2-32)$$

$$[\bar{G}_R] \equiv 2[\mathcal{J}][\bar{\phi}_\delta]^T[\Delta_G][\bar{G}][\Delta_G]^T[\phi_{\delta_1}] \quad (6.2-33)$$

The matrix $[MM_1]$ introduces rigid body inertia and incorporates the elements of the gyroscopic couple matrix appearing in equation (6.2-27). The matrix $[MM_2]$ introduces a linear, first-order approximation to the rigid body gravity perturbation forces arising from perturbations to the orientation of an aircraft in the gravity field. The matrix $[\bar{G}_R]$ introduces the perturbation gyroscopic couples due to rates of elastic deformation.

6.2.2.2 Linear perturbation rigid body equations of motion.—In this section the perturbation rigid body equations of motion, equation (6.2-29), are reduced to equations which are linear in the perturbation motion variables. Linearization is accomplished by assuming that the perturbation motion variables are so small that terms of second and higher order in these variables are negligibly small by comparison with the first-order terms.

The linearized equations are identical in form to equation (6.2-29), but the matrix $[MM_1]$ is redefined by deleting all elements containing perturbation motion variables. It follows that

$$[MM_1] \equiv \begin{bmatrix} 0 & MQ_1 & MW_1 & | & -MR_1 & 0 & -MV_1 \\ -MQ_1 & 0 & -MU_1 & | & MP_1 & MV_1 & 0 \\ 0 & 0 & 0 & | & 0 & 0 & 0 \\ \hline MR_1 & -MP_1 & 0 & | & 0 & -MW_1 & MU_1 \\ 0 & 0 & C & | & 0 & D & E \\ 0 & 0 & F & | & 0 & G & H \end{bmatrix} \quad (6.2-34)$$

where

$$A \equiv 2P_1 I_{XZ} + R_1 (I_{XX} - I_{ZZ}) + h_Z^G$$

$$B \equiv -2R_1 I_{XZ} + P_1 (I_{XX} - I_{ZZ}) - h_X^G$$

$$C \equiv -P_1 I_{XZ} + R_1 (I_{ZZ} - I_{YY}) - h_Z^G$$

$$D \equiv -Q_1 I_{XZ}$$

$$E \equiv Q_1 (I_{ZZ} - I_{YY}) - h_Y^G$$

$$F \equiv R_1 I_{XZ} + P_1 (I_{YY} - I_{XX}) + h_X^G$$

$$G \equiv Q_1 (I_{YY} - I_{XX}) + h_Y^G$$

$$H \equiv Q_1 I_{XZ}$$

6.2.2.3 Perturbation structural equations of motion.—The structural equations of motion, i.e., equations (4.2-84) and (4.2-85) listed in section 6.2, are expanded to obtain

$$\begin{aligned} [m_1]\{\ddot{u}_1\}_P + [G_3]\{\dot{u}_1\}_P + [K_1]\{u_1\}_P + [G_1]\{v\}_P = \\ = [\phi_{\delta_1}]^T(\{Q^A\}_P + \{Q^T\}_P) \end{aligned} \quad (6.2-35)$$

where

$$[G_1] \equiv [\phi_{\delta_1}]^T[\Delta_G][\dot{z}] \text{ and } [G_3] \equiv [\phi_{\delta_1}]^T[\Delta_G][\bar{G}]$$

and

$$\begin{aligned} \{\delta_2\}_P = [\tilde{C}_R]\{\{Q^A\}_P + \{Q^T\}_P - [\Delta_G][\bar{G}][\Delta_G]^T[\phi_{\delta_1}]\{\dot{u}_1\}_P - \\ - [m_\delta][\phi_{\delta_1}]\{\ddot{u}_1\}_P - [\Delta_G][G]\{v\}_P\} \end{aligned} \quad (6.2-36)$$

where $[\bar{G}]$ is the gyroscopic couple matrix defined by equation (6.2-24) and $[G]$ is the gyroscopic couple matrix defined by equation (6.2-23).

These equations, in combination with the rigid body equations of motion, represent the perturbation equations of motion for a flexible aircraft. Their integral with respect to time in the following, viz., in section 6.5, is used to assess the dynamic stability characteristics of an aircraft—section 6.5. It remains, however, to expand the aerodynamic forces appearing in these equations in the matrix form given by equations (6.2-4) and (6.2-5).

6.3 UNSTEADY PERTURBATION AERODYNAMIC FORCES

The central objective in this section is to derive formulas determining the elements of the aerodynamic matrices $[A_1^A]$ and $[a_1^A]$ introduced by equations (6.2-4) and (6.2-5). The derivation closely follows that of the static stability derivatives in section 5.6; in fact, some of the formulas derived in this section are identical in form to the static stability derivative formulas appearing in section 5.6.4.

6.3.1 Basic Aerodynamic and Structural Relations

The aerodynamic relation which is basic to the derivation is equation (3.5-63). This equation describes the aerodynamic forces generated at aerodynamic surface segments by unsteady perturbation motion of an aircraft about a steady, reference flight condition. The unsteady perturbation motion is, in part, due to elastic deformation governed by the structural equations of motion. The appropriate form of the structural equations of motion must therefore be combined with the perturbation aerodynamic equation—equation (3.5-63).

6.3.1.1 Basic structural relation.—The perturbation elastic deformation is given in section 4.2.4.2 as

$$\{\delta\}_P = [\tilde{C}_R](\{Q^S\}_P - [m_\delta][\phi_{\delta_1}]\{\ddot{u}_1\}_P) + [\phi_{\delta_1}]\{u_1\}_P \quad (4.2-85)$$

where $[\tilde{C}_R]$ is the residual flexibility matrix. Expanding the applied nodal forces as

$$\{Q^S\}_P = \{Q^A\}_P + \{Q^T\}_P + \{Q^G\}_P \quad (6.3-1)$$

(where the superscripts refer to forces arising from the aerodynamics, the thrust, and engine gyroscopic couples), the transformations given by equations (4.2-101) and (4.2-116) are introduced to obtain

$$\begin{aligned} \{\theta^*\}_P = & [\tilde{C}_{R\theta T}]\{f_T^A\}_P + [P_\theta][\tilde{C}_R](\{Q^T\}_P + \{Q^G\}_P \\ & - [m_\delta][\phi_{\delta_1}]^T\{\ddot{u}_1\}_P) + [\phi_{\theta_1}^*]\{u_1\}_P \end{aligned} \quad (6.3-2)$$

where

$$[\tilde{C}_{R\theta T}] \equiv [P_\theta][\tilde{C}_R][P_T]^T$$

and

$$[\phi_{\theta_1}^*] \equiv [P_\theta][\phi_{\delta_1}]$$

This structural relation is basic to the derivation to follow.

6.3.1.2 Combination of the aerodynamic and structural relations.—The elastic deformation $\{\theta^*\}_P$ can be eliminated from the aerodynamic relation, equation (3.5-63), by a direct substitution of the structural relation given by equation (6.3-2). The resulting expression must then be solved for the aerodynamic forces $\{f_T^A\}_P$. This solution requires the inverse of a large, full, nonsymmetric matrix.

The computational task involved in solving for the aerodynamic forces is considerably reduced by expressing the perturbation aerodynamic forces in the following sum:

$$\{f_T^A\}_P = \{f_T^A\}'_P + [T_{TF}]\{F^A\}'_P \quad (6.3-3)$$

where the perturbation aerodynamic forces appearing on the right are given by

$$\{F^A\}'_P \equiv \bar{q}_1 [T_{FP}][\bar{q}_c^{-1}][A_{P\theta}]\{\theta^*\}_P \quad (6.3-4)$$

— $\{\theta^*\}_P$ being the camber shape deformation arising from the applied perturbation forces shown by equation (6.3-1)—while $\{f_T^A\}'_P$ contains all remaining terms appearing in equation (3.5-63), viz.,

$$\begin{aligned}
\{f_T^A\}'_P = & \bar{q}_1 [TRANS_t] \left[2 \left(\bar{q}_t \frac{u}{U_1} + \bar{Y}_t \frac{r}{U_1} \right) \left(\{C_P^S\}_1^{iso} + [\Delta M_t] \left\{ \frac{\partial C_P^S}{\partial M} \right\}_1^{iso} \right) \right. \\
& \left. + \bar{q}_t \left(M_1 \left\{ \frac{\partial C_P^S}{\partial M} \right\}_1^{iso} \frac{u}{U_1} + M_1 \bar{Y}_t \left\{ \frac{\partial C_P^S}{\partial M} \right\}_1^{iso} \frac{r}{U_1} \right) \right] \\
& + \bar{q}_1 [T_{TF}] [T_{FP}] \left[2 \left(\bar{q}_c \frac{u}{U_1} + \bar{Y}_c \frac{r}{U_1} \right) \{C_P\}_1^{int} + M_1 \bar{q}_c \left\{ \frac{\partial C_P}{\partial M} \right\}_1^{int} \frac{u}{U_1} \right] \\
& + \bar{q}_1 [TRANS_{ID}] \left\{ 2 \left(\bar{q}_c \frac{u}{U_1} + \bar{Y}_c \frac{r}{U_1} \right) \{D\}_1 \right. \quad (6.3-5) \\
& \left. + \bar{q}_c \left[M_1 \left\{ \frac{\partial D}{\partial M} \right\}_1 \frac{u}{U_1} + [D_{P\theta}] \left(\{\theta^*\}_P + \{\psi_M\}_P \right) + \{\Delta D\}_P \right] \right\} + \\
& + \bar{q}_1 [T_{TF}] [T_{FP}] \left\{ 2 \left(\bar{q}_c \frac{u}{U_1} + \bar{Y}_c \frac{r}{U_1} \right) [A_{P\theta}] \{\psi\}_1 \right. \\
& \left. + \bar{q}_c \left[[A_{P\theta}] \{\psi_M\}_P + [\delta A_{P\theta}] \left([\phi_{\theta_1}^*] \{\dot{u}_1\}_P + \{\psi_M\}_P \right) \right. \right. \\
& \left. \left. + M_1 \left[\frac{\partial A_{P\theta}}{\partial M} \right] \{\psi\}_1 \frac{u}{U_1} \right] \right\}
\end{aligned}$$

where equation (3.5-66) has been used.

Combining equations (6.3-2) and (6.3-3) leads to the following result when use is made of the definition given by equation (6.3-4). The result is as follows:

$$\begin{aligned}
\{F^A\}'_P = & \bar{q}_1 [A_{F\theta}] [\tilde{C}_{R\theta T}] \left([T_{TF}] \{F^A\}'_P + \{f_T^A\}'_P \right) \\
& + \bar{q}_1 [A_{F\theta}] \left[[P_\theta] [\tilde{C}_R] \left(\{Q^T\}_P + \{Q^G\}_P - [m_\delta] [\phi_{\delta_1}] \{\ddot{u}_1\}_P \right) \right. \quad (6.3-6) \\
& \left. + [\phi_{\theta_1}] \{u_1\}_P \right]
\end{aligned}$$

where

$$[A_{F\theta}] \equiv [T_{TF}] [\bar{q}_c] [A_{P\theta}]$$

Solving for the aerodynamic forces $\{F^A\}'_P$ and substituting the result into equation (6.3-3) yields the perturbation aerodynamic forces expressed as

$$\begin{aligned}
\{f_T^A\}'_P = & \left([I] + \bar{q}_1 [T_{TF}] [\tilde{D}_R]^{-1} [A_{F\theta}] [\tilde{C}_{R\theta T}] \right) \{f_T^A\}'_P + \\
& + \bar{q}_1 [T_{TF}] [\tilde{D}_R]^{-1} [A_{F\theta}] \left[[P_\theta] [\tilde{C}_R] \left(\{Q^T\}_P + \right. \quad (6.3-7) \\
& \left. + \{Q^G\}_P - [m_\delta] [\phi_{\delta_1}] \{\ddot{u}_1\}_P \right) + [\phi_{\theta_1}^*] \{u_1\}_P \right]
\end{aligned}$$

where

$$[\tilde{D}_R] \equiv [[I] - \bar{q}_1 [A_{F\theta}] [\tilde{C}_{R\theta T}] [T_{TF}]]$$

6.3.1.3 Approximation to the leading edge correction.—Equation (6.3-7) expresses the perturbation aerodynamic forces without the explicit appearance of the elastic deformation arising from quasi-static, residual flexibility deformation except in the leading edge correction term. The leading edge correction term in equation (6.3-5) given by

$$\bar{q}_1 [TRANS_{ID}] [\bar{q}_c]_1 [D_{P\theta}] [\tilde{C}_{R\theta T}] [T_{TF}] \{F^A\}_P, \quad (6.3-8)$$

is neglected in the FLEXSTAB system analysis. Neglect of this term leaves out a portion of the leading edge correction. That which is left out arises from the residual elastic deformation produced by the perturbation aerodynamic forces, in turn, arising from residual elastic deformation—those aerodynamic forces given by equation (6.3-4) when $\{\theta^*\}_P$ is due to the residual flexibility only. This approximation introduces a small error into the leading edge correction but allows the matrix $[\tilde{D}_R]$ to be expressed in terms of forces normal to the mean camber surfaces of the thin bodies of a configuration in lieu of two components of force—one in the X_N -direction and one in the Z_N -direction of the local axis systems of the thin bodies.

Substituting the perturbation aerodynamic forces given by equation (6.3-5) into equation (6.3-7) and making use of the matrix identity

$$[\tilde{D}_R]^{-1} \equiv [[I] + \bar{q}_1 [\tilde{D}_R]^{-1} [A_{F\theta}] [\tilde{C}_{R\theta T}] [T_{TF}]] \quad (6.3-9)$$

and ignoring the leading edge correction term given by equation (6.3-8), the perturbation aerodynamic forces are found as

$$\begin{aligned} \{f^A\}_{T_P} = & \bar{q}_1 \left([I] + \bar{q}_1 [T_{TF}] [\tilde{D}_R]^{-1} [A_{F\theta}] [C_{R\theta T}] \right) \times \\ & \times \left\{ [TRANS_t] \left[2 \left([\bar{q}_t]_1 \frac{u}{U_1} + [\bar{Y}_t] \frac{r}{U_1} \right) \left(\{C_P^S\}_1^{iso} + \right. \right. \right. \\ & \left. \left. \left. + [\Delta M_t]_1 \left\{ \frac{\partial C_P^S}{\partial M} \right\}_1^{iso} \right) + M_1 [\bar{q}_t]_1 \left(\left\{ \frac{\partial C_P^S}{\partial M} \right\}_1 \frac{u}{U_1} + \right. \right. \right. \\ & \left. \left. \left. + M_1 [\bar{Y}_t] \left\{ \frac{\partial C_P^S}{\partial M} \right\}_1 \frac{r}{U_1} \right) \right] \right\} + [TRANS_{ID}] \left\{ \left[2 \left([\bar{q}_c]_1 \frac{u}{U_1} + \right. \right. \right. \\ & \left. \left. \left. + [\bar{Y}_c] \frac{r}{U_1} \right) \{D\}_1 + M_1 [\bar{q}_c]_1 \left\{ \frac{\partial D}{\partial M} \right\}_1 \frac{u}{U_1} \right] + \right\} \end{aligned}$$

$$\begin{aligned}
& + [\bar{q}_c]_1 [D_{P\theta}]_1 ([P_\theta][\tilde{C}_R] (\{Q^T\}_P + \{Q^G\}_P) + [\phi_{\theta_1}] \{u_1\}_P + \{\Delta D\}_P + \{\psi_M\}_P) \Big] \\
& + \bar{q}_1 [T_{TF}][\tilde{D}_R]^{-1} \Big\{ [T_{FP}] \Big[2 \left([\bar{q}_c]_1 \frac{u}{U_1} + \right. \\
& \quad \left. + [\bar{Y}_c] \frac{r}{U_1} \right) \{C_P\}_1^{int} + M_1 [\bar{q}_c]_1 \left\{ \frac{\partial C_P}{\partial M} \right\}_1^{int} \frac{u}{U_1} \Big] + \\
& \quad + \left(2[A_{Fe}]_1 + M_1 \left[\frac{\partial A_{F\theta}}{\partial M} \right]_1 \right) \{\psi\}_1 \frac{u}{U_1} + \\
& \quad + 2[T_{FP}][\bar{Y}_c][A_{P\theta}]_1 \{\psi\}_1 \frac{r}{U_1} + \\
& \quad + [A_{F\theta}] \Big[\{\psi_M\}_P + [\phi_{\theta_1}^*] \{u_1\}_P + [P_\theta][\tilde{C}_R] (\{Q^T\}_P + \{Q^G\}_P \\
& \quad - [m_\delta][\phi_{\delta_1}] \{\ddot{u}_1\}_P) \Big] + [\delta A_{F\theta}] \Big([\phi_{\theta_1}^*] \{\dot{u}_1\}_P + [P_\theta][\tilde{C}_R] \{\dot{Q}^G\}_P + \{\dot{\psi}_M\}_P \Big) \Big\}
\end{aligned} \tag{6.3-10}$$

This expression, describing the perturbation aerodynamic forces generated by unsteady perturbations about the steady reference flight condition of section 5, is fundamental to all of the development to follow in this section.

6.3.2 Aerodynamic Force Coefficient Matrices

This section contains a derivation of the force resultants computed from the distributed aerodynamic forces described by equation (6.3-10). These force resultants are generalized forces conjugate to the rigid body and free vibration mode shape amplitudes, i.e., the total aerodynamic force and couple at the center of mass and the aerodynamic forces which cause work to be done on the free vibration modes of the structure. The aerodynamic force resultants are linearly related to the perturbation motion variables by equation (6.3-10); thus, they can be expressed in terms of coefficients multiplying these variables. These aerodynamic force coefficients are derived in the following.

The aerodynamic force resultants are computed from the distributed aerodynamic forces of equation (6.3-10) using the following transformations:

$$\{F_B^A\}_P = [C_T] \{f_T^A\}_P \tag{6.3-11}$$

and

$$\begin{aligned}\{\bar{Q}_1^A\}_P &= [H_T]\{f_T^A\}_P \\ &= 2[\phi_{\delta_1}]^T\{Q^A\}_P\end{aligned}\quad (6.3-12)$$

where the matrix $[G_T]$, which transforms the distributed forces $\{f_T^A\}_P$ to a force and couple at the aircraft center of mass, is as previously defined by equation (5.3-13), viz.,

$$[G_T] \equiv 2[\mathcal{J}][\bar{\phi}^*]^T[T_{FT}], \quad (5.3-13)$$

and the matrix $[H_T]$, the transformation to generalized forces conjugate to the free vibration modes of the structure, is defined as

$$\begin{aligned}[H_T] &\equiv 2[\phi_{T_1}]^T \\ \text{and} \quad [\phi_{T_1}] &\equiv [P_T][\phi_{\delta_1}]\end{aligned}\quad (6.3-13)$$

The quantities appearing in these transformation matrices are as follows: the structural transformation matrix $[P_T]$ defined by equation (4.2-116), the rigid body and free vibration mode shape matrices $[\phi^*]$ and $[\phi_{\delta_1}]$, the factor 2 accounting for the fact that the mode shapes are expressed for only one side of the aircraft, the transformation from local axis system to Reference Axis System $[T_{FT}]$ defined by equation (3.5-30), and the transformation from Reference Axis System to Body Axis System $[\mathcal{J}]$ defined by equation (3.5-71).

The operations shown by equations (6.3-11) and (6.3-12) are applied to equation (6.3-10). These operations yield a set of column matrices multiplying the perturbation motion variables. These column matrices—the aerodynamic force coefficient matrices—are expanded into rigid plus aeroelastic increment* coefficient matrices following the approach of section 5.3.4 and are developed separately for the two cases of unsteady perturbation motion: longitudinal and lateral-directional. This development appears in the following four sections and leads to expressions of the following form:

$$\begin{aligned}\{F_B^A\}_P^S &= \{F_u^S\}_R^u + \cdots + [\Delta F^S \ddot{u}_1]_E \{\ddot{u}_1^S\}_P \\ \{F_B^A\}_P^A &= \{F_v^A\}_R^v + \cdots + [\Delta F^A \ddot{u}_1]_E \{\ddot{u}_1^A\}_P \\ \{\bar{Q}_1^A\}_P^S &= \{\bar{Q}_u^S\}_R^u + \cdots + [\Delta \bar{Q}^S \ddot{u}_1]_E \{\ddot{u}_1^S\}_P \\ \{\bar{Q}_1^A\}_P^A &= \{\bar{Q}_v^A\}_R^v + \cdots + [\Delta \bar{Q}^A \ddot{u}_1]_E \{\ddot{u}_1^A\}_P\end{aligned}$$

*Note that the aeroelastic increment is a quasistatic aeroelastic effect of residual flexibility; hence there is an aeroelastic increment for coefficients of free vibration mode shape amplitudes.

6.3.2.1 Longitudinal motion and rigid aircraft. – Assuming the unsteady perturbation motion to be restricted to longitudinal motion, the matrices appearing in equations (6.3-10), (6.3-11), and (6.3-12) are assumed to be expressed for the symmetric aircraft case—sections 3.4.1.5 and 4.2.5. Introducing this restriction and substituting equation (6.3-10) into equations (6.3-11) and (6.3-12) leads to the desired result. In carrying out these operations the flow incidence vector $\{\Psi\}_P$ is expanded as in section 3.5.2.1 to find the following:

a) Rigid body forces due to steady rigid body perturbation motions:

$$\begin{aligned} \{F_u^S\}_R = \bar{q}_1 [G_T] & \left\{ [TRANS_T] \left(2\{C_P^S\}_1^{iso} + M_1 \left\{ \frac{\partial C_P^S}{\partial M} \right\}_1^{iso} \right) + \right. \\ & + [TRANS_{ID}] \left(2\{D\}_1 + M_1 \left\{ \frac{\partial D}{\partial M} \right\}_1 \right) + \\ & + [T_{TF}] [T_{FP}] \left(2\{C_P\}_1^{int} + M_1 \left\{ \frac{\partial C_P}{\partial M} \right\}_1^{int} \right) + \\ & \left. + [T_{TF}] \left(2[A_{F\theta}] + M_1 \left[\frac{\partial A_{F\theta}}{\partial M} \right] \right) \{\Psi\}_1 \right\} \frac{1}{U_1} \end{aligned} \quad (6.3-14)$$

$$\{F_w^S\}_R = \bar{q}_1 \left[\left([G_{\theta R}] + [y_{\theta R}] \right) \{\Psi_\alpha\} + [G_T] \{\Delta D_\alpha\} \right] \frac{1}{U_1}$$

$$\{F_Q^S\}_R = \bar{q}_1 \left[\left([G_{\theta R}] + [y_{\theta R}] \right) \{\Psi_Q\} + [G_T] \{\Delta D_Q\} \right] \frac{1}{U_1}$$

where the superscript **S** refers to symmetry about the plane of symmetry of the aircraft and where, as in section 5.6.4.1,

$$[G_{\theta R}] \equiv [G_T] [T_{TF}] [A_{F\theta}]$$

and

$$[y_{\theta R}] \equiv [G_T] [TRANS_{ID}] [D_{P\theta}]$$

b) Rigid body forces due to unsteady rigid body perturbation motions:

$$\{F_w^S\}_R = \bar{q}_1 [\delta G_{\theta R}] \{\Psi_\alpha\} \frac{1}{U_1} \quad (6.3-15)$$

$$\{F_Q^S\}_R = \bar{q}_1 [\delta G_{\theta R}] \{\Psi_Q\} \frac{1}{U_1}$$

where

$$[\delta G_{\theta R}] \equiv [G_T] [T_{TF}] [\delta A_{F\theta}]$$

$$[\delta A_{F\theta}] \equiv [T_{FP}] [\delta A_{P\theta}]$$

c) Rigid body forces due to structural perturbation motions:

$$\begin{aligned}
 \{F_{u_1}^S\}_R &= \bar{q}_1 \left([G_{\theta R}] + [\mathcal{W}_{\theta R}] \right) [\phi_{\theta_1}^{*S}] \\
 \{F_{u_1}^S\}_R &= \bar{q}_1 \left[\left([G_{\theta R}] + [\mathcal{W}_{\theta R}] \right) [\phi_{d_1}^{*S}] \frac{1}{U_1} + [\delta G_{\theta R}] [\phi_{\theta_1}^{*S}] \right] \quad (6.3-16) \\
 \{F_{\ddot{u}_1}^{S*}\}_R &= \bar{q}_1 [\delta G_{\theta R}] [\phi_{d_1}^{*S}] \frac{1}{U_1} \\
 [\phi_{d_1}^{*S}] &\equiv [P_d^S] [\phi_{\delta_1}^S]
 \end{aligned}$$

d) Generalized structural forces due to steady rigid body perturbation motions:

$$\begin{aligned}
 \{\bar{Q}_u^S\}_R &= \bar{q}_1 [H_T] \left\{ [TRANS_t] \left(2\{C_P^S\}_1^{iso} + M_1 \left\{ \frac{\partial C_P}{\partial M} \right\}_1^{iso} \right) + \right. \\
 &\quad \left. + [TRANS_{ID}] \left(2\{D\}_1 + M_1 \left\{ \frac{\partial D}{\partial M} \right\}_1 \right) + \right. \\
 &\quad \left. + [T_{TF}] [T_{FP}] \left(2\{C_P\}_1^{int} + M_1 \left\{ \frac{\partial C_P}{\partial M} \right\}_1^{int} \right) + \right. \\
 &\quad \left. + [T_{TF}] \left(2[A_{F\theta}]_1 + M_1 \left[\frac{\partial A_{F\theta}}{\partial M} \right]_1 \right) \{\Psi\}_1 \right\} \frac{1}{U_1} \quad (6.3-17)
 \end{aligned}$$

$$\{\bar{O}_w^S\}_R = \bar{q}_1 \left[\left([H_{\theta R}] + [\mathcal{W}_{\theta R}] \right) \{\Psi_\alpha\} + [H_T] \{\Delta D_\alpha\} \right] \frac{1}{U_1}$$

$$\{\bar{Q}_Q^S\}_R = \bar{q}_1 \left[\left([H_{\theta R}] + [\mathcal{W}_{\theta R}] \right) \{\Psi_Q\} + [H_T] \{\Delta D_Q\} \right] \frac{1}{U_1}$$

where

$$[H_T] \equiv 2[\phi_\delta]^T [P_T]^T$$

$$[H_F] \equiv [H_T] [T_{TF}]$$

$$[H_{\theta R}] \equiv [H_F] [A_{F\theta}]$$

and

$$[\mathcal{W}_{\theta R}] \equiv [H_T] [TRANS_{ID}] [D_{P\theta}]$$

- e) Generalized structural forces due to unsteady rigid body perturbation motions:

$$\{\bar{Q}_W^S\}_R = \bar{q}_1 [\delta H_{\theta R}] \{\psi_\alpha\} \frac{1}{U_1}$$

$$\{\bar{Q}_Q^S\}_R = \bar{q}_1 [\delta H_{\theta R}] \{\psi_Q\} \frac{1}{U_1}$$

(6.3-18)

where

$$[\delta H_{\theta R}] \equiv [H_T][T_{TF}][\delta A_{FC}]$$

- f) Generalized structural forces due to structural perturbation motions:

$$[\bar{Q}_{u_1}^S]_R = \bar{q}_1 [H_{\theta R}^S][\phi_{\theta_1}^{*S}]$$

$$[\bar{Q}_{u_1}^S]_R = \bar{q}_1 \left([H_{\theta R}^S][\phi_{d_1}^{*S}] \frac{1}{U_1} + [\delta H_{\theta R}^S][\phi_{\theta_1}^{*S}] \right)$$

$$[\bar{Q}_{u_1}^S]_R = \bar{q}_1 [\delta H_{\theta R}^S][\phi_{d_1}^{*S}] \frac{1}{U_1}$$

(6.3-19)

6.3.2.2 Lateral-directional motion.—Assuming the unsteady perturbation motion to be restricted to lateral-directional motion, the matrices appearing in equations (6.3-10), (6.3-11), and (6.3-12) are assumed to be expressed for the antisymmetric aircraft case—sections 3.4.1.5 and 4.2.5. Introducing this restriction and substituting equation (6.3-10) into equations (6.3-11) and (6.3-12) leads to the desired result. In carrying out these operations the flow incidence vector $\{\psi\}_P$ is expanded as in section 3.5.2.1 to find the following:

- a) Rigid body forces due to steady rigid body perturbation motions:

$$\{F_V^A\}_R = \bar{q}_1 \left[([G_{\theta R}] + [g_{\theta R}]) \{\psi_\beta\} \frac{1}{U_1} - [G_T] \{\Delta D_\beta\} \frac{1}{U_1} \right]$$

$$\{F_P^A\}_R = \bar{q}_1 \left[([G_{\theta R}] + [g_{\theta R}]) \{\psi_P\} \frac{1}{U_1} - [G_T] \{\Delta D_P\} \frac{1}{U_1} \right]$$

$$\begin{aligned} \{F_R^A\}_R = & \bar{q}_1 [G_T] \left\{ [TRANS_t] \left[2[\bar{Y}_t] \{C_P^S\}_1^{iso} + \right. \right. \\ & \left. \left. + [\Delta M]_1 \left\{ \frac{\partial C_P^S}{\partial M} \right\}_1^{iso} \right] + [TRANS_{ID}] \left[2[\bar{Y}_c] \{D\}_1 + \right. \right. \\ & \left. \left. + [\bar{q}_c] \left([D_{P\theta}]_1 \{\psi_R\} - \{\Delta D_R\} \right) \right] + 2[T_{TF}][T_{FP}][\bar{Y}_c] \{C_P\}_1^{int} \right. \\ & \left. + 2[T_{TF}][T_{FP}][\bar{Y}_c][A_{P\theta}]_1 \{\psi\}_1 \right. \\ & \left. + [T_{TF}][A_{F\theta}] \{\psi_R\} \right\} \frac{1}{U_1} \end{aligned} \quad (6.3-20)$$

where, as in section 5.6.4.1,

$$[G_{\theta R}] \equiv [G_T][T_{TF}][T_{FP}][A_{P\theta}]$$

and

$$[g_{\theta R}] \equiv [G_T][TRANS_{ID}][D_{P\theta}]$$

b) Rigid body forces due to unsteady rigid body perturbation motions:

$$\begin{aligned} \{F_v^A\}_R &= \bar{q}_1 [\delta G_{\theta R}] \{\psi_\beta\} \frac{1}{U_1} \\ \{F_p^A\}_R &= \bar{q}_1 [\delta G_{\theta R}] \{\psi_P\} \frac{1}{U_1} \\ \{F_R^A\}_R &= \bar{q}_1 [\delta G_{\theta R}] \{\psi_R\} \frac{1}{U_1} \end{aligned} \quad (6.3-21)$$

where

$$[\delta G_{\theta R}] \equiv [G_T][T_{TF}][T_{FP}][\delta A_{P\theta}]$$

c) Rigid body forces due to structural perturbation motions:

$$\begin{aligned} [F_{u_1}^A]_R &= \bar{q}_1 \left([G_{\theta R}] + [g_{\theta R}] \right) [\phi_{\theta_1}^{*A}] \\ [F_{u_1}^A]_R &= \bar{q}_1 \left[\left([G_{\theta R}] + [g_{\theta R}] \right) [\phi_{d_1}^{*A}] \frac{1}{U_1} + [\delta G_{\theta R}] [\phi_{\theta_1}^{*A}] \right] \\ [F_{\ddot{u}_1}^A]_R &= \bar{q}_1 [\delta G_{\theta R}] [\phi_{d_1}^{*A}] \frac{1}{U_1} \\ [\phi_{d_1}^{*A}] &\equiv [P_d^A] [\phi_{\delta_1}^A] \end{aligned} \quad (6.3-22)$$

where the superscript A refers to free-vibration mode shapes antisymmetric with respect to the plane of aircraft symmetry.

d) Generalized structural forces due to steady rigid body perturbation motions:

$$\begin{aligned}
 \{\bar{Q}_V^A\}_R &= \bar{q}_1 \left[([H_{\theta R}] + [\mathcal{H}_{\theta R}]) \{\psi_\beta\} \frac{1}{U_1} - [H_T] \{\Delta D_\beta\} \frac{1}{U_1} \right] \\
 \{\bar{Q}_P^A\}_R &= \bar{q}_1 \left[([H_{\theta R}] + [\mathcal{H}_{\theta R}]) \{\psi_P\} \frac{1}{U_1} - [H_T] \{\Delta D_P\} \frac{1}{U_1} \right] \\
 \{\bar{Q}_R^A\}_R &= \bar{q}_1 [H_T] \left\{ [\text{TRANS}_t] \left[2[\bar{Y}_t] \{C_P^S\}_1^{\text{iso}} + \right. \right. \\
 &\quad \left. \left. + [\Delta M]_1 \left\{ \frac{\partial C_P^S}{\partial M} \right\}_1^{\text{iso}} \right] + [\text{TRANS}_{ID}] \left[2[\bar{Y}_c] \{D\}_1 + \right. \right. \\
 &\quad \left. \left. + [\bar{q}_c]_1 [D_{P\theta}]_1 \{\psi_R\} \right] + 2[T_{TF}][T_{FP}][\bar{Y}_c] \{C_P\}^{\text{int}} + \right. \\
 &\quad \left. + 2[T_{TF}][T_{FP}][\bar{Y}_c] [A_{P\theta}]_1 \{\psi\}_1 + [T_{TF}][A_{F\theta}] \{\psi_R\} \right\} \frac{1}{U_1}
 \end{aligned} \tag{6.3-23}$$

where

$$[H_{\theta R}] \equiv [H_T][T_{TF}][A_{F\theta}]$$

and

$$[\mathcal{H}_{\theta R}] \equiv [H_T][\text{TRANS}_{ID}][D_{P\theta}]$$

e) Generalized structural forces due to unsteady rigid body perturbation motions:

$$\begin{aligned}
 \{\bar{Q}_V^A\}_R &= \bar{q}_1 [\delta H_{\theta R}] \{\psi_\beta\} \frac{1}{U_1} \\
 \{\bar{Q}_P^A\}_R &= \bar{q}_1 [\delta H_{\theta R}] \{\psi_P\} \frac{1}{U_1} \\
 \{\bar{Q}_R^A\}_R &= \bar{q}_1 [\delta H_{\theta R}] \{\psi_R\} \frac{1}{U_1}
 \end{aligned} \tag{6.3-24}$$

where

$$[\delta H_{\theta R}] \equiv [H_T][T_{TF}][\delta A_{F\theta}]$$

f) Generalized structural forces due to structural perturbation motions:

$$[\bar{Q}_{u_1}^A]_R = \bar{q}_1 [H_{\theta R}] [\phi_{\theta 1}^{*A}]$$

$$[\bar{Q}_{u_1}^A]_R = \bar{q}_1 \left[\left([H_{\theta R}] + [H_{\theta R}] \right) [\phi_{d_1}^{*A}] \frac{1}{U_1} + [\delta H_{\theta R}] [\phi_{\delta 1}^{*A}] \right] \quad (6.3-25)$$

$$[\bar{Q}_{\ddot{u}_1}^A]_R = \bar{q}_1 [\delta H_{\theta R}] [\phi_{d_1}^{*A}] \frac{1}{U_1}$$

6.3.2.3 Aeroelastic increments to the unsteady perturbation aerodynamics.—The aeroelastic increments to the unsteady perturbation aerodynamics are derived by applying the expansion of the aeroelastic matrix, section 5.3.4, when the total flexibility of the structure is replaced by the residual flexibility, i.e.,

$$[\Delta \tilde{D}_R^{-1}]_1 \equiv [\tilde{D}_R]_1^{-1} - [I] \quad (6.3-26)$$

where the aeroelastic matrix is given by

$$[\tilde{D}_R] \equiv [I] - \bar{q}_1 [A_{F\theta}] [\tilde{C}_{R\theta T}] [T_{TF}] \quad (6.3-27)$$

The expansion procedure of section 5.3.4 then leads to the formulas appearing in the following two sections in which longitudinal and lateral-directional motions are treated separately as in sections 6.3.2.1 and 6.3.2.2.

6.3.2.4 Longitudinal motion aeroelastic increments.—Assuming the unsteady perturbation motion to be restricted to longitudinal motion, the matrices appearing in the following formulas are assumed to be expressed for the symmetric aircraft of sections 3.4.1.5 and 4.2.5.

a) Rigid body forces due to steady rigid body perturbation motion:

$$\begin{aligned} \{\Delta F_u^S\}_E &= \bar{q}_1^2 [G_T] [T_{TF}] [D_R]^{-1} [A_{F\theta}] [\tilde{C}_{R\theta T}] \left[[TRANS_t] \right. \\ &\times \left(2\{C_P^S\}_1^{iso} + M_1 \left\{ \frac{\partial C_P^S}{\partial M} \right\}_1^{iso} \right) + [TRANS_{ID}] \left(2\{D\}_1 + M_1 \left\{ \frac{\partial D}{\partial M} \right\}_1 \right) \left. \right] \frac{1}{U_1} \\ &+ \bar{q}_1 [G_T] [T_{TF}] [\Delta \tilde{D}_R^{-1}] \left[[T_{FP}] \left(2\{C_P\}_1^{int} + M_1 \left\{ \frac{\partial C_P}{\partial M} \right\}_1^{int} \right) \right. \\ &\{\Delta F_w^S\}_E = \bar{q}_1 [G_{R\theta E}] \{\psi_\alpha\} \frac{1}{U_1} + \left(2[A_{F\theta}]_1 + M_1 \left[\frac{\partial A_{F\theta}}{\partial M} \right]_1 \right) \{\psi\}_1 \left. \right] \frac{1}{U_1} \\ &\{\Delta F_Q^S\}_E = \bar{q}_1 [G_{R\theta E}] \{\psi_Q\} \frac{1}{U_1} \end{aligned} \quad (6.3-28)$$

where

$$[G_{R\theta E}] \equiv [G_T][T_{TF}][\tilde{\Delta D}_R^{-1}][A_{F\theta}]$$

while $[G_T]$ and $[\tilde{\Delta D}_R^{-1}]$ are defined by equations (6.3-13) and (6.3-26).

b) Rigid body forces due to unsteady rigid body perturbation motions:

$$\begin{aligned} \{\Delta F_{\dot{w}}^S\}_E &= \bar{q}_1 [\delta G_{R\theta E}] \{\psi_\alpha\}_{\dot{U}_1} \\ \{\Delta F_{\dot{Q}}^S\}_E &= \bar{q}_1 [\delta G_{R\theta E}] \{\psi_Q\}_{\dot{U}_1} \end{aligned} \quad (6.3-29)$$

where

$$[\delta G_{R\theta E}] \equiv [G_T][T_{TF}][\tilde{\Delta D}_R^{-1}][\delta A_{F\theta}]$$

c) Rigid body forces due to structural perturbation motions:

$$\begin{aligned} [\Delta F_{\dot{u}_1}^S]_E &= \bar{q}_1 [G_{R\theta E}] [\phi_{\theta_1}^{*S}] \\ [\Delta F_{\dot{u}_1}^S]_E &= \bar{q}_1 \left([G_{R\theta E}] [\phi_{d_1}^{*S}]_{\dot{U}_1} + [\delta G_{R\theta E}] [\phi_{\theta_1}^{*S}] \right) \\ [\Delta F_{\ddot{u}_1}^S]_E &= \bar{q}_1 [\delta G_{R\theta E}] [\phi_{d_1}^{*S}]_{\ddot{U}_1} \end{aligned} \quad (6.3-30)$$

where the superscript S refers to free-vibration mode shapes which are symmetric with respect to the plane of aircraft symmetry.

d) Generalized structural forces due to steady rigid body perturbation motions:

$$\begin{aligned} \{\Delta \bar{Q}_{\dot{u}}^S\}_E &= \bar{q}_1^2 [H_T][T_{TF}][\tilde{D}_R]^{-1} [A_{F\theta}] [\tilde{C}_{R\theta T}] \left[[TRANS_t] \left(2\{C_P^S\}^{iso} + \right. \right. \\ &\quad \left. \left. + M_1 \left\{ \frac{\partial C_P^S}{\partial M} \right\}_1^{iso} \right) + \bar{q}_1 [H_T][T_{TF}][\tilde{\Delta D}_R^{-1}] \right. \\ &\quad \left. \left[[T_{FP}] \left(2\{C_P\}_1^{int} + M_1 \left\{ \frac{\partial C_P}{\partial M} \right\}_1^{int} \right) \right. \right. \\ &\quad \left. \left. + \left(2[A_{F\theta}] + M_1 \left[\frac{\partial A_{F\theta}}{\partial M} \right] \right) \{\psi\}_1 \right] \right]_{\dot{U}_1} \end{aligned} \quad (6.3-31)$$

$$\{\Delta \bar{Q}_w^S\}_E = \bar{q}_1 [H_{R\theta E}] \{\psi_\alpha\}_{\dot{U}_1}$$

$$\{\Delta \bar{Q}_Q^S\}_E = \bar{q}_1 [H_{R\theta E}] \{\psi_Q\}_{\dot{U}_1}$$

where

$$[H_{R\theta E}] \equiv [H_T][T_{TF}][\Delta \tilde{D}_R^{-1}][A_{F\theta}]$$

and $[H_T]$ and $[\Delta \tilde{D}_R^{-1}]$ are defined by equations (6.3-12) and (6.3-26).

e) Generalized structural forces due to unsteady rigid body perturbation motions:

$$\{\Delta \bar{Q}_w^S\}_E = \bar{q}_1 [\delta H_{R\theta E}] \{\psi_\alpha\} \frac{1}{U_1} \quad (6.3-32)$$

$$\{\Delta \bar{Q}_Q^S\}_E = \bar{q}_1 [\delta H_{R\theta E}] \{\psi_Q\} \frac{1}{U_1}$$

where

$$[\delta H_{R\theta E}] \equiv [H_T][T_{TF}][\Delta \tilde{D}_R^{-1}][A_{F\theta}]$$

and $[H_T]$ and $[\Delta \tilde{D}_R^{-1}]$ are defined by equations (6.3-13) and (6.3-26).

f) Generalized structural forces due to structural perturbation motions:

$$[\bar{\Delta} Q_{u_1}^S]_E = \bar{q}_1 [H_{R\theta E}] [\phi_{\theta_1}^{*S}]$$

$$[\bar{\Delta} Q_{u_1}^S]_E = \bar{q}_1 \left([H_{R\theta E}] [\phi_{d_1}^{*S}] \frac{1}{U_1} + [\delta H_{R\theta E}] [\phi_{\theta_1}^{*S}] \right) \quad (6.3-33)$$

$$[\bar{\Delta} Q_{\ddot{u}_1}^S]_E = \bar{q}_1 [\delta H_{R\theta E}] [\phi_{d_1}^{*S}] \frac{1}{U_1}$$

where the superscript *S* refers to free-vibration mode shapes symmetric with respect to the plane of aircraft symmetry.

6.3.2.5 Lateral-directional motion aeroelastic increments.—Assuming the unsteady perturbation motion to be restricted to lateral-directional motion, the matrices appearing in the following formulas are assumed to be expressed for the antisymmetric aircraft case of sections 3.4.1.5 and 4.2.5.

a) Rigid body forces due to steady rigid body perturbation motion:

$$\begin{aligned}
 \{\Delta F_V^A\}_E &= \bar{q}_1 [G_{R\theta E}] \{\psi_\beta\} \frac{1}{U_1} \\
 \{\Delta F_P^A\}_E &= \bar{q}_1 [G_{R\theta E}] \{\psi_P\} \frac{1}{U_1} \\
 \{\Delta F_R^A\}_E &= \bar{q}_1 [G_{R\theta E}] \{\psi_R\} \frac{1}{U_1} + \bar{q}_1^2 [G_F] [\tilde{L}_R]^{-1} [A_{F\theta}] [\tilde{C}_{R\theta T}] \times \\
 &\times [TRANS_t] [\tilde{Y}_t] \left(2\{C_P^S\}_1^{iso} + M_1 \left\{ \frac{\partial C_P^S}{\partial M} \right\}^{iso} \right) \frac{1}{U_1} \\
 &+ 2\bar{q}_1 [G_F] [\tilde{\Delta D}_R^{-1}] \times [T_{FP}] [\tilde{Y}_c] \left(\{C_P\}_1^{int} + \{C_P\}_1 \right) \frac{1}{U_1}
 \end{aligned} \tag{6.3-34}$$

where

$$[G_{R\theta E}] \equiv [G_1] [T_{TF}] [\tilde{\Delta D}_R^{-1}] [A_{F\theta}]$$

while $[G_T]$ is defined by equations (6.3-13).

b) Rigid body forces due to unsteady rigid body perturbation motions:

$$\begin{aligned}
 \{\Delta F_V^A\}_E &= \bar{q}_1 [\delta G_{R\theta E}] \{\psi_\beta\} \frac{1}{U_1} \\
 \{\Delta F_P^A\}_E &= \bar{q}_1 [\delta G_{R\theta E}] \{\psi_P\} \frac{1}{U_1} \\
 \{\Delta F_R^A\}_E &= \bar{q}_1 [\delta G_{R\theta E}] \{\psi_R\} \frac{1}{U_1}
 \end{aligned} \tag{6.3-35}$$

where

$$[\delta G_{R\theta E}] \equiv [G_T] [T_{TF}] [\tilde{\Delta D}_R^{-1}] [\delta A_{F\theta}]$$

c) Rigid body forces due to structural perturbation motions:

$$\begin{aligned}
 [\Delta F_{u_1}^A]_E &= \bar{q}_1 [G_{R\theta E}] [\phi_{\theta_1}^{*A}] \\
 [\Delta F_{\dot{u}_1}^A]_E &= \bar{q}_1 \left[[G_{R\theta E}] [\phi_{d_1}^{*A}] \frac{1}{U_1} + [\delta G_{R\theta E}] [\phi_{\theta_1}^{*A}] \right] \\
 [\Delta F_{\ddot{u}_1}^A]_E &= \bar{q}_1 [\delta G_{R\theta E}] [\phi_{d_1}^{*A}] \frac{1}{U_1}
 \end{aligned} \tag{6.3-36}$$

where the superscript **A** refers to free-vibration mode shapes which are antisymmetric with respect to the plane of aircraft symmetry.

d) Generalized structural forces due to steady rigid body perturbation motions:

$$\begin{aligned}\{\Delta Q_V^A\}_E &= \bar{q}_1 [H_{R\theta E}] \{\psi_\beta\}_{U_1}^1 \\ \{\Delta Q_P^A\}_E &= \bar{q}_1 [H_{R\theta E}] \{\psi_P\}_{U_1}^1 \\ \{\Delta Q_R^A\}_E &= \bar{q}_1 [H_{R\theta E}] \{\psi_R\}_{U_1}^1\end{aligned}\quad (6.3-37)$$

$$\begin{aligned}\{\Delta Q_R^A\}_E &= \bar{q}_1 [H_{R\theta E}] \{\psi_R\}_{U_1}^1 + \bar{q}_1^2 [H_F] [\tilde{D}_R]^{-1} [A_{F\theta}] [\tilde{C}_{R\theta T}] \times \\ &\quad \times [TRANS_t] [\tilde{Y}_t] \left(2\{C_P^S\}^{iso} + M_1 \left\{ \frac{\partial C_P^S}{\partial M} \right\}^{iso} \right) \frac{1}{U_1} \\ &\quad + 2\bar{q}_1 [H_F] [\Delta D_R^{-1}] [T_{FF}] [\tilde{Y}_c] \left(\{C_P\}_1^{int} + \{C_P\}_1 \right) \frac{1}{U_1}\end{aligned}$$

e) Generalized structural forces due to unsteady rigid body perturbation motions:

$$\begin{aligned}\{\Delta Q_V^A\}_E &= \bar{q}_1 [\delta H_{R\theta E}] \{\psi_\beta\}_{U_1}^1 \\ \{\Delta Q_P^A\}_E &= \bar{q}_1 [\delta H_{R\theta E}] \{\psi_P\}_{U_1}^1 \\ \{\Delta Q_R^A\}_E &= \bar{q}_1 [\delta H_{R\theta E}] \{\psi_R\}_{U_1}^1\end{aligned}\quad (6.3-38)$$

f) Generalized structural forces due to perturbation structural motions:

$$\begin{aligned}[\Delta Q_{u_1}^A]_E &= \bar{q}_1 [H_{R\theta E}] [\phi_{\theta_1}^{*A}] \\ [\Delta Q_{u_1}^A]_E &= \bar{q}_1 \left([H_{R\theta E}] [\phi_{d_1}^{*A}] \frac{1}{U_1} + [\delta H_{R\theta E}] [\phi_{\theta_1}^{*A}] \right) \\ [\Delta Q_{u_1}^A]_E &= \bar{q}_1 [\delta H_{R\theta E}] [\phi_{d_1}^{*A}] \frac{1}{U_1}\end{aligned}\quad (6.3-39)$$

where the superscript A refers to free-vibration mode shapes which are antisymmetric with respect to the plane of aircraft symmetry.

6.3.3 Combined Aerodynamic Matrices

The aerodynamic force coefficient matrices developed in section 6.3.2 are combined in this section to form the aerodynamic matrices $[A_1^A]$ and $[A_2^A]$ appearing in equations (6.2-4) and (6.2-5). These matrices incorporate all of the terms appearing in the distributed aerodynamic forces described by equation (6.3-10). Thus, in addition to the aerodynamic force coefficient matrices, the matrices $[A_1^A]$ and $[A_2^A]$ contain the aeroelastic effects of the propulsion system gyroscopic couples and of the inertial loading from structural dynamics. The resulting matrices are as follows:

6.3.3.1 $[A_1^A]$, coefficient of $\{V\}_P$

$$[A_1^A] = [A_{R_1}] + [\Delta A_{E_1}] \quad (6.3-40)$$

where

$$[A_{R_1}] \equiv \begin{bmatrix} \{F_u^S\}_R & \{F_w^S\}_R & \{F_q^S\}_R & \{0\} & \{0\} & \{0\} \\ \{0\} & \{0\} & \{0\} & \{F_v^A\}_R & \{F_p^A\}_R & \{F_r^A\}_R \end{bmatrix} \quad (6.3-41)$$

$$[\Delta A_{E_1}] \equiv \begin{bmatrix} \{\Delta F_u^S\}_E & \{\Delta F_w^S\}_E & \{\Delta F_q^S\}_E & \{0\} & \{0\} & \{0\} \\ \{0\} & \{0\} & \{0\} & \{\Delta F_v^A\}_E & \{\Delta F_p^A\}_E & \{\Delta F_r^A\}_E \end{bmatrix} \quad (6.3-42)$$

+ [FG]

and

$$[FG] \equiv \bar{q}_1 ([G_{\theta R}] + [G_{R\theta E}]) [\tilde{C}_{R\theta G}][G] \quad (6.3-43)$$

$$[\tilde{C}_{R\theta G}] \equiv [P_\theta][\tilde{C}_R][\Delta_G]$$

6.3.3.2 $[A_2^A]$, coefficient of $\{V\}_P$

$$[A_2^A] = [A_{R_2}] + [\Delta A_{E_2}] \quad (6.3-44)$$

where

$$[A_{R_2}] \equiv \begin{bmatrix} \{0\} & \{F_w^S\}_R & \{F_q^S\}_R & \{0\} & \{0\} & \{0\} \\ \{0\} & \{0\} & \{0\} & \{F_v^A\}_R & \{F_p^A\}_R & \{F_r^A\}_R \end{bmatrix} \quad (6.3-45)$$

$$[\Delta A_{E_2}] \equiv \begin{bmatrix} \{0\} & \{\Delta F_W^S\}_E & \{\Delta F_Q^S\}_E & \{0\} & \{0\} & \{0\} \\ \{0\} & \{0\} & \{0\} & \{\Delta F_V^A\}_E & \{\Delta F_P^A\}_E & \{\Delta F_R^A\}_E \end{bmatrix} \quad (6.3-46)$$

and

$$[\delta FG] \equiv \bar{q}_1 \left([\delta G_{\theta R}] + [\delta G_{R\theta E}] \right) [\tilde{C}_{R\theta G}][G] + [\delta FG] \quad (6.3-47)$$

6.3.3.3 $[A_3^A]$, coefficient of $\{u_1\}_P$

$$[A_3^A] = [A_{R_3}] + [\Delta A_{E_3}] \quad (6.3-48)$$

where

$$[A_{R_3}] \equiv \begin{bmatrix} [F_{u_1}^S]_R & \text{zeros} \\ \text{zeros} & [F_{u_1}^A]_R \end{bmatrix} \quad (6.3-49)$$

and

$$[\Delta A_{E_3}] \equiv \begin{bmatrix} [\Delta F_{u_1}^S]_E & \text{zeros} \\ \text{zeros} & [\Delta F_{u_1}^A]_E \end{bmatrix} \quad (6.3-50)$$

6.3.3.4 $[A_4^A]$, coefficient of $\{\dot{u}_1\}_P$

$$[A_4^A] = [A_{R_4}] + [\Delta A_{E_4}] \quad (6.3-51)$$

where

$$[A_{R_4}] \equiv \left[\begin{array}{c|c} [F_{\ddot{u}_1}^S]_R & \text{zeros} \\ \hline \text{zeros} & [F_{\ddot{u}_1}^A]_R \end{array} \right] \quad (6.3-52)$$

$$[\Delta A_{E_4}] \equiv \left[\begin{array}{c|c} [\Delta F_{\ddot{u}_1}^S]_E & \text{zeros} \\ \hline \text{zeros} & [\Delta F_{\ddot{u}_1}^A]_E \end{array} \right] + [F\bar{G}] \quad (6.3-53)$$

and

$$[F\bar{G}] \equiv \bar{q}_1 \left([G_{\theta R}] + [G_{R\theta E}] \right) [\tilde{C}_{R\theta G}][\bar{G}\phi] \quad (6.3-54)$$

with $[\bar{G}\phi]$ defined by equation (6.2-28)

as

$$[\bar{G}\phi] \equiv [\bar{G}][\Delta_G]^T[\phi_{\delta_1}]$$

6.3.3.5 $[A_5^A]$, coefficient of $\{\ddot{u}_1\}_p$

$$[A_5^A] = [A_{R_5}] + [\Delta A_{E_5}] \quad (6.3-55)$$

where

$$[A_{R_5}] \equiv \left[\begin{array}{c|c} [\Delta F_{\ddot{u}_1}^S]_E & \text{zeros} \\ \hline \text{zeros} & [\Delta F_{\ddot{u}_1}^A]_E \end{array} \right] \quad (6.3-56)$$

$$[\Delta A_{E_5}] \equiv \left[\begin{array}{c|c} [\Delta F_{\ddot{u}_1}^S]_E & \text{zeros} \\ \hline \text{zeros} & [\Delta F_{\ddot{u}_1}^A]_E \end{array} \right] + [S_1] + [\delta F\bar{G}] \quad (6.3-57)$$

$$[S_1] \equiv -\bar{q}_1 \left([G_{\theta R}] + [G_{R\theta E}] \right) [Z_\theta] \quad (6.3-58)$$

with

$$[Z_\theta] \equiv [\tilde{C}_{R\theta Q}][m_\delta][\phi_{\delta_1}]$$

wherein $[m_\xi] = [m_e]$ in case of ISIC, and

$$[\delta F \bar{G}] \equiv \bar{q}_1 [S_2] [\bar{G} \phi] \quad (6.3-59)$$

with

$$[S_2] \equiv \left([\delta G_{\theta R}] + [\delta G_{R\theta E}] \right) [\tilde{C}_{R\theta G}]$$

and

$$[\bar{G} \phi] \equiv [\bar{G}] [\Delta_G]^T [\phi_{\delta_1}]$$

the gyroscopic matrix $[\bar{G}]$ being defined in equation (6.2-24).

6.3.3.6 $[a_1]$, coefficient of $\{\dot{V}\}_P$

$$[a_1^A] = [a_{R_1}] + [\Delta a_{E_1}] \quad (6.3-60)$$

where

$$[a_{R_1}] \equiv \begin{bmatrix} \{Q_u^S\}_R & \{Q_w^S\}_R & \{Q_Q^S\}_R & \{0\} & \{0\} & \{0\} \\ \{0\} & \{0\} & \{0\} & \{Q_V^A\}_R & \{Q_P^A\}_R & \{Q_R^A\}_R \end{bmatrix} \quad (6.3-61)$$

$$[\Delta a_{E_1}] \equiv \begin{bmatrix} \{\Delta Q_u^S\}_E & \{\Delta Q_w^S\}_E & \{\Delta Q_C^S\}_E & \{0\} & \{0\} & \{0\} \\ \{0\} & \{0\} & \{0\} & \{\Delta Q_V^A\}_E & \{\Delta Q_P^A\}_E & \{\Delta Q_R^A\}_E \end{bmatrix} \quad (6.3-62)$$

and

$$[QG] \equiv \bar{q}_1 \left([H_{\theta R}] + [H_{R\theta E}] \right) [\tilde{C}_{R\theta G}] [G] \quad (6.3-63)$$

with the gyroscopic matrix $[G]$ defined by equation (6.2-23).

6.3.3.7 $[a_2]$, coefficient of $\{\dot{V}\}_P$

$$[a_2^A] = [a_{R_2}] + [\Delta a_{E_2}] \quad (6.3-64)$$

where

$$[a_{R_2}] \equiv \begin{bmatrix} \{0\} & \{Q_W^S\}_R & \{Q_Q^S\}_R & \{0\} & \{0\} & \{0\} \\ \{0\} & \{0\} & \{0\} & \{Q_V^A\}_R & \{Q_P^A\}_R & \{Q_R^A\}_R \end{bmatrix} \quad (6.3-65)$$

$$[\Delta a_{E_2}] \equiv \begin{bmatrix} \{0\} & \{\Delta Q_W^S\}_E & \{\Delta Q_Q^S\}_E & \{0\} & \{0\} & \{0\} \\ \{0\} & \{0\} & \{0\} & \{\Delta Q_V^A\}_E & \{\Delta Q_P^A\}_E & \{\Delta Q_R^A\}_E \end{bmatrix} \quad (6.3-66)$$

and

$$[\delta QG] \equiv \bar{q}_1 \left([H_{\theta R}] + [H_{R\theta E}] \right) [\tilde{C}_{R\theta G}][G] + [\delta QG] \quad (6.3-67)$$

with the gyroscopic matrix $[G]$ defined by equation (6.2-23).

6.3.3.8 $[a_3^A]$ coefficient of $\{u_1\}_p$

$$[a_3^A] = [a_{R_3}] + [\Delta a_{E_3}] \quad (6.3-68)$$

where

$$[a_{R_3}] \equiv \begin{bmatrix} [Q_{u_1}^S]_R & \text{zeros} \\ \text{zeros} & [Q_{u_1}^A]_R \end{bmatrix} \quad (6.3-69)$$

and

$$[\Delta a_{E_3}] \equiv \begin{bmatrix} [\Delta Q_{u_1}^S]_E & \text{zeros} \\ \text{zeros} & [\Delta Q_{u_1}^A]_E \end{bmatrix} \quad (6.3-70)$$

6.3.3.9 $[a_4^A]$ coefficient of $\{\dot{u}_1\}_p$

$$[a_4^A] = [a_{R_4}] + [\Delta a_{E_4}] \quad (6.3-71)$$

where

$$[a_{R_k}] \equiv \left[\begin{array}{c|c} [Q_{u_1}^S]_R & \text{zeros} \\ \hline \text{zeros} & [Q_{u_1}^A]_R \end{array} \right] \quad (6.3-72)$$

$$[\Delta a_{E_k}] \equiv \left[\begin{array}{c|c} [\Delta Q_{u_1}^S]_E & \text{zeros} \\ \hline \text{zeros} & [\Delta Q_{u_1}^A]_E \end{array} \right] + [Q\bar{G}] \quad (6.3-73)$$

and

$$[Q\bar{G}] \equiv \bar{q}_1 \left([H_{\theta R}] + [H_{R\theta E}] \right) [\tilde{C}_{R\theta G}] [\bar{G}\phi] \quad (6.3-74)$$

with $[\bar{G}\phi]$ defined by equation (6.2-28)

as

$$[\bar{G}\phi] \equiv [\bar{G}][\Delta_G]^T [\phi_{\delta_1}]$$

6.3.3.10 $[a_5^A]$, coefficient of $\{\tilde{u}_1\}_p$

$$[a_5^A] = [a_{R_5}] + [\Delta a_{E_5}] \quad (6.3-75)$$

where

$$[a_{R_5}] \equiv \left[\begin{array}{c|c} [Q_{\tilde{u}_1}^S]_R & \text{zeros} \\ \hline \text{zeros} & [Q_{\tilde{u}_1}^A]_R \end{array} \right] \quad (6.3-76)$$

$$[\Delta a_{E_5}] \equiv \left[\begin{array}{c|c} [\Delta Q_{\tilde{u}_1}^A]_E & \text{zeros} \\ \hline \text{zeros} & [\Delta Q_{\tilde{u}_1}^A]_E \end{array} \right] + [\bar{S}_1] + [\delta Q\bar{G}] \quad (6.3-77)$$

$$[\bar{S}_1] \equiv -\bar{q}_1 \left([H_{\theta R}] + [H_{R\theta E}] \right) [Z_\theta] \quad (6.3-78)$$

with

$$[Z_\theta] \equiv [\tilde{C}_{R\theta Q}][m_\delta][\phi_{\delta_1}]$$

and

$$[\delta Q \bar{G}] \equiv \bar{q}_1 [\bar{S}_2][\bar{G}\phi]$$

with

$$[\tilde{S}_2] \equiv \left([\delta H_{\theta R}] + [\delta H_{R\theta E}] \right) [\tilde{C}_{R\theta G}]$$

and

$$[\bar{G}\phi] \equiv [\bar{G}][\Delta_G]^T[\phi_{\delta_1}]$$

6.3.4 Empirically Corrected Aerodynamic Force Coefficient Matrices

The corrected static perturbation aerodynamic forces of section 5.8.3.6 are incorporated into the aerodynamic force coefficient matrices appearing in the preceding. This operation leads to the modified forms for the aerodynamic force coefficient matrices listed in the following.

The empirical corrections affect only the steady aerodynamics; hence, the matrices involving unsteady aerodynamics are unchanged. Also, the matrix equations for the static stability derivatives in section 5.6.4 are identical with the equations describing their counterparts among the aerodynamic force coefficient matrices. This identity also holds for their corrected forms; hence, the corrected forms for these aerodynamic force coefficient matrices are given by the equations of sections 5.8.3.7 and 5.8.3.8. The aeroelastic increments to the static stability derivatives are described by equations nearly identical to those describing the aeroelastic increments to the corresponding aerodynamic force coefficient matrices. The sole difference is that the flexibility matrix is replaced by the residual flexibility matrix to obtain the aeroelastic increments to the aerodynamic force coefficient matrices. The corrected forms are, therefore, given by the equations of sections 5.8.3.9 and 5.8.3.10 when this substitution is incorporated.

The only corrected forms for the aerodynamic force coefficient matrices that do not appear in the preceding are those related to generalized structural forces, i.e., equations (6.3-17), (6.3-23), (6.3-31), and (6.3-37). The corrected forms for these equations are as follows:

$$\begin{aligned} \{\bar{Q}_u^S\}_R = \bar{q}_1 [H_T] & \left\{ [TRANS_t] \left(2 \{C_P^S\}_1^{iso} + M_1 \left\{ \frac{\partial C_P^S}{\partial M} \right\}_1^{iso} \right) + \right. \\ & + [TRANS_{ID}] \left[2 \left(\{D\}_1 - \{\Delta D\}_1 \right) + M_1 \left\{ \frac{\partial D}{\partial M} \right\}_1 \right] \left. \right\} \frac{1}{U_1} + \\ & + \bar{q}_1 [H_F] \left[[T_{FP}] \left(2 \{C_P\}_1^{int} + M_1 \left\{ \frac{\partial C_P}{\partial M} \right\}_1^{int} \right) + \right. \end{aligned}$$

$$\begin{aligned}
& + \left(2[A_{F\theta}]_1 + M_1 \left[\frac{\partial A_{F\theta}}{\partial M} \right]_1 \right) \{\Psi\}_1 + \\
& + \left(2[A_{F\Psi}]_1 + M_1 \left[\frac{\partial A_{F\Psi}}{\partial M} \right]_1 \right) \{\Psi'\}_1 + \\
& + 2[T_{FP}] \left(\{\Delta C_{P_o}\} + \{\Delta C_{P_\alpha}\} \alpha_1 \right) \left] \frac{1}{U_1} \right. \\
\{\bar{Q}_w^S\}_R &= \bar{q}_1 \left([H_{\theta R}] + [\mathcal{H}_{\theta R}] \right) \{\Psi_\alpha\} \frac{1}{U_1} - \bar{q}_1 [H_T] [\text{TRANS}_{ID}] \{\Delta D_\alpha\} \frac{1}{U_1} + \\
& + \bar{q}_1 \left([H_{\Psi R}] + [\mathcal{H}_{\Psi R}] \right) \{\Psi'_\alpha\} \frac{1}{U_1} + \\
& + \bar{q}_1 [H_F] [T_{FP}] \{\Delta C_{P_\alpha}\} \frac{1}{U_1}
\end{aligned}$$

where

$$[H_{\Psi R}] \equiv [H_F] [A_{F\Psi}]$$

and

$$[\mathcal{H}_{\Psi R}] \equiv [H_T] [\text{TRANS}_{ID}] [D_{P\Psi}]$$

$$\begin{aligned}
\{\bar{Q}_Q^S\}_R &= \bar{q}_1 \left([H_{\theta R}] + [\mathcal{H}_{\theta R}] \right) \{\Psi_Q\} \frac{1}{U_1} - \bar{q}_1 [H_T] [\text{TRANS}_{ID}] \{\Delta D_Q\} \frac{1}{U_1} + \\
& \bar{q}_1 \left([H_{\Psi R}] + [\mathcal{H}_{\Psi R}] \right) \{\Psi'_Q\} \frac{1}{U_1}
\end{aligned}$$

$$\begin{aligned}
\{\bar{Q}_v^A\}_R &= \bar{q}_1 \left([H_{\theta R}] + [\mathcal{H}_{\theta R}] \right) \{\Psi_\beta\} \frac{1}{U_1} - \bar{q}_1 [H_T] [\text{TRANS}_{ID}] \{\Delta D_\beta\} \frac{1}{U_1} + \\
& + \bar{q}_1 \left([H_{\Psi R}] + [\mathcal{H}_{\Psi R}] \right) \{\Psi'_\beta\} \frac{1}{U_1} + \\
& + \bar{q}_1 [H_F] [T_{FP}] \{C_{P_\beta}\} \frac{1}{U_1}
\end{aligned}$$

$$\begin{aligned}
\{\bar{Q}_P^A\}_R &= \bar{q}_1 \left([H_{\theta R}] + [\mathcal{H}_{\theta R}] \right) \{\Psi_P\} \frac{1}{U_1} - \bar{q}_1 [H_T] [\text{TRANS}_{ID}] \{\Delta D_P\} \frac{1}{U_1} + \\
& + \bar{q}_1 \left([H_{\Psi R}] + [\mathcal{H}_{\Psi R}] \right) \{\Psi'_P\} \frac{1}{U_1}
\end{aligned}$$

$$\begin{aligned}
\{\bar{Q}_R^A\}_R &= \bar{q}_1 [H_T] \left[[TRANS_t] [\bar{Y}_t] \left(2\{C_P^S\}_1^{iso} + M_1 \left\{ \frac{\partial C_P^S}{\partial M} \right\}_1 \right) + \right. \\
&\quad + [TRANS_{ID}] [\bar{Y}_t] \{D_1\} \left. \right] \frac{1}{U_1} + \\
&\quad + \bar{q}_1 \left([H_{\theta R}] + [\Psi_{\theta R}] \right) \{\Psi_R\} \frac{1}{U_1} + \\
&\quad + 2\bar{q}_1 [H_F] [T_{FP}] [\bar{Y}_C] \left(\{C_P\}_1^{int} + \{C_P\}_1 \right) \frac{1}{U_1} - \\
&\quad - \bar{q} [H_T] [TRANS_{ID}] \{\Delta D_R\} \frac{1}{U_1} \\
\{\Delta \bar{Q}_u^S\}_E &= \bar{q}_1^2 [H_F] [\tilde{D}_R]^{-1} [A_{F\theta}] [\tilde{C}_{R\theta T}] \left[[TRANS_t] \left(2\{C_P^S\}_1^{iso} + \right. \right. \\
&\quad + M_1 \left\{ \frac{\partial C_P^S}{\partial M} \right\}_1^{iso} \left. \right) \left. \right] + \\
&\quad + \bar{q}_1 [H_F] [\Delta \tilde{D}_R^{-1}] \left[[T_{FP}] \left(2\{C_P\}_1^{int} + M_1 \left\{ \frac{\partial C_P}{\partial M} \right\}_1^{int} \right) + \right. \\
&\quad + \left(2[A_{F\theta}]_1 + M_1 \left[\frac{\partial A_{F\theta}}{\partial M} \right]_1 \right) \{\Psi\}_1 + \\
&\quad + \left(2[A_{F\Psi}]_1 + M_1 \left[\frac{\partial A_{F\Psi}}{\partial M} \right]_1 \right) \{\Psi'\}_1 + \{\Delta C_{P_o}\} \\
&\quad + \{\Delta C_{P_\alpha}\}_\alpha \left. \right] \frac{1}{U_1} \\
\{\Delta \bar{Q}_w^S\}_E &= \bar{q}_1 [H_{R\theta E}] \{\Psi_\alpha\} \frac{1}{U_1} + \bar{q}_1 [H_{R\Psi E}] \{\Psi'_\alpha\} \frac{1}{U_1} + \\
&\quad + \bar{q}_1 [G_F] [\Delta \tilde{D}_R^{-1}] [T_{FP}] \{\Delta C_{P_\alpha}\} \frac{1}{U_1}
\end{aligned}$$

where

$$[H_{R\Psi E}] \equiv [H_F] [\Delta \tilde{D}_R^{-1}] [A_{F\Psi}]$$

$$\{\Delta \bar{Q}_Q^S\}_E = \bar{q}_1 [H_{R\theta E}] \{\Psi_Q\} \frac{1}{U_1} + \bar{q}_1 [H_{R\Psi E}] \{\Psi_Q'\} \frac{1}{U_1}$$

$$\begin{aligned} \{\Delta \bar{Q}_V^A\}_E = & \bar{q}_1 [H_{R\theta E}] \{\Psi_\beta\} \frac{1}{U_1} + \bar{q}_1 \left([H_{R\Psi E}] \{\Psi_\beta'\} + \right. \\ & \left. + [H_F] [\Delta \tilde{D}_R^{-1}]_1 [T_{FP}] [\bar{q}_c]_1 \{\Delta C_{P_\beta}\} \frac{1}{U_1} \right) \end{aligned}$$

$$\{\Delta \bar{Q}_P^A\}_E = \bar{q}_1 [H_{R\theta E}] \{\Psi_P\} \frac{1}{U_1} + \bar{q}_1 [H_{R\Psi E}] \{\Psi_P'\} \frac{1}{U_1}$$

$$\begin{aligned} \{\Delta \bar{Q}_R^A\}_E = & \bar{q}_1 [H_F] [\tilde{D}_R]^{-1} [A_{F\theta}] [\tilde{C}_{R,T}] [TRANS_t] [\bar{Y}_t] \times \\ & \times \left(2\{C_P^S\}_1^{iso} + M_1 \left\{ \frac{\partial C_P^S}{\partial M} \right\}^{iso} \right) \frac{1}{U_1} + \bar{q}_1 [H_{R\theta E}] \{\Psi_R\} \frac{1}{U_1} + \\ & + 2\bar{q}_1 [H_F] [\Delta \tilde{D}_R^{-1}] [T_{FP}] [\bar{Y}_c] \left(\{C_P\}_1^{int} + \{C_P\}_1 \right) \frac{1}{U_1} + \\ & + \bar{q}_1 [H_{R\Psi E}] \{\Psi_R'\} \frac{1}{U_1} \end{aligned}$$

6.3.5.1 Dynamic structural loads. — The FLEXSTAB system computes dynamic loads similar to the static loads of section 5.7.3 for the elastic axis method wherein the *net loads* are formed at the $\{\delta_{es}\}$ degrees of freedom.

The distributed dynamic airloads, including aeroelastic effects from propulsion system loads, $\{f_T^A\}_P$, are given by equation (6.3-10). These loads are transformed to yield applied structural loads using the transformation

$$\{Q^A\} = [P_T]^T \{f_T^A\}_P \quad (4.2-116)$$

where $\{Q^A\}$ describes the applied dynamic airloads at the elastic axis system when the transformation $[P_T]$ is generated as in section 4.3.5. Finally, the inertial loads are introduced by the transformation

$$[P] = [I] - [m_\delta][\bar{\phi}_\delta][M]^{-1}[\bar{\phi}_\delta]^T \quad (4.2-53)$$

and the net loads (i.e., $\{Q\}_P \equiv \{Q^A\}_P + \{Q^{inertial}\}_P$) are found as

$$\begin{aligned} \{Q\}_P &= [P] [P_T]^T \{f_T^A\}_P \\ &= [P] \{Q^A\}_P \end{aligned} \quad (6.3-79)$$

The dynamic loads are generated in coefficient form, i.e., as coefficients of the perturbation motion variables contained in the matrices $\{V\}_P$, $\{\dot{V}\}_P$, $\{u_1\}_P$, $\{\dot{u}_1\}_P$, and $\{\ddot{u}_1\}_P$ and of control surface deflections δ_e , δ_a , and δ_r . The development of the formulas which generate these dynamic load coefficients follows the development of the aerodynamic force coefficient matrices of section 6.3.2. The dynamic load coefficients are obtained from equations (6.3-14) through (6.3-36) by introducing the following substitutions:

$$(1) \quad [P_e]^T \rightarrow [G_T] \quad (6.3-80)$$

$$\text{wherein} \quad [P_e]^T \equiv [P] [P_T]^T \quad (4.3-208)$$

$$(2) \quad [L_F] \rightarrow [G_F] \text{ and } [H_F] \quad (6.3-81)$$

$$\text{wherein} \quad [L_F] \equiv [P_e]^T [T_{TF}] \quad (6.3-82)$$

$$(3) \quad [L_{\theta R}] \rightarrow [G_{\theta R}] + [Y_{\theta R}]$$

wherein

$$[L_{\theta R}] \equiv [L_F][A_{F\theta}] + [P_e]^T[\text{TRANS}_{ID}][D_{P\theta}]$$

(4)

$$[\delta L_{\theta R}] \rightarrow [\delta G_{\theta R}] \quad (6.3-83)$$

wherein

$$[\delta L_{\theta R}] \equiv [L_F][\delta A_{F\theta}]$$

(5)

$$[L_{\theta E}] \rightarrow [G_{R\theta E}] \quad (6.3-84)$$

wherein

$$[L_{\theta E}] \equiv [L_F][\tilde{\Delta D}_R^{-1}][A_{F\theta}]$$

(6)

$$[\delta L_{\theta E}] \rightarrow [\delta G_{R\theta E}] \quad (6.3-85)$$

wherein

$$[\delta L_{\theta E}] \equiv [L_F][\tilde{\Delta D}_R^{-1}][\delta A_{F\theta}]$$

In addition to the structural airloads, the loads due to the gyroscopic couples of the propulsion system, section 6.2.1.3, are computed as

$$[L_G] = \bar{q}_1 [L_\theta] [\tilde{C}_{R\theta G}] [G] \quad (6.3-86)$$

where

$$[L_\theta] \equiv [L_{\theta R}] + [L_{\theta E}]$$

and

$$[L_{\bar{G}}] \equiv \bar{q}_1 [L_\theta] [\tilde{C}_{R\theta G}] [\bar{G}\phi] \quad (6.3-87)$$

the quantities $[G]$ and $[\bar{G}\phi]$ being defined, respectively, by equation (6.2-23) and (6.2-28). Equation (6.3-86) yields the structural loads due to the values of the elements of the perturbation velocity vector, $\{V\}_p$. Equation (6.3-87) describes the structural loads due to the rates of change of the structural degrees of freedom, viz., $\{\dot{u}\}_p$. In both cases, the structural loads are those from the gyroscopic couples and attendant aeroelastic effects.

Because of the close analogy between the dynamic loads coefficient matrices and the aerodynamic force coefficient matrices of section 6.3.2, a separate derivation of the dynamic loads coefficient matrices is superfluous; the appropriate matrix equations are written, in comparison with the matrix equations of section 6.3.2, as follows:

$$\begin{aligned} \{L_u^S\}_R = & \bar{q}_1 [L_F] [T_{FP}] \left(2\{C_P\}_1^{\text{int}} + M_1 \left\{ \frac{\partial C_P}{\partial M} \right\}_1^{\text{int}} \right) + \left(2[A_{F\psi}] + M_1 \left[\frac{\partial A_{F\psi}}{\partial M} \right] \right) \{\psi\}_1 + \\ & + [T_{FP}] \left(\{\Delta C_{P_o}\} + \{\Delta C_{P_\alpha}\} \alpha_1 \right) + \\ & + \left(2[A_{F\theta}] + M_1 \left[\frac{\partial A_{F\theta}}{\partial M} \right] \right) \{\psi\}_1 \frac{1}{U_1} \end{aligned}$$

$$+ \bar{q}_1 [P_e]^T \left[[\text{TRANS}_t] \left(2\{C_P^S\}_1^{\text{iso}} + M_1 \left\{ \frac{\partial C_P^S}{\partial M} \right\}_1^{\text{iso}} \right) \right.$$

$$\left. + [\text{TRANS}_{ID}] \left(2\{D\}_1 + M_1 \left\{ \frac{\partial D}{\partial M} \right\}_1 \right) \right] \frac{1}{U_1}$$

$$\{L_W^S\}_R = \bar{q}_1 \left[[L_{\theta R}] \{\Psi_\alpha\} + [P_e]^T \{\Delta D_\alpha\} \right] \frac{1}{U_1} + \bar{q}_1 \left[[L_{\Psi R}] \{\Psi'_\alpha\} + [L_F] [T_{FP}] \{\Delta C_{P_\alpha}\} \right] \frac{1}{U_1}$$

$$\{L_Q^S\}_R = \bar{q}_1 \left[[L_{\theta R}] \{\Psi_Q\} + [P_e]^T \{\Delta D_Q\} \right] \frac{1}{U_1} + \bar{q}_1 [L_{\Psi R}] \{\Psi'_Q\} \frac{1}{U_1}$$

$$\{\Delta L_U^S\}_E = \bar{q}_1 [L_F] [\tilde{\Delta D}_R^{-1}] \left\{ \bar{q}_1 [A_{F\theta}] [\tilde{C}_{R\theta T}] \times \right.$$

$$\left[[\text{TRANS}_t] \left(2\{C_P^S\}_1^{\text{iso}} + M_1 \left\{ \frac{\partial C_P^S}{\partial M} \right\}_1^{\text{iso}} \right) \right.$$

$$\left. + [\text{TRANS}_{ID}] \left(2\{D\}_1 + M_1 \left\{ \frac{\partial D}{\partial M} \right\}_1 \right) \right] \frac{1}{U_1}$$

$$+ \left[[T_{FP}] \left(2\{C_P\}_1^{\text{int}} + M_1 \left\{ \frac{\partial C_P}{\partial M} \right\}_1^{\text{int}} \right) \right.$$

$$+ [T_{FP}] \left(\{\Delta C_{P_o}\} + \{\Delta C_{P_\alpha}\}_\alpha \right) + \left(2[A_{F\Psi}] + M_1 \left[\frac{\partial A_{F\Psi}}{\partial M} \right] \right) \{\Psi'\}_1$$

$$\left. + \left(2[A_{F\theta}]_1 + M_1 \left[\frac{\partial A_{F\theta}}{\partial M} \right]_1 \right) \{\Psi\}_1 \right] \frac{1}{U_1} \Big\}$$

$$\{\Delta L_W^S\}_E = \bar{q}_1 [L_{R\theta E}] \{\Psi_\alpha\} \frac{1}{U_1} + \bar{q}_1 [L_{R\Psi E}] \{\Psi'_\alpha\} \frac{1}{U_1} + \bar{q}_1 [L_F] [\tilde{\Delta D}_R^{-1}] [T_{FP}] \{\Delta C_{P_\alpha}\} \frac{1}{U_1}$$

$$\{\Delta L_Q^S\}_E = \bar{q}_1 [L_{R\theta E}] \{\Psi_Q\} \frac{1}{U_1} + \bar{q}_1 [L_{R\Psi E}] \{\Psi'_Q\} \frac{1}{U_1}$$

$$\{L_{\delta e}^S\}_R = \bar{q}_1 [L_{\theta R}] \{\Psi_{\delta e}\} + \bar{q}_1 [L_{\Psi R}] \{\Psi'_{\delta e}\}$$

$$\{\Delta L_{\delta e}^S\}_E = \bar{q}_1 [L_{R\theta E}] \{\psi_{\delta e}\} + \bar{q}_1 [L_{R\psi E}] \{\psi_{\delta e}'\}$$

$$\{L_W^S\}_R = \bar{q}_1 [\delta L_{\theta R}] \{\psi_\alpha\} \frac{1}{U_1}$$

$$\{L_Q^S\}_R = \bar{q}_1 [\delta L_{\theta R}] \{\psi_Q\} \frac{1}{U_1}$$

$$\{\Delta L_W^S\}_E = \bar{q}_1 [\delta L_{R\theta E}] \{\psi_\alpha\} \frac{1}{U_1}$$

$$\{\Delta L_Q^S\}_E = \bar{q}_1 [\delta L_{R\theta E}] \{\psi_Q\} \frac{1}{U_1}$$

$$\{L_{\delta e}^S\}_R = \bar{q}_1 [\delta L_{\theta R}] \{\psi_{\delta e}\}$$

$$\{\Delta L_{\delta e}^S\}_E = \bar{q}_1 [\delta L_{R\theta E}] \{\psi_{\delta e}\}$$

$$\{L_V^A\}_R = \bar{q}_1 [L_{\theta R}] \{\psi_\beta\} \frac{1}{U_1} + \bar{q}_1 [L_{\psi R}] \{\psi_\beta'\} \frac{1}{U_1} + \bar{q}_1 [L_F] [T_{FP}] \{\Delta C_{P_\beta}\} \frac{1}{U_1}$$

$$\{L_P^A\}_R = \bar{q}_1 [L_{\theta R}] \{\psi_P\} \frac{1}{U_1} + \bar{q}_1 [L_{\psi R}] \{\psi_P'\} \frac{1}{U_1}$$

$$\{L_R^A\}_R = \bar{q}_1 [L_{\theta R}] \{\psi_R\} \frac{1}{U_1} + \bar{q}_1 [P_e]^T \left[[TRANS_t] [\bar{Y}_t] \{C_P^S\}_1^{iso} + M_1 \left\{ \frac{\partial C_P^S}{\partial M} \right\}_1^{iso} \right.$$

$$\left. + [TRANS_{ID}] [\bar{Y}_t] \{D\}_1 \right] \frac{1}{U_1} + 2\bar{q}_1 [L_F] [T_{FP}] [\bar{Y}_C] \left(\{C_P\}_1^{int} \right.$$

$$\left. + \{C_P\}_1 \right) \frac{1}{U_1} - \bar{q}_1 [P_e]^T [TRANS_{ID}] \{\Delta D_R\} \frac{1}{U_1}$$

$$\{\Delta L_V^A\}_E = \bar{q}_1 [L_{R\theta E}] \{\psi_\beta\} \frac{1}{U_1} + \bar{q}_1 [L_{R\psi E}] \{\psi_\beta'\} \frac{1}{U_1} + \bar{q}_1 [L_F] [\Delta \tilde{D}_R^{-1}] [T_{FP}] \{\Delta C_{P_\beta}\} \frac{1}{U_1}$$

$$\{\Delta L_P^A\}_E = \bar{q}_1 [L_{R\theta E}] \{\psi_P\} \frac{1}{U_1} + \bar{q}_1 [L_{R\psi E}] \{\psi_P'\} \frac{1}{U_1}$$

$$\{\Delta L_R^A\}_E = \bar{q}_1 [L_{R\theta E}] \{\psi_R\} \frac{1}{U_1} + \bar{q}_1 [L_{R\psi E}] \{\psi_R'\} \frac{1}{U_1}$$

$$\{L_V^A\}_R = \bar{q}_1 [\delta L_{\theta R}] \{\psi_\beta\} \frac{1}{U_1}$$

$$\{L_P^A\}_R = \bar{q}_1 [\delta L_{\theta R}] \{\psi_P\} \frac{1}{U_1}$$

$$\{L_R^A\}_R = \bar{q}_1 [\delta L_{\theta R}] \{\psi_R\} \frac{1}{U_1}$$

$$\{\Delta L_V^A\}_E = \bar{q}_1 [\delta L_{R\theta E}] \{\psi_\beta\} \frac{1}{U_1}$$

$$\{\Delta L_P^A\}_E = \bar{q}_1 [\delta L_{R\theta E}] \{\psi_P\} \frac{1}{U_1}$$

$$\{\Delta L_R^A\}_E = \bar{q}_1 [\delta L_{R\theta E}] \{\psi_R\} \frac{1}{U_1}$$

$$\{L_{\delta a}^A\}_R = \bar{q}_1 [\delta L_{\theta R}] \{\psi_{\delta a}\}$$

$$\{L_{\delta r}^A\}_R = \bar{q}_1 [\delta L_{\theta R}] \{\psi_{\delta r}\}$$

$$\{\Delta L_{\delta a}^A\}_E = \bar{q}_1 [\delta L_{R\theta E}] \{\psi_{\delta a}\}$$

$$\{\Delta L_{\delta r}^A\}_E = \bar{q}_1 [\delta L_{R\theta E}] \{\psi_{\delta r}\}$$

$$[L_{u_1}^S]_R = \bar{q}_1 [L_{\theta R}] [\phi_{\theta_1}^{*S}]$$

$$[L_{u_1}^S]_R = \bar{q}_1 \left([L_{\theta R}] [\phi_{d_1}^{*S}] \frac{1}{U_1} + [\delta L_{\theta R}] [\phi_{\theta_1}^{*S}] \right)$$

$$[L_{u_1}^S]_R = \bar{q}_1 [\delta L_{\theta R}] [\phi_{d_1}^{*S}] \frac{1}{U_1}$$

$$[\Delta L_{u_1}^S]_E = \bar{q}_1 [L_{R\theta E}] [\phi_{\theta_1}^{*S}]$$

$$[\Delta L_{u_1}^S]_E = \bar{q}_1 \left([L_{R\theta E}] [\phi_{d_1}^{*S}] \frac{1}{U_1} + [\delta L_{R\theta E}] [\phi_{\theta_1}^{*S}] \right)$$

$$[\Delta L_{u_1}^S]_E = \bar{q}_1 [\delta L_{R\theta E}] [\phi_{d_1}^{*S}] \frac{1}{U_1}$$

$$[L_{u_1}^A]_R = \bar{q}_1 [L_{\theta R}] [\phi_{\theta_1}^{*A}]$$

$$[L_{u_1}^A]_R = \bar{q}_1 \left([L_{\theta R}] [\phi_{d_1}^{*A}] \frac{1}{U_1} + [\delta L_{\theta R}] [\phi_{\theta_1}^{*A}] \right)$$

$$[L_{u_1}^A]_R = \bar{q}_1 [\delta L_{\theta R}] [\phi_{d_1}^{*A}] \frac{1}{U_1}$$

$$[\Delta L_{u_1}^A]_E = \bar{q}_1 [L_{R\theta E}] [\phi_{\theta_1}^{*A}]$$

$$[\Delta L_{u_1}^A]_E = \bar{q}_1 \left([L_{R\theta E}] [\phi_{d_1}^{*A}] \frac{1}{U_1} + [\delta L_{R\theta E}] [\phi_{\theta_1}^{*A}] \right)$$

$$[\Delta L_{u_1}^A]_E = \bar{q}_1 [\delta L_{R\theta E}] [\phi_{d_1}^{*A}] \frac{1}{U_1}$$

6.3.5.2 *Unsteady pressure distribution.*—In addition to the pressure distribution in the steady, reference flight condition, the FLEXSTAB system computes the pressure distributions induced by accelerations. These pressure distributions are determined by the second term of equation (3.4-218), viz.,

$$\{C_F\} = [\delta A]\{\dot{\Psi}\}_P \frac{1}{U_1}$$

Applying the transformation from pressure to panel forces, equation (3.5-33), and introducing the residual flexibility form of the aeroelastic matrix, equation (6.3-7), the unsteady aerodynamic forces are found as

$$\{F^A\}_P = \bar{q}[\tilde{D}_R]^{-1}[\delta A_{F\theta}]\{\dot{\Psi}\}_P \quad (6.3-88)$$

Finally, using the transformation $[T_{\Delta P}]$, equation (5.7-17), the unsteady lifting pressures are found as

$$\{\Delta C_P\} = [T_{\Delta P}][\tilde{D}_R]^{-1}[\delta A_{F\theta}]\{\dot{\Psi}\}_P \quad (6.3-89)$$

Introducing the expansion of the flow incidence rate of section 3.5.2.1, the unsteady lifting pressure is expressed as that arising from components of $\{\dot{\Psi}_M\}_P$ and $\{\dot{\theta}^*\}_P$. This leads to the following relations:

$$\begin{aligned} \{\Delta C_{P_w}\} &= \frac{1}{U_1} [\Delta C_{P\theta}] \{\Psi_\alpha\} \\ \{\Delta C_{P_Q}\} &= \frac{1}{U_1} [\Delta C_{P\theta}] \{\Psi_Q\} \\ \{\Delta C_{P_{\dot{V}}}\} &= \frac{1}{U_1} [\Delta C_{P\theta}] \{\Psi_\beta\} \\ \{\Delta C_{P_{\dot{P}}}\} &= \frac{1}{U_1} [\Delta C_{P\theta}] \{\Psi_P\} \\ \{\Delta C_{P_{\dot{R}}}\} &= \frac{1}{U_1} [\Delta C_{P\theta}] \{\Psi_R\} \\ [\Delta C_{P_{\dot{u}_1}}] &= [\Delta C_{P\theta}] [\phi_{\theta_1}^*] \end{aligned} \quad (6.3-90)$$

and

$$[\Delta C_{P_{\dot{u}_1}}] = \frac{1}{U_1} [\Delta C_{P\theta}] [\phi_{d_1}^*]$$

where

$$[\Delta C_{P\theta}] \equiv [T_{\Delta P}][\tilde{D}_R]^{-1}[\delta A_{F\theta}]$$

6.4 LINEAR DYNAMIC ANALYSIS

The FLEXSTAB system performs a linear dynamic analysis by integrating the linear form of the equations of motion, section 6.2.2.2. Because the equations are linear, their integrals are found in terms of exponentials and are generated by solving an eigenvalue problem. The eigenvalues yield the natural frequencies and damping characteristics of characteristic modes of aircraft motion described by the eigenvectors. The final forms of the dynamic characteristics computed by the FLEXSTAB system are computed from the eigenvalues and eigenvectors deduced from the equations of motion.

The linear equations of motion are collected in section 6.4.1 from the development of the preceding sections. These equations are then formed into the systems of first-order, linear differential equations integrated in the FLEXSTAB system by solving the corresponding eigenvalue problems. This process is synonymous with rooting the characteristic equation obtained from the equations of motion, section 6.4.2. The dynamic stability characteristics, section 6.4.3, are computed from the characteristic roots (i.e., from the eigenvalues) and the characteristic modes of motion (i.e., the eigenvectors) are computed normalized with respect to the perturbation pitch attitude, θ_p , and the perturbation bank angle, ϕ_p . The dynamic stability derivatives and control effectiveness values are computed from the aerodynamic force coefficient matrices developed in section 6.3.2. This computation is based on transformations appearing in section 6.4.4.

6.4.1 Linear Equations of Motion

The linear equations of motion are given by equations (6.2-33) and (6.2-34), together with the aerodynamic matrix equations given by equations (6.2-4) and (6.2-5) whose coefficient matrices are defined in 6.3.3. As a collected set of equations they appear as follows:

$$\begin{aligned} [M]\{\dot{V}\}_P + [MM_1]\{V\}_P + [MM_2]\{r_0\}_P = \\ = [A_1]\{V\}_P + [A_2]\{\dot{V}\}_P + [A_3]\{u_1\}_P + \\ + [A_4]\{\dot{u}_1\}_P + [A_5]\{\ddot{u}_1\}_P \end{aligned} \quad (6.4-1)$$

and

$$\begin{aligned} [m_1]\{\ddot{u}_1\}_P + [K_1]\{u_1\}_P = [a_1]\{V\}_P + [a_2]\{\dot{V}\}_P + \\ + [a_3]\{u_1\}_P + [a_4]\{\dot{u}_1\}_P + [a_5]\{\ddot{u}_1\}_P \end{aligned} \quad (6.4-2)$$

where, from equations (6.2-34) and (6.2-35),

$$[A_4] = [A_4^A] - [\bar{G}_R], [a_1] = -[A_1^A] - [G_E], [G_E] \equiv [\phi_{\delta_1}]^T [\Delta_G] [G]$$

and

$$[a_4] = [a_4^A] - [\bar{G}_E], [\bar{G}_E] \equiv [\phi_{\delta_1}]^T [\Delta_G] [\bar{G}_\phi]$$

Equation (6.4-1) constitutes the rigid body equations of motion, while equation (6.4-2) constitutes the structural equations of motion. The objective of this section is to combine these two sets of equations of motion into a single matrix equation having the following form:

$$\{\dot{q}\} + [H]\{q\} = \{0\} \quad (6.4-4)$$

This equation poses an eigenvalue problem. The solution, in the form of eigenvalues and eigenvectors, implies the dynamic stability characteristics of an aircraft—a principal result computed in the FLEXSTAB system analysis.

In the following the equations of motion, as given by equations (6.4-1) and (6.4-2), are arranged in the eigenvalue problem form for six separate cases. These six cases derive from three possible cases of rigid body motion and two possible cases of structural behavior. The three possible cases of rigid body motion are longitudinal motion, lateral-directional motion, and coupled longitudinal and lateral-directional motions. The two possible cases of structural behavior are partially independent structural motion and totally dependent structural motion. In the case of partially independent motion, the $\{u_2\}_p$ degrees of freedom, section 4.2.4.3, are dependent variables while the $\{u_1\}_p$ degrees of freedom are independent variables. In the case of totally dependent motion, all structural degrees of freedom are dependent variables. The vector $\{q\}$ and the matrix $[H]$ are different in each of the six cases.

The six possible vectors $\{q\}$ are as follows: In the case of coupled longitudinal and lateral-directional motions with independent structural motion, the vector $\{q\}$ is given by

$$\{q\} \equiv \begin{bmatrix} u \\ w \\ q \\ v \\ p \\ r \\ \{\dot{u}_1^S\}_p \\ \{\dot{u}_1^A\}_p \\ \hline \theta_p \\ \phi_p \\ \psi_p \\ \{u_1^S\}_p \\ \{u_1^A\}_p \end{bmatrix} \quad (6.4-5)$$

where u , v , and w are perturbation translational velocities; p , q , and r are perturbation rotational velocities; ϕ_P , θ_P , and ψ_P are perturbations to the Euler angles, equation (2.2-1); and $\{u_1^S\}_P$ and $\{u_1^A\}_P$ are perturbations to the free-vibration mode deflection amplitudes—symmetric and antisymmetric, respectively. In the case of longitudinal motion the vector is given by

$$\{q^S\} \equiv \begin{bmatrix} u \\ w \\ q \\ \hline \{\dot{u}_1^S\}_P \\ \hline \theta_P \\ \hline \{u_1^S\}_P \end{bmatrix} \quad (6.4-6)$$

and for the case of lateral-directional motion it is given by

$$\{q^A\} \equiv \begin{bmatrix} v \\ p \\ r \\ \hline \{\dot{u}_1^A\}_P \\ \hline \phi_P \\ \hline \psi_P \\ \hline \{u_1^A\}_P \end{bmatrix} \quad (6.4-7)$$

For the case of totally dependent (i.e., quasi-static) structural behavior the vectors $\{u_1^S\}_P$, $\{u_1^A\}_P$, $\{\dot{u}_1^S\}_P$, $\{\dot{u}_1^A\}_P$ do not appear in the vector $\{q\}$. The primary objective of this section is to derive the $[H]$ coefficient matrices corresponding to each of the six cases.

6.4.1.1 Coupled motion and totally dependent structural behavior.—In the case of coupled motion and totally dependent structural behavior the vector $\{q\}$ is given by

$$\{q\} \equiv \begin{bmatrix} u \\ w \\ q \\ v \\ \hline p \\ r \\ \hline \theta_P \\ \hline \phi_P \\ \hline \psi_P \end{bmatrix} \quad (6.4-8)$$

and the $[H]$ coefficient matrix is expressed in terms of four partitions, viz.,

$$[H_1] \equiv \begin{bmatrix} [G_{11}] & [G_{12}] \\ [D_{31}] & [K_{32}] \end{bmatrix} \quad (6.4-9)$$

where the partition matrices are given by

$$[G_{11}] \equiv ([M] - [A_2])^{-1} ([A_1] - [MM_1]) \quad (6.4-10)$$

$$[G_{12}] \equiv -([M] - [A_2])^{-1} [MM_2] \quad (6.4-11)$$

$$[D_{31}] \equiv \begin{bmatrix} 0 & 0 & -\cos\phi_1 & 0 & 0 & \sin\phi_1 \\ 0 & 0 & -\sin\phi_1 \tan\theta_1 & 0 & -1 & -\cos\phi_1 \tan\theta_1 \\ 0 & 0 & -\sin\phi_1 \sec\theta_1 & 0 & 0 & -\cos\phi_1 \sec\theta_1 \end{bmatrix} \quad (6.4-12)$$

and

$$[K_{32}] \equiv (Q_1 \sin\phi_1 + R_1 \cos\phi_1) \begin{bmatrix} 0 & 1 & 0 \\ -\sec^2\theta_1 & -\tan\theta_1 & 0 \\ -\tan\theta_1 \sec\theta_1 & -\sec\theta_1 & 0 \end{bmatrix} \quad (6.4-13)$$

The matrices $[D_{31}]$ and $[K_{32}]$ are derived from the rigid body kinematics relating the rotation rates $\dot{\phi}_p, \dot{\theta}_p, \dot{\psi}_p$ to the rotation rates p, q, r , and the perturbations to the orientation of the Body Axis System relative to the Inertial Axis System, sections 2.2.1 and 2.2.2.

6.4.1.2 Coupled motion and independent structural motion.—In the case of independent structural motions and coupled rigid-body motion, the structural equations of motion, equation (6.4-2), are combined with the equations of the preceding section and the vector $\{q\}$ is given by equation (6.4-5). A matrix $[J]$ is formed of the coefficients of

$$\begin{bmatrix} \{\dot{V}\}_P \\ \vdots \\ \{\ddot{u}_1\}_P \end{bmatrix} \quad (6.4-14)$$

This matrix is formed of the partitions

$$[J] = \begin{bmatrix} [J_{11}] & [J_{12}] \\ [J_{21}] & [J_{22}] \end{bmatrix} \quad (6.4-15)$$

where

$$[J_{11}] \equiv [M] - [A_2]$$

$$[J_{12}] \equiv [A_5]$$

$$[J_{21}] \equiv -[a_2]$$

$$[J_{22}] \equiv [m_1] - [a_5]$$

The matrix $[J]$ contains the inertia—both mass and aerodynamic. Damping of the aircraft is described by the matrix $[D]$ having the partitions

$$[D] = \begin{bmatrix} [D_{11}] & [D_{12}] \\ [D_{21}] & [D_{22}] \end{bmatrix} \quad (6.4-16)$$

This matrix contains the coefficients of

$$\begin{bmatrix} \{V\}_P \\ \{\dot{u}_1\}_P \end{bmatrix} \quad (6.4-17)$$

Hence, as seen by reference to equations (6.4-1) and (6.4-2), the partitions of the matrix $[D]$ are given by

$$[D_{11}] \equiv [MM_1] - [A_1]$$

$$[D_{12}] \equiv -[A_4]$$

$$[D_{21}] \equiv -[a_1]$$

$$[D_{22}] \equiv -[a_4]$$

(6.4-18)

Stiffness of the aircraft is described by the matrix $[K]$ having the partitions

$$[K] = \begin{bmatrix} [K_{13}] & [K_{14}] \\ [K_{23}] & [K_{24}] \end{bmatrix} \quad (6.4-19)$$

This matrix contains the coefficients of

$$\begin{bmatrix} \{x_0\}_P \\ \{u_1\}_P \end{bmatrix} \quad (6.4-20)$$

where

$$\{r_o\}_P \equiv \begin{bmatrix} \theta_P \\ \phi_P \\ \psi_P \end{bmatrix}$$

Hence, as seen by reference to equations (6.4-1) and (6.4-2), the partitions of the matrix $[K]$ are given by

$$[K_{13}] \equiv [MM_2]$$

$$[K_{14}] \equiv -[A_3]$$

$$[K_{23}] \equiv [0] \quad (6.4-21)$$

$$[K_{24}] \equiv [K_1] - [a_3]$$

Combining the above relations (i.e., equations (6.4-14) through (6.4-21)), the equations of motion are obtained as follows:

$$\begin{bmatrix} [J_{11}] & [J_{12}] \\ [J_{21}] & [J_{22}] \end{bmatrix} \begin{bmatrix} \{\dot{V}\}_P \\ \{\ddot{u}_1\}_P \end{bmatrix} + \begin{bmatrix} [D_{11}] & [D_{12}] \\ [D_{21}] & [D_{22}] \end{bmatrix} \begin{bmatrix} \{V\}_P \\ \{\dot{u}_1\}_P \end{bmatrix} + \begin{bmatrix} [K_{13}] & [K_{14}] \\ [K_{23}] & [K_{24}] \end{bmatrix} \begin{bmatrix} \{r_o\}_P \\ \{u_1\}_P \end{bmatrix} = \{0\} \quad (6.4-22)$$

To these equations the following expressions are added relating $\{\dot{r}_o\}_P$ to $\{V\}_P$, $\{\dot{u}_1\}_P$ to $\{\dot{u}_1\}_P$ and $\{\ddot{r}_o\}_P$ to $\{\ddot{r}_o\}_P$:

$$\begin{bmatrix} \{\dot{r}_o\}_P \\ \{\ddot{r}_o\}_P \end{bmatrix} - \begin{bmatrix} [D_{31}] & [D_{32}] \\ [D_{41}] & [D_{42}] \end{bmatrix} \begin{bmatrix} \{V\}_P \\ \{\dot{u}_1\}_P \end{bmatrix} = \{0\} \quad (6.4-23)$$

where

$$[D_{31}] \equiv \begin{bmatrix} 0 & 0 & -\cos\phi_1 & 0 & 0 & \sin\phi_1 \\ 0 & 0 & -\sin\phi_1 \tan\theta_1 & 0 & -1 & -\cos\phi_1 \tan\theta_1 \\ 0 & 0 & -\sin\phi_1 \sec\theta_1 & 0 & 0 & -\cos\phi_1 \sec\theta_1 \end{bmatrix}$$

$$[D_{32}] \equiv [0]$$

$$[D_{41}] = [0]$$

$$[D_{42}] = -[I]$$

$$\begin{bmatrix} \{\dot{r}_0\}_P \\ \{\dot{u}_1\}_P \end{bmatrix} - \begin{bmatrix} [K_{33}] & [K_{34}] \\ [K_{43}] & [K_{44}] \end{bmatrix} \begin{bmatrix} \{r_0\}_P \\ \{u_1\}_P \end{bmatrix} = \{0\} \quad (6.4-24)$$

where

$$[K_{33}] \equiv (Q_1 \sin \phi_1 + R_1 \cos \phi_1) \begin{bmatrix} 0 & 1 & 0 \\ -\sec^2 \theta_1 & -\tan \theta_1 & 0 \\ -\tan \theta_1 \sec \theta_1 & -\sec \theta_1 & 0 \end{bmatrix}$$

$$[K_{34}] \equiv [0]$$

$$[K_{43}] \equiv [0]$$

$$[K_{44}] \equiv [0]$$

The matrix $[D_{31}]$ is identical to that defined by equation (6.4-12), while the matrix partition $[K_{33}]$ is identical with $[K_{32}]$ defined by equation (6.4-13). The equations of motion are now expressed in eigenvalue problem form, i.e., equation (6.4-4), as follows:

$$\{\dot{q}\} + \left[\begin{array}{cc|cc} [J]^{-1} & [D] & [J]^{-1} & [K] \\ \hline [D_{31}] & [0] & [K_{33}] & [0] \\ \hline [0] & -[I] & [0] & [0] \end{array} \right] \{q\} = \{0\} \quad (6.4-25)$$

The matrix appearing as the coefficient of $\{q\}$ is the desired coefficient matrix $[H]$ of the eigenvalue problem.

6.4.1.3 Longitudinal motion and totally dependent structural behavior.—The perturbation equations of motion can be reduced to those governing motion in the X, Z plane of the aircraft, i.e., longitudinal motion, when certain conditions are satisfied. One condition is on the reference flight condition and consists of the requirement that

$$P_1 = R_1 = 0, \quad \phi_1 = 0 \quad \text{and} \quad h_X^G = h_Z^G = 0 \quad (6.4-26)$$

Thus, the reference flight condition must consist of wings level, non-rolling, non-yawing flight, and the engine gyroscopic couples h_x^G and h_z^G must be zero or negligibly small. In addition, it is presumed that antisymmetric motion is unperturbed, i.e.,

$$v = 0, \quad p = r = 0, \quad \text{and} \quad \phi_p = 0 \quad (6.4-27)$$

In these cases, the rigid body equations of motion, equation (6.4-1), become, for totally dependent structural behavior,

$$\begin{aligned} [M^S]\{\dot{V}^S\}_P + [MM_1^S]\{V^S\}_P + [MM_2^S]\{r_0^S\}_P &= \\ &= [A_1]\{V^S\}_P + [A_2]\{\dot{V}^S\}_P \end{aligned} \quad (6.4-28)$$

where

$$[M^S] \equiv \begin{bmatrix} M & 0 & 0 \\ 0 & M & 0 \\ 0 & 0 & I_{YY} \end{bmatrix} \quad (6.4-29)$$

$$[MM_1^S] \equiv \begin{bmatrix} 0 & MQ_1 & MW_1 \\ -MQ_1 & 0 & -MU_1 \\ 0 & 0 & 0 \end{bmatrix} \quad (6.4-30)$$

and

$$[MM_2^S] \equiv \begin{bmatrix} -\cos\theta_1 & 0 \\ -\sin\theta_1 & 0 \\ 0 & 0 \end{bmatrix} Mg. \quad (6.4-31)$$

The equations of motion are expressed in terms of the vector

$$\{q^S\} \equiv \begin{bmatrix} u \\ w \\ q \\ \theta_P \end{bmatrix} \quad (6.4-32)$$

as

$$\{\dot{q}^S\} + [H_1^S]\{q^S\} = \{0\} \quad (6.4-33)$$

where $[H_1^S]$ is given by equation (6.4-9) but the partitions of $[H_1^S]$ corresponding to $[D_{31}]$ and $[K_{33}]$, become

$$[D_{31}^S] \equiv [00-1]$$

and

$$[K_{33}^S] \equiv 0$$

(6.4-34)

The coefficient matrix, therefore, is given by

$$[H_1^S] \equiv \left[\begin{array}{c|c} [G_{11}^S] & \{G_{12}^S\} \\ \hline [0 \ 0 -1] & 0 \end{array} \right] \quad (6.4-35)$$

wherein the partitions are as follows:

$$[G_{11}^S] \equiv ([M^S] - [A_2^S])^{-1} ([A_1^S] - [MM_1^S])$$

and

(6.4-36)

$$\{G_{12}^S\} \equiv -([M^S] - [A_2^S])^{-1} \{MM_2^S\}$$

6.4.1.4 Lateral-directional motion and totally dependent structural behavior.—Assuming that the conditions listed by equation (6.4-26) are satisfied and, in addition, that there is no reference flight condition sideslip, the longitudinal perturbation motion can be assumed unperturbed, i.e.,

$$u = w = 0, \quad q = 0 \text{ and } \theta_p = 0 \quad (6.4-37)$$

In these cases, the rigid body equations of motion, equation (6.4-1), become

$$\begin{aligned} [M^A]\{\dot{V}^A\}_P + [MM_1^A]\{V^A\}_P + [MM_2^A]\{r_o^A\}_P &= \\ &= [A_1^A]\{V^A\}_P + [A_2^A]\{\dot{V}^A\}_P \end{aligned} \quad (6.4-38)$$

where

$$[M^A] \equiv \begin{bmatrix} M & 0 & 0 \\ 0 & I_{XX} & -I_{XZ} \\ 0 & -I_{XZ} & I_{ZZ} \end{bmatrix} \quad (6.4-39)$$

$$[MM_1^A] \equiv \begin{bmatrix} 0 & -Mw_1 & MU_1 \\ 0 & -Q_1 I_{XZ} & Q_1 (I_{ZZ} - I_{YY}) \\ 0 & Q_1 (I_{YY} - I_{XX}) & Q_1 I_{XZ} \end{bmatrix} \quad (6.4-40)$$

and

$$[MM_2^A] \equiv \begin{bmatrix} \cos \theta_1 & 0 \\ 0 & 0 \\ 0 & 0 \end{bmatrix} Mg \quad (6.4-41)$$

The equations of motion are expressed in terms of the vector

$$\{q^A\} \equiv \begin{bmatrix} v \\ p \\ q \\ \phi_P \\ \psi_P \end{bmatrix} \quad (6.4-42)$$

as

$$\{\dot{q}^A\} + [H_1^A]\{q^A\} = \{0\} \quad (6.4-43)$$

where $[H_1^A]$ is given by equation (6.4-9) but the partitions of $[H_1^A]$, corresponding to $[D_{31}]$ and $[K_{32}]$, become

$$[D_{31}^A] \equiv \begin{bmatrix} 0 & -1 & -\tan \theta_1 \\ 0 & 0 & -\sec \theta_1 \end{bmatrix} \quad (6.4-44)$$

and

$$[K_{32}^A] \equiv \begin{bmatrix} 0 & 0 \\ 0 & 0 \end{bmatrix}$$

The coefficient matrix, therefore, is given by

$$[H_1^A] \equiv \begin{bmatrix} [G_{11}^A] & [C_{12}^A] \\ [D_{31}^A] & [K_{32}^A] \end{bmatrix} \quad (6.4-45)$$

wherein the partitions are as follows:

$$[G_{11}^A] \equiv ([M^A] - [A_2^A])^{-1} ([A_1^A] - [MM_1^A])$$

and

$$[G_{12}^A] \equiv - ([M^A] - [A_2^A])^{-1} [MM_2^A] \quad (6.4-46)$$

6.4.1.5 Longitudinal motion and independent symmetric structural motion.—In the case of longitudinal motion with independent structural motion, the structural equations of motion, equation (6.4-2), are reduced to the case of symmetric structural motions. They are then combined with the rigid body equations of motion when the latter are expressed for the case of longitudinal perturbations, section 6.4.1.3. The reference flight condition is assumed to satisfy equations (6.4-26), and structural perturbations are assumed to be such that $\{u^A\}_P = \{0\}$ for all time. The equations of motion are expressed in eigenvalue form, i.e., equation (6.4-4), as follows:

$$\{\dot{q}^S\} + [H_2^S]\{q^S\} = \{0\} \quad (6.4-47)$$

where the coefficient matrix has the form given by equation (6.4-25), i.e.,

$$[H_2^S] \equiv \begin{bmatrix} [J^S]^{-1} & [D^S] & [J^S]^{-1} & [K^S] \\ [D_{31}^S] & [0] & [K_{33}^S] & [0] \\ [0] & [-I] & [0] & [0] \end{bmatrix} \quad (6.4-48)$$

where $[J^S]$, $[D^S]$, and $[K^S]$ are formed following the definitions of equations (6.4-15), (6.4-16), and (6.4-19) but with the elements computed using the definitions given by equations (6.4-29), (6.4-30), and (6.4-31). The vector $\{q^S\}$ is given by equation (6.4-6), while the partitions $[D_{31}^S]$ and $[K_{33}^S]$ are those defined by equation (6.4-34).

6.4.1.6 Lateral-directional motion and independent antisymmetric structural motion.—In the case of lateral-directional motion with independent structural motion, the structural equations of motion, equation (6.4-2), are reduced to the case of antisymmetric motion and are combined with the rigid-body equations of motion when the latter are expressed for the case of lateral-directional perturbations, section 6.4.1.4. The reference flight condition is assumed to satisfy equations (6.4-26) with the added requirement that the reference flight condition sideslip velocity is zero— $V_1 = 0$ —and the structural perturbations are assumed to be such that $\{u^A\}_P = \{0\}$ for all time. The equations of motion are expressed in the eigenvalue form, i.e., equation (6.4-4) as follows:

$$\{\dot{q}^A\} + [H^A]\{q^A\} = \{0\} \quad (6.4-49)$$

where the coefficient matrix has the form given by equation (6.4-25), i.e.,

$$[H_2^A] \equiv \left[\begin{array}{cc|cc} [J^A]^{-1} & [D^A] & [J^A]^{-1} & [K^A] \\ \hline [D_{31}^A] & [0] & [K_{33}^A] & [0] \\ \hline [0] & -[I] & [0] & [0] \end{array} \right] \quad (6.4-50)$$

where $[J^A]$, $[D^A]$ and $[K^A]$ are formed following the definition of equations (6.4-15), (6.4-16), and (6.4-19) but with the elements computed using the definitions given by equations (6.4-39), (6.4-40), and (6.4-41). The vector $\{q^A\}$ is given by equations (6.4-7), while the partitions $[D_{31}^A]$ and $[K_{33}^A]$ are as defined by equations (6.4-44).

6.4.2 Characteristic Equation Rooting

The linear dynamic analysis performed by the FLEXSTAB system is an evaluation of the eigenvalues and eigenvectors of equation (6.4-4), i.e.,

$$\{\dot{q}\} + [H]\{q\} = \{0\}$$

The coefficient matrix $[H]$ is a nonsymmetric matrix having real elements, and the eigenvalues and eigenvectors are computed by the following sequence of operations*: (1) reduction to upper Hessenberg form; (2) generation of eigenvalues by QR iteration, (3) shifting and deflation, and (4) generation of eigenvectors by the inverse power method with shifts. The eigenvalues and eigenvectors are denoted as λ_i and $\{q\}_i$. The eigenvalues may be real numbers, or they may be found to be complex conjugate pairs of numbers. Since the motion implied by an eigenvalue and eigenvector consists of

$$\{q\}_i = \{q^*\}_i e^{\lambda_i t} \quad (6.4-51)$$

a real eigenvalue implies exponential time dependence, while a complex conjugate pair

$$\lambda_i = n_i \pm i\omega_i \quad (6.4-52)$$

implies harmonic time dependence with frequency ω_i and with an exponential variation in amplitude.

6.4.3 Dynamic Stability Characteristics

The dynamic stability characteristics computed by the FLEXSTAB system are as follows:

- a) time and number of cycles of each harmonic mode of motion (i.e., eigenvector $\{q\}_i$) to one-half (or double) and one-tenth amplitude
- b) frequency and period of each harmonic motion

*These operations are described in detail in section 9.5 of volume III.

- c) Logarithmic decrement and ratio of successive maximum amplitudes of each harmonic mode of motion
- d) undamped natural frequency of each harmonic mode of motion
- e) damping ratio of each mode
- f) phase and amplitude of modal coupling terms

These quantities are computed from the eigenvalues and eigenvectors as follows:

6.4.3.1 Times to one-half and one-tenth amplitude.—The periods of time to one-half amplitude ($t_{1/2x}$), to double amplitude (t_{2x}), and one-tenth amplitude ($t_{1/10x}$) are:

$$(t_{1/2x})_i \equiv \frac{\ln 2}{|\lambda_i|}, \quad (t_{2x})_i \equiv \frac{\ln 2}{|\lambda_i|}, \quad (t_{1/10x})_i \equiv \frac{\ln 10}{|\lambda_i|} \quad (6.4-53)$$

λ_i complex:

$$(t_{1/2x})_i \equiv \frac{\ln 2}{|n_i|}, \quad (t_{2x})_i \equiv \frac{\ln 2}{|n_i|}, \quad (t_{1/10x})_i \equiv \frac{\ln 10}{|n_i|} \quad (6.4-54)$$

For harmonic motion the number of cycles to one-half amplitude ($N_{1/2x}$), double amplitude (N_{2x}) and one-tenth amplitude ($N_{1/10x}$) are:

$$(N_{1/2x})_i \equiv \frac{\ln 2}{2\pi} \frac{\omega_i}{|n_i|}, \quad (N_{2x})_i \equiv \frac{\ln 2}{2\pi} \frac{\omega_i}{|n_i|}, \quad (N_{1/10x})_i \equiv \frac{\ln 10}{2\pi} \frac{\omega_i}{|n_i|} \quad (6.4-55)$$

6.4.3.2 Frequency and period.—The frequency of a harmonic motion is computed as

$$f_i = \frac{\omega_i}{2\pi} \text{ Hz} \quad (6.4-56)$$

and the period is computed as

$$T_i \equiv \frac{2\pi}{\omega_i} \text{ seconds} \quad (6.4-57)$$

6.4.3.3 Logarithmic decrement.—The logarithmic decrement δ_i (i.e., the natural logarithm of the ratio of successive maximum amplitudes of harmonic motion) is computed as

$$\delta_i = -2\pi \frac{n_i}{\omega_i} \quad (6.4-58)$$

6.4.3.4 Undamped natural frequency.—The undamped natural frequency of a harmonic motion is computed as

$$f_{n_i} = \frac{1}{2\pi} \sqrt{\omega_i^2 + n_i^2} \quad \text{Hz} \quad (6.4-59)$$

6.4.3.5 Damping ratio.—The damping ratio (i.e., the ratio of actual damping to critical damping for which harmonic motion is suppressed) is computed as

$$\zeta_i = -\frac{n_i}{\omega_i} \quad (6.4-60)$$

6.4.3.6 Phase and amplitude of modal coupling.—Each eigenvector $\{q\}_i$ is, in general, a vector with complex elements representing the relative amplitudes and phase relationships of the quantities describing a characteristic mode of aircraft perturbation motion. Considering the example of coupled motion with independent structural motions, section 6.4.1.2, the vector $\{q\}_i$ for the i^{th} characteristic mode of motion is given by

$$\{q\}_i = \{q^*\}_i e^{(n_i + i\omega_i)t} \quad (6.4-61)$$

where the asterisk denotes the elements to be complex numbers. The first element of $\{q^*\}_i$ is given by

$$u_i^* \equiv u_{Ri} + j u_{Ii}$$

where u_{Ri} is the real part and u_{Ii} is the imaginary part of the complex velocity component representing a perturbation to the forward velocity of the aircraft. The amplitude of this velocity component is given by

$$|u_i^*| = \sqrt{(u_{Ri})^2 + (u_{Ii})^2}$$

while the phase angle is given by

$$\phi_{ui} = \tan^{-1} \frac{u_{Ii}}{u_{Ri}}$$

The relative amplitudes and phase angles are computed by normalizing the elements of the eigenvectors with respect to one of the elements. In the FLEXSTAB system they are normalized with respect to the perturbation pitch attitude, θ_p , and the perturbation bank angle, ϕ_p .

6.4.4 Dynamic Stability Derivatives

The following dynamic stability derivatives are computed by the FLEXSTAB system. They are formed from the aerodynamic force coefficient matrices of section 6.3.2 and equations (5.6-24) and (5.6-36):

$$\begin{bmatrix} C_{D_u} \\ C_{L_u} \\ C_{m_u} \end{bmatrix} = U_1 [DER^S] \left(\{F_u^S\}_R + \{\Delta F_u^S\}_E \right) \quad (6.4-62)$$

$$\begin{bmatrix} C_{D_\alpha} \\ C_{L_\alpha} \\ C_{m_\alpha} \end{bmatrix} = U_1 [DER^S] \left(\{F_w^S\}_R + \{\Delta F_w^S\}_E \right) \sec^2 \alpha_1 \quad (6.4-63)$$

$$+ \frac{1}{\bar{Q}_1 S_w} \begin{bmatrix} \cos \alpha_1 & \sin \alpha_1 & 0 \\ \sin \alpha_1 & -\cos \alpha_1 & 0 \\ 0 & 0 & 0 \end{bmatrix} \left(\{F_B^A\}_{R_1} + \{\Delta F_B^A\}_{E_1} \right)$$

$$\begin{bmatrix} C_{D_q} \\ C_{L_q} \\ C_{m_q} \end{bmatrix} = \frac{2U_1}{\bar{C}} [DER^S] \left(\{F_Q^S\}_R + \{\Delta F_Q^S\}_E \right) \quad (6.4-64)$$

$$\begin{bmatrix} C_{Y_\beta} \\ C_{l_\beta} \\ C_{n_\beta} \end{bmatrix} = U_1 [DER^A] \left(\{F_v^A\}_R + \{\Delta F_v^A\}_E \right) \quad (6.4-65)$$

$$\begin{bmatrix} C_{Y_p} \\ C_{l_p} \\ C_{n_p} \end{bmatrix} = \frac{2U_1}{\bar{b}} [DER^A] \left(\{F_p^A\}_R + \{\Delta F_p^A\}_E \right) \quad (6.4-67)$$

$$\begin{bmatrix} C_{Y_r} \\ C_{l_r} \\ C_{r_r} \end{bmatrix} = \frac{2U_1}{b} [DER^A] \left(\{F_R^A\}_R + \{\Delta F_R^A\}_E \right) \quad (6.4-68)$$

$$\begin{bmatrix} C_{L_\alpha} \\ C_{D_\alpha} \\ C_{m_\alpha} \end{bmatrix} = \frac{2U_1^2}{\bar{c}} [DER^S] \left(\{F_W^A\}_R + \{\Delta F_W^A\}_E \right) \quad (6.4-69)$$

$$\begin{bmatrix} C_{Y_\beta} \\ C_{l_\beta} \\ C_{n_\beta} \end{bmatrix} = \frac{2U_1^2}{b} [DER^A] \left(\{F_V^A\}_R + \{\Delta F_V^A\}_E \right) \quad (6.4-70)$$

$$\begin{bmatrix} C_{Y_P} \\ C_{l_P} \\ C_{n_P} \end{bmatrix} = \frac{4U_1^2}{b^2} [DER^A] \left(\{F_P^A\}_R + \{\Delta F_P^A\}_E \right) \quad (6.4-71)$$

$$\begin{bmatrix} C_{Y_r} \\ C_{l_r} \\ C_{n_r} \end{bmatrix} = \frac{4U_1^2}{b^2} [DER^A] \left(\{F_R^A\}_R + \{\Delta F_R^A\}_E \right) \quad (6.4-72)$$

where

$$[DER^S] \equiv \frac{1}{\bar{a}_1 S_w} \begin{bmatrix} \sin \alpha_1 & -\cos \alpha_1 & 0 \\ -\cos \alpha_1 & -\sin \alpha_1 & 0 \\ 0 & 0 & \frac{1}{\bar{c}} \end{bmatrix} \quad (6.4-73)$$

and

$$[DER^A] \equiv \frac{1}{\bar{c}_i S_{wb}} \begin{bmatrix} 1 & 0 & 0 \\ 0 & \cos \alpha & \sin \alpha \\ 0 & -\sin \alpha & \cos \alpha \end{bmatrix} \quad (6.4-74)$$

Each of these dynamic stability derivatives is computed by FLEXSTAB for the following cases: flexible aircraft derivatives, rigid aircraft derivatives, and as aeroelastic increments. The computations and the computed results are completely analogous to the static stability derivatives of section 5.6, and the computed results are nondimensional in accord with table 5.6-1.

In addition to the dynamic stability derivatives, the system computes the following control effectiveness values:

$$\begin{bmatrix} C_{L\delta e} \\ C_{D\delta e} \\ C_{m\delta e} \end{bmatrix} = [DER^S] \left(\{F_{\delta e}^S\}_R + \{\Delta F_{\delta e}^S\}_E \right) \quad (6.4-75)$$

where

$$\{F_{\delta e}^S\}_R \equiv \bar{q}_1 \left([G_{\theta R}] + [G_{\delta R}] \right) \{\psi_{\delta e}\} + \bar{q}_1 \left([G_{\psi R}] + [G_{\delta \psi R}] \right) \{\dot{\psi}_{\delta e}\} \quad (6.4-76)$$

$$\{\Delta F_{\delta e}^S\}_E \equiv \bar{q}_1 [G_{R\theta E}] \{\psi_{\delta e}\} + \bar{q}_1 [G_{R\psi E}] \{\dot{\psi}_{\delta e}\} \quad (6.4-77)$$

$$\begin{bmatrix} C_{L\delta e} \\ C_{D\delta e} \\ C_{m\delta e} \end{bmatrix} = [DER^S] \left(\{F_{\delta e}^S\}_R + \{\Delta F_{\delta e}^S\}_E \right) \quad (6.4-78)$$

where

$$\{F_{\delta e}^S\}_R \equiv \bar{q}_1 [\delta G_{\theta R}] \{\psi_{\delta e}\} \quad (6.4-79)$$

$$\{\Delta F_{\delta e}^S\}_E \equiv \bar{q}_1 [\delta G_{R\delta E}] \{\psi_{\delta e}\} \quad (6.4-80)$$

$$\begin{bmatrix} C_{Y_{\delta a}} \\ C_{l_{\delta a}} \\ C_{n_{\delta a}} \end{bmatrix} = [DEF^A] \left(\{F_{\delta a}^A\}_R + \{\Delta F_{\delta a}^A\}_E \right) \quad (6.4-81)$$

where

$$\{F_{\delta a}^A\}_R \equiv \bar{q}_1 \left([G_{\theta R}] + [\mathcal{G}_{\theta R}] \right) \{\psi_{\delta a}\} + \bar{q}_1 \left([G_{\psi R}] + [\mathcal{G}_{\psi R}] \right) \{\psi'_{\delta a}\} \quad (6.4-82)$$

$$\{\Delta F_{\delta a}^A\}_E \equiv \bar{q}_1 [C_{R\theta E}] \{\psi_{\delta a}\} + \bar{q}_1 [G_{R\psi E}] \{\psi'_{\delta a}\} \quad (6.4-83)$$

$$\begin{bmatrix} C_{Y_{\delta a}} \\ C_{l_{\delta a}} \\ C_{n_{\delta a}} \end{bmatrix} = [DEF^A] \left(\{F_{\delta a}^A\}_R + \{\Delta F_{\delta a}^A\}_E \right) \quad (6.4-84)$$

where

$$\{F_{\delta a}^A\}_R \equiv \bar{q}_1 [\delta G_{\theta R}] \{\psi_{\delta a}\} \quad (6.4-85) \quad \{\Delta F_{\delta a}^A\}_E \equiv \bar{q}_1 [\delta G_{R\theta E}] \{\psi_{\delta a}\} \quad (6.4-86)$$

$$\begin{bmatrix} C_{Y_{\delta r}} \\ C_{l_{\delta r}} \\ C_{n_{\delta r}} \end{bmatrix} \equiv [DEF^A] \left(\{F_{\delta r}^A\}_R + \{\Delta F_{\delta r}^A\}_E \right) \quad (6.4-87)$$

where

$$\{F_{\delta r}^A\}_R \equiv \bar{q}_1 \left([G_{\theta R}] + [G_{\theta R}^*] \right) \{\psi_{\delta r}\} + \bar{q}_1 \left([G_{\psi R}] + [G_{\psi R}^*] \right) \{\psi_{\delta r}^*\} \quad (6.4-88)$$

$$\{\Delta F_{\delta r}^A\}_E \equiv \bar{q}_1 [G_{R\theta E}] \{\psi_{\delta r}\} + \bar{q}_1 [G_{R\psi E}] \{\psi_{\delta r}^*\} \quad (6.4-89)$$

$$\begin{bmatrix} C_{Y_{\delta r}} \\ C_{L_{\delta r}} \\ C_{n_{\delta r}} \end{bmatrix} \equiv [DER^A] \left(\{F_{\delta r}^A\}_R + \{\Delta F_{\delta r}^A\}_E \right) \quad (6.4-90)$$

where

$$\{F_{\delta r}^A\}_R \equiv \bar{q}_1 [SG_{\theta R}] \{\psi_{\delta r}\} \quad (6.4-91)$$

$$\{\Delta F_{\delta r}^A\}_E \equiv \bar{q}_1 [\delta G_{R\theta E}] \{\psi_{\delta r}\} \quad (6.4-92)$$

In addition to the above control effectiveness values, the FLEXSTAB system computes the following generalized aerodynamic forces conjugate with the free vibration mode shape amplitudes:

$$\{\bar{Q}_{\delta e}^S\}_R \equiv \bar{q}_1 \left([H_{\theta R}] + [H_{\theta R}^*] \right) \{\psi_{\delta e}\} + \bar{q}_1 \left([H_{\psi R}] + [H_{\psi R}^*] \right) \{\psi_{\delta e}^*\} \quad (6.4-93)$$

$$\{\Delta \bar{Q}_{\delta e}^S\}_E \equiv \bar{q}_1 [H_{R\theta E}] \{\psi_{\delta e}\} + \bar{q}_1 [H_{R\psi E}] \{\psi_{\delta e}^*\} \quad (6.4-94)$$

$$\{\bar{Q}_{\delta a}^A\}_R \equiv \bar{q}_1 \left([H_{\theta R}] + [H_{\theta R}^*] \right) \{\psi_{\delta a}\} + \bar{q}_1 \left([H_{\psi R}] + [H_{\psi R}^*] \right) \{\psi_{\delta a}^*\} \quad (6.4-95)$$

$$\{\Delta \bar{Q}_{\delta a}^A\}_E \equiv \bar{q}_1 [H_{R\theta E}] \{\psi_{\delta a}\} + \bar{q}_1 [H_{R\psi E}] \{\psi_{\delta a}^*\} \quad (6.4-96)$$

$$\{\bar{Q}_{\delta r}^A\}_R \equiv \bar{q}_1 \left([H_{\theta R}] + [H_{\theta R}^*] \right) \{\psi_{\delta r}\} + \bar{q}_1 \left([H_{\psi R}] + [H_{\psi R}^*] \right) \{\psi_{\delta r}^*\} \quad (6.4-97)$$

$$\{\Delta \bar{Q}_{\delta r}^A\}_E \equiv \bar{q}_1 [H_{R\theta E}] \{\psi_{\delta r}\} + \bar{q}_1 [H_{R\psi E}] \{\psi_{\delta r}\} \quad (6.4-98)$$

$$\{\bar{Q}_{\delta e}^S\}_R \equiv \bar{q}_1 [\delta H_{\theta R}] \{\psi_{\delta e}\} \quad (6.4-99)$$

$$\{\Delta Q_{\delta e}^S\}_E \equiv \bar{q}_1 [\delta H_{R\theta E}] \{\psi_{\delta e}\} \quad (6.4-100)$$

$$\{\bar{Q}_{\delta a}^A\}_R \equiv \bar{q}_1 [\delta H_{\theta R}] \{\psi_{\delta a}\} \quad (6.4-101)$$

$$\{\Delta \bar{Q}_{\delta a}^A\}_E \equiv \bar{q}_1 [\delta H_{R\theta E}] \{\psi_{\delta a}\} \quad (6.4-102)$$

$$\{\bar{Q}_{\delta r}^A\}_R \equiv \bar{q}_1 [\delta H_{\theta R}] \{\psi_{\delta r}\} \quad (6.4-103)$$

$$\{\Delta \bar{Q}_{\delta r}^A\}_E \equiv \bar{q}_1 [\delta H_{R\theta E}] \{\psi_{\delta r}\} \quad (6.4-104)$$

6.5 NONLINEAR DYNAMIC ANALYSIS

The nonlinear dynamic analysis is performed by integrating, by a numerical method, the nonlinear equations of motion. The numerical method is the fifth-order Runge-Kutta method and may be executed using a fixed step size or a variable step size. Initial conditions may be chosen as arbitrary initial values for the perturbation variables. Only one type of forcing function is currently used—that due to penetration of a discrete gust. The gust velocity distribution, section 6.5.2, may be a sine wave, a one-minus-cosine wave, or a modified square wave.

The nonlinear character of the equations of motion may arise from a combination of causes. Perturbations to the motions may be so large as to require the nonlinear equations for rigid body motion of section 6.2.2.1, or the rigid parts of the aerodynamic matrices, section 6.3.3, may be functions of the perturbation motion variables. In the latter case, the aerodynamic force coefficients are supplied to the FLEXSTAB system in tabular form much as in section 5.3.5.2—the nonlinear trim problem.

6.5.1 Nonlinear Equations of Motion

For a nonlinear dynamic analysis the equations of motion, equations (6.2-29), are expressed in the following special form:

$$\{\dot{V}\}_P = ([M] - [A_2])^{-1} ([A_5] \{\ddot{u}_1\}_P + [E]) \quad (6.5-1)$$

and

$$\begin{aligned} \{\ddot{U}_1\}_P = & \left[\{f_{m_1}\} - [a_5] - [a_2] \left([M] - [A_2] \right)^{-1} [A_5] \right]^x \\ & \times \left[[a_1]\{V\}_P + ([a_3] - [K_1])\{u_1\}_P \right. \\ & \left. + [a_4]\{\dot{u}_1\}_P + [a_2] \left([M] - [A_2] \right)^{-1} [E] \right] \end{aligned} \quad (6.5-2)$$

where

$$\begin{aligned} [E] \equiv & \left([A_1] - [MM_1] \right) \{V\}_P + [A_3]\{u_1\}_P \\ & + [A_4]\{\dot{u}_1\}_P - [MM_2]\{r_0\}_P \end{aligned} \quad (6.5-3)$$

Equation (6.5-1), when integrated, yields the perturbation rigid body velocity, while equation (6.5-2) yields the structural perturbations. These equations are coupled so that they are integrated simultaneously, and because the quantities which are computed are

$$\begin{aligned} & \dot{\vec{v}}_{CP}, \vec{v}_{CP}, \dot{\vec{\omega}}_P, \vec{\omega}_P, \dot{\vec{\theta}}_P, \vec{\theta}_P, \dot{\vec{\phi}}_P, \vec{\phi}_P, \dot{\vec{\psi}}_P, \vec{\psi}_P, \\ & \vec{r}_{OP}, |\vec{v}_C|, n_P \text{ (i.e., perturbation load factor)} \end{aligned}$$

and $\left(\frac{d\vec{r}_0}{dt} \right)_P$

the equations describing these quantities must be integrated as well, reference 2-2, section 4.12.

6.5.2 Nonlinear Aerodynamic Data

The aerodynamic forces contained in the equations of motion, viz., the matrices $[A_1^A]$ and $[A_2^A]$, are expressed as the sums

$$[A_1^A] = [A_{R_1}] + [\Delta A_{E_1}] \quad (6.5-4)$$

and

$$[A_2^A] = [A_{R_2}] + [\Delta A_{E_2}]$$

The elements of $[A_{R_1}]$ and $[A_{R_2}]$, section 6.3.2, contain the aerodynamic force coefficients for a rigid aircraft. These quantities may be supplied to the FLEXSTAB system expressed as functions of the perturbation motion variables. This functionality is expressed in tabular form with each element as a function of two variables contained in $\{V\}_P$ and $\{\dot{V}\}_P$, one of which is always w .

The rigid aircraft data are supplied to the FLEXSTAB system expressed in the Stability Axis System and in a nondimensional form consistent with table 5.6-1. This data may be used to construct any of the elements of $[AR_1]$ and $[AR_2]$ shown as non-zero in the following two equations:

$$[A_{R_1}] = \begin{bmatrix} F_{X_u}^A & F_{X_w}^A & F_{X_q}^A & | & F_{X_v}^A & F_{X_p}^A & F_{X_r}^A \\ F_{Z_u}^A & F_{Z_w}^A & F_{Z_q}^A & | & F_{Z_v}^A & F_{Z_p}^A & F_{Z_r}^A \\ M_{Y_u}^A & M_{Y_w}^A & M_{Y_q}^A & | & M_{Y_v}^A & M_{Y_p}^A & M_{Y_r}^A \\ \hline 0 & F_{Y_w}^A & 0 & | & F_{Y_v}^A & F_{Y_p}^A & F_{Y_r}^A \\ 0 & M_{X_w}^A & 0 & | & M_{X_v}^A & M_{X_p}^A & M_{X_r}^A \\ 0 & M_{Z_w}^A & 0 & | & M_{Z_v}^A & M_{Z_p}^A & M_{Z_r}^A \end{bmatrix} \quad (6.5-5)$$

$$[A_{R_2}] = \begin{bmatrix} 0 & F_{X_w}^A & F_{X_q}^A & | & 0 & 0 & 0 \\ 0 & F_{Z_w}^A & F_{Z_q}^A & | & 0 & 0 & 0 \\ 0 & M_{Y_w}^A & M_{Y_q}^A & | & 0 & 0 & 0 \\ \hline 0 & 0 & 0 & | & F_{Y_v}^A & F_{Y_p}^A & F_{Y_r}^A \\ 0 & 0 & 0 & | & M_{X_v}^A & M_{X_p}^A & M_{X_r}^A \\ 0 & 0 & 0 & | & M_{Z_v}^A & M_{Z_p}^A & M_{Z_r}^A \end{bmatrix} \quad (6.5-6)$$

Any three-element column in a partition of $[AR_1]$ and $[AR_2]$ may be described in the form of nonlinear tabular data, e.g.,

$$\{F_u^S\}_R \equiv \begin{bmatrix} F_{X_u}^A \\ F_{Z_u}^A \\ M_{Y_u}^A \end{bmatrix}_R \quad (6.5-7)$$

and

$$\{F_u^S\}_R = \{F_u^S(u, w)\}_R \quad (6.5-8)$$

In this example the values for the elements $\{F_u^S\}_R$ in $\{A_{R1}\}$, computed from equation (6.3-14), are replaced by values which are functions of the perturbation velocity components u and w .

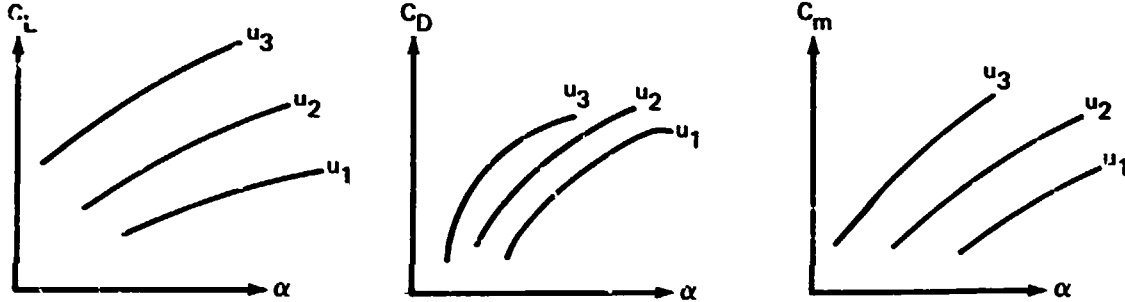
The tabular data define the following aerodynamic force coefficients:

$$\{C^S(i)\} \equiv \begin{bmatrix} C_L(i) \\ C_D(i) \\ C_m(i) \end{bmatrix} \quad \{C^A(i)\} \equiv \begin{bmatrix} C_Y(i) \\ C_\ell(i) \\ C_n(i) \end{bmatrix} \quad (6.5-9)$$

where, for example, $C_L(i)$ denotes the value of the lift coefficient for the i^{th} set of values of the variables chosen from $\{V_P\}$. The tables which may be supplied to the FLEXSTAB system, shown in graphical form, are the following:

6.5.2.1 Nonlinear steady aerodynamic data

- 1) Tables for constructing $\{F_u^S(u, w)\}_R$, $\{F_w^S(u, w)\}_R$:



$$C_L = C_L(\alpha, \hat{u}) \quad , \quad C_D = C_D(\alpha, \hat{u}) \quad , \quad C_m = C_m(\alpha, \hat{u}) \quad , \quad \hat{u} \equiv u/U_1, \\ \alpha \equiv \tan^{-1} w/U_1$$

- 2) Tables for constructing $\{F_P^S(w, P)\}_R$.

$$C_L = C_L(\alpha, \hat{p}) \quad , \quad C_D = C_D(\alpha, \hat{p}) \quad , \quad C_m = C_m(\alpha, \hat{p}), \quad \hat{p} \equiv \frac{pb}{2U_1}$$

- 3) Tables for constructing $\{F_W^A(w, v)\}_R, \{F_V^A(w, v)\}_R$:

$$C_Y = C_Y(\alpha, \beta) \quad C_\ell = C_\ell(\alpha, \beta) \quad , \quad C_{11} = C_n(\alpha, \beta), \quad \beta \equiv \tan^{-1} \frac{v}{U_1}$$

- 4) Tables for constructing $\{F_P^A(w, P)\}_R$.

$$C_Y = C_Y(\alpha, \hat{p}) \quad , \quad C_\ell = C_\ell(\alpha, \hat{p}) \quad , \quad C_n = C_n(\alpha, \hat{p})$$

- 5) Tables for constructing $\{F_P^S(w, P)\}_R$:

$$C_L = C_L(\alpha, \hat{p}) \quad , \quad C_D = C_D(\alpha, \hat{p}) \quad , \quad C_M = C_m(\alpha, \hat{p})$$

- 6) Tables for constructing $\{F_r^A(w, r)\}_R$:

$$C_Y = C_Y(\alpha, \hat{r}) \quad , \quad C_\ell = C_\ell(\alpha, \hat{r}) \quad , \quad C_n = C_n(\alpha, \hat{r}), \quad \hat{r} \equiv \frac{rb}{2U_1}$$

- 7) Tables for constructing $\{F_r^S(w, r)\}_R$:

$$C_L = C_L(\alpha, \hat{r}) \quad , \quad C_D = C_D(\alpha, \hat{r}) \quad , \quad C_m = C_m(\alpha, \hat{r})$$

- 8) Tables for constructing $\{F_v^S(w, v)\}_R$:

$$C_L = C_L(\alpha, \beta) \quad , \quad C_D = C_D(\alpha, \beta) \quad , \quad C_m = C_m(\alpha, \beta)$$

6.5.2.2 Nonlinear unsteady aerodynamic data

- 1) Tables for constructing $\{F_w^S(w, \dot{w})\}_R$:

$$C_L = C_L(\alpha, \hat{\alpha}), \quad C_D = C_D(\alpha, \hat{\alpha}), \quad C_m = C_m(\alpha, \hat{\alpha})$$

where

$$\hat{\alpha} \equiv \frac{\dot{w} \bar{c}}{2U_1^2}$$

- 2) Tables for constructing $\{F_q^S(w, \dot{q})\}_R$:

$$C_L = C_L(\alpha, \hat{q}), \quad C_D = C_D(\alpha, \hat{q}), \quad C_m = C_m(\alpha, \hat{q})$$

where

$$\hat{q} \equiv \frac{\dot{q} \bar{c}^2}{4U_1^2}$$

- 3) Tables for constructing $\{F_V^A(w, \dot{v})\}_R$:

$$C_Y = C_Y(\alpha, \hat{\beta}), \quad C_\ell = C_\ell(\alpha, \hat{\beta}), \quad C_n = C_n(\alpha, \hat{\beta})$$

where

$$\hat{\beta} \equiv \dot{v}b / 2U_1^2$$

- 4) Tables for constructing $\{F_P^A(w, \dot{p})\}_R$:

$$C_Y = C_Y(\alpha, \hat{p}), \quad C_\ell = C_\ell(\alpha, \hat{p}), \quad C_n = C_n(\alpha, \hat{p})$$

where

$$\hat{p} \equiv \frac{\dot{p}b^2}{4U_1^2}$$

- 5) Tables for constructing $\{F_r^A(w, \dot{r})\}_R$:

$$C_Y = C_Y(\alpha, \hat{r}), \quad C_\ell = C_\ell(\alpha, \hat{r}), \quad C_n = C_n(\alpha, \hat{r})$$

where

$$\hat{r} \equiv \frac{\dot{r}b^2}{4U_1^2}$$

6.5.2.3 Nonlinear aerodynamic data transformations.—The tabular data appearing in the above two sections are used to construct nondimensional dynamic stability derivatives which, in turn, are transformed to the aerodynamic force coefficients appearing as the elements of the matrices $[AR_1]$ and $[AR_2]$. The aerodynamic coefficients contained in equation (6.5-9) are transformed to aerodynamic forces letting

$$\Delta h \equiv (X_{cg} - X_{ref}) / \bar{c} \quad (6.5-10)$$

where X_{cg} and X_{ref} are the Reference Axis System coordinates of the aircraft center of mass and the reference point about which the moments ℓ , m , n of the aerodynamic data are measured. The transformations are

$$\begin{bmatrix} F_X(i) \\ F_Z(i) \\ M_Y(i) \end{bmatrix} = [\overline{DER}^S] \begin{bmatrix} C_L(i) \\ C_L(i) \\ C_m(i) \end{bmatrix} \quad (6.5-11)$$

where

$$[\overline{\text{DER}}^S] \equiv \overline{q}_1 S_W \begin{bmatrix} \sin \alpha_i & -\cos \alpha_i & 0 \\ -\cos \alpha_i & -\sin \alpha_i & 0 \\ \overline{c} \Delta h \cos \alpha_i & \overline{c} \Delta h \sin \alpha_i & \overline{c} \end{bmatrix}$$

and

$$\begin{bmatrix} F_Y(i) \\ M_X(i) \\ M_Y(i) \end{bmatrix} = [\overline{\text{DER}}^A] \begin{bmatrix} C_Y(i) \\ C_\phi(i) \\ C_n(i) \end{bmatrix} \quad (6.5-12)$$

where

$$[\overline{\text{DER}}^A] \equiv \overline{q}_1 S_W \begin{bmatrix} 1 & 0 & 0 \\ 0 & b \cos \alpha_i & -b \sin \alpha_i \\ \Delta h \overline{c} & b \sin \alpha_i & b \cos \alpha_i \end{bmatrix}$$

In addition to these force transformations, the nondimensional velocity components are transformed to dimensional velocity components as

$$\begin{aligned} u &= U_1 \hat{u} & v &= U_1 \beta \\ w &= U_1 \alpha & p &= \frac{2U_1 \hat{p}}{b} \\ q &= \frac{2U_1 \hat{q}}{\overline{c}} & r &= \frac{2U_1 \hat{r}}{b} \end{aligned} \quad (6.5-13)$$

and nondimensional acceleration components are transformed to dimensional acceleration components as

$$\begin{aligned} \dot{w} &= \frac{2U_1^2 \hat{\alpha}}{\overline{c}} & \dot{v} &= \frac{2U_1^2 \hat{\beta}}{b} \\ \dot{q} &= \frac{4U_1^2 \hat{q}}{\overline{c}^2} & \dot{p} &= \frac{4U_1^2 \hat{p}}{b^2} \\ & & \dot{r} &= \frac{4U_1^2 \hat{r}}{b^2} \end{aligned} \quad (6.5-14)$$

6.5.3 Excitation by Penetration of a Discrete Gust

The FLEXSTAB system has the capability of predicting the time history response of flexible aircraft to selected discrete gust fields. This is accomplished by modifying the equations of motion of section 6.5.1 to include the effects of gust penetration (i.e., by defining the gust as a finite, space-dependent incidence field) and then calculating its effects as the aircraft passes through. The formulation provides time history gust response capability for aircraft with pitch attitudes near zero or 90°. This enables (1) conventional airplane gust encounter calculations, or (2) the calculation of shear field gust effects encountered by launch configurations.

6.5.3.1 Coordinate systems.—Figure 6.5-1 illustrates the coordinate systems used. The axes of the Inertial Axis System are labeled (X', Y', Z'), and those of the Body Axis System are labeled (X_B, Y_B, Z_B). Section 2.2 and table 6.5-1 define the principal features of the two axis systems. The gust flow field is expressed in the coordinates of the Inertial Axis System, while the velocity of the aircraft and its geometry are expressed in the Body Axis System.

TABLE 6.5-1.—PRINCIPAL FEATURES OF THE INERTIAL AND BODY AXIS SYSTEMS FOR DESCRIBING A GUST FIELD

	Inertial Axis System	Body Axis System
Axes	X', Y', Z'	X_B, Y_B, Z_B
Unit vector	$\hat{i}', \hat{j}', \hat{k}'$	$\hat{i}_B, \hat{j}_B, \hat{k}_B$

The origin of the Body Axis System is located at (X'_0, Y'_0, Z'_0) of the Inertial Axis System. The vector

$$\vec{r}'_0 = X'_0 \hat{i}' + Y'_0 \hat{j}' + Z'_0 \hat{k}' \quad (6.5-15)$$

locates this point. The orientation of the Body Axis System is determined by the Euler angles ϕ, θ, ψ . It can be shown from figure 6.5-1 that any point (X_B, Y_B, Z_B) is related to the Inertial Axis System by the expression

$$\begin{bmatrix} X' \\ Y' \\ Z' \end{bmatrix} = \begin{bmatrix} X'_0 \\ Y'_0 \\ Z'_0 \end{bmatrix} + [T] \begin{bmatrix} X_B \\ Y_B \\ Z_B \end{bmatrix} \quad (6.5-16)$$

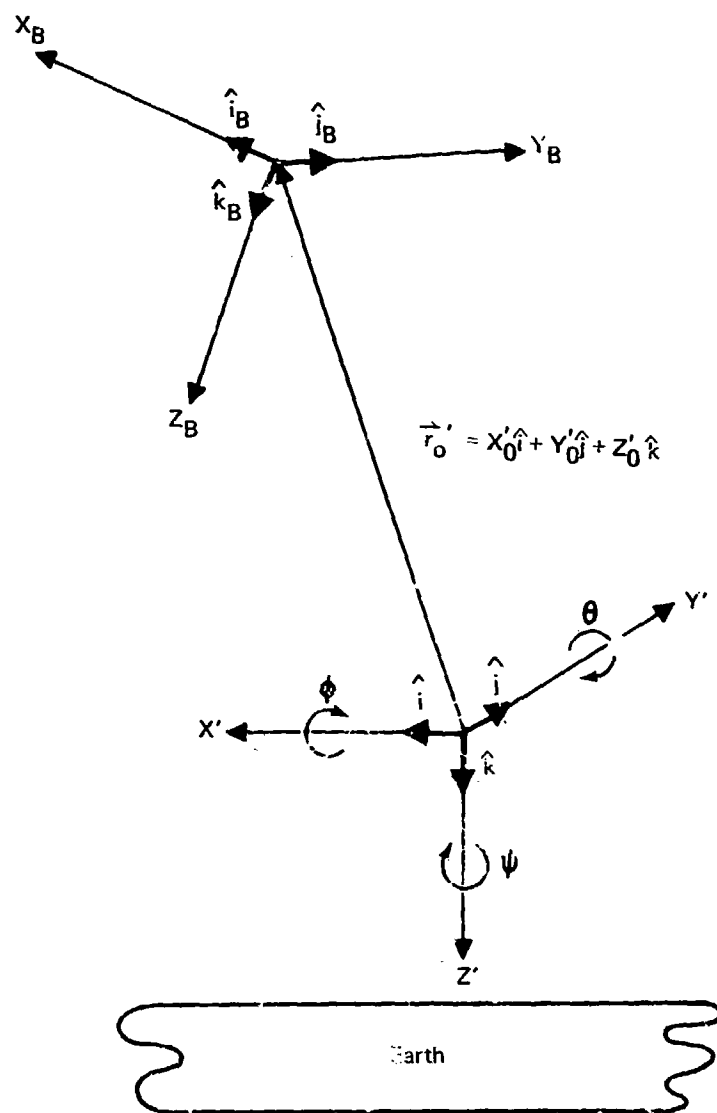


FIGURE 6.5-1.—COORDINATE SYSTEM DEFINITION

where the matrix $[T]$ is a rotational transformation matrix defined in terms of the Euler angles, equation (2.2-1).

6.5.3.2 Aircraft motion in a gust field.—As already noted, the gust flow field is described in the Inertial Axis System; hence, to evaluate the gust flow incidence at the aerodynamic surface segments, their coordinates in the Body Axis System must be transformed to the Inertial Axis System. This transformation depends on the velocity of the aircraft; and, since the aerodynamic theory is a first-order approximation, the transformation is based on a first-order approximation to aircraft velocity, viz.

$$\vec{V}_c = U_1 \hat{i}_B$$

The components of this velocity in the Inertial Axis System are given by

$$\begin{bmatrix} U' \\ V' \\ W' \end{bmatrix} = U_1 \begin{bmatrix} \cos\theta \cos\psi \\ \cos\theta \sin\psi \\ -\sin\theta \end{bmatrix} \quad (6.5-17)$$

in the Inertial Axis System.

For the gust problem, assume that the origins of the Body Axis System and the Inertial Axis System coincide when $t = 0$, and that, at all time $t > 0$, the airplane flies in a straight line through the gust. The origin of the Body Axis System may then be expressed as

$$\begin{bmatrix} X'_0 \\ Y'_0 \\ Z'_0 \end{bmatrix} = U_1 t \begin{bmatrix} \cos\theta \cos\psi \\ \cos\theta \sin\psi \\ -\sin\theta \end{bmatrix} \quad (6.5-18)$$

Therefore, any point (X_B, Y_B, Z_B) may be expressed as

$$\begin{bmatrix} X' \\ Y' \\ Z' \end{bmatrix} = U_1 t \begin{bmatrix} \cos\theta \cos\psi \\ \cos\theta \sin\psi \\ -\sin\theta \end{bmatrix} + [T] \begin{bmatrix} X_B \\ Y_B \\ Z_B \end{bmatrix} \quad (6.5-19)$$

In the FLEXSTAB system the gust field is assumed to be a function of X alone, figure 6.5-2. Since rectilinear flight is assumed through the gust, and since it is assumed that the airplane encounters the gust at exactly $t = 0$, the X location of the first point of the gust, X_{g1} , must coincide with the airplane's nose at $t = 0$. This point is found by substituting the coordinates of the airplane's nose $(X_{Bn}, 0, Z_{Bn})$ into equation (6.5-19).

$$\begin{aligned} X'_{g1} &= \cos\theta \cos\psi X_{Bn} \\ &+ (\cos\phi \sin\theta \cos\psi + \sin\phi \sin\psi) Z_{Bn} \end{aligned} \quad (6.5-20)$$

Assuming that the gust has length l_g the terminal point of the gust, X'_{g2} , is located at

$$X'_{g2} = X'_{g1} + l_g \quad (6.5-21)$$

The gust field is only defined when

$$X'_{g1} \leq X' \leq X'_{g2} \quad (6.5-22)$$

so it may be considered a function of ξ , where

$$\xi = X' - X'_{g1},$$

and

$$(6.5-23)$$

$$0 \leq \xi \leq l_g.$$

If (X_B, Y_B, Z_B) is a point on the aircraft, its coordinates in the Inertial Axis System are found using equation (6.5-19). If the X' coordinate of that point satisfies equation (6.5-22), it is within the gust field.

6.5.3.3 Gust field velocity components.—The velocity components of a gust are defined in the Inertial Axis System as (U_g, V_g, W_g) . These are expressed in the Body Axis System as

$$\begin{bmatrix} U_g \\ V_g \\ W_g \end{bmatrix} = [\bar{u}]^T \begin{bmatrix} U'_g \\ V'_g \\ W'_g \end{bmatrix} \quad (6.5-24)$$

The U_g component of a gust causes small dynamic pressure perturbations, while the V_g and W_g components cause sidewash and downwash perturbations. The dynamic pressure perturbations are of little importance to response of an aircraft, so the U_g component of the gust is set to zero. Assuming that most aircraft to be analyzed will have pitch attitudes near either zero or 90° , the U'_g gust component is also defined as zero.

If an aircraft has a pitch attitude, θ , of 90° , the arrangement shown by figure 6.5-2 leads to the nose of the aircraft remaining at the Inertial Axis System coordinate X'_g , for all time—the aircraft never penetrates the gust field. To preclude this situation and to permit gust penetration for very large pitch attitudes, if the pitch attitude relative to the earth's surface exceeds 70° , the Inertial Axis System is rotated so that X' points straight up. In this case, θ remains the Euler angle in the transformation from Body Axis System to Inertial Axis System, but θ is no longer the pitch attitude in the usual sense of airplane dynamics. In addition, it should be noted that even though arbitrary pitch attitudes are admissible in practice, they should be restricted to near zero or 90° when computing gust response. The reason for this restriction is an approximation described in the following, which neglects the effect of the gust field on the dynamic pressure.

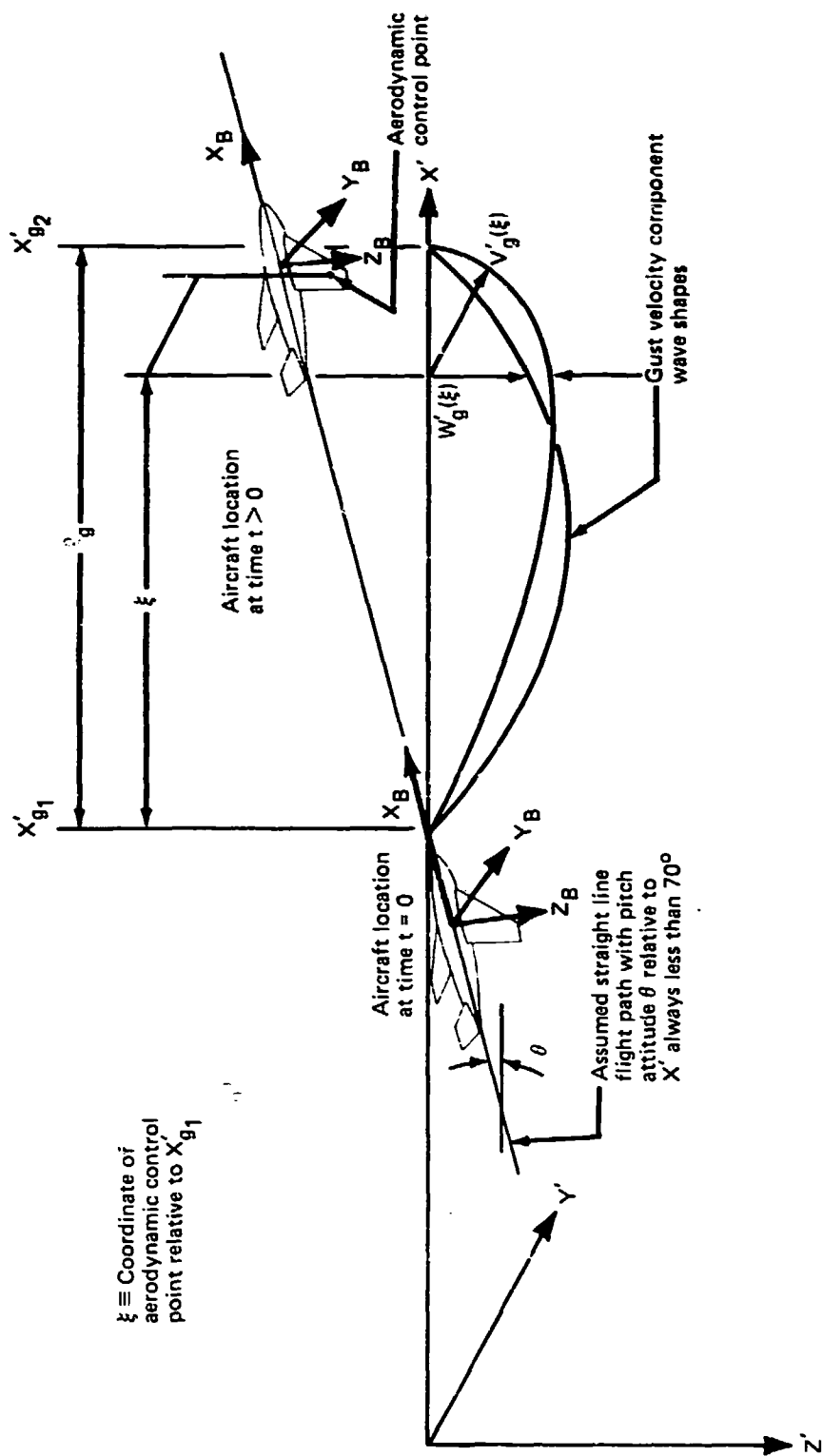


FIGURE 6.5-2.—GUST VELOCITY DISTRIBUTION RELATIVE TO FLIGHTPATH

6.5.3.4 Gust field flow incidence.—The V_g and W_g gust components are converted to incidence fields by using the equation

$$\psi_g = \frac{1}{U_1} \vec{v}_g \cdot \hat{n} \quad (6.5-25)$$

where

ψ_g is the incidence field, and

\hat{n} is the unit normal of the airplane's surface

Within small perturbation theory, the gust incidence rates are approximately

$$\dot{\psi}_g \approx \frac{1}{U_1} \dot{\vec{v}}_g \cdot \hat{n} \quad (6.5-26)$$

where

$$\dot{\vec{v}}_g \approx [T]^T \dot{\vec{V}}_g$$

The symmetric and antisymmetric components of a gust are used separately. Therefore, equations (6.5-25) and (6.5-26) must be separated into these components. Consider the i^{th} surface segment of the airplane shown in figure 6.5-3. Recalling that $U_g \approx 0$, the gust incidence may be expressed as follows:

$$\psi_g = -\frac{1}{U_\infty} (V_g \sin \theta_{DIH} + W_g \cos \theta_{DIH}) \quad (6.5-27)$$

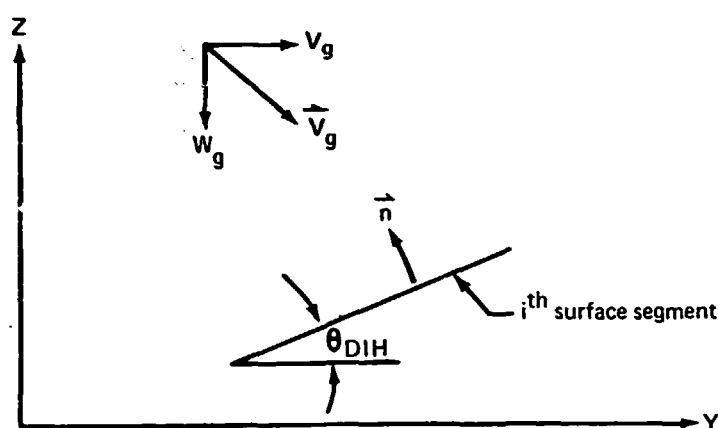


FIGURE 6.5-3.—RESOLUTION OF GUST ON AIRPLANE SURFACE

Since W_g is the symmetric gust component and V_g is the antisymmetric gust component, equation (6.5-27) may be written

$$\psi_g = \psi_g^S + \psi_g^A = -\frac{1}{U_1} W_g \cos \theta_{DIH} - \frac{1}{U_1} V_g \sin \theta_{DIH} \quad (6.5-28)$$

where ψ_g^S and ψ_g^A are the symmetric and antisymmetric gust incidences, respectively,

6.5.3.5 Gust field flow incidence rate.—Similarly, we may write

$$\begin{aligned} \dot{\psi}_g &= \dot{\psi}_g^S + \dot{\psi}_g^A \\ &= -\frac{1}{U_1} \dot{W}_g \cos \theta_{DIH} - \frac{1}{U_1} \dot{V}_g \sin \theta_{DIH} \end{aligned} \quad (6.5-29)$$

The term θ_{DIH} is most frequently used when discussing thin bodies. Equations (6.5-28) and (6.5-29) apply to slender bodies by defining $\theta_{DIH} \equiv 0^\circ$ for the symmetric problem, and $\theta_{DIH} \equiv 90^\circ$ for the antisymmetric problem.

6.5.3.6 Gust incidence vectors.—Using equation (6.5-23), the incidence vectors are written

$$\{\psi_g^S\} = -\frac{1}{U_1} \{W_g\} \otimes \{\psi_\alpha\}$$

and

$$\{\psi_g^A\} = -\frac{1}{U_1} \{V_g\} \otimes \{\psi_\beta\} \quad (6.5-30)$$

where the operator “ \otimes ” (defined in app. B) is an element multiply of two column matrices to form a third column matrix, and $\{\psi_\alpha\}$ and $\{\psi_\beta\}$ resolve the gust incidences into downwash and sidewash components.

Similar equations for the gust incidence rates can be found from equation (6.5-29).

$$\begin{aligned} \{\dot{\psi}_g^S\} &= -\frac{1}{U_1} \{\dot{W}_g\} \otimes \{\psi_\alpha\} \\ \{\dot{\psi}_g^A\} &= -\frac{1}{U_1} \{\dot{V}_g\} \otimes \{\psi_\beta\} \end{aligned} \quad (6.5-31)$$

The gust field described above allows V'_g and W'_g to be any arbitrary function of ξ , where ξ is defined by the equations (6.5-23), viz.,

$$\begin{aligned}\xi &= X' - X'_{g_1} \\ 0 &\leq \xi \leq l_g\end{aligned}\tag{6.5-23}$$

The parameters V'_g and W'_g are restricted to one of three forms: 1) sine wave, 2) one-minus-cosine wave, or 3) modified square wave.

6.5.3.7 Sine wave gust.—Figure 6.5-4 illustrates a sine wave gust. The parameters V_G , W_G , and l_g are supplied by the user. The equations describing this gust are

$$V'_g(\xi) = V_G \sin\left(\frac{2\pi\xi}{l_g}\right)$$

and (6.5-32)

$$W'_g(\xi) = W_G \sin\left(\frac{2\pi\xi}{l_g}\right)$$

The derivatives of V_g and W_g with respect to time are written

$$\dot{V}'_g(\xi) = \frac{2\pi V_G}{l_g} \cos\left(\frac{2\pi\xi}{l_g}\right) \frac{d\xi}{dt}$$

and (6.5-33)

$$\dot{W}'_g(\xi) = \frac{2\pi W_G}{l_g} \cos\left(\frac{2\pi\xi}{l_g}\right) \frac{d\xi}{dt}$$

The term $d\xi/dt$ is found by considering the motion of the airplane with respect to the Inertial Axis System, recalling that

$$\xi = X' - X'_{g_1}$$

Therefore (6.5-34)

$$\frac{d\xi}{dt} = \frac{dX'}{dt}$$

This can be found by taking the derivative of equation (6.5-19) with respect to time.

$$\frac{d\xi}{dt} = \frac{dX'}{dt} = U_1 \cos\theta \cos\psi \tag{6.5-35}$$

Finally, the complete equations for \dot{V}'_g and \dot{W}'_g can be written

$$\dot{V}'_g(\xi) = \frac{2\pi U_1 V_G}{l_g} \cos\theta \cos\psi \cos\left(\frac{2\pi\xi}{l_g}\right)$$

and

(6.5-36)

$$\dot{W}'_g(\xi) = \frac{2\pi U_1 W_G}{l_g} \cos\theta \cos\psi \cos\left(\frac{2\pi\xi}{l_g}\right)$$

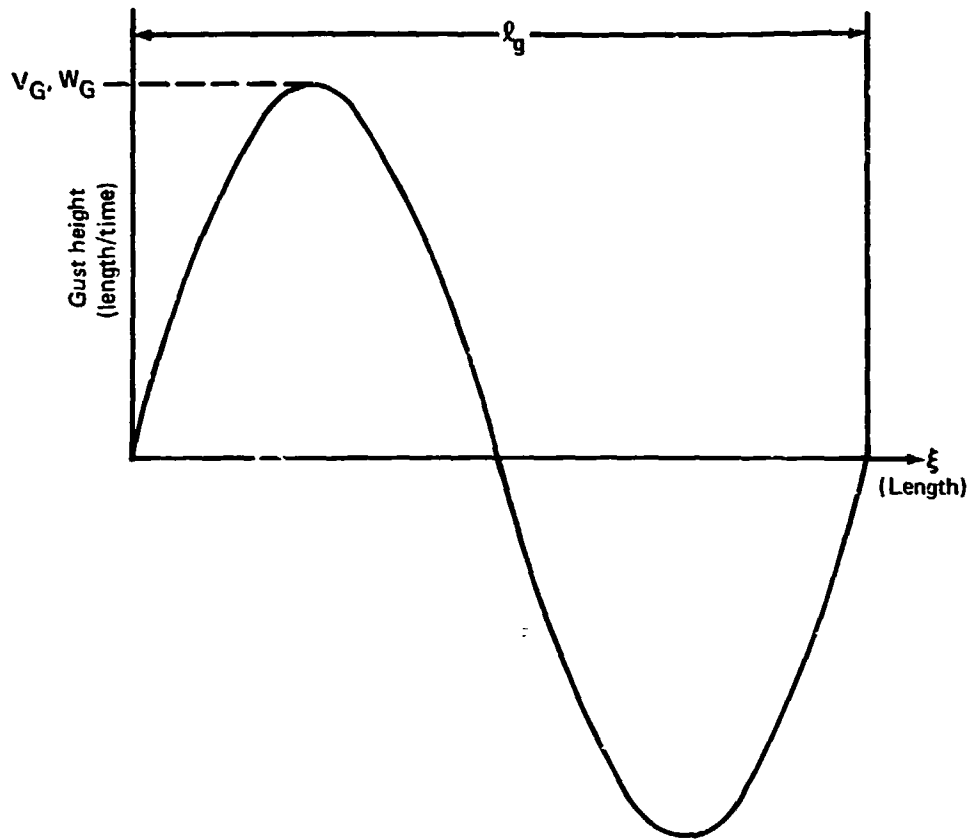


FIGURE 6.5-4.—SINE WAVE GUST DEFINITION

6.5.3.8 *One-minus-cosine wave gust.*—Figure 6.5-5 illustrates a one-minus-cosine gust. Once again, the parameters V_G , W_G , and l_g are supplied by the user. The equations describing this gust are

$$V'_g(\xi) = V_G \left[1 - \cos\left(\frac{2\pi\xi}{l_g}\right) \right]$$

and

$$W'_g(\xi) = W_G \left[1 - \cos\left(\frac{2\pi\xi}{l_g}\right) \right] \quad (6.5-37)$$

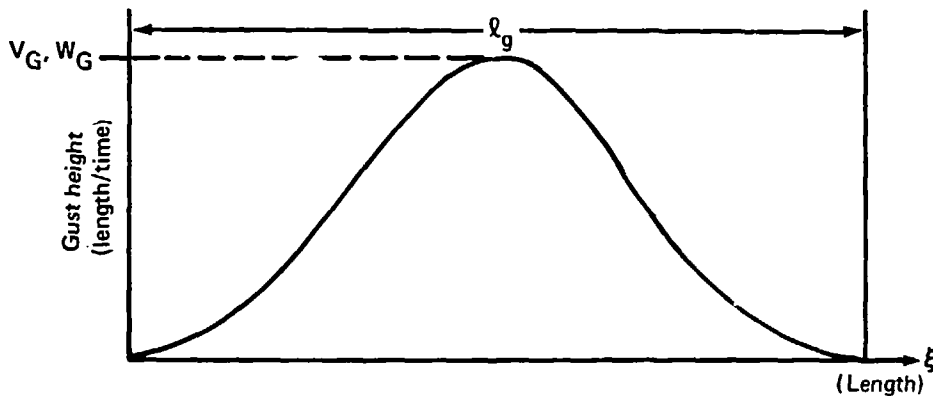


FIGURE 6.5-5.—ONE-MINUS-COSINE WAVE GUST DEFINITION

The derivatives with respect to time are found in the manner described for the sine wave. They are

$$\dot{V}'_g(\xi) = \frac{2\pi V_G U_1}{l_g} \cos\theta \cos\psi \sin\left(\frac{2\pi\xi}{l_g}\right)$$

and

(6.5-38)

$$\dot{W}'_g(\xi) = \frac{2\pi W_G U_1}{l_g} \cos\theta \cos\psi \sin\left(\frac{2\pi\xi}{l_g}\right)$$

6.5.3.9 Modified square wave gust.—Figure 6.5-6 illustrates the modified square wave. The parameters V_G , W_G , and l_g are supplied by the user. Note that the wave's length is $l_g + 29.0863$ meters. The wave is divided into four defining regions. These regions and amplitude definitions are listed below.

$$V'_{g1} = W'_{g1} = 0.0765\xi$$

$$V'_{g2} = W'_{g2} = \frac{1}{2}G_g \{1 - \cos[\frac{\pi}{30}(\xi + .9137)]\}$$

(6.5-39)

$$V'_{g3} = W'_{g3} = G_g$$

$$V'_{g4} = W'_{g4} = \frac{1}{2}G_g \{1 - \cos[\frac{\pi}{30}(\xi - l + 31.9137)]\}$$

where

$$G_g = V_G \text{ or } W_G$$

and

$$\left. \begin{array}{l} V'_{g1} = W'_{g1} \\ V'_{g2} = W'_{g2} \\ V'_{g3} = W'_{g3} \\ V'_{g4} = W'_{g4} \end{array} \right\} \text{ is valid for } \left\{ \begin{array}{l} 0 \leq \xi \leq 0.9215 \\ .9215 \leq \xi \leq 29.0863 \\ 29.0863 \leq \xi \leq l - .9137 \\ l - .9137 \leq \xi \leq l + 29.0863 \end{array} \right.$$

Note that all dimensions, except the input values, are in meters.

The derivatives of V'_g and W'_g with respect to time are

$$\begin{aligned}
 \dot{V}'_{g1} &= \dot{W}'_{g1} = .0765 U_{\infty} \cos \alpha \cos \beta \cos \psi \\
 \dot{V}'_{g2} &= \dot{W}'_{g2} = \frac{G}{60} U_{\infty} \cos \alpha \cos \theta \cos \psi \sin\left[\frac{\pi}{30}(\xi + .9137)\right] \\
 \dot{V}'_{g3} &= \dot{W}'_{g3} = 0 \\
 \dot{V}'_{g4} &= \dot{W}'_{g4} = \frac{G}{60} U_{\infty} \cos \alpha \cos \theta \cos \psi \sin\left[\frac{\pi}{30}(\xi - l + 30.9137)\right]
 \end{aligned} \tag{6.5-40}$$

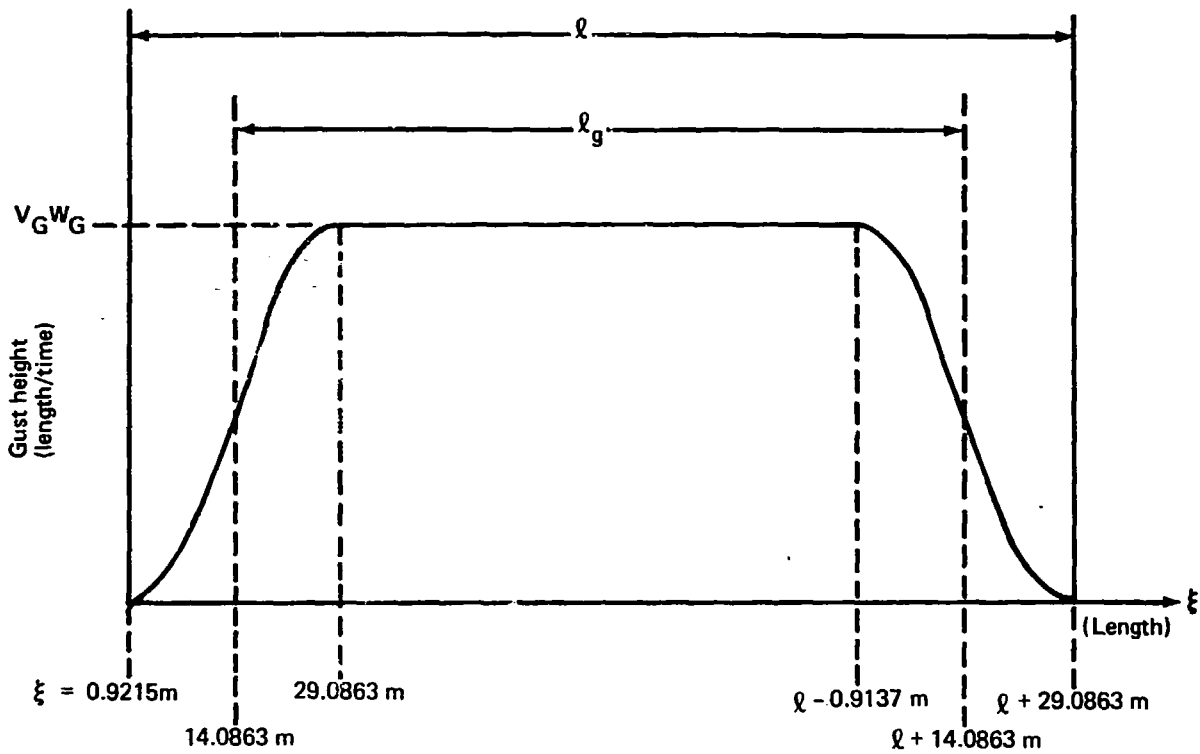


FIGURE 6.5-6.—MODIFIED SQUARE WAVE GUST DEFINITION

6.5.3.10 Gust-field-induced aerodynamic forces.—The aerodynamic forces, induced by flight through a gust field, are expressed in terms of matrices derived in this section. These matrices relate the perturbation of the aerodynamic forces to two quantities: (1) the flow incidence imposed by the gust field, and (2) the rate of change of flow incidence imposed by the gust field. These matrices are derived from the aerodynamic force coefficient matrices of section 6.3.2 and are written as combined aerodynamic matrices like those appearing in section 6.3.3. The derivation leads to the gust-field-induced aerodynamic forces expressed as

$$\{F_B^g\}_P = [A_6]\{V_g\} + [A_7]\{\dot{V}_g\} \quad (6.5-41)$$

and

$$\{\bar{Q}^g\}_P = [A_6]\{V_g\} + [A_7]\{\dot{V}_g\} \quad (6.5-42)$$

where

$$\{V_g\} \equiv \begin{bmatrix} \{U_g\} \\ \{W_g\} \\ \{V_g\} \end{bmatrix}$$

The elements of $\{V_g\}$ are the gust velocity components obtained by applying the transformation given by equation (5.5-24) transforming the gust velocity components of sections 6.5.3.7 through 6.5.3.9 from the Inertial Axis System to the Body Axis System.

As shown in section 6.5.3.6, the gust incidence matrices of equation (6.5-30) are identical, in form, with the angle of attack and angle of side slip incidence matrices given by equations (3.5-49) and (3.5-50). The partitions of the coefficient matrices $[A_i]$ and $[a_i]$ multiplying $\{W_g\}$ and $\{V_g\}$ are, therefore, the matrix coefficients of $\{\Psi_\alpha\}$ and $\{\Psi_\beta\}$ appearing in section 6.3.2. The coefficient matrices appearing in equations (6.5-41) and (6.5-42) are written as

$$[A_6] = \left[\begin{array}{c|c|c} [0] & [\bar{A}_6^W] & [0] \\ \hline [0] & [0] & [\bar{A}_6^V] \end{array} \right] \quad (6.5-43)$$

where

$$[\bar{A}_6^W] \equiv \bar{q}_1 \left([G_{\theta R}^S] + [Y_{\theta R}^S] + [G_{R\theta E}^S] \right) \approx \{\Psi_\alpha\} \frac{1}{U_1}$$

and

$$[\bar{A}_6^V] \equiv \bar{q}_1 \left([G_{\theta R}^A] + [Y_{\theta R}^A] + [G_{R\theta E}^A] \right) \approx \{\Psi_\beta\} \frac{1}{U_1}$$

where

$$[A_7] = \left[\begin{array}{c|c|c} [0] & [\bar{A}_7^W] & [0] \\ \hline [0] & [0] & [\bar{A}_7^V] \end{array} \right]$$

and

$$[\bar{A}_7^W] \equiv \bar{q}_1 \left([\delta G_{\theta R}^S] + [\delta G_{R\theta E}^S] \right) \approx \{\Psi_\alpha\} \frac{1}{U} \quad (6.5-44)$$

$$[\bar{A}_7^V] \equiv \bar{q}_1 \left([\delta G_{\theta R}^A] + [\delta G_{R\theta E}^A] \right) \approx \{\Psi_\beta\} \frac{1}{U}$$

$$[a_6] = \left[\begin{array}{c|c|c} [0] & [\bar{a}_6^W] & [0] \\ \hline [0] & [0] & [\bar{a}_6^V] \end{array} \right]$$

(6.5-45)

where

$$[\bar{a}_6^W] \equiv \bar{q}_1 \left([H_{\theta R}^S] + [W_{\theta R}^S] + [H_{R\theta E}^S] \right) \approx \{\Psi_\alpha\} \frac{1}{U_1}$$

and

$$[\bar{a}_6^V] \equiv \bar{q}_1 \left([H_{\theta R}^A] + [W_{\theta R}^A] + [H_{R\theta E}^A] \right) \approx \{\Psi_\beta\} \frac{1}{U}$$

$$[a_7] = \begin{bmatrix} [0] & [\bar{a}_7^w] & [0] \\ - & - & - \\ [0] & [0] & [\bar{a}_7^v] \end{bmatrix} \quad (6.5-46)$$

where

$$[\bar{a}_7^w] \equiv \bar{q}_1 \left([\delta H_{\theta R}^S] + [\delta H_{R\theta E}^S] \right) \equiv \{\psi_\alpha\} \frac{1}{U_1}$$

$$[\bar{a}_7^v] \equiv \bar{q}_1 \left([\delta H_{\theta R}^A] + [\delta H_{R\theta E}^A] \right) \equiv \{\psi_\beta\} \frac{1}{U_1}$$

The gust-induced aerodynamic forces given by equations (6.5-41) and (6.5-42) are combined with the nonlinear equations of motion of section 6.5.1. The matrix $[E]$ is replaced by the matrix $[E_g]$, where

$$[E_g] \equiv [E] + [A_6]\{V_g\} + [A_7]\{\dot{V}_g\}, \quad (6.5-47)$$

and the generalized structural excitation forces $\{\bar{Q}_g\}$ are added to equation (6.5-2). The resulting equations are integrated numerically, evaluating the elements of $\{V_g\}$ at each step of the integration. The values of $\{V_g\}$ follow from the ξ coordinate, equation (6.5-23), of each aerodynamic control point being substituted into equation (6.5-25).

GLOSSARY

Aerodynamic centroid—geometric location of the center of aerodynamic pressure acting on an *aerodynamic segment**—approximated as the geometric center of an *aerodynamic panel* and a *slender body* centerline segment; in volume II—*aerocentroids*

Aerodynamic derivatives—constants of proportionality between aerodynamic forces and small changes of aircraft and *trim parameters* from the value zero

Aerodynamic influence coefficients—Coefficients in any linear aerodynamic relation, but used herein as the coefficients linearly relating *lifting pressure coefficients* to *flow incidence*

Aerodynamic panel—quadrilateral segment of an *aerodynamic mean surface*, the quadrilateral having two edges parallel to the free stream direction

Aerodynamic problem—a boundary value problem consisting of a flow equation and boundary conditions specified on the aerodynamic surface of an aircraft, on its wake surface, and at large distances from the aerodynamic surface

Aerodynamic segment—portion of a *thin* or *slender body* over which the strength of a distributed *flow singularity* is controlled by a single parameter, viz., an *aerodynamic panel* on thin and slender body *mean surfaces* and the segment of a slender body between two adjacent points on the slender body centerline

Applied forces—*nodal forces* arising from *surface tractions* and body forces

Asymptotic expansion—a semi-convergent series the sum of whose terms represents an approximate solution to a boundary value problem

Bound vorticity—a vorticity distribution lying in a plane parallel to the free stream and having its surface of first-order pressure discontinuity (i.e., the surface across which the velocity component in the free stream direction is discontinuous) fixed to an aerodynamic *mean surface* of a *thin* or *slender body*

Body Axis System (X_B, Y_B, Z_B)—a right-handed, rectangular cartesian coordinate system constituting a *mean reference frame* and having its origin at the aircraft center of mass; the $X_B Z_B$ plane coincident with the aircraft plane of symmetry; and the X_B axis positive forward, into, and parallel to the free stream

Body-fixed axis system—a *mean reference frame*

Constant pressure panel—an *aerodynamic panel* having a uniform distribution of *bound vorticity*

Constrained flexibility matrix—flexibility matrix for a structure constrained from rigid body displacement

*Italicized terms are also defined in this glossary.

Control effectiveness—coefficients in linear relations between aerodynamic forces and small changes to control surface deflection angles

Control point—point (on the aerodynamic *mean surface* of a *thin* or *slender body* or on the surface of revolution representing the surface of a slender body) where an aerodynamic boundary condition is satisfied

Coordinated maneuver—an aircraft maneuver during which the bank angle is always such that the total acceleration vector (i.e., the sum of the acceleration due to gravity and of the acceleration due to flight path curvature) lies in the plane of aircraft symmetry

Cross flow—the component of flow in the plane normal to the free stream and in the region about a *slender body*

Cylindrical surface—a surface generated by moving a straight line parallel to itself along a curve that is not necessarily closed

Design point—the steady, *reference flight condition* selected as the *design point* flight condition (i.e., the flight condition whose aerodynamic loads are used to determine the *jig shape* of an aircraft)

Design point shape—the aerodynamic shape of an aircraft in the *design point* flight condition

Displacement relation—function describing the elastic displacement field interior to the boundaries of a structural *finite element* in terms of components of displacement at the *node points* of the finite element

Displacement vector—position of a material point in a deformed structure relative to its position in the structure before deformation

Elastic axis—the locus of points along a beam-like structure along which there is no extension arising from bending (i.e., the neutral axis in the Bernoulli-Euler law) and along which the centers of twist occur in torsion

Elastic displacement vector—*displacement vector* obtained by evaluating a displacement field satisfying the *mean reference frame* constraint conditions

Equivalent nodal forces—forces at structural *finite element node points* which perform work on the node point displacements equal to the work performed by forces distributed over the finite elements, viz., the finite element surface integral of one-half the scalar product of the distributed forces with the *displacement relations*

Finite element—geometric segments of a structure, lying between imaginary lines or planes intersecting at points called *node points*, whose structural properties are expressed in terms of forces and displacements at the node points

Flow singularity—a function describing a perturbation velocity field about a line or plane (i.e., a source or doublet distribution on a line or a source or vorticity distribution on a plane) and having a mathematical singularity at the line or plane

Flow incidence—the small angle through which a uniform free stream must be turned for the flow to become tangent to an aerodynamic surface

Fluid Axis System (x, y, z)—an inertial reference frame for aerodynamics coincident with the *Reference Axis System* at any instant of time under consideration and having a constant translational velocity relative to the *Inertial Axis System* equal to the present velocity of the Reference Axis System along its X axis

Free flexibility matrix—the flexibility matrix for a structure free of kinematic constraints (viz., such that sets of applied forces are in *self-equilibrium*)

Generalized (modal) coordinates—the amplitudes of deflection of the free vibration mode shapes of a structure

Induction problem—the *aerodynamic problem* whose solution determines the lifting pressure induced by an arbitrary interference flow

Inertial Axis System (X', Y', Z')—a right-handed, rectangular cartesian coordinate system fixed relative to an assumed flat, non-accelerating earth and taken as a reference frame for structural and rigid body dynamics

Inertially equivalent lumped masses—point masses, rigidly constrained to structural *node points*, whose kinetic energy, arising from node point velocity, is equal to the kinetic energy of the distributed mass of adjacent *finite elements* when the distributed mass has a velocity determined by the finite element *displacement relations*

Interference body (surface)—a closed *cylindrical surface* with generators parallel to the free stream, surrounding at least a portion of the length of a *slender body* and whose cross section is a mean of the cross section of the slender body portion lying between its ends; a cylindrical surface approximating the surface of a slender body over that portion of its length where interference flows are required to satisfy the *surface boundary condition*

Interference effects—the pressure distribution computed in the aerodynamic *induction problem*

Jig shape—the aircraft shape obtained when the *design point shape* is elastically deformed by removing the aerodynamic, inertial, and propulsion system loads of the *design point* flight condition

Junction point—*node points* where the *elastic axis* of *thin* and *slender bodies* are joined to one another in forming the elastic axis of a multiple thin and/or slender body configuration

Lateral-direction derivatives—*aerodynamic* or *stability derivatives* related to purely antisymmetric motion of an aircraft

Leading edge correction—streamwise component of aerodynamic force at the leading edge of a *thin body* required to correct the inviscid drag computed from the solution to the aerodynamic *lifting problem*

Lifting problem—the *aerodynamic problem* whose solution determines the lifting pressure distribution on a *thin* or *slender body* isolated in a uniform flow

Local axis system—a right-handed, rectangular cartesian coordinate system related to the *Reference Axis System* by an orthogonal transformation chosen so as to simplify the analytical description of the surface geometry and structural properties of *thin* and *slender bodies*

Longitudinal derivatives—*aerodynamic* and *stability derivatives* related to purely symmetric motion of an aircraft

Low frequency approximation—an approximate theory of unsteady aerodynamics valid when the unsteadiness is a slow time variation, viz., unsteadiness characterized by *reduced frequencies* small by comparison with unity

Mean interference surface of a slender body—see *interference body*

Mean reference frame—a coordinate system translating and rotating with an elastically deforming aircraft in such a way that the momentum of the aircraft at any instant of time is equal to the momentum of a rigid aircraft translating and rotating with the coordinate system; also, a moving coordinate system relative to which the kinetic energy of the aircraft is a minimum; the *Reference*, *Body* and *Stability Axis Systems* are mean reference frames

Mean surfaces—cylindrical surfaces aligned with the undisturbed free stream where the *surface boundary conditions* are specified in a linear, first-order aerodynamic theory

Mean wake surface—a cylindrical surface aligned with the undisturbed free stream where the wake boundary conditions are specified in the linear, first-order aerodynamic theory

Motion variables—a set of time-dependent variables which describe the motion of an aircraft relative to the *Inertial Axis System*, viz., the translation and rotation of the *mean reference frame* relative to the Inertial Axis System plus the elastic deformation motion relative to the mean reference frame

Net loads—sum of the *nodal forces* due to *surface tractions* and inertial body forces

Nodal displacement components—in a *finite element* representation of a structure, the components of translational and/or rotational displacement at the *node points* which, when substituted into the *displacement relations*, describe the deformation at all points of the structure

Nodal force components—in a *finite element* representation of a structure, the components of force and/or moment applied at the *node points*

Nodal mass matrix—matrix of *inertially equivalent lumped masses*, i.e., the matrix of mass quantities associated with the *node points*, in a *finite element* structural representation, which, when multiplied onto time rates of change of *nodal displacement components* describes the momentum of the structure

Node points—points where the applied forces and displacements are evaluated in the *finite element* representation of a structure

Panel centroid—*aerodynamic centroid*; also, panel geometric centroid and in volume II—*arocentroid*

Pressure coefficient—the deviation of the local pressure from static free stream pressure normalized with respect to the dynamic pressure of the free stream

Quadratic spline—a function of the X coordinate defined over three adjacent segments of the X axis (viz., X_1 to X_2 , X_2 to X_3 , and X_3 to X_4) varying smoothly and quadratically from zero value and slope at $X = X_1$ to a maximum value and zero slope at $X_2 < X < X_3$, and zero value and slope at $X = X_4$; functional description of the line doublet distributions on *slender body* centerlines used in constructing the solutions to the subsonic slender body aerodynamic *lifting problems* of the FLEXSTAB system

Quasi-steady maneuver—an unsteady maneuver in which the unsteadiness (i.e., the time rates of change of the translational and rotational velocities) is so small that time derivatives can be treated as negligibly small in the equations of motion

Reduced frequency—the frequency of a harmonic time dependence, ω , normalized with respect to the frequency with which an aircraft traverses the spatial distance, l , between the point where a cause of unsteadiness is located and the point where its effect is significant to the problem, i.e., $k = \omega l/U$ where for a wing alone undergoing pitch oscillations l is taken to be the mean wing chord

Reference Axis System (X, Y, Z)—a right-handed, rectangular cartesian coordinate system constituting a *mean reference frame* and having its origin located on the aircraft plane of symmetry, the X,Z plane coincident with the aircraft plane of symmetry, and the X axis positive aft aligned with the undisturbed free stream

Reference flight condition (state)—the steady, trimmed flight condition in which the static and dynamic stability of an aircraft is evaluated by the FLEXSTAB system

Reference junction point—one of the two *junction points* at the ends of the *elastic axis* of each *thin* and *slender body* used to describe the elastic axis of a multiple thin and slender body structural arrangement

Residual flexibility—the structural flexibility associated with free vibration mode shapes for which the generalized inertial and damping forces are negligibly small in the perturbation equations of motion

Rigid body mode shapes—displacement components, at points on an aircraft surface or at structural *node points*, arising from an infinitesimally small rigid body displacement which is either a rotation and translation of an aircraft at the center of mass or a displacement in terms of the constrained structural degrees of freedom

Self-equilibrium—term referring to a system of forces having vanishing resultant forces and couples at any point, e.g., the system of aerodynamic, propulsion system, and inertial forces acting on an aircraft in free flight

Singularity strength—parameters controlling the strengths of *flow singularity* distributions on *aerodynamic segments*

Slender body—an aircraft configuration component having an aspect ratio equal in order of magnitude to its thickness ratio, e.g., fuselages, nacelles, pods, tip tanks, etc.

Stability Axis System (X_S, Y_S, Z_S)—a right-handed, rectangular cartesian coordinate system constituting a *mean reference frame* and having its origin located on the aircraft plane of symmetry, the X_S, Z_S plane coincident with the plane of symmetry, and the X_S axis positive forward aligned with the free stream in the *reference flight condition*

Stability derivatives—constants of proportionality between aerodynamics forces and small changes of aircraft *motion variables* and *trim parameters* from their values in the *reference flight condition*

Steady, reference flight condition—see *reference flight condition*

Structural nodes—see *node points*

Structural reference frame—coordinate system used in deriving the structural theory

Subsonic edge—edge of a *thin body* having a sweep angle greater than the Mach cone angle of a supersonic free stream flow

Supersonic edge—edge of a *thin body* having a sweep angle less than the Mach cone angle of a supersonic free stream

Surface boundary condition—boundary condition on an *aerodynamic problem* requiring that the disturbed flow be tangent to the aerodynamic surface, neither penetrating it nor separating from it

Surface tractions—stresses applied to the external surface of a structure

Thickness problem—the *aerodynamic problem* whose solution determines the pressure distribution on a *thin* or *slender body*, the body having no camber or incidence and having only a symmetric thickness shape

Thin body—an aircraft configuration component having an aspect ratio at least an order of magnitude greater than its thickness ratio, e.g., wings, tail surfaces, sauts, etc.

Total nodal forces—*nodal forces* that are in equilibrium with the *applied forces* and the stresses at *finite element* boundaries

Trim parameters—all quantities appearing in the steady equations of motion which, for a particular aircraft, must have specified values in order for the equations of motion to be satisfied, i.e., velocity, rotation rate, control surface settings, bank angle, attitude, and thrust setting

Trim variables—six of the *trim parameters* which may be determined by solving the steady equations of motion treating these six parameters as unknowns

Trim solution—the values of the *trim variables* determined by solving the steady equations of motion

Wing-body problem—*aerodynamic problem* consisting of a wing-body combination used in the *asymptotic expansion* leading to the first-order approximate aerodynamic theory of the FLEXSTAB system

APPENDIX A

SYMBOLS

a :	speed of sound
$aR(X_M)$:	thickness shape of slender body, figure 3.2-5 and equation (3.2-17)
$a^{(-)}_{()}(X, Y, Z)$:	flow incidence induced at point (X, Y, Z) by unit flow singularity of type $(-)$ located at $()$, section 3.4
$a^{(-)}_{(\sim), ()}$:	flow incidence induced at control point (\sim) by unit flow singularity of type $(-)$ located at $()$, section 3.4
$[AIC]$:	aerodynamic influence coefficient matrix, equation (3.4-168)
AR :	aspect ratio, section 3.2.8
$[A]$:	intermediate form of aerodynamic influence coefficient matrix, equation (3.4-218)
$[\delta A]$:	intermediate form of unsteady aerodynamic influence coefficient matrix, equation (3.4-218)
$[A_{P\theta}]$:	steady aerodynamic influence coefficient matrix, equation (3.5-41) and section 3.5.2
$[A_{F\theta}]$:	steady aerodynamic matrix, equation (5.3-3)
$[\delta A_{P\theta}]$:	unsteady aerodynamic influence coefficient matrix, equation (3.5-41) and section 3.5.2
$[\int a^V_{(\sim), ()}]$:	matrix of integrated aerodynamic influence coefficients at control points (\sim) induced by vorticity distribution located at $()$, section 3.4.8

- $[A_i]$: rigid body aerodynamic force matrix, equation (6.2-4) and section 6.3.3
- $[a_i]$: generalized aerodynamic force matrix, equation (6.2-5) and section 6.3.3
- b : wing span
- $hG(X_M)$: camber shape of slender body, figure 3.2-5 and equation (3.2-15)
- $\{B\}$: matrix of small displacement components of an arbitrary point, equation (4.2-28)
- $\{\dot{B}\}$: matrix of velocity components of an arbitrary point relative to Inertial Axis System, equation (4.2-16)
- $[BSC_J]$: matrix related to isolated slender body aerodynamic thickness, equation (3.4-77)
- \bar{c} : reference chord length selected by user
- C_D : drag coefficient, section 5.1
- c_i : chord length at inboard edge of panel, figure 3.4-5
- \bar{c}_i : panel chord length along panel row geometric centroid, equation (3.4-10)
- $hI(X_M)$: camber shape of slender body figure 3.2-5 and equation (3.2-15)
- C_L : lift coefficient, section 5.1

C_l :	rolling moment coefficient, section 5.1
C_m :	pitching moment coefficient, section 5.1
C_n :	yawing moment coefficient, section 5.1
C_p :	pressure coefficient, equation (3.2-8)
$C_P^{(-)}()$:	pressure coefficient induced at aerodynamic segment centroid () by flow singularity of type (—), section 3.3.3
ΔC_p :	lifting pressure coefficient, equation (3.4-67)
C_Y :	side force coefficient, section 5.1
$\{C_P^{(-)}\}^{int}_{()}$:	matrix of interference pressure coefficients induced by flow singularities of type (—) located at (), section 3.4.6.2
$\{C_P^S\}^{iso}$:	matrix of pressure coefficients induced by thickness exclusive of interference (i.e., isolated thickness pressure coefficients), equation (3.4-173)
$[C]$:	constrained flexibility matrix, equation (4.2-60)
$[\tilde{C}]$:	unconstrained flexibility matrix, equation (4.2-64)
$[CPM]$:	pressure influence coefficient matrix, equation (3.4-167)
$[CPM^{(-)}_{(\sim), ()}]$:	matrix of pressure coefficients induced at aerodynamic segment centroids (—) by unit flow singularities of type (—) located at (), equation (3.4-37)
$[\tilde{C}_R]$:	unconstrained residual flexibility matrix, equations (4.2-81) and (4.2-83)

$[\tilde{C}_{\theta G}]$: unconstrained flexibility matrix in terms of aerodynamic surface segment rotations and gyroscopic couples, equation (5.3-1)

$[\tilde{C}_{\theta T}]$: unconstrained flexibility matrix in terms of aerodynamic surface segment rotations and forces, equation (5.3-1)

$[\tilde{C}_{dG}]$: unconstrained flexibility matrix in terms of aerodynamic surface segment translations and gyroscopic couples, equation (5.7-14)

$[\tilde{C}_{dT}]$: unconstrained flexibility matrix in terms of aerodynamic surface segment translations and forces, equation (5.7-14)

$[\tilde{C}_{R\theta G}]$: residual flexibility matrix in terms of aerodynamic surface segment rotations and gyroscopic couples, equation (6.3-43)

$[\tilde{C}_{R\theta T}]$: residual flexibility matrix in terms of aerodynamic surface segment rotations and forces, equation (6.3-2)

\vec{d} : elastic displacement vector, equation (2.3-14) and figure 2.3-3

$\{d^a\}$: components of elastic displacement vector evaluated interior to ath finite element, equation (4.2-5)

$\{d^*\}$: translational deformation matrix, equation (4.2-98)

$\{D\}$: leading edge correction forces, equation (3.4-224) and section 3.5.3.3

$\{\Delta D_\alpha\}$: increment leading edge correction force from angle of attack, section 3.5.3.3

$\{\Delta D_\beta\}$: increment leading edge correction force from angle of sideslip, section 3.5.3.3

$\{\Delta D_P\}$: increment leading edge correction force from roll rate, section 3.5.3.3

$\{\Delta D_Q\}$: increment leading edge correction force from pitch rate, section 3.5.3.3

$\{\Delta D_R\}$:	increment leading edge correction force from yaw rate, section 3.5.3.3
$[D_{ER}]$:	transformation matrix—Body Axis System components to Stability Axis System components, equations (6.4-73) and (6.4-74)
$[\overline{D_{ER}}]$:	transformation matrix—Stability Axis System components to Reference Axis System components, equations (6.5-11) and (6.5-12)
$[D_{P\theta}]$:	leading edge correction matrix, equation (3.5-71)
$[\tilde{D}]$:	aeroelastic matrix, equation (5.3-5)
$[\Delta \tilde{D}^{-1}]$:	incremental aeroelastic operator matrix, equation (5.3-32)
$[DX]$:	X-coordinate of aerodynamic pressure evaluation matrix, equation (3.4-210)
$F_I(X_I, Y_I)$:	normalized thickness shape of I^{th} thin body, section 3.2.4.2 and equation (3.4-14)
F_C^A :	total aerodynamic force at aircraft center of mass, equation (3.5-1)
$\{F_C^A\}$:	matrix of total aerodynamic force and couple components at aircraft center of mass expanded on Reference Axis System, equation (3.5-6)
$\{F_C^T\}$:	matrix of thrust force and couple components at aircraft center of mass expanded on Reference Axis System, equation (6.2-10)
$\{F_B^A\}$:	matrix of total aerodynamic force and couple components at aircraft center of mass expanded on Body Axis System, equation (5.3-11)

$\{F_B^G\} :$	matrix of gyroscopic force and couple components at aircraft center of mass expanded on Body Axis System, equation (5.4-21)
$\{F_B^T\} :$	matrix of propulsion system force and couple components at aircraft center of mass expanded on Body Axis System, equation (5.4-22)
$\{F^A\} :$	matrix of aerodynamic force normal components at centroids of aerodynamic segments, equation (3.5-38)
$\{f^A\} :$	matrix of aerodynamic force components at aerodynamic segment centroids expanded on Reference Axis System, equation (3.5-29)
$\{f_T^A\} :$	matrix of aerodynamic force components at aerodynamic segment centroids expanded on local axis systems, equation (3.5-39)
$\{f_T^A\}^{iso} :$	matrix of aerodynamic force components induced by thickness but not including thickness interference forces, equation (5.3-8)
$\{f_T^A\}^{int} :$	matrix of interference aerodynamic force components induced by thickness, equation (5.3-8)
$\vec{f}_{WIi}^A, \vec{f}_{BJj}^A :$	aerodynamic force at i^{th} (j^{th}), panel of I^{th} thin body (J^{th} slender body), equations (3.5-7) and (3.5-20)
$\vec{g} :$	gravitational acceleration vector, equation (4.2-2)
$G(X_M) :$	normalized camber shape of M^{th} slender body, figure 3.2-5
$[G_F] :$	rigid body aerodynamic force transformation matrix, equation (5.3-13)
$[G_T] :$	rigid-body aerodynamic force transformation matrix, equation (5.3-13)

$[G_\theta]$:	sum of $[G_{\theta E}]$ and $[G_{\theta R}]$, equations (5.3-13) and (5.3-31)
$[G_{\theta E}]$:	incremental aeroelastic operator, equation (5.3-32)
$[G_{\theta R}]$:	rigid aircraft aerodynamic force operator, equation (5.3-23)
$[G_{R\theta E}]$:	residual flexibility aeroelastic operator, equation (6.3-28)
$[\delta'_{\theta R}]$:	rigid-body, unsteady aerodynamic force operator, equation (6.3-21)
$[\delta G_{R\theta E}]$:	residual flexibility, unsteady aeroelastic operator, equation (6.3-29)
$[G]$:	propulsion system gyroscopic couple matrix, equation (6.2-23)
$[\bar{G}]$:	propulsion system gyroscopic couple matrix, equation (6.2-24)
$[\bar{G}_\phi]$:	propulsion system gyroscopic couple matrix, equation (6.2-28)
$[\bar{G}_R]$:	propulsion system gyroscopic couple matrix, equation (6.2-33)
$[G_E]$:	propulsion system gyroscopic couple matrix, equation (6.4-3)
$[\bar{G}_E]$:	propulsion system gyroscopic couple matrix, equation (6.4-3)
$[\frac{\partial G}{\partial \omega}]$:	propulsion system gyroscopic couple matrix for variable rotor spin rate, equation (5.4-16)
$[G_{\theta R}]$:	rigid-body aerodynamic force operator, equation (6.3-15)
\vec{h}_i^G :	angular momentum of i^{th} propulsion system rotor, equation (5.4-6)

$H_I(X_I, Y_I)$:	normalized camber shape of I^{th} thin body, section 3.2.4.2
$[H]$:	equations of motion coefficient matrix, equation (6.4-4)
$[H_T]$:	generalized aerodynamic force transformation matrix, equation (6.3-17)
$[H_{\theta R}]$:	generalized aerodynamic force operator, equation (6.3-17)
$[H_{R\theta E}]$:	residual flexibility aeroelastic, generalized aerodynamic force operator, equation (6.3-31)
$[\delta H_{\theta R}]$:	rigid-body, unsteady aerodynamic force operator, equation (6.3-24)
$[\delta H_{R\theta E}]$:	residual flexibility aeroelastic, generalized, unsteady aerodynamic force operator, equation (6.3-32)
$\hat{i}, \hat{j}, \hat{k}$:	unit base vectors of Reference Axis System
$\hat{i}, \hat{j}, \hat{k}'$:	unit base vectors of Inertial Axis System
$\hat{i}_B, \hat{j}_B, \hat{k}_B$:	unit base vectors of Body Axis System
$I_{XX}, I_{YY}, I_{ZZ}, I_{XZ}$:	moments and product of inertia of total aircraft expanded on Body Axis System, equation (2.3-13)
$[IDM]$:	integrated flow incidence matrix, equation (3.4-222)
$[ISC_{\theta}]$:	reduced integrated flow incidence coefficient matrix, equation (3.4-223)
$[ISC_{\psi}]$:	integrated flow incidence coefficient matrix, equation (3.4-223)

[INT]:	transformation of slender body interference surface pressures to aerodynamic forces on slender body centerlines, equation (3.5-35)
k:	reduced frequency, equation (3.2-46)
K:	kinetic energy, equation (4.2-i)
K_{rel}:	kinetic energy apparent to observer in Body Axis System, equation (2.3-8)
K⁽⁻⁾:	kernel function for a unit flow singularity of type (-), section 3.4
[K]:	reduced composite stiffness matrix, equations (4.2-14) and (4.2-58)
[k]:	generalized stiffness matrix, equation (4.2-76)
[K^a]:	stiffness matrix for ath structural finite element, equation (4.2-9)
[K_{δδ}]:	nonsingular stiffness matrix, equation (4.2-58)
[LSC]:	aerodynamic influence coefficient matrix, equation (3.4-170)
[δLSC]:	unsteady aerodynamic influence coefficient matrix, equation (3.4-216)
l_g:	gust wave length, section 6.5.3.2
L(Ni):	length of ith elastic axis segment on Nth body, equation (4.3-1)
ΔL(Ni):	length of elastic axis finite element, equation (4.3-1)

L_{BJ} :	length of J^{th} slender body centerline, equation (3.4-3)
L_{BJj} :	length of j^{th} segment of J^{th} slender body centerline, equation (3.4-3)
$m(\xi_{Ii}, \eta_{Ii})$:	source distribution strength, equation (3.4-15)
$[m_e]$:	reduced nodal mass matrix, equation (4.3-155)
$[m_\delta]$:	mass matrix, equation (4.2-20) and section 4.3.7
$[m_\delta^a]$:	nodal mass matrix for a $^{\text{th}}$ finite structural element, equation (4.2-18)
$[m]$:	generalized mass matrix, equation (4.2-79)
M :	total mass of aircraft, equation (2.3-10)
M :	Mach number apparent to Reference Axis System, equation (2.3-75)
M_∞ :	Mach number apparent to Fluid Axis System, equation (2.3-74)
\vec{M}_C^A :	total aerodynamic couple at aircraft center of mass, equation (3.5-2)
$[M]$:	total mass–inertia matrix, equation (4.2-26)
$\{M^G\}$:	propulsion system gyroscopic couple components, equations (4.2-119) and (4.3-117)
$[MM_1]$:	inertia matrix, equation (6.2-30)
$[MM_2]$:	gravity matrix, equation (6.2-32)

- \vec{n} : unit vector normal to surface, equation (2.3-32)
- \vec{n} : unit vector normal to surface before elastic deformation, equation (2.3-50)
- $[N^a]$: matrix of displacement functions for ath structural finite element, equation (4.2-5)
- $[NAF]$: thrust force transformation, equation (4.2-117) and section 4.3.6
- $\{NP\}$: thrust force coefficient matrix, equation (5.4-4)
- p : perturbation roll rate, section 2.3.2.5 and equation (6.2-7)
- P : roll rate, equation (2.2-3)
- \hat{p} : nondimensional roll rate, equation (2.3-67)
- $[P]$: structural mass transformation matrix, equations (4.2-53) and (4.2-63)
- $[P_d]$: structural transformation matrix—from nodal displacement components to aerodynamic control point translations, equation (4.2-100) and sections 4.3.5 and 4.4.2.3
- $[P_T]$: structural transformation matrix—from aerodynamic segment forces to structural node forces, equation (4.2-114) and sections 4.3.5 and 4.4.3
- $[P_\theta]$: structural transformation matrix—from nodal displacement components to aerodynamic control point rotations, equation (4.2-101) and sections 4.3.5 and 4.4.2.3
- q : perturbation pitch rate, section 2.3.2.5 and equation (6.2-7)

- \bar{q} : dynamic pressure apparent to Reference Axis System, equation (2.3-75)
- \bar{q}_∞ : dynamic pressure apparent to Fluid Axis System, equation (2.3-74)
- $\{q\}$: matrix of perturbation motion variables section 6.4.1
- $[\bar{q}]$: dynamic pressure distribution, equations (3.5-54) and (3.5-55)
- Q : pitch rate, equation (2.2-3)
- \hat{Q} : nondimensional pitch rate, equation (2.3-67)
- \vec{Q} : fluid velocity relative to Fluid Axis System, equation (2.2-4)
- $\{Q\}$: matrix of nodal force components applied to complete structure, equation (4.2-13)
- $\{Q^a\}$: matrix of nodal force components of ath finite structural element, equation (4.2-8)
- $\{Q^A\}$: matrix of aerodynamic force components at structural nodes, equations (4.2-116) and (6.2-3)
- $\{Q^G\}$: matrix of gyroscopic force components at structural nodes, equations (4.2-119) and (6.2-3)
- $\{Q_R\}$: matrix of nodal force components at structural constraint nodes, equation (4.2-59)
- $\{Q^S\}$: matrix of nodal force components applied by surface tractions, equation (4.2-41)
- $\{\bar{Q}_1\}$: matrix of generalized forces conjugate with the free vibration mode deflection amplitudes, equation (6.2-5)

- $\{Q^T\}$: matrix of thrust force components at structural nodes, equations (4.2-119) and (6.2-3)
- r : perturbation yaw rate, equations (2.3-26) and (6.2-7)
- $r(X_M)$: slender body thickness shape, equation (3.2-17)
- \vec{r} : position relative to aircraft center of mass, figure 2.3-3
- \vec{r}_i : position relative to Inertial Axis System, figure 2.3-1
- \vec{r}_0 : position of aircraft center of mass relative to Inertial Axis System, figure 2.3-3
- \vec{r} : position, before deformation, relative to aircraft center of mass, equation (2.3-14) and figure 2.3-3
- $\{r_o\}_P$: perturbation orientation matrix, equation (6.2-29)
- R : yaw rate, equation (2.2-3)
- \hat{R} : nondimensional yaw rate, equation (2.3-67)
- \vec{R} : position of aircraft center of mass relative to origin of Reference Axis System, equation (2.3-11)
- S : surface
- S^a : surface of ath structural finite element, section 4.2.2.1
- S_B : total mean surface of slender bodies, figure 3.3-1 and equation (3.3-10)

- S_{BJ} : mean surface of J^{th} slender body, equation (3.3-10)
- S_{BJj} : surface area of j^{th} panel of J^{th} slender body mean surface, section 3.4.1
- S_W : total mean surface of thin bodies, figure 3.3-1 and equation (3.3-9)
- S_{WI} : mean surface of I^{th} thin body, equation (3.3-9)
- S_{WII} : surface area of i^{th} panel of I^{th} thin body mean surface section 3.4.1
- $S_{(-)}$: strength of flow singularity of type (-) located at (), section 3.4
- $\{S_{(-)}\}$: matrix of flow singularity strengths of type (-) located at (), section 3.4
- $[J]$: coordinate transformation matrix—from Reference Axis System to Body Axis System, equation (3.5-75)
- $[SD]$: transformation matrix—Stability Axis System to Body Axis System, equations (5.3-44) and (5.3-45)
- t : time
- $\{T\}$: matrix of thrust forces, equations (4.2-119) and 4.3-122)
- $[T]$: coordinate transformation matrix—from Body Axis System to Inertial Axis System, equation (2.2-1)
- $[T_{fT}]$: aerodynamic force transformation matrix—from components in local axis systems to components in Reference Axis System, equation (3.5-30)

$[T_{FP}]$:	aerodynamic pressure transformation matrix—from surface pressure to normal components of force, equation (3.5-33)
$[T_{TF}]$:	aerodynamic force transformation matrix—from normal components of force to components in local axis systems, equation (3.5-32)
$[TRANS_{ID}]$:	leading edge correction transformation matrix—from leading edge panel forces to components in local axis systems, equation (3.5-40)
$[TRANS_t]$:	aerodynamic force transformation matrix—from thickness-induced pressures to force components in local axis systems, equation (3.5-31)
u, v, w :	components of nondimensional perturbation flow velocity relative to and expanded on Reference Axis System, equation (2.3-35)
u, v, w :	components of aircraft perturbation translational velocity relative to Inertial Axis System but expanded on Body Axis System, equation (6.2-7)
$u^{(-)}_{()}, v^{(-)}_{()}, w^{(-)}_{()}$:	components of nondimensional perturbation flow velocity induced by flow singularity of type (-) located at (), section 3.4
U_g, V_g, W_g :	gust flow velocity relative to Inertial Axis System but components expanded on Body Axis System, equation (6.5-24)
U'_g, V'_g, W'_g :	gust flow velocity relative to Inertial Axis System but components expanded on Inertial Axis System, equation (6.5-24)
u_i :	deflection amplitude of i^{th} free vibration mode shape, equation (2.3-64)
$\{u\}$:	matrix of deflection amplitudes of free vibration mode shapes treated as independent degrees of freedom, equation (4.2-69)
$\{u_1\}$:	subset of $\{u\}$, section 4.2.4.3

U :	linear approximation to strain energy, equation (4.2-15)
U^e :	exact strain energy, equation (4.2-1)
U, V, W :	aircraft translation velocity relative to the Inertial Axis System but components expanded on Body Axis System, equation (2.2-3)
\vec{v} :	nondimensional perturbation velocity of fluid relative to Fluid Axis System, equation (2.3-35)
v_n :	component of fluid nondimensional perturbation velocity (\vec{v}) along normal to surface, equation (2.3-37)
\hat{v}, \hat{w} :	amplitudes of surface velocity modes, equation (2.3-70)
$I_v(\vec{v}), I_w(\vec{v})$:	integrated nondimensional perturbation flow velocities, induced by vorticity distribution located at (), section 3.4
V :	volume
V^a :	volume of a th finite structural element, section 4.2.2.1
\vec{V} :	fluid velocity relative to Reference and Body Axis Systems, equation (2.2-4)
\vec{V}_C :	aircraft translational velocity relative to Inertial Axis System, equation (2.2-3)
\vec{V}_R :	velocity of Body Axis System relative to Fluid Axis System, equation (2.2-5)
\vec{V}^S :	surface velocity relative to Fluid Axis System, equation (2.3-38)
$\hat{v}\lambda_v\vec{V}, \hat{w}\lambda_w\vec{W}$:	components of surface velocity (\vec{V}^S) relative to Fluid Axis System, equation (2.3-70)

$\{V\}_P$	perturbation velocity matrix, equation (6.2-6)
W	wake surface, figure 3.3-1
W	work, section 4
x, y, z	Fluid Axis System coordinates, section 2.2.3
X, Y, Z	Reference Axis System coordinates, section 2.2.4
$\bar{X}, \bar{Y}, \bar{Z}$	Reference Axis System coordinates of point relative to aircraft center of mass, equation (2.3-60)
$\tilde{X}, \tilde{Y}, \tilde{Z}$	Lagrangian coordinates in Reference Axis System, equation (2.3-3)
x', y', z'	Inertial Axis System coordinates, section 2.2.1
$\tilde{x}', \tilde{y}', \tilde{z}'$	Lagrangian coordinates in Inertial Axis System, equation (2.3-1)
x_B, y_B, z_B	Body Axis System coordinates, section 2.2.2
x_{cg}, y_{cg}, z_{cg}	Reference Axis System coordinates of aircraft center of mass, figure 2.2-2
x_E, y_E, z_E	ESIC Reference Axis System coordinates, figure 4.4-9
x_M, y_M, z_M	M^{th} local slender body aerodynamic axis system, figure 3.2-5
x_N, y_N, z_N	N^{th} local thin body aerodynamic axis system, figure 3.2-4
$x_N(0), y_N(0), z_N(0)$	Reference Axis System coordinates of origin of N^{th} local axis system, figure 3.2-3
x_S, y_S, z_S	Stability Axis System coordinates, figure 2.2-4

x_{Ni}, y_{Ni}, z_{Ni} : local elastic axis coordinate system of i^{th} elastic axis segment of N^{th} body, figure 4.3-5

x_n^E, y_n^E, z_n^E : ESIC local thin body axis system, figure 4.4-9

$x_{Ii}(0), y_{Ii}(0), z_{Ii}(0)$: Reference Axis System coordinates of origin of i^{th} panel local axis system, equation (3.4-4)

Greek

$\alpha \equiv \tan^{-1} \frac{W}{U}$: angle of attack, equations (2.3-68) and (5.2-9)

$\beta \equiv \tan^{-1} \frac{V}{U}$: angle of sideslip, equations (2.3-68) and (5.2-9)

$\beta^2 \equiv 1 - M^2$: compressibility factor

γ : flight path angle, section 5.2.1

$\gamma(\xi_{Ii}, \eta_{Ii})$: vorticity distribution on i^{th} panel of I^{th} body, equation (3.4-51)

Γ_{Ni} : angle of sweep of i^{th} elastic axis segment of N^{th} thin body, figure 4.3-5

δ : first variation operator

δ_a : aileron deflection angle, equation (2.3-53)

δ_e : elevator deflection angle, equation (2.3-53)

δ_r : rudder deflection angle, equation (2.3-53)

$\vec{\delta}_c$: control surface deflection angle, equation (2.3-50)

- $\{\delta\}$: matrix of nodal displacement components for free, complete structure, equation (4.2-12) and section 4.2.2.2
- $\{\delta^c\}$: matrix of nodal displacement components for constrained, complete structure, equations (4.2-30) and (4.2-77) and section 4.2.2.2
- $\{\delta^a\}$: matrix of nodal displacement components for ath finite structural element, equation (4.2-5)
- $\{\bar{\delta}\}$: elastic axis nodal displacement components, equation (4.3-97)
- $\{\delta^*\}$: subset of elastic axis nodal displacement components, equation (4.3-97)
- $\{\delta_T\}$: subset of elastic axis nodal displacement components, equation (4.3-97)
- $\{\delta_e^*\}$: subset of elastic axis nodal displacement components, equation (4.3-97)
- $\{\delta_K^*\}$: subset of elastic axis nodal displacement components, equation (4.3-97)
- $\{\delta_P\}$: components of nodal displacement at Pth junction point, equation (4.3-45)
- $\{\delta_P^*\}$: subset of $\{\delta_P\}$, equation (4.3-45)
- $\{\delta_R\}$: matrix of structural constraint nodal displacement components, equation (4.2-59)
- $[\Delta_G]$: gyroscopic couple transformation matrix, equation (4.2-119)
- ϵ_i : ith aerodynamic perturbation parameter, equation (3.2-10)
- θ : pitch attitude, section 2.2.2

H :	nondimensionalizing camber ratio for thin body, section 3.2.3, equation (3.2-12)
$\hat{\theta}$:	camber ratio amplitude, equation (3.2-21)
θ_N :	dihedral angle of mean surface of N^{th} thin body, figure 3.2-3
θ_{Ii} :	Dihedral angle of i^{th} panel of I^{th} body, figure 3.4-3
$\vec{\theta}_E$:	elastic rotation at a point, equation (2.3-50)
$\{\theta^*\}$:	matrix of elastic rotations at control points, equations (3.5-44) and (4.2-99)
$\{\theta^G\}$:	elastic rotation of propulsion system rotors, equation (4.2-118)
$\lambda(\)$:	time function whose value and the values of its derivatives have order of magnitude unity for all time and govern perturbation parameter (), section 3.2.5, equation (3.2-21)
$\{\lambda\}$:	matrix of Lagrange multipliers, equation (4.2-42)
μ :	cylindrical coordinate of slender surface point, figure 3.2-5
$\mu^{()D}_{\xi\xi_{Jj}}$:	doublet distribution on j^{th} segment of J^{th} slender body centerline with axis in the () direction, section 3.3
ξ, η, ζ :	variables of integration in Reference Axis System
$\xi_{Ii}, \eta_{Ii}, \zeta_{Ii}$:	local coordinates of i^{th} panel of I^{th} thin body, figure 3.4-3
$\xi_{Jj}, \eta_{Jj}, \zeta_{Jj}$:	local coordinates of j^{th} interference surface panel, figure 3.4-5; also, local coordinates of j^{th} centerline segment of J^{th} slender body, figure 3.4-4
ρ :	fluid mass density, section 3

ρ_A :	aircraft material mass density, sections 2 and 4
τ :	thickness ratio of thin body, equation (3.2-12)
ϕ :	angle of bank, section 2.2.2
ϕ_i :	i^{th} perturbation velocity potential normalized with respect to freestream velocity and perturbation parameter ϵ_i and having order of magnitude unity, section 3.2.2
Φ :	total velocity potential, equation (3.2-5)
$\phi^{(-)}_{()}$:	velocity potential induced by flow singularity of type $(-)$ located at $()$, equation (3.3-12)
$\vec{\phi}_i$:	i^{th} free vibration mode shape displacement field, equation (2.5-64)
$[\phi_\delta]$:	complete set of free vibration mode shapes, equation (4.2-69)
$[\phi_{\delta_1}]$:	matrix of free vibration mode shapes treated as independent degrees of freedom, section 4.2.4.3
$[\phi_{\delta_2}]$:	matrix of free vibration mode shapes treated as dependent degrees of freedom, section 4.2.4.3
$[\bar{\phi}_\delta]$:	matrix of rigid-body mode shapes in terms of structural node displacements, equation (4.2-21)
$[\bar{\phi}_\delta^a]$:	matrix of rigid-body mode shapes for a th finite structural element, equation (4.2-17)
$[\bar{\phi}_i]$:	i^{th} node rigid body mode shape matrix, equations (4.2-16) and (4.2-21)

- $[\bar{\phi}^*]$: matrix of rigid-body mode shapes, relative to center of mass, in terms of aerodynamic segments, equations (3.5.6) and (5.6-22)
- $[\bar{\phi}_R^*]$: matrix of rigid-body mode shapes, relative to reference point, in terms of aerodynamic segments, equation (4.3-192)
- ω_i : i^{th} circular frequency, section 3.2.2.2
- $\bar{\omega}_i \equiv \frac{\omega_i}{U}$: small parameter related to i^{th} circular frequency, section 3.2.2.2
- $\vec{\omega}$: rigid-body rotation velocity of aircraft relative to Inertial Axis System, equation (2.2-3)
- $[\omega^2]$: diagonal matrix of squares of free vibration natural frequencies
- Ω : acceleration potential normalized with respect to freestream velocity, equation (3.2-60)
- Ψ : heading angle, section 2.2.2
- Ψ : angle of flow incidence, figure 2.3-4
- $\Psi \begin{pmatrix} - \\ \end{pmatrix} \begin{pmatrix} \end{pmatrix}$: flow incidence induced at control point () by flow singularity of type (—), section 3.4
- Ψ_g : gust flow incidence, equation (6.5-25)
- $\{\Psi\}$: matrix of flow incidences at panel centroids and slender body segment control points, equations (3.4-172), (3.5-42), and (3.5-43)
- $\{\Psi'\}$: matrix of flow incidences at all control points, equation (3.4-168)
- $\{\Psi_c\}$: matrix of flow incidences arising from camber shape, equation (3.5-44)

- $\{\Psi_M\}$: matrix of flow incidences arising from aircraft motion and control surface deflections, equation (3.5-45)
- $\{\Psi_\alpha\}$: matrix of flow incidence due to angle of attack, equation (3.5-45)
- $\{\Psi_\beta\}$: matrix of flow incidence due to sideslip, equation (3.5-45)
- $\{\Psi_P\}$: matrix of flow incidence due to roll rate, equation (3.5-45)
- $\{\Psi_Q\}$: matrix of flow incidence due to pitch rate, equation (3.5-45)
- $\{\Psi_R\}$: matrix of flow incidence due to yaw rate, equation (3.5-45)
- $\{\Psi_{\delta_e}\}$: matrix of flow incidence due to elevator deflection, equation (3.5-45)
- $\{\Psi_{\delta_a}\}$: matrix of flow incidence due to aileron deflection, equation (3.5-45)
- $\{\Psi_{\delta_r}\}$: matrix of flow incidence due to rudder deflection, equation (3.5-45)

Subscripts

- $()_1$: reference flight condition value of $()$
- $()_\infty$: freestream value of $()$
- $()_P$: perturbation value of $()$
- $()_i$: quantity related to i^{th} perturbation velocity potential
- $()_l$: value of $()$ at lower side of a surface, equation (3.5-9)

- $(\)_u$: value of $(\)$ at upper side of a surface, equation (3.5-9)
- $(\)_{BJj}$: value of $(\)$ associated with j^{th} aerodynamic segment of J^{th} slender body
- $(\)_{WIi}$: value of $(\)$ associated with i^{th} aerodynamic segment of I^{th} thin body
- $(\)_{BJBKjk}$: value of $(\)$ associated with j^{th} aerodynamic segment of J^{th} slender body influenced by k^{th} aerodynamic segment of K^{th} slender body
- $(\)_{WJWIji}$: value of $(\)$ associated with j^{th} aerodynamic segment of J^{th} thin body influenced by i^{th} aerodynamic segment of I^{th} thin body
- $[(\)_{B,B}]$: value of $(\)$ at all slender bodies influenced by all slender bodies
- $[(\)_{W,W}]$: value of $(\)$ at all thin bodies influenced by all thin bodies
- $[(\)_{BW,BW}]$: value of $(\)$ at all slender and thin bodies influenced by all slender and thin bodies

Superscripts

$()^A$: quantity related to aerodynamics

$()^G$: quantity related to gyroscopic couples

$()^T$: quantity related to thrust

$()^{(i)}$: i^{th} approximation in asymptotic frequency expansion

$()^*$: complex amplitude of $()$

Matrix Symbols

$\{ \}$: column matrix

$[\]$: row matrix

$[\]$: rectangular matrix

$\begin{bmatrix} & \\ & \end{bmatrix}$: diagonal matrix

$[\]^T$: transpose matrix

$[\]^{-1}$: inverse matrix

Operators

$\frac{D()}{Dt}$: Eulerian derivative of (), equation (3.2-29)

$\frac{d()}{dt}$: time rate of change of () apparent to observer fixed to an inertial reference frame, equation (2.3-2)

$\frac{\delta()}{\delta t}$: time rate of change of () apparent to an observer fixed to a moving reference frame, equation (2.3-5)

$(\dot{})$: time rate of change of ()—a function of time alone

$()_x, ()_y, ()_z, ()_t$: partial derivative of ()

$\llbracket () \rrbracket$: discontinuity (or jump) of () across a surface

$\delta()$: first variation of ()

\boxtimes : special matrix multiply, $[C] = \{A\} \boxtimes [B]$ such that $[C_{ij}] = [A_i B_{ij}]$, see Appendix B.

$\vec{\nabla}$: gradient operator

APPENDIX B

DEFINITION OF THE CIRCLE-CROSS PRODUCT MATRIX OPERATOR \otimes

B.1 INTRODUCTION

The purpose of this appendix is to define the matrix operator denoted by the symbol " \otimes ." This operator is hereinafter called the "circle-cross product" matrix operator. Reference has been made to this operator as an "element-by-element" matrix operator; however, this definition is only appropriate for a circle-cross product operation between two general matrices of order $m \times n$ where neither m nor n is equal to one. The circle-cross product matrix operator may be any one of the following:

- 1) A row operator
- 2) A column operator
- 3) An element-by-element or simply element operator

These three results of the circle-cross product matrix operator are defined in section B.3.

B.2 SYMBOLS AND DEFINITIONS

The following symbols will be used throughout this appendix:

$\begin{Bmatrix} \cdot \end{Bmatrix}$ denotes the column vector \cdot ; i.e., the specific case of a general matrix with m rows and only one column

$\begin{bmatrix} \cdot \end{bmatrix}$ denotes the row vector \cdot ; i.e., the specific case of a general matrix with only one row but n columns

$[\cdot]$ denotes the general matrix \cdot which has m rows and n columns

Conformability

Consider the fundamental definition of matrix multiplication

$$[A][B] = [C] \quad (B.2-1)$$

where the product $[C]$ exists if and only if the matrices $[A]$ and $[B]$ are conformable. Matrices $[A]$ and $[B]$ are said to be conformable for multiplication when the column size of the premultiplier, $[A]$, is equal to the row size of the postmultiplier, $[B]$. The size of the product $[C]$ is determined from both $[A]$ and $[B]$; viz, $[C]$ will have the same number of rows as $[A]$, and $[C]$ will have the same number of columns as $[B]$.

Then the product of [A] premultiplying [B] is [C]:

where

$$\begin{matrix} [A] & [B] & = & [C] \\ m \times p & p \times n & & m \times n \end{matrix} \quad (B.2-2)$$

and the elements of [C] are given by

$$c_{ij} = \sum_{k=1}^p a_{ik} b_{kj}, \quad \begin{matrix} i = 1, 2, \dots, m \\ j = 1, 2, \dots, n \end{matrix} \quad (B.2-3)$$

The rules of conformability for the circle-cross product matrix operator are developed in section B.3.

The definitions of the following matrix operations are used subsequently in the development of the operator: \otimes .

Premultiplication of a general matrix by a row vector:

$$\begin{matrix} [A] & [B] & = & [C] \\ 1 \times p & p \times n & & 1 \times n \end{matrix} \quad (B.2-4)$$

where

$$c_j = \sum_{k=1}^p a_k b_{kj}, \quad j = 1, 2, \dots, n \quad (B.2-5)$$

Postmultiplication of a general matrix by a column vector:

$$\begin{matrix} [A] & \{ B \} & = & \{ C \} \\ m \times n & n \times 1 & & m \times 1 \end{matrix} \quad (B.2-6)$$

where

$$c_i = \sum_{k=1}^n a_{ik} b_k, \quad i = 1, 2, \dots, m \quad (B.2-7)$$

Matrix addition (two matrices are conformable for addition if and only if they have identical row and column sizes):

$$\begin{matrix} [A] & + & [B] & = & [C] \\ m \times n & & m \times n & & m \times n \end{matrix} \quad (B.2-8)$$

where

$$c_{ij} = a_{ij} + b_{ij}, i = 1, 2, \dots, m \\ j = 1, 2, \dots, n \quad (B.2-9)$$

B.3 CONFORMABILITY AND OPERATOR DEFINITIONS

The circle-cross product matrix operator, \otimes , is defined below in terms of its use as a row, column or element operator; the necessary condition of conformability for each operation is established. The commutative, associative, and distributive properties of the circle-cross product operator are developed in sections B.4, B.5, and B.6, respectively. The use of mixed operations, i.e., the combined use of the circle-cross product operator with standard matrix operators, is discussed in section B.7.

B.3.1 A Row Operator

The circle-cross product as a row operator is defined for that operation between a column vector and a general matrix as shown in equations (B.3-1) through (B.3-4).

$$\left\{ A \right\}_{m \times 1} \otimes [B]_{m \times n} = [C]_{m \times n} \quad (B.3-1)$$

with

$$c_{ij} = a_i b_{ij}, i = 1, 2, \dots, m \\ j = 1, 2, \dots, n \quad (B.3-2)$$

and

$$[B]_{m \times n} \otimes \left\{ A \right\}_{m \times 1} = [C]_{m \times n} \quad (B.3-3)$$

with

$$c_{ij} = b_{ij} a_i, i = 1, 2, \dots, m \\ j = 1, 2, \dots, n \quad (B.3-4)$$

The column vector $\{A\}$ and the matrix $[B]$ are conformable for the circle-cross product row operation if and only if the row size of the column vector, $\{A\}$, is equal to the row size of the general matrix, $[B]$. The foregoing results are also valid if the general matrix $[B]$ is a column vector $\{B\}$; i.e., $n=1$.

This operation is equivalent to premultiplying $[B]$ by a diagonal matrix $[A']$ as shown below, where the diagonal matrix is formed from the elements of $\{A\}$ as,

$$\begin{bmatrix} A' \end{bmatrix}_{m \times m} = \begin{bmatrix} a_1 & a_2 & 0 \\ 0 & \ddots & \\ & & a_m \end{bmatrix}_{m \times m} \quad (\text{B.3-5})$$

or

$$a'_{ii} = a_i, i = 1, 2, \dots, m \quad (\text{B.3-6})$$

Thus, using equation (B.2-3), the operation

$$\begin{bmatrix} A' \end{bmatrix}_{m \times m} \begin{bmatrix} B \end{bmatrix}_{m \times n} = \begin{bmatrix} C \end{bmatrix}_{m \times n} \quad (\text{B.3-7})$$

where

$$c_{ij} = \sum_{k=1}^m a'_{ik} b_{kj}, i = 1, 2, \dots, m \quad (\text{B.3-8})$$

$$j = 1, 2, \dots, n$$

and realizing that the only nonzero terms in the summation over k result for $k=i$, and substituting from equation (B.3-6) yields,

$$c_{ij} = a_i b_{ij}, i = 1, 2, \dots, m \quad (\text{B.3-9})$$

$$j = 1, 2, \dots, n$$

is clearly equivalent to the circle-cross product operations shown in equations (B.3-1) through (B.3-4).

B.3.2 A Column Operator

The circle-cross product as a column operator is defined for that operation between a row vector and a general matrix as shown in equations (B.3-10) through (B.3-13).

$$\begin{bmatrix} A \end{bmatrix}_{1 \times n} \otimes \begin{bmatrix} B \end{bmatrix}_{m \times n} = \begin{bmatrix} C \end{bmatrix}_{m \times n} \quad (\text{B.3-10})$$

with

$$c_{ij} = a_j b_{ij}, i = 1, 2, \dots, m \quad (\text{B.3-11})$$

$$j = 1, 2, \dots, n$$

and

$$\begin{bmatrix} B \end{bmatrix}_{m \times n} \otimes \begin{bmatrix} A \end{bmatrix}_{1 \times n} = \begin{bmatrix} C \end{bmatrix}_{m \times n} \quad (\text{B.3-12})$$

with

$$c_{ij} = b_{ij} a_j, \begin{matrix} i = 1, 2, \dots, m \\ j = 1, 2, \dots, n \end{matrix} \quad (\text{B.3-13})$$

The row vector \underline{A} and the matrix $[B]$ are conformable for the circle-cross product column operation if and only if the column size of the row vector, \underline{A} , is equal to the column size of the general matrix, $[B]$. The foregoing results are also valid if the general matrix $[B]$ is a row vector \underline{B} ; i.e., $m=1$.

This operation is equivalent to postmultiplying $[B]$ by a diagonal matrix $\Gamma A'$ as shown below, where the diagonal matrix is formed from the elements of \underline{A} as,

$$\Gamma A' = \begin{matrix} \begin{bmatrix} a_1 & 0 & \dots & 0 \\ 0 & a_2 & \dots & 0 \\ \vdots & \vdots & \ddots & \vdots \\ 0 & 0 & \dots & a_n \end{bmatrix} \\ n \times n \qquad \qquad n \times n \end{matrix} \quad (\text{B.3-14})$$

or

$$a'_{jj} = a_j, j = 1, 2, \dots, n \quad (\text{B.3-15})$$

Thus, using equation (B.2-3), the operation

$$\begin{matrix} [B] & \Gamma A' \\ m \times n & n \times n \end{matrix} = \begin{matrix} [C] \\ m \times n \end{matrix} \quad (\text{B.3-16})$$

where

$$c_{ij} = \sum_{k=1}^n b_{ik} a'_{kj}, \begin{matrix} i = 1, 2, \dots, m \\ j = 1, 2, \dots, n \end{matrix} \quad (\text{B.3-17})$$

and recognizing that the only nonzero terms in the summation over k result for $k=j$, and substituting from equation (B.3-15) yields,

$$c_{ij} = b_{ij} a_j, \begin{matrix} i = 1, 2, \dots, m \\ j = 1, 2, \dots, n \end{matrix} \quad (\text{B.3-18})$$

is clearly equivalent to the circle-cross product operations shown in equations (B.3-10) through (B.3-13).

B.3.3 An Element Operator

The circle-cross product as an element operator is defined for that operation between two general matrices as shown in equations (B.3-19) and (B.3-20).

$$\begin{matrix} [A] & \otimes & [B] & = & [C] \\ m \times n & & m \times n & & m \times n \end{matrix} \quad (B.3-19)$$

with

$$c_{ij} = a_{ij} b_{ij}, i = 1, 2, \dots, m \\ j = 1, 2, \dots, n \quad (B.3-20)$$

Two matrices are conformable for the circle-cross product element operation if and only if they are the same size; i.e., both matrices are of order $m \times n$. The above results are also valid when *both* $[A]$ and $[B]$ are considered to be either row vectors ($[A]$, $[B]$) or column vectors ($\{A\}$, $\{B\}$); the resultant matrix $[C]$ would be a row vector $[C]$ or column vector $\{C\}$, respectively.

Therefore,

$$\begin{matrix} [A] & \otimes & [B] & = & [C] \\ 1 \times n & & 1 \times n & & 1 \times n \end{matrix} \quad (B.3-21)$$

where

$$c_j = a_j b_j, j = 1, 2, \dots, n \quad (B.3-22)$$

and

$$\begin{matrix} \{A\} & \otimes & \{B\} & = & \{C\} \\ m \times 1 & & m \times 1 & & m \times 1 \end{matrix} \quad (B.3-23)$$

where

$$c_i = a_i b_i, i = 1, 2, \dots, m \quad (B.3-24)$$

The expression given by equations (B.3-23) and (B.3-24) is used frequently within the FLEXSTAB theoretical development. This operation gave rise to the misnomer "element operator," which was used to describe the symbol \otimes .

B.4 COMMUTATIVE PROPERTY OF THE OPERATOR \otimes

The circle-cross product row operator is commutative; i.e.,

$$\begin{matrix} \{A\} & \otimes & [B] & \equiv & [B] & \otimes & \{A\} & = & [C] \\ m \times 1 & & m \times n & & m \times n & & m \times 1 & & m \times n \end{matrix} \quad (B.4-1)$$

This fact is verified when equation (B.3-2) is compared with equation (B.3-4), viz

$$c_{ij} = a_{ij} b_{ij} \equiv b_{ij} a_{ij}, i = 1, 2, \dots, m \\ j = 1, 2, \dots, n \quad (B.4-2)$$

Likewise, the circle-cross product column operator is commutative, i.e.,

$$\begin{bmatrix} A \end{bmatrix}_{1 \times n} \otimes \begin{bmatrix} B \end{bmatrix}_{m \times n} \equiv \begin{bmatrix} B \end{bmatrix}_{m \times n} \otimes \begin{bmatrix} A \end{bmatrix}_{1 \times n} = \begin{bmatrix} C \end{bmatrix}_{m \times n} \quad (\text{B.4-3})$$

This fact is verified when equation (B.3-11) is compared with equation (B.3-13), viz

$$c_{ij} = a_j b_{ij} \equiv b_{ij} a_j, \quad \begin{matrix} i = 1, 2, \dots, m \\ j = 1, 2, \dots, n \end{matrix} \quad (\text{B.4-4})$$

The circle-cross product element operator is also commutative; using equations (B.3-19) and (B.3-20) and interchanging notation for $\{A\}$ and $\{B\}$ since they are arbitrary yields,

$$\begin{bmatrix} A \end{bmatrix}_{m \times n} \otimes \begin{bmatrix} B \end{bmatrix}_{m \times n} \equiv \begin{bmatrix} B \end{bmatrix}_{m \times n} \otimes \begin{bmatrix} A \end{bmatrix}_{m \times n} = \begin{bmatrix} C \end{bmatrix}_{m \times n} \quad (\text{B.4-5})$$

or

$$c_{ij} = a_{ij} b_{ij} \equiv b_{ij} a_{ij}, \quad \begin{matrix} i = 1, 2, \dots, m \\ j = 1, 2, \dots, n \end{matrix} \quad (\text{B.4-6})$$

B.5 ASSOCIATIVE PROPERTY OF THE OPERATOR \otimes

The circle-cross product operator is associative; i.e.,

$$\left(\begin{bmatrix} A \end{bmatrix}_{m \times 1} \otimes \begin{bmatrix} B \end{bmatrix}_{m \times n} \right) \otimes \begin{bmatrix} C \end{bmatrix}_{1 \times n} \equiv \begin{bmatrix} A \end{bmatrix}_{m \times 1} \otimes \left(\begin{bmatrix} B \end{bmatrix}_{m \times n} \otimes \begin{bmatrix} C \end{bmatrix}_{1 \times n} \right) = \begin{bmatrix} D \end{bmatrix}_{m \times n} \quad (\text{B.5-1})$$

Equations (B.3-1) and (B.3-19) are used to demonstrate the identity of equation (B.5-1). The left-hand side (LHS) of the identity is evaluated as

$$\left(\begin{bmatrix} A \end{bmatrix}_{m \times 1} \otimes \begin{bmatrix} B \end{bmatrix}_{m \times n} \right) \otimes \begin{bmatrix} C \end{bmatrix}_{n \times 1} = \begin{bmatrix} D \end{bmatrix}_{m \times n} \quad (\text{B.5-2})$$

let

$$\begin{bmatrix} A \end{bmatrix}_{m \times 1} \otimes \begin{bmatrix} B \end{bmatrix}_{m \times n} = \begin{bmatrix} R \end{bmatrix}_{m \times n} \quad (\text{B.5-3})$$

using equation (B.3-1)

$$r_{ij} = a_i b_{ij}, \quad \begin{matrix} i = 1, 2, \dots, m \\ j = 1, 2, \dots, n \end{matrix} \quad (\text{B.5-4})$$

then substituting equation (B.5-3) into equation (B.5-2) yields

$$\begin{bmatrix} R \end{bmatrix}_{m \times n} \otimes \begin{bmatrix} C \end{bmatrix}_{n \times 1} = \begin{bmatrix} D \end{bmatrix}_{m \times n} \quad (\text{B.5-5})$$

Now using equation (B.3-12) and substituting from equation (B.5-4), the result for the LHS expansion is

$$d_{ij} = a_i b_{ij} c_j, i = 1, 2, \dots, m \\ j = 1, 2, \dots, n \quad (B.5-6)$$

The right-hand side (RHS) of the identity of equation (B.5-i) is evaluated as,

$$\{A\}_{m \times 1} \otimes ([B]_{m \times n} \otimes [C]_{n \times 1}) = [D]_{m \times n} \quad (B.5-7)$$

let

$$([B]_{m \times n} \otimes [C]_{n \times 1}) = [R]_{m \times n} \quad (B.5-8)$$

expand equation (B.5-8) using equation (B.3-12), thus

$$r_{ij} = b_{ij} c_j, i = 1, 2, \dots, m \\ j = 1, 2, \dots, n \quad (B.5-9)$$

substituting equation (B.5-8) into equation (B.5-7) yields

$$\{A\}_{m \times 1} \otimes [R]_{m \times n} = [D]_{m \times n} \quad (B.5-10)$$

Now using equation (B.3-1) and substituting from equation (B.5-9), the result for the RHS expansion is

$$d_{ij} = a_i b_{ij} c_j, i = 1, 2, \dots, m \\ j = 1, 2, \dots, n \quad (B.5-11)$$

Equations (B.5-6) and (B.5-11) are identical, demonstrating the associative property of the circle-cross product operator.

B.6 DISTRIBUTIVE PROPERTY OF THE OPERATOR \otimes OVER MATRIX ADDITION

The circle-cross product matrix operator is distributive over matrix addition (or subtraction); i.e.,

$$[A]_{m \times n} \otimes ([B]_{m \times n} + [C]_{m \times n}) \equiv [A]_{m \times n} \otimes [B]_{m \times n} + [A]_{m \times n} \otimes [C]_{m \times n} \quad (B.6-1)$$

To evaluate the LHS of equation (B.6-1), let

$$([B]_{m \times n} + [C]_{m \times n}) = [R]_{m \times n} \quad (B.6-2)$$

using equations (B.2-8) and (B.2-9),

$$r_{ij} = b_{ij} + c_{ij}, i = 1, 2, \dots, m \\ j = 1, 2, \dots, n \quad (B.6-3)$$

substitute equation (B.6-2) into the LHS of equation (B.6-1) and introduce an auxiliary matrix [D],

$$\begin{matrix} [A] & \otimes & [R] & = & [D] \\ m \times n & & m \times n & & m \times n \end{matrix} \quad (B.6-4)$$

using equations (B.3-19) and (B.3-20) and substituting from equation (B.6-3) yields the result for the LHS of the identity in equation (B.6-1)

$$d_{ij} = a_{ij} (b_{ij} + c_{ij}), i = 1, 2, \dots, m \\ j = 1, 2, \dots, n \quad (B.6-5)$$

To evaluate the RHS of equation (B.6-1), let

$$\begin{matrix} [A] & \otimes & [B] & = & [R] \\ m \times n & & m \times n & & m \times n \end{matrix} \quad (B.6-6)$$

and let

$$\begin{matrix} [A] & \otimes & [C] & = & [S] \\ m \times n & & m \times n & & m \times n \end{matrix} \quad (B.6-7)$$

by using equations (B.3-19) and (B.3-20) to evaluate equations (B.6-6) and (B.6-7) yield,

$$r_{ij} = a_{ij} b_{ij}, i = 1, 2, \dots, m \\ j = 1, 2, \dots, n \quad (B.6-8)$$

and

$$s_{ij} = a_{ij} c_{ij}, i = 1, 2, \dots, m \\ j = 1, 2, \dots, n \quad (B.6-9)$$

Now, forming an auxiliary matrix [D] by adding equations (B.6-6) and (B.6-7) and using equations (B.6-8) and (B.6-9) yields the result for the RHS of the identity of equation (B.6-1) as

$$d_{ij} = a_{ij} (b_{ij} + c_{ij}), i = 1, 2, \dots, m \\ j = 1, 2, \dots, n \quad (B.6-10)$$

Equations (B.6-5) and (B.6-10) are identical; thus, the distributive property of the circle-cross product matrix operator over matrix addition (or subtraction) is demonstrated.

B.7 THE OPERATOR \otimes COMBINED WITH STANDARD MATRIX OPERATIONS

The purpose of this section is to develop the meaning of the circle-cross product matrix operator when it is used in expressions which also contain standard matrix operations. Particular emphasis is placed upon the order of the matrix operations contained in the following expressions. The size of each matrix has been intentionally omitted below; however, each of the expressions shown is subsequently examined with specific regard to particular matrix sizes, and those orders of operations that result in nonconformable expressions (i.e., expressions which cannot be evaluated) are identified. The expressions are:

$$1) \quad [A] \{B\} \otimes \{C\} \quad (B.7-1)$$

$$2) \quad \{A\} \otimes [B] \{C\} \quad (B.7-2)$$

$$3) \quad [A] \{B\} \otimes \{C\} \quad (B.7-3)$$

$$4) \quad [A] \{B\} \otimes \{C\} \{D\} \quad (B.7-4)$$

$$5) \quad [A] [B] \otimes [C] \{D\} \quad (B.7-5)$$

Case 1

The expression shown in equation (B.7-1) is now developed for three sets of matrix sizes.

Let

$$\begin{matrix} [A] & \{B\} & \otimes & \{C\} & = & \{D\} \\ m \times n & n \times 1 & & m \times 1 & & m \times 1 \end{matrix}, m \neq n \quad (B.7-6)$$

Clearly, the order of operations to evaluate equation (B.7-6) must be

$$\begin{matrix} ([A] \{B\}) & \otimes & \{C\} & = & \{D\} \\ m \times n & n \times 1 & m \times 1 & & m \times 1 \end{matrix} \quad (B.7-7)$$

resulting in

$$\begin{matrix} \{[A] \{B\}\} & \otimes & \{C\} & = & \{D\} \\ m \times 1 & & m \times 1 & & m \times 1 \end{matrix} \quad (B.7-8)$$

Recall that the expression

$$\begin{matrix} [A] & \left(\{B\} \otimes \{C\} \right) \\ m \times n & n \times 1 \quad m \times 1 \end{matrix} \quad (B.7-9)$$

cannot be evaluated since $\{B\}$ and $\{C\}$ are not conformable for the circle-cross product row operation (see sec. B.3 I.)

Therefore, using equations (B.2-7) and (B.3-23), the expression given in equation (B.7-7) results in,

$$d_i = c_i \sum_{k=1}^n a_{ik} b_k, i = 1, 2, \dots, m \quad (\text{B.7-10})$$

Next, consider the expression of equation (B.7-1) with the following matrix sizes:

$$\begin{matrix} [A] & \{B\} & \otimes & \{C\} & = & \{D\} \\ m \times n & n \times 1 & & n \times 1 & & m \times 1 \end{matrix}, m \neq n$$

This expression can only be evaluated as

$$\begin{matrix} [A] & (\{B\} \otimes \{C\}) & = & \{D\} \\ m \times n & n \times 1 & & m \times 1 \end{matrix} \quad (\text{B.7-11})$$

resulting in

$$\begin{matrix} [A] & \left\{ \begin{matrix} n \times 1 \\ \{B\} \otimes \{C\} \end{matrix} \right\} & = & \{D\} \\ m \times n & n \times 1 & & m \times 1 \end{matrix} \quad (\text{B.7-12})$$

The expression

$$\begin{matrix} ([A] \{B\}) & \otimes & \{C\} \\ m \times n & n \times 1 & n \times 1 \end{matrix} \quad (\text{B.7-13})$$

cannot be evaluated because the matrix product $[A] \{B\}$ and the column vector $\{C\}$ are not conformable for the circle-cross product matrix operation.

Using equations (B.2-7) and (B.3-23), the expression given in equation (B.7-14) results in

$$d_i = \sum_{k=1}^n a_{ik} b_k c_k, i = 1, 2, \dots, m \quad (\text{B.7-14})$$

Next, consider the expression of equation (B.7-1) with the following matrix sizes.

$$\begin{matrix} [A] \{B\} & \otimes & \{C\} & = & \{D\} \\ n \times n & n \times 1 & n \times 1 & & n \times 1 \end{matrix} \quad (\text{B.7-15})$$

The order in which the operations are performed to evaluate this expression must be carefully specified. The result of the operation

$$\begin{matrix} ([A] \{B\}) & \otimes & \{C\} & = & \{D\} \\ n \times n & n \times 1 & n \times 1 & & n \times 1 \end{matrix} \quad (\text{B.7-16})$$

is given by equation (B.7-10) as,

$$d_i = c_i \sum_{k=1}^n a_{ik} b_k, i = 1, 2, \dots, n \quad (\text{B.7-17})$$

The result of the operation

$$\{A\} (\{B\} \otimes \{C\}) = \{D\}$$

is given by equation (B.7-14) as,

$$d_i = \sum_{k=1}^n a_{ik} b_k c_k, i = 1, 2, \dots, n \quad (\text{B.7-18})$$

Case 2

The expression given by equation (B.7-2) is not dependent upon the order in which it is evaluated. To evaluate equation (B.7-2), let

$$\left(\begin{matrix} \{A\} \\ m \times 1 \end{matrix} \otimes \begin{matrix} \{B\} \\ m \times n \end{matrix} \right) \begin{matrix} \{C\} \\ n \times 1 \end{matrix} = \begin{matrix} \{D\} \\ m \times 1 \end{matrix} \quad (\text{B.7-19})$$

Further, let

$$\begin{matrix} \{A\} \\ m \times 1 \end{matrix} \otimes \begin{matrix} \{B\} \\ m \times n \end{matrix} = \begin{matrix} \{R\} \\ m \times n \end{matrix} \quad (\text{B.7-20})$$

then

$$r_{ij} = a_i b_{ij}, i = 1, 2, \dots, m \\ j = 1, 2, \dots, n \quad (\text{B.7-21})$$

Substituting equation (B.7-20) into equation (B.7-19) and then substituting equation (B.7-21) into the result yields

$$d_i = \sum_{k=1}^n a_i b_{ik} c_k, i = 1, 2, \dots, m \quad (\text{B.7-22})$$

The same result is obtained by evaluating the expression

$$\begin{matrix} \{A\} \\ m \times 1 \end{matrix} \otimes \left(\begin{matrix} \{B\} \\ m \times n \end{matrix} \begin{matrix} \{C\} \\ n \times 1 \end{matrix} \right) = \begin{matrix} \{D\} \\ m \times 1 \end{matrix} \quad (\text{B.7-23})$$

Case 3

The expression shown in equation (B.7-3) must be evaluated as

$$\begin{matrix} [A] & (\{B\} \otimes [C]) \\ m \times p & p \times 1 \quad p \times n \quad m \times n \quad n > 1 \end{matrix} = [D], \quad (B.7-24)$$

Otherwise, the matrix product $[A] \{B\}$ would not be conformable with $[C]$ for the circle-cross product operation. Equation (B.7-24) is evaluated for $[D]$ using equations (B.3-1) and (B.2-2) to yield,

$$d_{ij} = \sum_{k=1}^p a_{ik} b_k c_{kj}, \quad \begin{matrix} i = 1, 2, \dots, m \\ j = 1, 2, \dots, n \end{matrix} \quad (B.7-25)$$

It is possible that the expression given by equation (B.7-3) can be evaluated to produce different results when the matrix sizes are as shown in equation (B.7-26).

$$\begin{matrix} [A] \{B\} \otimes [C] \\ n \times n \quad n \times 1 \quad n \times n \quad n \times n \end{matrix} = [D] \quad (B.7-26)$$

Evaluating

$$\begin{matrix} ([A] \{B\}) \otimes [C] \\ n \times n \quad n \times 1 \quad n \times n \quad n \times n \end{matrix} = [D] \quad (B.7-27)$$

yields

$$d_{ij} = c_{ij} \sum_{k=1}^n a_{ik} b_k, \quad \begin{matrix} i = 1, 2, \dots, n \\ j = 1, 2, \dots, n \end{matrix} \quad (B.7-28)$$

Whereas,

$$\begin{matrix} [A] (\{B\} \times [C]) \\ n \times n \quad n \times 1 \quad n \times n \quad n \times n \end{matrix} = [D] \quad (B.7-29)$$

may be evaluated as

$$d_{ij} = \sum_{k=1}^n a_{ik} b_k c_k, \quad \begin{matrix} i = 1, 2, \dots, n \\ j = 1, 2, \dots, n \end{matrix} \quad (B.7-30)$$

The correct order to evaluate this expression depends upon the desired results as given by equation (B.7-28) or (B.7-30).

Case 4

The expression given by equation (B.7-4) may be evaluated utilizing any of the following five forms (where all matrices are either n-square or n-vector as shown):

$$1) \quad \begin{matrix} ([A] \{B\}) \\ n \times n \quad n \times 1 \end{matrix} \otimes \begin{matrix} ([C] \{D\}) \\ n \times n \quad n \times 1 \end{matrix} = \begin{matrix} \{E\} \\ n \times 1 \end{matrix} \quad (B.7-31)$$

$$2) \quad [A] (\{B\} \otimes ([C] \{D\})) = \{E\} \quad (B.7-32)$$

$$3) \quad (([A] \{B\}) \otimes [C]) \{D\} = \{E\} \quad (B.7-33)$$

$$4) \quad [A] ((\{B\} \otimes [C]) \{D\}) = \{E\} \quad (B.7-34)$$

$$5) \quad ([A] (\{B\} \otimes [C])) \{D\} = \{E\} \quad (B.7-35)$$

These forms all have meaning; therefore, the important consideration is to establish a clear understanding of exactly which matrices are the object matrices (i.e., the prematrix and postmatrix) in the circle-cross product operation. Table B.7-1 shows the object matrices for equations (B.7-31) through (B.7-35).

The expressions given by equations (B.7-34) and (B.7-35) must yield identical results since they utilize the same circle-cross product matrix operation.

Equations (B.7-31) through (B.7-35) may be evaluated using the techniques developed earlier. These results are shown in table B.7-2 where the elements e_i define the column vector $\{E\}$ above.

Table B.7-2 also shows that forms "1" and "3" are equivalent. Forms "2", "4", and "5" are also equivalent; however, they are not equivalent to "1" or "3". One could, of course select matrix sizes that would result in nonconformable matrix operations.

Case 5

The expression of equation (B.7-5) must be evaluated in one specific order for the matrix sizes shown in equation (B.7-36), due to the conformability requirement of the circle-cross product operations.

$$\begin{matrix} [A] [B] \otimes [C] [D] \\ m \times p \quad p \times q \quad p \times q \quad q \times n \end{matrix} \Rightarrow [A] ([B] \otimes [C]) [D] \quad (B.7-36)$$

and

$$\begin{matrix} [A] [B] \otimes [C] [D] \\ m \times p \quad p \times n \quad m \times q \quad q \times n \end{matrix} \Rightarrow ([A] [B]) \otimes ([C] [D]) \quad (B.7-37)$$

**TABLE B.7-1 -- CASE 4: PREMATRICES AND POSTMATRICES
OF THE CIRCLE-CROSS PRODUCT OPERATOR**

Form	Prematrix	Postmatrix	Equation number
1	$\begin{bmatrix} A \end{bmatrix} \begin{Bmatrix} B \end{Bmatrix}$ $n \times n \quad n \times 1$	$\begin{bmatrix} C \end{bmatrix} \begin{Bmatrix} D \end{Bmatrix}$ $n \times n \quad n \times 1$	B.7-31
2	$\begin{Bmatrix} B \end{Bmatrix}$	$\begin{bmatrix} C \end{bmatrix} \begin{Bmatrix} D \end{Bmatrix}$	B.7-32
3	$\begin{bmatrix} A \end{bmatrix} \begin{Bmatrix} B \end{Bmatrix}$	$\begin{bmatrix} C \end{bmatrix}$	B.7-33
4	$\begin{Bmatrix} B \end{Bmatrix}$	$\begin{bmatrix} C \end{bmatrix}$	B.7-34
5	$\begin{Bmatrix} B \end{Bmatrix}$	$\begin{bmatrix} C \end{bmatrix}$	B.7-35

**TABLE B.7-2 — EVALUATIONS OF AN EXPRESSION WITH THE
CIRCLE-CROSS PRODUCT AND STANDARD MATRIX OPERATIONS**

Evaluations of: $\begin{bmatrix} A \end{bmatrix} \begin{Bmatrix} B \end{Bmatrix} \otimes \begin{bmatrix} C \end{bmatrix} \begin{Bmatrix} D \end{Bmatrix} = \begin{Bmatrix} E \end{Bmatrix}$
 $n \times n \quad n \times 1 \quad \quad n \times n \quad n \times 1 \quad \quad n \times 1$

Form	Result
1) $\left(\begin{bmatrix} A \end{bmatrix} \begin{Bmatrix} B \end{Bmatrix} \right) \otimes \left(\begin{bmatrix} C \end{bmatrix} \begin{Bmatrix} D \end{Bmatrix} \right) = \begin{Bmatrix} E \end{Bmatrix}$	$e_i = \sum_{k=1}^n \sum_{\ell=1}^n a_{ik} b_k c_{i\ell} d_{\ell}, i = 1, 2, \dots, n$
2) $\begin{bmatrix} A \end{bmatrix} \left(\begin{Bmatrix} B \end{Bmatrix} \otimes \left(\begin{bmatrix} C \end{bmatrix} \begin{Bmatrix} D \end{Bmatrix} \right) \right) = \begin{Bmatrix} E \end{Bmatrix}$	$e_i = \sum_{k=1}^n \sum_{\ell=1}^n a_{ik} b_k c_{k\ell} d_{\ell}, i = 1, 2, \dots, n$
3) $\left(\left(\begin{bmatrix} A \end{bmatrix} \begin{Bmatrix} B \end{Bmatrix} \right) \otimes \begin{bmatrix} C \end{bmatrix} \right) \begin{Bmatrix} D \end{Bmatrix} = \begin{Bmatrix} E \end{Bmatrix}$	$e_i = \sum_{k=1}^n \sum_{\ell=1}^n a_{i\ell} b_{\ell} c_{ik} d_k, i = 1, 2, \dots, n$
4) $\begin{bmatrix} A \end{bmatrix} \left(\left(\begin{Bmatrix} B \end{Bmatrix} \otimes \begin{bmatrix} C \end{bmatrix} \right) \begin{Bmatrix} D \end{Bmatrix} \right) = \begin{Bmatrix} E \end{Bmatrix}$	$e_i = \sum_{k=1}^n \sum_{\ell=1}^n a_{ik} b_k c_{k\ell} d_{\ell}, i = 1, 2, \dots, n$
5) $\begin{bmatrix} A \end{bmatrix} \left(\begin{Bmatrix} B \end{Bmatrix} \otimes \begin{bmatrix} C \end{bmatrix} \right) \begin{Bmatrix} D \end{Bmatrix} = \begin{Bmatrix} E \end{Bmatrix}$	$e_i = \sum_{k=1}^n \sum_{\ell=1}^n a_{ik} b_k c_{k\ell} d_{\ell}, i = 1, 2, \dots, n$

The order of operations must be carefully specified when all matrix sizes are $n \times n$, since the results produced for different orders of evaluation may be quite different. These differences are subsequently identified.

Consider equation (B.7-38) where all matrices are $n \times n$. Equation (B.7-38) may be evaluated using equations (B.2-2) and (B.3-19) as follows.

$$\begin{matrix} ([A] [B]) & \otimes & ([C] [D]) & = & [E] \\ n \times n & n \times n & n \times n & n \times n & n \times n \end{matrix} \quad (B.7-38)$$

Let

$$\begin{matrix} [R] & = & [A] [B] \\ n \times n & & n \times n & n \times n \end{matrix} \quad (B.7-39)$$

where

$$r_{ij} = \sum_{k=1}^n a_{ik} b_{kj}, \quad \begin{matrix} i = 1, 2, \dots, n \\ j = 1, 2, \dots, n \end{matrix} \quad (B.7-40)$$

and let

$$\begin{matrix} [S] & = & [C] [D] \\ n \times n & & n \times n & n \times n \end{matrix} \quad (B.7-41)$$

where

$$s_{ij} = \sum_{\ell=1}^n c_{i\ell} d_{\ell j}, \quad \begin{matrix} i = 1, 2, \dots, n \\ j = 1, 2, \dots, n \end{matrix} \quad (B.7-42)$$

Then, substituting equations (B.7-39) and (B.7-41) into equation (B.7-38) yields

$$\begin{matrix} [R] & \otimes & [S] & = & [E] \\ n \times n & & n \times n & & n \times n \end{matrix} \quad (B.7-43)$$

where

$$e_{ij} = r_{ij} s_{ij}, \quad \begin{matrix} i = 1, 2, \dots, n \\ j = 1, 2, \dots, n \end{matrix} \quad (B.7-44)$$

and substituting equations (B.7-40) and (B.7-42) into equation (B.7-44) provides the final result

$$e_{ij} = \sum_{k=1}^n a_{ik} b_{kj} \sum_{\ell=1}^n c_{i\ell} d_{\ell j}, \quad \begin{matrix} i = 1, 2, \dots, n \\ j = 1, 2, \dots, n \end{matrix} \quad (B.7-45)$$

or

$$e_{ij} = \sum_{k=1}^n \sum_{\ell=1}^n a_{ik} b_{kj} c_{i\ell} d_{\ell j}, \begin{matrix} i = 1, 2, \dots, n \\ j = 1, 2, \dots, n \end{matrix} \quad (\text{B.7-46})$$

Next evaluate equation (B.7-5) as

$$\begin{matrix} [A] & ([B] \otimes [C]) & [D] & = & [E] \\ n \times n & n \times n & n \times n & n \times n & n \times n \end{matrix} \quad (\text{B.7-47})$$

Again, using equation (B.2-2) and (B.3-19), let

$$\begin{matrix} [R] = [B] \otimes [C] \\ n \times n & n \times n & n \times n \end{matrix} \quad (\text{B.7-48})$$

where

$$r_{ij} = b_{ij} c_{ij}, \begin{matrix} i = 1, 2, \dots, n \\ j = 1, 2, \dots, n \end{matrix} \quad (\text{B.7-49})$$

Substituting equation (B.7-48) into equation (B.7-47) and evaluating left to right yields,

$$\begin{matrix} [A][R][D] = [E] \\ n \times n & n \times n & n \times n & n \times n \end{matrix} \quad (\text{B.7-50})$$

with

$$\begin{matrix} [S] = [A][R] \\ n \times n & n \times n & n \times n \end{matrix}$$

where

$$s_{ij} = \sum_{k=1}^n a_{ik} r_{kj}, \begin{matrix} i = 1, 2, \dots, n \\ j = 1, 2, \dots, n \end{matrix} \quad (\text{B.7-51})$$

further

$$e_{ij} = \sum_{\ell=1}^n s_{i\ell} d_{\ell j}, \begin{matrix} i = 1, 2, \dots, n \\ j = 1, 2, \dots, n \end{matrix} \quad (\text{B.7-52})$$

and the final result is obtained, after substituting equations (B.7-49) and (B.7-51) into equation (B.7-52), as

$$e_{ij} = \sum_{\ell=1}^n \sum_{k=1}^n a_{ik} b_{k\ell} c_{\ell j} d_{\ell j}, \begin{matrix} i = 1, 2, \dots, n \\ j = 1, 2, \dots, n \end{matrix} \quad (B.7-53)$$

Next evaluate equation (B.7-5) as,

$$\left(\begin{matrix} [A] & [B] \\ n \times n & n \times n \end{matrix} \right) \otimes \begin{matrix} [C] \\ n \times n \end{matrix} \begin{matrix} [D] \\ n \times n \end{matrix} = \begin{matrix} [E] \\ n \times n \end{matrix} \quad (B.7-54)$$

Let

$$\begin{matrix} [R] \\ n \times n \end{matrix} = \begin{matrix} [A] & [B] \\ n \times n & n \times n \end{matrix} \quad (B.7-55)$$

and

$$\begin{matrix} [S] \\ n \times n \end{matrix} = \begin{matrix} [R] \\ n \times n \end{matrix} \otimes \begin{matrix} [C] \\ n \times n \end{matrix} \quad (B.7-56)$$

Using equations (B.2-2) and (B.3-19) yields,

$$r_{ij} = \sum_{k=1}^n a_{ik} b_{kj}, \begin{matrix} i = 1, 2, \dots, n \\ j = 1, 2, \dots, n \end{matrix} \quad (B.7-57)$$

and

$$s_{ij} = r_{ij} c_{ij}, \begin{matrix} i = 1, 2, \dots, n \\ j = 1, 2, \dots, n \end{matrix} \quad (B.7-58)$$

or

$$s_{ij} = \sum_{k=1}^n a_{ik} b_{kj} c_{ij}, \begin{matrix} i = 1, 2, \dots, n \\ j = 1, 2, \dots, n \end{matrix} \quad (B.7-59)$$

Substituting equation (B.7-56) into equation (B.7-54) yields,

$$\begin{matrix} [S] & [D] \\ n \times n & n \times n \end{matrix} = \begin{matrix} [E] \\ n \times n \end{matrix} \quad (B.7-60)$$

where

$$e_{ij} = \sum_{\ell=1}^n s_{i\ell} d_{\ell j}, \begin{matrix} i = 1, 2, \dots, n \\ j = 1, 2, \dots, n \end{matrix} \quad (B.7-61)$$

thus, the final result is

$$e_{ij} = \sum_{\ell=1}^n \sum_{k=1}^n a_{ik} b_{k\ell} c_{i\ell} d_{\ell j}, \begin{matrix} i = 1, 2, \dots, n \\ j = 1, 2, \dots, n \end{matrix} \quad (\text{B.7-62})$$

Finally, evaluate equation (B.7-5) as,

$$\begin{matrix} [A] \\ n \times n \end{matrix} \left(\begin{matrix} [B] \\ n \times n \end{matrix} \otimes \begin{pmatrix} [C] [D] \end{pmatrix} \right) = [E] \quad \begin{matrix} n \times n \quad n \times n \end{matrix} \quad (\text{B.7-63})$$

Let

$$\begin{matrix} [R] \\ n \times n \end{matrix} = \begin{matrix} [C] \\ n \times n \end{matrix} \otimes \begin{matrix} [D] \\ n \times n \end{matrix} \quad (\text{B.7-64})$$

and

$$\begin{matrix} [S] \\ n \times n \end{matrix} = \begin{matrix} [B] \\ n \times n \end{matrix} \otimes \begin{matrix} [R] \\ n \times n \end{matrix} \quad (\text{B.7-65})$$

Then,

$$r_{ij} = \sum_{k=1}^n c_{ik} d_{kj}, \begin{matrix} i = 1, 2, \dots, n \\ j = 1, 2, \dots, n \end{matrix} \quad (\text{B.7-66})$$

and

$$s_{ij} = b_{ij} r_{ij}, \begin{matrix} i = 1, 2, \dots, n \\ j = 1, 2, \dots, n \end{matrix} \quad (\text{B.7-67})$$

or

$$s_{ij} = b_{ij} \sum_{k=1}^n c_{ik} d_{kj}, \begin{matrix} i = 1, 2, \dots, n \\ j = 1, 2, \dots, n \end{matrix} \quad (\text{B.7-68})$$

Substituting equation (B.7-65) into equation (B.7-63) yields

$$\begin{matrix} [A] \\ n \times n \end{matrix} \begin{matrix} [S] \\ n \times n \end{matrix} = [E] \quad n \times n \quad (\text{B.7-69})$$

where

$$e_{ij} = \sum_{\ell=1}^n a_{i\ell} s_{\ell j}, i = 1, 2, \dots, n$$

$$j = 1, 2, \dots, n \quad (B.7-70)$$

or

$$e_{ij} = \sum_{\ell=1}^n a_{i\ell} b_{\ell j} \sum_{k=1}^n c_{\ell k} d_{kj}, i = 1, 2, \dots, n$$

$$j = 1, 2, \dots, n \quad (B.7-71)$$

The final results are obtained by rewriting equation (B.7-71) as

$$e_{ij} = \sum_{\ell=1}^n \sum_{k=1}^n a_{i\ell} b_{\ell j} c_{\ell k} d_{kj}, i = 1, 2, \dots, n$$

$$j = 1, 2, \dots, n \quad (B.7-72)$$

The results of evaluating the expression of equation (B.7-5) as developed in equations (B.7-38) through (B.7-72) are summarized in table B.7-3.

TABLE B.7-3 — ADDITIONAL EVALUATIONS OF AN EXPRESSION WITH THE CIRCLE-CROSS PRODUCT AND STANDARD MATRIX OPERATIONS

Evaluations of: $[A] [B] \otimes [C] [D] = [E]$
 $n \times n \quad n \times n \quad n \times n \quad n \times n \quad n \times n$

Form	Result
$([A] [B]) \otimes ([C] [D]) = [E]$	$e_{ij} = \sum_{k=1}^n \sum_{\ell=1}^n a_{ik} b_{kj} c_{i\ell} d_{\ell j}, i = 1, 2, \dots, n$ $j = 1, 2, \dots, n$
$[A] ([B] \otimes [C]) [D] = [E]$	$e_{ij} = \sum_{\ell=1}^n \sum_{k=1}^n a_{ik} b_{k\ell} c_{\ell j} d_{ij}, i = 1, 2, \dots, n$ $j = 1, 2, \dots, n$
$(([A] [B]) \otimes [C]) [D] = [E]$	$e_{ij} = \sum_{\ell=1}^n \sum_{k=1}^n a_{ik} b_{k\ell} c_{i\ell} d_{\ell j}, i = 1, 2, \dots, n$ $j = 1, 2, \dots, n$
$[A] ([B] \otimes ([C] [D])) = [E]$	$e_{ij} = \sum_{\ell=1}^n \sum_{k=1}^n a_{i\ell} b_{\ell j} c_{\ell k} d_{kj}, i = 1, 2, \dots, n$ $j = 1, 2, \dots, n$

B.8 SPECIAL CONSIDERATIONS OF \otimes AS IT IS USED IN THE FLEXSTAB PROGRAM

Throughout the preceding development, three matrix types were treated:

- 1) Row vectors, $\underline{\cdot}$
- 2) Column vectors, $\{\cdot\}$
- 3) General $m \times n$ matrices where $m, n > 1$, $[\cdot]$

Circle-cross product operations for each of the three matrix types were developed to demonstrate several potential uses. However, the FLEXSTAB computer program does not require all of the circle-cross product operations that were defined.

The FLEXSTAB circle-cross product matrix operations, performed by subroutine TEMAB, are coded for the row operator (sec. B.3.1)

$$\begin{matrix} \{A\} & \otimes & [B] \\ m \times 1 & & m \times n \end{matrix} \quad (B.8-1)$$

or

$$\begin{matrix} [A] & \otimes & \{B\} \\ m \times n & & m \times 1 \end{matrix} \quad (B.8-2)$$

and the element operator (sec. B.3.3)

$$\begin{matrix} \{A\} & \otimes & \{B\} \\ m \times 1 & & m \times 1 \end{matrix} \quad (B.8-3)$$

or

$$\begin{matrix} [A] & \otimes & [B] \\ m \times n & & m \times n \end{matrix} \quad (B.8-4)$$

The circle-cross product column operator (sec. B.3.2)

$$\begin{matrix} \underline{A} & \otimes & [B] \\ 1 \times n & & m \times n \end{matrix} \quad (B.8-5)$$

or

$$\begin{matrix} [A] & \otimes & \underline{B} \\ m \times n & & 1 \times n \end{matrix} \quad (B.8-6)$$

is not used in the theoretical development (Vol. I) of the FLEXSTAB program. Therefore, this operation is not performed by subroutine TEMAB.

Some of the circle-cross product matrix operations shown in Volume I were coded in-line in subroutine LEC of the SD&SS program rather than calling TEMAB. This was done because partitions of matrices rather than full matrices were used.

B.9 INDEX TO THE USES OF THE CIRCLE-CROSS PRODUCT MATRIX OPERATOR WITHIN THE FLEXSTAB THEORETICAL DEVELOPMENT

The occurrence of the circle-cross product matrix operator, \otimes , in the text of Volume I is indicated in table B.9-1.

TABLE B.9-1. — USES OF CIRCLE-CROSS PRODUCT IN THE FLEXSTAB THEORETICAL DEVELOPMENT

Vol. I page no.	Vol. I equation no.	Type of operation
3-159	3.4-224	element, $\{A\} \otimes \{B\}$
3-162	3.4-235	element, $\{A\} \otimes \{B\}$
3-197	3.5-67	element, $\{A\} \otimes \{B\}$
3-198	3.5-70	element, $\{A\} \otimes \{B\}$
3-199	3.5-71	element, $\{A\} \otimes \{B\}$ and row $[A] \otimes \{B\}$
3-199	3.5-72	element, $\{A\} \otimes \{B\}$
5-83	5.8-26	row, $\{A\} \otimes [B]$
5-83	5.8-27	element, $\{A\} \otimes \{B\}$
5-83	5.8-29	element, $\{A\} \otimes \{B\}$
5-83	5.8-30	element, $\{A\} \otimes \{B\}$
5-84	5.8-32	element, $\{A\} \otimes \{B\}$
5-84	5.8-33	element, $\{A\} \otimes \{B\}$
6-77	6.5-30	element, $\{A\} \otimes \{B\}$
6-77	6.5-31	element, $\{A\} \otimes \{B\}$
6-84	6.5-43	row, $[A] \otimes \{B\}$
6-84	6.5-44	row, $[A] \otimes \{B\}$
6-84	6.5-45	row, $[A] \otimes \{B\}$
6-85	6.5-46	row, $[A] \otimes \{B\}$

B.10 INDEX TO THE EXPLICIT USES OF THE CIRCLE-CROSS PRODUCT MATRIX OPERATOR WITHIN THE FLEXSTAB CODE

Explicit uses of the circle-cross product matrix operator are defined as those matrix operations performed by subroutine TEMAB. The subroutine TEMAB is contained in the Matrix Operation Package (MOP). In FLEXSTAB, it is always accessed through the Automatic Matrix Management Package (AMMP) by a "CALL MOP (6HEMAB, . . .)" statement.

The circle-cross product matrix operator, \otimes , is used explicitly within the FLEXSTAB program SD&SS, subroutine DMAT only. Table B.10-1 indicates where the circle-cross product operator is used within subroutine DMAT, and it identifies the Volume I equation that is related to that operation.

**TABLE B.10-1. — USES OF CIRCLE-CROSS PRODUCT
IN THE FLEXSTAB CODE**

Program Card Location	Volume I ref.		Volume III ref.	
	Equation no.	Page no.	Flowchart no.	Page no.
DMAT 0365	3.5-71	3-199	9.3-46	9-130
DMAT 0373	3.5-71	3-199	9.3-46	9-130
DMAT 0492	3.5-70	3-198	9.3-46	9-131
DMAT 0514	3.5-70	3-198	9.3-46	9-131
DMAT 0536	3.5-71	3-199	9.3-46	9-132
DMAT 0544	3.5-71	3-199	9.3-46	9-132
DMAT 0579	5.8-26	5-83	9.3-46	9-132
DMAT 0587	5.8-26	5-83	9.3-46	9-132
DMAT 0766	3.5-71 ^a	3-199	9.3-46	9-133
DMAT 0774	3.5-71 ^a	3-199	9.3-46	9-133
DMAT 0809	5.8-26 ^a	5-83	9.3-46	9-133
DMAT 0817	5.8-26 ^a	5-83	9.3-46	9-133

^a Antisymmetric forms are not explicitly shown in Volume I

REFERENCES

- 1-1 Woodward, F.; LaRowe, E.; and Love, J. E.: Analysis and Design of Supersonic Wing-Body Combinations, Including Flow Properties in Near Field. Part I and II, NASA CR-73107, 1967.
- 1-2 MacNeal, R. H.: The Nastran Theoretical Manual. NASA SP-221, Sept. 1970.
- 1-3 Anon: SAMECS—Structural Analysis System—Theory Document. Boeing document D6-23757-2TN, June 6, 1969.
- 2-1 Sololnikoff, I. S.: Mathematical Theory of Elasticity. McGraw-Hill Book Company, Inc., 1956.
- 2-2 Etkin, B.: Dynamics of Flight. John Wiley and Sons, Inc., 1962.
- 2-3 Ashley, H.; and Landahl, M.: Aerodynamics of Wings and Bodies. Addison-Wesley Publishing Company, Inc. 1965.
- 2-4 Milne, R. D.: Dynamics of the Deformable Airplane, Parts I and II. Her Majesty's Stationery Office, London, 1964.
- 2-5 Lamb: Higher Mechanics. Cambridge University Press, 1929, pp. 175-177.
- 2-6 Hurty, W. C.; and Rubinstein, M.F.: Dynamics of Structures. Prentice-Hall, Inc., 1964.
- 3-1 Miles, J. W.: Potential Theory of Unsteady Supersonic Flow. Cambridge University Press, 1959.
- 3-2 Garrick, I. E.: High Speed Aerodynamics and Jet Propulsion, Volume 7. Princeton University Press, 1960.
- 3-3 Watkins, C. E.; Runyan, H. L.; and Woolston, D. S.: On the Kernel Function of the Integral Equation Relating the Lift and Downwash Distributions of Oscillating Finite Wings in Subsonic Flow. NACA Report 1234, 1955.
- 3-4 Watkins, C. E.; and Berman, J. H.: On the Kernel Function of the Integral Equation Relating Lift and Downwash Distributions of Oscillating Wings in Supersonic Flow. NACA Report 1257, 1956.
- 3-5 Garner, H. C.: Multhopp's Subsonic Lifting-Surface Theory of Wings in Slow Pitching Oscillations. ARC TR R&M 2885, 1956.

- 3-6 Row W. S.: Collocation Method for Calculating the Aerodynamic Pressure Distribution on a Lifting Surface Oscillating in Subsonic Compressible Flow. AIAA Symposium on Structural Dynamics and Aeroelasticity, Boston, Mass., August 1965.
- 3-7 Liepmann and Roshko: Elements of Gas Dynamics. GALCIT Aeronautical Series, John Wiley and Sons, Inc. 1958.
- 3-8 Woodward, F. A.: A Unified Approach to the Analysis and Design of Wing-Body Combinations at Subsonic and Supersonic Speeds. AIAA Paper No. 68-55, January 1968.
- 3-9 Sears, W. R.: General Theory of High Speed Aerodynamics, Volume VI. Princeton University Press, 1954.
- 3-10 Mercer, J. E.; Weber, J. A.; and Lesferd, E. P.: Aerodynamic Influence Coefficient Method Using Singularity Splines. NASA CR-2423, December 1973.
- 4-1 Goldstein: Classical Mechanics. Addison-Wesley Publishing Company, Inc., 1959.
- 4-2 Novozhilov, V. V.: Foundations of the Nonlinear Theory of Elasticity. Graylock Press, 1953.
- 4-3 Zienkiewicz, O. C.: Finite Element Methods in Structural and Continuous Mechanics. McGraw-Hill Book Company, Inc., 1967.
- 5-1 Hildebrand: Advanced Calculus for Engineers. Prentice-Hall, Inc. 1957.